School of Chemical, Environmental and Mining Engineering

A Fundamental Investigation into The Microwave Assisted Leaching of Sulphide Minerals

MOHAMMAD AL-HARAHSHEH

Thesis submitted to the University of Nottingham for
The degree of Doctor of Philosophy

September 2005

بسم الله الرحمن الرحيم

This Thesis is dedicated first and foremost to the authors ***Mother*** *"Om Mohammad". The thesis is also dedicated to the author's Wife "Om Sondos" and his daughters: Mariam, Sondos, Istabraq and Salsabeel.*

Abstract

Microwave assisted leaching has been investigated in an attempt to improve both the yield of extracted metal and reduce processing time. This is especially pertinent in view of the increased demands for metal and more environmentally friendly processes.

This work reports a fundamental study on the influence of microwave energy on the dissolution of sulphide minerals. Chalcopyrite and sphalerite were chosen as model materials due to their economic importance and the diversity of their heating behaviour in a microwave field (chalcopyrite being an excellent microwave heater and sphalerite being an extremely poor microwave receptor).

Chalcopyrite leaching has been carried out in ferric sulphate and ferric chloride under both microwave and conventional conditions. Conventionally, it was found that chalcopyrite dissolution in ferric sulphate seems to be limited by surface reaction control. More importantly, it has been shown that specific fracture planes on chalcopyrite particle surfaces experience selective leaching, which was revealed by SEM and ToF-SIMS surface analysis. The preferential attack on particular planes is speculated to be linked to different chemistry of some cleavage planes within the chalcopyrite crystal. In the ferric chloride system, however, it was found that cupric chloride, a reaction product of chalcopyrite with ferric sulphate, may play an important role in the dissolution process.

Leaching of both chalcopyrite and sphalerite in ferric sulphate under microwave conditions has shown enhanced recoveries of metal values compared to that produced conventionally. It has been demonstrated that the enhanced copper recovery from chalcopyrite during microwave treatment is as a result of the selective heating of the mineral particles over the solution which was found to be highly lossy. In addition, it is suggested that high loss leaching solutions will develop a superheated layer close to the periphery of the reaction vessel (due to the small penetration depth) which creates localised heating compared to the bulk solution temperature. The enhanced recovery of zinc from sphalerite seems to

occur as a result of only the presence of the superheated layer. If leaching takes place within this layer, an apparent rate increase will be noted with respect to the measured bulk temperature.

The hypotheses of selective heating (for chalcopyrite) and the effect of penetration depth (for chalcopyrite and sphalerite) were supported by the negligible difference between the activation energy values under microwave and conventional conditions for both chalcopyrite and sphalerite. Furthermore, the measurements of dielectric properties of the leaching solutions have shown that such solutions are highly lossy and characterised by a penetration depth of an order of about 3 mm. Finally, numerical electromagnetic simulations showed that chalcopyrite particles could be heated selectively when microwaved within highly lossy leaching solutions due to their high conductivity.

It is concluded that the dielectric properties of both the solid and liquid phases, the dimensions of the reactor and the position of solid particles within the reactor determine the leaching outcome. More importantly, it is likely that the enhanced recoveries observed are not likely to be as a result of a so called "non-thermal microwave effect" but rather as a result of thermal effects.

Affirmation

The work reported in this thesis is solely the work of the author and has not been published elsewhere except for the following publications

Al-Harahsheh, M. and Kingman, S. W. 2004. Microwave-assisted leaching – a review. Hydrometallurgy, 73(3-4), 189-203.

Al-Harahsheh M., Kingman S., Hankins N., Somerfield C., Bowater S. The influence of microwaves on the leaching kinetics of sulphide minerals. 2004. Abstract and oral presentation presented at the 4th World Congress on Microwave and Radio Frequency Applications .7-11 November, 2004, Austin, Texas, USA

Al-Harahsheh, M., Kingman, S., Hankins, N., Somerfield, C., Bradshaw, S. and Louw, W. 2005. The influence of microwaves on the leaching kinetics of chalcopyrite. Minerals Engineering. In Press, Corrected Proof, Available online 2 August 2005.

Al-Harahsheh, M, Rutten, F, Briggs, D, Kingman, S. 2005. Preferential oxidation of chalcopyrite surface facets characterised by ToF-SIMS and SEM. Proceedings of the 15th International Conference on Secondary Ion Mass Spectrometry (SIMS XV). 12-16 September 2005, Manchester, UK.

Acknowledgments

This thesis was only made possible through the help and support of many people. Foremost, the author would sincerely like to thank his supervisor, Samuel Kingman, who has guided and encouraged him throughout his PhD study, thank you Sam for your invaluable support. Many thanks also go to the author's second supervisor, Dr. Nick Hankins, for his supervision and guidance.

Many thanks also go to each of Chris Somerfield for his help in ICP analysis, Dr. Frank Rutten and Prof. David Briggs for their great help in ToF-SIMS analysis, Prof. Steven Bradshaw for the carrying out the electromagnetic simulation and arranging for the measurements of dielectric properties of liquids and Willim Louw for the help in measuring dielectric properties of liquids.

I would like to thank Al-Hussein Bin Talal University for their sponsorship and generous financial support.

Finally a personal great thanks to the Author's wife "Suzan", and daughters: Sondos, Istabraq and Salsabeel for their patient and endless supports. Thank you Suzan.

Contents

CHAPTER THREE

Conventional and Microwave Leaching of Sulphide Minerals 31

CHAPTER FOUR

CHAPTER FIVE

CHAPTER SEVEN

List of Figures

List of Tables

List of Appendices

CHAPTER ONE

Introduction

The extraction of metal values from sulphide minerals is carried out using two approaches; high temperature pyrometallurgical and hydrometallurgical processing. In recent years there has been an interest in hydrometallurgy; it has become more attractive mainly due to environmental drivers such as lower energy demands and less emission of gases such as SO_2. Other factors such as materials handling, dust formation and the possibility of treatment of complex and low grade ores also favour hydrometallurgy.

Among sulphide minerals, chalcopyrite ($CuFeS_2$) is considered the most economically important copper mineral in terms of the scale of availability. It accounts for the world's largest source of copper. Copper is traditionally extracted from chalcopyrite by pyrometallurgy using reveberatory furnaces and flash smelting technology. About 83% of the worldwide annual primary copper production, 15 million tonnes, is produced by smelting and half of that by flash smelting technology developed by Outokumpo (Hyvarinen and Hamalainen, 2005). Much effort has been directed toward the development of processes to hydrometallurgically leach chalcopyrite using various oxidants like oxygen, ferric sulphate, ferric and cupric chloride and others. However, attempts to do so have not been successful so far due to very slow reaction kinetics, economic or technical reasons. Significant work has been carried out to improve the dissolution kinetics of chalcopyrite in ferric ion media and also to explain the reasons behind the extremely slow reaction kinetics. Until now the passivation of chalcopyrite

leaching in ferric sulphate is not completely understood and is a subject of debate. The passivation was explained by the formation of a product layer which slowed the oxidation process. There was no conclusive evidence of the nature of the passivation and the way to overcome this passivation. Several techniques have been used to increase the reactivity of chalcopyrite such as: organic extracting additions, sulfidising chalcopyrite activation, mechanical activation, the use of ozone as an oxidant (Havlik and Ukasik, 2001), or the use of promoters (silver ions, surfactants, carbon particles, iron powder or hematite) (Havlik and Kammel, 1995; Hiroyoshi et al., 2000)

Research into the application of microwave energy in chemical processing started as early as 1967 (Ford and Pei, 1967). The research into the application of microwaves in extractive metallurgy started in 1982 (Kruesi and Frahm, 1982a; Kruesi and Frahm, 1982b). It has been reported that the application of microwave energy reduces the processing time and improves the recovery of metal values. Of particular interest is the mechanism by which microwave energy interacts with metallurgical systems, and the effect of microwaves on the chemical reaction. This is a subject of significant discussion. Some authors claim that the tremendous acceleration of the reaction rate is due the presence of "non-thermal" microwave effects which significantly reduce the activation energy of the chemical reaction. Others denied the presence of the so called "non-thermal" microwave effect and explain the observed acceleration as a superheating effect where the temperature is no longer limiting the reaction conditions.

The application of microwaves to enhance the leaching kinetics of chalcopyrite has been reported recently (Antonucci and Correa, 1995; Bradshaw and Beckmann, 1998; Harrison, 1997; Havlik et al., 2002; Lovas et al., 2003; Weian, 1997; Yianatos and Antonucci, 2001). A review paper has also been published by Al-Harahsheh and Kingman (2004) which discussed the recent findings of many research studies into the microwave leaching of minerals. It was concluded that there is great disagreement with respect to the influence of microwaves on hydrometallurgical systems and there is no clear explanation of the reason behind

the higher recovery of the metal value during microwave leaching compared to conventional leaching.

It is the aim of this work to carry out a fundamental investigation into the influence of microwaves on the leaching of sulphide minerals. The understanding of the mechanisms by which microwaves act upon leaching systems is of particular importance for more efficient microwave processing and also to be able to determine the optimum microwave leaching conditions and potential scale up.

In order to carry out this work, two model sulphide minerals were chosen: chalcopyrite and sphalerite. Both minerals account for most of the copper and zinc production in the world. In terms of microwave heating characteristics, chalcopyrite was found to heat readily in microwave fields, whereas, sphalerite is considered to be one of the poorest microwave couplers among the sulphide minerals.

Two leaching systems were chosen to carry out this research. These are ferric sulphate and ferric chloride, with more focus on ferric sulphate. In order to investigate the effect of microwaves on leaching systems, it was felt very important to understand the conventional leaching systems. As mentioned earlier a great discrepancy was found in the literature regarding the leaching kinetics of chalcopyrite, as well as the reason behind the slow reaction kinetics. Therefore, an extensive conventional leaching study was carried out upon the leaching kinetics of chalcopyrite. In addition, surface analysis study of chalcopyrite was carried out using a powerful surface analysis technique, Time of Flight Secondary Ion Mass Spectrometry (ToF-SIMS) and also Scanning Electron Microscopy (SEM).

The leaching of both chalcopyrite and sphalerite will be carried out under conventional and microwave conditions, the results will then be compared. Furthermore a comprehensive study of the dielectric properties of both leaching solutions and solid materials will be carried out. Microwave heating of the leaching solutions will then be investigated without solids under different conditions, followed by a numerical simulation study which will be carried out in collaboration with Prof. Steven Bradshaw (2005), Stellenbosch University, South

Africa. Finally, conventional and microwave leaching results, dielectric properties measurement data, microwave heating of liquids data, numerical simulation results and other data from the literature will be analysed in order to provide an understanding of the mechanisms behind the interaction of microwave energy with sulphide minerals in leaching solutions.

.

CHAPTER TWO

Principles of Microwaves and Microwave Heating

2.1 Microwave Spectrum and Electromagnetic Waves

Microwaves are a form of electromagnetic energy, which travels in high frequency waves. The wave lengths of microwaves are between 1 mm and 1 m with corresponding frequencies between 300 GHz and 300 MHz respectively.

Figure 2-1 shows a logarithmic scale of the electromagnetic spectrum. The frequencies allocated for microwave heating are designated as ISM "industrial, scientific and medical". ISM frequency bands are listed in Table 2-1. The most commonly used frequencies for heating purposes are 915 MHz (896 in the UK) and 2.45 GHz, which correspond to wave lengths of 32.78 and 12.24 cm. These frequencies were chosen by international agreement to minimise the interference with communication systems (Meredith, 1998). The longer wavelength of 915 MHz frequency is commonly used in industrial ovens where deeper penetration is required. The higher frequency 2.45 GHz is more practical for domestic ovens and is also used widely in industry as the wavelength of this frequency (12.2 cm) is more suitable for domestic ovens, where the cavity must be at least two wavelengths in two dimensions to work efficiently.

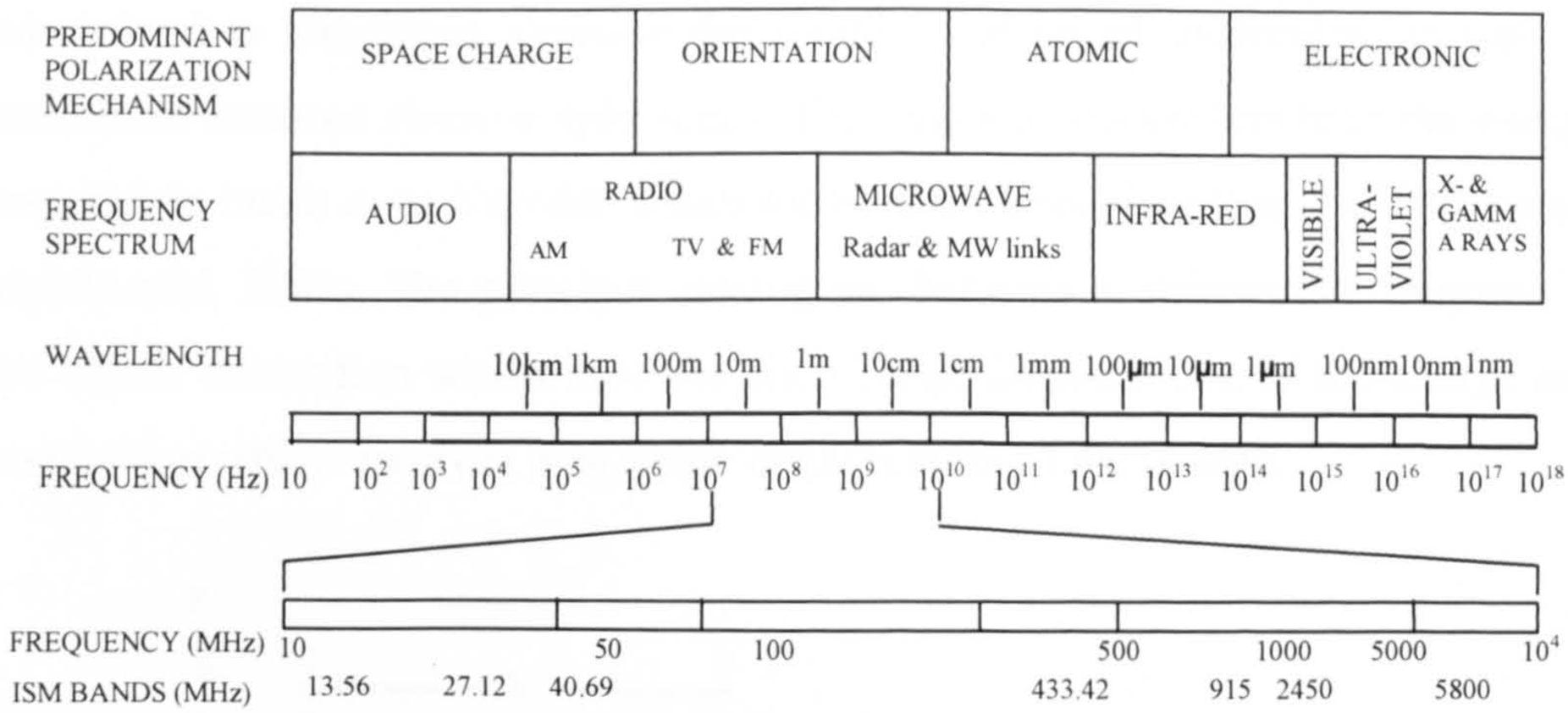

Figure 2-1 The electromagnetic spectrum (Meredith, 1998)

A propagating electromagnetic wave has two components, an electric field (E; V/m) and a magnetic field (H; A/m). These components are vectors and are always perpendicular to each other (see Figure 2-2). In free space the propagating wave has a velocity (c) of about 3.0×10^8 m/s, and this is the maximum speed at which energy can travel. The relationship between the frequency and the wavelength is represented by the following equation (Sucher and Fox, 1963):

$$\lambda = c / f \qquad \textbf{Equation 2-1}$$

where: λ is the wavelength in free space (m), c is the speed of light (m/s), f is microwave frequency (1/s or Hz)

Table 2-1 ISM frequency bands (Saltiel and Datta, 1999)

Designation	Band	Central frequency
UHF-Ultra high frequency	433.05-434.79 MHz	433.92 MHz
UHF-Ultra high frequency	902-928 MHz	915 MHz
UHF-Ultra high frequency	2400-2500 MHz	2.450 GHz
SHF-Super High Frequency	5725-5875 MHz	5.8 GHz
SHF-Super High Frequency	24-24.25 GHz	24.125 GHz
EHF-Extremely high frequency	61-61.5 GHz	61.25 GHz
EHF-Extremely high frequency	122-123 GHz	122.5 GHz
EHF-Extremely high frequency	244-246 GHz	245 GHz

2.2 Principles of Microwave Heating

Microwave heating is a process within a family of electro-heat techniques, such as induction, radio frequency, direct resistance, and infrared heating, which utilize specific parts of the electromagnetic energy (Fletcher, 1995). Microwaves are non ionising irradiation and correspond to photon energies typically between about 1.24×10^{-6} and 1.24×10^{-3} eV (Chemat and Esveld, 2001). These energies

correspond to transitions between the rotational states of molecules, as well as transitions between electron spin states. Their values also are less than the energy required to break even Van der Waals molecular forces (less than 2 eV) (Chemat and Esveld, 2001). The principal heating mechanisms at microwave frequencies are dipole orientation which involves short range displacement of the charge and conduction which involves long range displacement of the charge.

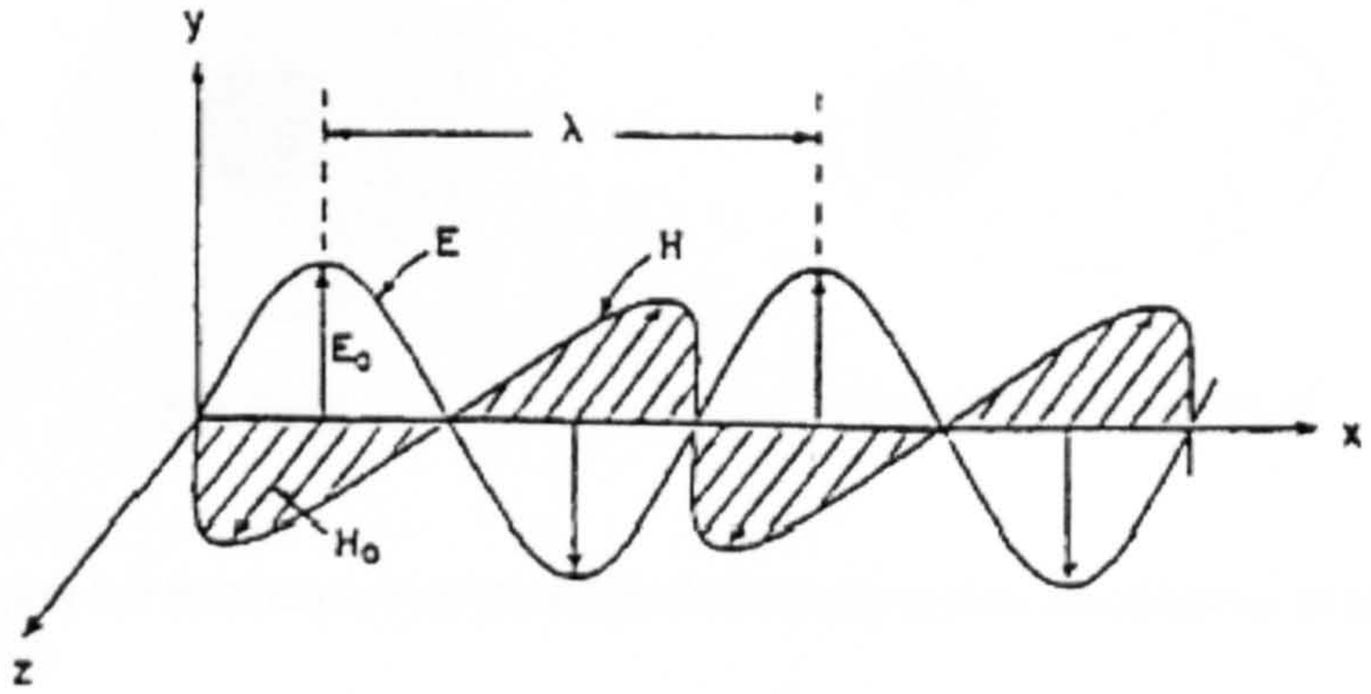

Figure 2-2 Electromagnetic wave components: E-electric field, H-magnetic field, λ-wavelength (Ryynanen, 2002)

2.2.1 Dielectric Polarisation

Dielectric material is one which contains either permanent or induced dipoles which when placed between two electrodes acts as a capacitor. In other words, the material allows charge to be stored and dc conductivity is observed between the plates (Gabriel et al., 1998). Microwave heating of dielectric materials, therefore, arises from the ability of the electric field to polarize the charge of the material where polarisation cannot follow the rapid change of the electric field. The main types of dielectric polarisation are: electron polarisation, atomic polarisation, orientation polarisation and space charge or Maxwell-Wagner polarisation (Metaxas and Meredith, 1983; Saltiel and Datta, 1999).

2.2.1.1 Electronic Polarisation

Matter consists of positive atomic nuclei surrounded by a negative electron cloud. Electronic polarisation occurs when an applied electric field displaces the electron cloud centre of an atom relative to the centre of the nucleus inducing dipole

moment (von Hippel, 1954). Figure 2-1 shows a schematic representation of an atom after it was exposed to an electric field. This kind of polarisation occurs at high frequencies (close to the ultraviolet) and it is of little significance at microwave frequencies.

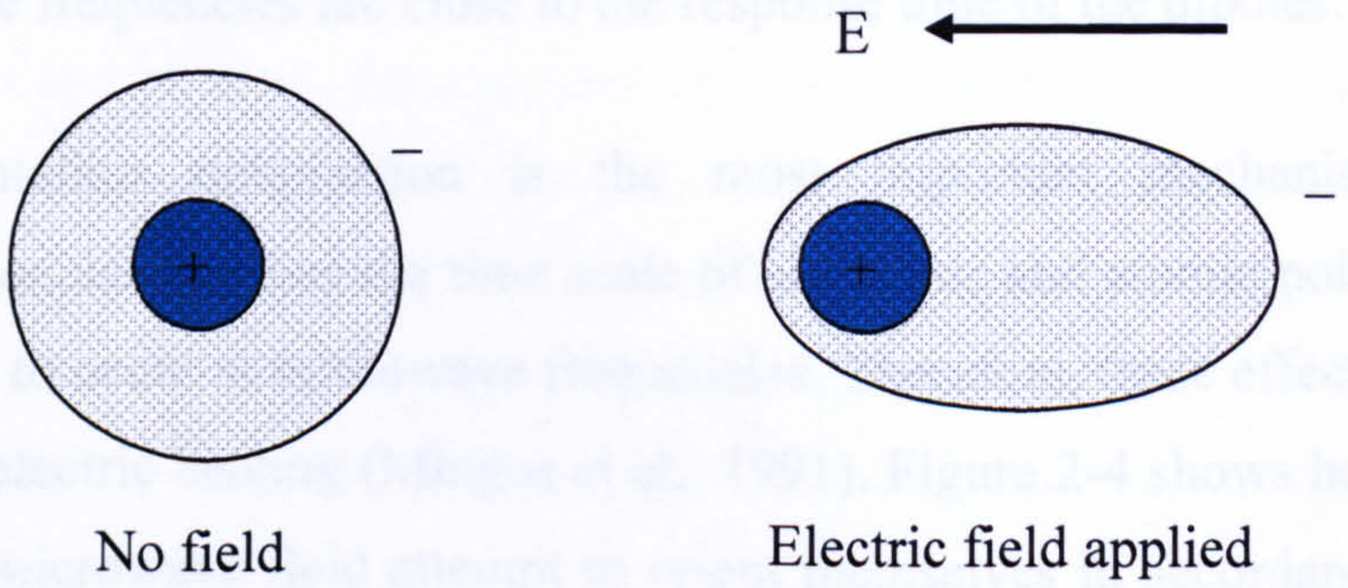

Figure 2-3 Schematic representation of the electronic mechanism of polarisation (von Hippel, 1954)

2.2.1.2 Atomic Polarisation

When atoms of different types form a molecule, they will not normally share their electrons symmetrically, because the electron clouds will be displaced toward the stronger binding atoms in an eccentric fashion. Therefore, atoms acquire charges of different polarity (von Hippel, 1954). Atomic polarisation is induced due to the separation of negative and positive ions in a molecule as a result of an applied electric field which tends to change the equilibrium state of the atoms themselves. Atomic polarisation involves the displacement of nuclei relative to the other nuclei in a molecule. This type of polarisation occurs predominantly at infra-red frequency band and is referred to as ionic polarisation

2.2.1.3 Orientation Polarisation

Dipole alignment or orientation polarisation occurs in dielectrics containing permanent dipoles due to the highly asymmetric charge distribution in a molecule which makes them sensitive to the alternating electric field where they tend to reorient themselves to follow the phase change. At low frequencies, dipoles are able to align themselves in phase with the electric field. Whilst some energy is

gained by the molecule by this behaviour, and some is also lost in collisions, the overall heating effect is small. At very high frequencies, dipoles do not have enough time to respond to the change in electric field and therefore do not rotate. As the motion of dipoles is inhibited, there is no energy transfer and therefore no heat is generated. In the range between the two extremes is the microwave region where frequencies are close to the response time of the dipoles. (Whittaker, 1997).

Orientation polarisation is the most important mechanism at microwave frequencies because the time scale of electronic and atomic polarisations is far too great to occur at microwave frequencies. Therefore, these effects do not contribute to dielectric heating (Mingos et al., 1991). Figure 2-4 shows how polar molecules in a microwave field attempt to orient themselves in accordance with the rapidly changing electric field.

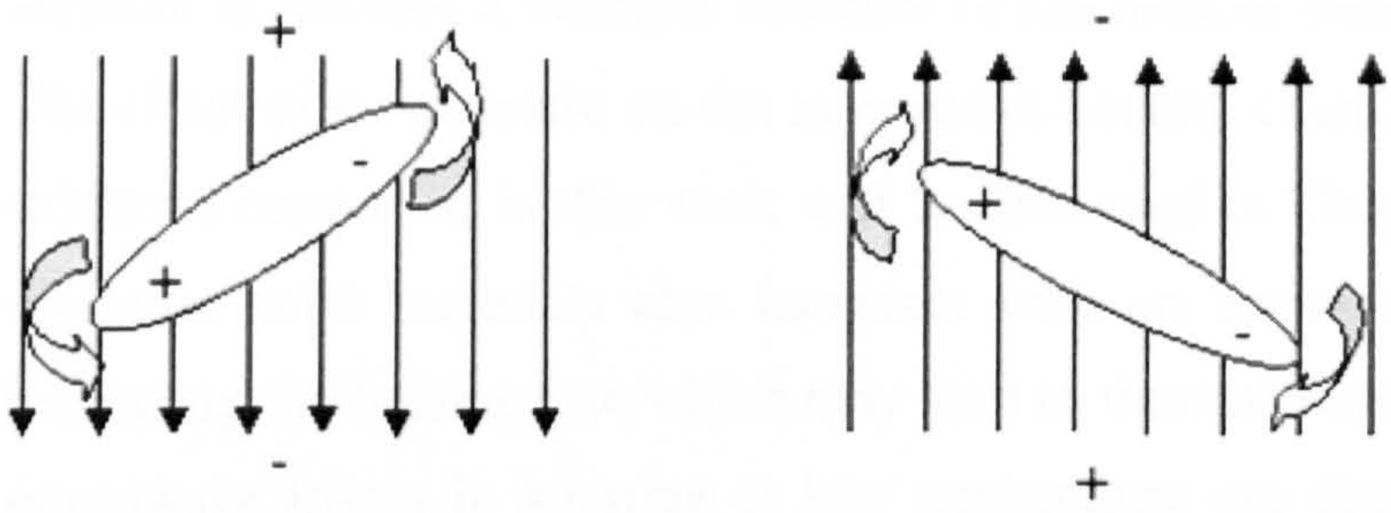

Figure 2-4 Movement of a dipole in an electromagnetic field (Schaefer, 1999)

2.2.1.4 Space Charge Polarisation

Maxwell-Wagner or space charge polarisation arises from the build up of charges at an interface between components in heterogeneous systems comprising a small fraction of a conduction phase in a non conducting medium. Space charge polarisation relates to the build up of charged particles at the interfaces in heterogeneous dielectrics which have different permittivity and conductivity values. For example, conductive metal particles dispersed within transparent sulphur powder. Neither of these materials will heat when irradiated on its own. However, the combination is readily heated. The actual mechanism is a combination of conduction and dipolar effects. This polarisation takes place mainly at frequencies of less than 50 MHz (Metaxas and Meredith, 1983).

2.2.2 Ionic Conduction

Ionic conduction is another important microwave heating mechanism. When an electrical conductor is subjected to microwave irradiation, charge carriers (electrons or ions) move under the influence of electric field resulting in polarisation. The induced current causes heating due to any electric resistance. For high conducting materials, such as metals, microwaves do not penetrate to the surface. Instead microwaves will be reflected which may cause some arcing on the surface (Whittaker, 1997). Water heats by a dipolar mechanism and this will be discussed in Section 2.5. However, addition of ions to water increases its conductivity and therefore causes the ionic solution to heat by Joule heating coupled with dipole losses.

The increase of temperature also increases the conductivity thus allowing the ionic solution to become a stronger absorber of microwave energy as they are heated. The effect of temperature on the microwave heating characteristics of some ionic solutions concerned in this work will be discussed in Chapter 6. Conductivity of dielectric solid materials also increases with an increase of temperature, thus increasing the heating rate which may lead to thermal runaway. For example, the microwave losses in alumina at low temperature are due to dipolar relaxation. However, as the temperature increases conduction losses increase rapidly and become more important than dipolar losses. The increase of alumina conductivity with temperature is associated with the thermal activation of the electrons which pass from the oxygen $2p$ valence band to the $3s3p$ conduction band (Mingos and Baghurst, 1991).

2.3 Dielectric Properties of Materials

The electrical behaviour of materials when they are exposed to electromagnetic field is characterised by the following parameters: permittivity (ε, F/m), permeability (μ, H/m) and conductivity (σ, S/m). Permittivity is the ratio of electric displacement to electric field strength and it describes the interaction of the material with the electric field. Similarly, the permeability is the ratio between

the magnetic flux density and magnetic field strength and it describes the interaction with the magnetic field. The electrical conductivity is closely related to the permittivity and characterises free-electron conductive properties (Saltiel and Datta, 1999)

Materials with low values of conductivity are classified as dielectrics, whereas, those with high values of conductivity are called conductors (Meredith, 1998).

2.3.1 Permittivity and Loss Factor

The permittivity of a material is composed of a real part (ε', dielectric constant) and an imaginary part (ε'', dielectric loss factor). Dielectric constant and loss factor are used to express the dielectric response of materials in microwave fields. The dielectric constant measures the ability of the material to store microwave energy or in other words it measures the ability of material to be polarised. The latter measures the ability of material to dissipate the stored energy into heat (Galema, 1997; Metaxas and Meredith, 1983). Permittivity (ε^*) can be expressed as:

$$\varepsilon^* = \varepsilon_a^{'} - j\varepsilon_a^{''} \qquad \textbf{Equation 2-2}$$

Where $j = \sqrt{-1}$. Alternatively,

$$\varepsilon^* = \varepsilon_O(\varepsilon_r^{'} - j\varepsilon_{eff}^{''}) \qquad \textbf{Equation 2-3}$$

where $\varepsilon_a^{'}$ is dielectric constant (F/m), $\varepsilon_a^{''}$ is loss factor (F/m), ε_O is the permittivity of free space (8.86×10^{-12} F/m), $\varepsilon_r^{'}$ is the relative dielectric constant, $\varepsilon_{eff}^{''}$ is the effective relative dielectric loss factor (throughout the thesis the relative dielectric constant and effective relative loss factor will be designated as ε' and ε'' respectively).

The effective relative loss factor characterizes the loss contribution from all of various mechanisms mentioned above in Section 2.2. Since it is difficult to separate the losses due to conduction from those caused by polarisation using experimental techniques (such as cavity perturbation and coaxial probe

technique), all losses can be summed together, thus expressing ε'' as follows (Metaxas and Meredith, 1983):

$$\varepsilon''(\omega) = \varepsilon_d^{"}(\omega) + \varepsilon_e^{"}(\omega) + \varepsilon_a^{"}(\omega) + \varepsilon_s^{"}(\omega) + \frac{\sigma}{\varepsilon_O \omega} \qquad \textbf{Equation 2-4}$$

where ω is the angular frequency (rad.s^{-1}) . Subscripts: *(d), (e), (a)* and *(s)* refer to dipolar, electronic, atomic and space charge (Maxwell-Wagner) polarisation respectively.

The loss tangent provides an indication of how well a material dissipates stored energy into heat (Chan, 2000):

$$\tan\delta = \frac{\varepsilon''}{\varepsilon'} \qquad \textbf{Equation 2-5}$$

In a way similar expressing the dielectric loss under the influence of electric field, a complex permeability can be defined to describe loss in ferromagnetic materials (Saltiel and Datta, 1999):

$$\mu = \mu' - j\mu'' = \mu_O(\mu_r' - j\mu_{eff}'') \qquad \textbf{Equation 2-6}$$

where μ' is the permeability (H/m), μ'' is the effective magnetic loss factor due to relaxation and resonance processes under the influence of an alternating magnetic field. μ_O is the permeability of the free space ($4\pi \times 10^{-7}$ H/m).

2.3.2 Penetration Depth

When an electromagnetic wave propagates into a dielectric material, its amplitude diminishes due to the absoption of power into the material. In absence of reflection, the field intensity and its associated power flux density fall exponentially with distance from the surface. The rate of decay of the power dissipation is a function of both the relative permittivity and the loss factor. The penetration depth (D_P, m) is defined as the distance from the material surface where the absorbed electric field falls to 1/e of the electric filed at the surface. D_P is given by (Meredith, 1998):

$$D_p = \frac{c}{2\pi f\sqrt{2\varepsilon'}\left[\sqrt{1+\tan^2\delta}-1\right]^{1/2}} \qquad \textbf{Equation 2-7}$$

When $\varepsilon''/\varepsilon' << 1$, Equation 2-8 simplifies to:

$$D_p = \frac{c(\varepsilon')^{1/2}}{2\pi f\varepsilon''} \qquad \textbf{Equation 2-8}$$

It follows that the penetration depth is inversely proportional to frequency. In general, the penetration depth at frequencies below 100 MHz is of the order of meters and presents little problem for power penetration unless loss factors are extremely high (Metaxas and Meredith, 1983). At microwave frequencies, D_P is correspondingly smaller and often the size of the treated material is larger than the penetration depth which could result in non-uniform heating. The greatest rate of heating is often achieved at high frequencies, for example, for water the greatest heating occurs at 18 GHz where the dielectric loss factor is at its maximum value. However, the penetration depth at such frequencies is so low that only thin layer of the material will heat (Mingos and Baghurst, 1991; Thostenson and Chou, 1999).

In conventional furnaces, heat is transferred to the material by thermal radiation. The penetration depth of infrared radiation (f=10^{13} s^{-1}) is very small ($D_P << 10^{-4}$m) in the majority of solids, which means a very thin layer of the material will heat up and the rest of the material will be heated at a rate which depends on the heat transfer properties of the material. Obviously, this can result in significant temperature gradients. In the microwave frequency range D_P varies from meters to millimetres depending on the frequency, temperature, chemical composition and microstructure (Bykov et al., 2001). Minimization of temperature gradient across a material as a result of microwave heating can therefore give more uniform heating. The penetration depth of microwave energy at various frequencies into pyrite has recently been investigated (Cumbane, 2003). It was shown that penetration depths within the order of several centimetres are possible but are highly frequency dependant. Tests were carried out at frequencies of 615 MHz, 1.4 and 2.21 GHz and the penetration depth was calculated to reduce from 14 cm

at 615 MHz to about 4 cm at 2.21 GHz. This suggests that if large pieces of material are to be treated, then lower frequency energy should be used.

2.3.3 Skin Depth

Skin heating occurs when high frequency currents flow through a conductor causing an eddy current to flow in the opposite direction. These currents remain confined to the near-surface in a thin skin. The skin depth δ_S (m) is defined as the depth into the conductor from the surface at which the current density is 1/e (=0.368) of its value at the surface (Meredith, 1998). It is given by the following formula:

$$\delta_S = \sqrt{\frac{2}{\sigma\omega\mu_0}} \qquad \textbf{Equation 2-9}$$

where: σ is the conductivity, S/m; ω is the angular frequency, rad.s^{-1} ($\omega = 2\pi f$), μ_0 is the permeability of free space ($4\pi\times10^{-7}$ H/m).

The eddy current heating effect is more pronounced when the dimensions of the metallic sample are comparable with the skin depth. In other words, as the skin depth increases the conduction losses diminish meaning that the conductivity of the material is low enough to produce the required eddy currents. However, the conductivity of metallic materials increases exponentially with an increase in temperature according to the following equation (Mahan, 1976; Tebble, 1969):

$$\sigma = \sigma_0 EXP(-Ep/KT) \qquad \textbf{Equation 2-10}$$

where Ep is the activation energy (J) and K is Boltzmanns constant ($1.38\text{x}10^{-23}$ J/K)

In addition, from Equation 2-9 it can be seen that the skin depth depends on the conductivity and the frequency. Therefore, eddy current losses are more likely to become important at high temperatures as seen from Equations 2-9 and 2-10.

The skin depth is not the same as the penetration depth discussed in Section 2.3.2. Penetration depth effect arises essentially from the dielectric losses which causes the dissipation of the power (see Section 2.7).

2.4 Material Interactions with Microwaves

Depending on the response to microwave heating, materials can be classified into three groups with respect to their interaction with the microwave field (Figure 2-5): transparent or low loss materials where microwaves pass through without any losses; conductors which reflect microwaves without any penetration; and absorbing or high loss materials, which absorb microwaves and dissipate them into heat depending on the value of dielectric loss factor. There is a fourth category of materials when a material contains two or more phases with different dielectric properties. In this case microwaves can selectively heat the high loss phase passing through the low loss one without significant losses (Clark et al., 2000).

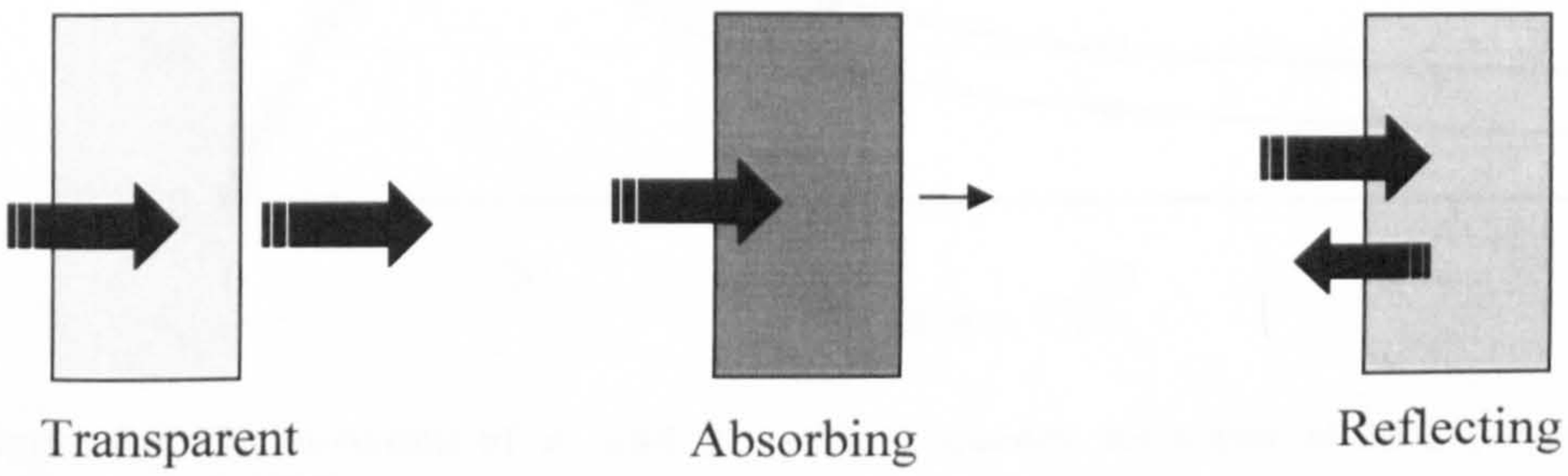

Figure 2-5 Schematic illustration of the interaction of transparent (insulator), absorbing (dielectric), and reflecting (conductors) materials with microwave irradiation.

2.5 Microwave Heating of Liquids

Some liquids contain permanent dipole moments in their structure. Their magnitude depends on the size and symmetry of the molecule. For example, carbon tetrachloride (CCl_4) and methane (CH_4) are non-polar and have zero dipole moment, whereas, water (H_2O) is polar because it has no charge symmetry and exhibit dipole moments. Loss factor of a polar liquid depends strongly on its

dipole moments in conjunction with its dependence on the frequency and relaxation time (Metaxas and Meredith, 1983). On the other hand, the liquid ability to absorb microwaves is determined by induced or permanent dipole moments because polarisation of dielectrics arises from the rotation of dipoles in an electric field which involves the physical rotation of molecular dipoles (Gabriel et al., 1998). When frequency increases, the molecular forces imbedding the dipole orientation become more predominant and the contribution to the orientation of permanent dipoles to the storing ability (dielectric constant) becomes less predominant (Hasted, 1973). An example on that the behaviour of water dielectric properties is shown in Figure 2-6.

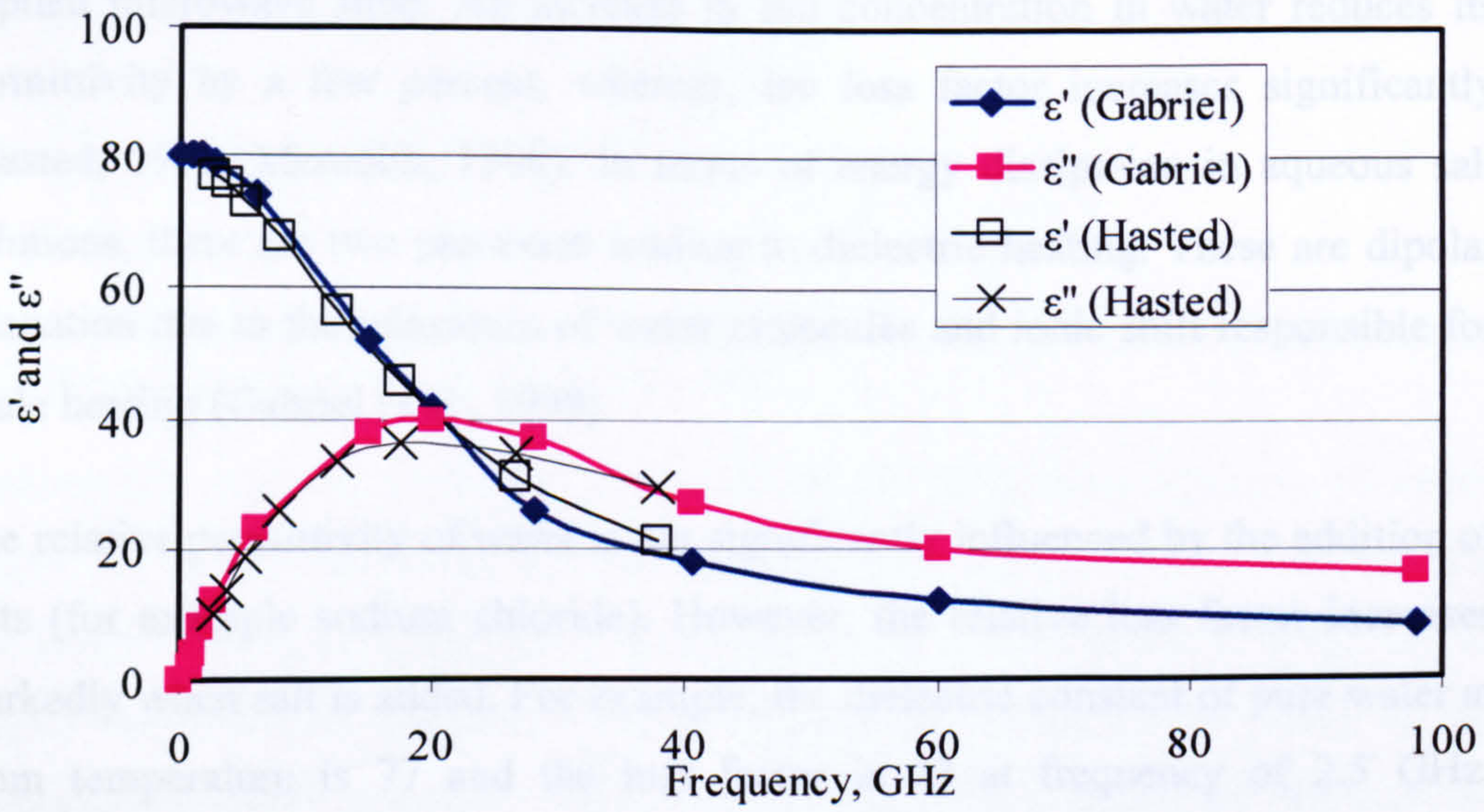

Figure 2-6 The variation of ε' and ε'' with frequency for water at 20°C (Gabriel et al., 1998; Hasted, 1973)

The behaviour of dielectric constant (ε') and loss factor (ε'') for water is well reproduced by the Debye equations (Gabriel et al., 1998; Metaxas and Meredith, 1983).

$$\varepsilon' = \varepsilon_\infty + \frac{\varepsilon_S - \varepsilon_\infty}{1+\omega^2\tau^2} \qquad \textbf{Equation 2-11}$$

$$\varepsilon'' = \frac{(\varepsilon_S - \varepsilon_\infty)\omega\tau}{1+\omega^2\tau^2} \qquad \textbf{Equation 2-12}$$

where ε_s and ε_∞ are the dielectric constants at d.c. and very high frequencies respectively; τ is the relaxation time (s).

Relaxation time is the delay in the response of the medium to electromagnetic stimulation. The relaxation time of water at temperature 20°C is about 9×10^{-12}s which means the relaxation frequency of water is about 18 GHz (Hasted, 1973). Therefore, the maximum conversion of microwave into thermal energy occurs at this frequency.

The introduction of ions into water has a significant effect on its dielectric properties and structure. This, therefore, affects water heating characteristics in an applied microwave field. An increase in ion concentration in water reduces its permittivity by a few percent, whereas, the loss factor increases significantly (Hasted, 1973; Meredith, 1998). In terms of energy dissipation in aqueous salt solutions, there are two processes leading to dielectric heating. These are dipolar relaxation due to the relaxation of water molecules and ionic shift responsible for Joule heating (Gabriel et al., 1998).

The relative permittivity of water is not significantly influenced by the addition of salts (for example sodium chloride). However, the relative loss factor increases markedly when salt is added. For example, the dielectric constant of pure water at room temperature is 77 and the loss factor is 13 at frequency of 2.5 GHz. However, for 0.5 M sodium chloride solution the corresponding values of dielectric constant and loss factor are 68 and 54 measured at the same conditions (Meredith, 1998). The penetration depth of water is reduced significantly by the introduction of ionic salts. The reason for that is the dramatic increase in dielectric loss factor when sodium or potassium chloride is added to the water (see Figure 2-7) (Gabriel et al., 1998).

According to Hasted (1973) the slight decrease in the dielectric constant following the addition of ions is that the ions orient the water molecules around them, thereby reducing their ability to orient in the applied electric field, and so reducing the dielectric constant by a local high-field effect. The contribution of conducting

loss to the relative effective loss factor becomes more evident with the increase of ions concentration due to the marked increase of conductivity (Boughriet et al., 1999). Therefore, the introduction of ions into water leads to marked effect on the heating rate.

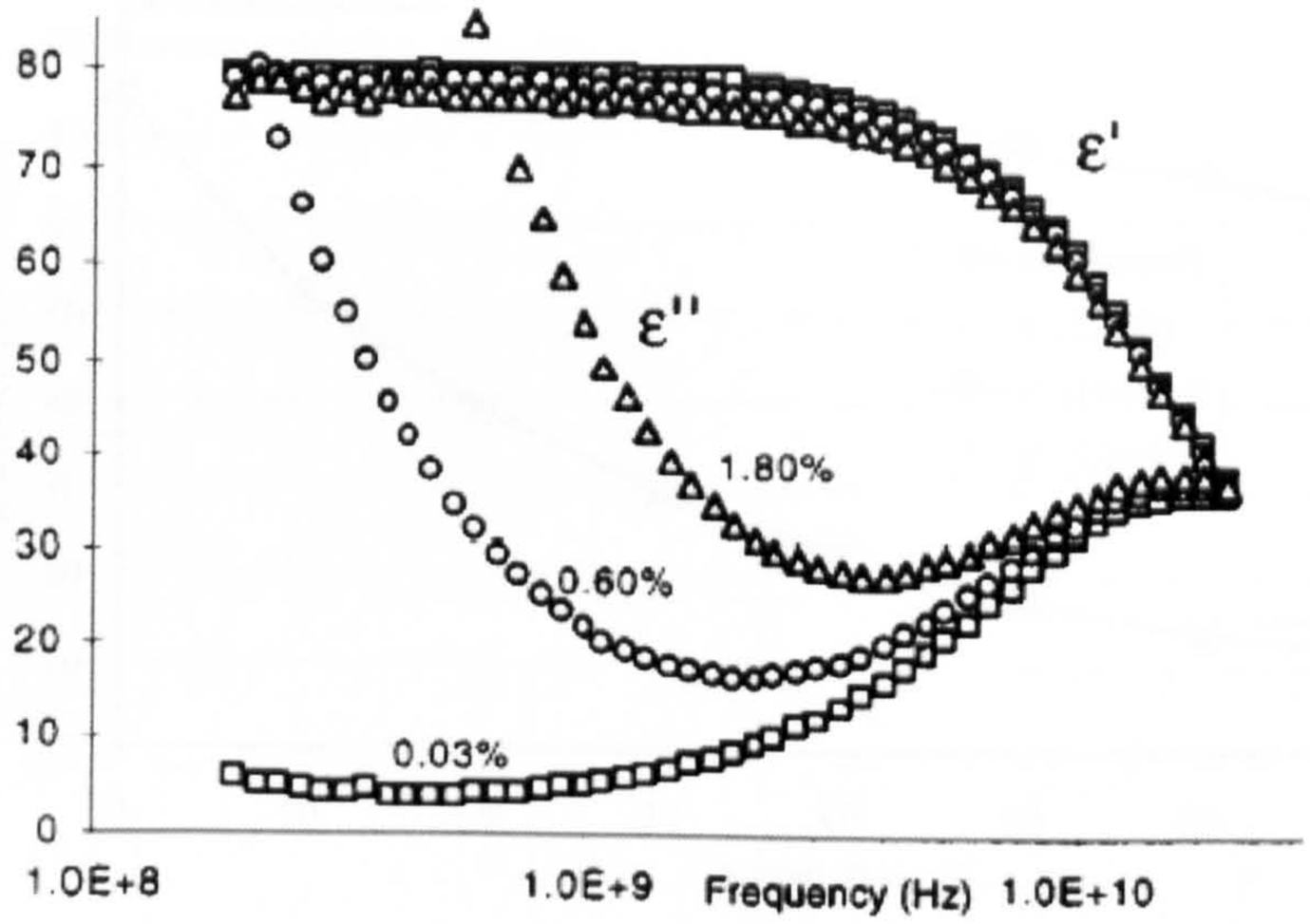

Figure 2-7 Experimental values of the dielectric constant and loss factor for KCl solutions with differing concentrations (Gabriel et al., 1998)

Temperature also has significant influence on the dielectric properties of water. Figure 2-8 shows that as the temperature increases, both dielectric constant and loss factor experience drops. The drop in loss factor is more dramatic compared to that of the dielectric constant. This in turn has an effect on the value of the penetration depth of microwaves through the water. These issues are discussed in more details in Chapter 6.

The drop in the loss factor as the temperature increases is linked to the reduction in relaxation time, with the later being inversely proportional to the temperature according to the following Equation 2-13 (Hasted, 1973):

$$\tau = \frac{4\pi \bar{r}^3 \eta}{KT} \qquad \textbf{Equation 2-13}$$

where $\bar{r}$ is molecular radius (m), η is viscosity (kg/(m.s)), K is Boltzman constant (1.3807×10^{-23}J.K^{-1}), and T is temperature (K).

It is believed that the relaxation time is related to the number of hydrogen bonds which are required to break to obtain mobile water molecules that are able to reorient with the applied electric field (Buchner et al., 1999).

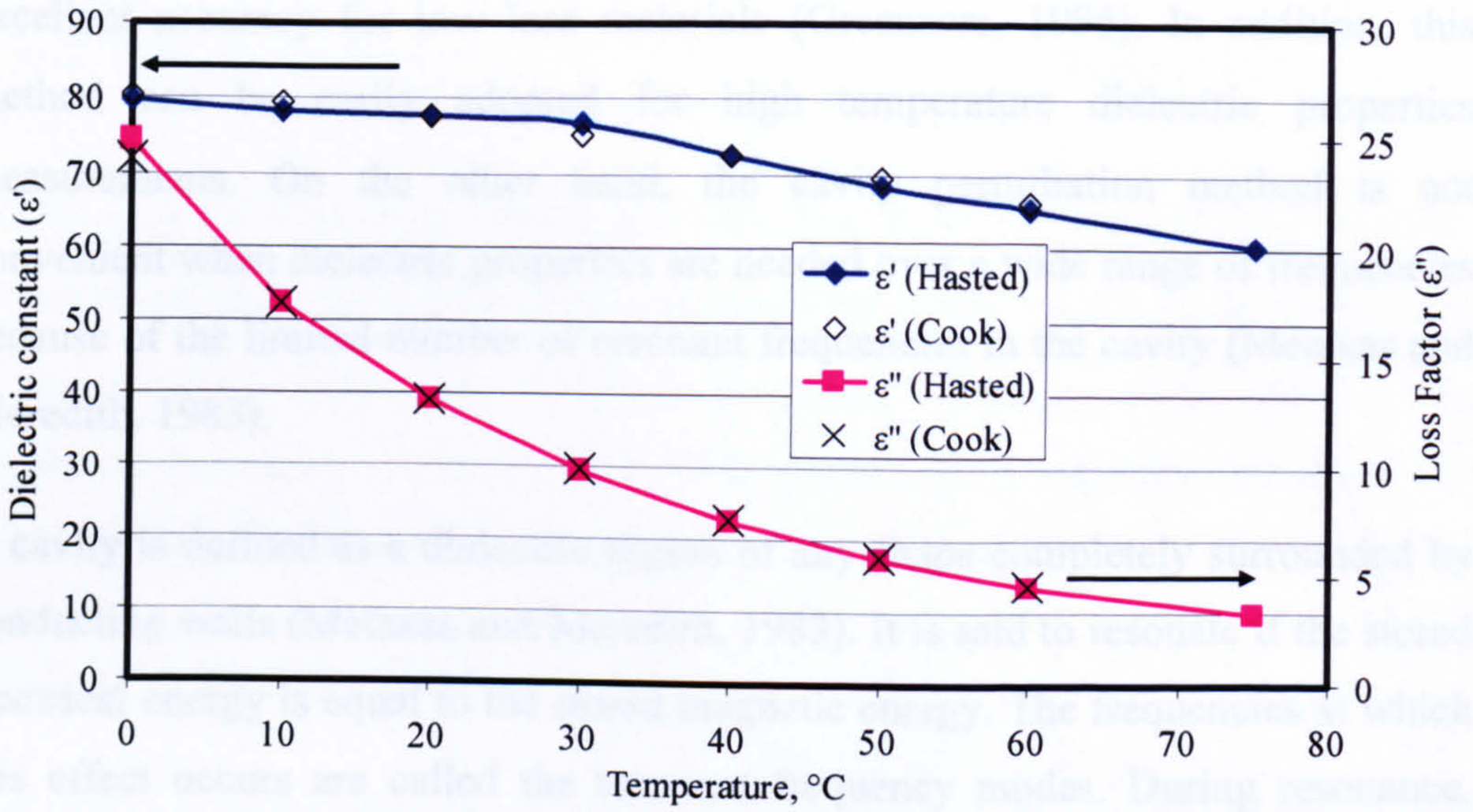

Figure 2-8 The effect of temperature on the dielectric properties of water at a frequency of 3 GHz ((Cook, 1952; Hasted, 1973)

2.6 Methods for Measurements of Dielectric Properties

Knowledge of a material dielectric property is critical for proper design of microwave applicators. The measurement of dielectric properties is not an easy task and it requires specialised techniques. The choice of dielectric properties measurement technique depends on the required frequency and the properties of the material. For frequencies of less than 100 MHz, Bridge and *Q*-metre methods are employed but are not used for measurements at microwave frequencies. Measurements using coaxial lines, wave-guides or resonant cylindrical cavity techniques are considered to be the most suitable for frequencies above 100 MHz (Metaxas and Meredith, 1983). The permittivity of the sample is calculated from the measured reflection for non resonant methods and from the measured resonant frequency and Q-factor for resonant methods. In the following sections two methods are considered in some detail as they are employed to measure the dielectric properties of the solids and liquids used in the current research.

2.6.1 Cavity Perturbation

The cavity perturbation method has long been regarded as a suitable tool for investigating the dielectric properties of materials and is capable of providing excellent accuracy for low loss materials (Greenacre, 1996). In addition, this method can be easily adopted for high temperature dielectric properties measurements. On the other hand, the cavity perturbation method is not convenient when dielectric properties are needed over a wide range of frequencies because of the limited number of resonant frequencies in the cavity (Metaxas and Meredith, 1983).

A cavity is defined as a dielectric region of any shape completely surrounded by conducting walls (Metaxas and Meredith, 1983). It is said to resonate if the stored electrical energy is equal to the stored magnetic energy. The frequencies at which this effect occurs are called the resonant frequency modes. During resonance, energy is dissipated in the walls of the cavity. This loss gives rise to quality factor (Q) of the cavity (see Equation 2-14), which is a direct measurement of its looseness. The insertion of a sample into the cavity alters the energy dissipation characteristics of the cavity as well as the resonant frequency and knowledge of these alterations allows the dielectric properties of the sample to be estimated.

$$Q = \omega \frac{Energy\_stored}{Energy\_Dissipated} \qquad \textbf{Equation 2-14}$$

The resonant cylindrical cavity technique is based on this simple perturbation theory, which assumes that the change in the stored energy in the cavity between the loaded and unloaded conditions is very small. This means that the electromagnetic fields in the cavity with and without the sample must be approximately equal. Therefore, the dimensions of the sample must be small compared with the size of the cavity resulting in a small frequency shift. In addition, the symmetry of the sample within the cavity is important (Metaxas and Meredith, 1983).

Dielectric properties (dielectric constant and loss factor) can be calculated if the resonant frequency shift and the Q factor after the insertion of the sample are

known. This can be carried out using the following equations (Equations 2-15 & 2-16)

$$\varepsilon' = 1 + 2 * J_1^2 * (X_{l,m}) * \frac{\overline{V}_0}{\overline{V}_S} * \frac{f_0 - f_s}{f_0} \qquad \textbf{Equation 2-15}$$

$$\varepsilon'' = J_1^2 * (X_{l,m}) * \frac{\overline{V}_0}{\overline{V}_S} * (\frac{1}{Q_s} - \frac{1}{Q_0}) \qquad \textbf{Equation 2-16}$$

where: J_1 is the first order Bessel function, $X_{(l,m)}$ is the m^{th} root of the first order Bessel function ($J_1(x)=0$), $\overline{V}_0$ is the volume of the cavity (mm^3), $\overline{V}_S$ is the volume of the sample (mm^3), f_0 is resonance frequency of empty cavity (Hz), f_s is resonance frequency of empty cavity(Hz), Q_0 and Q_s are quality factors of the empty cavity and the cavity with a sample.

2.6.2 Coaxial Line Method

This method is also called the Roberts and von Hippel method and the open-ended coaxial probe (Metaxas and Meredith, 1983). It involves the examination of standing waves in a transmission line (or waveguide) terminated by a section filled with the dielectric material under investigation. A schematic diagram of the apparatus and the standing pattern associated with it is shown in Figure 2-9.

The open ended coaxial probe method has been used for measuring the dielectric properties of solids (Arai et al., 1993; Bringhurst and Iskander, 1996; Santos et al., 2002) and liquids (Boughriet et al., 1999; Price, 1973; Raicu, 1995). The main attractive features of coaxial probe technique are (Greenacre, 1996):

It is a broad band technique which allows a very wide frequency sweep in a few seconds, whereas the resonant methods are not convenient when data is needed at many frequencies.

Coaxial probe method is suited to measure dielectric properties of high loss material. However, large numbers of dielectric property measurement techniques, including the cavity perturbation, are suited to measuring low loss materials.

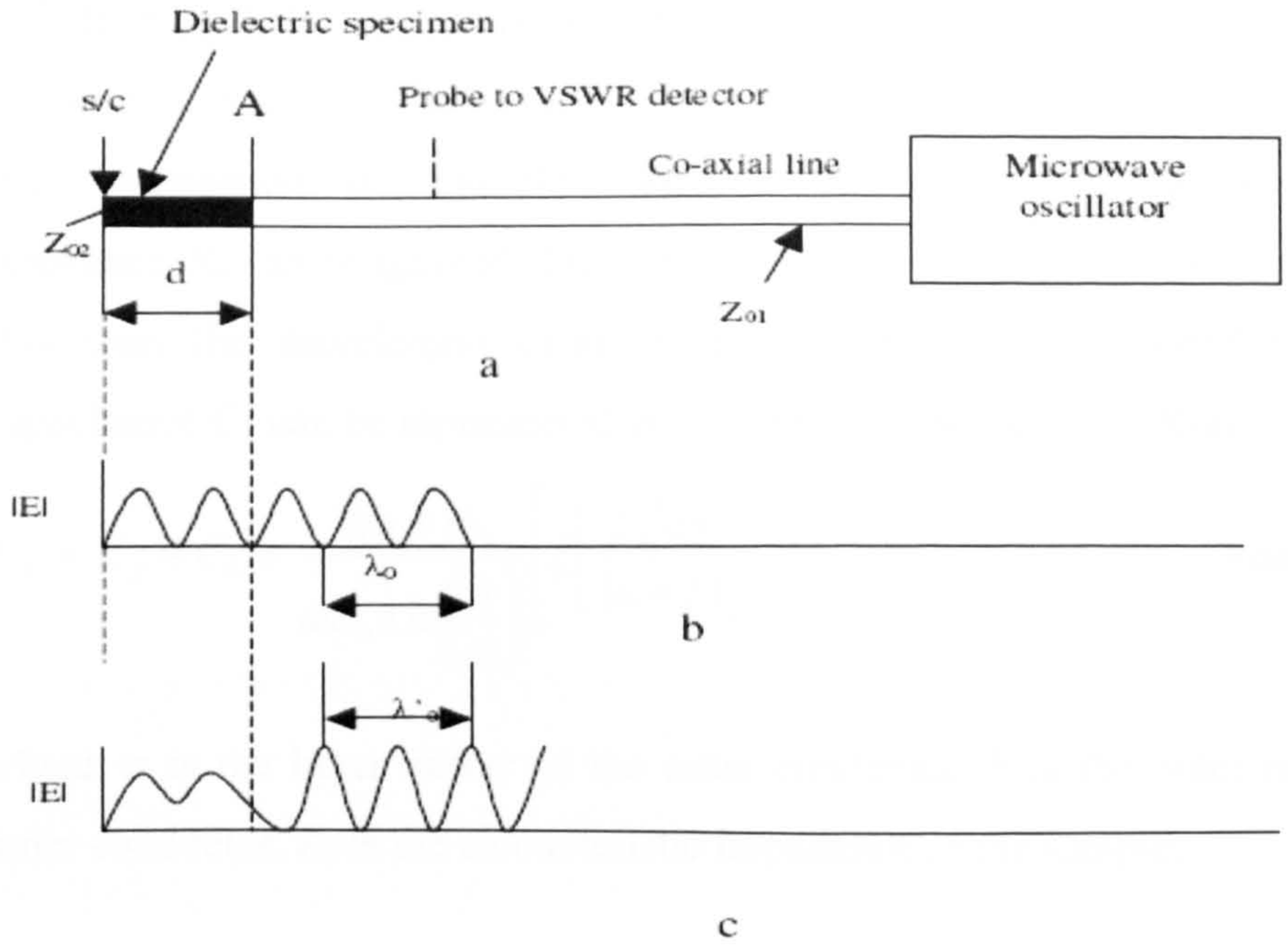

Figure 2-9 Coaxial line method for dielectric properties measurements: (a) general form of the apparatus, (b) standing wave pattern with empty slotted coaxial line, (c) standing wave pattern with dielectric specimen of length d at the end of the slotted coaxial line (Metaxas and Meredith, 1983)

The schematic diagram of the open ended coaxial probe itself is shown in Figure 2-10 (left). It consists of an inner conductor, an outer conductor forming a flange at the right end and an insulator filling between the two conductors.

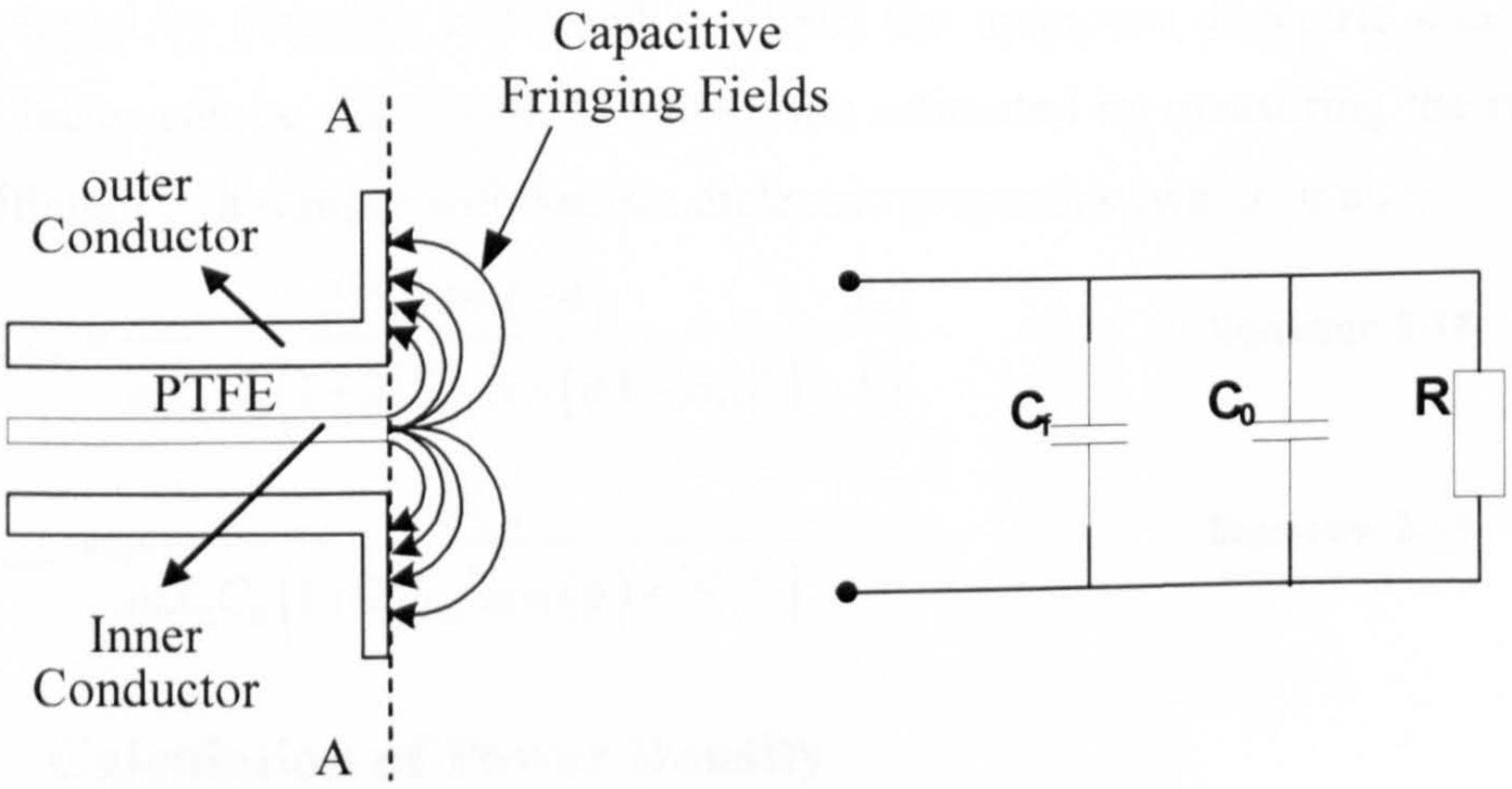

Figure 2-10 Flanged coaxial probe and equivalent lumped element representation (Louw, 2005; Stuchly and Stuchly, 1980).

The equivalent electrical circuit according to the lump capacitance method is shown in Figure 2-10 (right). C_f is the capacitive fringing field in the coaxial line

(PTFE or air dielectric), C_0 is the fringing capacitance outside the probe (inside air or sample) and R is radiation loss. The capacitive fringing field outside the probe (C_0) interrogates the sample material during measurement. The radiation resistance, R, can be ignored if the diameter of the inner conductor is considerably less than the wavelength (Stuchly and Stuchly, 1980). Therefore the total capacitance C_T can be represented as follows in Equation 2-17 (Rimbi, 2003).

$$C_T = C_f + C_0 = \frac{8(a+b)}{\omega Z_0 \lambda \ln\left(\frac{a}{b}\right)}\left[\xi\left(\frac{2\sqrt{ab}}{(a+b)}\right)-1\right] \qquad \textbf{Equation 2-17}$$

where: a is the inner radius of the outer conductor, b is the outer radius of the inner conductor, Z_0 is the characteristic impedance of the sample.

In the coaxial line method the dielectric constant and loss factor of the sample are obtained from the measurement of the reflection coefficient (S_{11}) at a defined reference plane similar to that shown in Figure 2-10 (usually at the interface of the test dielectric (plane A-A)). The reflection coefficient is defined as the ratio of the reflected to the incident electric fields and it is closely related to the voltage standing wave ratio (Sucher and Fox, 1963). The reflection coefficient may be measured by a slotted line or network analyser. Using Equations 2-18 & 2-19 developed by (Stuchly and Stuchly, 1980) the unknown dielectric constant and loss factor can be calculated. C_f and C_0 are estimated by measuring the reflection coefficient of a sample with known dielectric properties (water or air).

$$\varepsilon'_{unknown} = \frac{2|S_{11}|\sin(-\phi)}{\omega Z_0 C_0\left(1+2|S_{11}|\cos(\phi)+|S_{11}|^2\right)} - \frac{C_f}{C_0} \qquad \textbf{Equation 2-18}$$

$$\varepsilon''_{unknown} = \frac{1-|S_{11}|^2}{\omega Z_0 C_0\left(1+2|S_{11}|\cos(\phi)+|S_{11}|^2\right)} \qquad \textbf{Equation 2-19}$$

2.7 Calculation of Power Density

The average power density *Pd* (volumetric absorption of microwave energy W/ m^3) produced in a material when exposed to microwave energy is defined in Equation 2-20 as (Metaxas and Meredith, 1983):

$$Pd = 2\pi f \varepsilon_0 \varepsilon'' E^2, \qquad \textbf{Equation 2-20}$$

where E is electric field strength inside the material (V/m)

If the material exhibits magnetic losses, the effect of magnetic field must be considered, especially for materials exhibiting high magnetic susceptibility. Equation 2-20 can be rewritten as follows:

$$Pd = 2\pi f \varepsilon_0 \varepsilon'' E^2 + 2\pi f \mu_0 \mu''_{eff} H^2 \qquad \textbf{Equation 2-21}$$

where H is magnetic field strength, (A/m)

If the material is highly conductive the loss mechanism is different as discussed in Section 2.2.2 where the electrons loose their energy by resistive dissipation due to the collision with other electrons and atoms in the lattice structure. Therefore, the lump loss factor in this case will be composed only from the contribution of conductive loss shown in Equation 2-4. The volumetric average power density can be written as (if the material is non-magnetic):

$$P = \sigma E^2 \qquad \textbf{Equation 2-22}$$

2.8 Calculation of Temperature Change

The temperature rise of a material in a conventional heating system can be expressed as follows in Equation 2-23

$$\frac{dT}{dt} = \frac{Pd}{\overline{C} \cdot \rho} \qquad \textbf{Equation 2-23}$$

where: dT is the temperature change (K), dt is the time increment (s), Pd power density (W/m^3), $\overline{C}$ specific heat capacity (J/kg.K), ρ density (kg/m^3).

By substitution of Equation 2-20 into Equation 2-23, the temperature change of a material treated in a microwave cavity can be estimated as:

$$\frac{dT}{dt} = \frac{2\pi f \varepsilon_0 \varepsilon'' E^2}{\overline{C}.\rho} \qquad \textbf{Equation 2-24}$$

Equation 2-24 shows that the temperature rise of the material treated depends on its physical properties, dielectric properties as well as the internal electric field generated inside the material. Practically, the dielectric properties can change significantly with temperature and the internal electric field is very difficult to measure. In addition, for systems involving fast exothermic chemical reactions with high energies of formation of products, Equation 2-24 does not take into account the heat generated due to chemical reaction. The heat effect due to chemical reaction can be expressed as:

$$\overline{Q} = -\sum_i n_i \Delta H^0_{T,i} \frac{dX_i}{dt} \qquad \textbf{Equation 2-25}$$

where: $\overline{Q}$ is the volumetric heat effect due to chemical reaction (W/m^3), n_i is the molar number of reactant i, $\Delta H^0_{T,i}$ is the heat of formation of reaction (J/mole), and X_i is fraction converted.

In addition, the heating system can experience various heat losses such as losses due to radiation and convection losses. If the heat losses are lumped together and denoted as q, then the net power responsible for temperature rise can be expressed as;

$$P = Pd + \overline{Q} - q \qquad \textbf{Equation 2-26}$$

Therefore the overall microwave heating rate can be obtained as:-

$$\frac{dT}{dt} = \frac{1}{\overline{C}.\rho}(Pd + \overline{Q} - q) \qquad \textbf{Equation 2-27}$$

2.9 Microwave Equipment

This section will address the major parts of any microwave system. In addition, the generation of microwave energy will be briefly described.

2.9.1 Main Components of a Microwave System

The main components of a microwave system are: the magnetron, the circulator, the waveguide, and the applicator. Figure 2-11 shows a block diagram of a typical

microwave system. The magnetron represents the microwave source where electromagnetic waves are generated. The waveguide acts as a transmission device for microwaves to the applicator. Between the applicator and the magnetron often there is an adjustable tuner and circulator. The tuners role is to match the impedance of the generator and transmission line to the impedance of the load. The purpose of the circulator is to redirect any excess microwave energy which is not absorbed by the load and reflected back to the magnetron causing its damage.

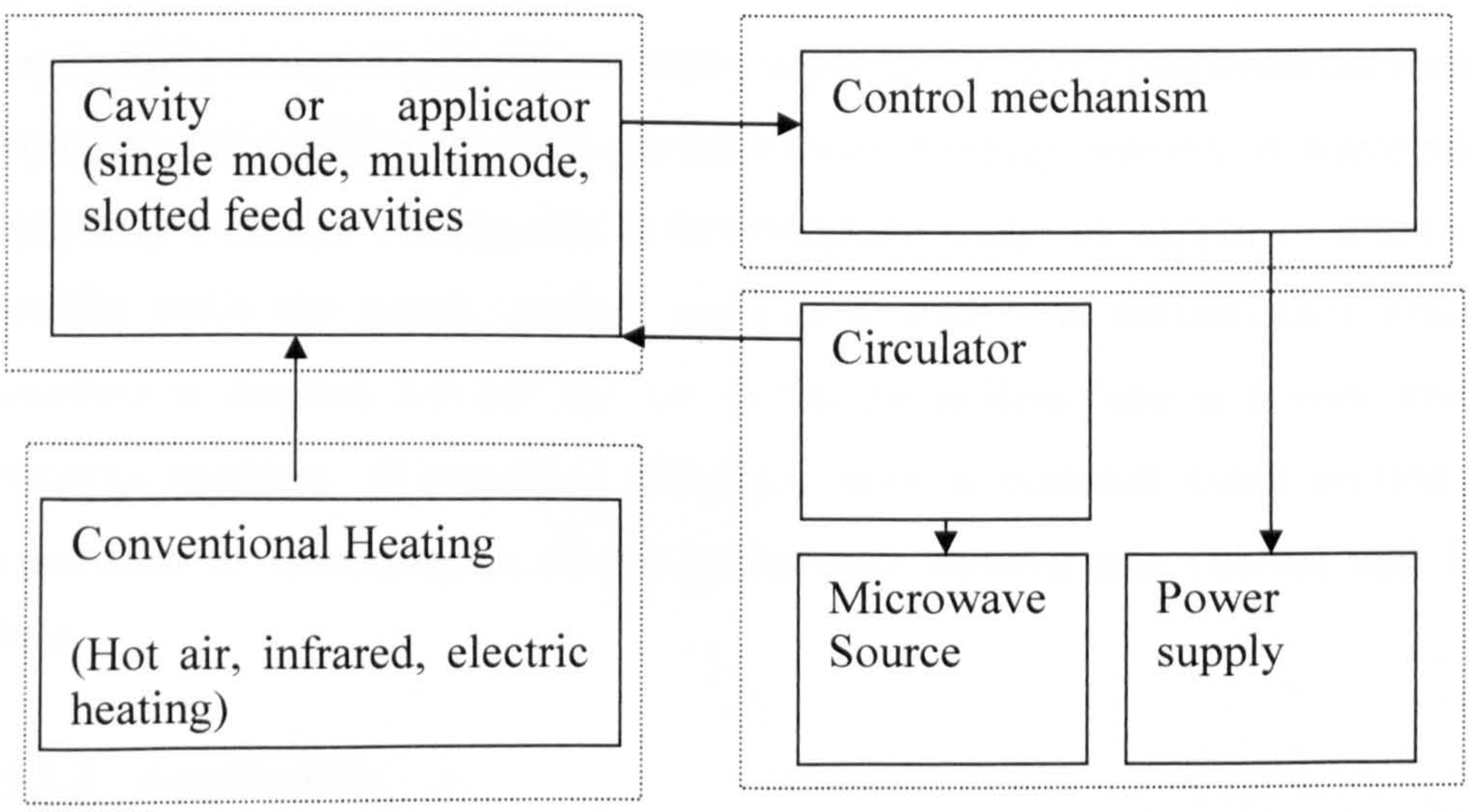

Figure 2-11 Typical block diagram of microwave systems (Chan and Reader, 2000)

2.9.1.1 Microwave Generators

There are number of electronic devices that are capable of generating electromagnetic waves at microwave frequencies. Solid state devices are not presently able to generate the high power required by microwave heating applications (Saltiel and Datta, 1999). The maximum power that a solid state device can generate is about 500 W (Porch, 2005). The microwave devices currently used for heating are vacuum tubes. They are classified by the trajectory of electron beam path to linear and crossfield. Linear tubes include klystrons and traveling wave tubes. They are more expensive and less compact when they are compared with crossfield generators, magnetrons. Magnetrons can deliver high power output with excellent frequency stability couples with low cost and high

compactness (Meredith, 1998; Saltiel and Datta, 1999). A description about the principle of operation of some microwave generators is given in Appendix 2-1.

2.9.1.2 Waveguides

Once microwave energy has been produced, it has to be transmitted to the applicator. There are two types of transmission devices that are used for microwave propagation: transmission lines such as coaxial cables and waveguides. At microwave frequencies the losses occurring in coaxial cables are significant especially at high power because the current density used results in unacceptable losses as the microwave propagates through transmission medium. Therefore, waveguides are used for microwave heating systems. A waveguide is essentially a hollow rectangular or circular tube made of copper or aluminium. Metallic walls are nearly perfect conductors with low transmission losses as described in Section 2.4 and the air within the hollow tube is a very low loss dielectric medium. Waveguides generally have a constant cross section with dimensions at least quarter of the operational wavelengths (Saltiel and Datta, 1999).

2.9.1.3 Applicators

The applicator transfers the electromagnetic energy to the workload. The size and shape of the applicator depends on the operating frequency, the dielectric properties, and size and shape of the processed material (Saltiel and Datta, 1999). The design of the applicator is critical for microwave heating. The temperature field within the material undergoing the heating is linked to the distribution of electromagnetic fields within the applicator. Common microwave applicators include waveguides, travelling wave applicators, multimode and single mode resonant cavities. For material processing, the most common types are the resonant cavities.

2.9.1.3.1 Multi Mode Cavity

Multimode applicators are the most commonly used microwave heating cavities. Mechanically a multimode applicator is a metallic box of various sizes with walls that are able to reflect the microwaves with minimal losses. The applicator is usually made of aluminum, copper, stainless steel or epoxy coated metals. However, the choice of materials of construction is determined by characteristics of the loaded material as well as by other considerations such as hygiene and durability (Metaxas and Meredith, 1983)

Multimode applicators usually have different accessories that can be attached to them, such as mode stirrers and turn tables. The simplest example of a multimode cavity is the domestic oven. This type of cavity is described as a multimode cavity because it sustains a number of modes within the frequency range of the magnetron. These modes result from multiple reflections from the oven walls producing standing-wave patterns. The mode is a well-defined geometric pattern of electromagnetic energy inside the cavity

Multimode cavities can be used to process large samples. The cavity dimensions are generally larger than the operation frequency allowing the generation of a large number of modes. Due to the complex pattern, consisting of many electromagnetic fields with various intensities, the material location within the cavity affects the heating efficiency and uniformity. However, to establish more uniform heating patterns mode stirrers and turntables can be used. A mode stirrer is a rotating metallic blade introduced into the oven to continuously perturb the electromagnetic field within the cavity. The movement of the work load also assists the heating uniformity because the position of the standing wave is determined mainly by the cavity walls.

2.9.1.3.2 Single Mode Cavity

Single mode cavities support only one mode at the source frequency. Their attraction is that the field pattern is well defined inside the cavity. Precise knowledge of electromagnetic field configurations enables the material to be

placed in the position of maximum field strength. This allows the maximum heating rate to be achieved at all times. A magnetic field is also present inside the cavity with its maximum located at a different position to the electric field maximum. This can be useful for heating magnetic materials (Metaxas and Meredith, 1983).

Compared to the multimode cavity, a single mode cavity (TE) can establish much higher electric field strengths for the same power applied. Therefore, the single mode cavity is widely used for processing small volumes of low and medium loss materials. For example, it is used for heating filamentary materials, ceramic material, and liquids flowing through small tubes. The main disadvantage is that only small size samples can be treated (Chan and Reader, 2000).

Monomode cavities can be rectangular and cylindrical. Figure 2-12 shows a 1 kW TE_{10} single mode cavity and is used in the current research.

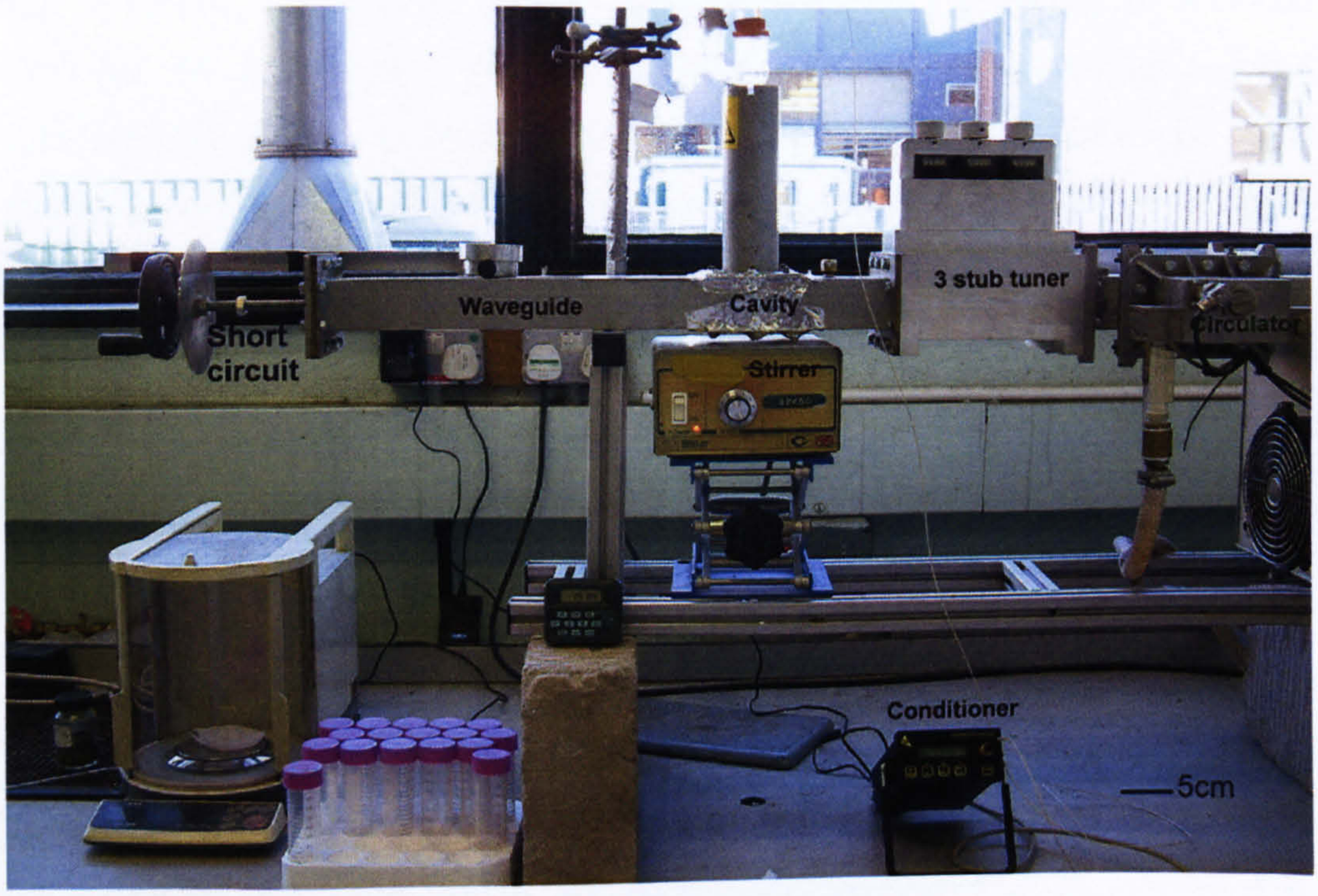

Figure 2-12 Cylindrical single mode cavity TE_{10}

2.10 Conclusions

The basic principles of microwave heating have been discussed. Heating of different materials has been detailed with the emphasis on the behaviour of liquids and aqueous solutions. Various methods for the measurements of dielectric properties have been introduced. Particular attention in the experimental work for this thesis will be toward using coaxial probe method to evaluate the dielectric properties of liquids used in microwave leaching experiments. Coaxial probe method is more suitable for measurements of loss materials and also it is possible to measure dielectric properties over a wide range of frequencies. Cavity perturbation is the other method which will be considered here. Although this method is limited to a number of frequencies, accurate measurements of the dielectric properties of loss materials can be obtained. Some details of the theory behind these methods of measurements were presented. In addition, the specifics of microwave generation, transmission and application have been presented.

CHAPTER THREE

Conventional and Microwave Leaching of Sulphide Minerals

3.1 Overview

In this chapter a general background of the conventional leaching of chalcopyrite and sphalerite is presented. This is then followed by a summary of methods available for activation of chalcopyrite, the sulphide mineral which is most resistive to leaching. As it is foreseen that microwave heating could be a potential method proposed for chalcopyrite activation, intensive discussion about the latest findings in microwave assisted leaching of chalcopyrite and other minerals and compounds is presented.

The conclusions drawn from this chapter form an important part of the justifications of the need to carry out the experimental work presented within this thesis.

3.2 Introduction

Compared with pyrometallurgy, hydrometallurgical extraction of metals from their ores is potentially highly attractive. This attractiveness is attributed to economic, environmental, and technical reasons (Habashi, 1993). Hydrometallurgy is often less costly and less harmful to the environment due to the avoidance of hazardous gaseous emissions such as SO_2. In addition, metals can be obtained directly in pure form from leach solution or recovered from

impure leach solution. Factors such as the relatively mild corrosion issues compared to refractory lining consumption in smelting operations; low temperature processing; low handling cost of leaching products; possibility of treatment of low grade ores and the massive scale of operation make leaching potentially more preferable than high temperature smelting.

However, some problems may arise during hydrometallurgical operations. These include: low recovery of extracted metal, difficulties in solid liquid separation and the effect of impurities on the ease of purification. The main disadvantage of hydrometallurgical operations is probably the process times required to achieve high metal recovery since these processes are often carried out at low temperatures compared to pyrometallurgical processes.

Leaching of sulphide minerals involves the process of extracting a soluble constituent from a sulphide ore or concentrate by means of a solvent. This process can be achieved under reducing conditions (in absence of oxidizing agents) or under oxidizing conditions in the presence of an oxidizing agent. In the latter case sulphur is produced as a by product either as elemental sulphur or it can oxidise further to a sulphate form.

3.3 Conventional Leaching of Chalcopyrite

Chalcopyrite is one of the most important copper minerals in terms of the scale of use and availability. Generally, chalcopyrite is treated by pyrometallurgical processes often in reverberatory furnaces or by using flash smelting techniques (Davenport et al., 1976). However, recently, there has been interest in the hydrometallurgical leaching of sulphide minerals due to the requirement to avoid SO_2 emissions and the fall in demand for H_2SO_4 produced as a by-product during smelter operations (Dutrizac, 1989a). Conversion of SO_2 to H_2SO_4 requires a high capital cost, which often can not be justified economically, whereas, elemental sulphur formed during ferric ion leaching can be discarded with the tailings without the environmental problems encountered in the disposal of SO_2 produced by smelting operations (Lu et al., 2000a). If required elemental sulphur can also

be separated physically by hot sulphur vacuum filtration (Palencia et al., 1998). In addition, there is a need to process lower grade sulphide concentrates that cannot be economically treated by smelting technology (Peacey et al., 2003)

The most common lixiviants used for chalcopyrite leaching are chloride, sulphate, amine and nitrate. Despite the favorable kinetics of ammonia leaching and the formation of hematite out of solution, this process consumes considerable amounts of ammonia due to the formation of $(NH_4)_2SO_4$, which needs to be decomposed (Habashi and Toor, 1979; Tiwari et al., 1980). In addition, the process also requires special equipment for handling equipment due to the explosive nature of ammonia and oxygen mixtures (Tiwari et al., 1980). Nitric acid is a powerful oxidizing agent which can successfully dissolve many sulphide minerals with acceptable kinetics. However, it is very expensive and small losses can affect the economics of the process (Habashi, 1993).

From an economic point of view the most practical oxidants are ferric ions (Dutrizac, 1992). However, the leaching rate of chalcopyrite is very slow when using ferric sulphate and is also slow in ferric chloride media. Therefore, several methods have been used to increase reaction rates, by separation or oxidation of sulphur to soluble sulphuric acid, such as:-organic extracting additions, sulfidizing chalcopyrite activation, mechanical activation, the use of ozone as an oxidant (Havlik and Kammel, 1995), the use of promoters (silver ions, surfactants, carbon particles, iron powder or hematite) (Hiroyoshi et al., 2000), and leaching in presence of nanosized silica (Misra and Fuerstenau, 2005).

3.3.1 Leaching of Chalcopyrite in Ferric Sulphate

Leaching of chalcopyrite in sulphate media involves the use of sulphuric acid as a leaching reagent in addition to an oxidant, which can be ferric sulphate, oxygen or bacteria. In this section ferric sulphate as an oxidant will by discussed.

Several investigators have studied ferric sulphate leaching (Dutrizac, 1978; Dutrizac, 1981; Dutrizac, 1989a; Dutrizac et al., 1969; Hackl et al., 1995; Hirato et al., 1987b; Hiroyoshi et al., 1997; Hiroyoshi et al., 2001; Munoz et al., 1979;

Tiwari et al., 1980). The attractiveness of this system is principally due to the ability to regenerate sulphuric acid during electro-winning (Munoz et al., 1979). In addition, high purity copper can be recovered from solution, copper recovery from sulphate media (by solvent extraction/electro-wining) is straight forward (Hackl et al., 1995), most of the oxidized sulphide ion is reported as elemental sulphur (Dutrizac, 1989a; Lu et al., 2000a), in addition to low cost process and minimal corrosion problems.

The principle disadvantage of ferric sulphate leaching is its slower reaction rate comparing to ferric chloride leaching. This is probably due to the formation of a passivating layer (elemental sulphur) on the surface of the particles, which retards the reaction rate (50 hrs was needed to achieve 90% extraction from 14μm chalcopyrite) (Dutrizac et al., 1969) and the transport of reactants. Therefore, there has been a focus on the activation of chalcopyrite (fine grinding, use of chemical catalysts such as addition of silver ions to catalyse the reaction and convert chalcopyrite to another sulphide (thermal treatment)) (Dutrizac, 1989a).

3.3.1.1 The Reaction

The main reaction, which describes leaching of chalcopyrite in ferric sulphate, was proposed as (Dutrizac, 1981; Dutrizac, 1989a; Munoz et al., 1979; Palmer et al., 1981):

$CuFeS_2 + 2Fe_2(SO_4)_3 \rightarrow CuSO_4 + 5FeSO_4 + 2S^0$ **Reaction 3-1**

However, Reaction 3-2 is also thermodynamically possible and may take place (Munoz et al., 1979):

$CuFeS_2 + 8Fe_2(SO_4)_3 + 8H_2O \rightarrow CuSO_4 + 17FeSO_4 + 8H_2SO_4$ **Reaction 3-2**

According to Dutrizac (1989a), the dominant chalcopyrite leaching reaction is the first reaction (about 94% of sulphur being formed as elemental sulphur). Lu et al. (2000a) also reported that the amount of sulphur formed during chalcopyrite leaching is about 95% of the available sulphide sulphur. Reaction 3-2 represents the formation of sulphate during the leaching process (~6% SO_4^{-2}) but this does not depend on the leaching time. Tiwari (1980) also reported a formation of 2.5% SO_4^{-2}. However, Sullivan and Jones reported 30-35% and 18% SO_4^{-2} respectively

(cited in Tiwari et al., 1980). On the other hand, Kametani and Aoki (1985) found that all the sulphur from chalcopyrite was oxidized to elemental sulphur, and pyrite was the source sulphate, which formed when the suspension potential was over 0.45V.

3.3.1.2 Elemental Sulphur Formation

The relative amount of sulphur formed during ferric sulphate leaching is not dependent on the particle size and ferric ion concentration. However, the morphology of the formed sulphur strongly depends upon the particle size and the leaching medium (Dutrizac, 1989a; Dutrizac, 1990). For example, no continuous sulphur layer was formed on large surfaces comparing to the chloride media, but the sulphur was formed mostly as globules. However, Dutrizac (1990) suggested that the continuous sulphur layer formed in chloride media might be more permeable to deposit the solution to chalcopyrite particle surface. However, smaller particles were completely covered by sulphur layer. Therefore, the reaction rate is reasonably fast at the beginning of the leaching process, and then becomes very slow as the reaction continues.

With regards to the nature of sulphur layer formed on the chalcopyrite surface it is suggested that this layer is comprised of copper polysulfide, CuS_n (Hackl et al., 1995). XPS analysis conducted by Balaz et al. (1996) revealed the existence of sulphur in three chemical forms, S^{2-}, S^0 and S^{6+}, when experiments were performed with combined bacterial and chemical leaching. Other investigators, such as Antonijevic et al. (1994), suggest the sulphur to be elemental in nature. Biegler and Swift (1979) observed the properties of sulphur to vary with experimental conditions. When standing over a period of days, sulphur lightened in color due to the transformation of its amorphous plastic form to the yellow rhombic form. As can be noted, there is no real consensus among investigators as to the nature of the sulphur associated with the passive layer that is formed during chalcopyrite leaching. Nevertheless, it has been concluded that the slow reaction kinetics of chalcopyrite is due to the formation of a passive layer on the reacted

surface. This issue will be further discussed in Chapter 4 based on the investigation of mineral surfaces using SEM and ToF-SIMS studies.

3.3.1.3 Effect of Particle Size

Munoz et al (1979) found out that the apparent rate constant of chalcopyrite dissolution in ferric sulphate was inversely proportional to the square of the initial particle size (4, 12 and 40μm). Dutrizac (1981) confirmed that the rate is directly proportional to the leached area. However, Jones and Peters (1976) report that there is no particle size effect below 300μm. According to Dutrizac (1981) this is due to dry screening in Jones and Peters' experiments, where the very fine particles were not completely separated from the larger particles. Thus their results (Jones and Peters') were based on a mixed size of large and very fine particles. Lu et al. (2000a) reported that the total copper extracted after 9 hours for particles of d_{50} =4.03 and 15.1μm was nearly the same, although the rate was different.

3.3.1.4 Character of the Leaching Rate Curve

The leaching rate curve is a plot of copper reacted (moles, or fraction reacted) versus leaching time. Jones and Peters (1976) found that the leaching rate curve of massive chalcopyrite specimen in acidic ferric sulphate exhibited linear characteristics over a long period of time (55 days). In contrast, Dutrizac (1981) and Dutrizac and MacDonald (1978) and Munoz et al. (1979) reported that the kinetics were parabolic over about 100 hrs using ground chalcopyrite. However, Hirato et al. (1987b) found that the leaching rate curve of chalcopyrite crystals in 1M $Fe_2(SO_4)_3$ and 0.2M H_2SO_4 exhibited parabolic character over the first 100 hrs then the rate was found to increase linearly over an extended period of time. This can be explained by the fact that the work carried out by Dutrizac (1981) and Munoz (1979) finished after 100hrs whereas; Jones and Peter (1976) reported an existence of an induction period. According to Hirato et al. (1987b) the growth of the dense sulphur layer formed during the first 100 hrs caused to peel off leaving rough surface after which no thick layer was formed.

3.3.1.5 Effect of Ferric Sulphate Concentration

Generally, it would be expected that as Fe^{+3} concentration increases an increase in the reaction rate will follow. However, according to Munoz et al. (1979) the reaction rate of chalcopyrite dissolution in ferric sulphate is independent of the ferric ion concentration, which is unusual. They suggest that the rate-limiting step is the transport of electrons through the elemental sulphur layer. In the same study, it was suggested that the activation energy of the system (83.7 kJ/mole) is approximately the same as the activation energy for transport of electrons through an elemental sulphur layer (96.3kJ/mole). Dutrizac (1981) also reported that the leaching rate is marginally dependent on the ferric ion concentration ($leaching.rate \propto [Fe^{+3}]^{0.12}$). In earlier work Dutrizac (1969) found that rate of the reaction is limited by the ferric ion concentration to the order of 2 ($leaching.rate \propto [Fe^{+3}]^{2}$) when it is below 0.01M, then it becomes independent to the concentration of ferric ions. Hirato et al. (1987b) found that below a concentration of 0.1 M Fe^{+3}, the reaction rate increased with first order dependence then declined at a higher concentrations.

3.3.1.6 Effect of Ferrous Sulphate

Addition of $FeSO_4$ even in small quantities causes a rapid drop in the rate of chalcopyrite dissolution in ferric sulphate (Dutrizac, 1981). Hirato et al. (1987b) also found that ferrous ions suppress chalcopyrite oxidation. However, Beckstead et al. (1976-cited in Dutrizac (1981)) obtained essentially identical leaching curves when 20 or 100 g/l Fe^{+2} as $FeSO_4$ was added to sulphate medium at 93°C. By contrast, Hiroyoshi et al. (1997) reported that the addition of ferrous sulphate enhances the leaching of chalcopyrite. These controversial opinions may indicate that the conditions of the reaction are different in terms of solution potential, pH, presence of impurities, and dissolved oxygen. This is indicated by different results achieved with different chalcopyrite samples.

Hiroyoshi et al. (2000) suggested that ferrous ions enhance chalcopyrite leaching by the formation of Cu_2S, which is more amenable to oxidation than chalcopyrite.

Thermodynamically, this is possible when redox potential is lower than the critical point, which is a function of ferrous and cupric ion concentrations. The proposed model by Hiroyoshi et al. (2000) for chalcopyrite leaching is shown below:

$$CuFeS_2 \xrightarrow{\text{Reduction}} Cu_2S \xrightarrow{\text{Oxidation}} Cu^{+2}$$

Reaction 3-3

Recently, Hiroyoshi et al. (2001) reported that chalcopyrite leaching can be enhanced by controlling the concentration ratio of ferrous to ferric ions or the redox potential of solution and found that ferrous ions suppress the oxidation of chalcopyrite when cupric ion concentration is low. Hiroyoshi et al. (2001) explained the results obtained by Dutrizac (1981) and Hirato et al. (1987b) by the fact that the volume of solution is too high such that the accumulated cupric ions are not concentrated to form Cu_2S according to the following reaction (Hiroyoshi et al., 2000):

$$CuFeS_2 + 3Cu^{+2} + 3Fe^{+2} \rightarrow 2Cu_2S + 4Fe^{+3}$$ **Reaction 3-4**

Earlier work carried out by Kametani and Aoki (1985) suggests that the reaction rate depends on the suspension potential of the solution which depends on the ratio of $[Fe^{3+}]/[Fe^{2+}]$. Also the maximum rate constant is attained at a very narrow range of suspension potential with an optimum value of about 0.43V. A further increase in suspension potential up to 0.45V drastically reduces the rate constant where pyrite oxidation starts, and then the rate constant increases at a slower rate. Pinches et al. (2001) confirmed that the suspension potential must be controlled in a narrow range between 0.35 and 0.45V. Therefore, Dutrizac's (1981) results concerning the negative effect of ferrous ion concentration can be explained in terms of suspension potential, which decreases with the addition of ferrous ions in the range above 0.45V.

3.3.1.7 Effect of Sulphuric Acid Concentration

Acid concentration has no influence on the leaching rate of chalcopyrite dissolution in ferric sulphate at least up to 1M (Dutrizac, 1978; Dutrizac, 1981).

However, the presence of H^+ ions is important to prevent hydrolysis and/or oxidation according to the following equations (Klauber et al., 2001):

$$Fe^{+2} + 2H_2O = Fe(OH)_2 + 2H^+ \qquad \textbf{Reaction 3-5}$$

$$2H_2O + Fe(OH)_2 + O_2 = 2Fe(OH)_3 \qquad \textbf{Reaction 3-6}$$

3.3.1.8 Effect of Temperature

The reaction rate of chalcopyrite dissolution in ferric sulphate has been found to be highly dependent on temperature (Dutrizac, 1978; Dutrizac, 1981; Hirato et al., 1987b; Munoz et al., 1979). With an increase in temperature the reaction rate increases. There is scatter in the values of activation energy reported in literature. A summary of the values of activation energy reported by investigators are listed in Table 3-1.

The reported activation energy (Ea) of the reaction varies between 65 and 88 kJ/mole. Scatter in the results may be attributed to the method of calculation especially when the conversion is far from unity. This latter can lead to an error in determining the rate-limiting step and therefore an incorrect calculation of the apparent rate constant and activation energy (Prosser, 1996). Other possible factors that could effect the uncertainty of activation energy are the presence of impurities, such as galena, which could cause a precipitation of lead sulphate on the surface, and the presence of additional unaccounted components in the solid. These could consume reactants or cause errors in mass accounting, and therefore affect the rate constants. Further details regarding the uncertainty in evaluating the activation energy are discussed by Prosser (Prosser, 1996).

Table 3-1 Summary of some investigations on chalcopyrite leaching in ferric sulphate

Material, system and observation	T, °C	Ea, kJ/mol.	Suggested rate limiting process	Author
Synthetic chalcopyrite, rotating disk, independent of Fe^{+3}, Parabolic kinetics	50-94	71±13	Transport control. Diffusion of ferrous ions through sulphur layer	Dutrizac et al (1969)
Natural, Continuous flow of solution through packed bed of particles (1.44×4.76 μm), rate is independent on $Fe^{+3}$and H_2SO_4	32-52	75	Surface reaction controlled. Surface saturation followed by chemical reaction	Lowe (1970)
Natural (Transvaal $CuFeS_2$). Suspended particles (5 to 40μm) in stirred reactor, Parabolic kinetics	27-91.5	84	Transport controlled. Diffusion of ferric ion through sulphur layer	Baur et al (1974)
Natural (massive piece of 1.0cm cubes) and particulate (30-1680μm), Some sulphur oxidized to SO_4. No particle size dependence bellow 300 μm. Linear kinetics up to 40 pct reacted	90	-	Electrochemical surface reaction	Jones and Peters (1976)
Natural, monosize $FeCuS_2$ particles and attritor ground particles (1-40μm). Rate is independent on Fe^{+3}, Fe^{+2}, Cu^{+2} and H^+. Well-defined rate dependence on particle size. Parabolic kinetics	60-90	84	Transport control. Diffusion of ferric ion through sulphur layer	Beckstead et al (1976)
Natural (Pima concentrate), prepared by wet screening, 12 μm particles, rate is inversely proportional to the r^2. 0.25M $Fe_2(SO_4)_3$ -1.0 M H_2SO_4	60-90	83.7	Reaction rate is limited by transport of electrons through sulphur layer	Munoz (1979)
Natural, from different localities and impurity level, 0.1M $Fe_2(SO_4)_3$ -0.3 M H_2SO_4	65- 95	65		Dutrizac (1982)
Natural, two stages: first leach in 1M $Fe_2(SO_4)_3$ and 0.2 M H_2SO_4 at 70°C until linear rate achieved then transfer the crystals to (1.0, 0.1 and 0.01) M $Fe_2(SO_4)_3$ and 0.2 M H_2SO_4. Different activation energy with different $Fe_2(SO_4)_3$ and related to the second stage	50-78	76.8-87.7	Second stage chemically controlled	Hirato (1987)
Natural, 0-1M $Fe_2(SO_4)_3$,.05-1M H_2SO_4	20-99	12 in the T range 20-40	Leaching agent diffusion onto leaching surface	Havlik et al (1996))
		69 in the T range 40-99	Chemical reaction kinetics on the leaching surface	

3.3.1.9 Reaction Mechanism

The reaction mechanism of chalcopyrite oxidation in ferric sulphate has been a subject of great debate in the literature and widely different interpretations of kinetic data are presented. Some researchers claim that the diffusion of either ferric or ferrous ions through the sulphur layer is the rate-limiting step (Baur et al., 1974; Beckstead et al., 1976; Dutrizac et al., 1969). Others have reported that the reaction is limited by surface chemical reaction (Havlik et al., 2001; Hirato et al., 1987b) while some reports show that electrochemical or electron transfer is the limiting step (Jones and Peters, 1976; Munoz et al., 1979; Parker et al., 1981b). Electron transfer could occur through a series of sequential steps, in which, disulphide is oxidized by ferric ions with the aid of the oxygen from water (Parker et al., 2003). Table 3-1 summarizes the results of some investigators regarding the mechanism, which controls the reaction

3.3.1.10 Effect of Additives

Various promoters have been used to improve the recovery of copper from chalcopyrite. In the following sections, the effect of addition of chloride, silver and nano sized silica will be discussed.

3.3.1.10.1 Chloride Addition

Schultze et al. (1995) reported that addition of chloride ions increases the recovery of copper from chalcopyrite by 94% at a temperature of 50°C and pH=1.7. Lu et al. (2000a) also showed that the percentage copper extracted increased from 30% without sodium chloride additions to 98% with addition of 1 M NaCl in the system of 0.8 M H_2SO_4 over 9 hours at 95°C. This was suggested to be due to the formation of a crystalline and porous sulphur layer, whereas; in the absence of chloride ions particles were completely coated by sulphur layer. There is no further effect when the concentration of chloride ions was increased to more than 0.5 M.

3.3.1.10.2 Effect of Silver Ions

The leaching process of chalcopyrite in ferric sulphate in the presence of silver ions in a ferric sulphate system proceeds according to the following reactions (Hiroyoshi et al., 2002):

$CuFeS_2 + 4Ag^+ \rightarrow Cu^{2+} + Fe^{2+} + 2Ag_2S$ **Reaction 3-7**

$2Ag_2S + 4Fe^{3+} \rightarrow Fe^{2+} + 4Ag^+ + 2S$ **Reaction 3-8**

The copper extraction rate is higher with silver ions because the mixed layer of S and Ag_2S is suggested to be porous and non-protective (Miller and Portillo, 1979 - sited in Hiroyoshi et al. 2002).

Furthermore, Parker et al. (1981b) reported that Ag_2S is an excellent electron conductor, which means faster electron transfer between ferrous and ferric ions. According to the authors, Ag_2S provides cathodic sites on the surface of chalcopyrite, leading to higher corrosion potential which means faster leaching of the chalcopyrite. On the other hand, Hiroyoshi et al. (2002) proposed the formation of an intermediate product, Cu_2S, due to chalcopyrite reduction at low potentials and subsequent oxidation of Cu_2S and silver ions to remove H_2S formed during the reduction, which increased the critical potential of Cu_2S formation.

The amount of copper extracted increases with an increase in silver ion concentration until a certain limit when copper extraction becomes less dependent on silver ion concentration (Carranza et al., 1997). The optimum results were achieved with 2 mg silver/g concentrate. To recover the silver from residues, sulphur must be removed first by means of solvent extraction, and then silver can be recovered by leaching in $NaCl\text{-}H_2SO_4$ mixtures (Palencia et al., 1998). The addition of silver ions is however, not economic unless they are contained naturally within the ore.

3.3.1.11 Effect of Nanosize Silica Particles

Very recently it has been reported that the addition of nanosize silica particles (50 nm in size) with a concentration of 17.5g/l increased the recovery of copper from

chalcopyrite by 50% compared with that without nanosize particles (Misra and Fuerstenau, 2005). It was shown that chalcopyrite particles were not covered by elemental sulphur in the presence of silica nanosize particles in both ferric sulphate and ferric chloride systems. However, there was no explanation given for this phenomenon. Furthermore, the nanosize particles were not characterized both before and after treatment.

Based on this work, it can be speculated that the nanosize silica may have acted as an active surface for sulphur deposition. This might also suggest that chalcopyrite oxidation in ferric ion media occurs through an intermediate step involving the production of products like H_2S. Hydrogen sulphide would then oxidize to produce elemental sulphur which would deposit on nanosize silica particles instead of the chalcopyrite surface.

3.3.2 Ferric Chloride Leaching

Chloride systems involve the use of hydrochloric acid as a leaching reagent to prevent hydrolysis with ferric chloride as the oxidant. Compared to ferric sulphate leaching, this system is quicker and more aggressive, ferric chloride can be regenerated, and pyrite is not attacked (Godocikova et al., 2002). Chlorides are corrosive but this can be overcome by the use of polymers and plastic materials. In addition, the iron is dissolved and has to be separated (Habashi and Toor, 1979). However, elements like Ag, Pb, As, and Sb are soluble in chloride media and can report to the final product (Dutrizac, 1992).

Several researchers have investigated chloride leaching (Dutrizac, 1978; Dutrizac, 1981; Dutrizac, 1990; Havlik and Kammel, 1995; Havlik et al., 1995; O'Malley and Liddell, 1987; Palmer et al., 1981) and there are several processes (pilot and large laboratory scale), which involve use of the chloride system; these include CYMET process, Cuprex process, Cominco process, MINTEK process, Outokumpo process, and Intec process (Peacey et al., 2003). The only commercial process was the CLEAR process which again was closed in 1982 due to major problems including: gypsum fouling in the tank house, silver contamination of the final product and washing of the final product (Dutrizac, 1992; Peacey et al.,

2003). The most recent chloride process is HydroCopper™ developed by Outokumpo® is still in a demonstration plant stage (Hyvarinen and Hamalainen, 2005)

3.3.2.1 The Reaction

The leaching reaction of chalcopyrite with ferric chloride is (Havlik and Kammel, 1995):

$$CuFeS_2 + 4FeCl_3 \rightarrow CuCl_2 + 5FeCl_2 + 2S^0 \qquad \textbf{Reaction 3-9}$$

The reaction below although thermodynamically less likely could also occur (Havlik and Kammel, 1995):

$$CuFeS_2 + 3FeCl_3 \rightarrow CuCl + 4FeCl_2 + 2S^0 \qquad \textbf{Reaction 3-10}$$

This reaction is more likely when using more concentrated solutions (Cl- concentration) especially when simultaneous milling with ferric chloride for over 8hrs is used (Maurice and Hawk, 1999a; Maurice and Hawk, 1999b). In addition, similar to ferric sulphate leaching of chalcopyrite, in ferric chloride medium SO_4^{2-} could be generated in quantities of less than 5 % (Dutrizac, 1992)

3.3.2.2 Effect of Ferric Chloride Concentration

The reaction rate of chalcopyrite dissolution in ferric chloride increases considerably by increasing the concentration of $FeCl_3$ (from 0.001-0.2 M) (Dutrizac and MacDonald, 1978). This is different to the ferric sulphate system where the leaching rate has less dependence on the ferric sulphate concentration (Dutrizac, 1981; Dutrizac and MacDonald, 1978; Munoz et al., 1979). According to Havlik et al. (1995), with an increase in Fe^{+3} the rate increases until about 0.7 M. Dutrizac (1990) reported that the amount of copper extracted was doubled when the ferric chloride concentration was increased from 0.1 to 2 M. Palmer et al. (1981) also reported that the rate was proportional to the square root of Fe^{+3} concentration (0.02-0.5M). However, Ngoc et al. (1990) reported that maximum recovery of Cu and Zn from low-grade complex ores is achieved when ferric ion concentration reaches 4 M with order dependence ($[Fe^{+3}]^x$) of 0.37 for Cu and 0.14 for Zn. Hirato et al. (1986) also found that the rate of reaction was about 0.5

with respect to ferric ion concentration. On the other hand, Jain et al. (1993) and Ermilov et al. (1969) reported a reaction order of unity. This wide range of reaction orders reported in the literature is probably due to different impurity level in the chalcopyrite used where ferric ions would be consumed by other constituents presented in the solid.

3.3.2.3 Character of the Leaching Rate Curve

The leaching rate curve of chalcopyrite in chloride media exhibit a parabolic character ($[Cu]_{aq} = kt^{0.5}$) (Havlik et al., 1995). These observations were based on 4 hrs leaching time. Palmer also confirmed this (5hrs) (Palmer et al., 1981). Dutrizac (1981) observed that the leaching curve of a disk of synthetic chalcopyrite was linear with a slight curvature over about 70 hrs, which may be related to the porosity of the disk. Ngoc et al. (1990) also observed linear kinetics for leaching of copper from low-grade concentrate in 4M $FeCl_3$ (2 hrs) according to surface reaction control from the shrinking core model. This model will be discussed in Chapter 4.

3.3.2.4 Effect of HCl Concentration

Dutrizac (1978) reported that when concentration of HCl was increased from 0.1 to 3M the copper extraction increased from 61 to 73% in ferric chloride system. Lower concentrations were avoided to prevent hydrolysis. However, O'Malley and Liddell (1987) and Havlik and Kammel (1995) reported that there is no effect of HCl alone without oxidant on the characteristics of chalcopyrite (no leaching).

3.3.2.5 Effect of Additives

3.3.2.5.1 Effect of NaCl Addition

The addition of 100g/l NaCl to 1M $FeCl_3$- 0.2M HCl leaching solution increases copper extraction from 65% to 78% over 2hrs leaching but further increase had no tangible effect (Ngoc et al., 1990). Hirato et al (1986) also reported that the presence of 2 M NaCl in 0.1 M $FeCl_3$ doubled the reaction rate of chalcopyrite dissolution in ferric chloride. Neither Ngoc et al (1990) nor Hirato et al (1986)

have given any explanation for the enhancement observed. However, it could be possible that the NaCl enhances the formation of complexes resulting in better leachability of chalcopyrite (Skrobian et al., 2005).

3.3.2.5.2 Effect of Ozone

One of the advantages of ozone oxidation is that it takes place at room temperature. According to Havlik and Ukasik (2001) leaching of chalcopyrite takes place in several stages. It is suggested that chalcopyrite was oxidised by ozone in the first stage of leaching according to the reaction below: -

$3CuFeS_2 + 8O_3 \rightarrow 3CuSO_4 + 3FeSO_4$ **Reaction 3-11**

Subsequently, ozone is dissolved in solution, whereas, ferric ions become involved in the oxidation process generating ferrous ions, which in turn was oxidised by ozone to ferric ions again. After achieving the equilibrium ozone participates directly as an oxidant.

3.3.2.5.3 Effect of Sulphate Ions

Dutrizac (1978) reported that the addition of magnesium sulphate ($MgSO_4$) to 0.1 M $FeCl_3$-0.3 M HCl at a temperature of 85°C reduced the amount of dissolved copper until the concentration of $MgSO_4$ reached 2.0 M. At this point the leaching rate becomes similar to that in ferric sulphate media. Industrially $CaCl_2$ or CaO are used to precipitate gypsum ($CaSO_4.H_2O$) to collect any sulphate formed during the leaching process in chloride systems (Dutrizac, 1990).

3.3.2.5.4 Effect of Organic Solvents

The purpose of the addition of organic solvents is to dissolve the elemental sulphur formed on the surface of chalcopyrite particles during leaching. With the addition of carbon tetrachloride, the copper extraction rate increased by more than 45% and the apparent activation energy for the system was found to be Ea=31.2 kJ/mole (Havlik and Kammel, 1995).

3.3.2.6 Effect of Particle Size

The effect of particle size on the leaching rate of chalcopyrite was found to be the same as for the ferric sulphate system (Dutrizac, 1981). Palmer et al. (1981) also observed that the leaching rate to be proportional to the inverse of particle size. However, leaching of very fine particles could after some time be passivated by formation of a complete envelope of sulphur (Dutrizac, 1990).

3.3.2.6.1 Mechanical Activation

Mechanical activation has been used as a mean for acceleration of dissolution of chalcopyrite during leaching due to an increase in surface area. Maurice and Hawk (1998; 1999b) reported that the reaction rate of chalcopyrite dissolution in ferric chloride increases after autogenous milling not only due to the increase in surface area and reactivity of concentrate, but also through lattice distortion resulting from deformation. Furthermore, it has been reported that fine grinding enhances dissolution of chalcopyrite due an enhanced microtopography formation on the surface of milled particles. Tromans and Meech (2002) observed that the enhanced microtopography is more likely to occur on fine particles of few microns which in turn increases the effective surface area leading to enhanced dissolution. It is possible that a prolonged grinding process may enhance the formation of more reactive fracture planes which are more reactive and require higher energy to create.

3.3.2.6.2 Effect of Temperature

The leaching rate of chalcopyrite in ferric chloride increases with an increase in temperature (Havlik et al., 1995; Ngoc et al., 1990). High extraction efficiency was observed at the boiling temperature of chloride medium (110°C) (Ngoc et al., 1990). Similarly to the sulphate system, the reported values of activation energy vary considerably (see Appendix 3-1). The scatter of the data relates to the fact that some authors did not consider the two mechanisms (Havlik and Kammel, 1995). It could also be due to some of the factors discussed in Section 3.3.1.8.

3.3.2.6.3 Effect of Locality

Chalcopyrite obtained from different sources varies in its chemical composition, impurity level, and even crystallographic structure (Ferreira, 1972). Paynter (1974 - cited in Dutrizac 1982), in his review reported that the reactivity of chalcopyrite to leaching was affected by the locality (origin). On the other hand, Dutrizac (Dutrizac, 1982) leached eleven chalcopyrite samples obtained from different localities in both ferric chloride and ferric sulphate systems at different temperatures. It was observed that the leaching rates of these samples were similar when the rates were corrected for the amount of $CuFeS_2$ in the sample.

3.3.2.6.4 Effect of Agitation

O'Malley and Liddell (1987) found that at agitation speeds higher than 550 rpm there is no effect on the recovery of copper from chalcopyrite. Ngoc et al. (1990) noticed that the recovery of copper, from an off grade concentrate, increases with increase in agitation speed until an optimum speed after which the rate of reaction start to decrease. The optimum stirring speed was found to be 700 rpm. Similar observations were noted by Haver and Wong (1971). This phenomenon was explained by a synergetic action of $CuCl_2$ at low stirring speed which is produced according to Reaction 3-9 then it reacts with chalcopyrite as a second oxidant (Roman and Banner, 1973) according to Reaction 3-12. This interesting effect is further investigated in Chapter 4 of this thesis.

$$CuFeS_2 + 3CuCl_2 \rightarrow 4CuCl + FeCl_2 + 2S^0 \qquad \textbf{Reaction 3-12}$$

Nevertheless, it should be noted that the level of mixing is influenced by several factors including: the dimensions of both the impeller and the reactor, the position of the impeller in the reactor, the design of the impeller as well as the stirring speed (Harnby et al., 1997). Furthermore, the effect of reaction products, in autocatalytic reactions, and the effect of heat generation due to exothermic reactions on the rate of reaction should be taken into account.

3.3.2.6.5 Elemental Sulphur Formation

Different studies suggest that over 90% of sulphur found as a product of leaching occurs as elemental sulphur (Dutrizac, 1990). It was found that 95-97% of the oxidized sulphur reports as elemental sulphur and only about 3-5% reports as SO_4^{-2} according to the following reaction:

$$CuFeS_2 + 16FeCl_3 + 8H_2O \rightarrow CuCl_2 + 17FeCl_2 + 2H_2SO_4 + 12HCl \quad \textbf{Reaction 3-13}$$

Dutrizac (1990) suggested that chloride media in the temperature range used did not attack sulphur. There is no or very little influence of HCl and $FeCl_3$ concentration, particle size and the presence of oxygen on the amount of elemental sulphur produced, whereas, the morphology of the formed sulphur is strongly affected by the particle size. The formation of well-formed large sulphur crystals suggests that the sulphur is deposited from the solution as a result of the following two reactions:

$$CuFeS_2 + 4HCl \rightarrow CuCl_2 + FeCl_2 + 2H_2S_{aq} \quad \textbf{Reaction 3-14}$$

$$2H_2S_{aq} + 4FeCl_3 = 4FeCl_2 + 4HCl + 2S^0 \quad \textbf{Reaction 3-15}$$

On the other hand, other studies suggest that the passivation of chalcopyrite is due to the formation of a metal-deficient sulphide layer (Lu et al., 2000b). After dipping chalcopyrite in CS_2 and further leaching in mixed chloride and sulphate media the mineral was still passive. These findings counteract the results achieved when Havlik et al. (1995) leached chalcopyrite in presence of CCl_4 and the copper extraction was found to increase from 16.2 to 23.2% at 80°C, whereas Klauber et al. (2001) found no identification for either metal-deficient sulphides or polysulphides. However, using X-ray Photoelectron spectroscopy it was detected that the chalcopyrite particles were covered by elemental sulphur and disulphides (S_2^{-2}) (Klauber et al., 2001).

3.4 Activation of Chalcopyrite

It has been shown that chalcopyrite leaching in ferric ion media is a slow process and there have been many research studies conducted in an attempt to increase the reactivity of chalcopyrite. The increase of leaching temperature, fine grinding, and

addition of promoters during the course of leaching such as: silver ions organic solvents and silica nanosize particles were investigated in an attempt to increase the reaction rate. Furthermore, activation of chalcopyrite prior to leaching by thermal treatment has been tested. Thermal activation of chalcopyrite can be achieved by addition or removal of Cu, Fe and S from chalcopyrite to produce more amenable compounds for leaching. Table 3-2 summarizes some of the methods employed to activate chalcopyrite by thermal treatment.

All these methods are either expensive to implement or did not give the desired results in terms of copper recovery. Recently there have been a few attempts to use microwave energy to activate chalcopyrite either as a pretreatment method or insitu during leaching process. A detailed review of this is presented in Section 3.6.2.

Table 3-2 Activation methods for chalcopyrite (Dutrizac, 1992)

Method	Comments	Author
Activation with sulphur	Pyrite and various Cu-S phases (nukundamite ($(Cu,Fe)_4S_4$), idaite (Cu_5FeS_6), bornite (Cu_5FeS_4), covellite (CuS), etc.)	Jolley et al (1991), Demopoulos et al (1983)
Activation with covellite	Covellite reacts to form bornite and pyrite. Rapid copper leaching and good iron rejection achieved in $CuSO_4$ leach	Parker et al (1975)
Activation with copper	Reaction forms Cu_2S and FeS; hence high soluble Fe concentration realized during leaching. Significant rate increase during O_2-H_2SO_4 leaching	Bjorling et al (1968)
Activation with iron	Forms Cu_2S or Cu in addition to FeS. Copper is recovered by $FeCl_3$ leaching or floatation	Pemsler (1975), Neou-Singoua et al (1990)
Activation with carbon	Activated carbon increases the leaching rate in ferric sulphate media by up to 400%	Wan et al (1985)
Activation by sulphur removal in vacuum or in inert gas	Treatment at 800°C forms intermediate solid solution, bornite and FeS. Enhanced leaching rate noted in H_2SO_4-O_2 system	Gabler et al (1975)

3.5 Conventional Leaching of Sphalerite

Sphalerite (ZnS) is the most economically important zinc mineral. Currently, the majority of sphalerite ores are treated through flotation producing high grade concentrates. Zinc is produced from sphalerite by pyrometallurgical and hydrometallurgical means. Pyrometallurgical processes involve the reduction of zinc from roasted concentrate by carbon in horizontal retorts; vertical retorts, electrothermic furnaces or the Imperial Smelting furnace (ISF)(Gill, 1980). Using this method of production, zinc is recovered only from zinc oxide and any sulphide or sulphate is lost. The roast-leach-electrolysis process as a method of zinc production can be considered as a combined pyro and hydrometallurgical process. Using this method sphalerite concentrate is roasted in a fluidised bed at high temperature by hot air to convert zinc sulphide to zinc oxide, zinc sulphate and zinc ferrite, and then the roasted concentrate is leached by two stages of acid digestion.

Primary zinc production in the world is about 6627600t/y (Dutrizac et al., 2003; International-Zinc-Association, 2005). About 80% of it originates from roast-leach-electrolysis process, whereas, zinc produced by pyrometallurgical operation is in continuous decline due to the environmental problems involved. The roast-leach process also suffers from the generation of SO_2, which is either used for sulphuric acid production or escapes into atmosphere.

Recently there has been an interest in hydrometallurgical production of zinc. An improvement has occurred in oxygen pressure leaching which has found wide industrial application (Palencia and Dutrizac, 1991). Oxygen pressure leaching of sphalerite oxidises sulphide sulphur to its elemental form at low temperatures according to the following reaction:

$$ZnS + H_2SO_4 + 1/2O_2 \rightarrow ZnSO_4 + H_2O + S^0 \qquad \textbf{Reaction 3-16}$$

However this reaction is very slow and higher temperature and oxygen pressure are required to compensate for the poor kinetics. Leaching is carried out usually at a temperature below 150°C to produce a good yield of elemental sulphur.

Similarly, atmospheric ferric sulphate and chloride leaching of sphalerite has been given significant attention in recent years (Buban et al., 2000; Ferron, 2000). Sphalerite leaching in ferric ion media is more preferable in terms of kinetics point of view especially at the boiling temperature of the solution. However, sphalerite leaching in ferric media requires huge amount of Fe^{3+}, which makes the treatment of the leach solution more difficult and reduces the economic potential. Ferrous iron is produced either from the reduced ferric ions or from the dissolution of iron contained in the sphalerite concentrate. If Fe^{3+} is regenerated it will be very advantageous (Ferron, 2000).

Several investigators have studied direct oxidative leaching of sphalerite using ferric chloride and ferric sulphate (Dutrizac and MacDonald, 1978; Jin et al., 1984). In the following two sections atmospheric leaching of sphalerite in ferric sulphate and ferric chloride are reviewed.

3.5.1 Ferric Chloride Leaching

3.5.1.1 Reaction

The reaction of sphalerite oxidation with ferric chloride is as follows (Dutrizac and MacDonald, 1978; Jin et al., 1984; Rath et al., 1981):

$$ZnS + 2FeCl_3 \rightarrow ZnCl_2 + 2FeCl_2 + S^0 \qquad \textbf{Reaction 3-17}$$

According to Dutrizac and MacDonald (1978) most of the sulphur reports as elemental sulphur in the leach residue (85-95% sulphide sulphur). They suggest that the presence of H_2S became more apparent when HCl concentration exceeds 1 M. Some of H_2S oxidised to elemental sulphur and the remaining escaped from the vessel. The standard free energy change for the above reaction is 90kJ/mol. and the equilibrium constant is about 10^{16} at a temperature of 298°C (Bobeck and Su, 1985).

3.5.1.2 Effect of Temperature

The reaction of sphalerite in ferric chloride has been found to be dependant upon temperature. The activation energy calculated from temperature dependence found

in literature is given in Appendix 3-2. From analysing the data presented in Appendix 3-2, generally, one can say that the activation energy decreases as the iron content of the sphalerite increased when leached in ferric chloride. However, there are some exceptions that may be related to the presence of other impurities such as copper minerals, galena, and pyrite.

Most research studies in this area suggest that Reaction 3-17 is chemically controlled. However, others claim electrochemical control (Crundwell, 1988a). This is because the reaction rate was enhanced when UV light, which was used to irradiate the leaching system. UV light irradiation creates free electrons and holes in the valence band of sphalerite (Crundwell, 1987a) knowing that the band gap of sphalerite is about 4 eV (Shuey, 1975).

3.5.1.3 Effect of Ferric Chloride Concentration

It was found that the reaction of sphalerite oxidation in ferric chloride depends on the ferric ion concentration. According to Dutrizac and MacDonald (1978) the reaction order with respect to Fe^{3+} is 0.36 over a concentration range of 0.001-3 M $FeCl_3$. Warren et al. (1985) and Jin et al (1984) also found that the reaction order was 0.5 with respect to Fe^{3+} across a concentration range of between 0.05 and 0.8 M. However, according to Rath et al. (1981) the reaction order of zinc sulphide in ferric chloride with respect to Fe^{3+} (0.2-0.8 M) is 1.37 when the whole leaching time was included. However Rath et al. (1981) found that the reaction order was 1.12 when calculating the rate constant after 5 minutes, which is close to unity. The difference in result for reaction order between Rath et al and others could be related to the fact that Rath et al (1981) used synthetic material, whereas, others used natural sphalerite.

3.5.1.4 Effect of Agitation

There is a general agreement regarding the effect of stirring speed on the reaction rate of sphalerite dissolution in ferric chloride. It was reported that a stirring speed of 300 rpm is enough to eliminate the mass transfer effect through the fluid film layer (Bobeck and Su, 1985; Jin et al., 1984; Rath et al., 1981). However,

previously, Dutrizac and MacDonald (1978) found that for a sintered disk, the leaching rate was independent of the stirring speed. Nevertheless, the rate of a mass transport controlled reaction for a rotating disk can be calculated using the Levich equation (Levich, 1962):

$$k = 0.620\overline{D}^{2/3}\overline{v}^{-1/6}W^{1/2}(C_B - C_S) \qquad \textbf{Equation 3-1}$$

where $\overline{D}$ is diffusion coefficient, (cm^2/s), $\overline{v}$ is kinematic viscosity ($cm^2.s^{-1}$). W is the disk rotating speed (rad./s) ($W=2\pi f/60$), (C_B-C_S) is the difference between the bulk concentration and the concentration at the surface

3.5.1.5 Effect of Iron Substitution

Iron can substitute zinc in the sphalerite crystal lattice as (Zn, Fe)S. Dutrizac and MacDonald (1978) suggest that sphalerite dissolution in ferric chloride is more or less independent on the amount of iron substituted in (Zn, Fe)S. However, in a more recent study Palencia and Dutrizac (1991) studied the effect of iron content in the solid solution of sphalerite upon the dissolution rate. They leached 15 sphalerite samples having iron contents ranging from .04 to 12.5% in $FeCl_3$-HCl at a temperature of 80°C. It was found that the leaching rate was significantly increased with the increase in iron content. They normalized data to the surface area and after statistical treatment the data was found to fit the following equation:

$$k(gg^{-1}m^{-2}h^{-1}) = -0.001 + 0.657\times[\%Fe] \qquad \textbf{Equation 3-2}$$

where: k is the rate constant, [%Fe] is the iron content in sphalerite

Palencia and Dutrizac (1991) concluded that the linear relationship was indicative of electrochemical control because it was consistent with rate control by charge transfer at the surface of the sphalerite. They observed that the samples containing copper and silver did not follow the general observed relationship. This was explained by the presence of some sulphide precipitation of these elements. Crundwell (1988b) also postulated that the sphalerite dissolution rate was first order with respect to the number of occupied sites in the *d* orbital conduction band, which means that the rate is proportional to iron content of sphalerite in the absence of other electrically active impurities.

3.5.2 Ferric Sulphate Leaching

3.5.2.1 Reaction

The reaction of sphalerite with ferric sulphate is as follows (Dutrizac and MacDonald, 1978; Jin et al., 1984; Rath et al., 1981):

$ZnS + Fe_2(SO_4)_3 \rightarrow ZnSO_4 + 2FeSO_4 + S^0$ **Reaction 3-18**

Sulphur is formed in its elemental form, however, Dutrizac et al. (2003) suggest the formation of hydrogen sulphide at the beginning which then oxidises to elemental sulphur reacting with ferric ions. They also suggest the formation of SO_2 as reaction product (less than 5%) and/or SO_4^{2-} according to Reaction 3-19 (Dutrizac et al., 2003):

$ZnS + 8Fe^{2+} + 4\ H_2O \rightarrow Zn^{2+} + 8Fe^{2+} + SO_4^{2-} + 8\ H^+$ **Reaction 3-19**

3.5.2.2 Effect of Ferric Sulphate Concentration

Kametani and Kobayashi (1988) found that the rate constant varies at a power of 0.5 to the Fe^{3+} concentration <10g/l, whereas it was independent at higher Fe^{3+} concentrations. This implies that the reaction is not electrochemically controlled at higher ferric ion concentrations. However, Crundwell (1987b) suggests that the reaction rate of sphalerite in ferric sulphate is proportional to the sum of the Fe^{3+} and $FeHSO_4$ complexes with a reaction order of 0.5 based on an electrochemical model.

3.5.2.3 Effect of Temperature

As found with ferric chloride dissolution of sphalerite, the reaction was found to be dependent on temperature. The activation energy reported by various investigations is presented in Appendix 3-3. The activation energy of ferric sulphate is also affected by the iron content in the sphalerite crystal lattice. This subject will be discussed in more detail in Section 3.5.2.5.

3.5.2.4 Effect of Agitation Speed

According to Verbaan and Crundwell (1986) turbulence has no effect on the leaching kinetic of sphalerite in ferric sulphate, which means that the oxidation is not limited by the liquid film layer. It appears that the effect of agitation on the kinetics of sphalerite dissolution in ferric sulphate is not clearly studied. Most researchers who studied the kinetics of sphalerite dissolution in ferric sulphate used agitated systems; ((Kammel et al., 1987) – 800 rpm; (Lochmann and Pedlik, 1995) -700rpm; (Dutrizac et al., 2003) – 800 rpm; (Markus et al., 2004) – 420 rpm). However, none of these investigators has clearly stated the degree of the influence of agitation on the dissolution kinetics. This issue is investigated in Chapter 5.

3.5.2.5 Effect of Iron Substitution

As found with the ferric chloride system, the iron content of sphalerite affects the leaching rate. Kammel et al (1987) studied the effect of the iron content of sphalerite on its leaching rate in ferric sulphate (5 g/l $Fe_2(SO_4)_3$ and 50g/l H_2SO_4) at a temperature 70°C where the iron content varied from 0.11 to 10.3%. They found the following relationship:

$$Zn\ extraction\ (\%) = A + B*\log[\%Fe] \qquad \textbf{Equation 3-3}$$

This relationship is valid in absence of Cu^{2+}. A and B are constants.

Similarly, Kametani and Kobayashi (1988) concluded that the rate of sphalerite leaching in ferric sulphate (10 g/l $Fe_2(SO_4)_3$ and 100 g/l H_2SO_4) at a temperature of 90°C increased linearly as the iron content increased from 0.79 to 13.4%. They related this result to electrical conductivity and concluded that the leaching rate is proportional to the electrical conductivity. Xiong et al. (1989) found there was no good correlation between the reactivity and the conductivity. The rate of sphalerite dissolution in 20 g/l $Fe_2(SO_4)_3$ and 90 g/l H_2SO_4 at a temperature of 68°C increased 3 times when the iron content increased from 0.51 to 7.17 % Fe. The conductivity at room temperature increased from 10^{-12} to 10^{-7} ohm^{-1} cm^{-1} when iron content increased from 0.51 to 10%.

Palencia and Dutrizac (1991) also studied the iron content effect in solid solution of sphalerite on the dissolution rate. They leached 15 sphalerite samples having iron contents ranging from .04 to 14.7% in both $Fe_2(SO_4)_3$ - H_2SO_4 at a temperature of 80°C. It was found that the leaching rate was significantly increased with the increase in the iron content. They normalized data to the surface area and after statistical treatment the data was found to fit the following equation:

$k(gg^{-1}m^{-2}h^{-1}) = 0.219 + 0.258\ [\%Fe]$ **Equation 3-4**

where k is the rate constant

To conclude it is obvious that the iron content in sphalerite has a positive influence on the leaching rate. This is indicative of the electrochemical nature of the reaction and it is controlled by charge transfer at the sphalerite surface (Dutrizac et al., 2003). Furthermore, this effect is related to the number of occupied sites in the *d*-orbital of the conduction band of the (Zn, Fe)S, because iron is present in *d*-orbital (Crundwell, 1987a).

3.5.2.6 Effect of Lead and Copper Content

If galena is present as an impurity with sphalerite it will react with ferric sulphate forming lead sulphate. The solubility of $PbSO_4$ in sulphate solutions is very small and it tends to precipitate on the sphalerite particle surface. Crundwell (1987b) reported that the presence of lead in the sphalerite could passivate its leaching in ferric sulphate solution due to the formation of lead sulphate or lead jarosite. However, this cannot be a problem in ferric chloride solution because of the formation of $PbCl_2$ which soluble in chloride media.

On the other hand, it was reported that copper sulphate catalyses the aqueous oxidation of ZnS as the following reactions:

$ZnS + CuSO_4 \rightarrow ZnSO_4 + CuS$ **Reaction 3-20**

$CuS + 2O_2 \rightarrow CuSO_4$ **Reaction 3-21**

3.6 Application of Microwaves in Extractive Metallurgy

3.6.1 Introduction

Research into heating of minerals with microwave energy started in 1966 when Connell et al. obtained a US patent for apparatus for the treatment of ore. The apparatus was designed to convert hematite ore to magnetite and metallic iron. Ford and Pie (1967) applied microwaves to several oxides and sulphide minerals using two 800 W 2.45 GHz magnetrons. The temperature was measured using an infrared radiation thermometer. Ford and Pie (1967) found that dark coloured ore heated faster than lighter ore (see Appendix 3-4). Chen et al. (1984) applied microwave irradiation to 40 minerals and compounds. They concluded that most silicates, carbonates and sulphates are microwave transparent, whereas, most sulphide and arsenide minerals were readily heated in microwave fields (see Appendix 3-4). Walkiewicz et al. (1988) subjected 135 reagent grade chemicals and 19 minerals to microwave irradiation. Generally, it was found that many ore minerals are lossy and good absorbers, whereas, gangue minerals (silicate type) heated poorly. McGill et al. (1988) studied the effect of power level on the heating rate of reagent grade chemicals and minerals. Appendix 3-4 summarises some of the early findings on microwave heating of minerals and compounds.

Various authors have suggested potential applications of microwave energy in mineral extraction and several review papers can be found in this area (Haque, 1999; Kingman, 2005; Kingman and Rowson, 1998; Xia and Pickles, 1997). It was indicated that microwave energy could have potential applications in comminution, drying, pre-treatment of refractory gold ores, coal desulphurisation, leaching, roasting, carbon reactivation, carbothermic reduction of oxides and waste and slag management. The above authors concluded in most cases that microwaves may have the potential to reduce the energy cost of comminution, enhance mineral surface chemistry and facilitate new forms of metal extraction in a controlled environment.

3.6.2 Microwave Leaching of Chalcopyrite and Other Copper Sulphide Minerals

The first attempt to use microwave energy to improve copper recovery from its ores was conducted by Kruesi et al. (1982a) . These workers obtained a US patent for the recovery of copper from its oxide and sulphide ores using microwaves. Various methods for treating different ores and concentrates were presented. For example, 120g of copper ore containing 1.6% copper, 53 % of which was in the form of oxides and 47% in the form of sulphide was blended with 11 g of concentrated sulphuric acid and 3 g of iron as $FeCl_2$. The mixture was irradiated for 10 minutes at a power level of 600 W and a frequency of 2.45 GHz under a chlorine atmosphere. The mixture was then cooled and leached in a brine solution achieving 86% of copper soluble. Another example was where 100 g of copper ore, containing 0.6% copper mainly in the form of chalcopyrite, was ground to 1680 μm then mixed with 1g of iron in the form of $FeCl_2$. The dry mixture was then irradiated under a chlorine atmosphere for 6 minutes at 600 W and at a frequency of 2.45 GHz. The remaining solids were then leached in brine solution and 91% copper was found to be soluble.

Walkiewicz et al. (1988) microwave treated chalcopyrite ore containing 24% Cu mixed with ferric chloride hexahydrate ($FeCl_3.6H_2O$). The experiments were carried out in 1 kW 2.45 GHz commercial multimode oven, and the temperature was measured and monitored continuously using type K type thermocouple with an ungrounded tip sheathed in Inconel 702, which was inserted in the sample through the roof of the oven. The temperature reached 224°C after 10 minutes and the copper extraction reached 30%. However, when the same mixture was heated in a muffle furnace for 10 minutes, the maximum temperature reached was 255°C but only 22%Cu of the copper was extracted. According to authors, this indicates that increase in copper extraction is not related to the heat delivered by microwaves but by some other non-thermal effect. Walkiewicz et al (1988) reported an accuracy of ±2% in their temperature measurement. However, it should be noted that to prevent electrical field concentration and therefore arcing between the tip of the thermocouple and the surface of the material either an

insulating layer needs inserting in between or an air gap must be left (Binner et al., 2003). Either approach reduces the sensitivity and accuracy of the temperature measurement. Furthermore, the metallic shield disturbs the microwave field pattern inside the cavity and also causes localised field concentration which if it does not cause arcing will certainly cause enhanced local heating of the material close to the tip.

Worner (1990) mixed 85% copper concentrate, containing 24% Cu, 29% Fe, 33% S and minor amounts of Pb, Zn and gangue minerals, with 15% finely ground peat and formed the mixture into pellets of 2 cm diameter. The pellets were irradiated in a laboratory 650 W multimode microwave oven. As a result sulphur and sulphur dioxide were emitted. After 6.5 minutes the pellets were removed from the oven. The reaction continued and after two minutes all the carbon was burned out. The product was subjected to leaching in a solution of ammonia and ammonium carbonate. Copper was found to completely dissolve with the resulting blue solution being separated from the iron oxide residue.

Antonucci and Correa (1995) heated chalcopyrite and concentrated sulphuric acid in an adapted domestic microwave oven (up to 1 kW at 2.45GHz) across a temperature range of 200 to 260°C for about 20 minutes. The product was then leached in water at a temperature of 60°C and at a pH of 1.6. The copper extraction was between 90 and 99% with high copper concentrations in the solution (9-14g/l). All the elemental sulphur formed was captured and sulphur dioxide was produced in low volumes and any pyrite contained in the concentrate remained unreacted. However, the energy consumption was 5 times higher than thermodynamic calculations and the penetration depth was less than the material thickness. Leaching reactions of the sulphide minerals contained within the concentrate in concentrated sulphuric acid are as follows:

$$CuFeS_2 + 4H_2SO_4 \rightarrow CuSO_4 + FeSO_4 + 2S^0 + 2SO_2 + 4H_2O \qquad \textbf{Reaction 3-22}$$

$$Cu_2S + 4H_2SO_4 \rightarrow 2CuSO_4 + S^0 + 2SO_2 + 4H_2O \qquad \textbf{Reaction 3-23}$$

$$CuS + 2H_2SO_4 \rightarrow CuSO_4 + S^0 + SO_2 + 2H_2O \qquad \textbf{Reaction 3-24}$$

An industrial multimode microwave oven was used with a maximum power output of 50 kW at a frequency of 915 MHz for the pilot scale study (Antonucci and Correa, 1995). The cavity volume was 3.22 m^3. The maximum copper extraction efficiency achieved was 70%. This was achieved at the following conditions: acid paste/concentrate ratio-1.34; power level- 7 kW; irradiation time-13 minutes and cross energy consumption- 0.602 kWh/kg. However, the quantity of copper concentrate used for this experiment and the method for calculating the energy consumption were not given.

Antonucci (2004) recently demonstrated, in a pilot plant experiment, that it is possible to leach copper concentrate in continuous form under atmospheric pressure and a temperature of about 230°C using concentrated sulphuric acid. The copper recovery was shown to reach up to 97% within one hour of microwave heating. Carbon additives were used to reduce SO_2 to elemental sulphur.

Florek et al. (1996b) observed that microwave pre-treatment of tetrahedrite ($Cu_2S.Sb_2S_3$) had a positive effect on the recovery of As and Sb. When tetrahedrite was treated in a 900W Panasonic multimode microwave oven at a frequency of 2.45GHz for 30 seconds, and subsequently leached in a solution of sodium sulphide, the recovery of As and Sb was 15% and 6% higher than without microwave irradiation. Cu_2S remained as a solid phase. The authors concluded that the different effect could not be connected with the phase change. However, there was no explanation given for the enhancement observed.

Harrison (1997) investigated the effect of microwave pre-treatment of copper sulphide minerals on copper recovery after subsequent leaching. The pre-treatment was carried out in a 2.6 kW Panasonic multimode microwave oven at 2.45 GHz. 3 g samples of untreated and treated bornite, chalcocite chalcopyrite, and pyrite were leached in 50 ml solution of cupric chloride (118g/l $CuCl_2$ and 25g/l HCl, 40g/l $CaCl_2$). After 120 minutes the leached masses of the untreated samples as a percentage of the original mass were approximately 22% of the bornite, 25% of the chalcocite, 10% of the chalcopyrite, and 1% of the pyrite compared to 23 % of bornite, 34 % of chalcocite, 14% of chalcopyrite, and 2% of

pyrite for the treated samples. The increase in dissolved amount was explained by the increase of the surface area after microwave treatment. This explanation would be possible for relatively large particle sizes where micro cracks would form; however, Harrison used a particle size of 250-355 μm where micro cracks are unlikely to form. It is possible that the slight increase in the reactivity could be related to surface oxidation enhanced by surface heating.

Harrison (1997) also examined the effect of microwaves on the leaching of chalcopyrite in acidified ferric sulphate. 50g of Norwegian chalcopyrite containing 28% copper at a size of -355+250 μm was microwaved at 1.3 and 2.6 kW for 10, 20 and 30 seconds. The product was then leached in a solution of 0.25 M $Fe_2(SO_4)_3$ and 1.0 M H_2SO_4 for 180 minutes. The amount of copper extracted increased with an increase in microwave exposure time and also with the increase in power level, although the increase was insignificant (see Figure 3-1).

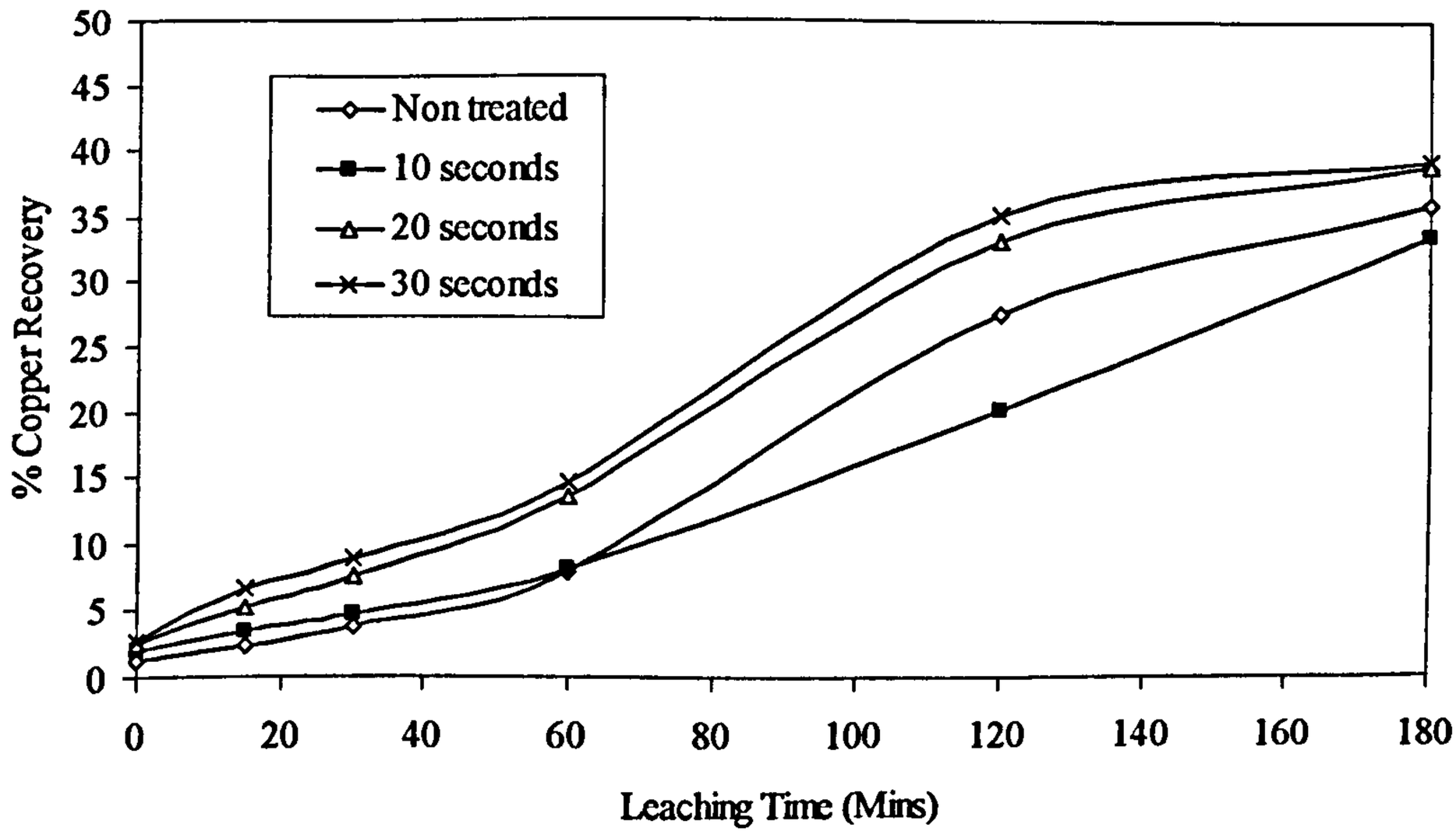

Figure 3-1 Influence of microwave time on copper recovery for treated (power level-2.6 kW) and non-treated chalcopyrite in ferric sulphate solution at 89 °C (Harrison, 1997)

Kingman (1998) also investigated the effect of microwave pre-treatment on the copper recovery from chalcopyrite concentrate. Chalcopyrite concentrate at a size of 45–63 μm, from Mount Isa Mines, Australia, containing about 23.7% copper was microwaved for 10, 20 and 30 seconds, then leached in a solution of 0.25 M

$Fe_2(SO_4)_3$ and 1.0 M H_2SO_4 at various temperatures. It was observed that the initial reaction rate of chalcopyrite leaching was much faster for microwaved samples than that of untreated ones. This was probably due to the oxidation of chalcopyrite to bornite after microwave pre-treatment which is more amenable to leaching than chalcopyrite. Furthermore, the activation energy calculated for the leaching reaction of the pre- treated chalcopyrite was found to be similar to the activation energy of bornite. However, the reason for lower final copper recovery of the microwave treated chalcopyrite was not given (see Figure 3-2).

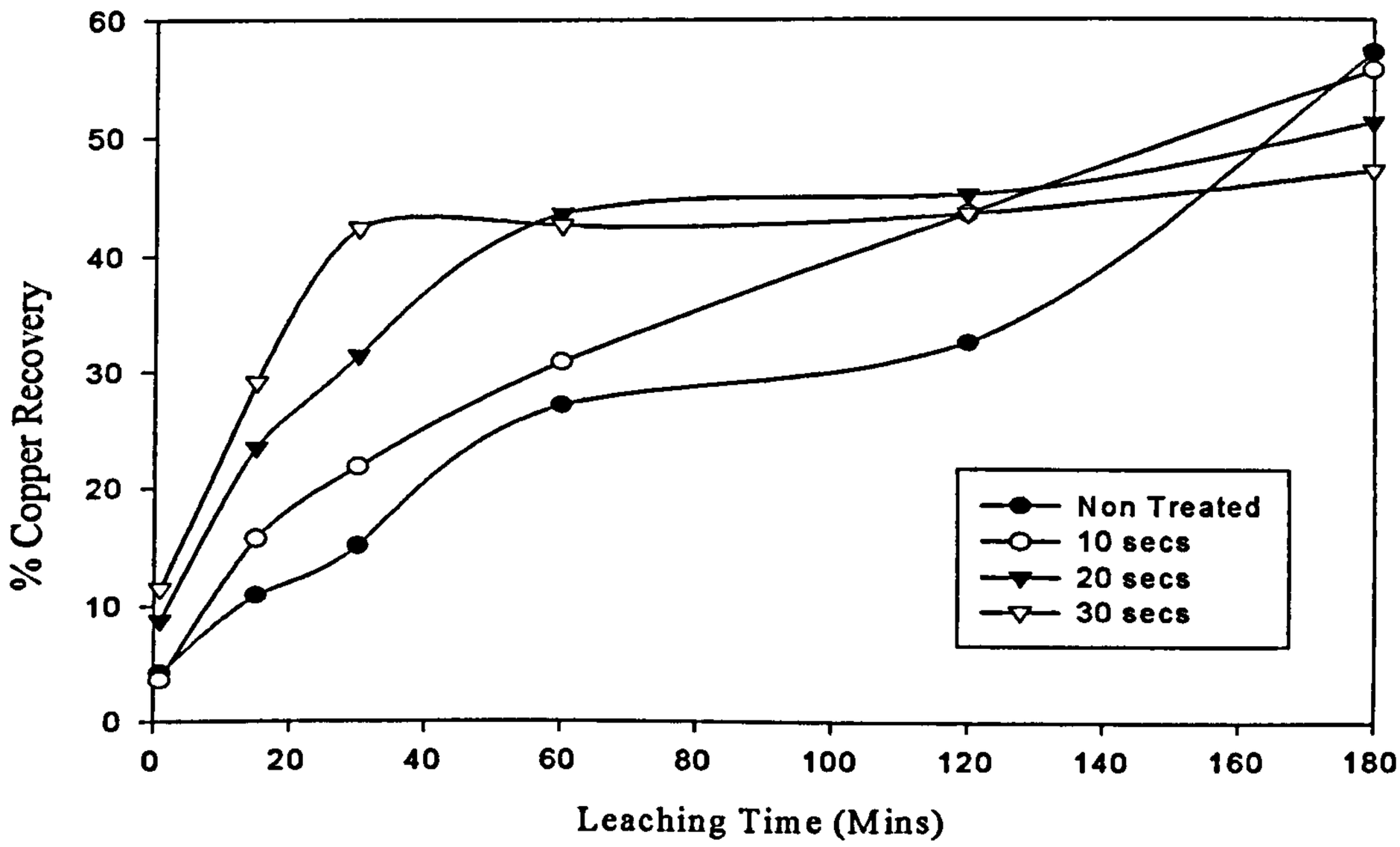

Figure 3-2 Influence of leaching time on copper recovery for treated (2.6 kW) and non-treated chalcopyrite in ferric sulphate solution at 90 °C (Kingman, 1998)

Harrison (1997) noticed this effect when microwave treated chalcopyrite samples were quenched in water before leaching in ferric sulphate and this was explained by the formation of $CuSO_4$, which dissolved in water before leaching.

The leaching rate of chalcopyrite in Figure 3-1 and Figure 3-2 is different, although microwave treatment and leaching conditions are the same (power level, microwave treatment time, leaching temperature and concentration of the leaching solution). This difference may be due to the different particle size, the mineralogy of the chalcopyrite concentrate or a combination of both factors. Another important factor that might be considered is the location of the samples in

microwave cavity because the field distribution inside the cavity is different and depends on the applicator design and the size of the load (Chan and Reader, 2000).

Weian (1997) investigated the effect of microwave heating on the leaching of a complex copper sulphide concentrate containing mainly chalcocite (79%) and chalcopyrite. It was found that that copper extraction reached 99% within 45 minutes when a leaching solution of 120g/l $FeCl_3$ was irradiated in a refitted commercial microwave oven at an output power of 700 W. The leaching temperature was 105°C, which was measured at the end of treatment. In comparison it was found that 2 hours were required to achieve the same results by conventional heating. According to the author this may be due to the creation of large convection thermal currents, which agitated the surface of the particles and swept away the formed sulphur layer. Nadkarni (1984) came to this conclusion in an earlier paper. Tremendous accelerations of sample dissolution in the microwave field were explained by the fact that in heterogeneous reaction systems the effect of microwaves causes different heating rate of liquids and solids, which generate gradient temperature between the two phases. This creates large thermal convection currents, which can agitate and sweep away the reaction products exposing new surface to the solution. On the other hand, it was claimed that microwave heating alone could not break chemical bond because the quantum energy of microwaves is less than the energy required to break chemical bonds (Chemat and Esveld, 2001).

Similar results were achieved by Hwang et al. (2002). The author investigated the leaching kinetics of oxygenated chalcocite under microwave-hydrothermal conditions in $CuCl_2$-NaCl-HCl solution with a corresponding concentration of 0.25, 0.4 and 1.0 M. Thick, stirred (300 rpm) leaching slurries (50-100g/l) under an oxygen pressure (approx. 3 bar) were irradiated in a multimode microwave oven at 4 kW and 2.45 GHz to reach the required leaching temperature. Fast leaching kinetics were observed with low initial concentrations of cupric and chloride ions. Complete leaching of copper was achieved after 1 hour for a solution containing 50g/l of mineral, while 3 hours were required to totally

dissolve copper from a solution containing 100g/l mineral. The fast leaching kinetics were attributed to the super heating effect of copper ions, which became more significant as temperature rises.

Microwave heating has been also tested in an attempt to improve the leaching kinetics of chalcopyrite by sulfidizing decomposition according to the following Reaction 3-25 (Bradshaw and Beckmann, 1998):

$CuFeS_2 + S \rightarrow CuS + FeS_2$ **Reaction 3-25**

When chalcopyrite is heated with sulphur at 425°C, covellite originates which covers the pyrite core. The former is easily leached in $FeCl_3$ or $CuCl_2$ with an efficiency of more than 99%. The estimated energetic requirement was low (23 kWh/t). However, temperature must be strictly controlled because an increase of temperature to over 445°C causes the formation of bornite and idaite. Additionally a problem with sulphur that smelted and evaporated was found to occur.

Yianatos et al. (2001) leached chalcopyrite from molybdenite concentrate in sulphuric acid. Reactions 3-22, 3-24 and 3-26 describe the leaching process:

$2FeSO_4 + 2H_2SO_4 \rightarrow Fe_2(SO_4)_3 + SO_2 + 2H_2O$ **Reaction 3-26**

The experiments were carried out in a modified multimode microwave oven with a power level of between 147 and 850 W. A multi speed agitator was used to stir the system. Copper and iron were dissolved in the same proportion (1:1.5), whereas, pyrite was not dissolved. After exposure to microwaves for 15 minutes 95% of copper was dissolved from the molybdenite concentrate, whereas 40 minutes was required to reach a similar level when applying conventional electrical heating at 200°C. The dissolution of finer particles was faster than in standard leaching because of larger surface area. It was observed that the elemental sulphur formed during the first stage of leaching of chalcopyrite was dissolved after 8 minutes of microwave treatment probably via Reaction 3-27. This process was less progressive (only 60% SO_2 generated) when using nitrogen (2001).

$S + 2H_2SO_4 \rightarrow 3SO_2 + 2H_2O$ **Reaction 3-27**

Popovicova and Havlik (2001) and Havlik et al. (2002) leached chalcopyrite containing 30% copper in ferric chloride (0-1.0 M) in an adapted domestic microwave oven (900W). In each experiment 3 g of chalcopyrite and 200 ml of leaching solution were used. The copper extraction increased with an increase in power level. About 19% of the total copper was leached at a power level of 90 W in 0.5 M $FeCl_3$ - 0.5 M HCl within 2 hrs compared to about 34% at 900 W (within the same other conditions). It was found that the rate constant increased very quickly with an increase in ferric ion concentration up to 0.25 M. Above 0.25 M the increase became less progressive. Popovicova and Havlik (2001) and Havlik et al. (2002) compared microwave leaching with other methods and results are shown in Figure 3-3 (lines 2-7).

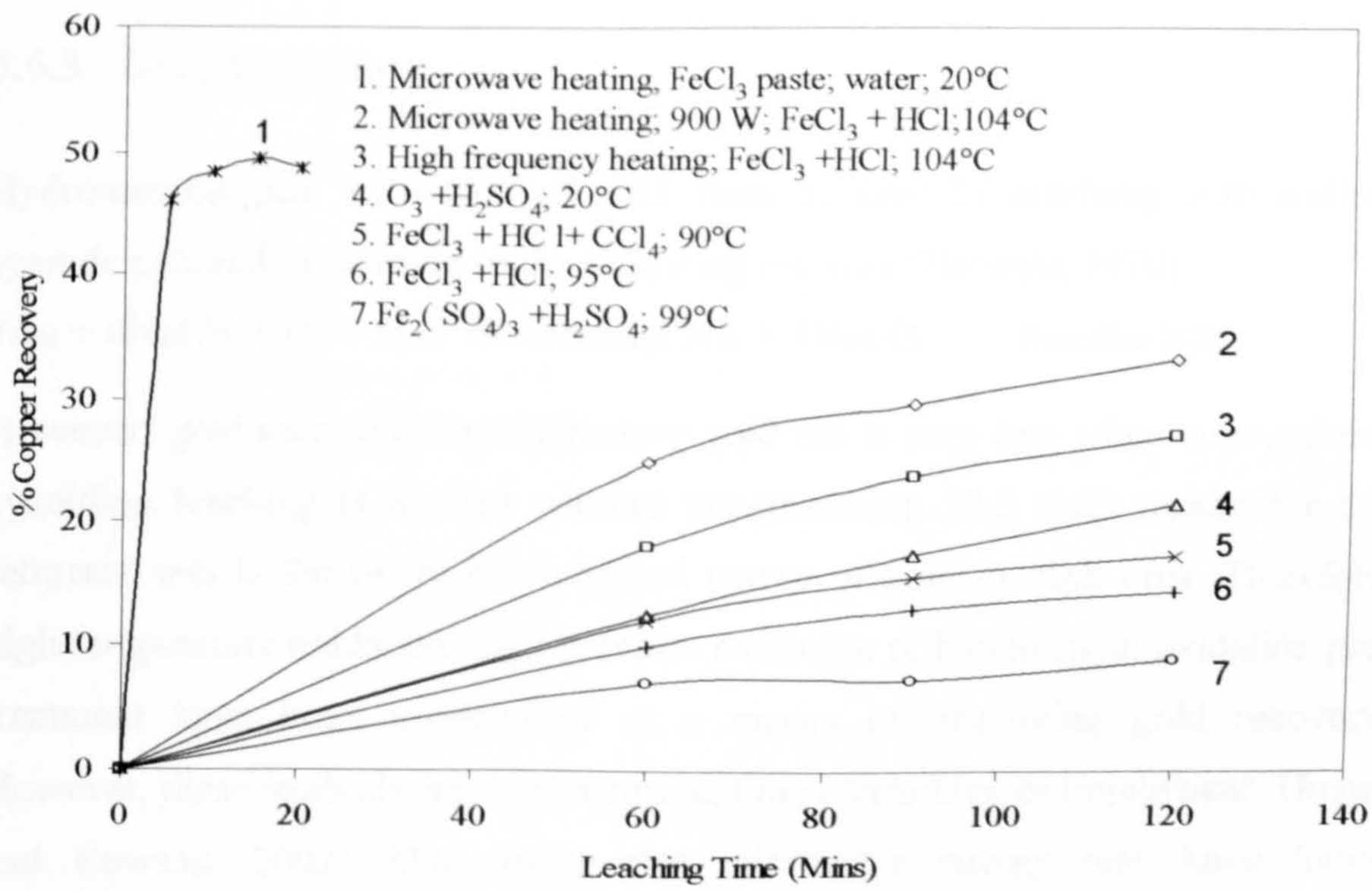

Figure 3-3 Comparison of the most effective chalcopyrite leaching curves of various leaching agents (Havlik et al., 2001; Havlik et al., 2002).

In a different study Havlik et al. (2001) heated a dry mixture of ferric chloride and chalcopyrite in a microwave field for a short time (the time is not stated by the authors). Highly soluble compounds were produced which were leached in water at a temperature of 25°C. The achieved copper leaching efficiency was better than that achieved by leaching under conventionally heating conditions (see Figure 3-3,

line 1). However, there was no attempt given to explain the reason for the enhancement observed.

Lovas et al. (2003) investigated the effect of microwaves on the leaching of chalcopyrite in both 0.25 M $Fe_2(SO_4)_3$ and 0.25 M $FeCl_3$. They conducted their experiments in a laboratory multimode microwave oven of type Whirlpool AVM 435 with a pulse system at a frequency of 2.45 GHz. The temperature was measured by means of an optical fibre. They showed that microwaves had a positive influence on the leaching kinetics of chalcopyrite in both chloride and sulphate systems. However, there was no attempt to explain the lower recovery of copper in both systems from chalcopyrite at a temperature of 71°C under microwave conditions compared to that of standard leaching conditions.

3.6.3 Gold Leaching

Hydrometallurgical extraction of gold from its ores by leaching with sodium cyanide proceeds according to the following reaction (Habashi, 1970):

$4Au + 8NaCN + O_2 + H_2O \rightarrow 4NaAu(CN)_2 + 4NaOH$ **Reaction 3-28**

However, gold recovery from refractory gold ore is very low when conventional cyaniding leaching is applied without pre-treatment. The main reason for this refractoriness is the finely disseminated nature of gold in such ores. Therefore, high temperature oxidation, high pressure oxidation or biochemical oxidation pre-treatment have been investigated as a means of improving gold recovery. However, these methods are cost intensive, time consuming or impractical (Huang and Rowson, 2002). One reason that microwave energy may have found successful application in gold extraction is that gold bearing minerals tend to be good microwave absorbers, whereas gangue minerals commonly found in gold ores are microwave transparent (Haque, 1999; Huang and Rowson, 2000). Pyrite and arsenopyrite are the main gold bearing minerals.

Chen et al. (1984) reported that when arsenopyrite was microwaved at a power level of 80 W, it heated readily and sulphur and arsenic fumed, leaving new phases of pyrrhotite and ferroarsinide. Similarly, pyrite has also been shown to

heat quickly with the evolution of sulphur fumes and pyrrhotite products. Haque (1987) also studied microwave pre-treatment of refractory gold concentrate. It was found that the weight loss after irradiation was about 20%, which corresponds to complete volatisation of As and S as As_2O_3 and SO_2, whereas iron was converted to Fe_2O_3. After subsequent cyanidation leaching, 98% gold recovery was achieved. When concentrate was irradiated in a nitrogen atmosphere the major products were pyrrhotite, As_2S_3 and sulphur with 89% of gold being recovered after subsequent cyanidation. However, 99% of gold extraction was achieved when the same concentrate was mixed with sodium hydroxide and irradiated at a power level of 5 kW for 5 minutes, and subsequent water leaching. Water-soluble Na_3AsO_4, Na_2SO_4 and $FeSO_4$ were formed instead of As_2O_3 and SO_2.

Beeby (1992) examined the effect of short microwave pulses on the leachability of gold from gold bearing ores. It was found that when Ora Banda gold ore was exposed to short pulses of microwave energy for 3 seconds after every 30-second interval, for 10 minutes, the amount of gold recovered increased by 62% compared to the amount recovered without microwave exposure. Microwave pulses were applied at a power level of 1300 W (2×650W) and the corresponding energy for every pulse is estimated to be about 3.9kJ/pulse. The leachability was assessed by dissolution of wet ground ore with a mean particle size of 76 μm in 0.005 M NaCN at a pH of 10.5 and a temperature of 22°C. Microwave pulses result in differential thermal expansion within the ore as a result of the varying loss factor of the constituents in the ore. In addition, these pulses may create high temperature internal gas phases, which led to structural distortion and breakdown of the ore. This process would occur if locked moisture droplets are present within the ore which would generate high vapour pressure at such a high level energy per pulse (3.9 kJ/pulse) (Lester et al., 2005).

Huang (2000) and Huang and Rowson (2000) also investigated the effect of microwave irradiation on gold recovery from refractory ore obtained from Lihir Gold Mine, Papua New Guninea. The ore was sized between 0.2-16 mm and was irradiated for a period of between 0 and 70 minutes in either a monomode or multimode microwave cavity. The ore was then ground to 80% passing 75 μm and

leached in a cyanide solution of pH 11-12. The optimum results produced were an 81% gold extraction after microwave pre-oxidation compared to 37% for untreated ore. It was found that irradiation time and particle size of the pretreated samples has a significant effect on the gold recovery. The enhancement of gold leachability was probably due to the increase in surface area as a result of pyrite and arsenopyrite oxidation and formation of a porous hematite structure, according to the following reactions:

$FeS_2 + O_2 \rightarrow FeS + SO_2$ **Reaction 3-29**

or $FeS_2 \rightarrow FeS + S$ **Reaction 3-30**

$S + O_2 \rightarrow SO_2$ **Reaction 3-31**

then: $4FeS + 7O_2 \rightarrow 2Fe_2O_3 + 4SO_2$ **Reaction 3-32**

An alternative process for pre-treatment of refractory gold ores is to use nitric acid to oxidise marcasite, pyrite and arsenopyrite. Huang (2000) and Huang and Rowson (2002) studied hydrometallurgical decomposition of pyrite and marcosite in a microwave field. A Microwave Accelerated Reaction Systems (MARS) produced by CEM operating at a power level of 1200W and a frequency of 2.45 GHz was used for the leaching experiments. In this device temperature and pressure can be controlled and monitored by variation of power level. Samples of pyrite and marcasite with different particle size ranges (20-63, 90-125, and 180-250 μm) were leached in nitric acid (0.25, 0.5, 1.0, 2, 3 and 4 M) at different temperatures (70-110°C). The leached particles were washed with deionised water and dried at a temperature of below 50°C so that the sulphur was kept stable. The dried samples were then slowly heated below 220°C to vaporize sulphur to allow calculating of the amount of elemental sulphur formed. It was found that the reaction rate increased with an increase in nitric acid concentration and temperature, whereas reaction rate was found to be inversely proportional to the particle size. With regard to reaction kinetics, it was found that the rate-limiting step was chemical reaction on the particle surface for both pyrite and marcasite. Marcasite was found to have a higher apparent reaction rate than pyrite despite being chemically identical.

Huang and Rowson (2002) suggested that microwaves only heat the system and did not effect the reaction mechanism or chemically activate the dissolution of minerals because microwave energy itself does not break chemical bonds. This is supported by the view that quantum microwave energy within the microwave frequencies (300 MHz- 300 GHz) is 1.24×10^{-6} to 1.24×10^{-3}eV. These energies are much lower than the ionization energies of covalent bond energies like OH (5 eV), hydrogen bonds (2eV), Van der Vaals bonds (<2eV) and even lower than the energies associated with Brownian motion at 37°C (2.7×10^{-3}eV) (Chemat and Esveld, 2001).

Huang and Rowson (2002) found no significant change in the activation energy of the dissolution reaction of pyrite in nitric acid, with and without microwave heating. The acceleration of the leaching reaction rate, for microwave leached experiments was suggested to be due to the super heating effect produced in nitric acid in a microwave field. In addition, the different dielectric properties of liquid and solid may have resulted in localized temperature differences which create strong convection currents at the surface of the microwaved solid. This promotes diffusion of the reaction product away from the surface. The authors also found that microwave radiation failed to reduce the formation of elemental sulphur or indeed dissolve it which may reduce the leaching rate of gold from the decomposed marcasite and pyrite. Joret et al. (1997) also concluded that the increase of the dissolution rate of Co_3O_4 and CeO_2 in nitric acid is not related to a specific microwave effect.

On the other hand, Kuslu and Bayramoglu (2002) found that the activation energies for both classical and microwave heated vessels for the leaching of pyrite in ferric sulphate solution were approximately 33 and 19kJ/mol respectively. They found that the reaction rate for dissolution of pyrite in ferric sulphate was chemically controlled and that the reaction order with respect to ferric ion and sulphuric acid was the same for both conventional and microwave heating. Other researchers support the idea of a non-thermal influence of dielectric heating in chemical reactions. Specially designed experiments have been used to study the non-thermal effect of microwaves. For example, Shibata et al. (1996) investigated

the effect of microwave power on the disintegration kinetics of sodium hydrogen carbonate. It was found that the activation energy of this reaction under microwave heating was less than that found for resistive heating and in addition the reaction rate was found to be much faster. Temperature was measured in various places using a glass-alcohol thermometer with a very fine thermo junction (20μm in diameter) completely shielded except for its hot tip. The tremendous acceleration of the reaction rate was explained by the fact that when the polarized dipoles in the molecules rotate as microwave energy was applied, the probability of the contact between molecules and atoms might be increased as a consequence of the reduction in activation energy. Therefore, the microwave effect was said to originate by lowering of the Gibbs energy of activation of the reactions through either storage of microwave energy as vibrational energy of molecules (enthalpy effect) or by alignment of molecules (entropy effect) (Fini and Breccia, 1999; Galema, 1997).

At EMR Technology Corporation Canada, arsenopyrite gold ore was subjected to microwave pre-treatment under very low oxygen conditions at an energy level below 50 kJ/kg for a sub-second time. The product contained pyrrhotite, elemental sulphur and arsenic, which was then acid washed to remove the elemental sulphur and arsenic then retreated again to oxidize pyrrhotite to magnetite (Tranquilla, 1997). The main advantages of this process were suggested to be low energy cost (about Cdn $ 0.5/tonne), the low SO_2 emission and the ore being processed at lower temperature than conventional roasting. An estimate of operational costs for a microwave treatment plant capable of processing 200 tones/day of ore concentrate compared to costs for roasters, autoclaves and bio-oxidation processes are shown in Figure 3-4. EMR put into operation a pilot plant for microwave pre-treatment of pyrite and arsenopyrite gold ores in 1997 which incorporated two microwave generators with a power level of 75 kW at a frequency of 915 MHz and using fluidised bed based cavity.

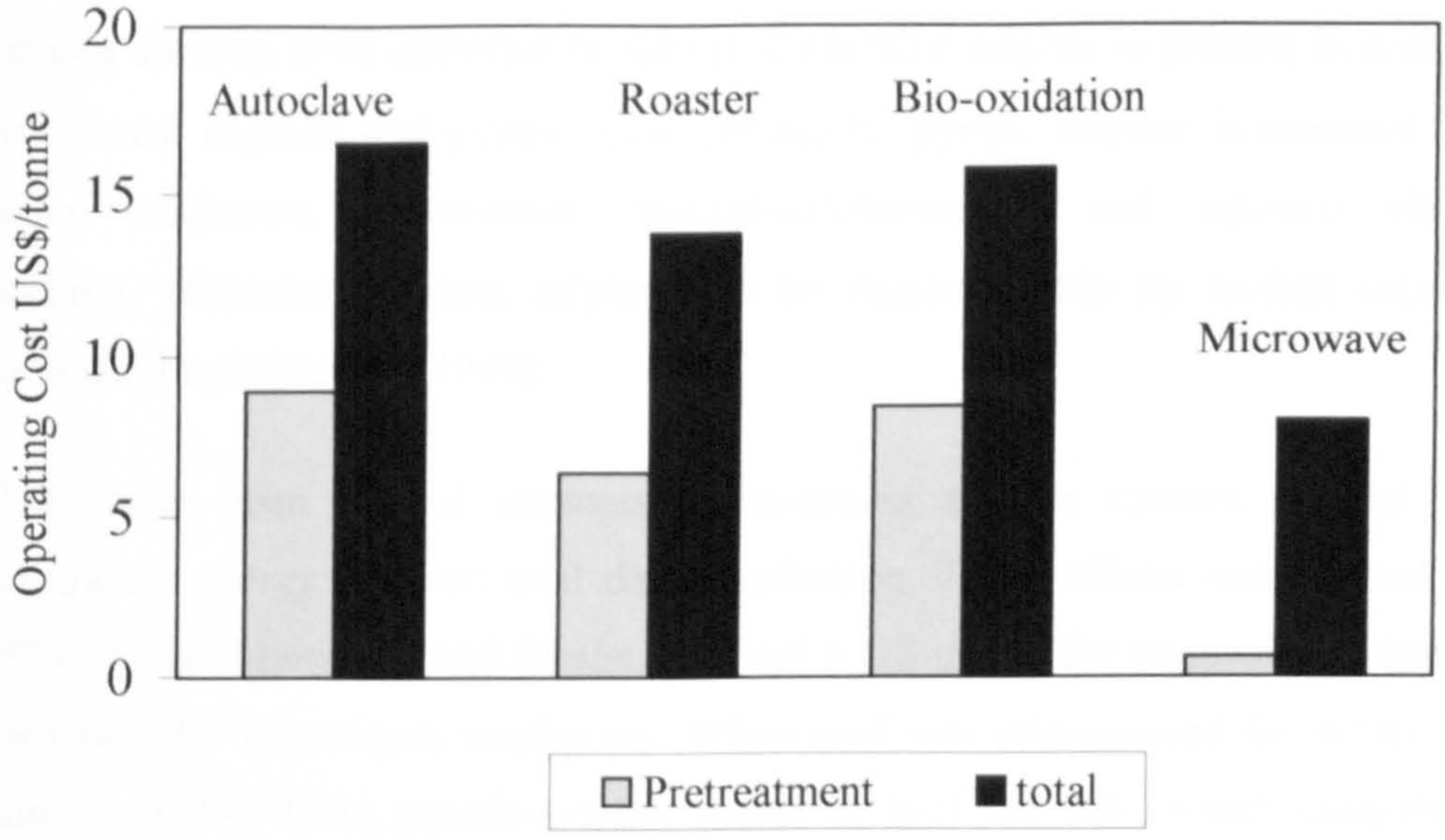

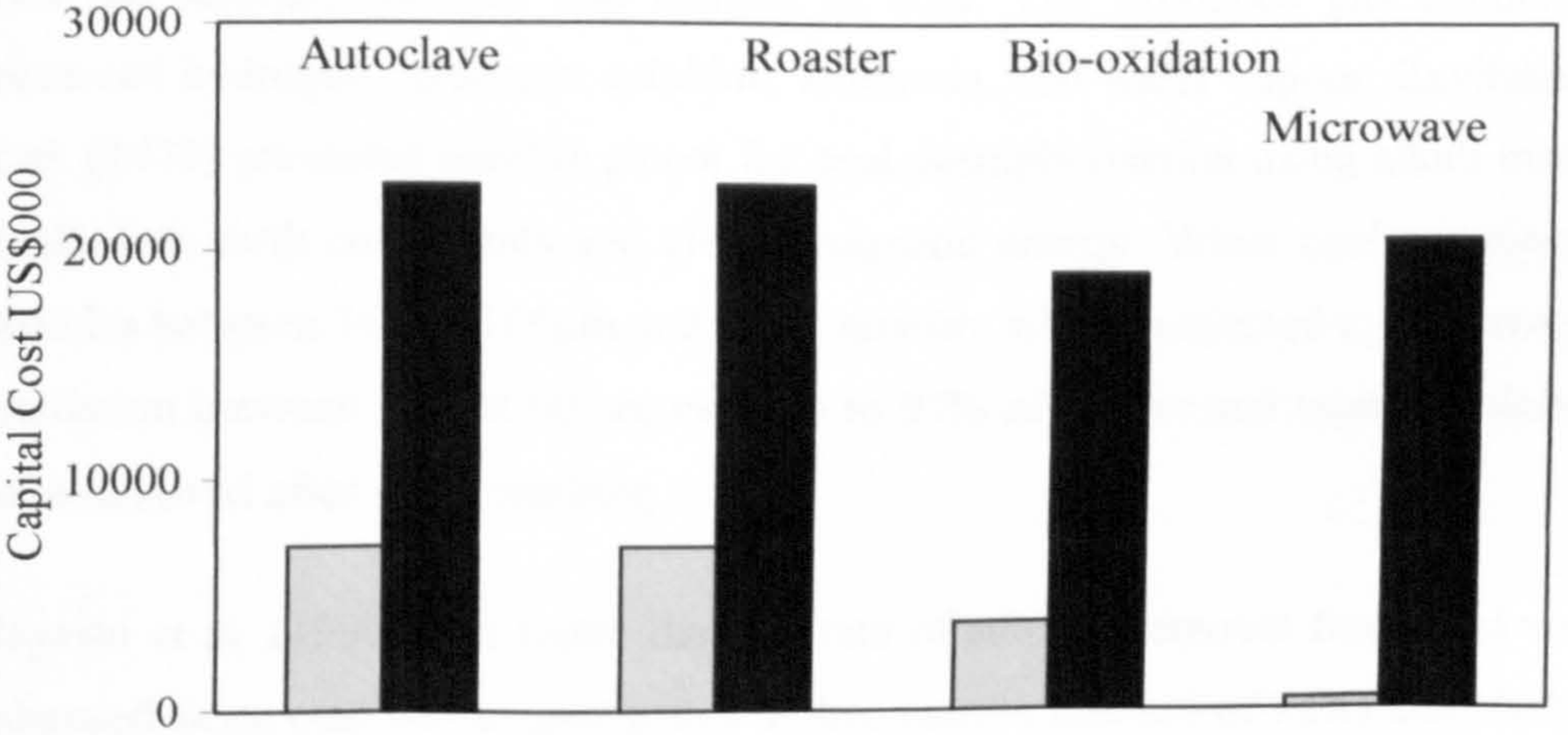

Figure 3-4 Comparative cost estimate for major gold ore pre-treatment technologies for a plant throughput of 200 tpd of concentrate (Tranquilla, 1997)

3.6.4 Coal Desulphurisation

The presence of sulphur in coal leads to SO_2 emissions into the atmosphere during burning causing environmental problems. Generally sulphur is present in coal in two forms: organic and pyritic. Conventionally, pyritic sulphur is removed by partial oxidation, chlorination, hydrodesulphurisation, and aqueous alkali leaching. However, organic sulphur can be removed only by molten caustic methods (Hayashi et al., 1990).

There have been several attempts to minimize sulphur content in coal by microwave energy to assist coal desulphurisation. These efforts were started in (1978) when Zavitsanos and Bleiler obtained a US patent for removal of sulphur from coal by microwave irradiation. When coal was microwaved for 40 to 60 seconds at 2.45 GHz, pyritic sulphur fumed as H_2S and SO_2, which were then recovered as elemental sulphur. Up to 50% of sulphur was removed using this technique. In the same year Kirkbride (1978) presented an invention whereby microwave energy was used with hydrogen to remove sulphur. Coal was dried prior to admixing with hydrogen and then microwave treated. Hydrogen reacted with the sulphur, nitrogen and oxygen in coal. The produced gas contained unreacted hydrogen, hydrogen sulphide, ammonia, and water vapour. Zavitsanos et al. (1979) presented another patent for coal desulphurisation using alkali metal or alkaline earth compounds and electromagnetic energy. When coal containing particles between 74 and 149μm and alkali mixture where subjected to microwave irradiation between 30 and 60 seconds, up to 97% of pyritic and organic sulphur were removed after water washing.

Hayashi et al. (1990) also found that the rate of sulphur removal from coal was enhanced when coal was treated with a molten caustic mixture of KOH and NaOH under microwave irradiation. This was suggested to facilitate the contact between coal and molten caustics. It was suggested that the rate-determining step was not chemical reaction but mass transfer of the caustics and coal. Rowson and Rice (1990a; 1990b) confirmed this when coal was mixed with strong caustic solution (KOH or NaOH) and microwaved at a power level of 500 W and at a frequency of

2.45 GHz for 60 seconds. They obtained up to 70% reduction in the total sulphur content of raw coal after magnetic separation, where pyrite was altered pyrrhotite.

Weng and Wang (1992) carried out further investigations regarding inorganic sulphur removal from coal using microwave treatment and diluted hydrochloric acid washing. They found that pyrite was converted to pyrrhotite ($Fe_{1-x}S$) and troilite (FeS) according to the following reaction:

$FeS_2 \rightarrow Fe_{1-x}S \rightarrow FeS$ **Reaction 3-33**

This reaction progressed towards FeS formation with an increase in radiation time. A 97% decrease in inorganic sulphur content was achieved after 100 seconds treatment combined with successive acid washing. These results were supported by Mossbauer spectral analysis. However, Weng et al. (1992) and Weng (1993) suggested that Fe-S bonds of pyrite molecules were broken due to the polarization of the electric field portion of the microwave, which may contradict other researchers' opinion (Chemat and Esveld, 2001; Huang and Rowson, 2000; Huang, 2000). Despite this controversy, Weng and Wang (1993) further investigated ways in which to increase coal desulphurisation efficiency, by incorporating magnetic separation after microwave irradiation and chemical acid leaching.

Ferrando et al. (1996) and Andres et al.(1996) obtained 99% removal of pyritic and 70% removal of organic sulphur by reacting coal with HI in a sealed reactor in H_2 with microwave heating for 10 minutes. Sulphur was removed as H_2S and elemental sulphur. Further solvent extraction was required to remove the free sulphur in the coal. Elsamak et al. (2003) confirmed that concentrated HI leaching of coal reduced the total sulphur to carbon ratio (S_{total}/C) to a lower value than raw coal and concluded that microwave desulphurisation of coal is much faster than thermal treatment, which is probably due to a localised super heating effect.

Laban and Atkin (2000) developed a three-stage method for the direct determination of sulphur forms in coal using microwave acid digestion and Inductively Coupled Plasma Atomic Emission Spectrometry (ICP-AES). 5 M HCl was used to dissolve sulphate sulphur, followed by 2 M HNO_3 to extract pyrite

sulphur and finally concentrated HNO_3, HCl, HF and boric acid were used to leach organic sulphur. Solutions from each stage were analysed using ICP-EAS. The first application of microwave energy for sample preparation in analytical chemistry was reported in (1975) by Abu Samra et al.

3.6.5 Leaching of Nickel, Cobalt and Manganese

Nickel and cobalt have been recovered from laterite ores by smelting operations to obtain ferronickel-cobalt, these are then selectively dissolved with ammonia-ammonium carbonate. Alternatively, nickel and cobalt can be recovered by applying microwave radiation to the mixture of laterite, ferric chloride and sodium chloride. When the mixture was microwaved for 4 to 8 minutes, chlorides were formed which were subsequently leached in water (Kruesi and Frahm, 1982b). Manganese and cobalt can also be recovered in a similar way from deep sea nodules. Gomez (1995) obtained a US patent for a leaching process for nickel, cobalt and manganese ore containing high levels of magnesium. In this case, microwave heating was applied directly to the leaching slurry containing sulphuric and hydrochloric acids. Metal extraction increased considerably compared with conventional leaching at temperatures of between 230 and 250°C.

Kruesi and Kruesi (1986) investigated the leaching of laterite ores in ammonium chloride using microwave energy as a heating source. Laterites containing nickel, cobalt, iron and magnesium oxides were mixed with ammonium chloride and irradiated at a power level of 1200 W for 4-5 minutes under a nitrogen atmosphere. The product was then leached in water at a temperature of 80°C for 30 minutes. It was found that 66% nickel and 78% cobalt were extracted. Microwave pulses (30 seconds) were examined to avoid any possible thermal runaway effect. After irradiation of a similar mixture with a total pulsing time of 5 minutes in an air atmosphere, 70% of nickel and 85% of cobalt were extracted after only 15 minutes water leaching. These results are comparable to conventional treatment after 300°C in a rotary kiln for 2 hours.

3.6.6 Extractions of Lead and Zinc from their Ores and Compounds

Peng and Liu (1992) investigated effect of microwaves on the leaching kinetics of sphalerite (76-98μm) in a solution of 1.0 M FeCl3 and 0.1 M HCl at 95°C. It was observed that the total zinc extracted after one-hour of microwave treatment reached 90%, whereas under conventional leaching conditions the maximum zinc recovery was about 52%. The reaction was found to be first order and the activation energy of the reaction was calculated to be 51 kJ/mole, which suggests that the reaction was chemically controlled. In a similar study (Peng and Liu, 1997), it was found that microwave leaching kinetics of sphalerite in ferric sulphate were much faster than those produced by conventional leaching. The results showed that 92% of zinc was leached within 90 minutes when microwaves were applied compared to 41% total zinc recovery under conventional conditions. It has been suggested, that compared to other sulphide minerals, sphalerite is a poor adsorber of microwave energy (Walkiewicz et al., 1988). After 7 minutes of microwave exposure in a1 kW microwave oven, a 25 g sample of sphalerite reached a maximum temperature of only 88°C. This may indicate an existence of a microwave effect which enhanced the kinetics of the leaching process. In addition it is likely that the heating rate of sphalerite in a microwave field is sensitive to the iron content of the mineral. In Chapters 5 and 6 of this thesis an effort has been made to understand the interaction mechanism between microwaves and leaching systems like sphalerite and ferric sulphate.

Another alternative source of zinc is from zinc silicate ores. However, when such ore is treated by hydrometallurgical processes, minimisation of the dissolution of iron and silica and increased zinc recovery can be a problem. Using a quick leach method the dissolution of silica could be reduced. However, iron dissolution increases which is not preferable. Hua et al. (2002) applied microwave heating to quick leach zinc from silicate ores in diluted sulphuric acid. The zinc extraction increased with a combination of reduction in silica gel formation and iron dissolution. The authors obtained 99% zinc extraction after 15 minutes microwave leaching. The iron and silica in solution were as low as 0.3% and 0.1%, respectively.

Electric arc furnace (EAF) dust contains considerable amounts of lead and zinc and it is considered a hazardous waste. Zinc occurs in EAF dust mainly as zincite (ZnO) and magnetite- franclinite ($ZnFe_2O_4$). Lead occurs as lead oxide (PbO). It was observed that the leaching kinetics of zinc and lead in caustic solutions were significantly improved when microwave energy was used as a heating source (Xia and Pickles, 2000). The leaching efficiency was strongly dependent on the power, caustic concentration and solid liquid ratio. According to the authors this may be due to super heating of liquids, extremely violent behavior and interaction of the microwaves with the EAF dust solids in the solution (temperature of particles higher than would be achieved in conventional heating). Mingos et al. (1991) and Baghurst et al. (1992) reported earlier that any acceleration of reaction rate might be due to super heating. The super heating effect was observed when some organic solvents and water were heated in a microwave cavity (Baghurst and Mingos, 1992). For example, it was found that ethanol heated to 103°C without boiling (boiling point 79°C), methanol 84°C (boiling point 65°C) and water 104°C. This may be due to the absence of a nucleation surface compared with conventional heating or because the liquid heats up so quickly that convection to the top surface and subsequent vaporization are insufficient to dissipate the excess energy (Mingos and Baghurst, 1991). Temperature measurements were conducted using fiber-optic techniques.

3.6.7 Recovery of Plutonium from Waste Nuclear Materials

Sturcken (1992) obtained a US patent for plutonium recovery from crucibles used for processing spent nuclear fuel. The porous crucible material was immersed into a solution contained HBF_4 and HNO_3 in a Teflon pressure vessel. The admixture was heated to 200°C and at a pressure of about 700 kPa by applying microwave energy for at least 30 minutes. Plutonium was then recovered from the acid. The inventor believed that the high recovery was a function of the structure and dielectric constant of the solvent and solute and also due to the direct delivery of the heat the mixture. The oscillating nature of microwaves and the thermal gradient could also have a positive effect on the dissolution kinetics.

3.7 Conclusions

There has been significant amount of work carried out in an attempt to find more economic and environmental friendly ways in which treat chalcopyrite by hydrometallurgical processes. Many media have been tested to improve the leaching kinetics of chalcopyrite and despite much success at laboratory scale; no one method was efficient from an economic and scale up point of view.

It can be also concluded that there is an incomplete understanding of the processes involved, which leaves a gap for researchers to investigate the problems again from different angles. Therefore, it was decided to repeat some of the research work that has been carried out again for two main reasons. Firstly, to establish a consistency and agreement with some of the published data so that more confidence can be built to help in analysis of microwave leaching work. Secondly, it is attempted to explain some of the phenomena that are left in literature without proper clarification in order to develop better understanding.

With regards to the application of microwave energy in mining and metallurgy, it is still in the early stages. The information presented in section 3.6 shows that microwaves have potential application in mineral processing and extraction of metals such as copper, gold, nickel, cobalt, lead, zinc and manganese. Also the use of microwaves for coal desulphurisation seems to be promising. It has been shown that many research studies have been conducted to examine microwave-assisted leaching. However, there are no or limited industrial applications of the technology. This is may be due to a lack of understanding of the influence of microwaves on a particular leaching reaction system. The explanations that are used to justify the acceleration of the reaction rate under microwaves are:

- The existence of a non-thermal effect which reduces the activation energy of the reaction;
- The super heating effect occurring during dielectric heating making the temperature no longer representative of the reaction conditions;

- The large temperature gradient between solids and liquids assisting the mass transport from the reaction interface due to the generation of large thermal currents;
- The increase in surface area due to cracks initiated when solid particles contain more than one phase with different heating rates.

It is believed that the lack of reliable temperature measurement is the main reason behind the misunderstanding regarding the real microwave effect in any reaction system. Control and measurement of temperature in microwave fields is a major challenge because the electric field induced can cause serious errors or damage the thermocouples unless they have been carefully designed. Non-thermal microwave effects are still under debate and not clearly proven.

Non-thermal effects are not important if microwave irradiation is used as a convenient way to deliver heat. However, understanding of the interaction of microwaves with materials and chemical systems is required to optimize the operation involved in order to achieve the best results with minimum energy consumption. This is because microwave energy is expensive in terms of capital cost and energy conversion factors. However, despite the debates that are ongoing, it appears that microwave energy has unique advantages that are waiting for greater exploitation.

CHAPTER FOUR

Chalcopyrite Leaching

4.1 Overview

This chapter will consider leaching of chalcopyrite in acidic ferric ion media under both conventional and microwave conditions. Although the conventional leaching of chalcopyrite in ferric ion media is widely covered in the literature as shown in Chapter 3, there are still some issues which are not completely understood and require further investigation. Therefore, part of this chapter is concerned with the various factors which influence the leaching kinetics (and the mechanism of chalcopyrite leaching) in both ferric sulphate and ferric chloride. This then forms a platform for the understanding of microwave leaching of chalcopyrite.

A detailed account of chalcopyrite material preparation from its sources is presented. In addition, the analytical methods employed are included. This is followed by experimental work which details leaching of chalcopyrite in ferric sulphate under both conventional and microwave conditions. This section also includes a detailed surface analysis study using Scanning Electron Microscopy (SEM) and Time of Flight Secondary Ion Mass Spectrometry (ToF-SIMS). Furthermore, a study of chalcopyrite leaching in ferric chloride under both microwave and conventional leaching conditions is considered. Particular attention has been given to the effect of agitation on the leaching kinetics of chalcopyrite in this system.

4.2 General Materials and Methods

4.2.1 Materials

Three chalcopyrite samples are considered in this chapter. These are: a pure natural chalcopyrite crystal, a chalcopyrite concentrate and a synthetic chalcopyrite. The natural chalcopyrite crystal was obtained from a mineral dealer Gregory, Bottley & Lloyd (GBL)/UK. The samples prepared from this chalcopyrite will be designated as GBL chalcopyrite throughout this thesis. Apart from chalcopyrite, this sample contained small sphalerite crystals (0.5-5mm) and quartz. The origin of GBL chalcopyrite is believed to be Bulgaria. The chalcopyrite concentrate was prepared from a copper sulphide ore. The ore was obtained from North America/Kennecott Utah Copper Corporation (KUCC) and designated as MZ2HE. This designation will be used throughout this thesis. It contained about 2.9% chalcopyrite and 0.6% pyrite in a matrix of quartz, feldspar and Fe-rich mica. Finally, the synthetic chalcopyrite was prepared from pure copper, iron and sulphur compounds.

4.2.1.1 Preparation of GBL Chalcopyrite

GBL chalcopyrite was prepared from the supplied crystals by careful hand grinding using an agate pestle and mortar. Sphalerite and quartz contained in the sample were removed with the aid of a hand magnifier at several stages during hand grinding. The careful hand cleaning was continued until the size of particles reached 100% passing 1mm where it was very difficult to find any sphalerite inclusions. Chalcopyrite was then ground down to 100% passing 106 μm using agate pestle and mortar. The sample was subsequently divided into the following size fractions using wet sieving: -106+75, -75+53, -53+38 and -38 μm. After being washed with acetone, the fractions were collected on a filter paper using a vacuum filter. Each fraction was then dried in a vacuum dryer at 30°C before being manually well mixed and divided into small batches of about 5 grams, and stored in a vacuum desiccator.

4.2.1.2 Preparation of Chalcopyrite Concentrate from MZ2HE Ore

The as received sample of MZ2HE ore was 100 % passing 50 mm. The mineralogy data provided by the supplier of the sample is presented in Appendix 4-1. Figure 4-1 shows the flow diagram presented in the processing procedure to prepare the chalcopyrite concentrate from the as received ore. About 25 kg of the ore was crushed first using a clean laboratory Jaw Crusher down to 100% passing 1 mm by passing the ore through the crusher and sieving in closed circuit. The product (< 1 mm) was then sieved on vibrating Russell screens using 180 μm sieve cloth. The oversize was wet ground using a laboratory ball mill. The product was then subjected to froth flotation to separate chalcopyrite from the gangue minerals. The detailed procedure for flotation is presented in Appendix 4-2. Pressure filtration was then performed to separate the solid from liquid. The solids were then dried in a vacuum oven at a temperature of 30°C. The initial concentrate was then subjected to re flotation to minimize entrained gangue. The refloated product was again filtered and vacuum dried, stored in air tight glass jars for further processing.

4.2.1.3 Preparation of Synthetic Chalcopyrite.

Synthetic (pure) chalcopyrite was prepared by the School of Chemistry at the University of Nottingham. It was prepared according to the procedure described by Adams et al (1972) using pure compounds of Cu, Fe and S. The heat source used was a domestic microwave oven.

4.2.2 Physical Characterization of Chalcopyrite

4.2.2.1 XRD Analysis

X-Ray Diffraction (XRD) analysis is a semi-quantitative technique for identification of minerals and compounds crytallographically. Details about the theory and the principles of XRD are available in many text books such as Cullity and Stock (2001).

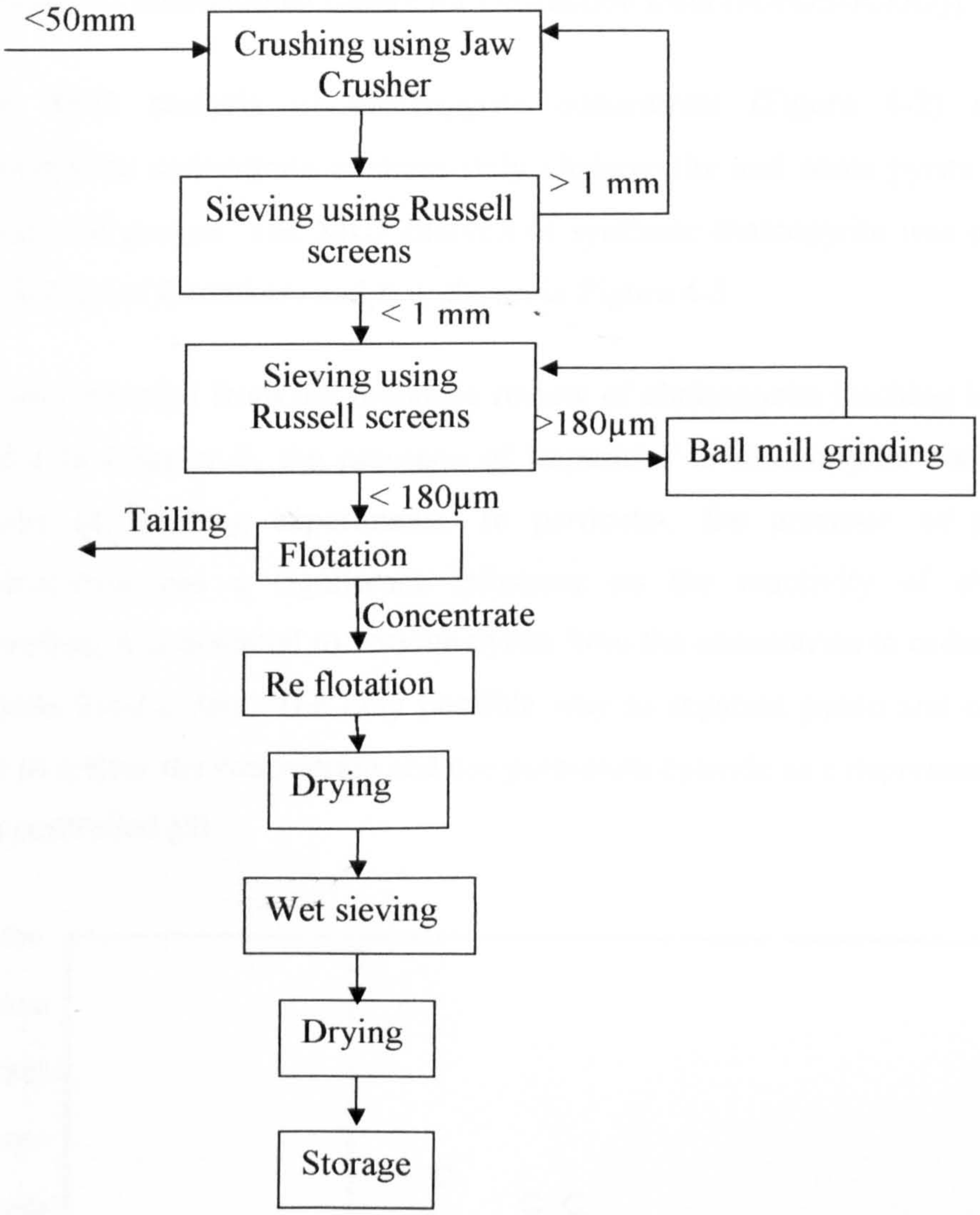

Figure 4-1 Procedure for preparing chalcopyrite concentrate from MZ2HE ore

Representative samples, taken after prolonged manual mixing, obtained from chalcopyrite sources GBL and MZ2HE were taken prior to final sizing. The representative samples were ground further to suit XRD sample requirements. A computer controlled Hiltonbrooks® generator with a Philips® PW 1050 diffractometer with an automatic divergence slit, and Cu anode producing X-rays of wavelength λ= 1.54056 A° was used. The diffractometer was operating at 40 kV and 20 mA, and automatic routines allowed scanning for values 2θ from 5° to 95° using a step size of 0.05° and scan speed of 2°/min. The diffraction data was analysed by Diffraction Technology "Traces V.3®" X-ray analytical software. Identification of the minerals contained in the sample was achieved by comparing

the X-ray spectrum with a database (Joint Committee on Powder Diffraction Standards - International Centre for Diffraction Data (JCPDS-ICDD)).

The XRD analysis of chalcopyrite concentrate (Figure 4-2) shows that chalcopyrite concentrate contains only chalcopyrite and some pyrite with small amount of gangue. The XRD analysis of synthetic chalcopyrite was provided by the School of Chemistry and it is shown in Figure 4-3.

As was revealed from the literature review of chalcopyrite leaching in ferric ion media in Chapter 3, the presence of impurities in chalcopyrite could bias the results of leaching experiments. In particular, the presence of pyrite with chalcopyrite has a significant influence on the reactivity of chalcopyrite. Therefore, it is essential to remove pyrite from the concentrate in order to achieve reliable kinetic data. The only possible way to separate pyrite and chalcopyrite was to refloat the concentrate and use potassium cyanide as a depressant for pyrite at a controlled pH.

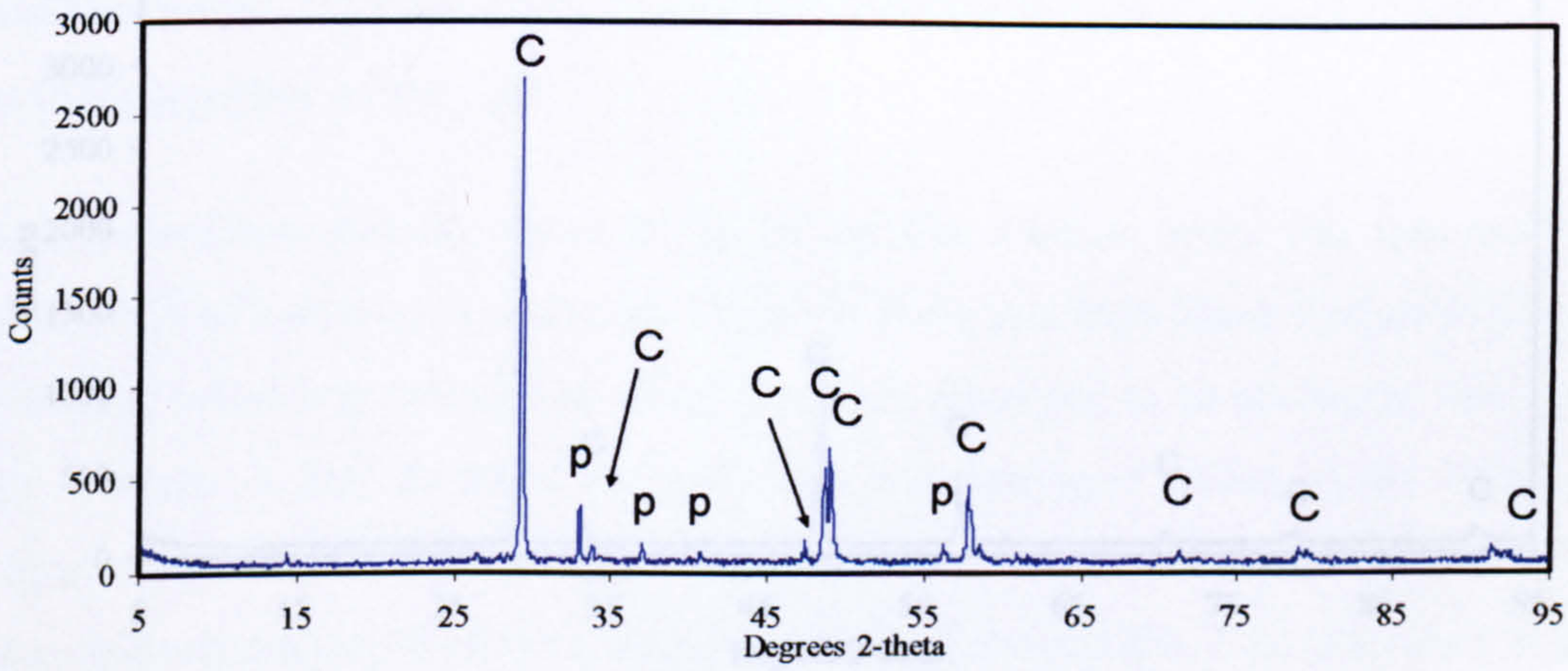

Figure 4-2 XRD pattern of MZ2HE chalcopyrite concentrate after double flotation (C-chalcopyrite, P-pyrite)

Due to the hazard associated with use of cyanide and the cost of disposal of the water used during flotation experiments it was decided to use GBL chalcopyrite for all leaching experiments unless otherwise stated. It has no pyrite or any other copper sulphide minerals as shown in the XRD analysis (see Figure 4-4) and chemical analysis thereafter (Section 4.2.3.4).

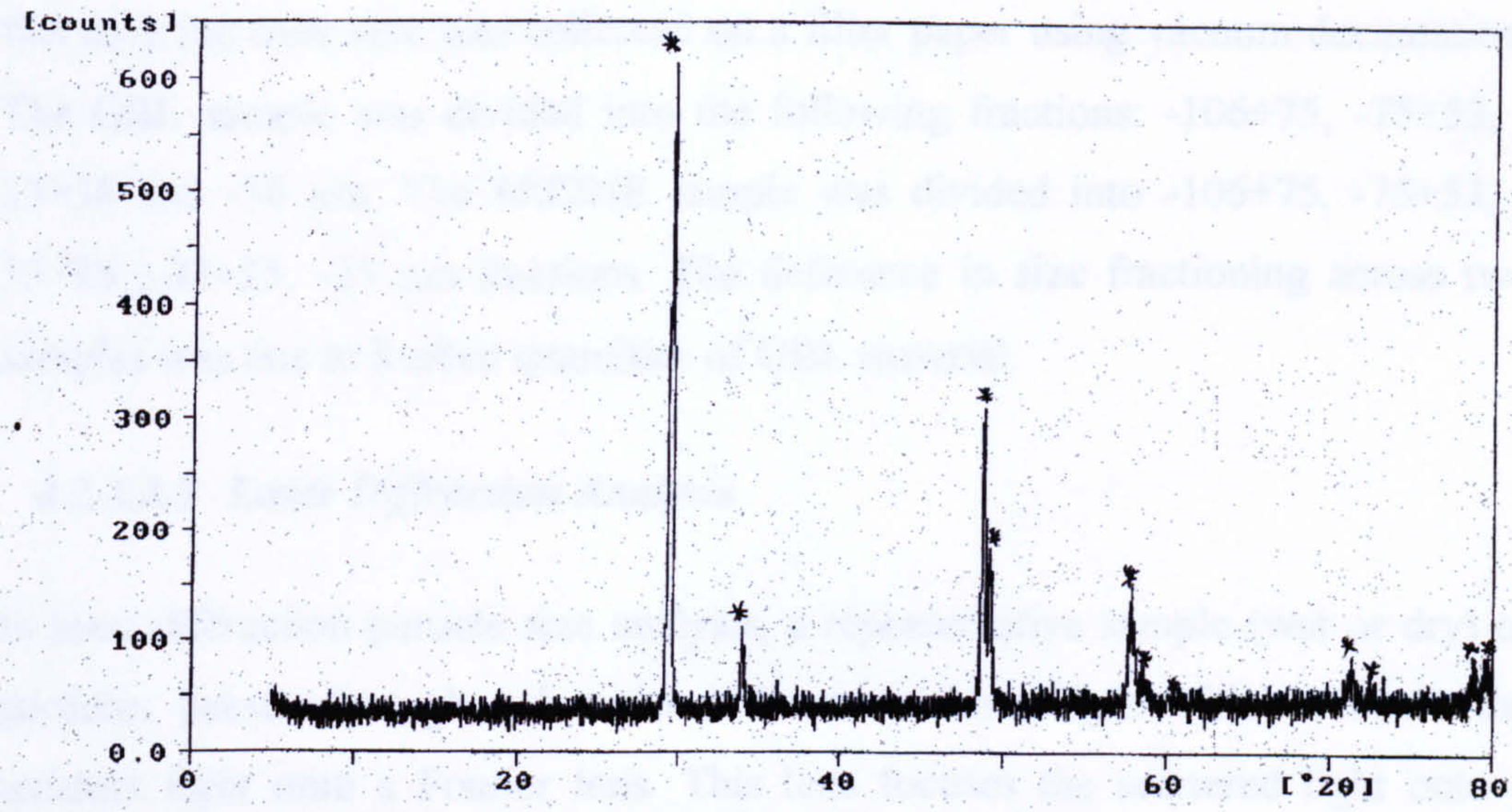

Figure 4-3 XRD pattern of pure synthetic chalcopyrite made by microwave firing of stoichiometric amounts of pure Cu, Fe and S (*- denotes chalcopyrite peaks)

The XRD pattern of GBL chalcopyrite appeared free of any impurities and can be compared to the XRD pattern of synthetic chalcopyrite shown in Figure 4-3. The chemical analysis of GBL chalcopyrite confirmed its purity (Section 4.2.3.4).

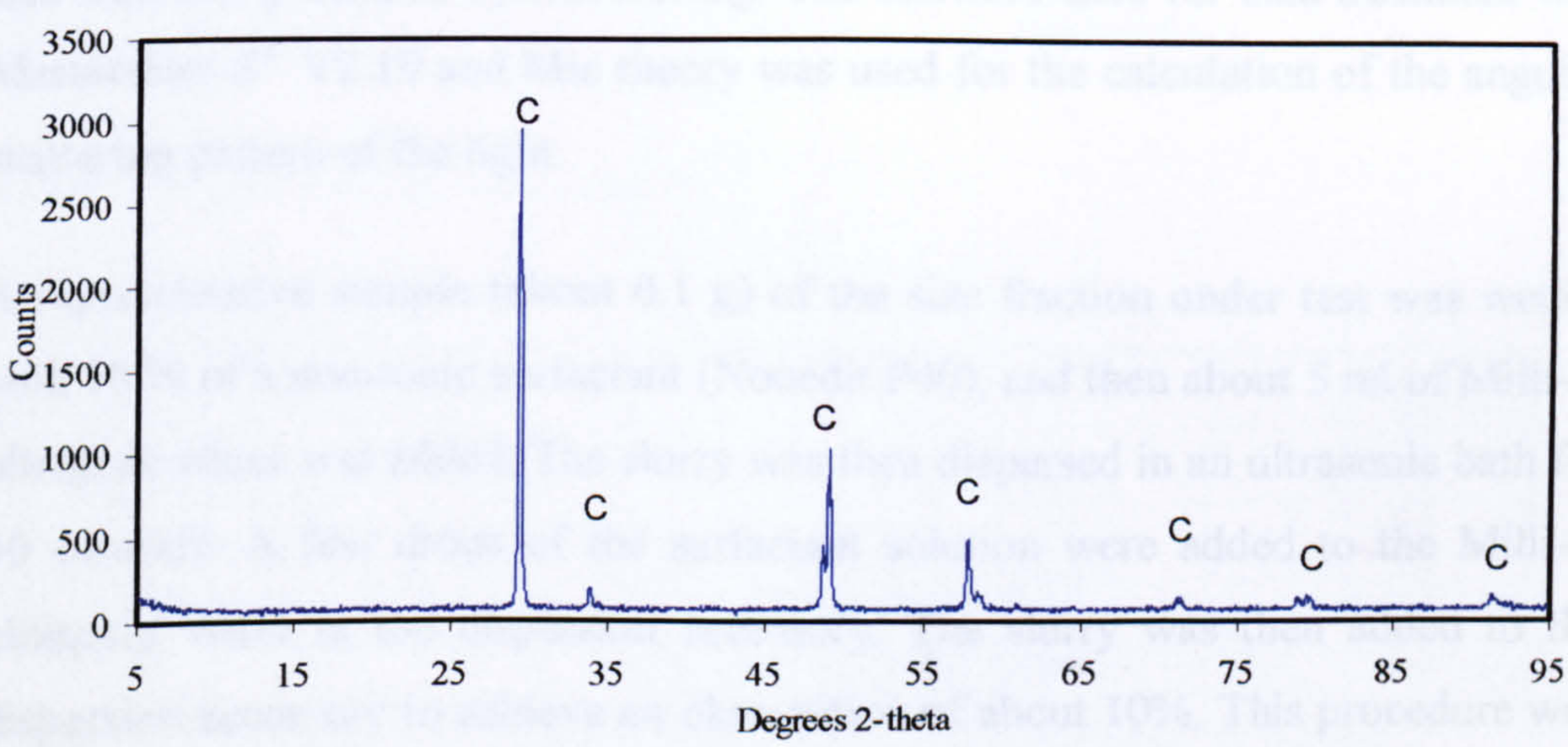

Figure 4-4 XRD pattern of GBL chalcopyrite obtained from Gregory, Bottley & Lloyd. (C-denotes chalcopyrite peak)

4.2.2.2 Particle Size Analysis

4.2.2.2.1 Sieve Analysis

Chalcopyrite samples (GBL and MZ2HE concentrate) were divided into individual size fractions by wet sieving. The wet sieving procedure was carried out according to British Standard BS 1796-1 except for the drying stage where in

this case the over size was collected on a filter paper using vacuum decantation. The GBL sample was divided into the following fractions: -106+75, -75+53, -53+38 and -38 μm. The MZ2HE sample was divided into -106+75, -75+53, -53+38 ,-38+25, -25 μm fractions. The deference in size fractioning across two samples was due to limited quantities of GBL material.

4.2.2.2.2 Laser Diffraction Analysis

In laser diffraction particle size analysis, a representative sample (wet or dry) of particles passes through a broadened beam of laser light which scatters the incident light onto a Fourier lens. This lens focuses the scattered light onto a detector array and, using an inversion algorithm, a particle size distribution is inferred from the collected diffracted light data. The diffraction angle is inversely proportional to the particle size (Allen, 1997).

A Malvern Mastersizer® was used to characterize the distribution of the individual size fractions produced by wet sieving. The software used for data treatment was Mastersizer-S® V2.19 and Mie theory was used for the calculation of the angular scattering pattern of the light.

A representative sample (about 0.1 g) of the size fraction under test was wetted with 10 % of a non-ionic surfactant (Nonedit P40), and then about 5 ml of Milli-Q ultrapure water was added. The slurry was then dispersed in an ultrasonic bath for 30 seconds. A few drops of the surfactant solution were added to the Milli-Q ultrapure water in the dispersion accessory. The slurry was then added to the dispersion accessory to achieve an obscuration of about 10%. This procedure was employed to prevent agglomeration during the analysis. Three samples were analysed from each size fraction. The size distribution of the GBL and MZ2HE fractions are given in Figure 4-5 and Figure 4-6.

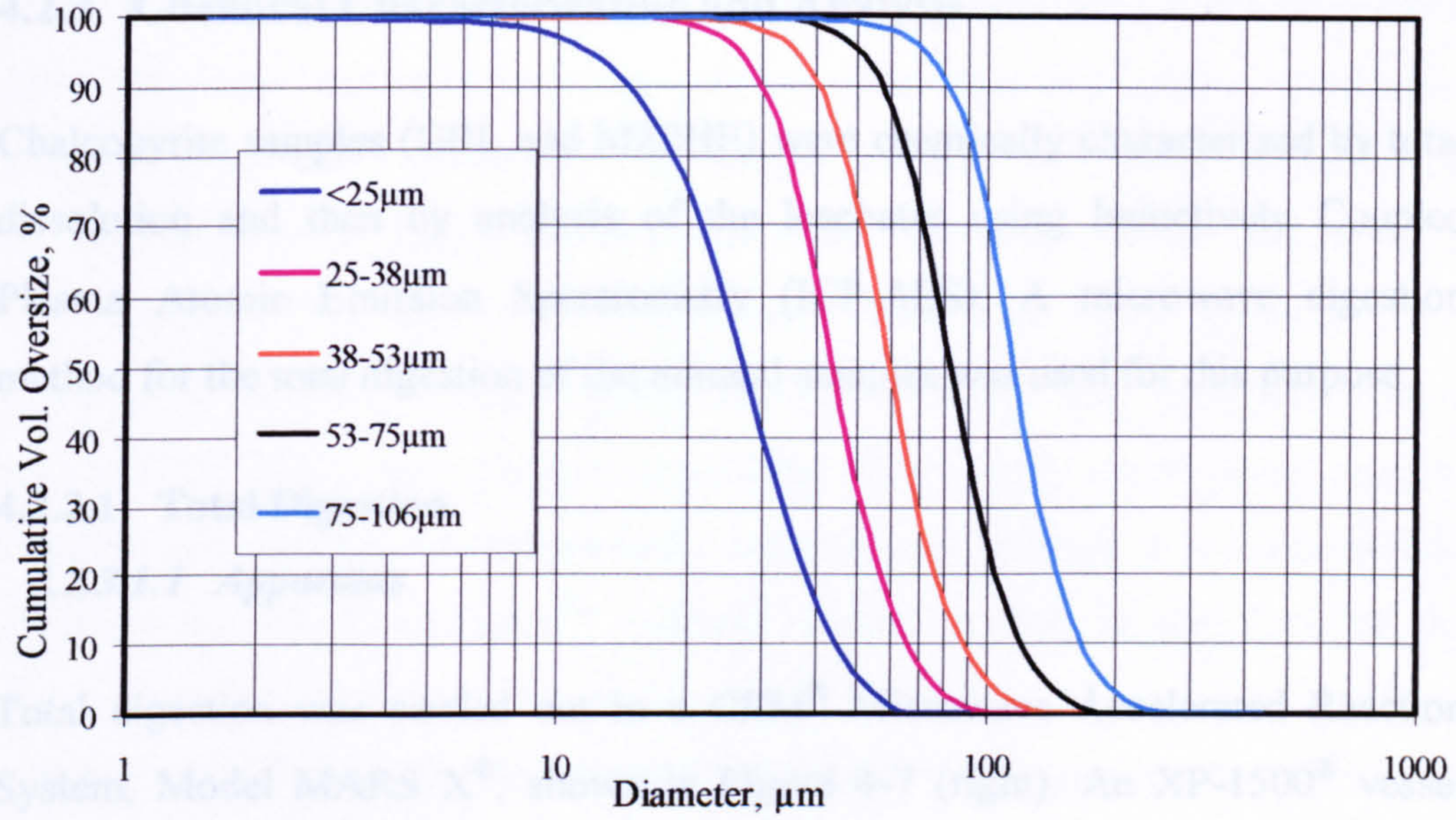

Figure 4-5 Cumulative volume oversize and frequency of the MZ2HE concentrate size fractions analysed by Malvern® laser diffraction

The diameter D(3,2) was used to characterize the surface area diameter and it is calculated as (Rauwle, 2000):

$$D(3,2) = \frac{\sum d^3}{\sum d^2}$$ **Equation 4-1**

where d is particle diameter (µm).

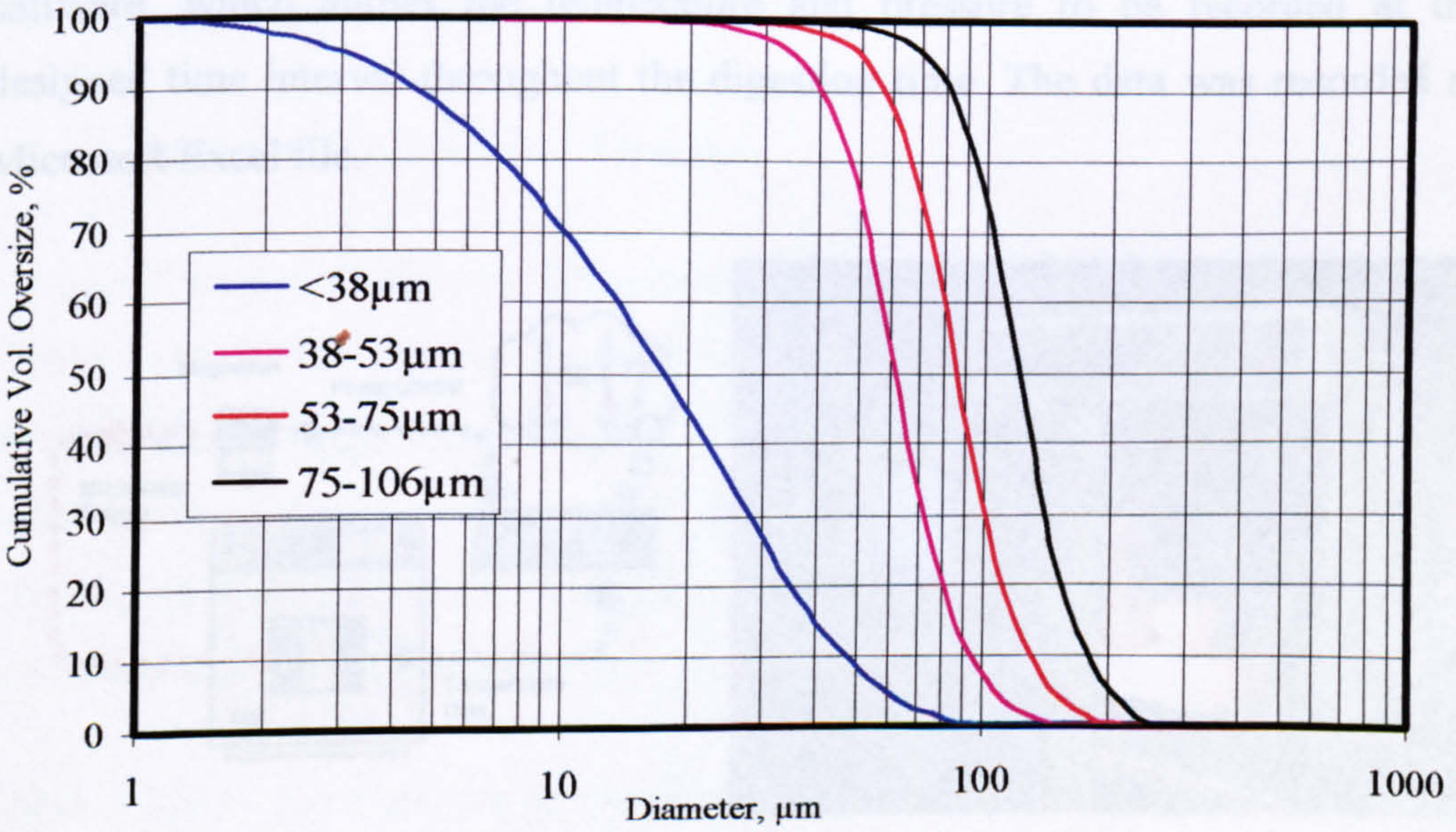

Figure 4-6 Cumulative volume oversize and frequency of the GBL size fractions analysed by Malvern® laser diffraction

4.2.3 Chemical Characterization and Analysis

Chalcopyrite samples (GBL and MZ2HE) were chemically characterized by total dissolution and then by analysis of the leachates using Inductively Coupled Plasma Atomic Emission Spectrometry (ICP-AES). A microwave digestion method for the total digestion of the mineral samples was used for this purpose.

4.2.3.1 Total Digestion

4.2.3.1.1 Apparatus

Total digestion was carried out in a CEM® Microwave Accelerated Reaction System, Model MARS X®, shown in Figure 4-7 (right). An XP-1500® vessel made of a transparent and chemical resistant material (Teflon PFA®) was used as the digestion vessel. This vessel can operate up to a maximum pressure of about 55 bar and a temperature of about 240°C. The system was capable of holding up to 12×80ml of these digestion vessels on a turn table at any one time. Each vessel consisted of a base, cap and relief valve. The caps were tightened with a torque wrench to insure the same torque was applied to each vessel, which then controls the relief pressure. Three levels of magnetic stirring are available if required. The MARS X® can be operated through a personal computer (PC) using MarsLink® software, which allows the temperature and pressure to be recorded at the designed time interval throughout the digestion time. The data was recorded as Microsoft Excel file.

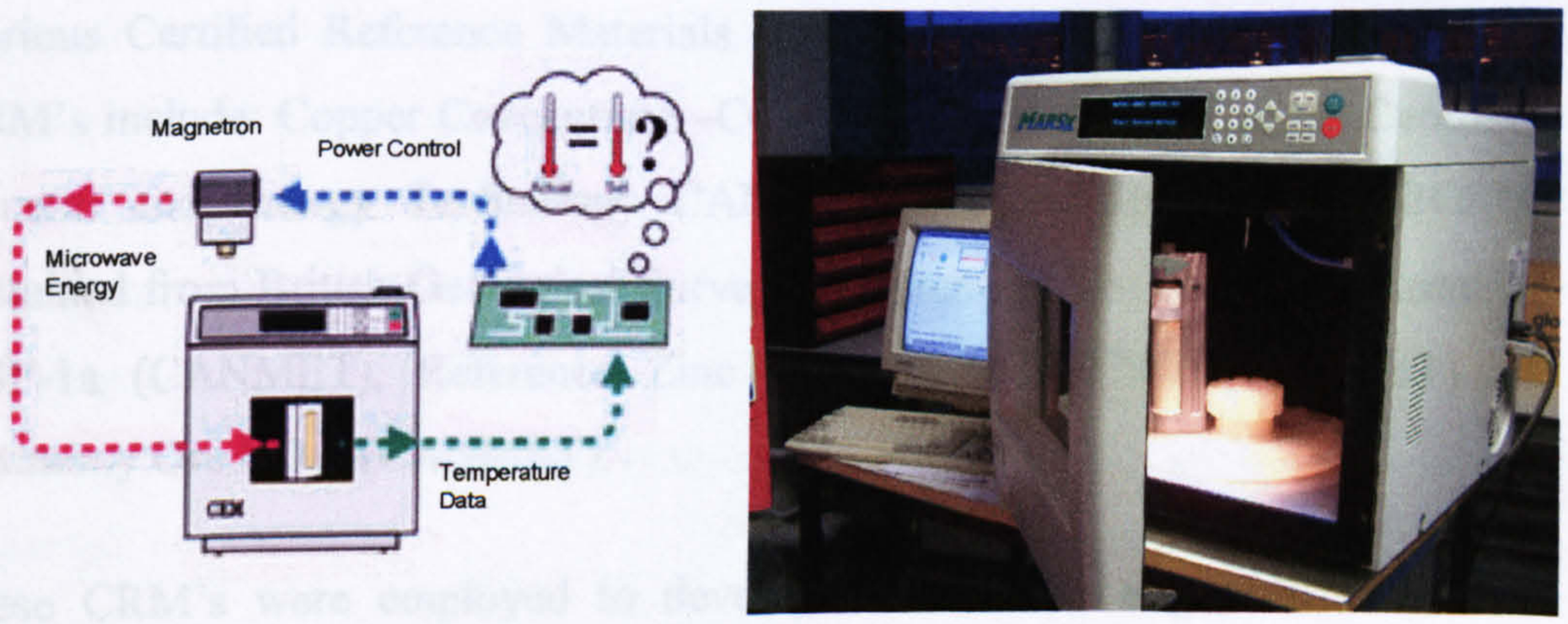

Figure 4-7 Microwave Accelerated Reaction System (MARS X®) (right) and the schematics of the temperature control (left) ((CEM)

This MARS® system is designed mainly for laboratory use for the purpose of extracting, digesting, hydrolyzing or a drying wide range of materials. Its primary purpose is the rapid preparation of various samples for variety of analytical procedures. MARS® system delivers 3 levels of l microwave power; 300, 600 and 1200 watts at a frequency of 2450 MHz. Each power level can be varied from 1% to 100% of its value. MARS® system is supplied was a fiber optic temperature sensor (EST-1500) and pressure transducer (EPS-1500) which were used to monitor and control the temperature and pressure through a microcomputer. Additionally, the TempGuard™ infrared sensor located in the floor of the microwave cavity monitors the temperature in each of the 12 vessels as they pass across it every 7 seconds. The temperature control loop is shown schematically on Figure 4-7 (left). The temperature and pressure sensors are attached to one of the vessels (control vessel).

4.2.3.1.2 Reagents and Materials

All the acids used were reagent grades with the following concentrations: nitric acid, HNO_3-69.5% (AnalaR®), hydrochloric acid, HCl-33% (AnalarR®), hydrofluoric acid, HF- 40% (AristaR®), boric acid, H_3BO_3-99.99% (AristaR®). Milli-Q ultrapure water (18.2 $M\Omega cm^{-1}$) was used for making up the solutions and for washing volumetric flasks.

4.2.3.1.3 Certified Reference Materials

Various Certified Reference Materials (CRM's) were employed in this study. CRM's include: Copper Concentrate –CCU-1c (obtained from Canada Centre for Mineral and Energy Technology CANMET), Copper Concentrate -BGS100 (obtained from British Geological Survey), Reference Zinc-Tin-Copper-Lead ore –MP-1a (CANMET), Reference Zinc Concentrate -CZN-1 (CANMET) and Antimony Ore CD-1 (CANMET).

These CRM's were employed to develop and validate a general microwave digestion protocol for sulphide ores and concentrates. In addition CCU-1c CRM

was used to assess the accuracy of the total digestion of GBL and MZ2HE chalcopyrite.

4.2.3.1.4 Method Development

A total digestion method was developed to facilitate the digestion of ores of widely ranging composition (copper ore, zinc ores and other ores and concentrates) used in this research. Therefore, an ore containing chalcopyrite, pyrite, pyrrhotite, sphalerite, quartz, calcite and minor content of other minerals was chosen for method development. A description of the sample preparation procedure and XRD analysis of this ore are shown in Appendix 4-3.

During method development only the controlled vessel was used for digestion with a maximum power level of 300W. Method development involved using concentrated nitric, hydrochloric and hydrofluoric acids in various proportions to obtain the optimum acid composition, which dissolved all the minerals associated with the ore. The mass of the ore used for digestion was 0.2 grams weighed using a four decimal place electronic balance with an error of ±0.0001g.

Firstly, 20 ml of concentrated HNO_3 was added to 0.2 g of the ore sample in the control vessel. The vessel was then microwaved according to the following program: ramp the temperature to 200°C in 15 minutes (heating rate is about 13.3°C/minute) using up to 300 W microwave power. The temperature was maintained at 200°C for a further 30 minutes. The maximum pressure achieved inside the vessel was about 27 bar. The temperature profile during heating and cooling is shown on Figure 4-8. On completion, the microwave was then switched off and the solution was left to cool until the temperature decreased to room temperature. The vessel contents were then quantitatively transferred to a 100 ml polypropylene volumetric flask using 10% nitric acid solution. Nitric acid alone did not dissolve all minerals associated in the sample and a white residue remained

Therefore, in the second attempt 5 ml of hydrofluoric acid (HF) was used in addition to 20 ml nitric acid. The same heating and cooling conditions were used.

There was still some residue remaining with a blue to black color. Thirdly, the volume of HF was increased to 10 ml but again complete dissolution was not achieved. A mixture of 10 ml HNO_3 +10 ml HF + 5 ml HCl was then used. This resulted in total dissolution with no visible residue. The quantity of HF was then reduced to 5 which still gave total digestion.

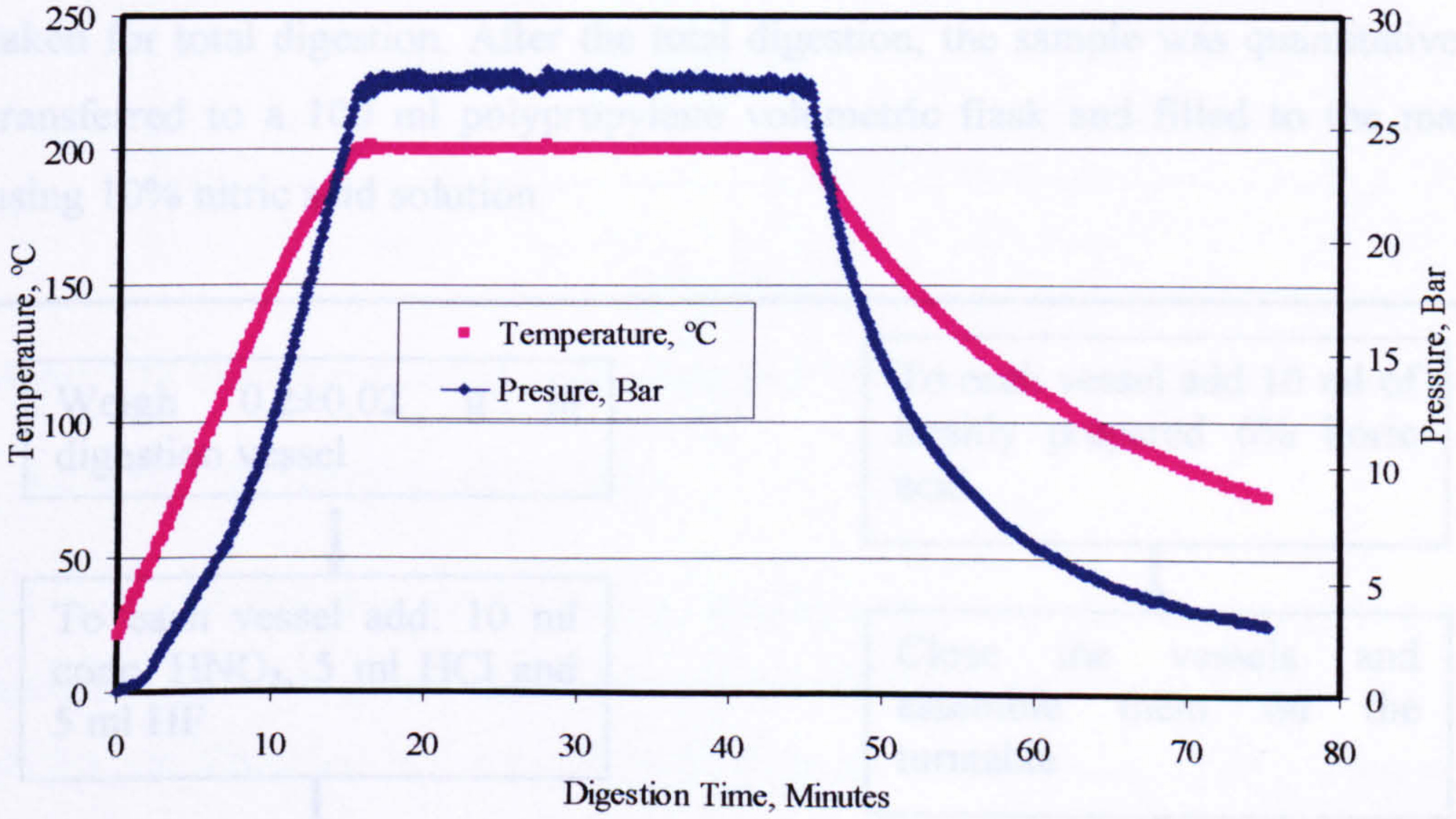

Figure 4-8 Heating and cooling profile of the first stage of the microwave total digestion method

In the final stage of the method development, CRM CCU-1c (Appendix 4-4) obtained from CANMET was digested. The same heating and cooling conditions were used to dissolve 0.2 g of CCU-1C. About 10 ml of a freshly made 6% orthoboric acid was added to the solution in the leach vessel. The new mixture was heated again to 170°C within 7 minutes (heating rate was about 24.3 °C/minute) and kept for a further 10 minutes at this temperature. The temperature profile of the heating and cooling is shown in Figure 4-10. The addition of boric acid had a dual purpose. The acid was required to dissolve any fluoride precipitations of second group elements such as CaF_2 that would have precipitated during the first stage of the digestion. It was also required to complex any free fluoride ions making the final leachate less hazardous to handle (Laban and Atkin, 1999).

4.2.3.1.5 Procedure

The procedure developed and used to digest samples is summarized in Figure 4-9. This procedure can be used to digest 12 samples at a power level of 1200 W.

Three samples from each size fraction of GBL chalcopyrite (-106 +75, -75+53, -53+38, -38μm) and MZ2HE (-106+75, -75+53, -53+38, -38+25, -25μm) were taken for total digestion. After the total digestion, the sample was quantitatively transferred to a 100 ml polypropylene volumetric flask and filled to the mark using 10% nitric acid solution.

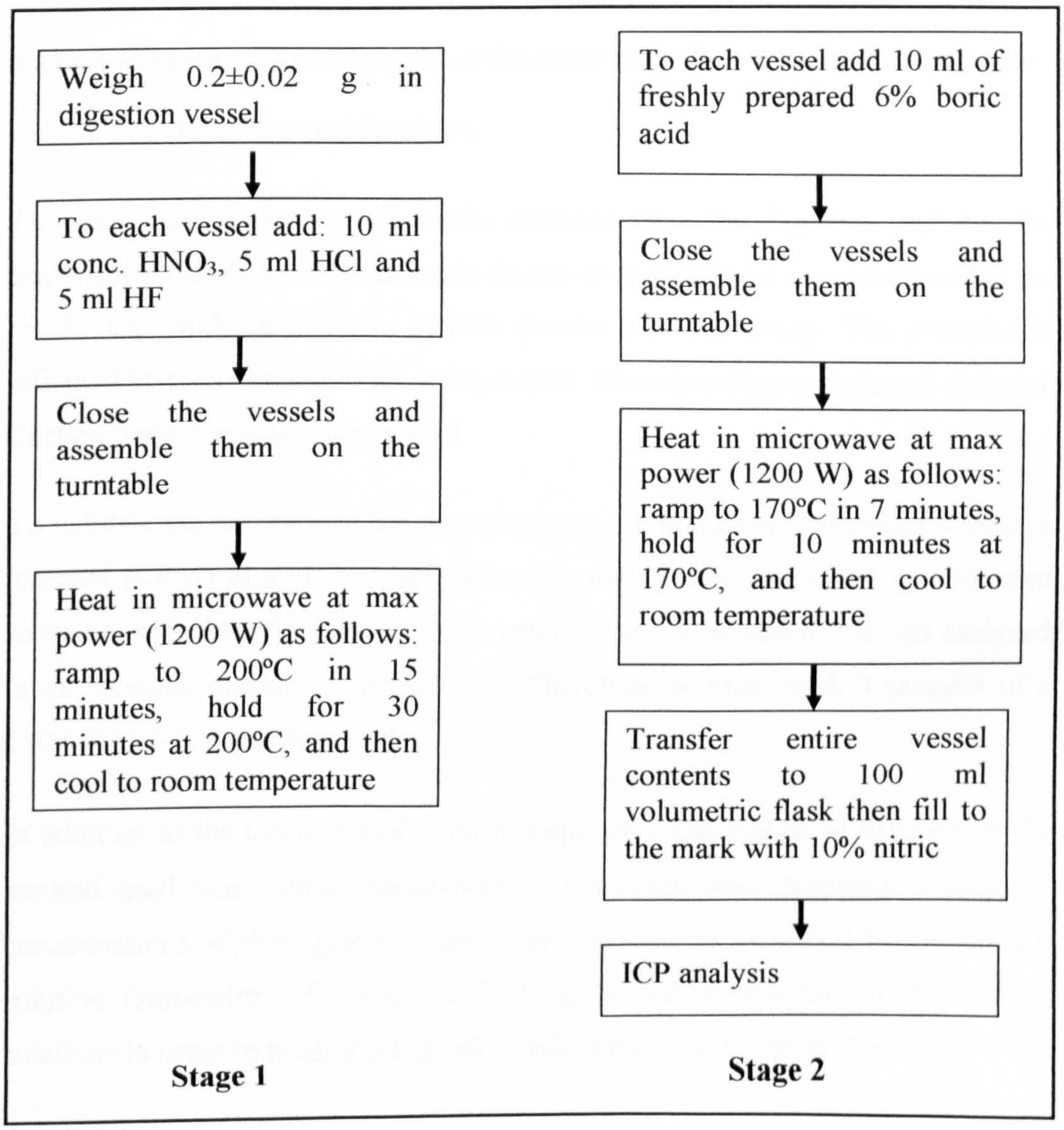

Figure 4-9 Total element digestion procedure

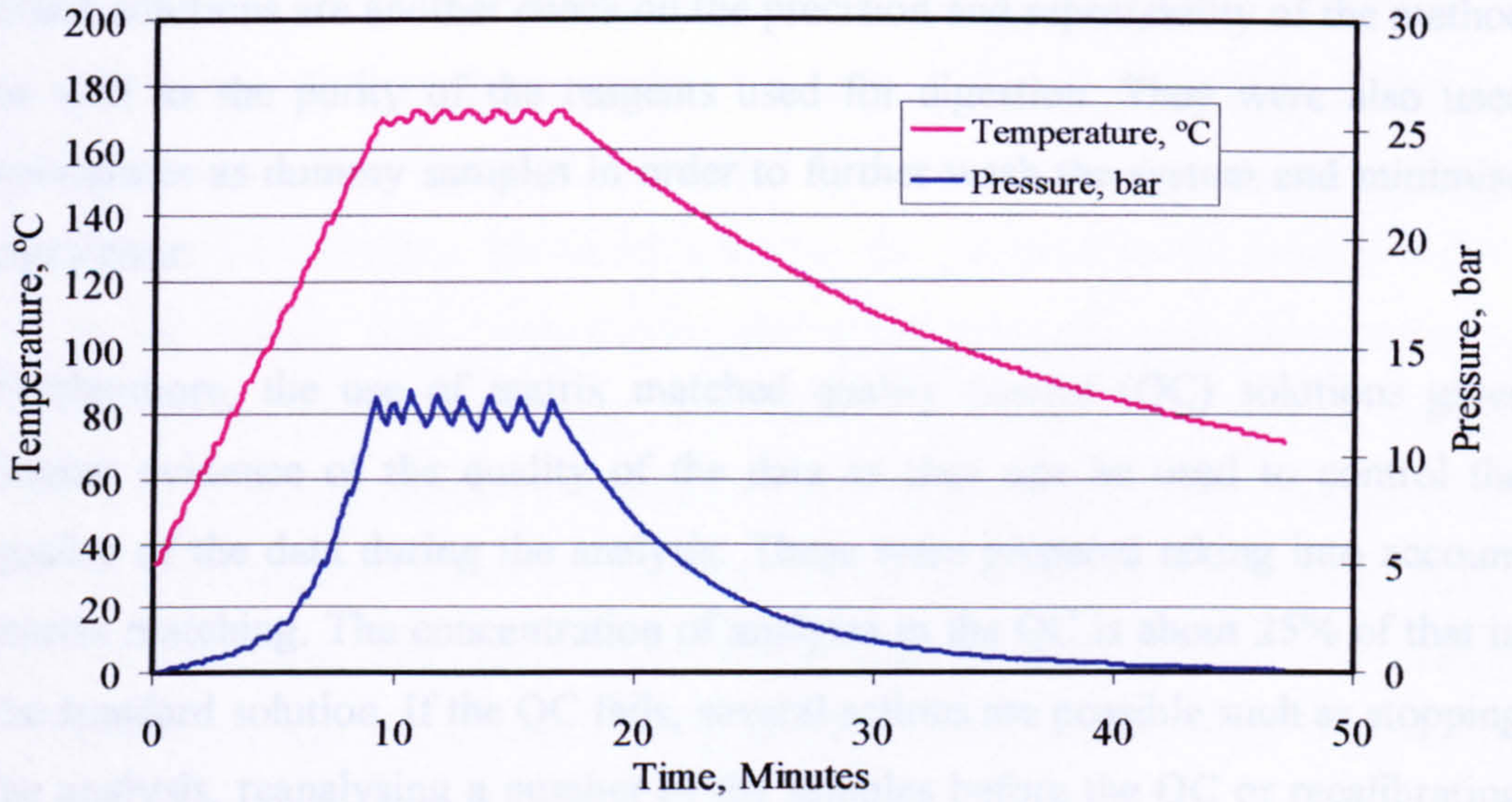

Figure 4-10 Heating and cooling profile of the second stage of the microwave total digestion

4.2.3.1.6 Accuracy and Precision

To ensure the quality of the results obtained from the digestion and that the analytical methods give a reasonable degree of confidence it is imperative that the results are validated in terms of their precision and accuracy. The precision is reflected by the reproducibility of the results. Therefore three samples of each size fraction were digested and analysed

To validate the accuracy of the digestion method, digestion of certified reference material (CRM) of known composition was undertaken. The CRM was selected so that it resembles the samples to be analysed and to ensure that it was analysed in an identical manner to the samples. Therefore, in each batch 3 samples of a CRM (CCU-1c) were included.

In addition to the use of CRM's, other steps were undertaken to ensure that the method used was robust. Multi-element standards were prepared at element concentrations slightly greater than those expected to be found in the sample solution (Appendix 4-5). The standards were matrix matched to the sample solutions in order to minimize the risk of affecting the calibration method.

The blank contained the same reagents used during the total digestion stages to ensure the blanks were matrix matched to the standard and sample solution. The

blank solutions are another check on the precision and repeatability of the method as well as the purity of the reagents used for digestion. They were also used sometimes as dummy samples in order to further wash the system and minimise carry over.

Furthermore, the use of matrix matched quality control (QC) solutions gives further evidence of the quality of the data as they can be used to control the quality of the data during the analysis. These were prepared taking into account matrix matching. The concentration of analytes in the QC is about 25% of that in the standard solution. If the QC fails, several actions are possible such as stopping the analysis, reanalysing a number of the samples before the QC or recalibrating and reanalysing again.

The duplicate analysis of the samples was then subjected to statistical analysis to assess the precision. The standard deviation and the percent relative standard deviation (%RSD) are used here as an estimate of the precision of the data. The relative standard deviation is the same as the coefficient of variation (%CV) and they can be expresses mathematically as:

$$\%RSD = \%CV = \frac{S}{\bar{x}}100\% \qquad \textbf{Equation 4-2}$$

where S is the standard deviation and $\bar{x}$ is the mean

4.2.3.2 ICP Analysis

Once the samples were totally digested they can be quantitatively analysed using ICP-AES. The basis of the technique is that when an atom is exited, and then returned to its ground state it emits a characteristic radiation of an intensity which is proportional to the number of emitted atoms and hence concentration. In inductively coupled plasma the sample is atomised in a plasma formed in argon. The sample is introduced as an aerosol and temperatures of up to 10000°C can be generated ensuring complete atomisation of the sample without any interference effect of chemical reaction (Abkar, 1998). The technique is capable of analyzing a wide range of elements since each element has an exclusive set of wavelengths at

which radiation is emitted as the atoms return to their ground state. Quantification is achieved by comparing the radiation intensity of the sample with the calibration curve formed with a standard containing a known concentration of the element and blank. The standard and blank solutions are prepared in the same matrix in which the sample was digested. The instrument analyses each element in the solution simultaneously through the use of polychromator, which enables detection of energy emitted at a characteristic wavelength for each analyte. ICP-AES is advantageous in that the technique offers a number of wavelength choices for every element. The characteristic wavelength for each element was selected taking into account signal intensity and possible spectral interference. Interference by emission peaks from other species in the sample with lines close to the one of interest can be avoided by the judicious selection of background correction points either side of the peak. Should the interfering peak be very close to the wavelength of interest, another wavelength that is free of interference will have to be chosen. Wavelengths used for the quantitative analysis for total digestion are presented in Appendix 4-5.

The ICP-AES instrument used was a Perkin Elmer Optima® 3300 DV which was equipped with an AutoSampler (AS-90 Plus®) capable of holding up to 106 samples. This enabled large number of samples to be analysed automatically. The analytical run was controlled with software (Perkin Elmer ICP winLab®) which enables parameters such as the number of repeats, wash time and quality control limits to be defined for the run. The concentration of each element in the sample solution was measured three times and the mean result is quoted throughout this thesis. The instrument was programmed to recalibrate after every 10 samples. A quality control standard was introduced between each two calibrations. At the end of the analytical run, the calibration and quality control data were examined for robustness. The intensity of each element, the standard deviation of the three replicates and the elements concentrations in the quality control samples were scrutinized for consistency.

The detection limit of an element in solution is defined as the lowest concentration level of the analyte that can be determined to be statistically different from the

analytical blank (Miller and Miller, 1993). A separate analytical run was performed to experimentally evaluate the detection limit where the blank was analysed as a sample. This was generally carried out at the end of each analytical run when the instrument was behaving in a similar manner to that of the analysis period. The detection limit was calculated as three times the standard deviation measured when 10 analyses of the element in blank are taken. The detection limit (D_L) of the mineral sample was then calculated as shown in Equation 4-1.

$$D_L(ppm)\,in\,the\,sample = D_L(ppm)\,in\,solution \times \frac{total\,sample\,volume(ml)}{digested\,mass(g)} \quad \textbf{Equation 4-3}$$

The detection limits, in the solution and sample, of the elements under test are listed in Appendix4-5.

The operating conditions of the ICP used in this work are presented in Table 4-1.

Table 4-1 The operating conditions of the ICP

RF power	1300 W
Plasma Argon	15 l/min
Auxiliary Argon	0.5 l/min
Nebulizer Argon	0.8 l/min
Sample flow rate	1 ml/min
Wash time	40 seconds
Read delay	110 seconds

4.2.3.3 Method Validation

In an attempt to validate the total digestion method developed in section 4.2.3.1, six CRM's were microwave digested according to the procedure shown in Figure 4-9. The CRM's were obtained from CANMET (CCU-1c, CD-1, CZN-1, CPB-1 and MP-1a) and the British Geological Survey (BGS100). To ensure that analyst bias was minimised and to examine the robustness of the digestion method 12 digestion batches were created (each batch contained 12 samples). The first 6 batches were created so that two CRM's (6 samples×2 CRM's) were digested in one batch. Two batches were arranged as: 3 samples×4 CRM's. Three batches were randomised using Microsoft Excel so that at least one sample was included in any of these batches. Finally, one batch was included as a blank which had the same solution content used for digestion but without any solid sample. At least 18 samples from CRM were totally digested.

Due to the wide range of concentrations of each element, every sample was analysed twice in separate analytical runs along with two groups of quality control and standard solutions. The two analytical runs were designed to measure the minor and major elements separately. One standard solution contained high concentrations of the following elements: Al, Cu, Fe, Pb, S, and Zn. The second standard solution contained low concentrations of the elements under investigation (Al, As, Ca, Cd, Cr, Co, Cu, Fe, Mg, Mn, Mo, Ni, Pb, S, Sb, Zn). Additionally two quality control (QC) solutions and one blank were prepared. The chemical composition of the standard solutions, QCs and blank are listed in Appendix 4-5.

It was noticed that the samples prepared from CRM MP-1a yielded lower recoveries than the samples prepared from other CRM's. MP-1a contained a high content of silicon. This caused slight drift in the recovery of elements due to so called matrix effect where the background was shifted. Therefore, new standards containing high concentration of silicon to match the matrix were prepared. The samples from MP-1a were reanalysed using this new standard (Appendix 4-6).

To evaluate the cross contamination between samples during digestion, caused by improper cleaning of the vessels and any possible impurities in the reagents used through out the method, a blank run was performed according to the sequence presented in Figure 4-9 but without 0.2 g of sample. For example, it was found that the maximum carry over of copper among 12 samples could reach 76 ppm with an average of less than 14 ppm which is less than the detection limit. That is to say, if a sample contains 0 ppm of copper, the maximum carry over would be 76 ppm of that element. This suggests that the carry over would affect the elements with low concentration in the sample. Therefore, extra care is required when digesting a variety of samples of different levels of concentrations and composition. Table 4-2 shows the analytical summary of 12 blank samples which were analysed by the ICP method for elements with high concentrations. Some of the average values are below the detection limit (BDL). Similar results were obtained when the analysis was performed for low concentration elements and is

presented in Appendix 4-7. Generally the measured concentration is below the detection limit.

Table 4-2 Summary of the chemical analysis of the digested blank samples

Element	Average, ppm	Maximum Value, ppm	Detection limit, ppm	CV, %
Al	BDL	19.2	17.5	7.5
Cu	13.4	76.7	4.6	52.5
Fe	BDL	43.7	1.5	16.6
Pb	BDL	32.6	3.8	153.8
S	136.8	212.0	116	381.9
Zn_{334}	BDL	161.5	18.6	13.7
Zn_{206}	BDL	43.7	21.3	5.5

The chemical analysis of 6 CRM obtained by total digest using the developed method is presented in Tables 4-3 to 4-8. The reference values of CRMs in these tables are marked as R (recommended value) or P (provisional value). Generally speaking the reproducibility of results is good and all the CV values are below 5% with exception to limited cases where the analyte concentration is within the range of the detection limit.

Table 4-3 The chemical analysis of MP-1a

Element	n	Mean, %	CV, %	Max, %	Min, %	Reference values, %	Recovery, %
Zn	17	18.29	3.06	18.93	17.72	19.02^{R}	96.15
Pb	17	4.31	2.43	4.48	4.17	4.33^{R}	99.49
Cu	17	1.40	4.80	1.50	1.33	1.44^{R}	97.44
As	17	0.94	3.84	0.98	0.88	0.84^{R}	111.82
Bi	17	0.034	4.89	0.037	0.031	0.032^{R}	105.47
Mo	17	0.031	4.14	0.034	0.029	0.029^{R}	107.44

Table 4-4 The chemical analysis of CCU-1c

Element	n	Mean, %	CV, %	Max, %	Min, %	Reference values, %	Recovery, %
Al	19	0.15	8.93	0.19	0.13	0.18^{P}	80.94
Ca	19	0.104	3.87	0.112	0.100	0.107^{R}	97.38
Cd	19	138ppm	2.11	143ppm	133ppm	$136ppm^{R}$	101.09
Co	19	18ppm	3.77	19ppm	16ppm	$18ppm^{P}$	97.13
Cr	19	29ppm	2.50	31ppm	28ppm	$30ppm^{P}$	97.91
Cu	19	25.87	2.67	26.89	25.01	25.62^{R}	100.96
Fe	19	28.42	2.31	29.41	27.67	29.34^{R}	96.85
Mg	19	0.60	1.68	0.62	0.59	0.62^{R}	97.75
Mn	19	0.012	1.76	0.012	0.012	0.012^{R}	97.93
Ni	19	11ppm	7.18	13ppm	10ppm	$11ppm^{P}$	105.56
Pb	19	0.35	2.75	0.38	0.34^{P}	0.34^{P}	101.62
S	19	31.73	1.67	32.59	30.90	33.30^{R}	95.28
Zn	19	3.91	1.86	4.07	3.79	3.99^{R}	98.09

Table 4-5 The chemical analysis of CD-1

Element	n	Mean, %	CV, %	Max, %	Min, %	Reference values, %	Recovery, %
As	23	0.66	3.64	7.31	0.62	0.66^{R}	100.00
Fe	23	2.69	1.57	2.99	2.61	2.80^{P}	95.91
S	23	3.06	3.02	3.48	2.93	3.10^{P}	98.98
Sb	23	3.43	2.73	3.86	3.25	3.57^{R}	95.95

Table 4-6 The chemical analysis of CZN-1

Element	n	Mean, %	CV, %	Max, %	Min, %	Reference values, %	Recovery, %
Al	20	0.130	4.40	0.140	0.121	0.132^{R}	97.97
As	20	0.026	4.92	0.029	0.024	0.026^{R}	100.98
Ca	20	0.165	3.48	0.173	0.154	0.179^{P}	92.14
Cd	20	0.128	2.29	0.132	0.123	0.132^{R}	96.60
Cu	20	0.141	2.91	0.149	0.135	0.144^{R}	97.91
Fe	20	10.73	1.80	11.13	10.28	10.93^{R}	98.20
Pb	20	7.37	1.38	7.61	7.18	7.45^{R}	98.91
S	20	29.20	3.74	29.34	27.93	30.20^{R}	96.68
Zn	20	44.13	2.32	45.42	42.37	44.74^{R}	98.63
Mg	20	0.180	2.18	0.186	0.173	0.193^{P}	93.03
Mn	20	0.208	2.32	0.216	0.201	0.219^{R}	94.86
Sb	20	0.0300	41.29	0.043	0.011	0.025^{R}	119.18

Table 4-7 The chemical analysis of CPB-1

Element	n	Mean, %	CV, %	Max, %	Min, %	Reference values, %	Recovery, %
Al	19	0.149	3.632	0.159	0.138	0.148^{R}	100.438
As	19	0.059	5.511	0.065	0.053	0.056^{R}	104.518
Ca	19	0.626	2.544	0.647	0.586	0.629^{P}	99.437
Cd	19	0.015	2.377	0.015	0.014	0.014^{R}	102.167
Cu	19	0.257	3.188	0.270	0.241	0.254^{R}	101.050
Fe	19	8.295	2.280	8.513	7.705	8.430^{R}	98.398
Mg	19	0.088	2.585	0.091	0.082	0.090^{P}	96.835
Mn	19	0.038	2.042	0.039	0.036	0.039^{P}	96.261
Pb	19	62.212	1.917	64.045	60.124	64.740^{R}	96.095
S	19	17.588	2.217	18.322	17.013	17.80^{R}	98.811
Sb	19	0.341	2.942	0.357	0.319	0.360^{R}	94.655
Zn	19	4.234	1.840	4.359	4.034	4.420^{R}	95.784

Table 4-8 The chemical analysis of BGS100

Element	n	Mean, %	CV, %	Max, %	Min, %	Reference values, %	Recovery, %
Al	17	0.96	2.02	1.01	0.94	0.97^{R}	99.12
As	17	77ppm	15.31	103ppm	61ppm	94 ppm^{R}	81.56
Ca	17	0.27	2.30	0.28	0.27	0.27^{R}	99.60
Cd	17	5.8ppm	10.93	7.2ppm	4.8ppm	$5.20ppm^{P}$	111.20
Co	17	86ppm	2.76	91ppm	83ppm	$99ppm^{R}$	87.30
Cr	17	9.2ppm	2.57	9.6ppm	8.6ppm	$8.1ppm^{R}$	113.40
Cu	17	35.86	2.22	37.58	34.13	35.90^{R}	99.88
Fe	17	19.63	1.84	20.42	18.48	20.04^{R}	97.94
Mg	17	0.491	1.99	0.523	0.481	0.507^{R}	97.01
Mn	17	218ppm	3.50	238ppm	207ppm	214 ppm^{P}	101.94
Ni	17	28ppm	5.065	33ppm	27ppm	28 ppm^{R}	103.15
S	17	26.872	1.811	27.811	25.992	28.07^{R}	95.73
Zn	17	624ppm	2.994	661ppm	581ppm	$665ppm^{R}$	93.89

4.2.3.4 Chemical Composition of GBL chalcopyrite

The average chemical composition of all the size fractions of GBL chalcopyrite is listed in Table 4-9. The percentage of each element is calculated according to Equation 4-4. The detailed chemical composition including all replicates is listed in Appendix 4-8. The theoretical chemical composition of chalcopyrite is 34.62% Cu, 30.43%Fe and 34.95%S. Apart from these elements GBL chalcopyrite contained less than 0.14% Zn and the rest are BDL. The calculated molar ratio of Cu, Fe and S from the chemical analysis showed that stoichiometry of GBL chalcopyrite is very close to the theoretical value and the variation is within analytical error. The lower chalcopyrite content in size class 75-106μm can be explained by the presence of some quartz. Otherwise the deviation of 100% chalcopyrite is within analytical error.

$$Concentration.(\%) = Concentration.(ppm) \times \frac{sample.volume(ml)}{1000000 \times mass.(g)} \times 100\% \quad \textbf{Equation 4-4}$$

Table 4-9 The average chemical composition of GBL chalcopyrite.

Particle size ,μm	Cu, %	Fe, %	S, %	Zn, %
Theoretical	34.62	30.43	34.95	0
<38	34.29±0.09	29.44±0.36	35.00±0.45	0.15±0.00
38-53	34.84±0.19	29.98±0.0.04	35.59±0.10	0.14±0.00
53-75	34.94±0.15	29.89±0.26	35.35±0.500	0.15±0.00
75-106	34.29±0.30	29.24±0.39	33.97±0.54	0.14±0.00
Analysed CCU-1c	25.78±0.20	28.73±0.28	33.58±0.41	4.05±0.06
Reported CCU-1c	25.62±0.12	29.34±0.68	33.30±0.50	3.99±0.19

4.2.3.5 Chemical Composition of MZ2HE Chalcopyrite

The average chemical composition of all size fractions prepared from MZ2HE is listed in Table 4-10. It is interesting to note that the copper content decreases with the increase in particle size, whereas the sulphur and iron content generally remain constant. This suggests the pyrite content increases with the increase in particle size. The detailed chemical composition with all the replicates is listed in Appendix 4-9.

Table 4-10 The average chemical composition of MZ2HE chalcopyrite concentrate.

Particle size, μm	Cu,%	Fe,%	S,%	Zn,%
theoretical	34.62	30.43	34.95	0
<25	31.08±0.37	29.09±0.32	33.35±0.51	0.16±0.00
25-38	29.94±0.38	29.55±0.27	34.08±0.28	0.08±0.00
38-53	28.78±0.27	29.84±0.55	34.04±0.42	0.07±0.00
53-75	27.64±0.23	30.11±0.13	34.32±0.84	0.07±0.00
75-106	25.49±0.27	29.42±0.46	33.83±0.57	0.07±0.00

4.2.4 Analytical Method

4.2.4.1 Copper Analysis by ICP

During chalcopyrite leaching, periodic samples were taken. These samples were analysed using ICP-AES. Some modifications were made to the main analytical technique used for total digestion to account for matrix effects and analysis time and to minimise uncertainty. The samples of one leaching experiment were analysed in ascending order by increasing the copper concentration. Furthermore calibration was repeated after analysing each group of samples from one leaching experiment (5 to 9 samples).

In order to investigate the effect of iron content on copper analysis, 5 standard solutions with 25 ppm copper and an iron concentration ranging from 0 to 3000 ppm were made. These standard solutions were analysed using a calibration obtained from the standard which contained 3000 ppm iron. It was found that the copper signal measured in each of the 5 standard solutions was different on Cu_{327} and Cu_{213} with the Cu_{213} line being more sensitive to the iron change in the solution. Therefore, to minimise the matrix effect during copper analysis in the samples containing different concentrations of ferric ions, different standard and quality control solutions were prepared. This was particularly important to do for samples representing leaching experiments designed to study the effect of ferric ion concentration on copper recovery. Although this was time consuming, it was important to introduce this procedure to minimise matrix effect.

4.2.4.2 Iron Analysis by Dichromate Titration

Dichromate titration is a well known technique used for the determination of ferrous ion concentration in solutions containing trivalent iron (Vogel, 1961). This technique was used to determine the concentration of ferrous ions produced as a result of chalcopyrite oxidation. The concentration of Fe^{+2} is very difficult to determine by ICP-AES in a matrix of high Fe^{+3}. A summary of the titration method is presented in Appendix 4-10. Potassium dichromate was used as a titrate. It was standardised against ferrous ammonium sulphate $Fe(NH_4)_2(SO_4)_2$. The standardisation procedure is also presented in Appendix 4-10. Equation 4-5 was used to calculate the quantity of ferrous iron produced:

$$N_{Fe} = \frac{T_{Fe} \times V_{Dichr}}{M_{Fe}} D_f \times V_{final} \qquad \textbf{Equation 4-5}$$

where N_{Fe} is the number of Fe^{+2} moles of (moles), T_{Fe} is the titration factor as determined in Appendix 4-10 (µg/ml), V_{Dichr} is the volume of dichromate required to titrate 1 ml of a diluted leach solution (ml/ml), D_f is the dilution factor of the sample, V_{final} is the final volume of the leach solution (ml), M_{Fe} is the molecular mass of iron (µg/mole).

4.2.4.3 Sulphur Determination by UV Spectrophotometry

The mass of elemental sulphur formed during the oxidation of sulphide minerals can be determined by several techniques. Sulphur can be evaporated at a temperature of about 170°C under vacuum (Lotens and Wesker, 1987). The mass of sulphur is then determined as the difference between the mass of the residue before and after the evaporation. Sulphur also can be separated by passing hot steam (140°C) through a bed of leach residue retained on a fritted glass disk to smelt the sulphur particles and the layer surrounding the mineral particles (Romero et al., 2003). The sulphur droplets can be then collected and the mass is then determined. The most commonly used method for the separation of sulphur is by dissolving it using organic solvents such as carbon disulphide (Dutrizac, 1978; Dutrizac, 1989a; Dutrizac, 1989b; Hiroyoshi et al., 1997; Ngoc et al.,

1990), perechloroethylene (Hackl et al., 1995) and toluene (Rath et al., 1981). The mass of sulphur is then determined as the difference in mass residue before and after extraction or by determining the concentration of sulphur in the organic solvent by UV spectrophotometry. In this thesis elemental sulphur was extracted by toluene and determined using UV spectophotometry. The solubility of sulphur in toluene is shown in Table 4-11

Table 4-11 Solubility of sulphur in toluene (Linke, 1965)

Temperature, °C	S (g) in 100 g of toluene
20	1.827
23	1.889
25	2.018
35	2.722
54	4.85

4.2.4.3.1 Soxhlet Extraction of Sulphur

The elemental sulphur was extracted from leach residue by toluene using a Soxhlet extractor. The leach residue was collected on a double layer of Whatman® filter paper (No 452) and then washed thoroughly with 10 times volume of Milli-Q ultrapure water to remove any remaining sulphate sulphur trapped on the surface of the particles. The residue was then dried in a vacuum dryer at room temperature to remove all the moisture. The residue was then put in a thimble. The thimble was then put in the siphon part of the Soxhlet apparatus (Soxhlet diagram is shown in Appendix 4-11). The flask was filled with about 200 ml of high purity toluene (HPLC grade) and then was heated gradually on a heating mantle until the toluene reached boiling point. The toluene vapours ascended through the side arm of the extractor then condensed and dripped into the thimble. When the extractor was filled to the top of the side arm, the solvent now containing dissolved sulphur from the sample siphons over into the flask. The apparatus permits to make a series of extractions with fresh solvents. The extraction was stopped after at least 24 hours of extraction. The flask was then allowed to cool, and the solvent was the poured into 250 ml volumetric flask. All parts of the system where washed with fresh toluene and poured into the flask as well. The flask was then filled to the mark and the content was then transferred to a 250 ml amber bottle.

4.2.4.3.2 Determination of Sulphur

Ultraviolet spectrophotometry is based on the ability of materials to absorb photons of light. For each material the maximum absorbance of light occurs at a characteristic wavelength (λ_{max}). If the intensity of incident light is (I_0) and the corresponding transmitted intensity when passing through a sample is (I), then according to the Beer's law the absorbance of light (A) is linearly related to concentration of the absorbing species C as (Skoog et al., 2000):

$$A = \log\frac{I_0}{I} = \bar{\varepsilon}\bar{b}C \qquad \textbf{Equation 4-6}$$

where $\bar{\varepsilon}$ is the molar absorptivity (L $mol^{-1}cm^{-1}$), $\bar{b}$ is the path length (cm)

The concentration of sulphur in toluene was determined using a single beam SHIMADZU® UV Visible Spectrophotometer (UV mini-1240®) at a wavelength of 360 nm in 10×10mm cell. A standard sulphur solution in toluene was prepared from high purity crystalline sulphur (>99.998% S obtained from Aldrich®), from which 5 standard solutions were prepared with concentrations which varied from 10 to 1500 µg/ml (Appendix 4-11). The Absorbance was then measured for the standard solutions and for a blank sample to draw a calibration curve (Appendix 4-12).

4.2.4.4 Surface Analysis by Scanning Electron Microscopy

Samples were prepared by mounting on to pin type SEM stubs using carbon adhesive tabs. Samples were examined in a Philips XL30 SEM using a beam voltage of 20 kV and in the Secondary Electron Emission and Back Scattered modes. Non conductive samples like sphalerite were gold coated as well to produce a conductive surface suitable for SEM analysis.

Qualitative elemental analysis was performed by using Oxford Instruments ISIS EDX (Energy Dispersive X-ray Analysis) system powered with a Si(Li) Crystal spectrometer and an ultra-thin entrance window allowing detection of elements as light as carbon.

4.2.4.5 Surface Analysis by Time of Flight Secondary Ion Mass Spectrometry

Secondary Ion Mass Spectrometry (SIMS) is a surface analysis method for analysing the elemental and chemical composition of materials, in particular their surface. The mass spectrometry of ionised particles which are emitted when the sample surface is bombarded by monoenergetic (primary) particles which are usually ions like Ar^+, Ga^+, Cs^+ (Vickerman and Briggs, 2001; Vickerman et al., 1989). The primary ions penetrate the material and transfer their kinetic energy to atoms at the surface via a collision cascade. As a result secondary particles are sputtered from the surface. These sputtered particles can be electrons, neutral species (atoms or molecules), atomic and cluster ions (see Figure 4-11). The majority of the sputtered particles are neutral and only the ionized particles are detected and analysed by the mass spectrometer. The secondary ion mass spectrum gives information about the elemental and chemical surface composition (Vickerman and Briggs, 2001).

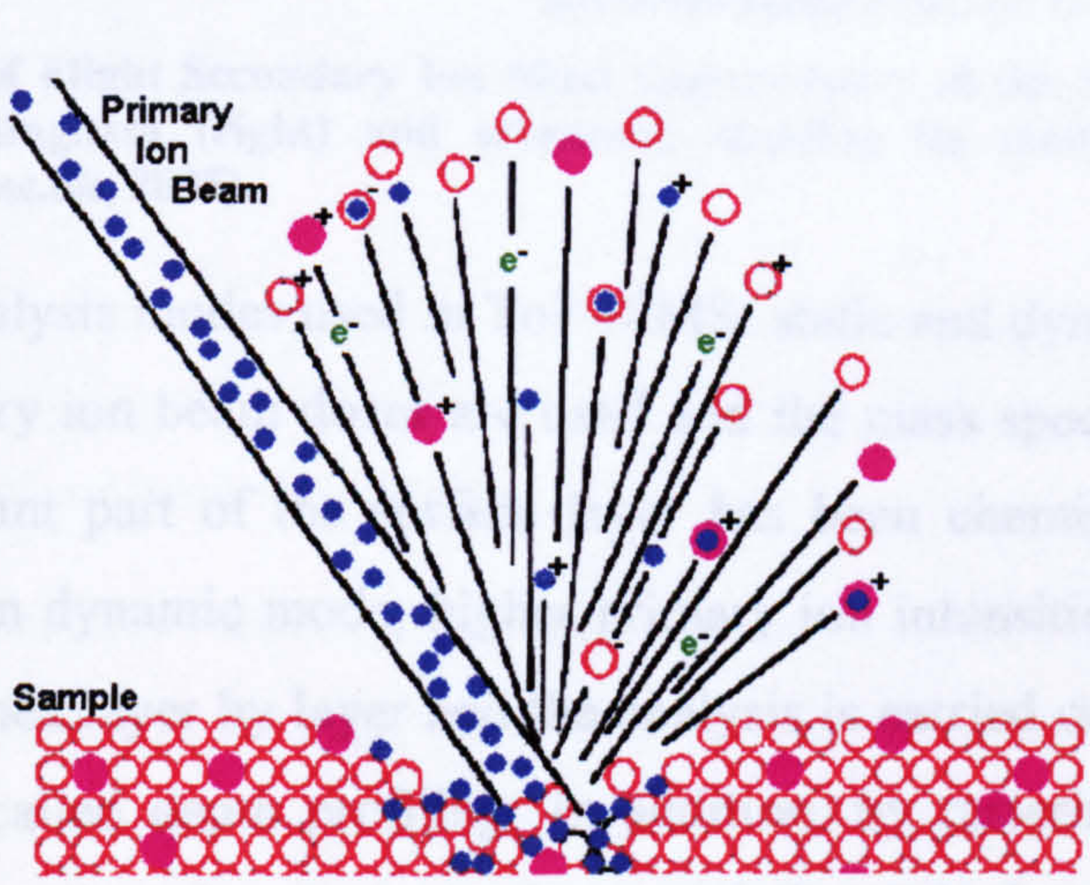

Figure 4-11 Schematic diagram showing the principles of secondary ion mass spectrometry (Eaglabs, 2005)

In Time of Flight Secondary Ion Mass Spectrometry (ToF-SIMS) the ion masses are measured by the time of flight. The technique is based on pulsed primary ion beams. The generated secondary ions are accelerated by a 3-8 keV field to a constant kinetic energy for all ions, and then they fly through a free field space before they hit the detector where their intensity is measured as a function of time of flight. Because ions with different masses have different velocities at a

particular kinetic energy according to the equation of kinetic energy, the measured time of flight can be converted easily to their masses (Vickerman and Briggs, 2001). Figure 4-12 (left) shows schematically the path of the primary ion from the ion gun to the target from where the secondary ions are emitted and extracted by an electric field through transport optics to the detector. The main advantage of ToF-SIMS compared to other surface mass spectrometry techniques is that it offer a unique combination of wide mass range, high mass resolution and high transmission (Vickerman and Briggs, 2001).

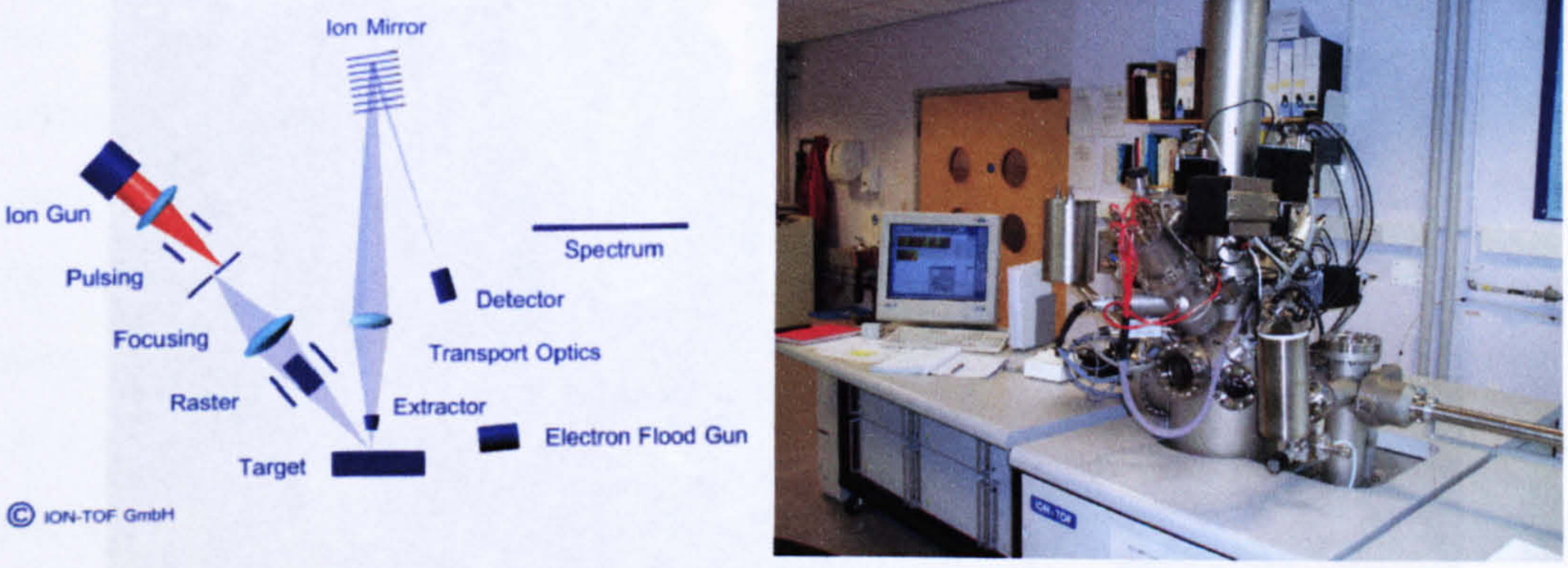

Figure 4-12 Time of Flight Secondary Ion Mass Spectrometry at the School of Pharmacy-University of Nottingham (right) and schematic showing its main components (left) ((www.nottingham.ac.uk, 2005).

There are two analysis modes used in ToF-SIMS: static and dynamic. In the static mode, low primary ion beam doses are used and the mass spectrum is measured before a significant part of the surface layer has been chemically modified or sputtered away. In dynamic mode, higher primary ion intensities are used where the surface is etched layer by layer and the analysis is carried out with increasing depth, which is called depth profiling. In addition, by rastering the ion beam, spectra from each point of analysis can be recorded and the lateral distribution of different elements can be visualised by ion imaging. The later can be combined by depth profiling to get a three dimensional distribution of elements. In the static mode, this allows for the mapping of atoms and molecules across the sample surface.

4.3 Conventional Leaching of Chalcopyrite in Ferric Sulphate

4.3.1 Experimental Method

Conventional leaching experiments were carried out in a simple leaching apparatus shown in Figure 4-13. It consists of a 500 ml round bottomed reaction vessel and a five necks lid. The reaction vessel was immersed in a thermostatic water bath, which controlled the temperature within ±1°C.

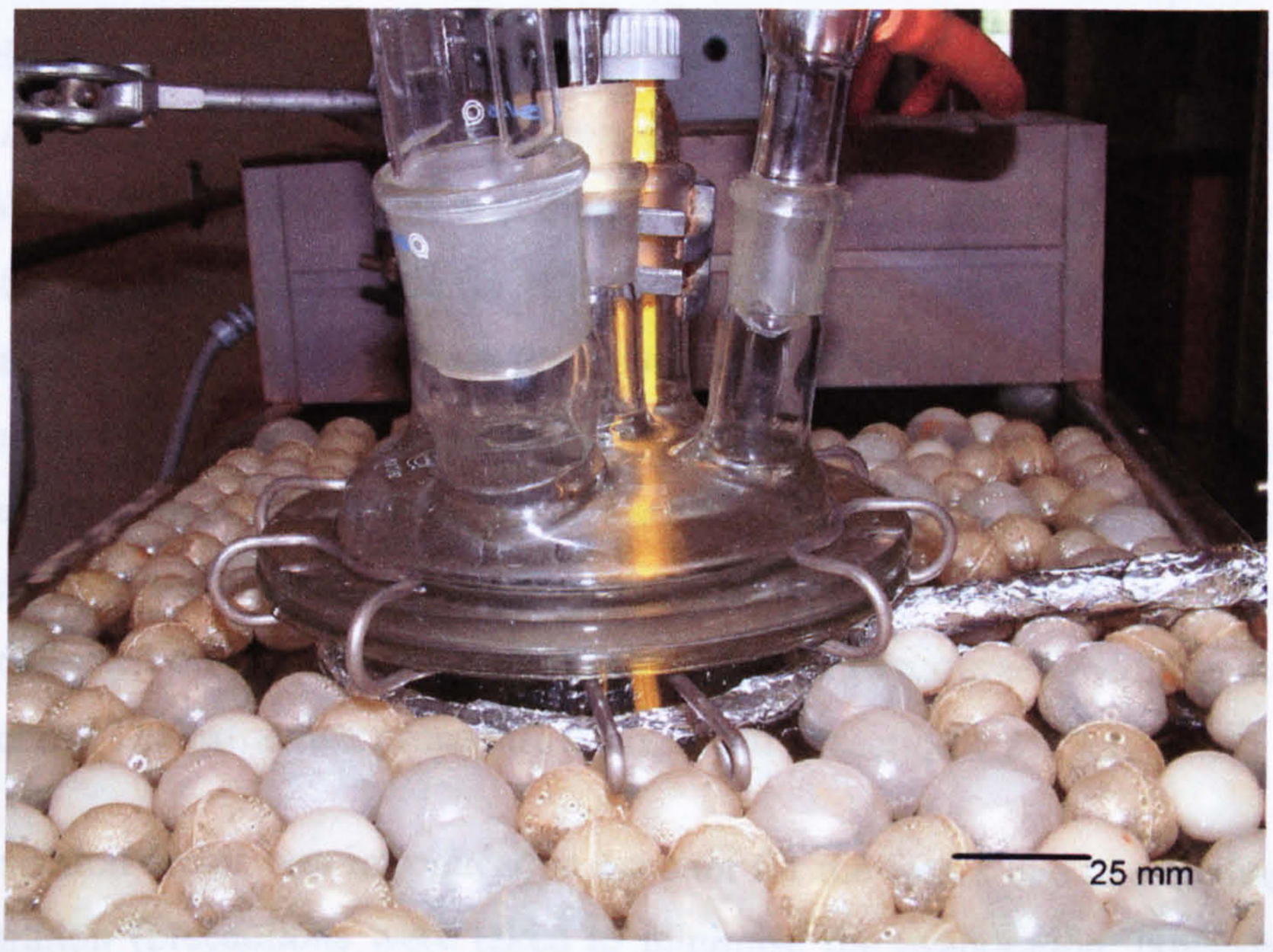

Figure 4-13 Conventional leaching apparatus

The degree of agitation of the mixture was maintained using a two-bladed anchor glass propeller. Agitation was applied to suspend the particles and prevent their caking and to eliminate any possible gross solution inhomogeneities. The shaft of the propeller passed through the central neck in the lid and was connected to a variable speed stirrer supplied with a digital tachometer and speed control.

In the other four necks of the lid were a condenser to control evaporation, a mercury thermometer to check the temperature of the solution, a closed neck that was opened only to withdraw samples, and a final neck which was used for gas purging.

The leaching of chalcopyrite was carried out as follows: The starting volume of the leaching solution used was 250 ml. It consisted of 0.5 M sulphuric acid and various molar concentrations of ferric sulphate. The leaching solution was first purged with helium for about 15 minutes to minimize the dissolved oxygen prior to leaching. The solution was then left for about 10 minutes to allow thermal equilibrium to be established. One gram of chalcopyrite, with the required particle size was then added to the leaching solution after the leaching temperature had been reached. Small volumes of sample (1.8 ml aliquots) were taken periodically for chemical analysis. Samples were diluted further in 8 ml of 0.5 M sulphuric acid and then centrifuged for 5 minutes to separate any particulates taken during sampling. A volume of 5 ml was then was taken from each centrifuge tube and transferred to a sample bottle for ICP analysis as described in Section 4.2.4.1. A further volume of (2×1 ml) from the centrifuged sample was taken for titration to determine Fe^{2+} in the leaching solution as described in Section 4.2.4.2. At the end of the experiment, larger volumes of sample were sometimes taken for titration especially in the cases where the final recovery was below 2%. The residue was then collected on a double layer of Whatman® filter paper grade (452) for sulphur extraction. The extraction procedure is presented in section 4.2.4.3.1.

A correction factor was introduced to account for the losses due to sampling and evaporation (precautions were taken to minimise the evaporation, however, the losses during purging with helium were significant). The formula to account for there loses is as follows:

$$V_i = V_0 - V_{purg} - t_i \times \frac{dV}{dt} - V_{is-1} \qquad \textbf{Equation 4-7}$$

where V_i is the volume of leaching solution prior to i^{th} sample (ml) , V_0 is the initial solution volume (250 ml), V_{purg} is the volume lost during the 15 minutes purging with helium (found by repeating blank experiments and it was about 2/3 of the total losses during the whole experiment time- in average about 10 ml) , t_i is the sampling time (minutes), $\frac{dV}{dt}$ is the estimated evaporation rate (ml/min),

V_{is-1} is the volume of samples taken before i^{th} sample (ml) (about 12.6 ml for the sample taken at time 180 minutes).

Evaporation rate was estimated as follows:

$$\frac{dV}{dt} = \frac{V_0 - V_{end} - V_w - V_{purg} - V_{si}}{t} \qquad \textbf{Equation 4-8}$$

where V_{end} - is the volume of solution collected at the end of the experiment (ml), V_w is the volume lost on wetting the filter paper and the flask of the vacuum filter (about 3 ml), V_{si} is the total samples volume (ml) and t was the time of the experiment (180 min).

The fraction of copper extracted was calculated as the ratio of extracted copper to the initial content of copper in the sample.

$$X = \frac{m_0 - m}{m_0} \qquad \textbf{Equation 4-9}$$

where m_0 is the initial mass of copper in the leached chalcopyrite sample.

4.3.2 Experimental Results

This section is concerned with the effect of various parameters on the leaching kinetics of chalcopyrite in ferric sulphate. In addition, an attempt was made to find the rate limiting step of the reaction of chalcopyrite oxidation in an acidic ferric sulphate solution. Surface analysis studies were carried out in an attempt to elucidate the nature of the sulphur layer formed during the leaching process. In this study GBL chalcopyrite was used for all experiments.

4.3.2.1 The Effect of Ferric Sulphate Concentration

The effect of ferric sulphate concentration on the leaching rate of chalcopyrite was carried out in 0.5 M H_2SO_4 leaching solution containing various concentrations of $Fe_2(SO_4)_3$ (0, 0.0025, 0.01, 0.075, 0.1, 0.15, 0.25, 0.30 M) at a temperature of 90°C. The particle size used was <38μm. Experimental results are shown in Figure 4-14. It can be seen that above a 0.1 M concentration of ferric sulphate

there is no further positive effect on the leaching rate. Adversely, the amount of copper extracted is slightly reduced when ferric sulphate increased above 0.15 M.

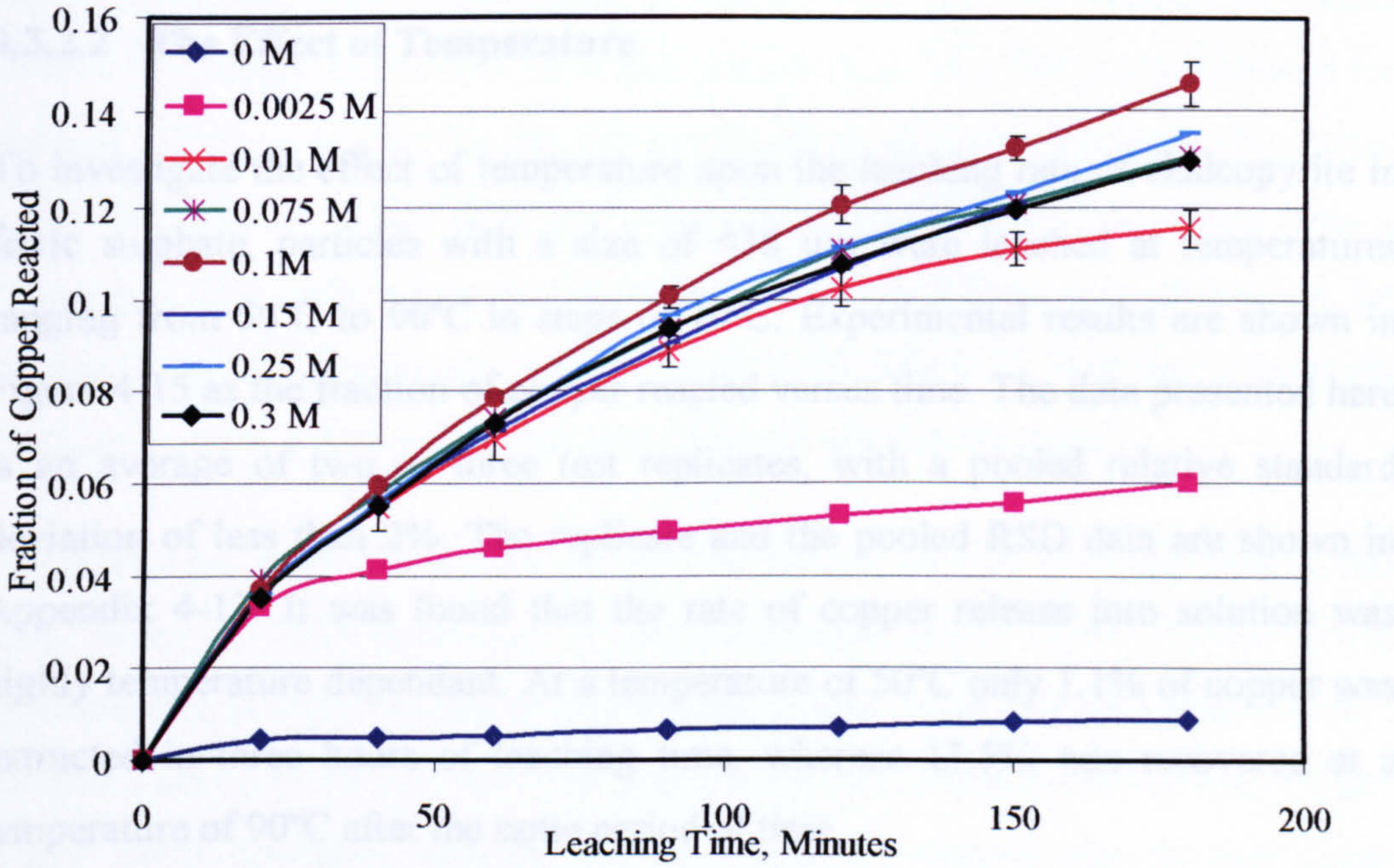

Figure 4-14 The effect of ferric sulphate concentration on conventional leaching of chalcopyrite as a function of time (T= 90°C, particle size <38μm)

It seems that the reduction in leaching rate when leaching was conducted with 0.0025 M solution was due to ferric ion depletion (the calculated remaining Fe^{3+} molarities after 20 minutes of leaching was about 8×10^{-5} M).

When leaching of chalcopyrite was conducted in the absence of ferric sulphate the amount of copper dissolved was about 1% after 3 hours of leaching at a temperature of 90°C. This means that the oxidation which occurred without ferric sulphate was negligible. The amount of copper extracted may be related to the presence of some oxygen and/or due to the presence of some sulphate presence at the particles surface. The main contribution of copper dissolved into solution could be from sulphate formed on the surface prior to leaching. This is because in the first 20 minutes 50% of copper was already in the solution (see Figure 4-14). Wadsworth (1972) reported that in the absence of any iron species in the leaching solution, oxygen reacts with the mineral surface forming intermediates (H_2O_2 and HO_2) in a series of single-electron charge transfer steps. This results in a relatively slow electron discharge from oxygen due to the oxygen-oxygen double bond.

Therefore, even with oxygen acted as an oxidant, the reaction will be very slow to occur.

4.3.2.2 The Effect of Temperature

To investigate the effect of temperature upon the leaching rate of chalcopyrite in ferric sulphate, particles with a size of <38 μm were leached at temperatures ranging from 50°C to 90°C in steps of 10°C. Experimental results are shown in Figure 4-15 as the fraction of copper reacted versus time. The data presented here is an average of two or three test replicates, with a pooled relative standard deviation of less than 2%. The replicate and the pooled RSD data are shown in Appendix 4-13. It was found that the rate of copper release into solution was highly temperature dependant. At a temperature of 50°C only 1.1% of copper was extracted in three hours of leaching time, whereas 13.5% was recovered at a temperature of 90°C after the same period of time.

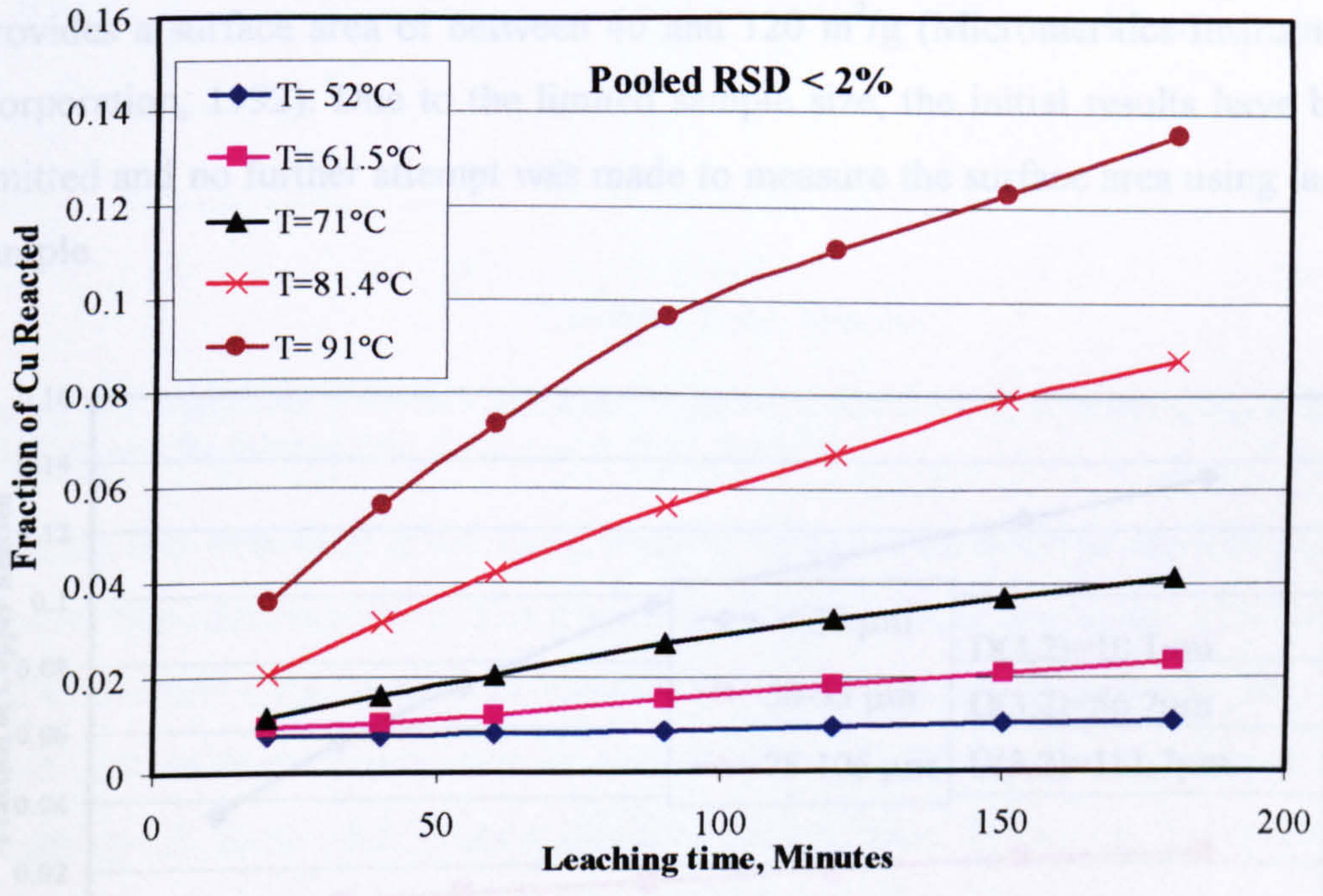

Figure 4-15 The effect of temperature on the conventional leaching of chalcopyrite as a function of time ($C_{Fe2(SO4)3}$: 0.25 M, particle size: <38μm)

4.3.2.3 The Effect of Particle Size

The effect of particle size on the leaching rate of chalcopyrite was studied by using a leaching solution of 0.25 M $Fe_2(SO_4)_3$ - 0.5M H_2SO_4 at a temperature of

90°C. Three size fractions were chosen to verify the effect of particle size on the leaching rate. Figure 4-16 shows the effect of particle size on the amount of copper extracted from chalcopyrite. It can be seen that the fraction of copper reacted is strongly dependant upon the particle size. The difference between the fraction of copper reacted for the <38 and 38-53 μm size fractions could be related to the high content of fine particles in the <38μm fraction which is clearly seen in Figure 4-6. The surface area diameters D(3,2), obtained from laser diffraction, for the leached size fractions are given in Figure 4-16. The D (3,2) of the <38μm size fraction is about 5 time lower than that of 38-53 μm size fraction.

Attempts were made to measure the surface area of the size fractions used in this study using the BET technique. A Micromeritics® ASAP 2000 instrument was implemented to carry out the measurements. It was found that the surface area of the size fraction (< 38 μm) was less than 1 m^2/g. According to the Micromeritics® ASAP 2000 operation manual, the recommended sample size is one which provides a surface area of between 40 and 120 m^2/g (Micromeritics-Instrument-Corporation, 1992). Due to the limited sample size, the initial results have been omitted and no further attempt was made to measure the surface area using larger sample.

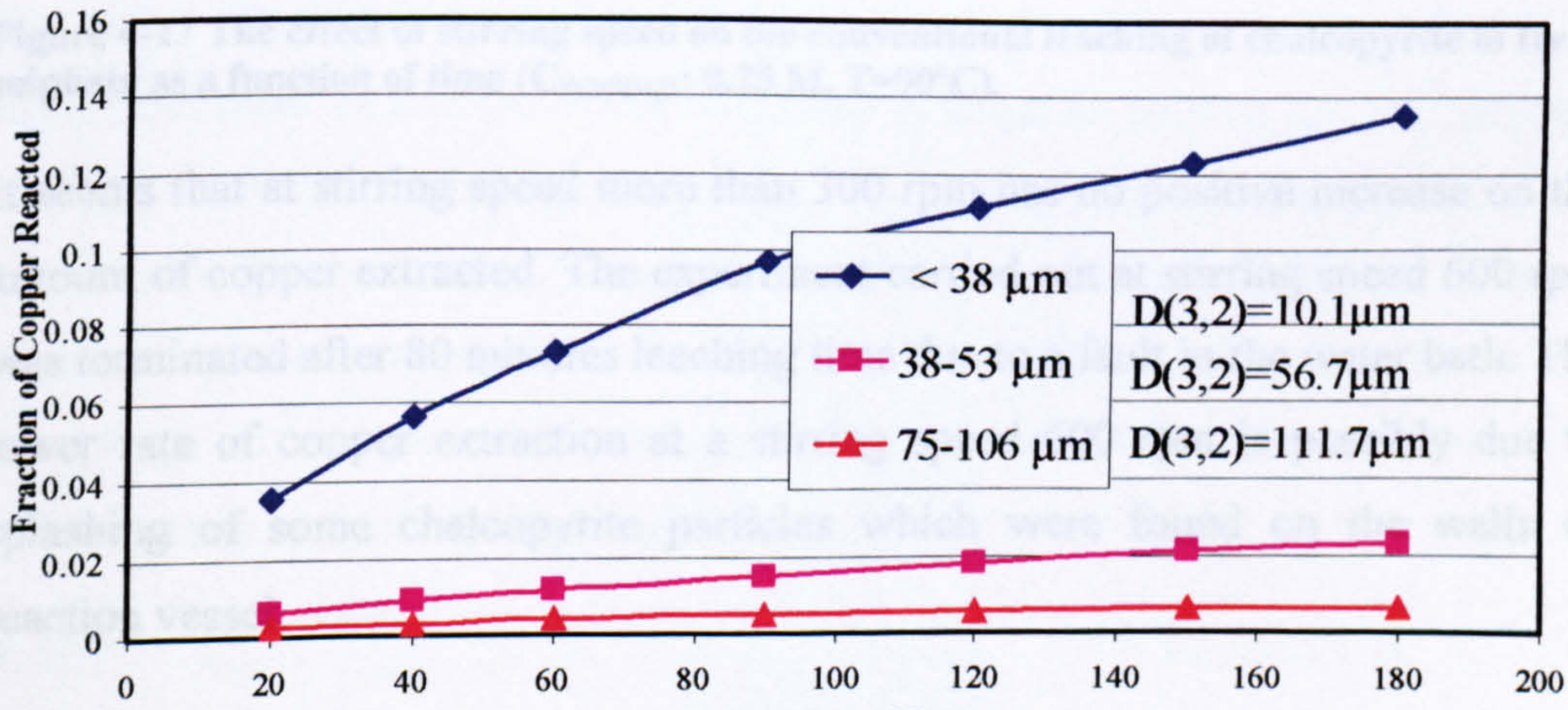

Figure 4-16 The effect of particle size on the leaching of chalcopyrite as a function of time ($C_{Fe2(SO4)3}$: 0.25 M, T=90°C).

4.3.2.4 The Effect of Agitation

Stirring of the leaching mixture was performed to eliminate the effect of diffusion of the reaction products through the so-called fluid film or boundary layer (Levenspiel, 1999). Experiments were carried out at a temperature of 90°C in 0.25M $Fe_2(SO_4)_3$ - 0.5M H_2SO_4. Figure 4-17 shows the experimental results.

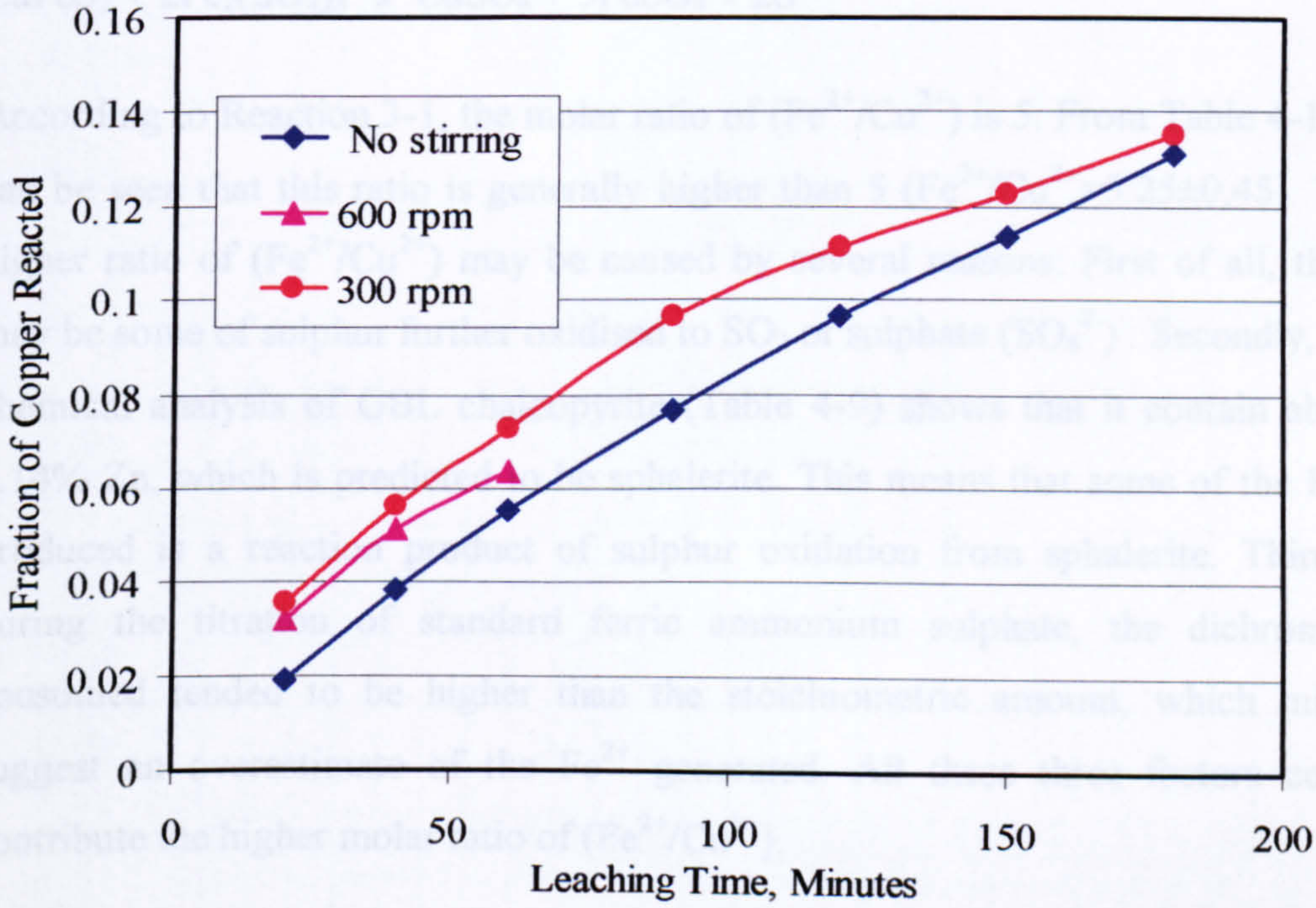

Figure 4-17 The effect of stirring speed on the conventional leaching of chalcopyrite in ferric sulphate as a function of time ($C_{Fe2(SO4)3}$: 0.25 M, T=90°C).

It seems that at stirring speed more than 300 rpm has no positive increase on the amount of copper extracted. The experiment carried out at stirring speed 600 rpm was terminated after 80 minutes leaching time due to a fault in the water bath. The lower rate of copper extraction at a stirring speed 600 rpm is possibly due to splashing of some chalcopyrite particles which were found on the walls of reaction vessel.

It has been shown in previous studies (Dutrizac, 1978) that stirring speed has negligible effect on the reaction rate of chalcopyrite dissolution in ferric sulphate when stirring speed is higher than 300 rpm. These observations are confirmed in this work.

4.3.2.5 Reaction Stoichiometry

The known reaction products (S^0, $Fe^{2+}$and Cu^{2+}) from chalcopyrite dissolution in ferric sulphate have been measured. The molar ratio of these products is presented in Table 4-12. It was shown in Chapter 3 (Section 3.3.2.1) that the predominant leaching reaction of chalcopyrite in ferric sulphate is Reaction 3.1.

$$CuFeS_2 + 2Fe_2(SO_4)_3 \rightarrow CuSO_4 + 5FeSO_4 + 2S^0$$

According to Reaction 3-1, the molar ratio of (Fe^{2+}/Cu^{2+}) is 5. From Table 4-12 it can be seen that this ratio is generally higher than 5 (Fe^{2+}/Cu^{2+}=5.25±0.45). The higher ratio of (Fe^{2+}/Cu^{2+}) may be caused by several reasons: First of all, there may be some of sulphur further oxidised to SO_2 or sulphate (SO_4^{2-}) . Secondly, the chemical analysis of GBL chalcopyrite (Table 4-9) shows that it contain about 0.14% Zn, which is predicted to be sphalerite. This means that some of the Fe^{2+} produced is a reaction product of sulphur oxidation from sphalerite. Thirdly, during the titration of standard ferric ammonium sulphate, the dichromate consumed tended to be higher than the stoichiometric amount, which might suggest an overestimate of the Fe^{2+} generated. All these three factors could contribute the higher molar ratio of (Fe^{2+}/Cu^{2+}).

Assuming that Reactions 3-1 and 3-2 take place, one can judge the amount of sulphate formed as a result of the oxidation of sulphide sulphur (S^{2-}) to sulphate (SO^{2-}_4). Since the direct determination of (SO^{2-}_4) produced by Reaction 3-2 is not possible by ICP because of its high concentration in the initial leaching solution, the ratio of reaction products (like Fe^{2+}/Cu^{2+}) could be used to calculate the percentage of sulphate formed using Equation 4-10 derived from the stoichiometry in Reactions 3-1 and 3-2 :

$$\%SO_4^{2-} = 4.55\left(\frac{Fe^{2+}}{Cu^{2+}}\right) - 22.72 \qquad \textbf{Equation 4-10}$$

The average amount of sulphate formation is about 5%, which agrees with the values suggested by Dutrizac (1989a) and Tiwari et al (1980) (see Section 3.3.1.1).

Table 4-12 Ratio of reaction products of chalcopyrite leaching in ferric sulphate under conventional conditions : Fe/Cu, S/Cu and Fe/S

Leaching conditions			Results of analysis: number of mmoles			Ratio of elements		
Concentration, mole/l	T, °C	Particle size, µm	Cu	Fe	S	Fe/Cu	S/Cu	Fe/S
0	91	<38	0.047	0.069		1.479		
0.0025	91	<38	0.302	1.319		4.371		
0.0075	91	<38	0.728	3.847		5.282		
0.01	91	<38	0.613	3.055	0.989	4.987	1.615	3.089
0.01	91	<38	0.629	3.175	1.128	5.046	1.793	2.815
0.01	91	<38	0.602	3.198		5.309		
0.1	91	<38	0.727	3.719		5.115		
0.1	91	<38	0.772	4.003	1.388	5.187	1.798	2.884
0.1	91	<38	0.796	4.359	1.488	5.474	1.869	2.930
0.15	91	<38	0.704	3.674		5.215		
0.25	48	75-106	0.013	-	0.026	-	2.009	0.000
0.25	52	<38	0.056	0.256	0.113	4.615	2.029	2.274
0.25	52	<38	0.056	0.269	0.113	4.821	2.019	2.387
0.25	61.5	<38	0.125	0.654	0.230	5.249	1.845	2.846
0.25	61.5	<38	0.121	0.717	0.249	5.913	2.056	2.876
0.25	71	<38	0.207	1.157	0.438	5.589	2.115	2.642
0.25	71	<38	0.230	1.280	0.373	5.559	1.621	3.430
0.25	81.3	<38	0.474	2.473	0.789	5.215	1.665	3.133
0.25	81.3	<38	0.452	2.625	0.849	5.810	1.878	3.093
0.25	91	38-53	0.123	0.765		6.208		
0.25	91	<38	0.465	2.669	0.708	5.743	1.524	3.768
0.25	91	<38	0.539	2.761	0.907	5.121	1.682	3.045
0.25	91	<38	0.549	3.058	0.937	5.568	1.706	3.264
0.25	91	<38	0.671	3.752		5.593		
0.25	91	<38	0.716	3.749		5.236		
0.30	91	<38	0.812	3.435		4.231		

On the other hand, the theoretical molar ratio of S^0/Cu^{2+} according to Reaction 3-1 is 2. Generally, the experimental values of the molar ratio of S^0/Cu^{2+} are close to 2. The lower ratio of S^0/Cu^{2+} less than 2 in some instances as seen in Table 4-12 could be attributed to several factors: if some of elemental sulphur produced from the oxidation process was amorphous it would not dissolve compared to rhombic and monoclinic forms(Tuller, 1954). Recent studies have shown the sulphur tends to form polysulphides before it has been liberated completely from the surface (Smart et al., 2000), which means that part of the sulphur is being partially oxidized on the surface without breaking the bonds with unreacted Cu and Fe. Thirdly, during the experiment there were some losses of reacted particles during sampling, which might contribute to the underestimate of sulphur. Finally, it was noticed that the sulphur tends to adhere to the vessel walls and mainly on the neck used for the condenser which also suggests losses.

The relative amount of sulphur formed and subsequently extracted was not found to be dependant on the particle size or ferric sulphate concentration. From the above discussion, one can say that the suggested reaction stoichiomerty is reasonably acceptable.

4.3.2.6 Sulphur Formation and Morphology

The study of sulphur formation on chalcopyrite during ferric sulphate conventional leaching was carried out in 0.25 M $Fe_2(SO_4)_3$ – 0.5 M H_2SO_4 at a temperature of 90°C. This study is aimed to assist the understanding of the kinetics of chalcopyrite leaching in ferric sulphate.

Figure 4-18 shows an SEM micrograph of unleached chalcopyrite particles (38-53μm) prepared from GBL chalcopyrite. When chalcopyrite of particle size 38-53μm was leached for 3 hours in 0.25 M $Fe_2(SO_4)_3$ – 0.5 M H_2SO_4 leaching solution at a temperature of 90°C, the particles seemed not to have been attacked, especially their edges and corners as shown in Figure 4-19. Only a few sulphur particles or globules (a few microns size) were observed as shown by the white arrow in Figure 4-19. The amount of copper extracted was only about 2%.

On the other hand, when chalcopyrite particles of <38μm where leached under the same conditions, some particles are shown to be attacked heavily (Figure 4-20) and certain areas are covered with sulphur, which caused the particles to agglomerate and adhere to each others. However, some particles seem not to be attacked, except their edges where their sharpness was reduced

Figure 4-18 Back scattered electron micrograph of unleached GBL chalcopyrite particles (38-53μm).

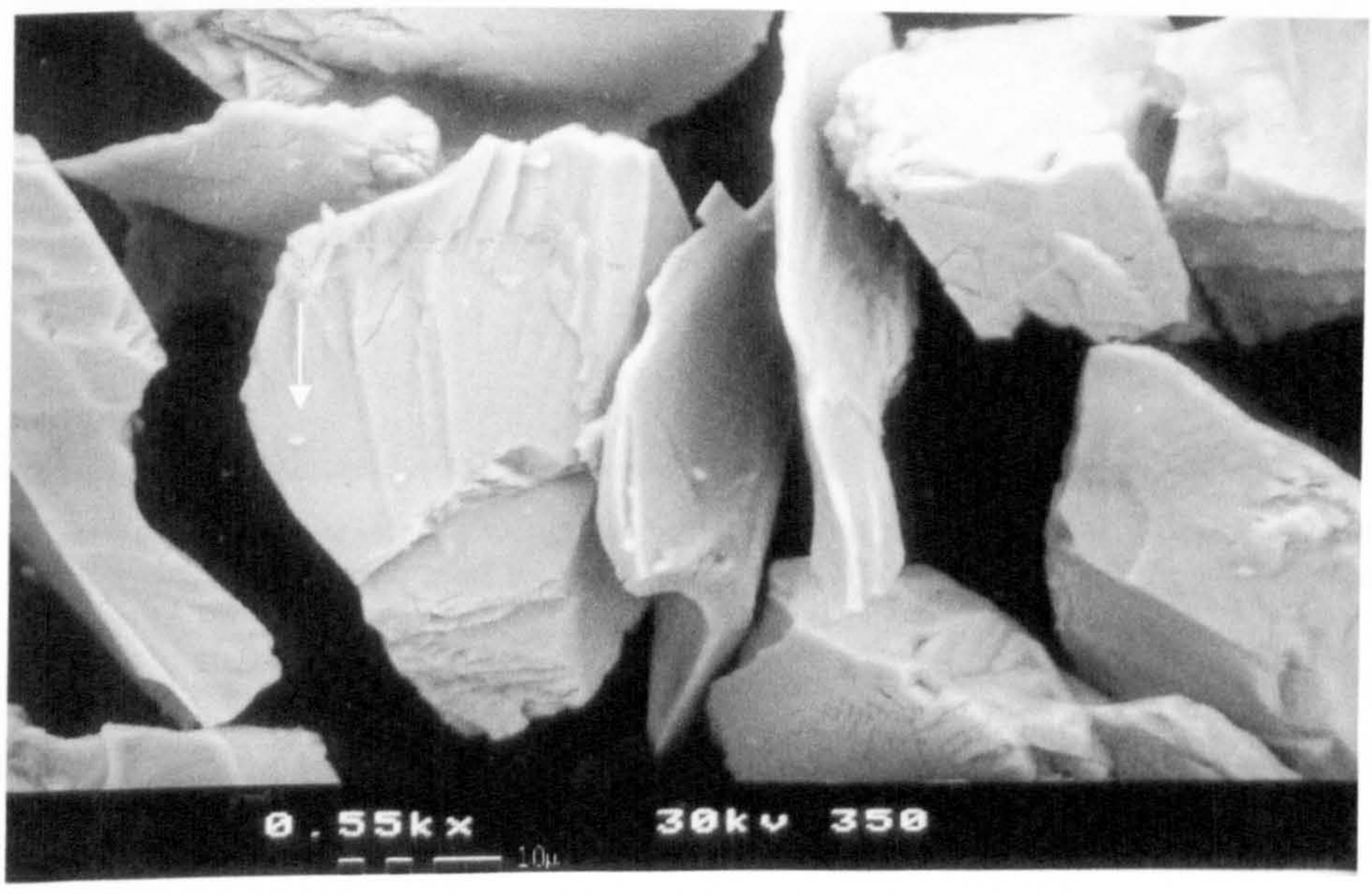

Figure 4-19 Back scattered electron micrograph of the surface of GBL chalcopyrite particles (38-53μm), leached in 0.25M Fe2(SO4)3 – 0.5M H2SO4 at a temperature of 90°C for 3 hours

Figure 4-20 Back scattered electron micrograph of the surface of GBL chalcopyrite particles (<38µm), leached in 0.25 M $Fe_2(SO_4)_3$ – 0.5 M H_2SO_4 at a temperature of 90°C for 3 hours.

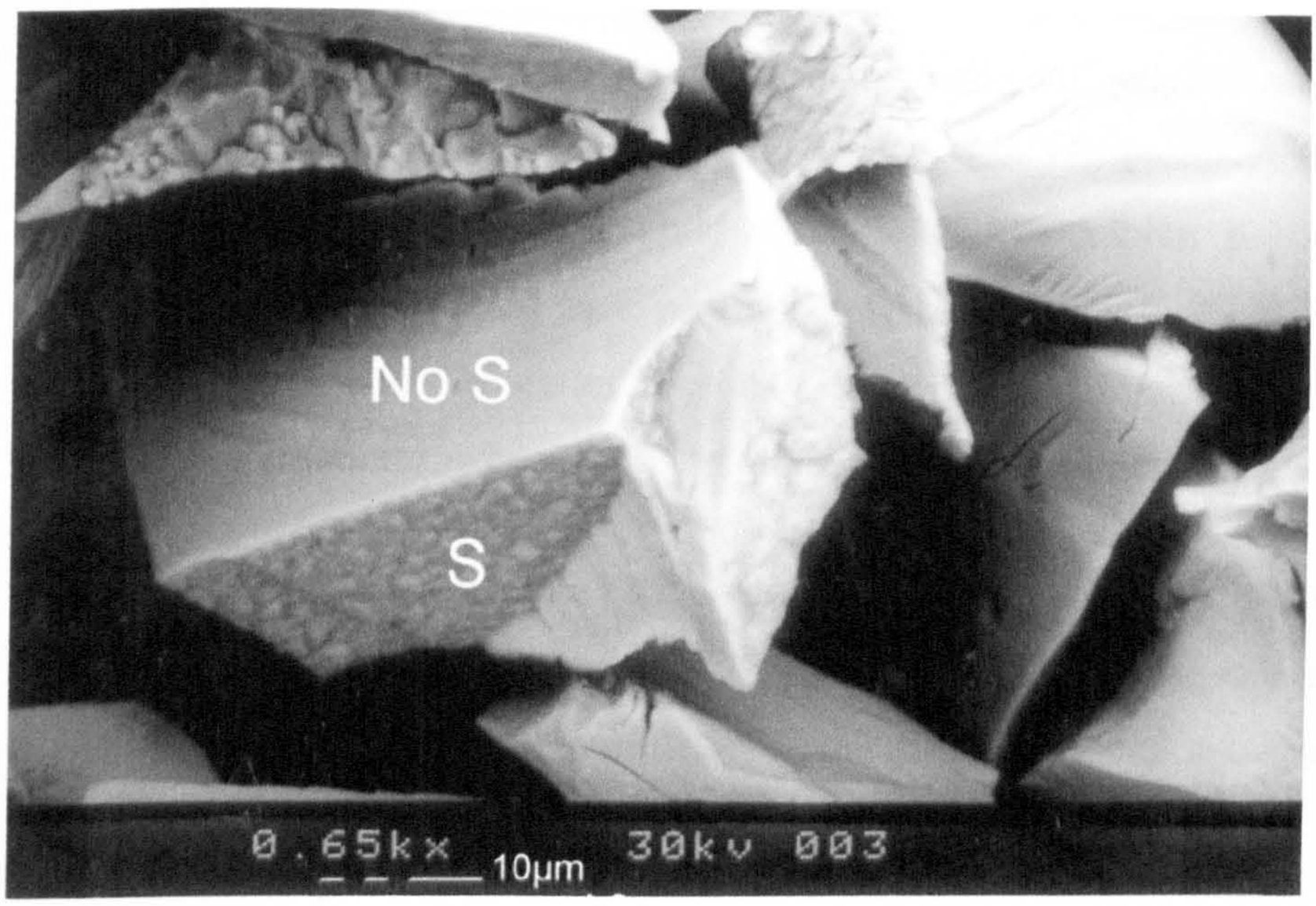

Figure 4-21 Back scattered electron micrograph of the surface of GBL chalcopyrite particles (38-53µm), leached in 0.25M $Fe_2(SO_4)_3$ – 0.5 M H_2SO_4 at temperature 90°C for 10 hours.

Figure 4-21 shows chalcopyrite particles (38-53µm) leached for 10 hours in the same leaching solution, but in a completely closed vessel and without stirring. The sulphur seems to form on specific parts or planes of some particles, whereas, other planes are shown to be not covered with sulphur or attacked.

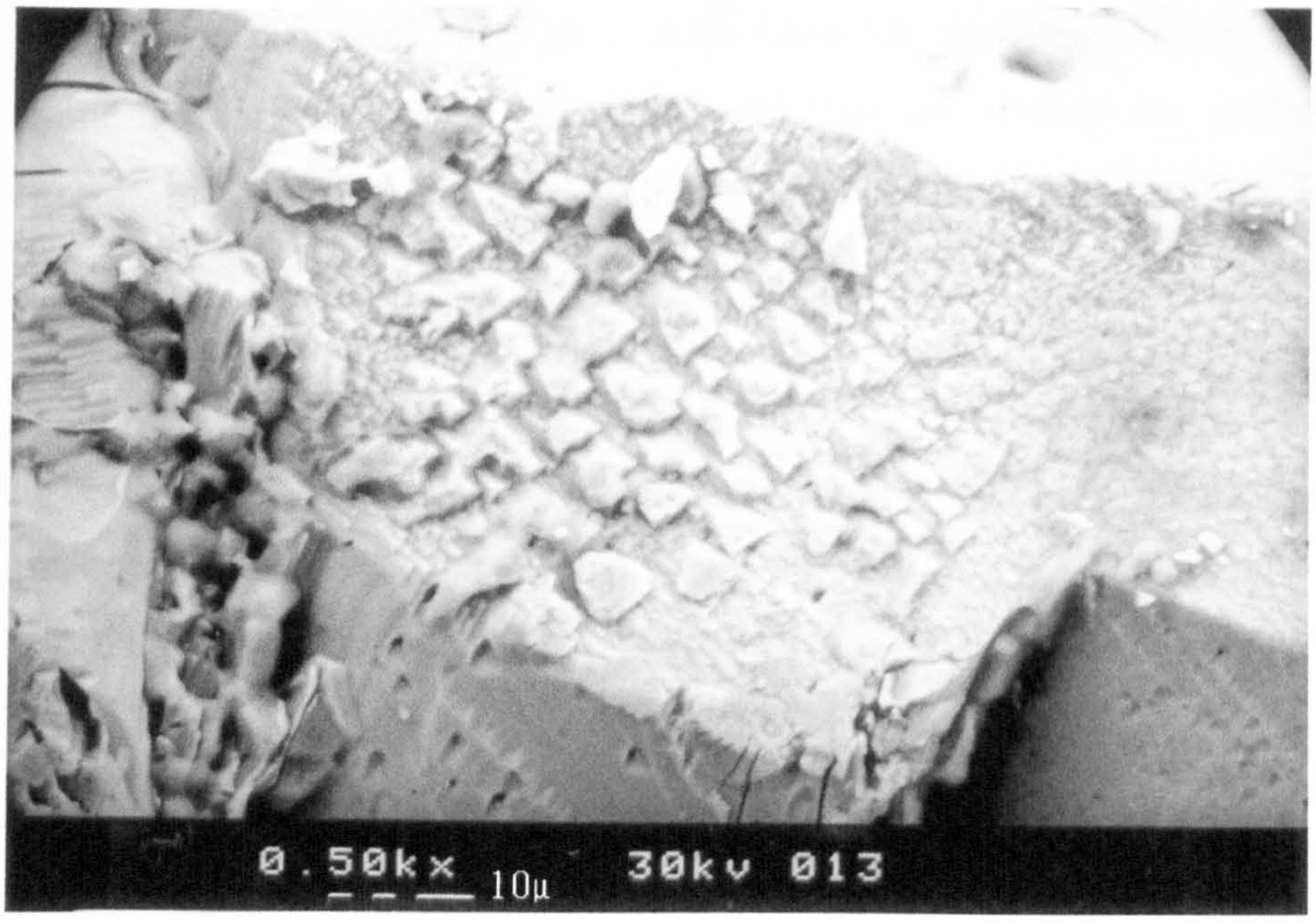

Figure 4-22 Back scattered electron micrograph of the surface of a massive piece of GBL chalcopyrite leached in 0.25M $Fe_2(SO_4)_3$ – 0.5 M H_2SO_4 at a temperature of 90°C for 96 hours.

To investigate the preferential deposition or formation of sulphur on the leached particle surface, massive particles were leached for 96 hours under the same conditions as ground particles. Only a few euhedral sulphur particles (a few microns in size) were found on a very clean surface, which looks as if it was not attacked. Figure 4-22 shows an edge of a massive chalcopyrite piece, which is attacked preferentially, whereas the neighbour planes were not attacked.

The preferential attack of some active sites or planes and/or the sulphur deposition on some areas is a very interesting phenomenon which requires more detailed investigation. It will be discussed further in the discussion section of this chapter.

4.3.2.7 A Study of Reaction Kinetics

The dissolution of sulphide minerals in liquids forms a heterogeneous system. The oxidation reaction occurs at the interface between liquid and solid (Fogler, 2000; Levenspiel, 1999). This dissolution process can occur with generation of a product layer on the particle surface, which may hinder the reaction. The best two models that can describe solid-liquid reactions are shrinking particle and shrinking core models. The rate limiting steps in the systems described by the shrinking particle

model are; diffusion through a film layer or surface reaction control. The shrinking core model describes systems that are limited by surface reaction control, diffusion control through a product layer (ash layer) or diffusion through a liquid film layer.

In the case of chalcopyrite leaching in ferric ion media, it was shown in Chapter three (Section 3.3) that sulphur is produced as a solid reaction product on the chalcopyrite surface. Therefore, it is reasonable to apply the shrinking core model to try and describe the reaction kinetics of chalcopyrite in ferric sulphate.

For a spherical particle, depending on the rate-limiting step, the shrinking core model can be expressed as follows (see Appendix 4-14 for full derivation):

For surface reaction control:

$$1-(1-X)^{1/3}=k_S t \qquad \textbf{Equation 4-11}$$

For diffusion control through the ash layer:

$$1-3(1-X)^{2/3}+2(1-X)=k_D t \qquad \textbf{Equation 4-12}$$

For film diffusion control:

$$X=k_f t \qquad \textbf{Equation 4-13}$$

where $X=1-(\frac{r_c}{r})^3$ is the fraction reacted at time t (min) , r is the initial particle radius (m), r_c is the radius of unreacted core (m),and k_S , k_D and k_f are the apparent rate constants (1/min).

The apparent rate constants are given according to the following equations:

$$k_S=\frac{bk''MC}{\rho r} \qquad \textbf{Equation 4-14}$$

$$k_D=\frac{6bD_eMC}{\rho r^2} \qquad \textbf{Equation 4-15}$$

$$k_f=\frac{3bkMC}{\rho r} \qquad \textbf{Equation 4-16}$$

where b is the stoichiometric coefficient, k'' is the intrinsic rate constant (m/min), C is the bulk concentration of reactant in liquid phase (mole/m^3), M is the solid molar mass (kg/mole) ρ is the density of reacted particle (kg/m^3), D_e is the effective diffusivity (m^2/min), and k is the mass transfer coefficient of liquid film(m/min).

To establish which rate limiting step controls the reaction, the left hand side of one of Equations 4-11, 4-12 and 4-13 is plotted against time on the right hand side giving a straight line. The slope of this line represents the apparent rate constant. For the rate-limiting step, it is related to reaction activation energy, E_A, by Arrhenius law:

$$k = A_0 \exp(-\frac{E_A}{RT})$$ **Equation 4-17**

where A_0 is a constant and R is the universal gas constant (8.314 Jmol^{-1}K^{-1}).

The activation energy can be found by plotting $\ln k$ against $\frac{1}{T}$. The slope of the straight line represents $(-\frac{E_A}{R})$, from where activation energy E_A can be found easily.

When various shrinking core models were fitted to the rate data presented in Figure 4-15 (these relating to different types of limiting step) plots of the data in the appropriate form yielded straight lines with good correlation coefficients. For example, a model in which the rate-limiting step corresponded to diffusion through the sulphur product layer (Equation 4-12) yielded a highly linear plot with correlation coefficients higher than 0.98 (see Appendix 4-15). A difficulty arises in data interpretation, however, because the highest conversion of chalcopyrite (X) was less than 15% (for conventional leaching). This means that it is very difficult to distinguish between the different forms of the model: all yield quasi-linear plots over a small range in X. Furthermore, electron microscopy analysis was carried out (see Section 4.3.2.6), in which, it was found that the residual chalcopyrite particles were almost free of sulphur deposition (with the exception

of some isolated islands and planes). Diffusion control is thus dismissed as a rate limiting step. In view of this, a model involving surface reaction control was instead chosen to describe the kinetic data. This is represented by the Equation 4-12 and a plot of $1-(1-X)^{1/3}$ versus time is shown in Figure 4-23. The choice of surface reaction control is also supported by the fact that a linear relationship was obtained between the apparent rate constant and the inverse particle radius as shown in Figure 4-24. This is consistent with Equation 4-12 which shows that the apparent rate constant k_s is inversely proportional to the particle radius. The particle radius used is obtained from a Malvern calculation of the surface area diameter D(3,2) as discussed in Section 4.2.2.2.2.

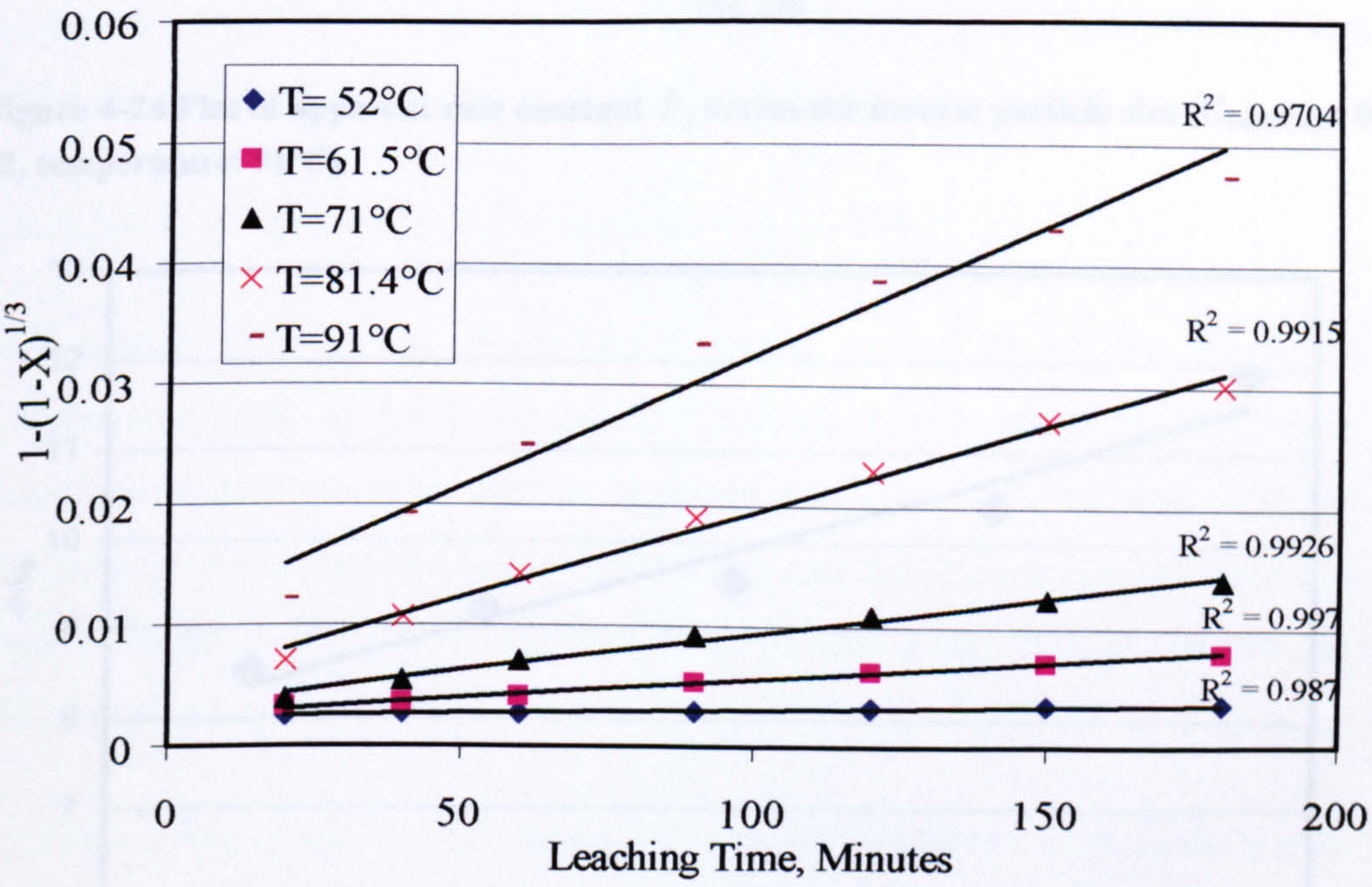

Figure 4-23 Plot fitted using a shrinking core model with a limiting step of surface reaction: conversion vs. time data in Figure 4-15 at various temperatures

The regression analysis of the data presented in Figure 4-23 yielded straight lines with correlation coefficients higher than 0.97. The apparent rate constants k_s were calculated from the slopes of the "best-fit" straight lines in Figure 4-23. An Arrhenius plot was then drawn as shown in Figure 4-25, from which the apparent activation energy of 79.5 kJ/mole was determined. This value of activation energy

is within the range of the values of activation energy value found in the literature (Table 3.1).

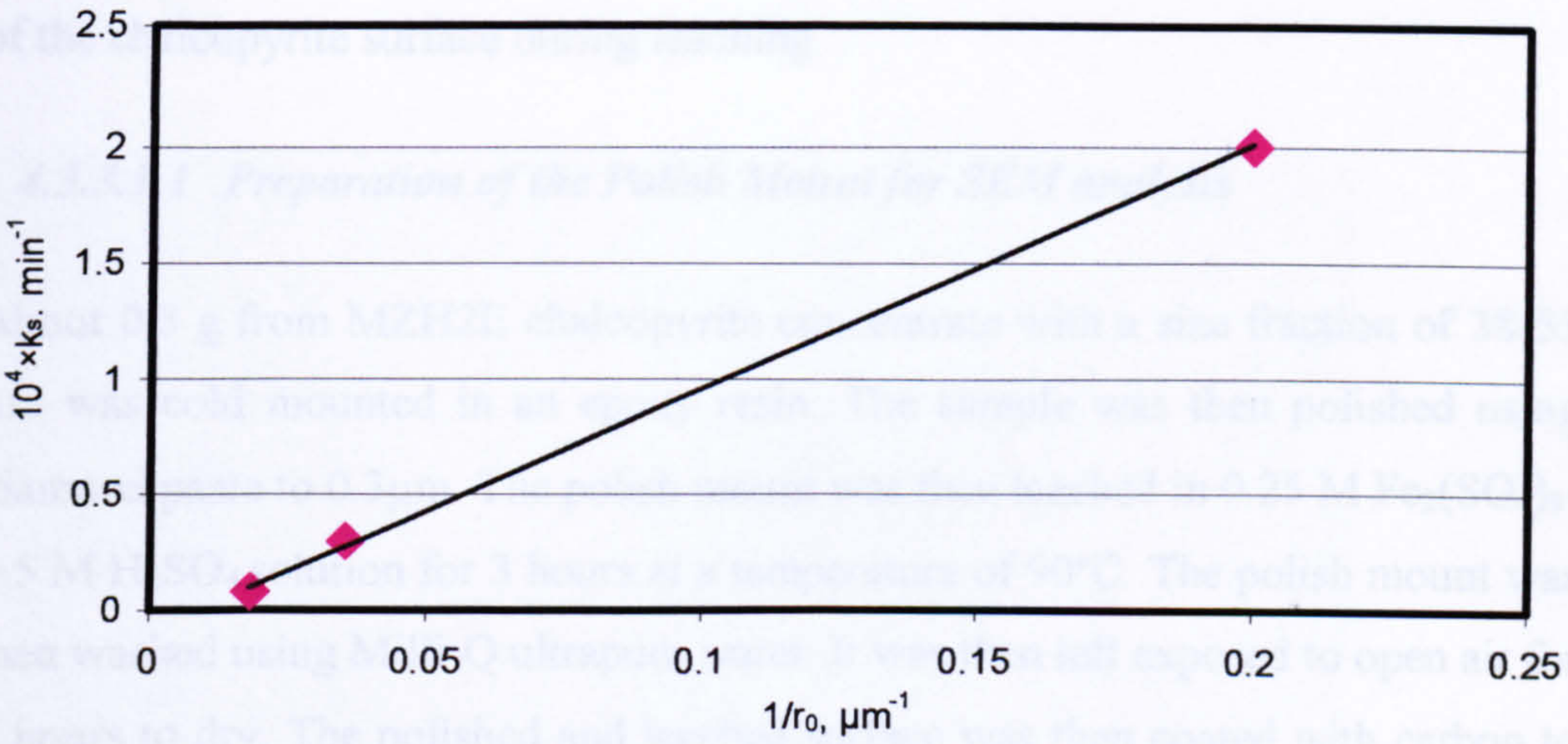

Figure 4-24 Plot of apparent rate constant k_S versus the inverse particle size ($C_{Fe2(SO4)3}$: 0.25 M, temperature: 91°C).

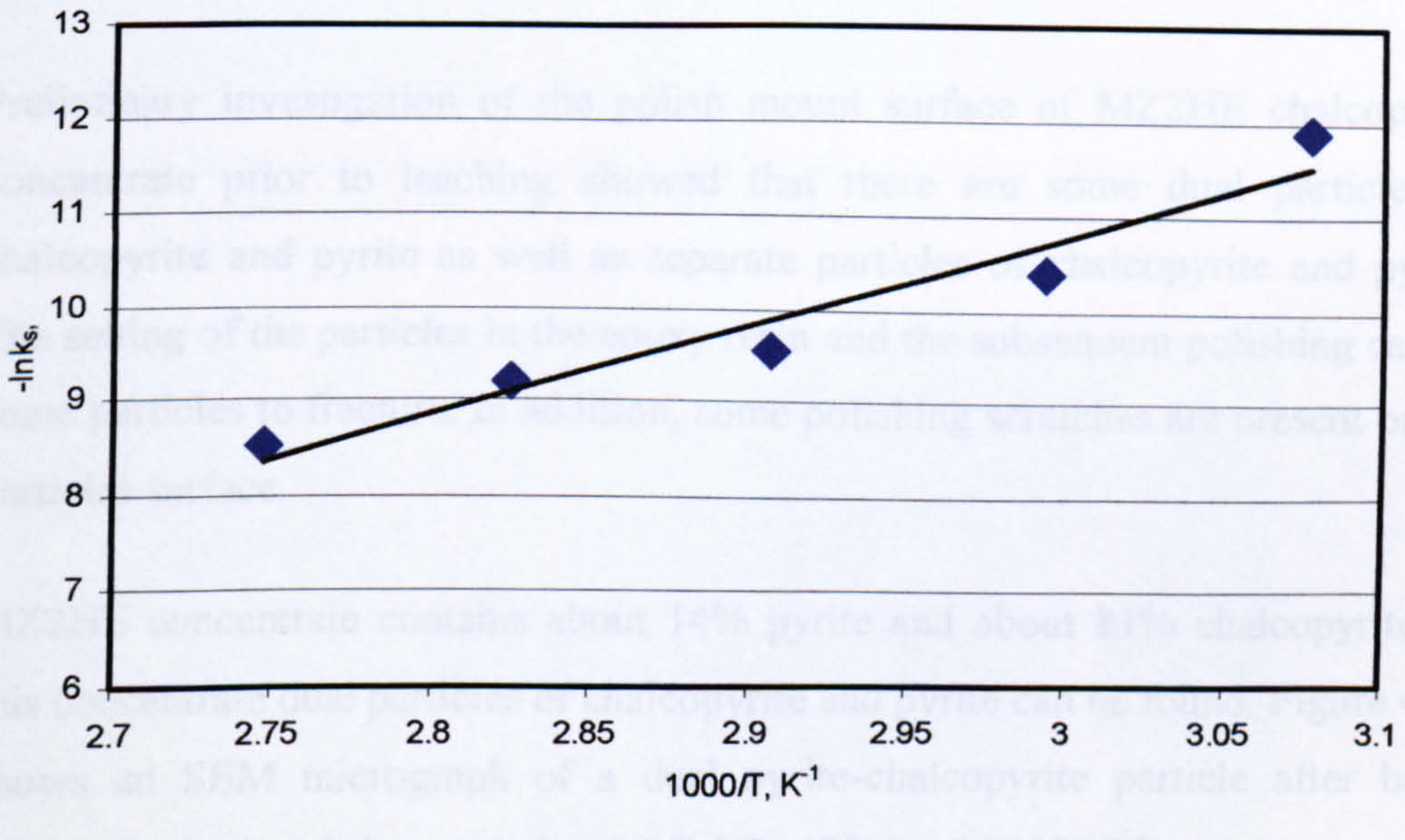

Figure 4-25 Arrhenius plot of the conventional leaching of chalcopyrite in ferric sulphate based on the apparent rate constants calculated from Figure 4-23.

4.3.3 Scanning Electron Microscopy Investigation of MZ2HE Chalcopyrite

Scanning Electron Microscope (SEM) analysis was carried out on MZ2HE chalcopyrite concentrate to provide further information to assist the understanding

of the mechanism of chalcopyrite leaching in ferric sulphate. It was shown in Chapter 3 (Section 3.3.1) that the mechanism of chalcopyrite leaching in ferric ion media is not fully understood and in particular the reason behind the passivation of the chalcopyrite surface during leaching.

4.3.3.1.1 Preparation of the Polish Mount for SEM analysis

About 0.3 g from MZH2E chalcopyrite concentrate with a size fraction of 38-53 μm was cold mounted in an epoxy resin. The sample was then polished using diamond paste to 0.3μm. The polish mount was then leached in 0.25 M $Fe_2(SO_4)_3$-0.5 M H_2SO_4 solution for 3 hours at a temperature of 90°C. The polish mount was then washed using Milli-Q ultrapure water. It was then left exposed to open air for 2 hours to dry. The polished and leached surface was then coated with carbon to make the surface conductive and ready for SEM analysis.

4.3.3.1.2 Results of SEM Investigation on MZ2HE

Preliminary investigation of the polish mount surface of MZ2HE chalcopyrite concentrate prior to leaching showed that there are some dual particles of chalcopyrite and pyrite as well as separate particles of chalcopyrite and pyrite. The setting of the particles in the epoxy resin and the subsequent polishing caused some particles to fracture. In addition, some polishing scratches are present on the particles surface.

MZ2HE concentrate contains about 14% pyrite and about 81% chalcopyrite. In this concentrate dual particles of chalcopyrite and pyrite can be found. Figure 4-26 shows an SEM micrograph of a dual pyrite-chalcopyrite particle after being leached in ferric sulphate solution 0.25M $Fe_2(SO_4)_3$ -0.5M H_2SO_4 at a temperature of 90°C for three hours. Chalcopyrite (middle of the micrograph) is shown to be heavily attacked compared to pyrite.

However, chalcopyrite particles which are not in contact with pyrite are shown to be unattacked as illustrated in Figure 4-27 . The polish scratches can still be seen on the chalcopyrite particle surface. Again this experiment shows preferential

oxidation of chalcopyrite surface, but in this case chalcopyrite is preferentially attacked when it is in contact with pyrite. It is possible here that chalcopyrite and pyrite form a galvanic pair where chalcopyrite acts as an anode and pyrite acts as a cathode.

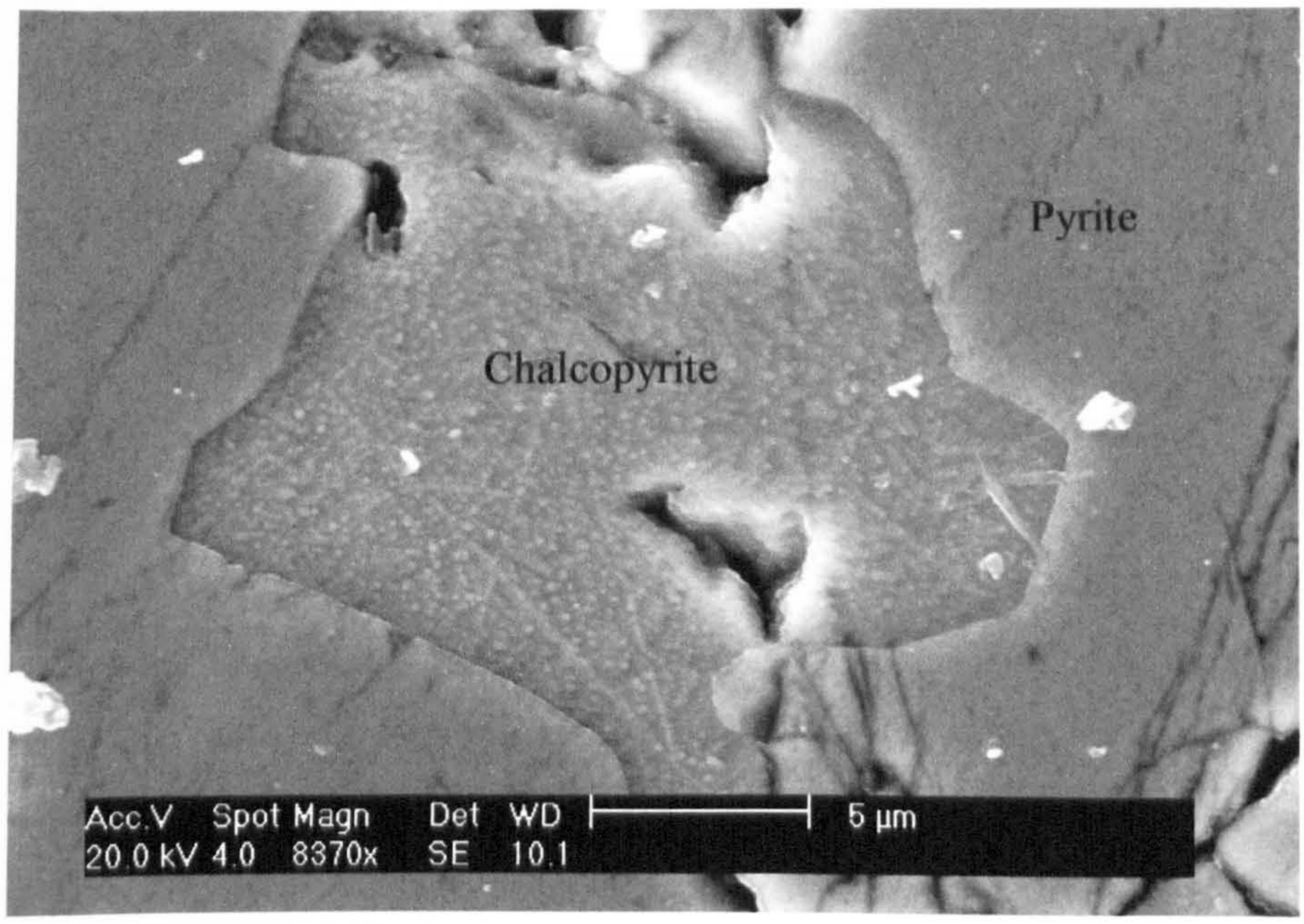

Figure 4-26 Secondary electron image of a polished composite chalcopyrite-pyrite particle after being leached in 0.25M Fe2(SO4)3 -0.5M H2SO4 at a temperature of 90°C for 3hrs. Note attacked chalcopyrite

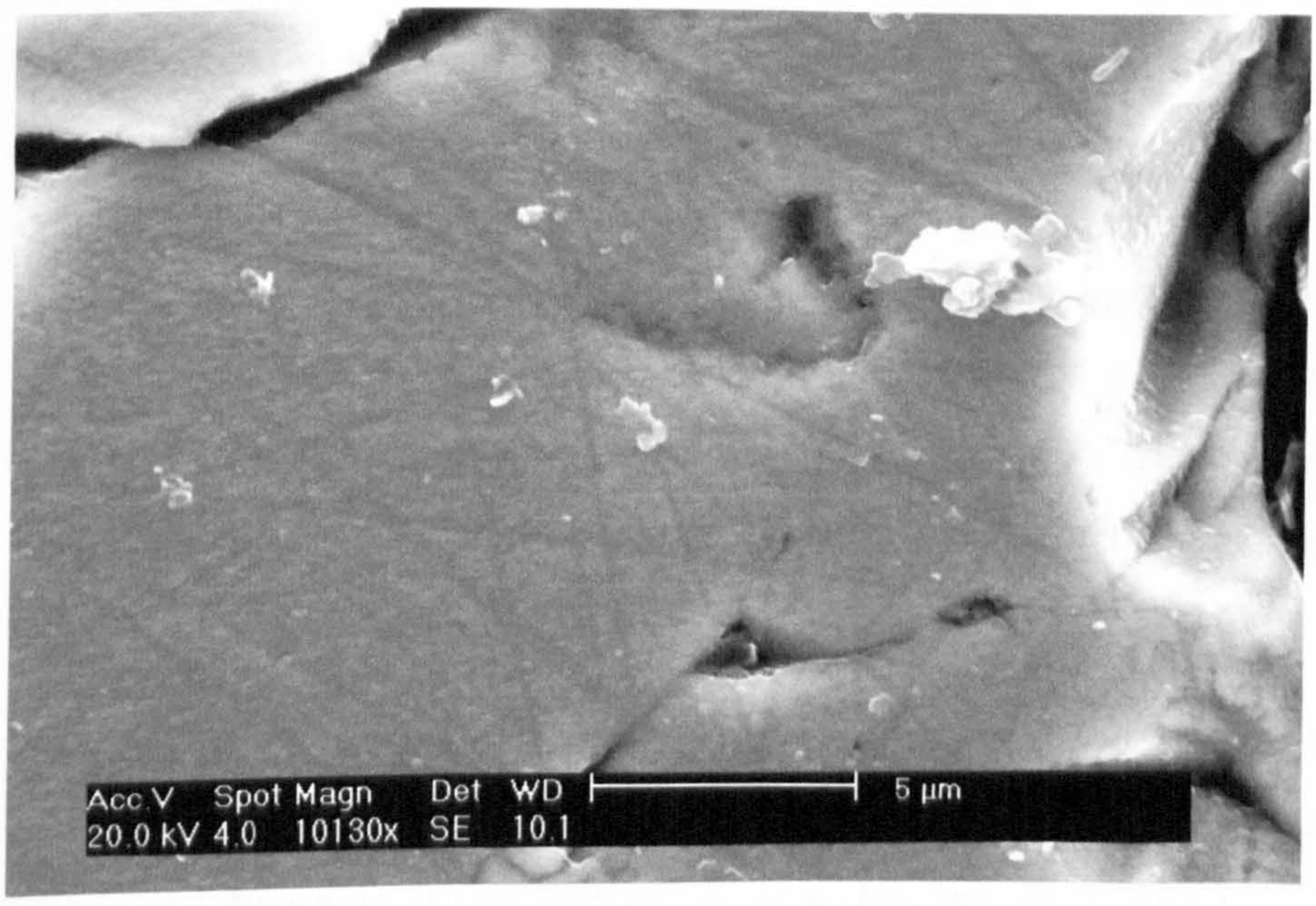

Figure 4-27 Secondary electron image of a polished separate chalcopyrite particle after being leached in 0.25M Fe2(SO4)3 -0.5M H2SO4 at a temperature of 90°C for 3hrs.

4.3.4 ToF-SIMS Surface Analysis Study

4.3.4.1 Materials and Method

A surface analysis study upon GBL chalcopyrite was performed with an ION-ToF IV ToF-SIMS (Time of Flight Secondary Ion Mass Spectrometry) instrument equipped with a gallium liquid metal ion gun. An introduction to the ToF-SIMS technique was given in Section 4.3.4.5. The instrument is shown in Figure 4-12. Mass spectra and chemical maps were generated from the raw data using IonSpec-IonImage® V.4 software supplied by ION ToF GmbH, Munster.

At first attempts were made to examine ground chalcopyrite particles similar to those used for the SEM study (in Sections 4.3.6.6 and 4.3.7). The particles were mounted on an indium foil, however, the signal to noise ratio per particle was low. Therefore larger particles (75-106μm) were analysed, the signal to noise in this case improved slightly. However, when the samples where leached and analysed again, they were found to be heavily contaminated with hydrocarbons. The sources of hydrocarbons were probably the vacuum pump used for solid liquid separation and the atmosphere in the laboratory.

To avoid any possible contamination and to improve the signal to noise level a freshly prepared chalcopyrite sample was used for further ToF-SIMS analysis. The chalcopyrite sample was prepared by fracturing a piece of GBL chalcopyrite crystal sample (~5mm) using a carefully cleaned pestle and mortar. The freshly fractured particle was mounted and transferred to the ToF-SIMS chamber for analysis immediately after breakage. When the required vacuum was achieved ($<10^{-7}$mbar), the sample surface was bombarded with a primary ion beam produced using a gallium gun with an AC current of 1.5 pA and voltage 25 kV to analyse an area of 500×500 μm^2.

After the sample was analysed, it was removed from the chamber and the position of the sample within the sample holder was carefully recorded by photographic means and diagrams. It was then subjected to leaching in 0.25 M $Fe_2(SO_4)_3$-0.5 M H_2SO_4 at a temperature of 90°C for 3hrs. The sample was then carefully removed

from the solution and washed several times with Milli-Q ultrapure water and left to air dry for about 30 minutes. The sample was then mounted in exactly the same position as before leaching using the recorded photographs and diagrams. It was then loaded into ToF-SIMS chamber for analysis

4.3.4.2 Analysis of the Freshly Cleaved Chalcopyrite Surface

Images were acquired from a number of locations on the sample surface in order to identify any differences on the chalcopyrite surfaces. The analysed areas included two distinctly different sites as gained from $C_3H_5^-$ maps (see Figure 4-28 and Appendix 4-16). Spectra were then generated from the raw dataset recorded during image acquisition from the two regions of interest. Two types of area were identified on the freshly fractured chalcopyrite surface, each site seeming to have distinctly different reactivity. One picked up significant amount of hydrocarbons (HC) from the air. This is expected normally to find on the surfaces exposed to the open atmosphere. This area was found to be rich in HCs and oxidized species (mainly oxy-sulphur species). Surprisingly, the other area resembled what might be expected from a pure chalcopyrite surface. The intensity of HC signals in this area was very weak. Figure 4-28 shows a comparison of the positive spectra of these two types of areas. The bottom spectrum (pane B) predominantly shows peaks associated with Cu and Fe whereas, pane A (Figure 4-28) shows several HC peaks as well as peaks for Cu and Fe. The normalized intensities of the ions to the total intensity shows very high contribution of the Fe and Cu (see Figure 4-29). A lower contribution of Fe and Cu to the total ion signal compared to the area of low HC is observed as shown in Figure 4-29.

Several normalizations were carried out during data analysis process, including to the total counts, to the total corrected intensity of ions having more than 100 counts and single ion intensities (Fe^+, S^-). All normalizations essentially showed similar trends. The negative spectrum of the areas with low and high HC contamination is shown in Table 4-30. The contribution of O^-, S^- and HS^- to the total signal on the surface with a low HC content is higher than that of high HC area (see Figure 4-31). When the intensity of the negative species of the areas with

high HC content was normalized to the total corrected intensity and compared to that of the areas with low HCs, a significant increase in the amount of oxidized species (SO_x and FeO_x) and S_n species was found (Figure 4-32). The ratio of negative species like O^-, S^-, HS^-, Cl^- and F^- was very close to unity suggesting similar relative availability of these species in the both areas. However, the ratio of oxidized sulphur species like S_n^-, MS_n^- and SO_n^- was up to 7 times higher in the areas with high HC content. This is indicative of superior oxidation and higher reactivity of those sites with high HC content after being exposed to air. Further evidence of the superior oxidation was obtained when the sum of the intensity of $S_n^- + MS_n^-$ and SO_n^- species found on the spectra of both kind of areas were compared (Table 4-13). The total normalized signals of $\sum S_n^- + HS_n^-$ species are generally the same for both kinds of surfaces. However, the signals of $\sum SO_n^-$ and $\sum MS_n^-$ obtained from the HC regions are about 2.6 and 3 times higher than the one obtained from the area with low HC content respectively.

Table 4-13 Comparison of low and high HC areas in terms of S_n^- and SO_n^- on the chalcopyrite surface before treatment

Species	High HC area	Low HC area	Ratio
	CI/Cl_{total}, %		
$\sum S_n^- + HS_n^-$	20.9	21.2	.99
$\sum SO_n^-$	12.44	4.85	2.57
$\sum MS_n^-$	0.54	0.18	3.00
$\frac{\sum S_n^-}{\sum SO_n^-}$	1.7	4.4	0.39

The concentration maps of negative and positive signal are attached in Appendices 4-16. The brighter the area on the map for the particular species the higher is the concentration of that species in that particular area.

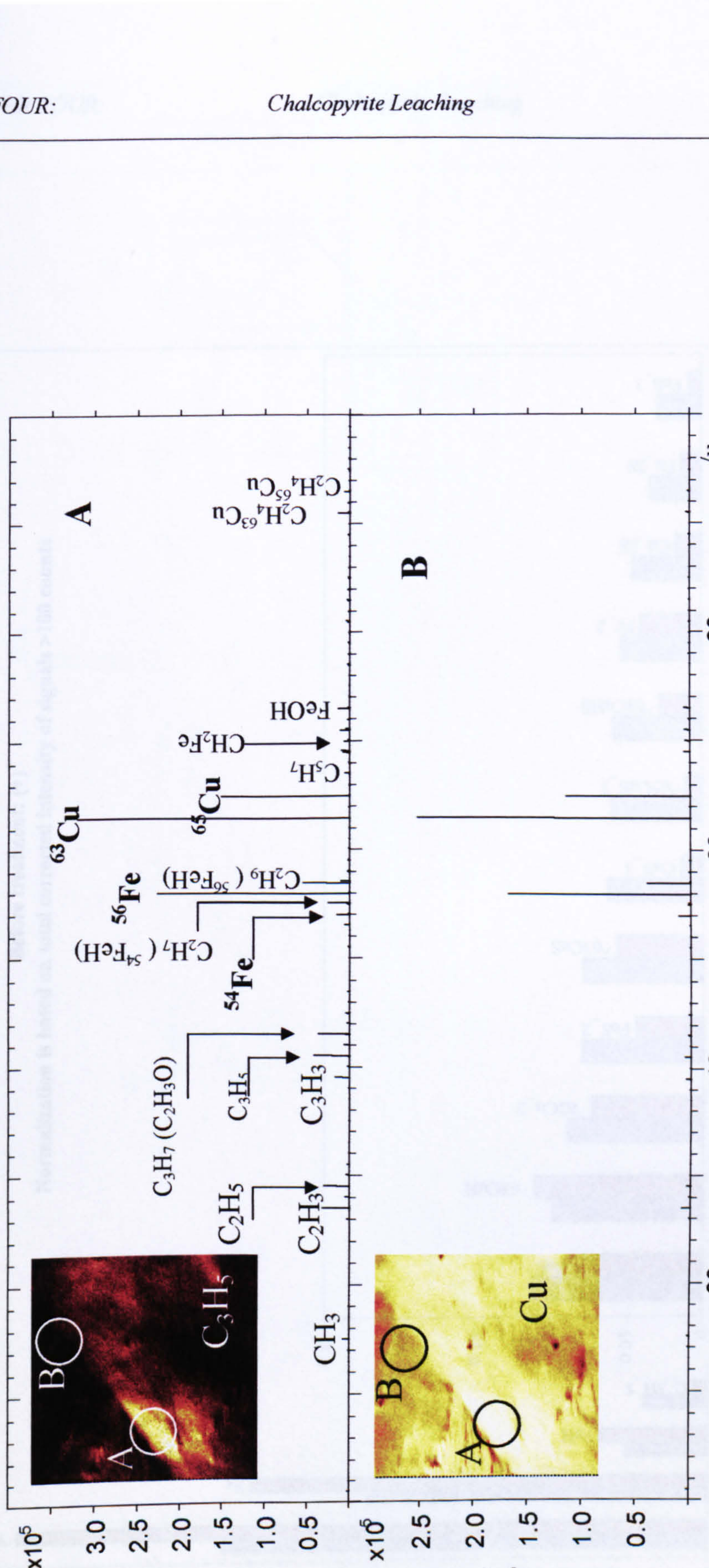

Figure 4-28 Positive spectra of a freshly fractured chalcopyrite surface obtained from areas with (A) high and (B) low levels of HCs. Peak identifiers in brackets denote minor components

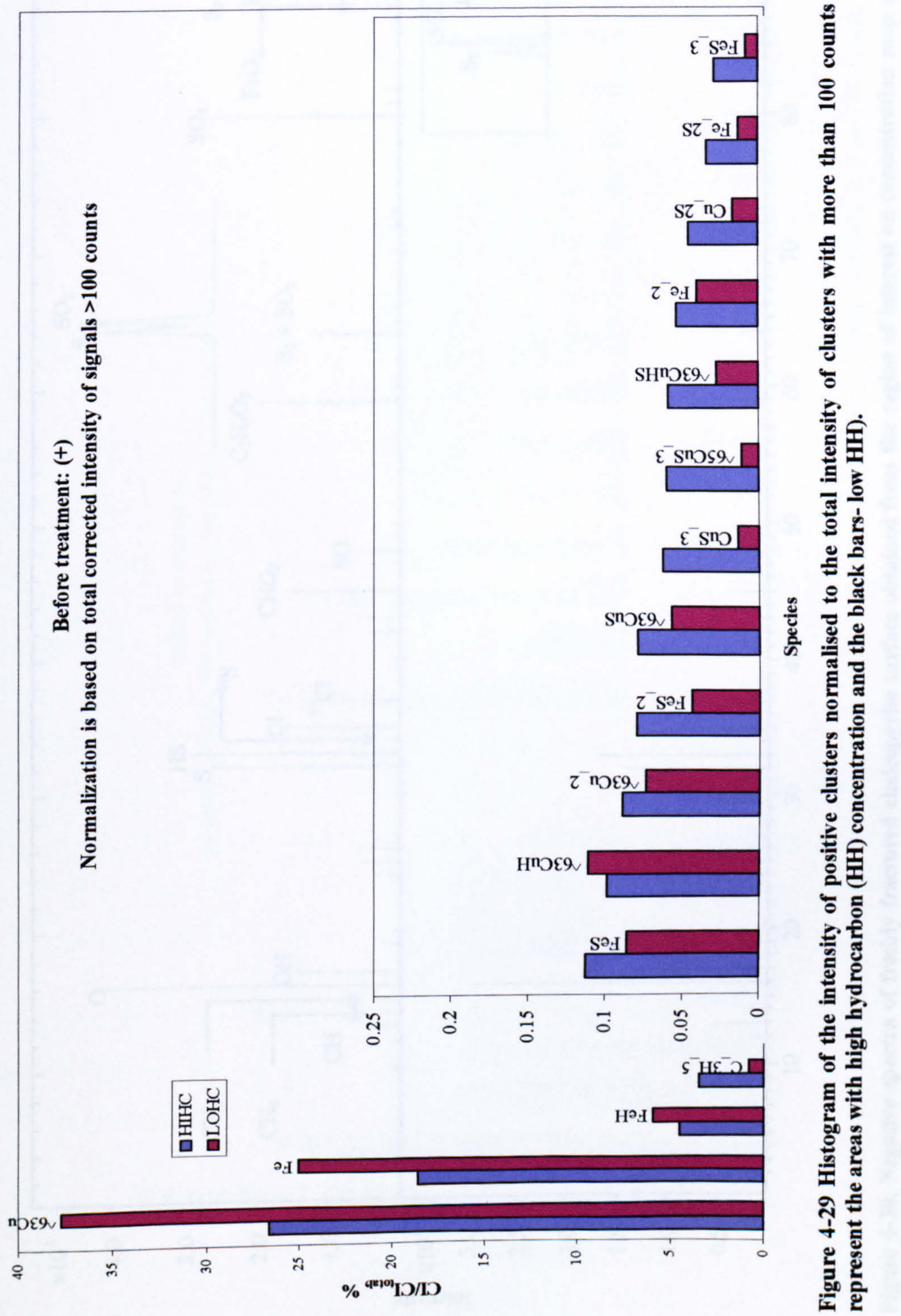

Figure 4-29 Histogram of the intensity of positive clusters normalised to the total intensity of clusters with more than 100 counts (blue bars represent the areas with high hydrocarbon (HH) concentration and the black bars- low HH).

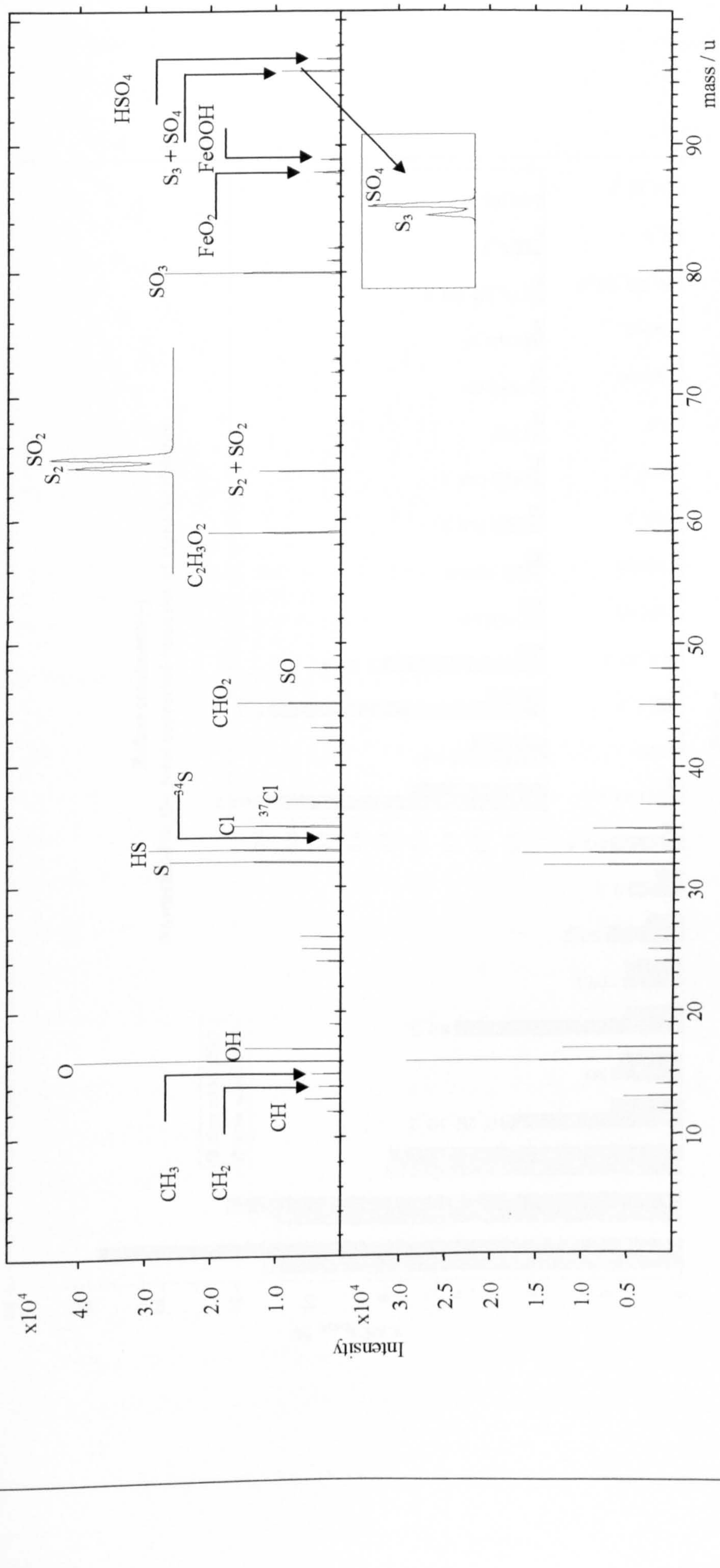

Figure 4-30. Negative spectra of freshly fractured chalcopyrite surface obtained from the region of interest on concentration map (A- an area with high concentration of HCs, B-an area low in HCs)

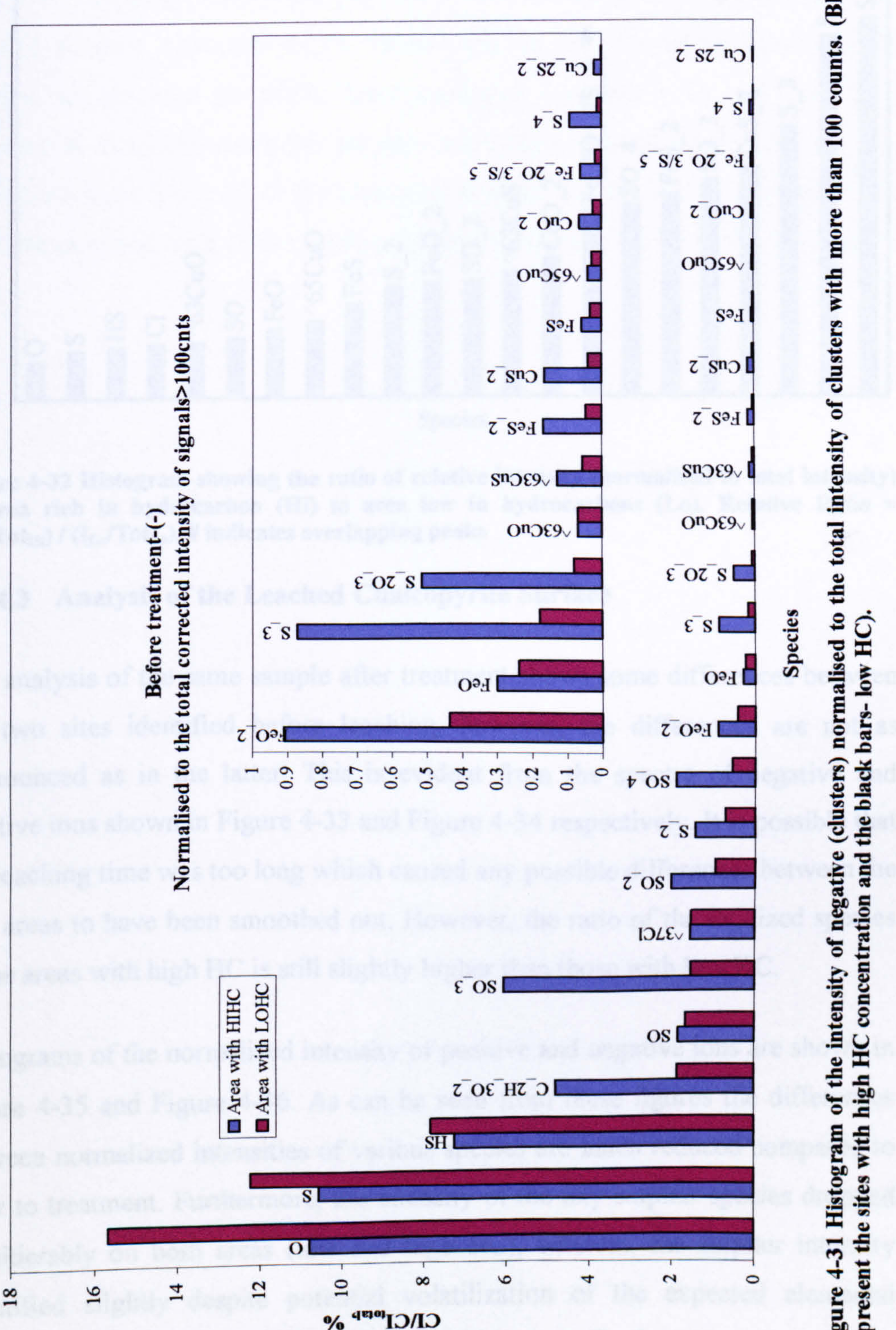

Figure 4-31 Histogram of the intensity of negative (clusters) normalised to the total intensity of clusters with more than 100 counts. (Blue bars represent the sites with high HC concentration and the black bars- low HC).

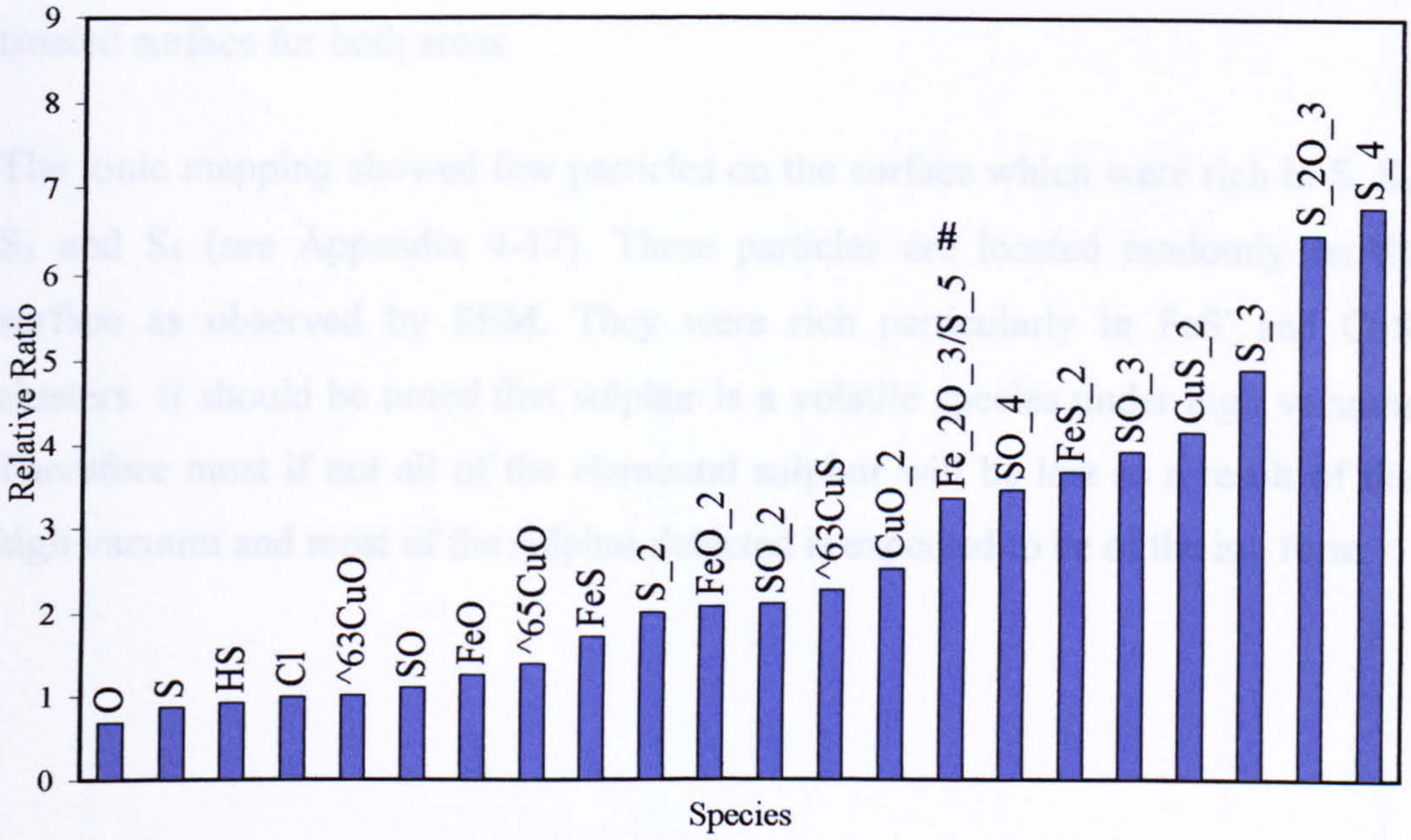

Figure 4-32 Histogram showing the ratio of relative intensity (normalised to total intensity) of area rich in hydrocarbon (Hi) to area low in hydrocarbons (Lo). Relative Ratio = $(I_{Hi}/Tot_{Hi}) / (I_{Lo}/Tot_{Lo})$. # indicates overlapping peaks

4.3.4.3 Analysis of the Leached Chalcopyrite Surface

The analysis of the same sample after treatment shows some differences between the two sites identified before leaching, however, the differences are not as pronounced as in the latter. This is evident from the spectra of negative and positive ions shown in Figure 4-33 and Figure 4-34 respectively. It is possible that the leaching time was too long which caused any possible differences between the two areas to have been smoothed out. However, the ratio of the oxidized species in the areas with high HC is still slightly higher than those with low HC.

Histograms of the normalized intensity of positive and negative ions are shown in Figure 4-35 and Figure 4-36. As can be seen from these figures the differences between normalized intensities of various species are much reduced compared to prior to treatment. Furthermore, the intensity of the oxy-sulphur species dropped considerably on both areas (low and high HC), whereas, the sulphur intensity magnified slightly despite potential volatilization of the expected elemental sulphur on the surface after three hours leaching time. Furthermore, it was found that the normalized intensity of S_n^- is essentially the same for the two surfaces

before and after treatment, whereas, SO_n^- almost disappeared in the spectra of the treated surface for both areas.

The ionic mapping showed few particles on the surface which were rich in S, S_2, S_3 and S_4 (see Appendix 4-17). These particles are located randomly on the surface as observed by SEM. They were rich particularly in FeS^- and CuS^- clusters. It should be noted that sulphur is a volatile species under high vacuum. Therefore most if not all of the elemental sulphur will be lost as a result of this high vacuum and most of the sulphur detected is expected to be of the ion form.

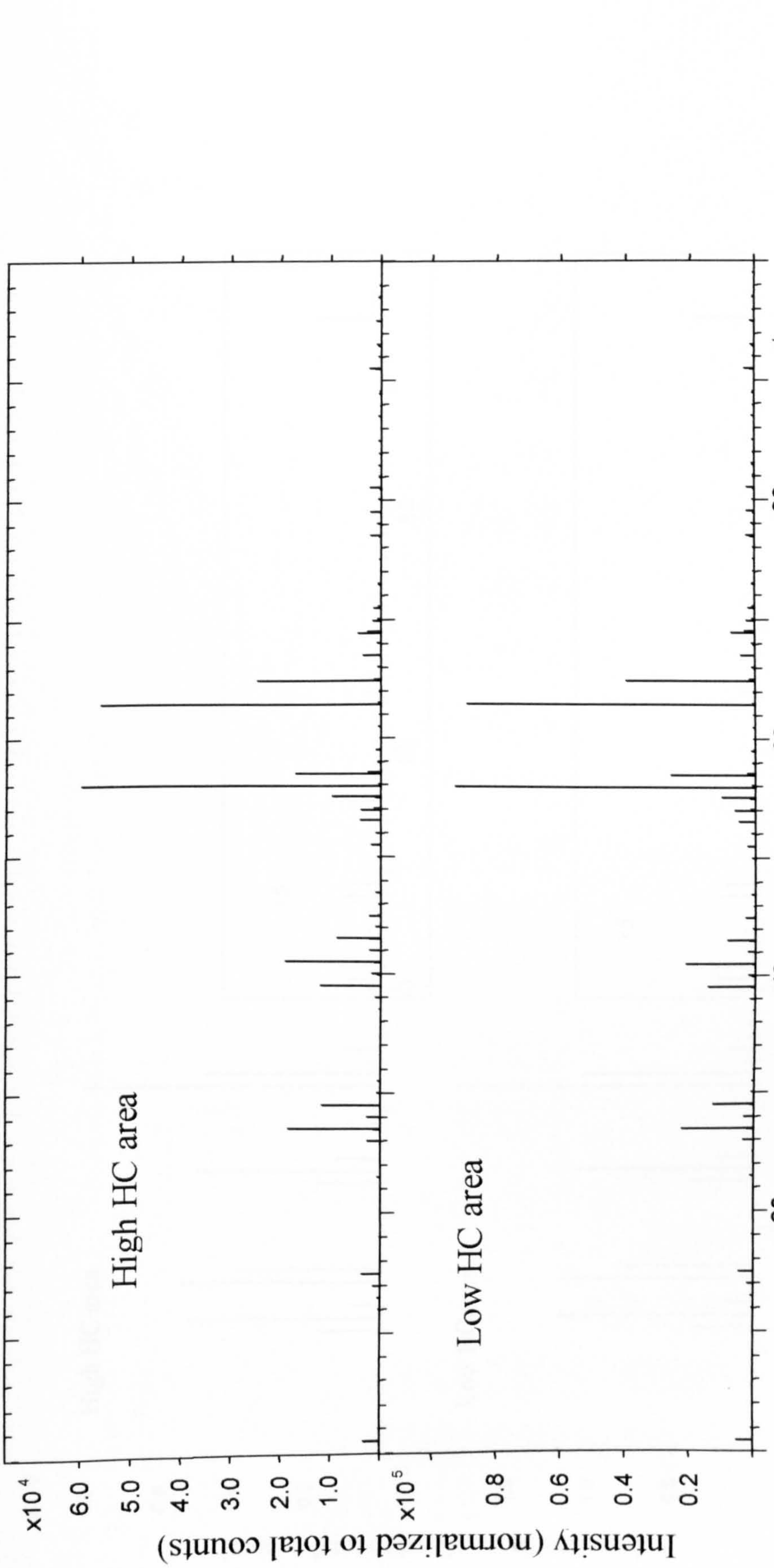

Figure 4-33 ToF-SIMS positive spectra obtained from the surface of chalcopyrite after being leached in 0.25 M $Fe_2(SO_4)_3$-0.5 M H_2SO_4 for 3 hours at a temperature of 90°C.

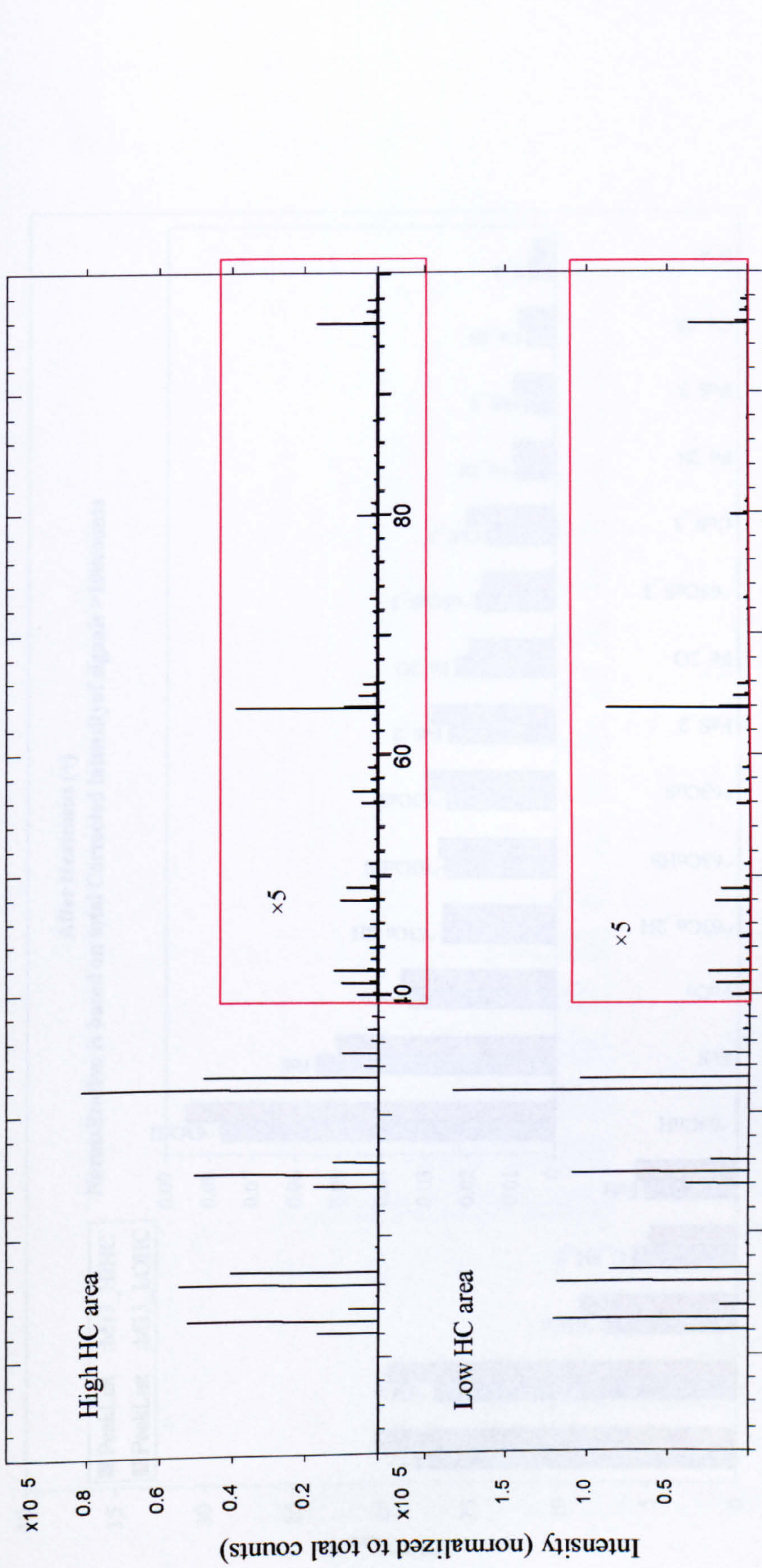

Figure 4-34 ToF-SIMS negative spectra obtained from the surface of chalcopyrite after being leached in 0.25 M $Fe_2(SO_4)_3$-0.5 M H_2SO_4 for 3 hours at a temperature of 90 (note that the signal intensity was multiplied by 5 after mass 40m/u)

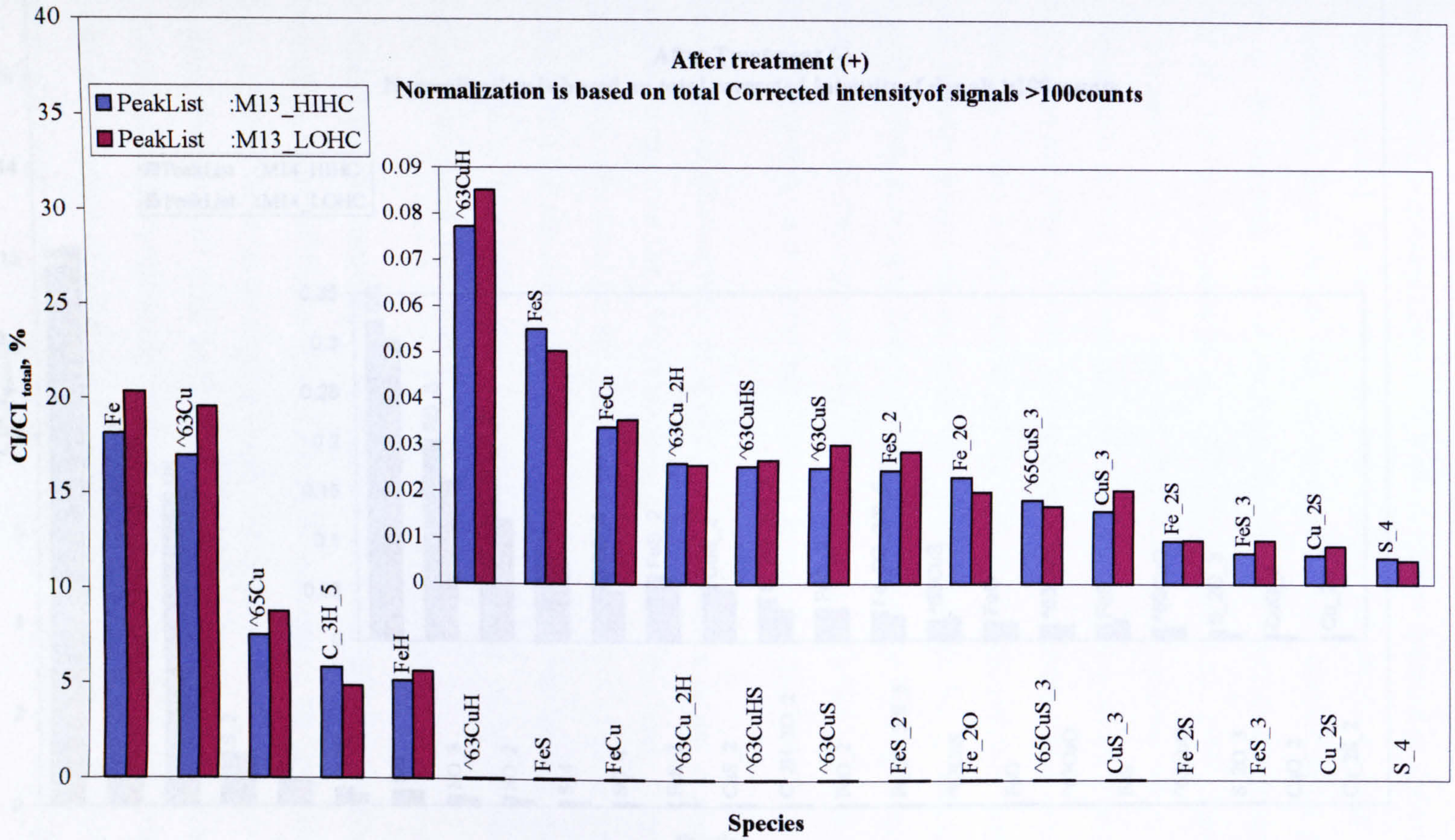

Figure 4-35 Histogram of the intensity of positive ions normalised to the total intensity of more than 100 counts. (Blue bars represent the sites with high HC concentration and the black bars- low HC). (After leaching).

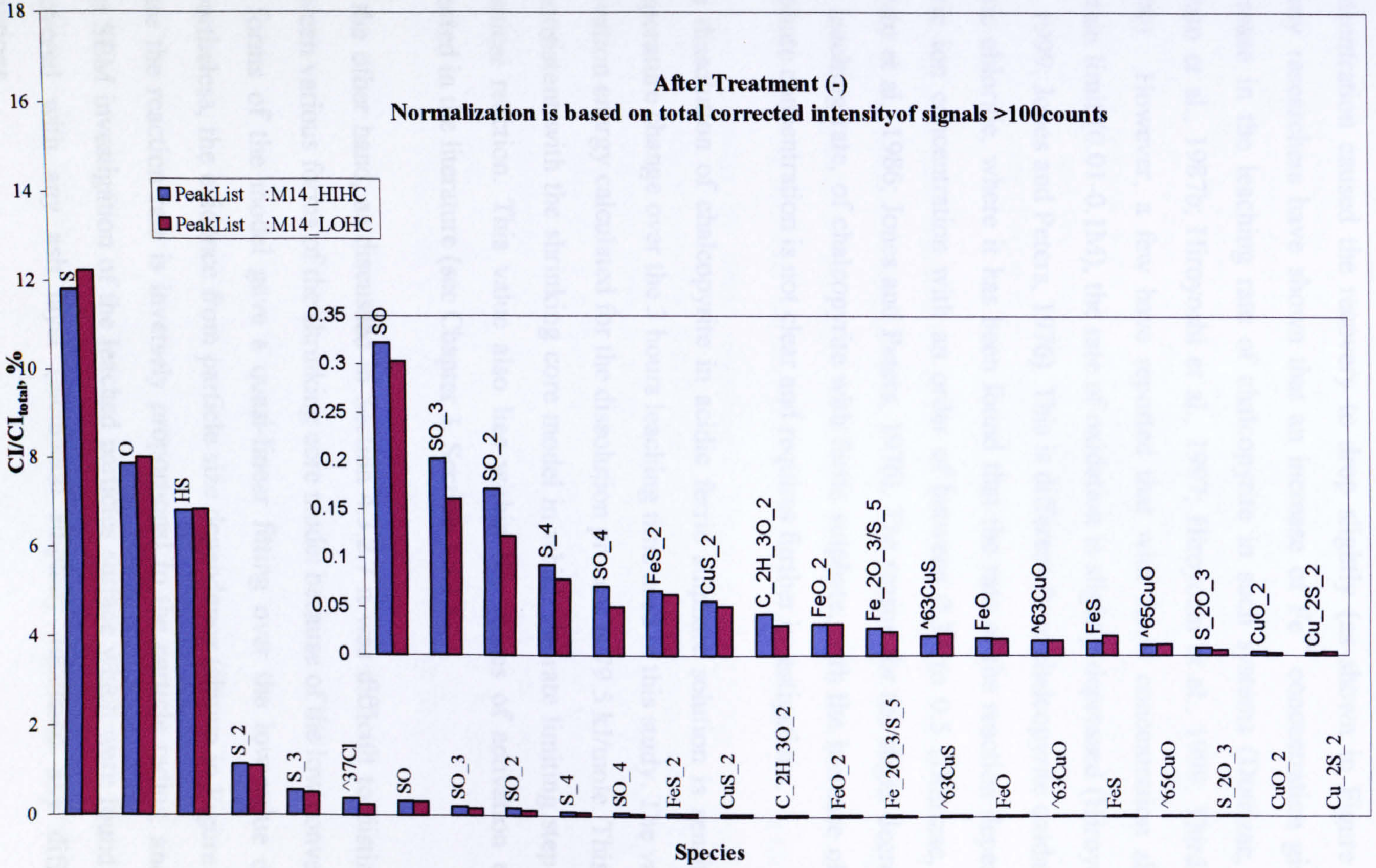

Figure 4-36 Histogram of the intensity of negative ions normalised to the total intensity of clusters with more than 100 counts (blue bars represent the sites with high HC concentration and the black bars- low HC). (After leaching)

4.3.5 Discussion

The experimental results in Section 4.3.2.1 show that the recovery of copper from chalcopyrite when it was leached in ferric sulphate is dependant on ferric sulphate concentration until a concentration of 0.1 M. A further increase in ferric sulphate concentration caused the recovery to drop slightly (as shown in Figure 4-14). Many researchers have shown that an increase of Fe^{3+} concentration gives no increase in the leaching rate of chalcopyrite in such systems (Dutrizac, 1981; Hirato et al., 1987b; Hiroyoshi et al., 1997; Hiroyoshi et al., 1999; Third et al., 2000) . However, a few have reported that with ferric concentration above a certain limit (0.01-0.1M), the rate of oxidation is slightly depressed (Hiroyoshi et al., 1999; Jones and Peters, 1976). This is different from chalcopyrite oxidation in ferric chloride, where it has been found that the rate of the reaction depends on ferric ion concentration with an order of between 0.37 to 0.5 (Dutrizac, 1981; Hirato et al., 1986; Jones and Peters, 1976). The reason for the slight decrease in the leaching rate, of chalcopyrite with ferric sulphate, with the increase of ferric sulphate concentration is not clear and requires further investigations.

The dissolution of chalcopyrite in acidic ferric sulphate solution is sensitive to temperature change over the 3 hours leaching time used in this study. The value of activation energy calculated for the dissolution process is 79.5 kJ/mole. This value is consistent with the shrinking core model in which the rate limiting step is the chemical reaction. This value also lies within the values of activation energy reported in the literature (see Chapter 3, Section 3.3.1.8).

On the other hand, as discussed in Section 4.3.2.7 it was difficult to distinguish between various forms of the shrinking core model because of the low conversion. All forms of the model gave a quasi-linear fitting over the low value of X. Nevertheless, the evidence from particle size dependence (shown in Figure 4-24) where the reaction rate is inversely proportional to the particle radius, and also from SEM investigation of the leached particles surface which were found to be uncovered with any ash layer (elemental sulphur) dismissed any diffusion limitations.

Besides, the copper recovery from chalcopyrite when leached in ferric sulphate at a temperature of 90°C for 3 hours is very low. As shown in Figures 4-19 to 4-22 the sulphur formed on the chalcopyrite particle surface covers specific and limited areas of some particles or probably some specific planes, whereas other parts of the surface seems to be not attacked. This suggests that sulphur formation or deposition is not the reason behind the slow reaction kinetics, especially, at the early stages of leaching. Furthermore, the idea that sulphur formation retards the reaction rate, as discussed in Chapter 3, does not explain the following points: a layer of sulphur is formed in all other copper sulphide minerals, however, only chalcopyrite suffers from such slow reaction kinetics; the rate of diffusion of Fe^{3+} through the sulphur layer is four times higher than chalcopyrite dissolution (Linge, 1976); and the removal of sulphur in the course of reaction does not affect reaction rate (Parker et al., 1981a).

Furthermore a close examination of the SEM micrographs, shown in Figure 4-21 where the particles were leached for 10 hours at a temperature of 90°C, suggests a preferential attack at particular fracture planes on the same particle. The heterogeneity of minerals surface chemistry was observed during flotation of sulphide minerals by other researchers. Duan et al. (2003) observed large differences in the amount and distribution of dialkyl dithiophosphate (DTP) on the surface of chalcopyrite particles when they were examined by ToF-SIMS. These workers also observed a difference in surface chemistry between three size fractions of chalcopyrite (<10, 20-30 and >50μm). This was similar to previous work of Boulton et al.(2003) where large differences in the amount and distribution of collectors (Potassium Isobutyl Xanthate (KIBX)) on pyrite and galena surfaces were observed. Similar phenomena were also observed by Piantadosi et al (Piantadosi et al., 2000). They observed large differences in collector adsorption for both Isobutyl Xanthate (IBX) and Diisobutyl Dithiophosphinate (DBPhos) between different faces of galena particles. It was also found that there was a large variation in collector concentration on different particles from the same size fraction. The non-uniform distribution of flotation reagents on the surface of sulphide minerals was attributed to mineral surface

heterogeneity arising from defects, impurities, lattice imperfections and small variations in stoichiometry (Piantadosi and Smart, 2002).

In the light of the above observations, the influence of surface heterogeneity upon the reactivity of chalcopyrite surfaces was examined further in this study. The results of the SEM study on MZ2HE concentrate leached in ferric sulphate (Section 4.3.3) shows a pronounced enhancement on the reactivity of chalcopyrite when it has electrical contact with pyrite. This phenomenon was observed previously ((Berry et al., 1978; Mehta and Murr, 1983; Murr and Mehta, 1982; Murr and Mehta, 1983). The enhanced reactivity of chalcopyrite when it is in an electrical contact with pyrite is due to the galvanic interaction between the two minerals. Mehta (1983) reported that the rest potentials of pyrite and chalcopyrite in 1 M H_2SO_4 solution are 0.63 and 0.52 V respectively. That is to say that the chalcopyrite acts as an anode where it corrodes faster than pyrite which is acting as a cathode. However, when pyrite did not have contact with chalcopyrite it corroded faster than chalcopyrite (see Appendix 4-18). It is suggested that a semiconductor with a higher rest potential will provide cathodic sites on the chalcopyrite surface.

With reference to the nature of the sulphur formed on chalcopyrite (as discussed in Section 4.3.2.6) one can notice preferential attack on particular planes as shown in Figures 4.20 & 4-21. Some facets are seen to have sulphur formed or deposited, whereas, other planes (as shown in Figure 4-22) are heavily attacked but with no signs of sulphur formation or deposition on the surface. This is quite interesting and could be caused by different reactions occurring on different chalcopyrite surface facets.

Additionally, on the basis of the ToF-SIMS results of the freshly fractured GBL chalcopyrite, it was found that various sites have different reactivities in terms of the amount of hydrocarbon absorbed on the surface and the relative amount of oxidized species. The difference in reactivity of various sites on the chalcopyrite surface as well as other sulphide minerals could be related to the chemistry of different cleavage planes.

Chalcopyrite has a tetragonal structure with lattice parameters: a=5.289 and c= 10.423 and a space group of $I\bar{4}2d$ (Hall and Stewart, 1973). A schematic of the chalcopyrite unit cell is shown on Figure 4-37. Chalcopyrite is known to be brittle and preferentially displays conchoidal fracture. Shukri and Champness (1997) studied the structure of $CuInSe_2$ which has distinct similarities with $CuFeS_2$. These workers found that the main cleavage planes are {101}, {112} and less frequently a plane of {110}. They found that the plane {110} does in fact consist of ridges in the direction of <110> where the micro planes on either side of the ridges were {112} planes. Analogously it is reasonable to assume that the main cleavage planes in chalcopyrite are {101} , {112} and less frequently {110} .

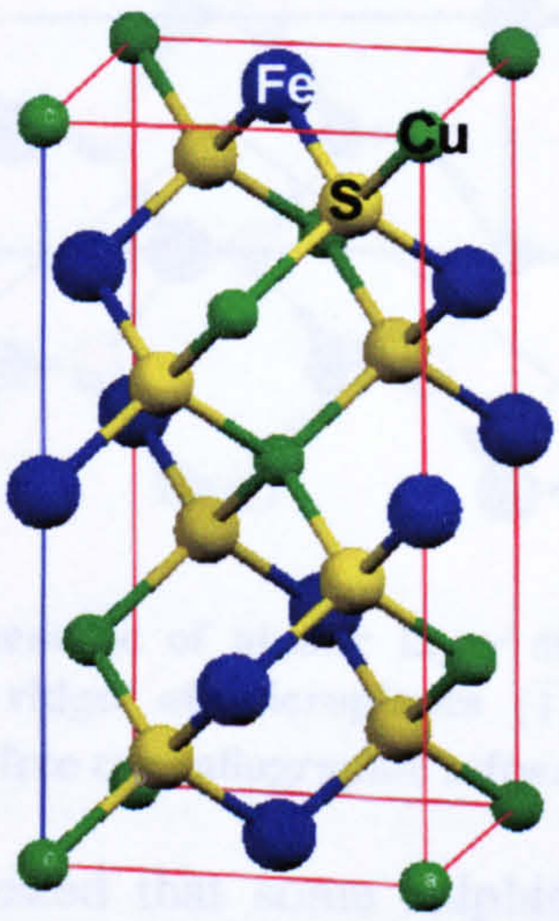

Figure 4-37 Schematic of chalcopyrite crystal structure: (sulphur-yellow, iron-blue, copper-green) (the structure is generated using crystallographic software Mercury® v1.4 and the crystallographic data was obtained from Chemical Database Service (Hall and Stewart, 1973))

Based on the observations of Shukri and Champness (1997) if chalcopyrite surface exhibit cleavage along $(\bar{1}10)$, the zigzag surface is formed from orthogonal micro planes $\{\bar{1}12\}$ and $\{1\bar{1}2\}$ as shown in Figure 4-38. The Cu-S bond in chalcopyrite $CuFeS_2$ (about 53.1 kJ/mole for a diatomic molecule) is weaker than the Fe-S bond (100 kJ/mole for a diatomic molecule). Therefore it would be energetically easier per unit area (in one unit cell) to generate zigzag cleavage plane with $\{112\}$ ridges along (110) than $\{110\}$ planes because in the first case it is

required to break only one Fe-S bonds and 3 Cu-S bonds whereas in the second case 2 Fe-S bonds 2 Cu-S bonds are required to break.

One can notice that the first layer of the micro plane $\{\bar{1}12\}$ is dominated by sulphur atoms whereas the top two layers of the micro plane $\{1\bar{1}2\}$ are dominated by alternate Cu and Fe atoms while sulphur appears on the layer below.

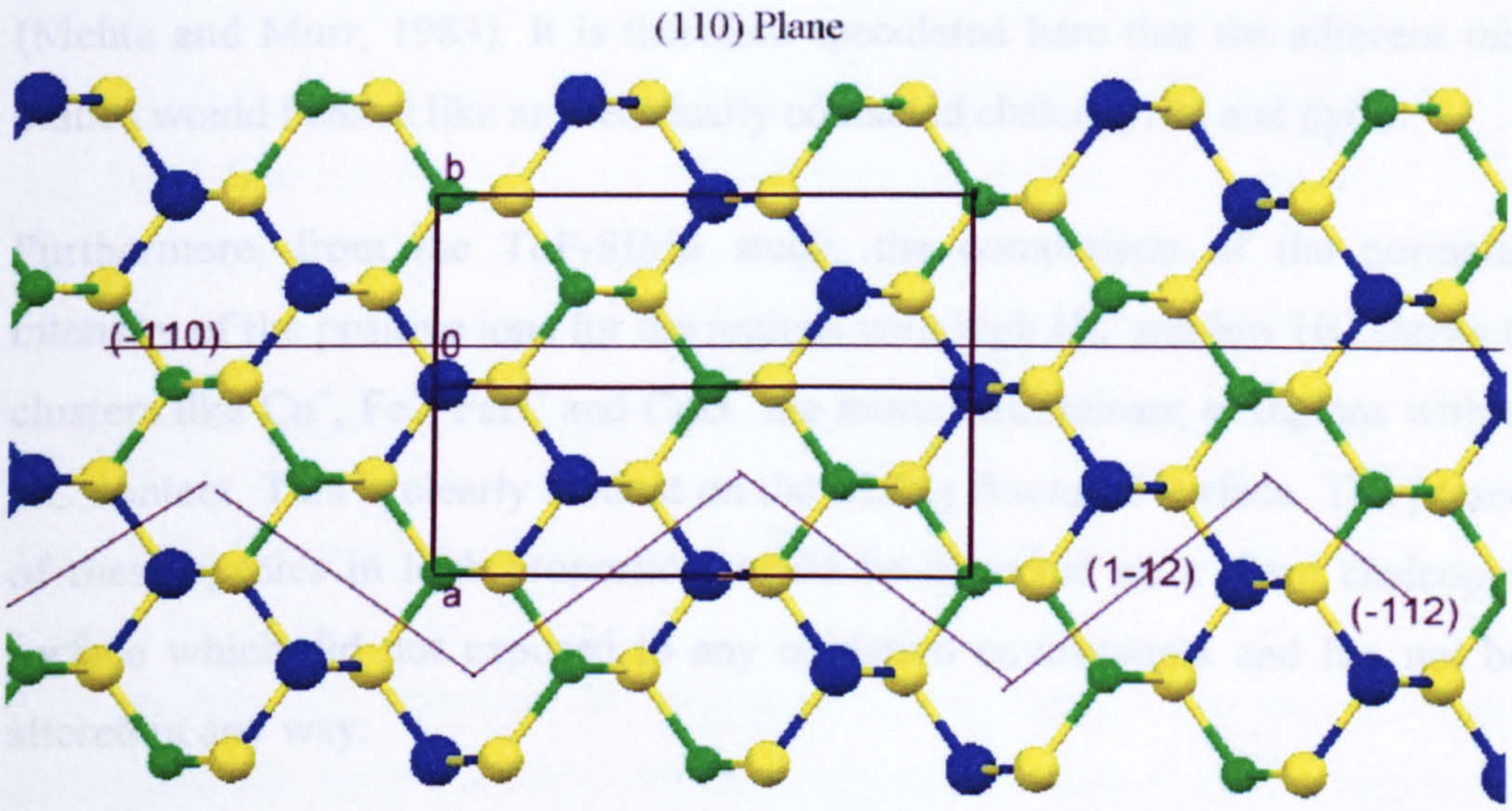

Figure 4-38 Ball and stick schematic of atomic layer of the 110 plane of chalcopyrite fractured along $\{\bar{1}10\}$ forming ridges of microplanes $\{\bar{1}12\}$ and $\{1\bar{1}2\}$. The graph was generated using Mercury® V 1 a free crystallographic software

Vaughan et al (1997) suggested that some sulphide surfaces are amenable to substantial relaxation and possibly reconstruction. The reconstruction would involve movement of electrons and possibly formation of new phases on the first atomic monolayer. Klauber (2003) proposed a surface reconstruction of freshly cleaved chalcopyrite surfaces which resulted in formation of a pyrite like structure with about 50% pyrite content. According to Klauber (2003) planes like {112} are less likely to experience this reconstruction but fracture along planes like {101}, {110} and {001} would experience the reconstruction readily.

Assuming that reconstruction would occur along plane (110) (in this case along $(\bar{1}10)$), it can be speculated that a pyrite-like structure would form on the micro planes, which have higher sulphur availability to form the S_2^{2-}. If this is the

case, the first layer on that micro plane would gain the properties of pyrite whereas, the micro plane $\{1\,\bar{1}\,2\}$ would behave like chalcopyrite.

In addition, this was shown in the experiments carried out on the polished mount when chalcopyrite and pyrite are in contact (as shown on Figure 4-26). It has been previously reported that when chalcopyrite and pyrite are in electrical contact they form a galvanic pair with chalcopyrite being corroded leaving pyrite unattacked (Mehta and Murr, 1983). It is therefore speculated here that the adjacent micro planes would behave like an electrically contacted chalcopyrite and pyrite.

Furthermore, from the ToF-SIMS study, the comparison of the normalized intensity of the positive ions for the regions with high HC and low HC shows that clusters like Cu^+, Fe^+, FeH^+ and CuH^+ are more predominant at regions with low HC content. This is clearly evident on the freshly fractured surface. The presence of these species in high proportion would be expected on a clean chalcopyrite surface which did not exposed to any oxidation environment and has not been altered in any way.

However, clusters like Fe_2O^+, CuS_2^+, Fe_2S^+, FeS_2^+, CuS^+, Cu_2S^+ and FeS_3^+ can be seen in higher proportion at sites with high HC (see Figure 4-29). These facts suggest that the later kind of surface has experienced more alteration and some oxidation. It is therefore possible to speculate that such surfaces might represent the case where the reconstruction process, proposed by Klauber (2003), has occurred.

Similar trends can be traced from the normalized intensity of negative ions. The species like O^-, S^-, HS^- are in higher portions on the nontreated surface containing low HC compared to that of high HC. However, the oxidized oxy-sulphur species and S_n^- and clusters like FeO^-, CuS^-, CuO^-, FeS_2^-, CuS_2^-, FeS^-, CuO_2^-, and $Fe_2O_3^-$ form higher proportion in the regions with high HC content.

The situation after treatment on both high and low HC areas shows the same trend in observations as found before treatment in terms of the level of oxidation and

the presence of HC. However, the magnitude of the differences diminishes to comparable values between the two areas.

It is interesting to note that the thiosulphate cluster $S_2O_3^-$ is quite evident on the surface with high HC intensities. This thiosulphate is expected to form as a result of pyrite oxidation (Rimstidt and Vaughan, 2003). Therefore, it can be speculated here that $S_2O_3^-$ could be an intermediate oxidation product of pyrite-like surfaces that have resulted from the proposed reconstructed surface. When the normalized signal of $S_2O_3^-$ was compared before and after treatment, on the surface with HC it was found that the $S_2O_3^-$ had diminished from the surface after treatment. This is probably because $S_2O_3^-$ is not stable in an acidic environment and is transferred momentary to a sulphate state. Nevertheless, this evidence supports the idea the phase pyrite has an important role in the chalcopyrite oxidation process.

4.4 Microwave Leaching of Chalcopyrite in Ferric Sulphate

This section will consider the influence of microwaves on the leaching of chalcopyrite in ferric sulphate. All materials used in this study are the same as those used in the study of conventional leaching of chalcopyrite.

4.4.1 Experimental Apparatus and Method

The microwave system used for microwave leaching experiments was a MARS X® described in Section 4.2.3.1.1. This system utilises a multimode cavity. The MARS system has several advantages which make it ideal to use as a microwave leaching apparatus. First of all, the temperature is measured continuously and accurately inside the Teflon PFA® vessel. Continuous bulk temperature measurement during microwave irradiation is a major problem in microwave processing. This is because the use of normal thermocouples inside microwave fields suffers from the possibility of high error (see Section 3.6.2) because of electric field concentration at the tip of the thermocouple which could give false readings because of the enhanced localized heating. This problem is overcome in the MARS system by using a fibre optical sensor. Temperature was calibrated against the thermometer used to measure the temperature in the conventional

leaching experiments. This was done to avoid any possible drift in the measured temperature which is important when comparing the results of microwave and conventional leaching.

Furthermore, the microwave power in the MARS system can be applied continuously at any power level below 1200W. By using this system the microwave pulsing is avoided which causes the leaching system to heat instantly to high temperature. The pulsing system causes uncontrolled temperature change of the system. The application of agitation is also possible using stirrer bars.

To carry out leaching at constant temperature with minimal switching on/off of microwave power, a specific percentage of 300 W was used for each temperature. Furthermore, experiments were carried out in the control vessel only because the fibre optic temperature sensor is incorporated solely in this vessel. The heating parameters used during different microwave leaching experiments are shown in Table 4-18. Using this procedure, the power applied is just enough to keep the temperature constant with a minimum switching on and off of microwave power. An example of the temperature profile achieved over three hours leaching time is shown in Appendix 4-19. The temperature profile was produced by recording the temperature using a PC connected to the MARS system with the use of MarsLink® software.

Table 4-14 Heating parameters used during microwave leaching. Power level 300 W

Required leaching temperature, °C	The (%) of 300 W Power level used
50	2
60	3
70	4
80	5
90	7

A volume of 50 ml was first heated in the microwave field in order to reach the designated leaching temperature, and then a mass of 0.2 g of a closely-sized chalcopyrite was added to the solution. The sample was leached with continuous microwave energy for a set time, and then samples were taken for Cu and Fe analysis. The sampling procedure used was the same as for the standard leaching

conditions. However, after each sampling time a new solution with a new chalcopyrite sample was used to avoid the effect of changes in time and temperature during the removal of the leaching vessel for sampling.

4.4.2 Experimental Results

This section presents the findings of microwave leaching of GBL chalcopyrite in ferric sulphate.Three main factors were studied; the effect of temperature, the effect of particle size and effect of agitation. Furthermore, a reproducibility study is presented which was also carried out to confirm the precision of the experimental results.

It is worth emphasising that every point, in any graph reporting the results of microwave leaching experiments, represents a separate experiment. That is to say to construct one leaching curve under certain conditions, 5 separate identical experiments were carried out at time intervals of: 30, 60, 90, 120, and 180 minutes.

4.4.2.1 Effect of Temperature

The effect of temperature on the leaching rate of chalcopyrite was carried out in 0.25 M $Fe_2(SO_4)_3$ - 0.5M H_2SO_4 leaching solution. The particle size used was <38μm. Reaction temperatures ranged from 50°C to 90°C with steps of 10°C. The dissolution curves of the microwave leaching of chalcopyrite are shown in Figure 4-39. The temperature dependence pattern is similar to that seen in conventional leaching except that the recovery is slightly higher. At a temperature of 51°C only 1.4% of copper was extracted in 3 hours leaching time, whereas 16.9% was recovered at a temperature of 90°C over the same period of time.

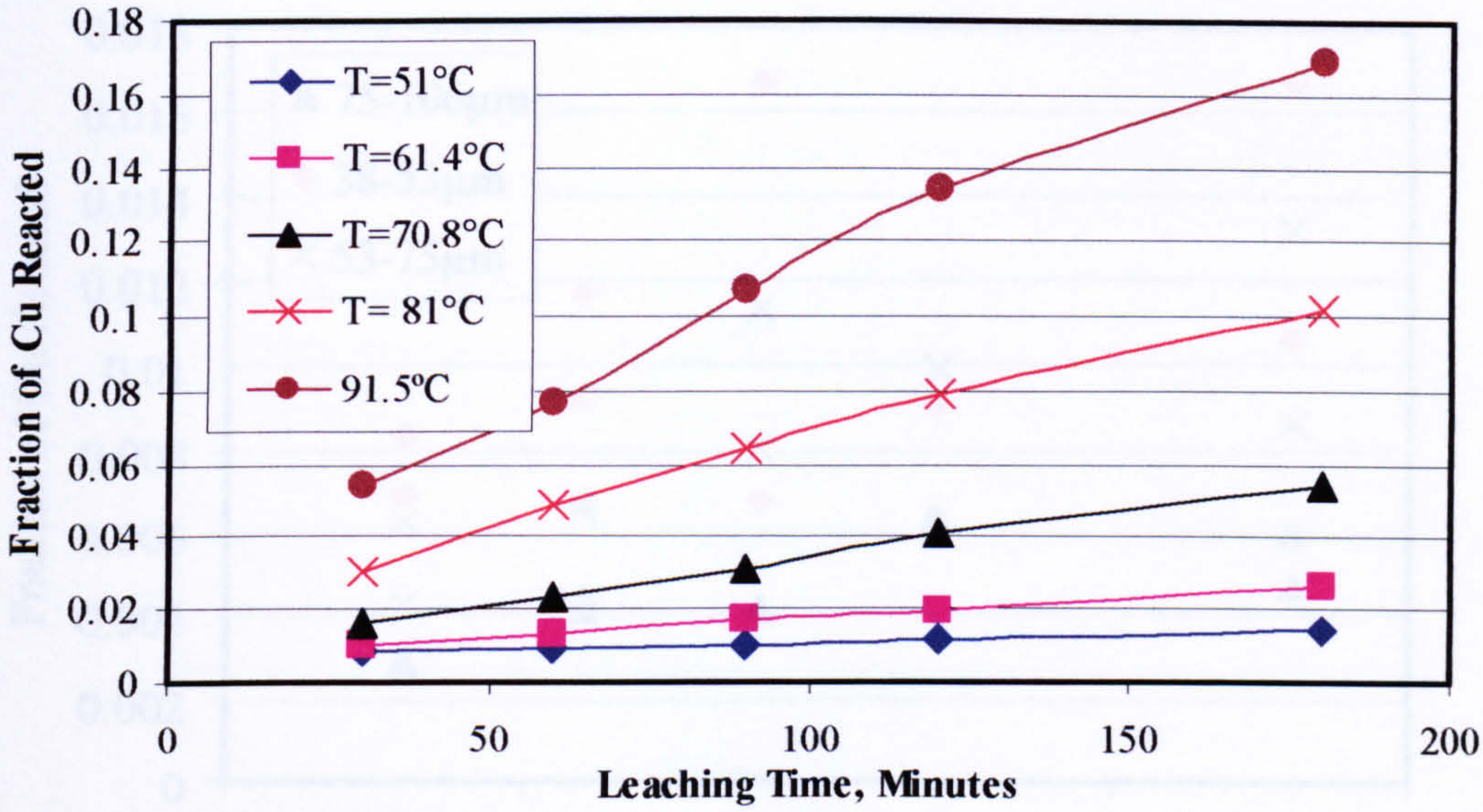

Figure 4-39 The effect of temperature on microwave leaching of GBL chalcopyrite as a function of time ($C_{Fe2(SO4)3}$:0.25M, Particle size:<38µm)

4.4.2.2 The Effect of Particle Size

GBL chalcopyrite, in various particle size ranges (75-106, 53-75, 38-53µm), was used to investigate the effect of particle size on chalcopyrite leaching within a microwave field. Leaching was carried out at a temperature of 90°C. The results are presented in Figure 4-40. Generally speaking the leaching rate was seen to increase with a decrease in particle size. However, the reproducibility of the results was poor compared to that of the < 38 µm fraction (see Figure 4-39). Furthermore, no clear and unambiguous distinction could be made between the various particle sizes, as shown in Figure 4-40, in terms of the fraction of copper reacted although the trend of increasing recovery from smaller particles could still be seen. In fact, this can be attributed to the specific interaction of microwaves with both the leaching solution and the chalcopyrite as will become clear in following discussion in Section 4.4.6.

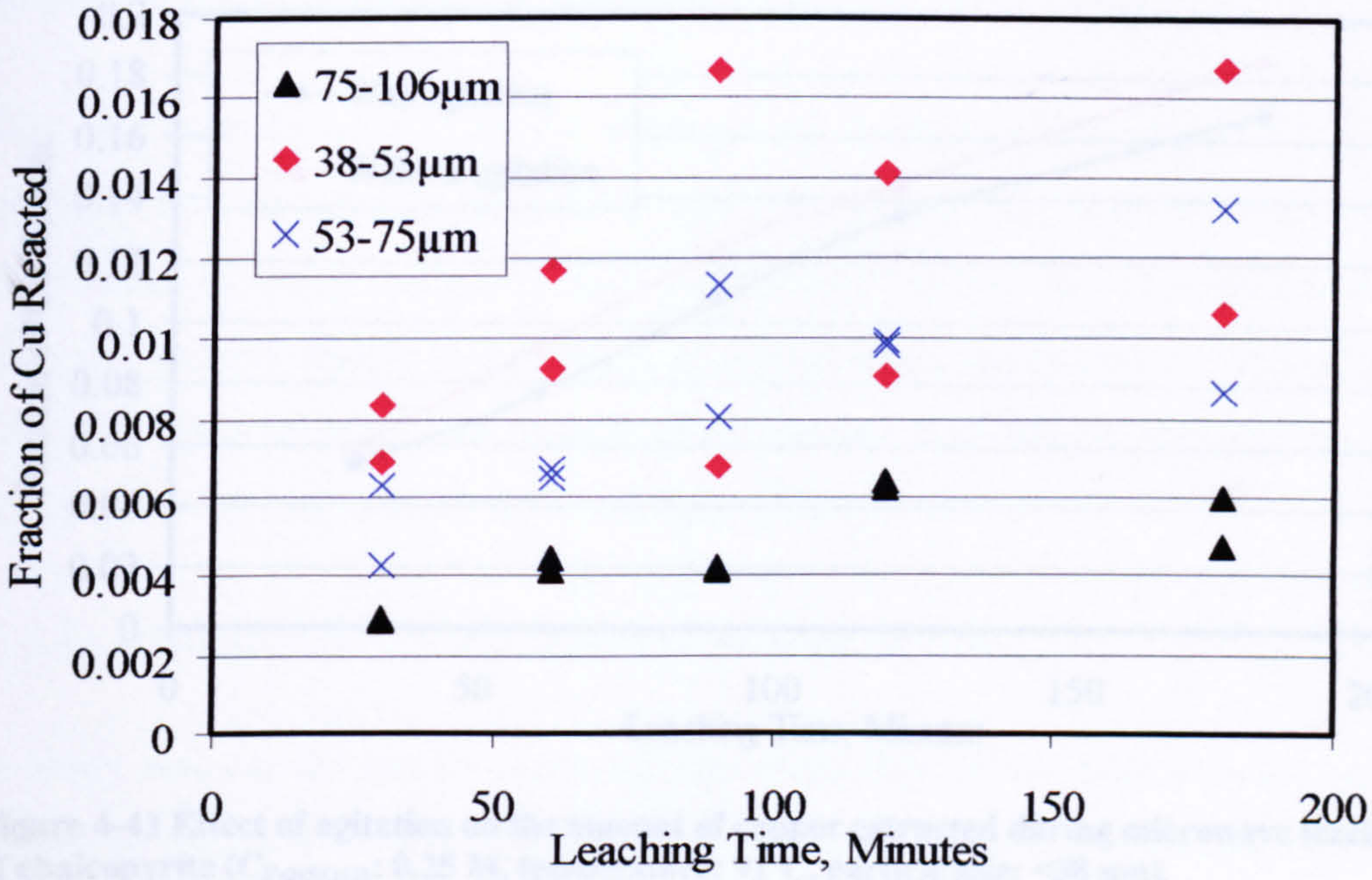

Figure 4-40 The effect of particle size on the leaching of GBL chalcopyrite in ferric sulphate as a function of time (T= 91°C: $C_{Fe2(SO4)3}$:0.25M)

4.4.2.3 The Effect of Agitation

The effect of agitation on chalcopyrite leaching in microwaves was investigated using 0.25 M ferric sulphate solutions at a temperature of 90°C. The results are presented in Figure 4-41. When no stirring was applied the copper recovery was up to 10% higher than when stirring was applied. This is contrary to the results obtained for conventional leaching. In the latter case, greater agitation leads to greater mass transfer efficiency, so that any diffusion-limiting effects through liquid film layer become further reduced and final conversions are higher. Joret et al (1997) also observed that the dissolution of Co_3O_4 and CeO_2 were faster when no mechanical stirring was applied. However, no comments where given to explain the observed phenomena. This apparent anomaly will be discussed later in Section 4.4.6. The reproducibility of the result presented in Figure 4-41 is addressed in Section 4.4.4.

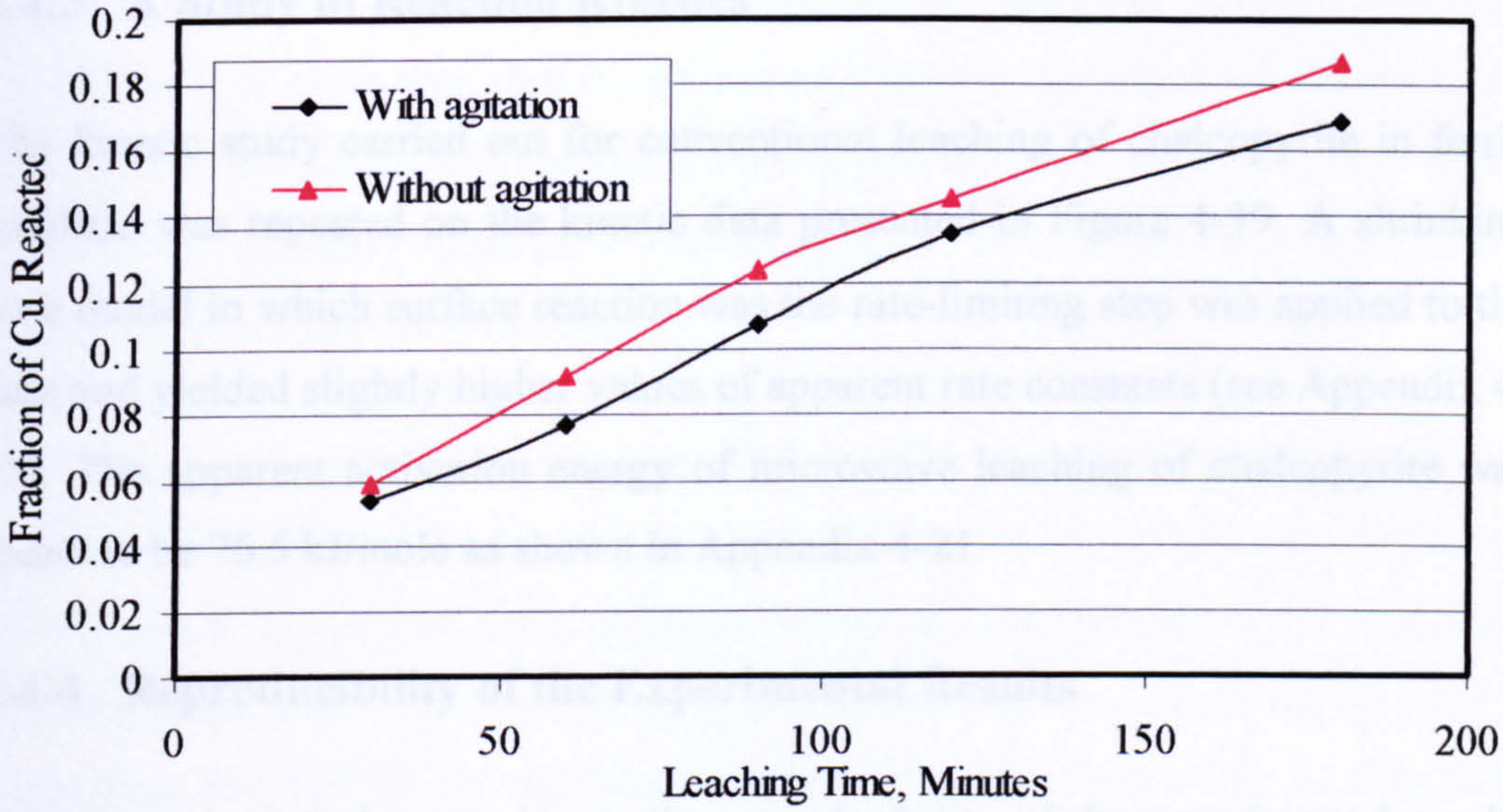

Figure 4-41 Effect of agitation on the amount of copper extracted during microwave leaching of chalcopyrite ($C_{Fe2(SO4)3}$: 0.25 M, temperature: 91°C, particle size: <38 µm).

4.4.2.4 Ratio of Reaction Products

A summary of the molar ratio of Fe/Cu calculated for microwave leaching of chalcopyrite in ferric sulphate can be found in Table 4-15. A detailed table of Fe/Cu molar ratio is presented in Appendix 4-20

Table 4-15 Molar ratio of Fe/Cu calculated for GBL chalcopyrite when leached in ferric sulphate for 3 hours

T, °C	51.0	61.4	70.8	81.0	91.5				
Stirring	Yes				NO	Yes			
Particle size, µm	<38					75-106	38-53	53-75	
Fe/Cu	3.6	5.2	5.6	5.7	5.2	5.4	5.5	5.7	5.3

Similar to the conventional leaching of GBL chalcopyrite in ferric sulphate (see Section 4.3.2.5) the molar ratio is slightly higher than the theoretical value calculated from Reaction 3-1 except at a temperature of 51°C where Fe/Cu is equal to 3.6±0.1 . This could be related to the presence of sulphate layer on chalcopyrite surface which is released into the solution without any Fe^{3+} consumption. The sulphate film is more pronounced on the Fe/Cu ratio at a temperature of 50°C because the copper and iron produced by Reaction 3-1 is comparable in quantity to those released directly without oxidation reaction. The reasons behind the slight increase in Fe/Cu were discussed in Section 4.3.2.5.

4.4.3 A Study of Reaction Kinetics

The kinetic study carried out for conventional leaching of chalcopyrite in ferric sulphate was repeated on the kinetic data presented in Figure 4-39. A shrinking core model in which surface reaction was the rate-limiting step was applied to the data and yielded slightly higher values of apparent rate constants (see Appendix 4-21). The apparent activation energy of microwave leaching of chalcopyrite was found to be 76.5 kJ/mole as shown in Appendix 4-21.

4.4.4 Reproducibility of the Experimental Results

A study was carried out to insure the reproducibility of the experimental results shown in Figure 4-39 and Figure 4-41 which are related to microwave leaching experiments. The reproducibility study was carried out using a new freshly prepared GBL chalcopyrite sample. A sample of a size fraction < 38 μm was prepared from the same GBL chalcopyrite sample as described in Section 4.2.1.1. The reproducibility study was carried out under microwave and conventional conditions. The results for microwave and conventional leaching are presented in Table 4-16.

It is important to note that the absolute values of the data presented in Table 4-16 cannot be compared directly to the previous results of similar experiments. This is because the chalcopyrite sample used in this case was prepared as another batch which means that the size distribution could be different from the first batch.

Table 4-16 The reproducibility of the experimental results for conventional and microwave leaching of chalcopyrite ($C_{Fe2(SO4)3}$: 0.25 M, particle size: <38 μm and 91°C, 3hrs)

	Microwave leaching		Conventional leaching
Stirring	Stirred	Not stirred	400 RPM
Fraction of Cu Reacted	0.141	0.174	0.119
	0.156	0.169	0.121
	0.145	0.168	0.118
			0.123
Average	0.147	0.170	0.120
Standard deviation	0.008	0.003	0.002
%RSD	5.284	1.891	1.848

Furthermore, it can be seen that the experimental results here are consistent with the previous results of conventional and microwave leaching of GBL chalcopyrite

in ferric sulphate. With regards to the effect of agitation under microwave conditions it is clear that copper recovery is higher at stagnant conditions when chalcopyrite was leached in ferric sulphate. In addition, the copper recovery under conventional leaching conditions is lower than that carried out under microwave conditions (with and without stirring).

The results are consistent and reproducible. The maximum relative standard deviation (%RSD) of the repeats is 5.3%. This value represents the %RSD of microwave leaching data with agitation. However, the %RSD of the data from stagnant microwave leaching and agitated conventional leaching is about 3 times lower than the %RSD for microwave agitated leaching data. This is consistent with the assumption that chalcopyrite is heated selectively within a high loss leaching solution.

4.4.5 Comparison between Microwave and Conventional Leaching of Chalcopyrite.

Leaching of chalcopyrite in microwaves and under conventional conditions can reasonably be regarded as similar in terms of temperature control, materials used, sampling and analytical procedures. It is, therefore, reasonable to directly compare the results of microwave and conventional leaching. Figure 4-42 shows a comparison between the rate of copper leaching from GBL chalcopyrite in ferric sulphate solution at different temperatures, with and without the influence of microwaves. It clearly demonstrates the positive influence of microwave energy on copper recovery over the range of temperatures used. However, this positive influence is not great as shown in Figure 4-42. After three hours the amount of copper extracted at 90°C is about 17% under microwave conditions compared to 13.5% conventionally.

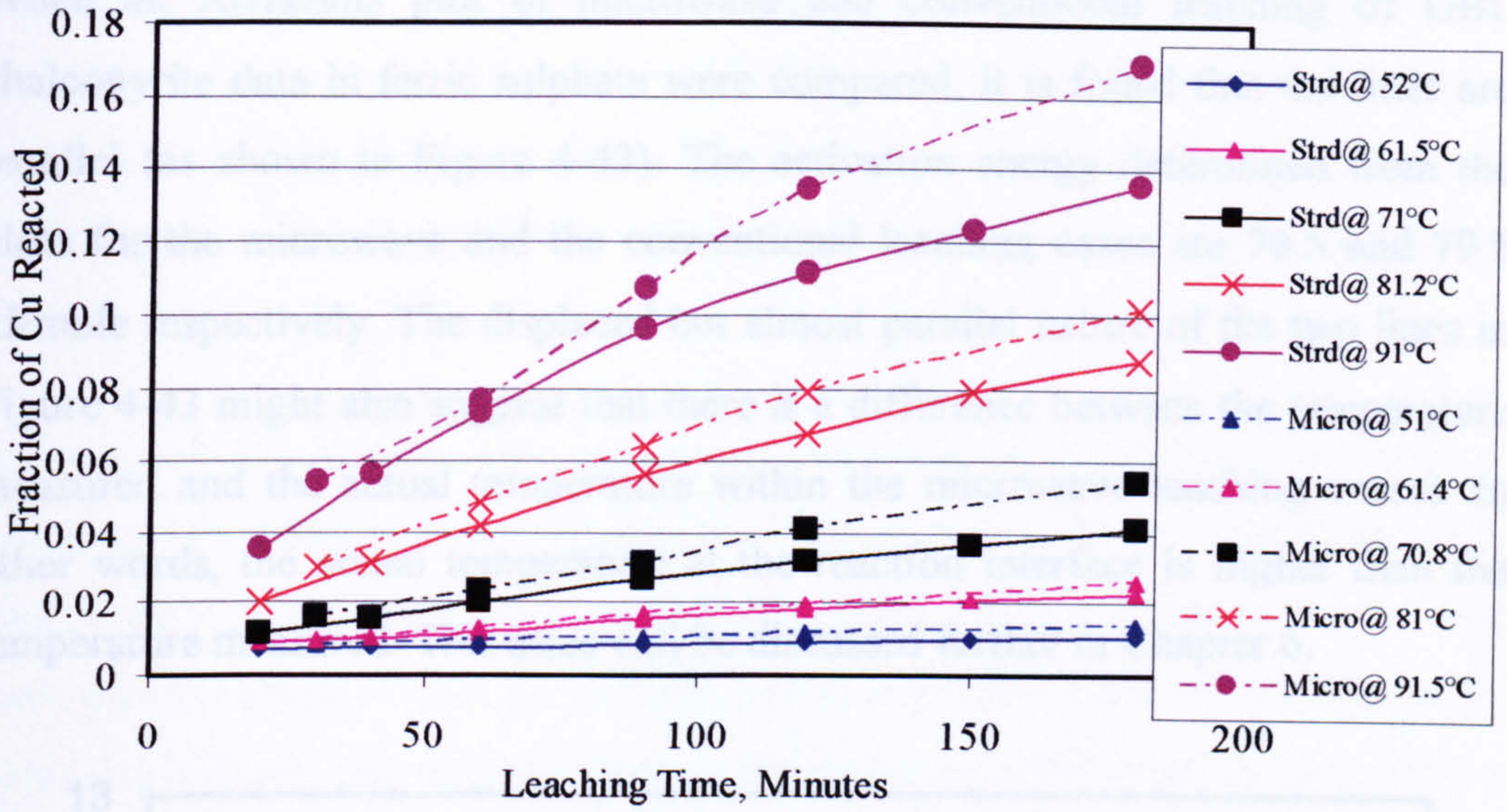

Figure 4-42 Comparison between microwave leaching and conventional leaching of chalcopyrite at various temperatures as a function of time ($C_{Fe2(SO4)3}$: 0.25 M, particle size: <38 µm).

Nevertheless, the difference in recovery between the two cases is reproducible as shown in Table 4-16 and consistently higher under microwave conditions. To examine the significance level of the difference in the average values of leaching rates at microwave and standard conditions, a statistical test, using null hypothesis assuming a significance level of 5%, was performed (see Appendix 4-22). The highest value of the standard deviation shown in Table 4-16 was used to compare the leaching rates. It was found that the difference between them is statistically significant. Therefore, this difference cannot be ignored, which confirms that the slight positive increase in leaching rate has not resulted from an experimental error.

The mechanisms by which microwaves interact with a chemically reactive system are still a matter of controversy. As discussed in Section 3.6, some researchers claim the existence of a non-thermal microwave effect by which the activation energy can be significantly reduced. Others deny the existence of this microwave effect and explain the remarkable acceleration of reaction rate by microwave induced thermal effects or so-called superheating effect (Huang and Rowson, 2002; Joret et al., 1997).

When an Arrhenius plot of microwave and conventional leaching of GBL chalcopyrite data in ferric sulphate were compared, it is found that the lines are parallel (as shown in Figure 4-43). The activation energy determined from the plots for the microwave and the conventional leaching cases are 76.5 and 79.5 kJ/mole respectively. The displaced but almost parallel nature of the two lines in Figure 4-43 might also suggest that there is a difference between the temperature measured and the actual temperature within the microwave leaching vessel. In other words, the actual temperature at the reaction interface is higher than the temperature measured. This issue will be discussed further in Chapter 6.

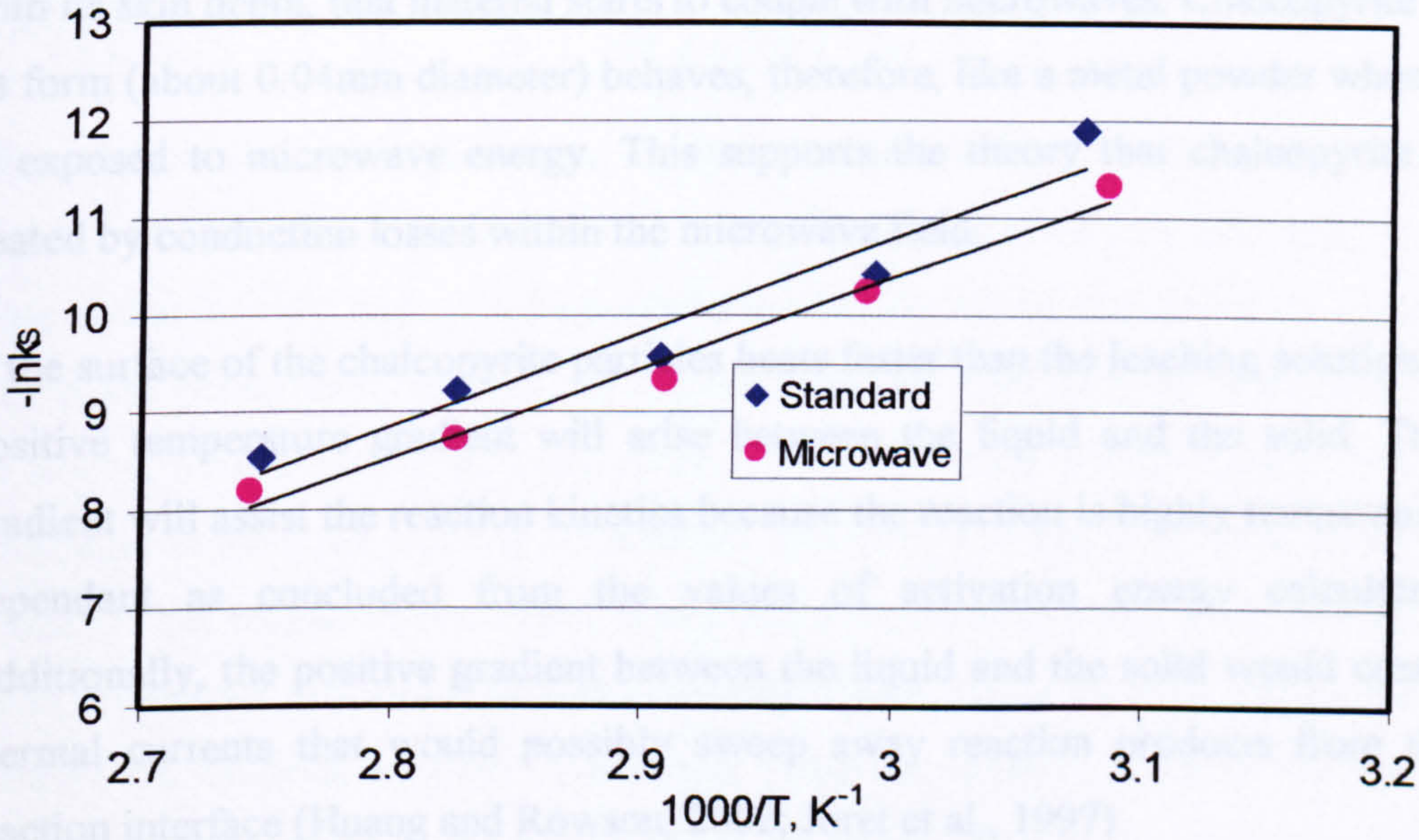

Figure 4-43 Comparison of Arrhenius plots for microwave and conventional leaching of GBL chalcopyrite in ferric sulphate ($C_{Fe2(SO4)3}$: 0.25 M, Particle Size: <38 μm)

When the values of activation energy for microwave and conventional leaching conditions were compared based on the standard deviations presented in Table 4-16, the difference was found to be statistically insignificant. Therefore, one can assume that the variation in activation energy is within the experimental error.

4.4.6 Discussion

Previous studies on the rate of chalcopyrite heating in microwave fields have shown that chalcopyrite heats very rapidly and its temperature can reach up to 1000°C in a matter of seconds (Harrison, 1997; Walkiewicz et al., 1988). It has

also been reported that chalcopyrite behaves as a conductor because its electrical conductivity is about 1000 S/m (Shuey, 1975). Such a high value of conductivity suggests that chalcopyrite particles heat in microwaves by a conduction loss mechanism or in other words by surface heating (see Section 2.2.2 and Section 2.3.3).

The value of skin depth (δ_S) for chalcopyrite was calculated according to Equation 2-9. It was found to be about 0.3 mm at a frequency of 2.45 Hz. This means that 63% of the incident microwave power is dissipated within the first 0.3 mm of the chalcopyrite particle. When the particle size of a metallic material is comparable with its skin depth, that material starts to couple with microwaves. Chalcopyrite in its form (about 0.04mm diameter) behaves, therefore, like a metal powder when it is exposed to microwave energy. This supports the theory that chalcopyrite is heated by conduction losses within the microwave field.

If the surface of the chalcopyrite particles heats faster than the leaching solution, a positive temperature gradient will arise between the liquid and the solid. This gradient will assist the reaction kinetics because the reaction is highly temperature dependant as concluded from the values of activation energy calculated. Additionally, the positive gradient between the liquid and the solid would create thermal currents that would possibly sweep away reaction products from the reaction interface (Huang and Rowson, 2002; Joret et al., 1997)

On the other hand, water based liquids heat very rapidly in microwave fields, while the microwave penetration depth (D_p) is quite small (Section 2.5). For pure water as calculated from the data reported in Meredith (1998), the D_p is about 1.3 cm at room temperature and 4.8 cm at a temperature of 85°C. Both these figures are calculated at a frequency of 2.5 GHz (see Table 4-17). However, when NaCl is added to water the heating rate increases rapidly due to the increase in conduction losses, whereas, the penetration depth drops dramatically. This drop is due to the considerable increase in loss tangent (see Section 2.3.1). For example, the penetration depth into 0.5 M salt solution is about 3.5 mm (the data used for calculating penetration depth is taken from (Meredith, 1998)). It is interesting to

note, in Table 4-17, that at a lower frequency (1GHz) the penetration depth in distilled water and 0.1 M NaCl solution increases when compared to at a frequency of 2.5 GHz, whereas, it decreases for more concentrated salt solutions. This is again is linked to the much higher loss tangent of concentrated solution at a frequency of 1 GHz.

Table 4-17 Dielectric properties and penetration depth of selected solutions (Meredith, 1998)

Material	T, °C	1 GHz			2.5 GHz		
		ε'	ε"	D_p, cm	ε'	ε"	D_p, cm
Distilled water	25	77	5.2	8.2	77	13	1.3
Distilled water	85	56	1	35.7	56	3	4.8
0.1 M NaCl	25	76	30	1.4	76	20	0.8
0.3 M NaCl	25	70	70	0.63	70	17	0.9
0.5 M NaCl	25	68	140	0.093	68	54	0.3

The solution used for chalcopyrite leaching contains 0.5 M [Fe^{3+}], 1.0 M [SO_4^{2-}] and 0.5 M [H^+] dissolved in distilled water. The conductivity of this solution is expected to be very high. Analogously to the sodium chloride solution mentioned above, the penetration depth of the applied ferric sulphate solution is expected to be low as well. If this is the case, most of the microwave power applied will be dissipated in the outer shell of the solution. Knowing that the fibre optic sensor is located in the middle of the vessel, which has a diameter of about 4 cm, there will be a temperature difference between the temperature sensor location and the outer shell of the leaching solution. In addition, when the solution is stirred the bigger particles tend to move to the outer shell of the vessel. Taking the above two facts one can conclude that either the leaching mixture as a whole system has a higher temperature than the bulk temperature or the solid particles have a higher temperature than the liquid. Indeed, it is possible that both situations operate simultaneously. Whichever is the case, the actual reaction temperature will be higher than the bulk temperature measured.

Therefore, two factors appear to play a significant role in the leaching kinetics of chalcopyrite under microwave conditions. These are the selective heating of the surface of chalcopyrite particles and the penetration depth of microwaves through a high loss leaching solution. The first factor is clearly evident from Figure 4-41 where higher recovery of copper was achieved when chalcopyrite was leached

without agitation. In this case, chalcopyrite is located at the bottom of the reaction vessel where all the particles are located within the zone of microwave penetration. So, in spite of the mass transfer limitation in terms of the diffusion of ferric ions through the film layer to the chalcopyrite surface, the conversion is higher.

The second factor can be inferred from Figure 4-42 where the recovery of copper is higher in the case of microwave leaching for all of the temperature ranges covered. Furthermore, this positive influence could not be related to a change in the activation energy of the reaction. In addition, the almost parallel nature of the Arrhenius plots for both the microwave and conventional leaching cases suggests that the reaction temperature in the microwave case is higher than the actual bulk temperature, the latter being measured at the centre point of the reaction vessel.

4.5 Conventional Leaching of Chalcopyrite in Ferric Chloride

This section presents the effect of temperature and stirring speed on the leaching kinetics of chalcopyrite in ferric chloride. A kinetic study was also carried out in order to determine the rate limiting step of chalcopyrite oxidation in ferric chloride. All leaching solutions used in this study were prepared in a matrix of 0.5 M HCl. The chalcopyrite materials used in this study are GBL and MZ2HE chalcopyrites. The experimental apparatus and procedure were previously described (Section 4.3.1).

4.5.1 Experimental Results

4.5.1.1 Effect of Temperature

The effect of temperature upon the copper recovery from GBL chalcopyrite in ferric chloride under conventional conditions was studied using particles with a size of <38 μm leached at temperatures of: 70, 80 and 90°C for 3 hours. The experimental results are shown in Figure 4-44. As shown in this graph, the copper recovery is highly sensitive to temperature. About 7.4% of copper was extracted from chalcopyrite at a temperature of 71.7°C in three hours of leaching time, whereas about 22% was recovered at a temperature of 90°C after the same period

of time. These values are higher than those observed during ferric sulphate leaching.

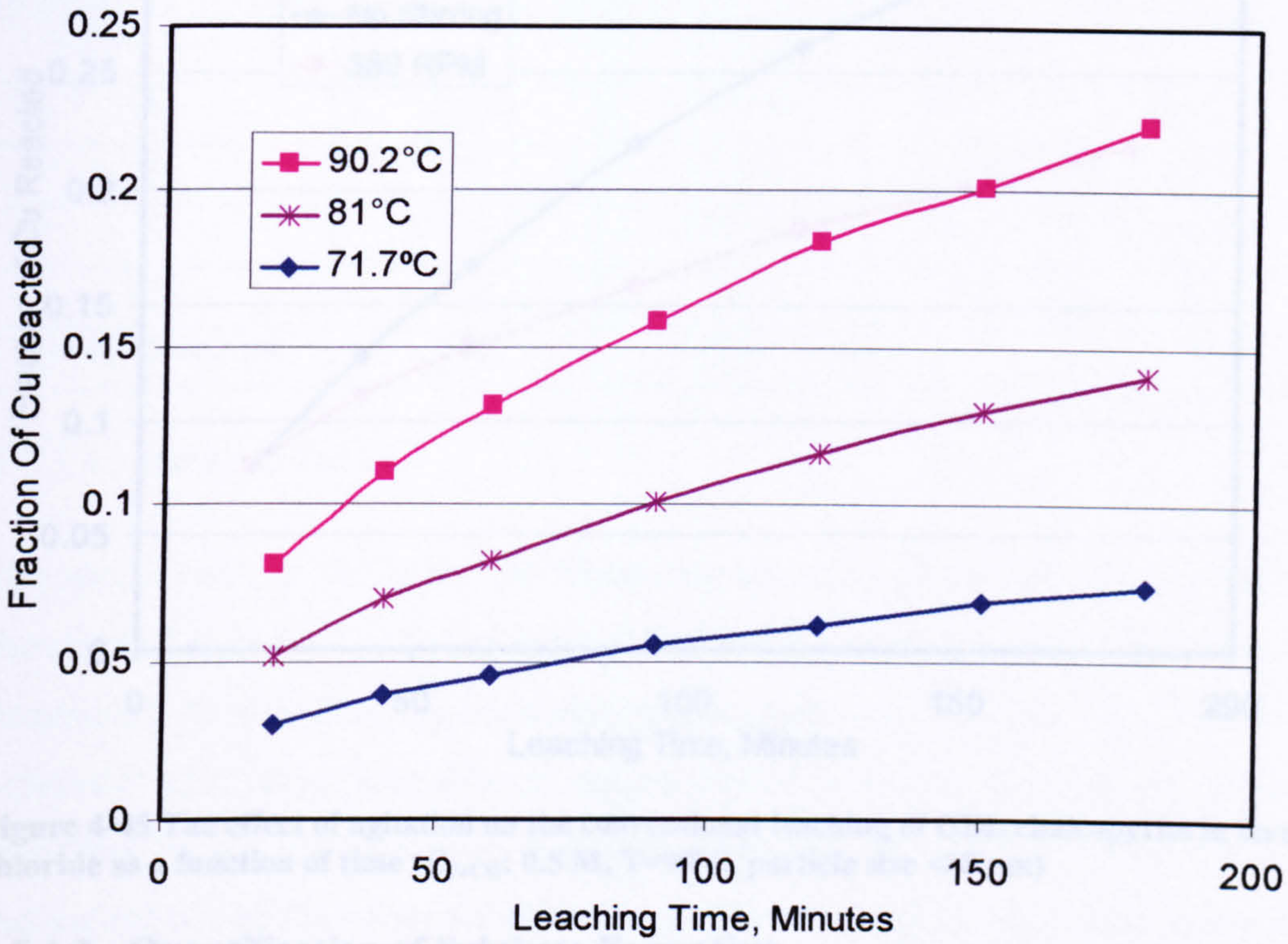

Figure 4-44. The effect of temperature on the conventional leaching of GBL chalcopyrite in ferric chloride as a function of time (C_{FeCl3}=0.5 M, particle size <38μm)

4.5.1.2 Effect of Agitation

The effect of stirring on the copper recovery from chalcopyrite when leached in ferric chloride was studied at a temperature of 90°C in 0.5 M $FeCl_3$-0.5 M HCl. The experimental results are shown in Figure 4-45. Unexpectedly, agitation had a negative effect on the amount of copper extracted.

Due to the limitation on the quantity of GBL chalcopyrite available, this phenomenon was investigated further using MZ2HE chalcopyrite concentrate (see Section 4.5.3). The residues from the leaching experiment with a stirring speed of 380 rpm were examined by SEM. It was found that the particles formed spherical particle agglomerates (see Appendix 4-23).

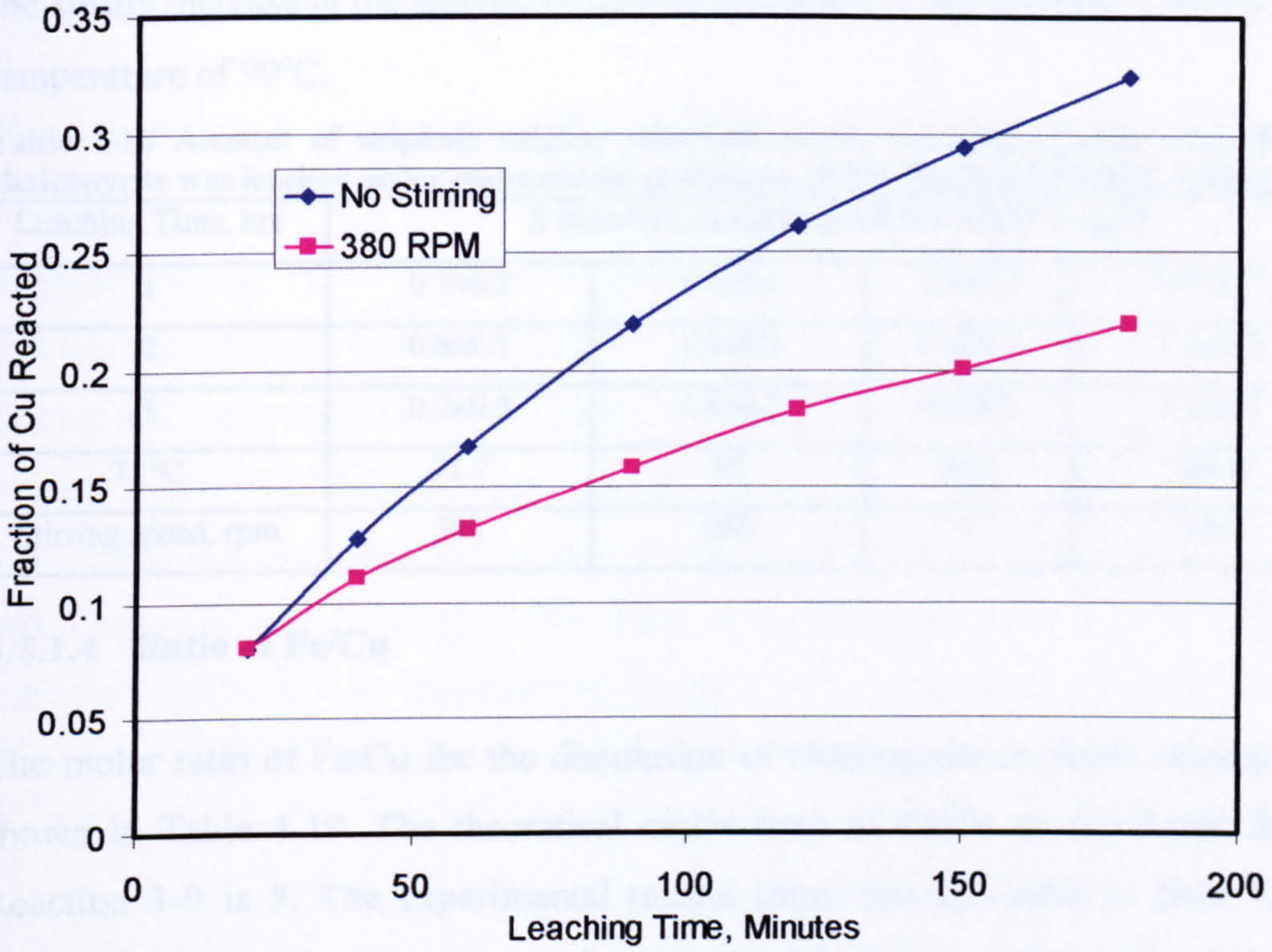

Figure 4-45 The effect of agitation on the conventional leaching of GBL chalcopyrite in ferric chloride as a function of time (C_{FeCl3}: 0.5 M, T=90°C, particle size <38 µm)

4.5.1.3 Quantification of Sulphate Formation

As opposed to ferric sulphate, in ferric chloride leaching of chalcopyrite, it is possible to measure sulphate present in the leaching solution formed as a result of sulfur oxidation. This is because the matrix of the leaching solution is chloride based. The source of sulphate could be a result of sulphide oxidation to sulphate and/or as a result of the dissolution of any sulphates which were formed prior to leaching. As discussed earlier (Section 3.3.1.1 and Section 4.3.2.5), there is a possibility of sulphide oxidation to sulphate during ferric sulphate leaching of chalcopyrite. In this study, it was attempted to measure the sulphate present in the ferric chloride leaching solution by ICP. The experimental results are shown in Table 4-18. However, the concentration of sulphur in the leaching solution is close to the detection limit (sulphur detection limit in solution is 0.33 µg/ml or 0.8mg/g chalcopyrite in the current case) and consequently the confidence variance could reach 70%. In spite of this limitation, one may conclude that some sulphur in the sulphide is oxidized to a sulphate state. This is clearly evident from

the steady increase in the amount of sulphur dissolved in the leaching solution at a temperature of 90°C.

Table 4-18 Amount of sulphate sulphur dissolved in the leaching solution when GBL chalcopyrite was leached under conventional conditions (0.5 M $FeCl_3$-0.5 M HCl, <38µm)

Leaching Time, hrs	S dissolved in leaching solution (SO_4^{2-}) mg/g			
1	0.7±0.2	1.1±0.1	1.4±0.1	0.9±0.7
2	0.8±0.1	1.4±0.4	1.8±0.1	1.1±0.2
3	0.7±0.5	1.4±0.2	2.0±0.3	1.3±0.7
T, °C	71.7	81	90.2	90.2
Stirring speed, rpm	380	380	0	380

4.5.1.4 Ratio of Fe/Cu

The molar ratio of Fe/Cu for the dissolution of chalcopyrite in ferric chloride is shown in Table 4-19. The theoretical molar ratio of Fe/Cu as calculated from Reaction 3-9 is 5. The experimental results show that this ratio is close to 5 especially after taking into account the amount of ferric ions consumed in sulphur oxidation to the sulphate state. However, this ratio is slightly higher than the theoretical one at the lower temperature (Fe/Cu = 5.44 @71.7°C). The reason for this is not clear and requires further investigation.

The dissolution of chalcopyrite in ferric chloride also involves the formation of sulphate ions as shown in Section 4.5.1.3. The quantity of sulphate formed is estimated to be less than 6% of the total oxidized sulphide. This is in agreement with the values reported in the literature (Dutrizac, 1992).

Table 4-19 Molar ratio of reaction products as measured or calculated when chalcopyrite was leached in 0.5 M $FeCl_3$-0.5 M HCl for 3 hrs at standard conditions

T, °C	Stirring, rpm	Cu (measured, mmole/g chalcopyrite)	Fe (measured, mmole/g chalcopyrite)	SO_4^{2-} (measured, mmole/g chalcopyrite)	Fe Required to oxidize S to SO_4^{2-} (Calculated, mmole/g chalcopyrite)	Fe/Cu	(Fe/Cu) corrected	$\frac{SO_4^{2-}}{S+SO_4^{2-}}$, %
90.2	0	1.71	8.59	0.06	0.43	5.02	4.81	3.5
90.2	380	1.16	5.51	0.04	0.29	4.76	4.55	3.4
81	380	0.74	3.92	0.04	0.31	5.28	4.92	5.7
71.7	380	0.39	2.23	0.02	0.14	5.75	5.44	5.0

4.5.2 Kinetic Study

The kinetic study on the dissolution of GBL chalcopyrite in ferric chloride (conventional) was carried out for comparison with microwave leaching (see Appendix 4-24). This is due to the negative influence of agitation on the leaching kinetics of chalcopyrite dissolution in ferric chloride (Section 4.5.1.2) and incomplete understanding of the reason behind this phenomenon. If the stirring causes the leached particles to agglomerate, the dissolution kinetics would involve a complex diffusion process which would be difficult to account for in the shrinking core model. On the other hand, if the stirring inhibits any synergetic action of $CuCl_2$ as was discussed in Section 3.3.2.6.4, then the process would involve more than one reaction which again is difficult to account for in the shrinking core model. Nevertheless, the value of the activation energy estimated for chalcopyrite dissolution in ferric chloride, based on the conditions in Section 4.5.1.1, is found to be about 69 kJ/mole. This value is in good agreement with the published literature values presented in Chapter 3 (see also Appendix 3-1).

4.5.3 Effect of Agitation on the Leaching of Chalcopyrite in Ferric Chloride.

4.5.3.1 Open Vessel Conditions

The aim of this study is to investigate the effect of agitation on the leaching of chalcopyrite in ferric chloride under conventional conditions. An open vessel means here that the vessel is not tightly closed which could allow some escape or ingress of air and/or vapour. When GBL chalcopyrite was leached in ferric chloride at different stirring speeds, it was found that the copper recovery was higher under stagnant conditions compared with that under agitation (380 rpm).

MZ2HE chalcopyrite concentrate (<25μm) was used here to further investigate the observed phenomenon due to limitations in the quantity of GBL chalcopyrite (<38μm) available. The agitation also had a negative effect on the copper recovery from MZ2HE (see Figure 4-46). At high stirring speed (570 rpm), the

copper recovery improved slightly compared to that at 360 rpm, but remained below that without agitation.

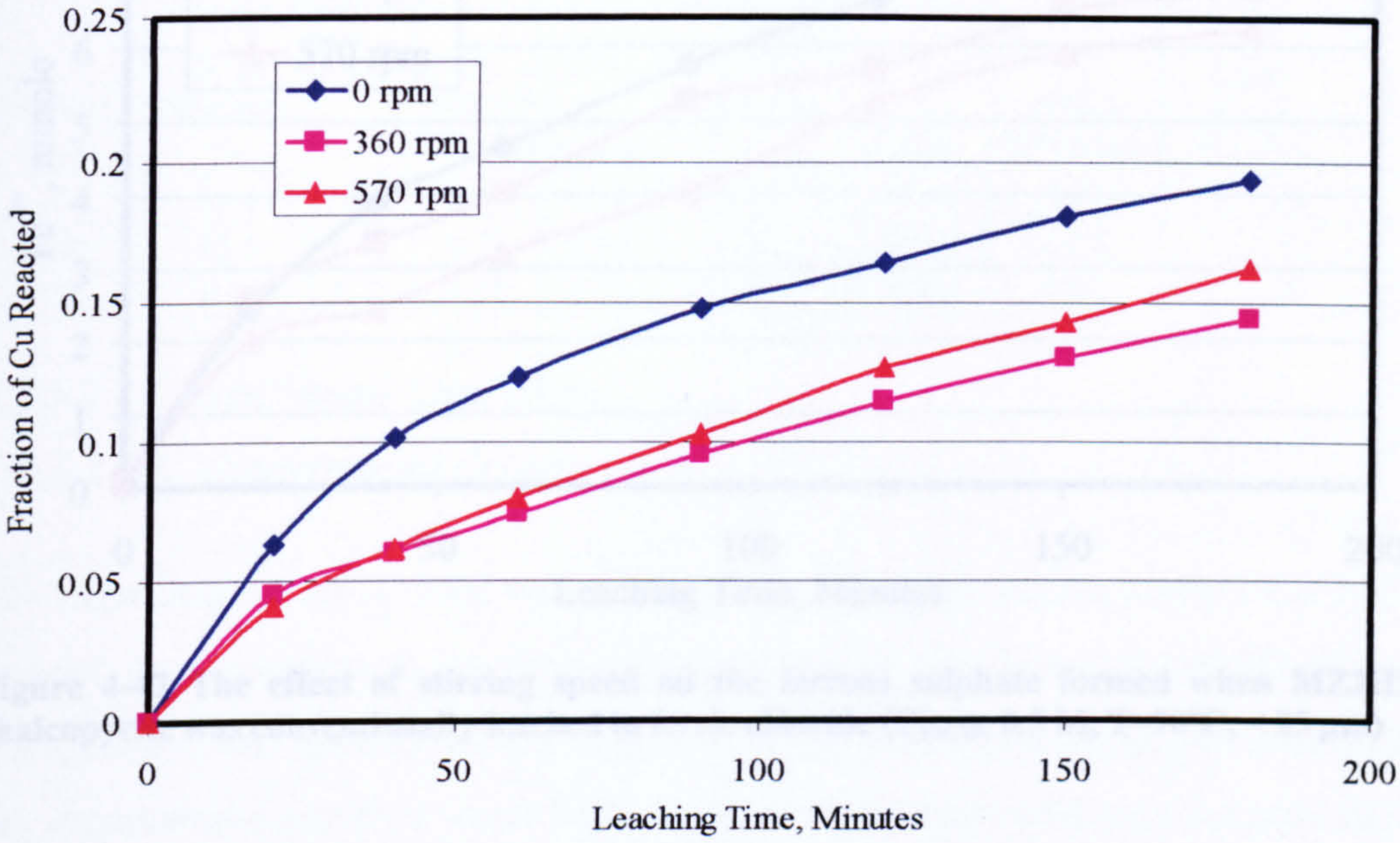

Figure 4-46 The effect of stirring speed on the copper recovery from MZ2HE chalcopyrite when conventionally leached in ferric chloride (C_{FeCl3}: 0.5 M, T=90°C, < 25 µm)

Similarly, the ferrous iron concentration in the leaching solution behaved in a similar pattern to that of copper with the exception that at a stirring speed of 570 rpm the ferrous concentration was lower than that at 360rpm (see Figure 4-47). However, the behaviour of sulphate formed during leaching is more complicated as shown in Figure 4-48. The initial rate of sulphate formation is higher at stirred conditions then drops compared to the stagnant case.

The molar ratio of dissolution reaction products is shown in Table 4-20. The ratio of Fe/Cu and the relative amount of sulphate in the MZ2HE chalcopyrite case are considerably higher than in the case of GBL chalcopyrite leaching. This fact is particularly evident under agitation conditions. However, when no agitation was applied, the Fe/Cu ratio becomes similar in both cases whereas the relative amount of sulphate is higher (about 24% compared to 3.5%). Further investigation was required to investigate the observed phenomena. In order to minimise the number of possible variables that could affect the leaching, a new simple experimental set up was prepared as presented in Section 4.5.3.2.

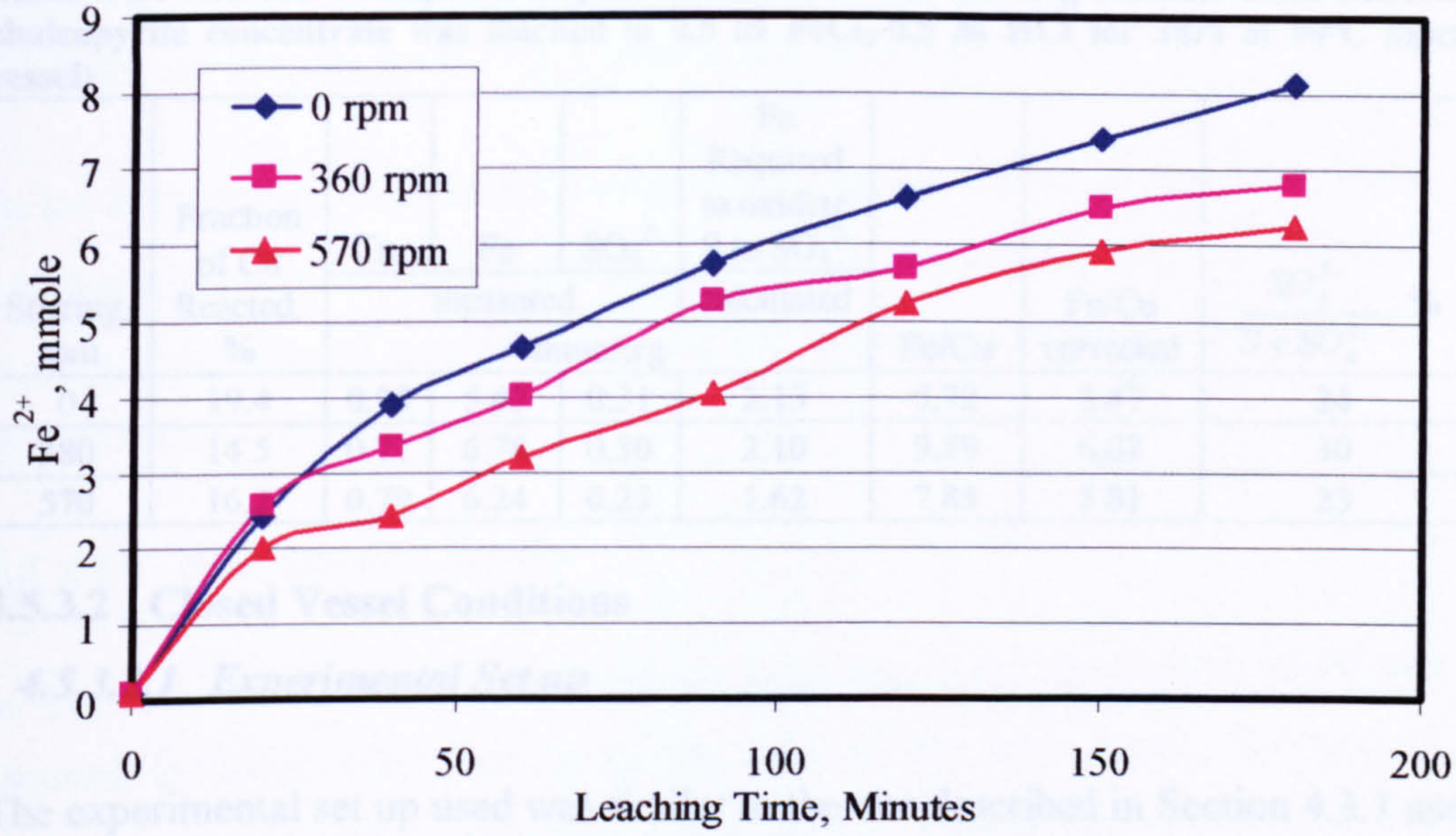

Figure 4-47 The effect of stirring speed on the ferrous sulphate formed when MZ2HE chalcopyrite was conventionally leached in ferric chloride (C_{FeCl3}: 0.5 M, T=90°C, < 25 µm)

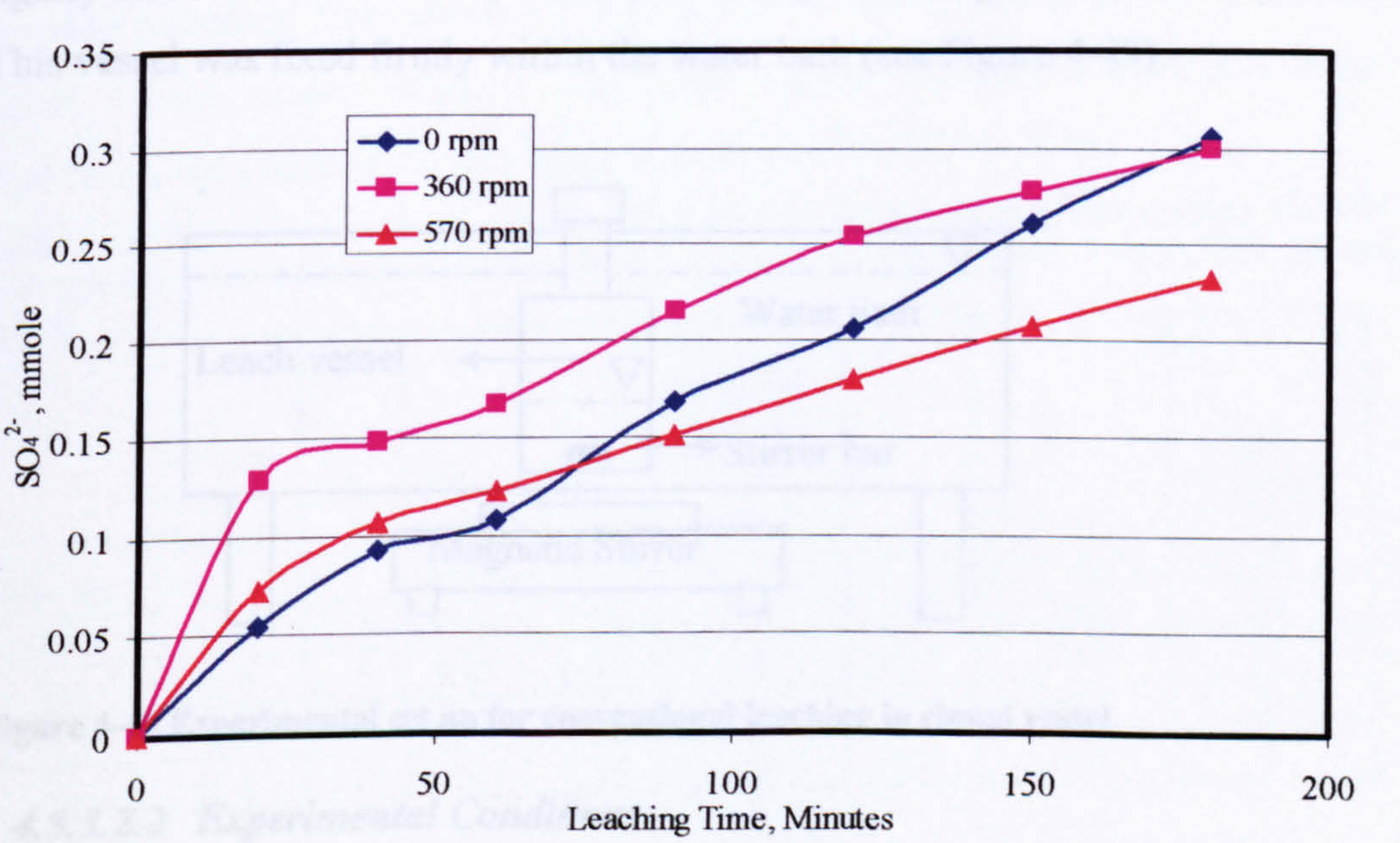

Figure 4-48 The effect of stirring speed on the amount of SO_4^{2-} generated from MZ2HE chalcopyrite when conventionally leached in ferric chloride (C_{FeCl3}: 0.5 M, T=90°C, < 25 µm)

Table 4-20 Amount of sulphate sulphur dissolved in the leaching solution when MZ2HE chalcopyrite concentrate was leached in 0.5 M $FeCl_3$-0.5 M HCl for 3hrs at 90°C (open vessel)

Stirring, rpm	Fraction of Cu Reacted, %	Cu,	Fe	SO_4^{2-}	Fe Required to oxidize S to SO_4^{2-}	Fe/Cu	Fe/Cu corrected	$\frac{SO_4^{2-}}{S+SO_4^{2-}}$, %
		measured			calculated			
		mmole/g						
0	19.4	0.95	5.42	0.31	2.13	5.72	3.47	24
380	14.5	0.71	6.78	0.30	2.10	9.59	6.62	30
570	16.2	0.79	6.24	0.23	1.62	7.85	5.81	23

4.5.3.2 Closed Vessel Conditions

4.5.3.2.1 Experimental Set up

The experimental set up used was similar to the one described in Section 4.3.1 and as used for conventional leaching experiments with the following modifications: the agitation was applied using a magnetic stirrer which was arranged underneath the thermostat-controlled water bath, the leaching vessel used was a single neck flat-bottomed flask supplied with a screw-type plastic cover, which could be tightly closed so that no escape of vapour and gases or ingress of air was possible. This vessel was fixed firmly within the water bath (see Figure 4-49).

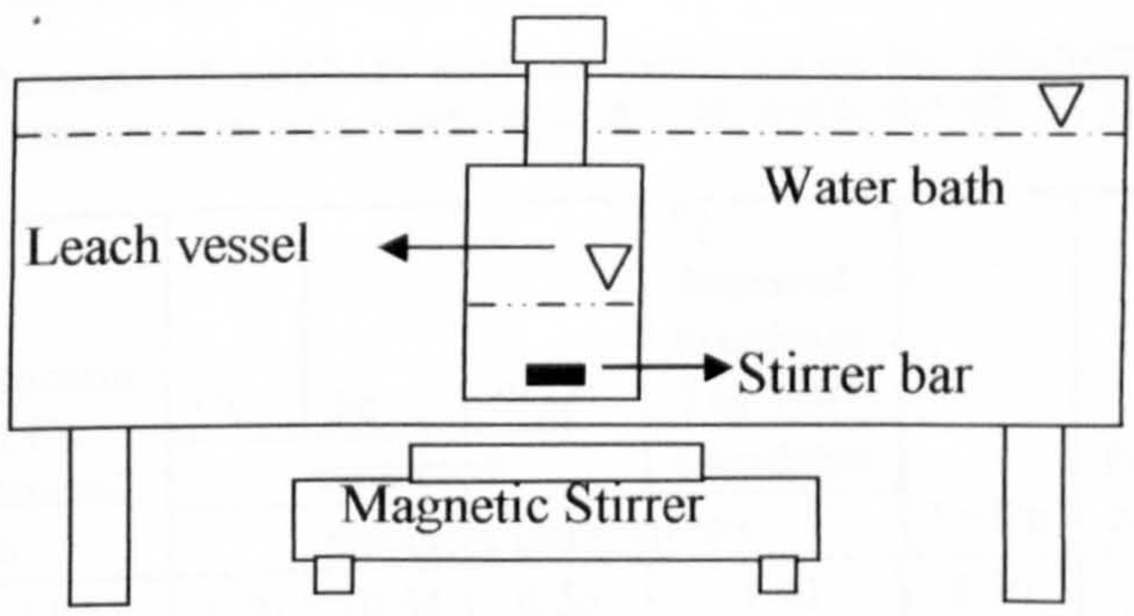

Figure 4-49 Experimental set up for conventional leaching in closed vessel

4.5.3.2.2 Experimental Conditions

100 ml of 0.5 M $FeCl_3$-HCl was poured in the vessel and immersed in the water bath for about 10 minutes (to allow the solution to reach the required temperature (90°C)). The vessel was then opened, and about 0.4 g of MZ2HE chalcopyrite concentrate (<25μm) was added to the leaching solution. The vessel was then

tightly closed. After 3 hours of leaching time, the vessel was removed from the water bath and samples for ICP and titration analyses were taken.

Two leaching experiments where carried out using this set up. In one experiment the leaching mixture was agitated using a stirrer bar at a stirring speed of 700 rpm. The second experiment was carried out under stagnant conditions. Each of these experiments was repeated twice.

4.5.3.2.3 Experimental Results.

The experimental results of the leaching experiments in the closed vessel are presented in Table 4-21. Similar to the case of the open vessel, the copper recovery is higher without agitation. About 24% of copper was recovered in the closed agitated vessel compared to about 41% copper recovered without agitation. The estimated amount of sulphate formed during the leaching process of MZ2HE chalcopyrite concentrate in the closed vessel conditions was found to be more than three times higher when stirring was applied. Surprisingly, the copper recovery increased from about 19 % in the open vessel case to about 42% in the closed vessel, under stagnant conditions. Under agitated and closed vessel conditions, the copper recovery again rose from about 16 to 24 %.

Table 4-21 Amount of sulphate sulphur dissolved in the leaching solution when MZ2HE chalcopyrite concentrate was leached in 0.5 M $FeCl_3$-0.5 M HCl for 3hrs at 90°C (closed vessel)

Stirring	Fraction of Cu Reacted, %	Cu, measured	Fe measured	SO_4^{2-} measured	Fe Required to oxidize S to SO_4^{2-} calculated	Fe/Cu	Fe/Cu corrected	$\frac{SO_4^{2-}}{S+SO_4^{2-}}$, %
		mmole/g chalcopyrite						
Yes	24.5	1.20	10.54	0.56	3.90	8.80	5.54	32
Yes	23.7	1.16	9.91	0.41	2.87	8.56	6.01	26
No	40.2	1.97	10.65	0.18	1.28	5.42	4.76	9
No	42.0	2.05	11.29	0.18	1.26	5.49	4.88	8

4.5.3.3 Discussion

The negative effect of agitation on the recovery of copper from chalcopyrite is surprising. Traditionally, one may expect an increase in the conversion when the diffusion through the liquid film layer is eliminated by agitation. One might

expect a higher conversion under stagnant conditions if the chemical reaction is very fast and exothermic. In this case, the heat released due to the chemical reaction would raise the temperature at the reaction interface so that the actual reaction temperature was higher than the bulk one. The heat of formation calculated for chalcopyrite oxidation by ferric chloride (Reaction 3-9) is about -165 kJ/mole. This enthalpy value does not suggest that the rise in temperature at the solid surface due to the exothermic reaction is high enough that an enhanced copper recovery would be observed. Furthermore, the apparent rate constant calculated for chalcopyrite leaching at a temperature of 90°C is about $5.23\times10^{-6}s^{-1}$ as calculated from the kinetic data in Figure 4-44. This is not high enough to expect an appreciable rise in temperature at the reaction interface.

On the other hand, the observed agglomeration of leached particles caused by agitation might be the reason for the drop in the copper recovery when GBL chalcopyrite was leached. This would result in reducing the surface area exposed to oxidation. However, when the leaching experiments were repeated using MZ2HE chalcopyrite at a higher agitation speed (570rpm), a slight improvement in the copper recovery was achieved. However, the copper recovery in this case was still well below the value without agitation (Figure 4-46). The amount of sulphate generated in the system after 3 hours leaching time seemed to increase slightly at a stirring speed of 380 rpm and drop slightly for a stirring speed 570 rpm. However, the rate of sulphate generation is different, as shown in Figure 4-48.

On the other hand, in the closed vessel where a minimal amount of oxygen could participate in the oxidation reaction, the situation is different (see Table 4-21). The amount of sulphate generated in solution is much higher when stirring is applied (more than 250 % higher).

The amount of iron generated in the closed vessel is slightly higher in the non-agitated conditions (only 10% higher), whereas, the copper recovery is more than 180% higher under stagnant conditions (Table 4-21). The XRD and chemical analysis of MZ2HE chalcopyrite concentrate shows that it contains some pyrite. It

is estimated that the fraction <25μm of MZ2HE chalcopyrite concentrate contains about 5% pyrite as calculated from the chemical analysis. This means that pyrite could participate in the leaching process although it is known that pyrite is of slow reactivity in chloride systems (Dutrizac, 1992). The oxidation of pyrite is known to generate mainly sulphate rather than elemental sulphur according to the following overall Reaction 4-1 (Dutrizac, 1989b; Rimstidt and Vaughan, 2003).

$FeS_2 + 14Fe^{3+} + 8H_2O \rightarrow 15Fe^{2+} + 16H^+ + 2SO_4^{2-}$ **Reaction 4-1**

Therefore one can suggest that the high level of sulphate in the leaching solution is associated with pyrite oxidation. Generation of sulphate during chalcopyrite oxidation, as revealed in Sections 4.5.1.3 & 4.5.1.4 is negligible and could not exceed more than 5% of the total oxidized sulphide.

The above facts regarding the leaching of MZ2HE would suggest that agitation had a negative effect on chalcopyrite leaching, whereas it had a positive effect on pyrite oxidation. It could therefore be concluded that the agglomeration of particles as discussed in Section 4.5.1.2 is not the reason behind the lower reaction rate in the agitated case. This is because pyrite particles would be entrained in the agglomerate leading to lower sulphate concentrations in solution. Furthermore, the agglomeration was no longer observed after the agitation was increased to 570 rpm in the open vessel and 700 rpm in the closed vessel conditions. Coagulation of chalcopyrite and pyrite has been recently investigated by Mitchell et al (Mitchell et al., 2005) in flotation separation. These workers found that the two minerals heterocoagulate in acidic media which make their separation by flotation at a pH below 4 impossible. This fact would again suggest that if agglomeration is observed in the chalcopyrite/pyrite system, the agglomerate would involve both minerals as the leaching solution used is highly acidic (0.5 M HCl).

Pyrite, when oxidized in acidic media, produces sulphate. From the experiments in the closed vessel under agitated conditions where the oxygen is limited in the system, it can be seen that SO_4^{2-} concentration steadily increases. This fact suggests that the oxygen source in sulphate is not only the dissolved oxygen but also from water. This supports the proposed model for pyrite oxidation by Rimstidt (2003). Furthermore, the presence of SO_4^{2-} in the solution suggests the

formation of several intermediate products such as: $S_2O_3^{2-}$, SO_3^{2-}, HSO_3^{1-}, $S_4O_6^{2-}$ and S_3O_6). However, these species are not stable and could not be measured (Parker et al., 2001)

The arguments presented in this section do not address two issues. These are the higher recovery of copper under non agitating conditions in both open and closed vessels and also the considerable increase in copper recovery in the closed vessel under non-agitating conditions compared to that from the open vessel. Regarding the first issue, one can present the following hypothesis: Under stagnant conditions the Fe^{3+} concentration is high (0.5 M). Due to the slow reaction kinetics of chalcopyrite leaching in ferric chloride, it can be assumed that the Fe^{3+} concentration across the liquid film layer is equal to the bulk concentration. Furthermore, according to Reaction 3-9, $CuCl_2$ is produced, which is known to be a powerful oxidant (Hirato et al., 1987a; Lundstrom et al., 2005). The chalcopyrite oxidation reaction using cupric chloride proceeds according to Reaction 4-2:

$$CuFeS_2 + 3CuCl_2 \rightarrow 4CuCl + FeCl_2 + S_2 \qquad \textbf{Reaction 4-2}$$

Under non-agitation conditions, it is possible that $CuCl_2$ accumulates at the reaction surface within the liquid film layer (see schematic in Figure 4-50). The rate of chalcopyrite oxidation by cupric chloride is dependant on $CuCl_2$ concentration. According to Hirato et al. (1987a) the reaction rate of chalcopyrite in cupric chloride was found to be half order $[CuCl_2]^{0.5}$. Therefore, with no agitation, Reaction 4-2 proceeds at a faster rate than the agitated case, whereas agitation may reduce the concentration of $CuCl_2$ at the chalcopyrite surface by diluting it with the bulk solution. Furthermore, chalcopyrite leaching with cupric chloride is faster than its leaching with ferric chloride at equal concentrations of both (Hirato et al., 1987a; Parker et al., 1981a).

It can therefore be concluded that the enhanced reaction rate of chalcopyrite leaching in ferric chloride without agitation is due to chalcopyrite oxidation by two parallel reactions (Reaction 3-9 and Reaction 4-2). If the action of $CuCl_2$ is the only reason behind the enhanced recovery then this phenomenon would diminish if a sensible background of $CuCl_2$ is added to the leaching system. Ngoc et al (1990) studied the effect of $CuCl_2$ on the recovery of copper when

chalcopyrite was leached in 1M $FeCl_3$-0.2 M HCl at a temperature of 106°C and a stirring speed of 700 rpm. These authors observed that the copper recovery increased with an increase in $CuCl_2$ addition, especially up to 0.25 M $CuCl_2$, and further increase was seen to have negligible effect. The observations of Ngoc et al (1990) agree with the observations of this work.

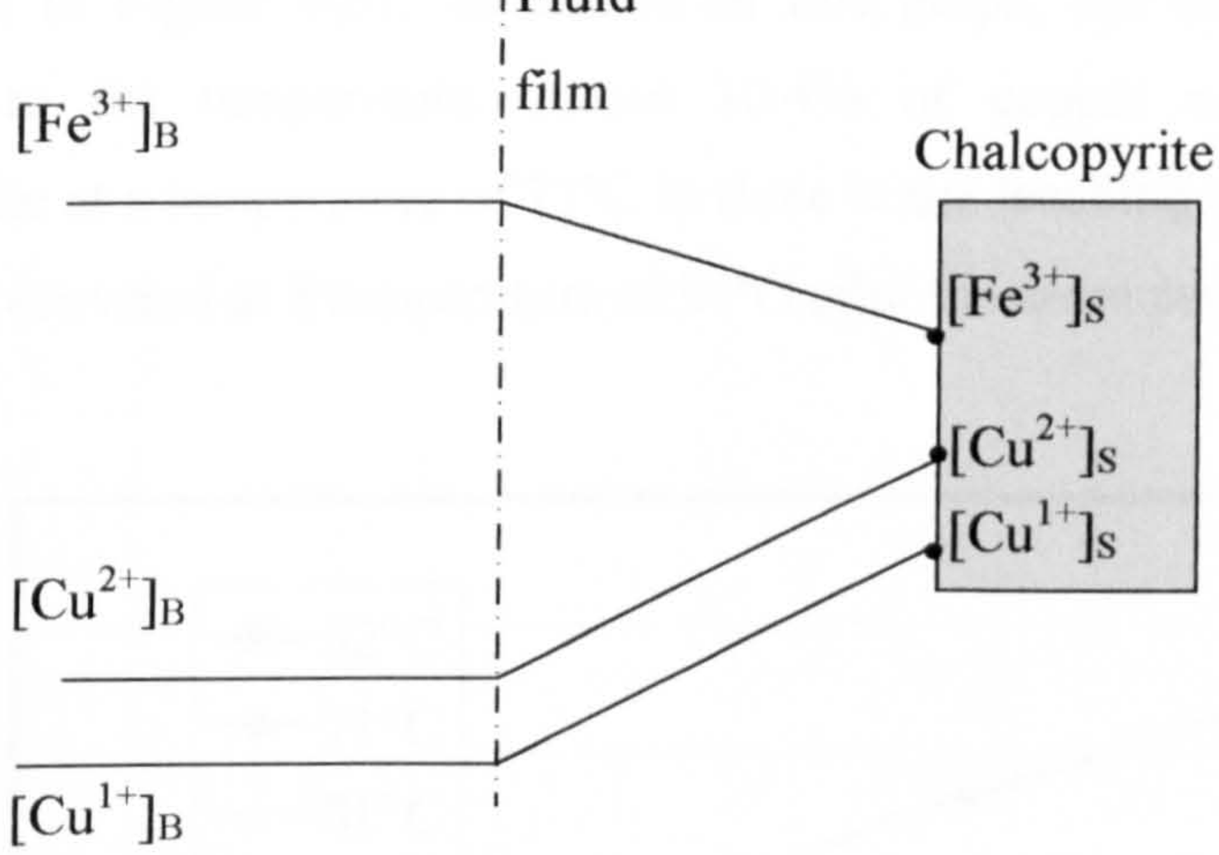

Figure 4-50 Mass transfer of reactants and products of chalcopyrite leaching in ferric chloride with no agitation

Furthermore, there is no explanation for the considerable increase in copper recovery when chalcopyrite was leached in a closed vessel. A systematic study is required to further investigate this interesting result.

4.6 Microwave Leaching of Chalcopyrite in Ferric Chloride

The effect of microwaves on the leaching of chalcopyrite in ferric chloride leaching solution was investigated. All leaching experiments were carried out in a leaching solution, containing 0.5 M $FeCl_3$ prepared in 0.5 M HCl, as described in Section 4.4.1.

The aim of this study was to examine the effect of microwaves on the leaching of chalcopyrite in ferric chloride and to present a comparison between conventional and microwave leaching results.

4.6.1 Experimental Results

4.6.1.1 Effect of Temperature

The effect of temperature upon the copper recovery from GBL chalcopyrite in ferric chloride was studied using a sample of particles size <38 μm leached for 3 hours at temperatures of 50; 70, 80 and 90°C respectively. Experimental results are shown in Figure 4-51. As shown in this graph, the copper recovery was sensitive to the temperature. About 10.4% of copper was extracted from chalcopyrite at a temperature of 71°C in three hours leaching time, whereas about 34% was recovered at a temperature of 91°C after the same period of time.

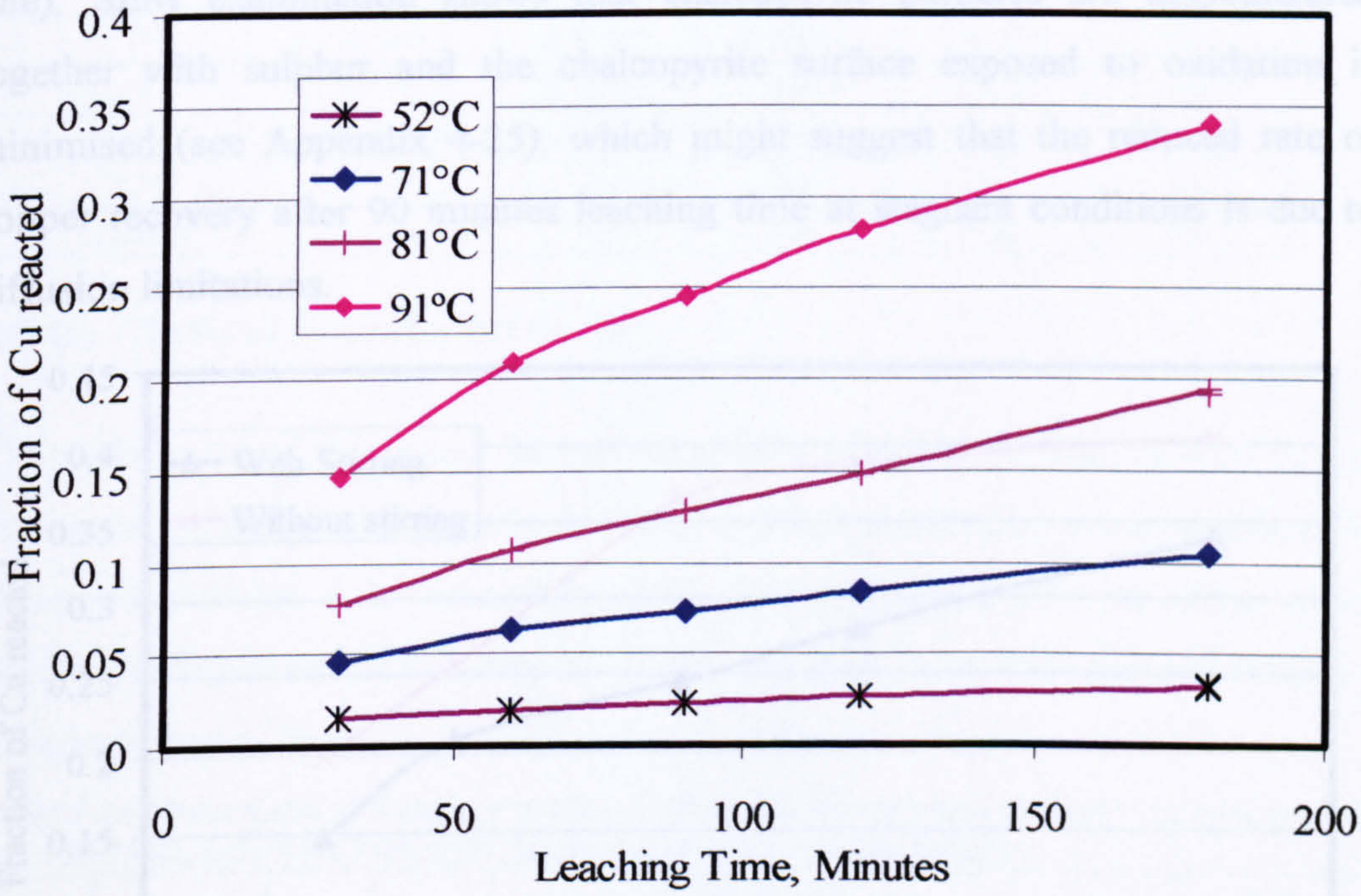

Figure 4-51 The effect of temperature on the microwave leaching of GBL chalcopyrite in ferric chloride as a function of time (C_{FeCl3}=0.5M, particle size <38μm)

4.6.1.2 Effect of Agitation

The effect of agitation on the copper recovery from GBL chalcopyrite when leached in ferric chloride was studied at a temperature of 90°C. The experimental results are shown in Figure 4-45. Similar to the conventional leaching experiments, stirring had a negative effect on the amount of copper extracted and the reaction rate. In this case, however, the higher recovery of copper in the

stagnant case may be linked to more than one factor. The selective heating of chalcopyrite discussed in Section 4.4.6 might have a role here as well as the possibility of chalcopyrite oxidation by cupric chloride produced by Reaction 4-2. Furthermore, the leaching vessel in the microwave leaching experiments is closed, which means that the unexplained phenomena observed during conventional leaching of ferric chloride might also be taking place. It is very difficult to distinguish which process is predominant and further work is required to quantify this.

Although the rate of copper recovery under stagnant microwave conditions is high during the first 90 minutes, it then starts to decrease as shown in Figure 4-52 (red line). SEM examination shows that chalcopyrite particles are agglomerated together with sulphur and the chalcopyrite surface exposed to oxidation is minimised (see Appendix 4-25), which might suggest that the reduced rate of copper recovery after 90 minutes leaching time at stagnant conditions is due to diffusion limitations.

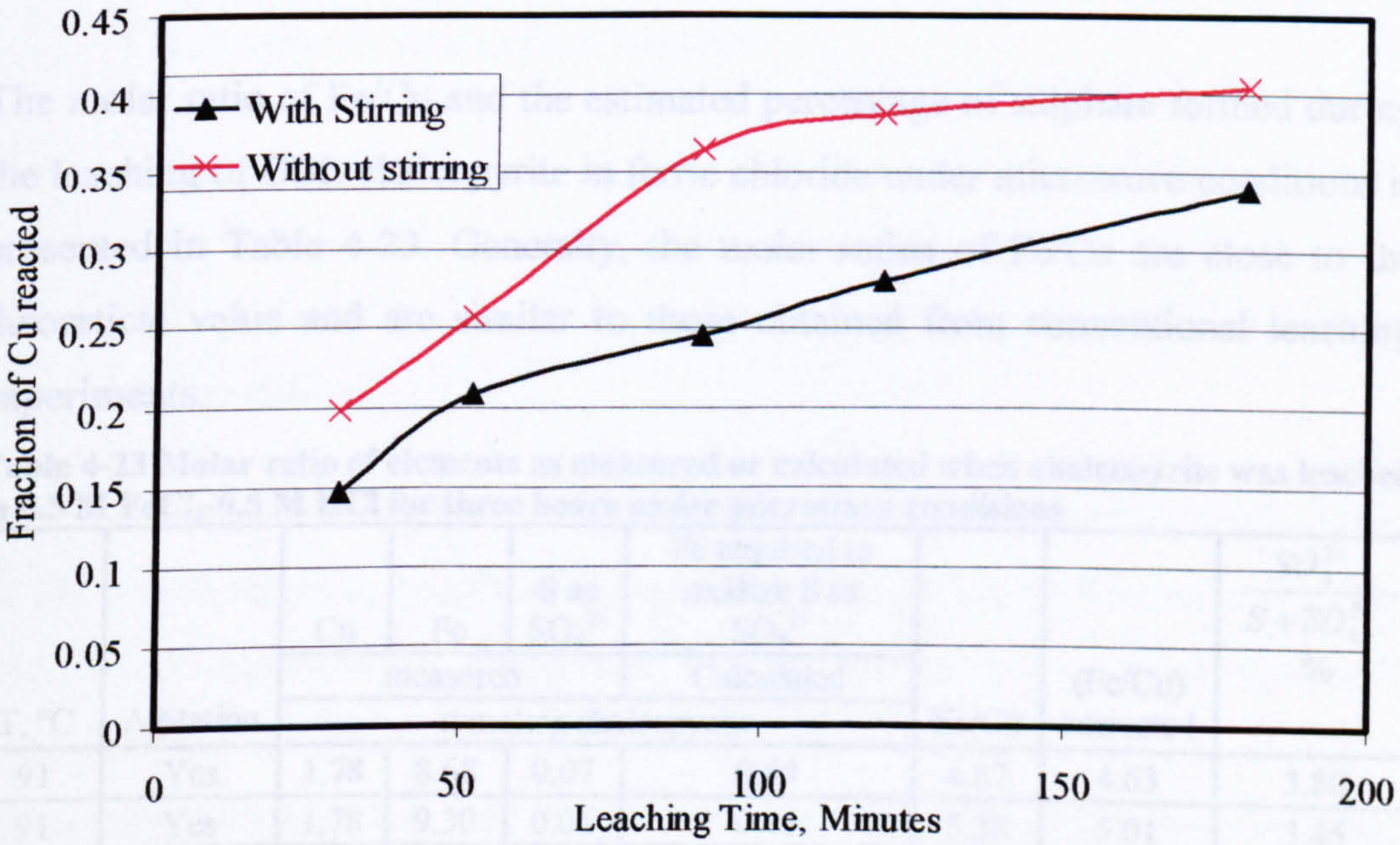

Figure 4-52 The effect of agitation on the microwave leaching of GBL chalcopyrite in ferric chloride as a function of time (C_{FeCl3}: 0.5 M, T=90°C, particle size <38 µm)

4.6.1.3 Quantification of Sulphate Formation

As discussed earlier (Section 4.5) the sulphur dissolved in ferric chloride leaching solution can be measured by ICP. The results of sulphate formed during microwave leaching experiments are presented in Table 4-22. The detection limit of sulphur analysis by ICP is about 0.8 mg/g chalcopyrite. For leaching experiments carried out at 80 and 90°C where the measured concentration is well above the detection limit, a steady increase in the concentration of dissolved sulphur is noticed. In addition, the results are reproducible.

Table 4-22 Amount of sulphate dissolved in leaching solution when GBL chalcopyrite was leached under microwave conditions (0.5 M $FeCl_3$-0.5 M HCl, <38μm)

Leaching Time, hrs	S dissolved in chloride leaching solution (SO_4^{2-}), mg/g chalcopyrite				
1	0.3±0.5	0.6±0.2	0.8±0.2	1.2±0.2	1.8±0.3
2	0.5±0.1	0.8±0.2	0.7±0.4	1.6±0.0	2.2±0.5
3	0.7±0.0	0.7±0.3	1.4±0.4	2.0±0.4	2.7±0.2
3	0.5±0.3	0.9±0.3	1.4±0.4	2.3±0.4	2.7±0.1
T,°C	52	71	81	91	91
Stirring	Yes	Yes	Yes	Yes	No

4.6.1.4 Ratio of Reaction Products

The molar ratio of Fe/Cu and the estimated percentage of sulphate formed during the leaching of GBL chalcopyrite in ferric chloride under microwave conditions is presented in Table 4-23. Generally, the molar ratios of Fe/Cu are close to the theoretical value and are similar to those obtained from conventional leaching experiments.

Table 4-23 Molar ratio of elements as measured or calculated when chalcopyrite was leached in 0.5 M $FeCl_3$-0.5 M HCl for three hours under microwave conditions

T, °C	Agitation	Cu (measured)	Fe (measured)	S as SO_4^{2-} (measured)	Fe required to oxidize S to SO_4^{2-} (Calculated)	Fe/Cu	(Fe/Cu) corrected	$\frac{SO_4^{2-}}{S+SO_4^{2-}}$, %
		mmole/g chalcopyrite						
91	Yes	1.78	8.68	0.07	0.49	4.87	4.63	3.80
91	Yes	1.78	9.30	0.06	0.45	5.23	5.01	3.45
91	No	2.12	11.12	0.08	0.59	5.24	5.00	3.83
81	Yes	1.02	5.76	0.04	0.30	5.66	5.41	4.02
81	Yes	1.01	5.82	0.04	0.30	5.80	5.54	4.04
71	Yes	0.55	2.99	0.02	0.16	5.44	5.20	3.93
71	Yes	0.55	3.00	0.03	0.21	5.47	5.15	5.12
52	Yes	0.17	0.96	0.02	0.15	5.75	4.98	11.32
52	Yes	0.17	0.99	0.02	0.12	5.68	5.09	8.96

The quantity of sulphate sulphur dissolved in the solution is generally less than 5% with the exception of the leaching carried out at a temperature of 50°C. At this temperature, the estimated percentage of sulphate is on average about 10%. This is more likely due to the fact that the measured value of S by ICP is below the detection limit, which would suffer from high error.

4.6.2 Kinetic Study

Similar to the case for conventional leaching of GBL chalcopyrite in ferric chloride, the kinetic data were examined using the shrinking core model in which the rate limiting step is the chemical reaction. The plots of kinetic data to calculate the apparent rate constant and the activation energy are presented in Appendix 4-26. The value of activation energy calculated from the Arrhenius plot is about 63 kJ/mole, which suggests that the reaction is chemically controlled. This value agrees with most of the values reported in literature (see Appendix 3-1).

4.6.3 Comparison between Microwave and Conventional Leaching of Chalcopyrite in Ferric Chloride

The comparison between microwave and conventional leaching of GBL chalcopyrite in ferric chloride in terms of fraction of copper reacted is shown in Figure 4-53. The enhancement in copper recovery is clearly evident under microwave conditions.

As opposed to ferric sulphate, in the ferric chloride leaching system, the isolation of the vessel seems to positively affect the copper recovery (Section 4.5.3). The microwave experimental conditions can be regarded as closed (isolated). Therefore, the enhancement observed in the copper recovery cannot be attributed to microwaves alone. It is very possible that there is a contribution resulting from the isolation of the vessel.

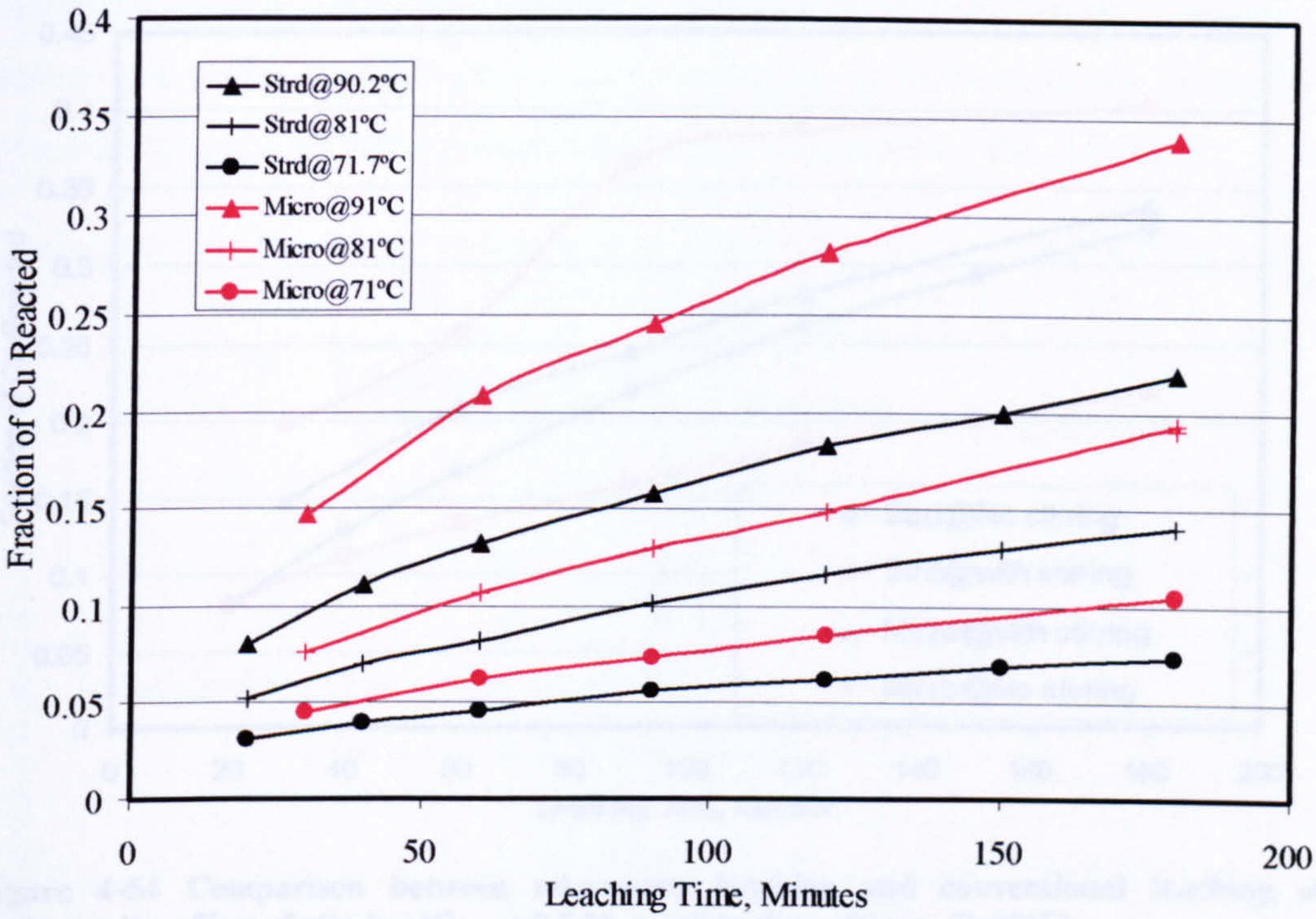

Figure 4-53 Comparison between microwave and conventional leaching of chalcopyrite at various temperatures as a function of time (C_{FeCl3}: 0.5 M, particle size: <38 µm).

Direct comparison of the activation energy in both microwave and conventional leaching in this case shows that it is lower under microwave conditions. However, there is a principal difference in both cases in that the microwave leaching vessel is closed. The comparison here is therefore misleading and cannot be made because, as was shown earlier, the isolation of the vessel caused enhanced copper recovery under conventional conditions (see Section 4.5.3).

The comparison of the molar ratio of the products and the estimated quantity of sulphate in chloride solution seems to suggest that microwave heating did not influence the types of reactions occurring during microwave leaching of chalcopyrite in ferric chloride.

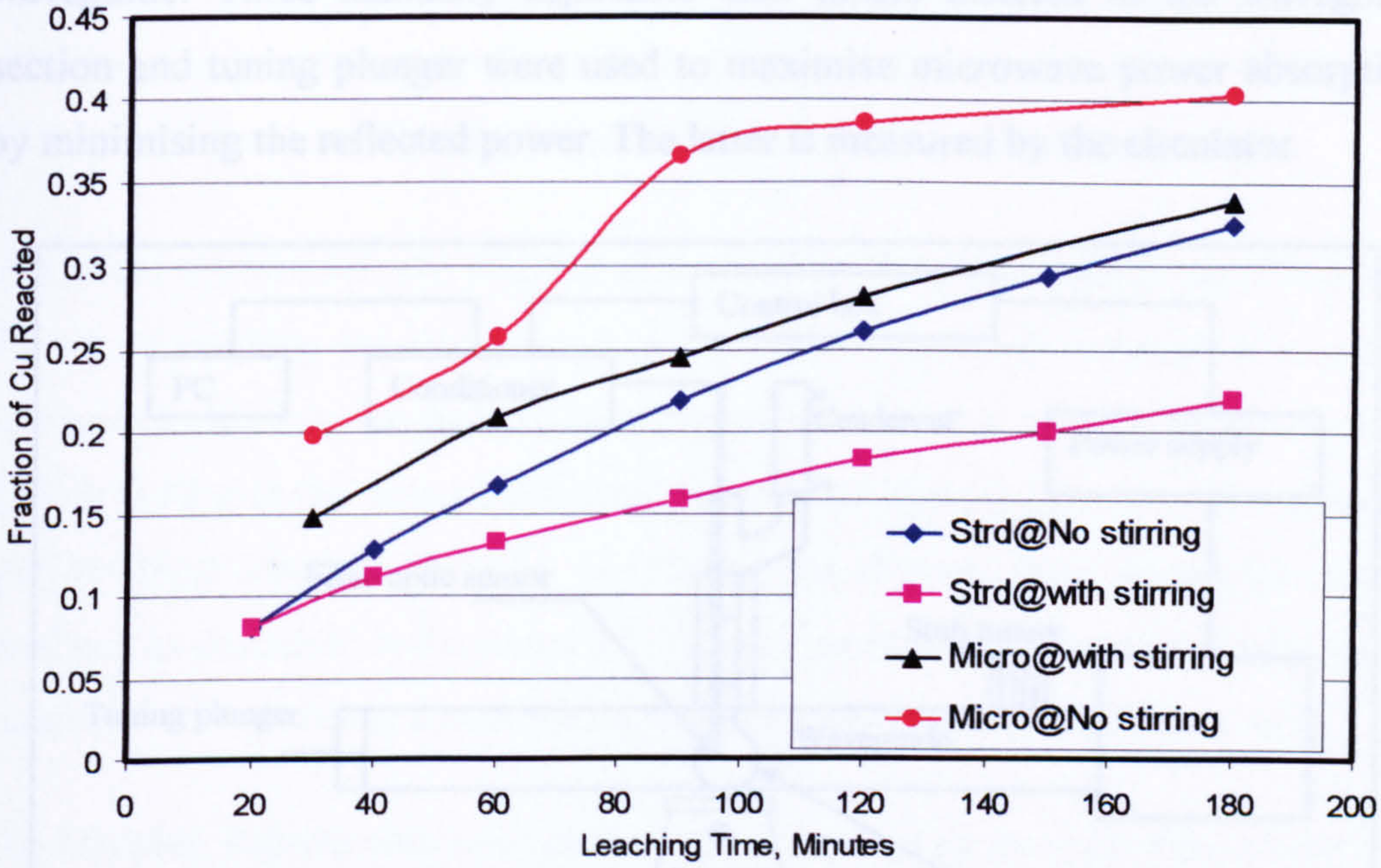

Figure 4-54 Comparison between microwave leaching and conventional leaching of chalcopyrite- effect of stirring (C_{FeCl3}: 0.5 M, particle size: <38 μm, T=90°C).

4.7 Single Mode Cavity Work

As discussed in Section 2.9.1.3, single mode cavities support one mode where the electric field pattern is well defined, whereas in multimode the electric field pattern is complex and many modes or areas of high electric field can be developed inside the applicator. Therefore, it was necessary to carry out some leaching experiments in a single mode cavity to investigate the difference in the leaching outcome between multimode and single mode cavities. Furthermore, the effect of microwaves is expected to be better defined. All experiments carried out so far were in multimode cavity represented by the MARS X® system. In this section, the experiments were carried out in 1 kW cylindrical TE_{10} single mode cavity.

4.7.1 Experimental Apparatus and Method

The experimental microwave apparatus is shown in Figure 2-14. A schematic of that apparatus is shown in Figure 4-55. It consists of a microwave generator operated at 2.45 GHz with adjustable power in the range of 0-1 kW; a WR340 standard rectangular waveguide; a cylindrical applicator (TE_{10}) located within the

waveguide. Three manually adjustable stub tuners inserted in the waveguide section and tuning plunger were used to maximise microwave power absorption by minimising the reflected power. The latter is measured by the circulator.

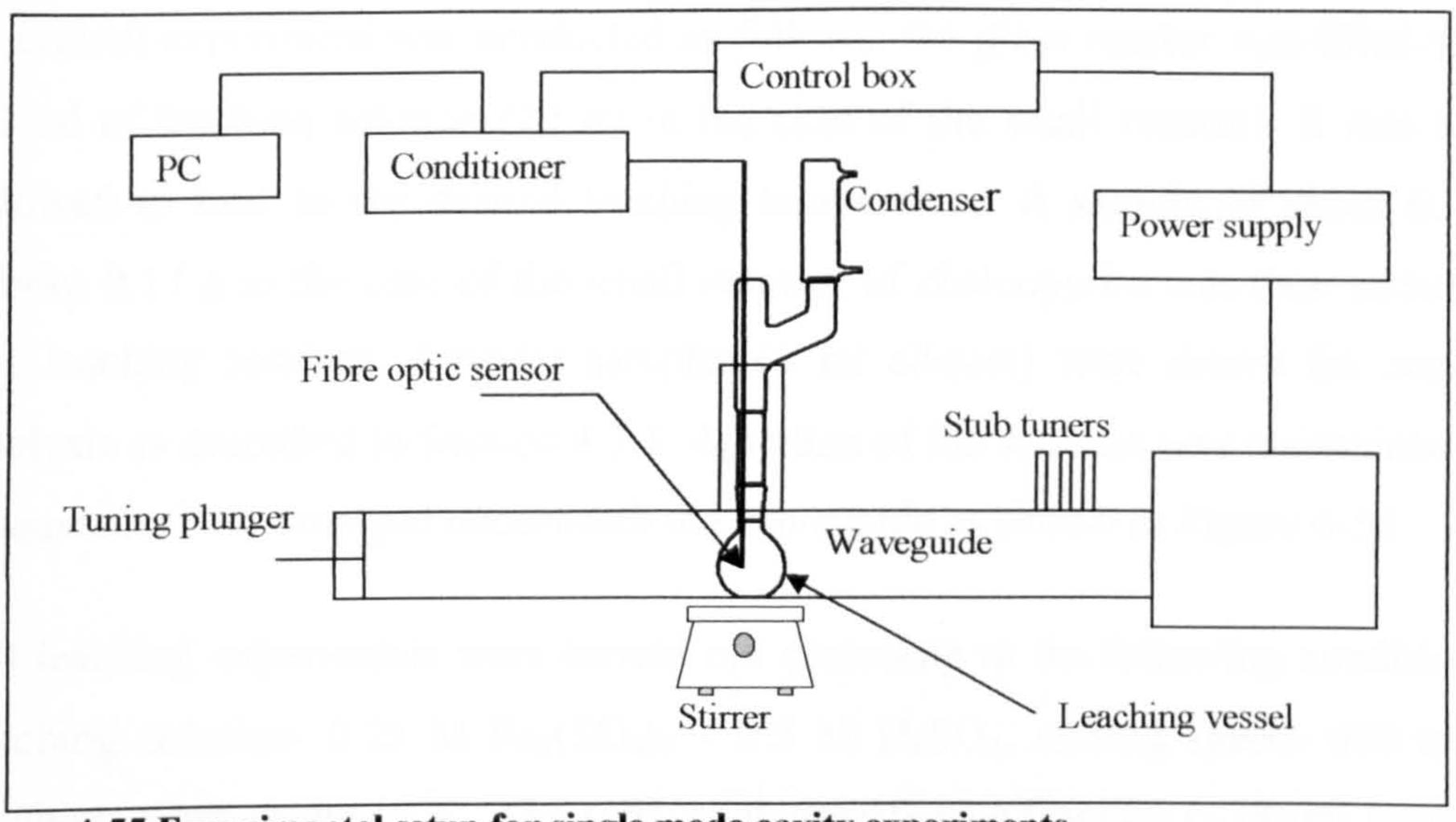

Figure 4-55 Experimental setup for single mode cavity experiments

The microwave system was equipped with a temperature controller system designed in cooperation with the School of Electrical and Electronic Engineering at the University of Nottingham. A detailed description of the design of the temperature controller system in presented in Appendix 4-27. It consisted of a FISO® fiber optic temperature sensor connected to a FTI-10® signal conditioner which allowed the measurement of the temperature inside the leaching vessel located in the microwave cavity with an accuracy of ±1°C. The measured temperature is sent to a control box where it is compared to a set temperature. A signal from the control box (programmed chip) is then sent to the magnetron power supply to regulate the incident power. This was done so that minimal switching on/off of the power would occur. A hyper link was created between the conditioner and a PC to allow continuous monitoring of the measured temperature. An example of the temperature profile obtained is shown in Appendix4-28

The leaching experiments were carried out using two reactors with different diameters. The first reactor was a 50 ml flat bottom narrow neck flask with diameter of about 50 mm (large reactor). The second reactor was a round bottom

cylindrical tube (small reactor) with an internal diameter of about 20 mm. The reactor was positioned in the middle of the cavity and connected through an extension tube to a reflux condenser to minimize the evaporation losses.

A typical experiment was conducted as follows: the glass reactor was filled with 50 ml of leaching solution (20 ml in the case of the small reactor). It was then allowed to heat to the desired leaching temperature. A sample of about 0.2 g (about 0.13 g in the case of the small reactor) of chalcopyrite was then added to the leaching solution. Periodic samples (1 ml aliquot) were drawn for copper analysis as described in Section 4.3.1. Agitation of the solution was maintained by magnetic stirrer arranged underneath the waveguide as shown in Figure 4-55.

All leaching experiments were carried out according to the following conditions: leaching solution- 0.25 M $Fe_2(SO_4)_3$ – 0.5 M H_2SO_4, stirring speed- 600 rpm, leaching temperature-91°C. The GBL chalcopyrite size fraction (<38μm) used in this study is the same one used to examine the reproducibility of the experimental results in Section 4.4.4. Therefore direct comparison of results of the overall copper recovery is permissible only with the data obtained using the same sample.

4.7.2 Experimental Results and Discussion

The effect of reactor size on the recovery of copper was studied in order to investigate further the effect of penetration and selective heating of chalcopyrite. The experimental results of the copper recovery achieved in both the large and small reactors are presented in Figure 4-56. The results clearly show that the recovery of copper during microwave leaching of GBL chalcopyrite in the small reactor is higher than that obtained in the large reactor. The experiments were repeated twice in each case and show acceptable reproducibility in the data. It is worth mentioning here that a small amount of chalcopyrite was found on the side walls of the small reactor above the liquid level. This probably caused slightly reduced copper recoveries. Nevertheless, the effect of reactor size is evident.

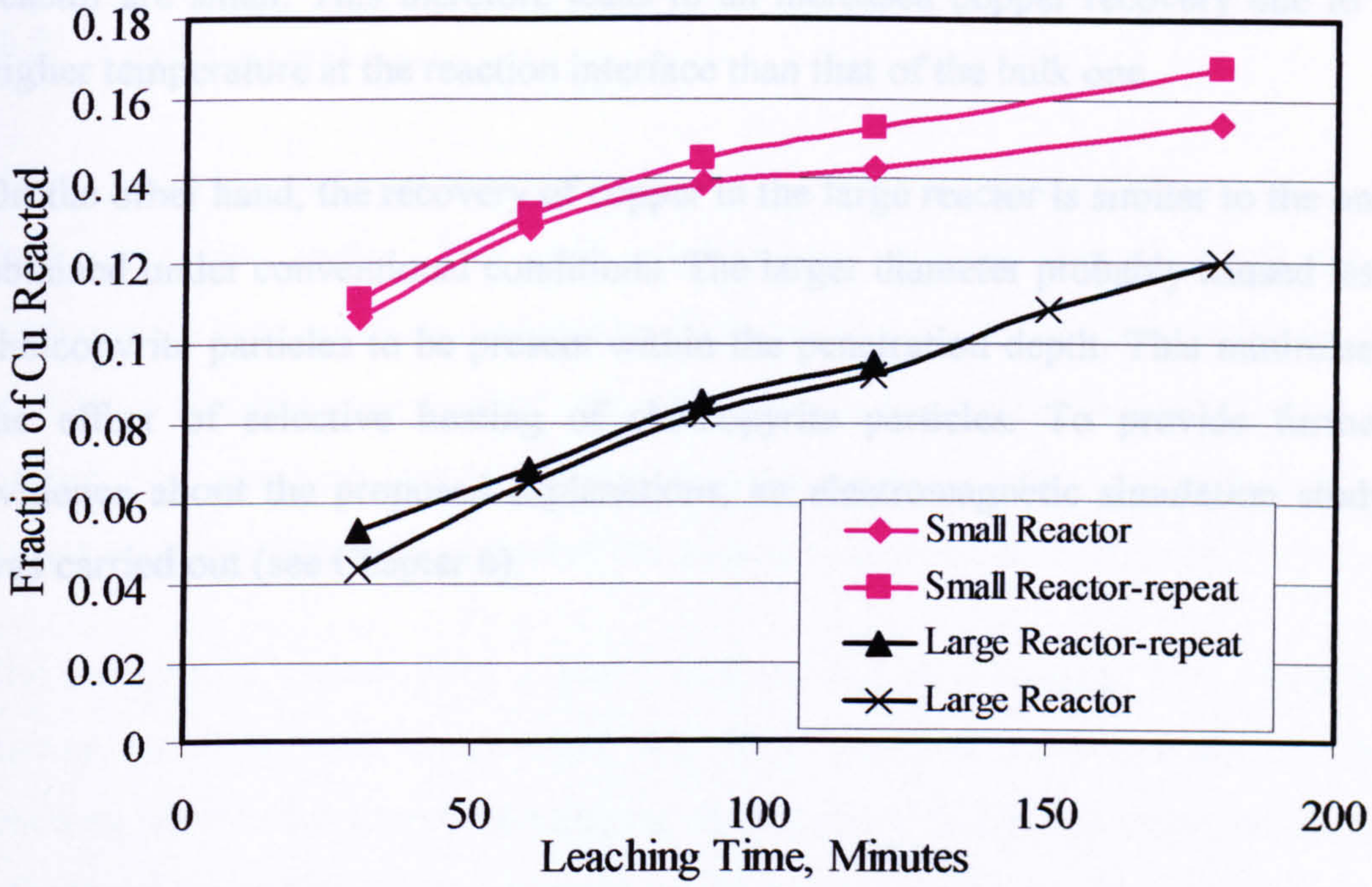

Figure 4-56 Effect of reactor size on the recovery of copper from GBL chalcopyrite when leached in single mode microwave cavity ($C_{Fe2(SO4)3}$:0.25M, particle size:<38µm, 91°C, 3 hours)

The recovery of copper in the large reactor is comparable to that obtained under conventional conditions (see Table 4-16). The average copper recovery from chalcopyrite when leached in ferric sulphate under conventional conditions after three hours leaching time was about 12% which is the same recovery achieved in the single mode cavity using the large reactor.

On the other hand, the copper recovery obtained after three hours leaching time in the small reactor was about 16% on average. This value is slightly higher than the recovery obtained in multimode cavity under agitation conditions (about 14.7% as in Table 4-16). This difference may be amplified even further if the losses on the vessel walls mentioned earlier are taken into account.

Referring back to the discussion given in Section 4.4.6, the effect of chalcopyrite selective heating in the microwave field is expected to be more pronounced if the particles fall within the penetration depth of microwaves. This is consistent in the situation of the small reactor (reactor radius= 10mm) where the dimensions of the

reactor are small. This therefore leads to an increased copper recovery due to a higher temperature at the reaction interface than that of the bulk one.

On the other hand, the recovery of copper in the large reactor is similar to the one obtained under conventional conditions. The larger diameter probably caused less chalcopyrite particles to be present within the penetration depth. This minimises the effect of selective heating of chalcopyrite particles. To provide further evidence about the proposed explanations, an electromagnetic simulation study was carried out (see Chapter 6).

4.8 Conclusions

This chapter has demonstrated the main analytical and experimental methods used throughout this thesis. The main chalcopyrite used in this study is GBL chalcopyrite because of its high purity confirmed by XRD and chemical analysis. A microwave digestion method was developed and validated in order to digest copper, zinc and lead ores and concentrate. This method offers a fast, clean and robust sample preparation procedure for chemical analysis using ICP-AES.

The leaching of chalcopyrite in ferric sulphate has been studied. The effects of stirring, particle size, temperature and ferric sulphate concentration on the leaching kinetics have been investigated. It was found that the reaction rate is not influenced by agitation when stirring speed exceeds 300 rpm. The reaction rate was found to be inversely proportional to the particle size. Furthermore, the effect of ferric sulphate concentration above 0.1 M is negligible and any further increase in Fe^{3+} concentration seems to correspond to a slight drop in the reaction rate. The reason behind this slight drop is not clear. The reaction rate was found to be highly sensitive to temperature change and the activation energy calculated was about 79.5 kJ/mole suggesting that rate of reaction is not limited by any diffusion process and is rather surface reaction controlled. This was confirmed by SEM analysis of the leach residue. The surface was not found to be covered by sulphur and only few sites or planes were found to be aggressively attacked.

The ToF-SIMS analysis on a freshly fractured GBL chalcopyrite piece shows the presence of regions of different reactivity and ability to be oxidized confirming the selective attack on chalcopyrite surface during the leaching process. It is speculated that this selectivity in reactivity of various planes and regions on the chalcopyrite surface is probably linked to the electrochemical properties of various fracture surfaces created during size reduction process. Furthermore, the SEM study showed enhanced reactivity of chalcopyrite when it is in intimate contact with pyrite phase because of the galvanic interaction between the two minerals.

ToF-SIMS results coupled with SEM analysis on GBL and MZ2HE chalcopyrite seem to support the reconstruction mechanism of chalcopyrite surfaces, which was proposed to occur on particular cleavage planes ((Klauber, 2003). The areas would be more reactive than other planes and thus attacked during leaching.

The application of microwave heating to chalcopyrite leaching has a positive effect on the reaction kinetics. Although the increase in copper recovered from chalcopyrite is low under microwave conditions, it is consistently higher than conventional leaching over the temperature range used. Furthermore, the difference between the reaction rates achieved within microwave and conventional leaching conditions was found to be statistically significant. However, this influence seems to be of a thermal nature. The increase in copper recovery during microwave leaching is due to a combination of two factors. Primarily, the limitation of microwave penetration through a high loss leaching solution which causes a temperature difference between the outer shell of the leaching solution and the bulk temperature measured. This is evident from the parallel nature of the Arrhenius plot and the similar values of apparent activation energy for both microwave and conventional leaching conditions. This suggests that microwave energy has no effect on the intrinsic leaching mechanism.

Secondly, the selective heating of chalcopyrite in such a high loss leaching solution potentially explains the higher copper recovery under microwave conditions, which is demonstrated by the higher recovery of copper when no agitation was applied. In addition, this is supported by the high conductivity of chalcopyrite which causes chalcopyrite to heat mainly by conductive losses.

The leaching of chalcopyrite in ferric chloride has been studied to a lesser extent. The reaction rate was also found to be sensitive to temperature change. However the agitation was found to have a negative influence on the leaching rate. This result is consistent for both GBL and MZ2HE materials. It is suggested that the higher rate of reaction under stagnant conditions was due to another oxidation reaction between $CuCl_2$ and chalcopyrite. The chalcopyrite oxidation by $CuCl_2$ is more evident at stagnant conditions because of the higher concentration of $CuCl_2$

at the chalcopyrite surface when the system is not agitated. Surprisingly, anaerobic leaching (where the leaching vessel was isolated from air being drawn in and from gases escaping) has resulted in an enhanced copper recovery after 3 hours leaching time under both stagnant and agitated conditions. This phenomenon could not be explained and further research is required.

It was therefore very difficult to verify if microwaves had positive effect on the reaction kinetics of chalcopyrite dissolution in ferric chloride. This is because the microwave leaching vessel is closed which affected the copper recovery without microwaving the system. In addition the negative influence of agitation will influence the selective heating of chalcopyrite and the penetration depth effects being observed.

Microwave treatment of chalcopyrite in a single mode cavity has been demonstrated. The reactor size had an effect upon the chalcopyrite leaching outcome. Furthermore, the results of leaching in the small reactor seem to support the hypothesis of the selective heating of chalcopyrite and the effect of penetration depth on the overall leaching kinetics.

CHAPTER FIVE

Sphalerite Leaching

5.1 Overview

This chapter will consider the leaching of sphalerite in ferric sulphate under both conventional and microwave conditions. In Chapter 4 the leaching of chalcopyrite was studied extensively (Section 4.5.2) and the effects of various parameters were investigated. It was found that factors such as the effect of agitation and temperature could be used to explain the effect of microwaves on the leaching of chalcopyrite. For this reason the current study is limited to the investigation of the effect of agitation and temperature on the leaching of sphalerite in ferric sulphate under both microwave and conventional conditions.

The aim of this chapter is to investigate the effect of microwaves on the leaching of sphalerite in ferric sulphate, based on the observed effect of microwaves on the leaching of chalcopyrite in ferric sulphate, to widen the understanding obtained from chalcopyrite study.

5.2 Material Preparation

The sphalerite used in this study was a piece of museum grade sphalerite obtained from the mineral dealer Gregory, Bottley and Lloyd, UK. The visual examination (by eye) of the sphalerite piece did not reveal a presence of any other minerals apart from few quartz pieces that were easily removed. The purity of the

sphalerite sample was confirmed by XRD analysis and chemical analysis thereafter.

The sphalerite sample was prepared using the same procedure which was used to prepare GBL chalcopyrite samples (Section 4.2.1.1). Sphalerite sample was then divided into several size fractions using wet sieving. The size fractions used in this study were 53-38 μm (for SEM examination) and <25μm (for leaching experiments and SEM examination). A narrower size distribution (<25μm) was used for sphalerite leaching compared to GBL chalcopyrite (<38μm) because the original sphalerite sample was large enough to prepare a significant quantity of narrow size distribution.

5.3 Physical Characterization of Sphalerite

5.3.1 XRD Analysis

A representative sample of sphalerite was manually taken, after prolonged mixing in a jar, prior to wet sieving, for XRD analysis which was carried out according to the procedure presented in Section 4.2.2.1. The XRD pattern of the sample is given in Figure 5-1, which shows its high purity (see XRD pattern of reference sphalerite shown in Appendix 5-1)

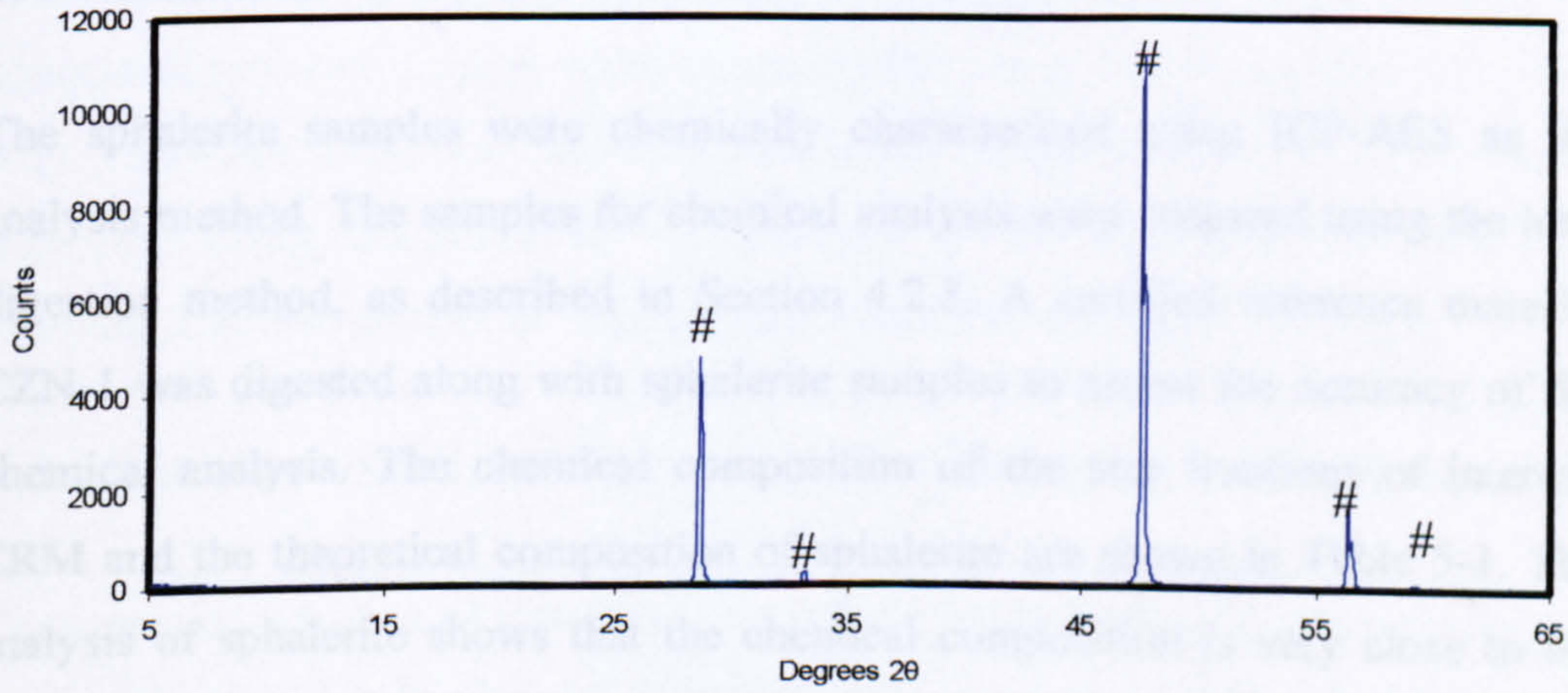

Figure 5-1 XRD pattern of sphalerite (#-denotes peaks of pure sphalerite)

5.3.2 Laser Diffraction Analysis

The size distributions of the <25 and 38-53µm sphalerite samples were characterized by Malvern® laser diffraction, according to the procedure presented in Section 4.2.2.2.2. The size distribution of the sphalerite samples are shown in Figure 5-2. The average D(3,2) of the size fractions, <25 and 38-53µm, were found to be 7 and 30µm respectively.

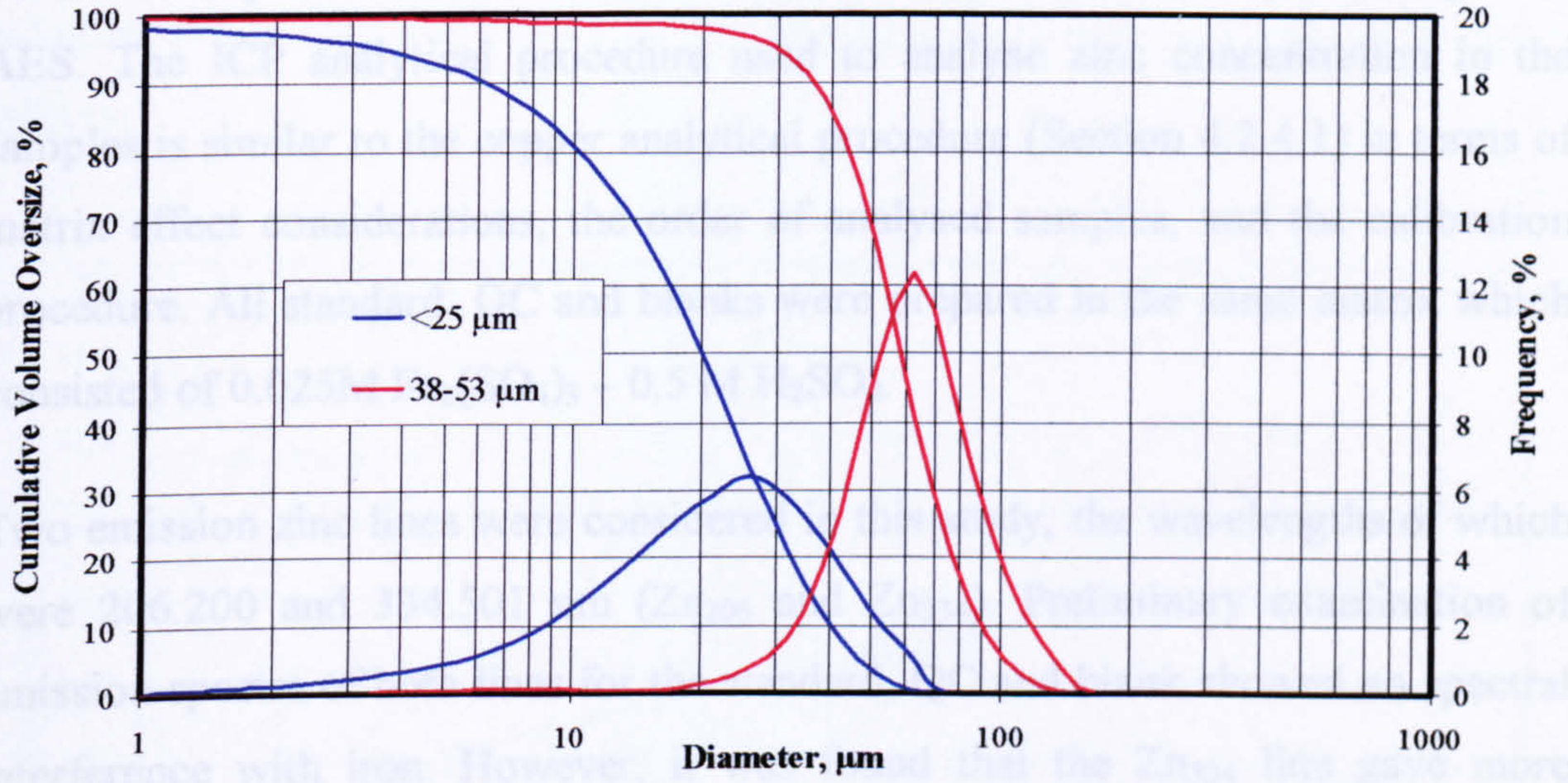

Figure 5-2 Frequency and cumulative volume undersize of sphalerite size fractions as analysed by Malvern® laser diffraction

5.4 Chemical Characterization

The sphalerite samples were chemically characterized using ICP-AES as the analysis method. The samples for chemical analysis were prepared using the total digestion method, as described in Section 4.2.3. A certified reference material CZN-1 was digested along with sphalerite samples to assess the accuracy of the chemical analysis. The chemical composition of the size fractions of interest, CRM and the theoretical composition of sphalerite are shown in Table 5-1. The analysis of sphalerite shows that the chemical composition is very close to the theoretical values (32.9% S and 67.09%Zn). Furthermore, the iron content in the crystal lattice was found to be less than 0.1%.

Table 5-1 The average chemical composition of sphalerite

Particle size, µm	Cu %	Fe %	S %	Zn %
Pure ZnS	-	-	32.90	67.09
<25	0.05±0.00	0.09±0.00	31.99±0.13	66.88±0.30
38-53	0.03±0.00	0.06±0.00	31.73±0.15	66.58±0.48
CRM analyzed	0.12±0.00	11.57±0.07	29.35±0.20	43.47±0.32
CRM-Certificate	0.144±0.00	10.93±0.06	30.20±0.20	44.74±0.11

5.5 Zinc Analysis by ICP-AES

Periodic samples were withdrawn during leaching for zinc analysis using ICP-AES. The ICP analytical procedure used to analyse zinc concentration in the samples is similar to the copper analytical procedure (Section 4.2.4.1) in terms of matrix effect considerations, the order of analysed samples, and the calibration procedure. All standard, QC and blanks were prepared in the same matrix which consisted of 0.025M $Fe_2(SO_4)_3$ – 0.5 M H_2SO_4.

Two emission zinc lines were considered in this study, the wavelengths of which were 206.200 and 334.501 nm (Zn_{206} and Zn_{334}). Preliminary examination of emission spectra of both lines for the standard, QC and blank showed no spectral interference with iron. However, it was found that the Zn_{334} line gave more accurate values of the zinc in the QC when the zinc concentrations in the QC were scrutinized at the end of the analytical runs. Further investigation, to check the linearity for both lines, showed that Zn_{334} holds linear characteristics (intensity vs. concentration) over a much wider concentration range than Zn_{206} (See Appendix 5-2). Therefore, Zn_{334} was chosen as a main line for data treatment as the linearity was particularly important for the analysis of the sphalerite total digestion samples. The zinc content of these digestion samples was about 1300 ppm.

5.6 Conventional Leaching of Sphalerite in Ferric Sulphate

Conventional leaching of sphalerite was carried out according to the experimental method described in Section 4.3.1. In this section, only the effects of agitation and effect of temperature were investigated. All the leaching experiments were carried out in 0.25 M $Fe_2(SO_4)_3$ – 0.5 M H_2SO_4.

5.6.1 Effect of Temperature

The effect of temperature on the rate of zinc extraction from sphalerite when leached in ferric sulphate was investigated over a temperature range of 50 to 90°C with a particle size of < 25 μm. Figure 5-3 shows the dissolution curves of sphalerite in ferric sulphate at different temperatures. The rate of zinc extraction greatly accelerated as the temperature increased. At a temperature of 50°C the zinc released into solution was found to be about 19% after three hours leaching time whereas about 74% was recovered at a temperature of 90°C after the same period of time.

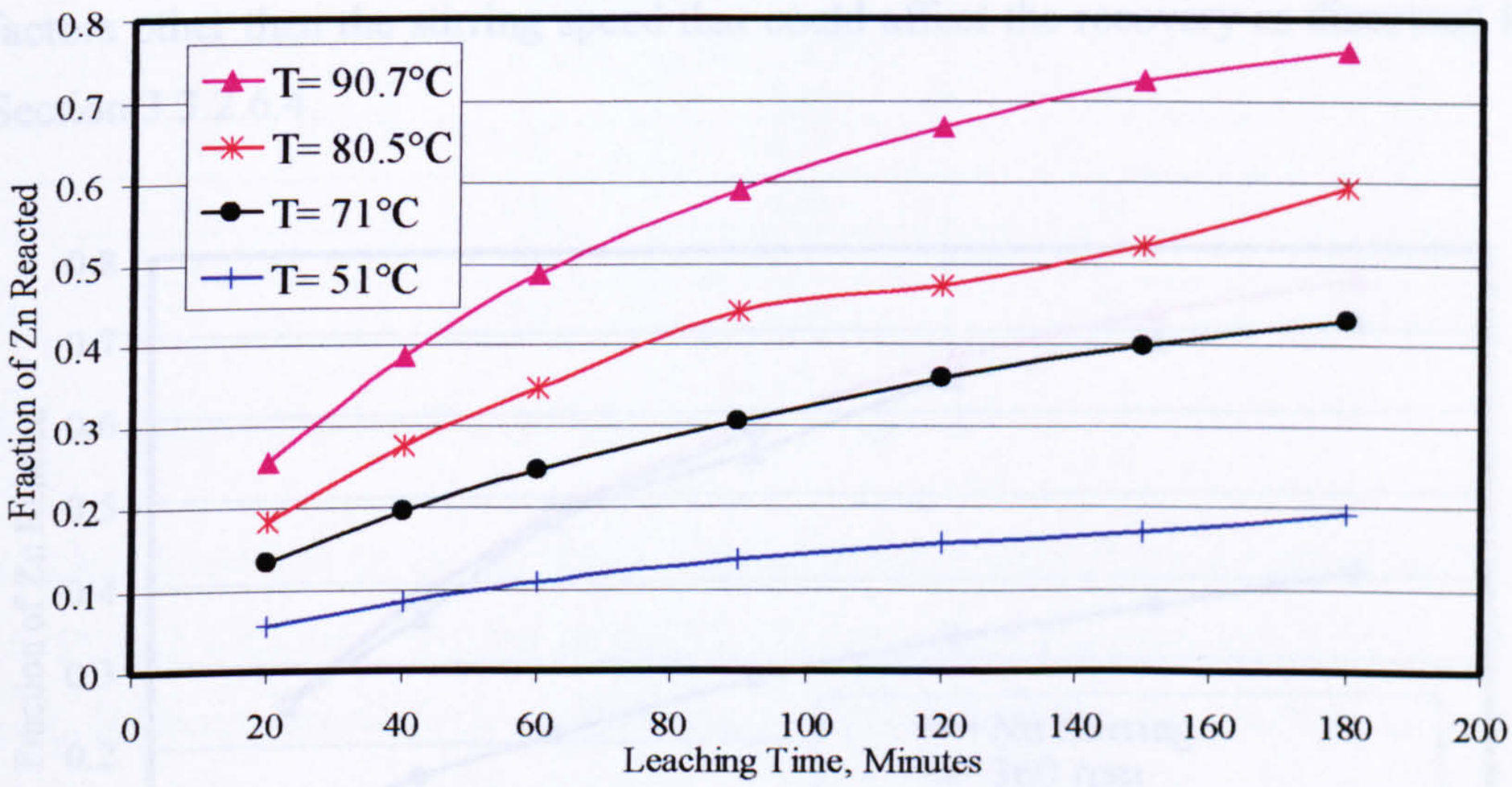

Figure 5-3 The effect of temperature on the conventional leaching of sphalerite as a function of time ($C_{Fe2(SO4)3}$: 0.25 M, particle size: <25μm)

5.6.2 Effect of Agitation

The effect of agitation on the leaching kinetics of sphalerite was determined at a temperature of 90°C using material with a particle size of <25μm. The experimental results are shown in Figure 5-4, this figure clearly shows that the leaching rate was affected by agitation. In the absence of agitation the dissolution reaction proceeded at a slower rate, which suggests that the participation of mass transfer through the liquid film layer is influential upon the reaction kinetics under stagnant conditions. Furthermore, the rate of reaction at a stirring speed of 360 rpm was found to be close to that at 550 rpm (see Figure 5-4). The replicate

experiment at 360 rpm gave essentially similar zinc recoveries to 550 rpm. It should be noted, however, this experiment was terminated due to a fault in water bath system after about 100 minutes leaching time.

The result obtained in this work seem to contradict with those of the Verbaan and Crundwell (1986) who reported that zinc recovery is independent of stirring speed. On the other hand, the current results agree with the work of (Bobeck and Su, 1985; Jin et al., 1984; Rath et al., 1981) where it was reported that the rate of reaction was influenced by agitation up to a stirring speed of 300 rpm (see Section 3.5.1.4). It is not clear why agitation did affect the rate of reaction in Verbaan and Crundwell (1986) experiments. However, it should be realised that there are other factors other than the stirring speed that could affect the recovery as discussed in Section 3.3.2.6.4.

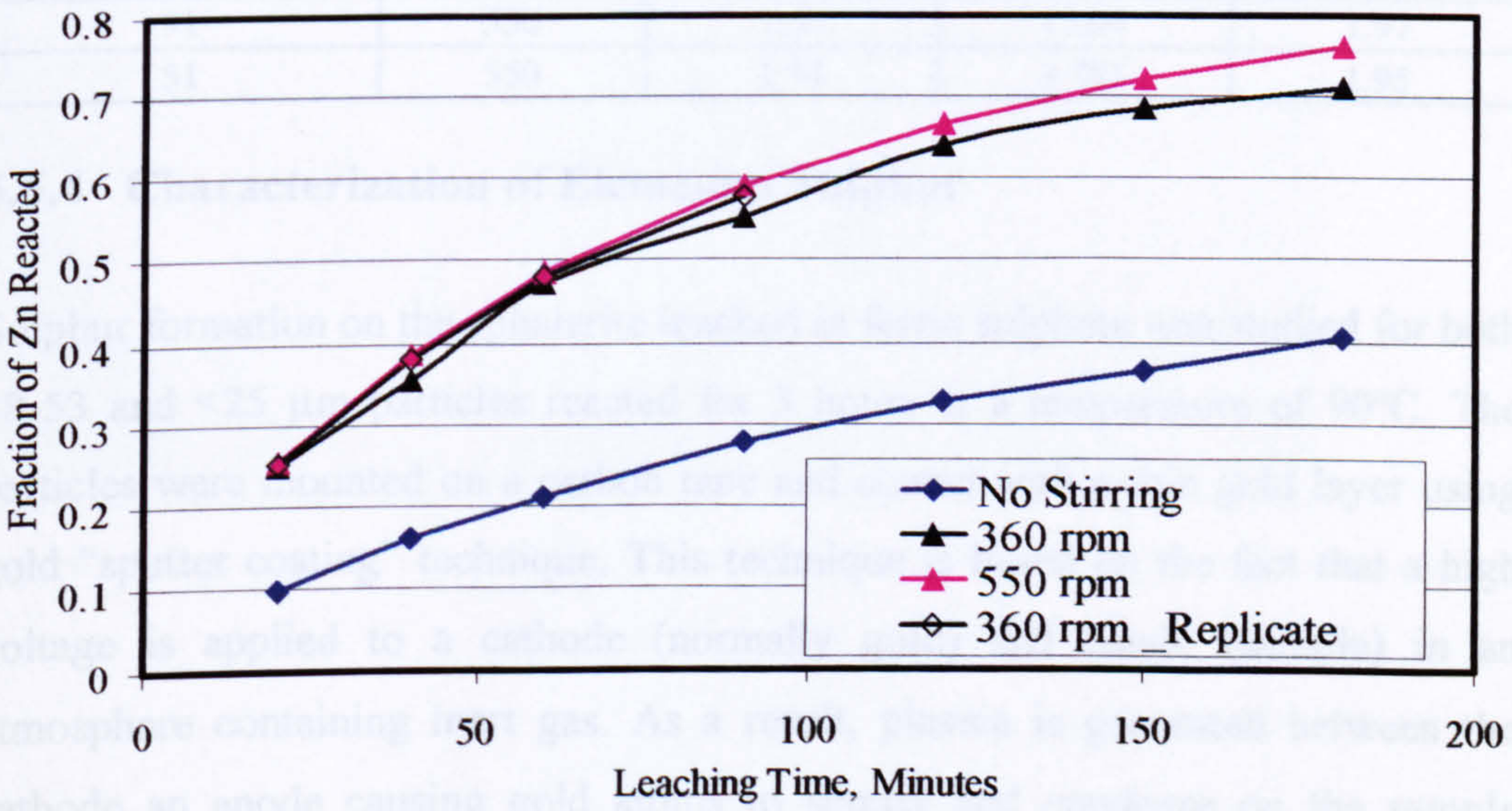

Figure 5-4 The effect of stirring speed on the conventional leaching of sphalerite in ferric sulphate as a function of time ($C_{Fe2(SO4)3}$: 0.25 M, T=90°C, particle size: < 25µm).

5.6.3 Ratio of Reaction Products

The calculated molar ratio of reaction products Fe^{2+}/Zn^{2+} is presented in Table 5-2. The theoretical molar ratio of Fe^{2+}/Zn^{2+} according to Reaction 3-18 is 2. The experimental value of the calculated ratio is very close to the theoretical (Fe^{2+}/Zn^{2+}=2). At a temperature of 90°C the ratio of Fe^{2+}/Zn^{2+} is slightly higher

than two. If any sulphate formation has occurred it would be of maximum value of 3% of the total amount of reacted sulphur. This was estimated according to Equation 5-1, which was derived based on the stoichiometry of Reactions 3-18 and 3-19:

$$\%SO_4^{2-} = 16.67\left(\frac{Fe^{2+}}{Zn^{2+}}\right) - 33.33 \qquad \textbf{Equation 5-1}$$

The amount of sulphate formed is impossible to measure directly against the high background sulphate concentration (0.25 M $Fe_2(SO_4)_3$- 0.5 M H_2SO_4) by ICP or any other method.

Table 5-2 Molar ratio of reaction products as measured when sphalerite was leached in 0.5 M $Fe_2(SO_4)_3$-0.5 M H_2SO_4 for 3 hrs under conventional conditions

Temperature, °C	Stirring speed, rpm	Zn^{2+}, mmole	Fe^{2+}, mmole	Fe^{2+}/Zn^{2+} Ratio
91	0	4.10	8.49	2.07
91	360	7.17	15.52	2.17
71	550	4.38	8.41	1.92
91	550	7.63	15.04	1.97
51	550	1.94	3.781	1.95

5.6.4 Characterization of Elemental Sulphur

Sulphur formation on the sphalerite leached in ferric sulphate was studied for both 38-53 and <25 μm particles reacted for 3 hours at a temperature of 90°C. The particles were mounted on a carbon tape and coated with a thin gold layer using gold "sputter coating" technique. This technique is based on the fact that a high voltage is applied to a cathode (normally gold) and anode (sample) in an atmosphere containing inert gas. As a result, plasma is generated between the cathode an anode causing gold atoms to sputter and condense on the sample surface (Goldstain et al., 2003). Gold coating was required to improve the surface conductivity of the sphalerite particles. The phases ZnS and elemental sulphur were identified by the Energy Dispersive X-ray (EDAX) analysis

Figure 5-5 illustrates 38-53 μm sphalerite particles prior to leaching. The particles are generally flat and show some flat cleavage surfaces and other textured surfaces. Figure 5-6 shows four sphalerite particles (38-53μm) after the leaching process. The particles are linked together by a sulphur bridge and the particles are

shown to be partially covered with sulphur. Figure 5-7 shows the surface of the same particles, shown in Figure 5-6 at a higher magnification where the original texture structure still can be seen. The surface is not totally enveloped with a sulphur layer, but rather it is covered with batches of sulphur deposited randomly on the surface. Similarly, the particles from the <25μm size fraction were found to be partially covered with sulphur and some original texture still can be seen (see Figure 5-8). The EDAX Spectra of the area marked by ZnS in Figure 5-8 confirm that this surface is mostly sphalerite with an intense sulphur signal (Figure 5-9).

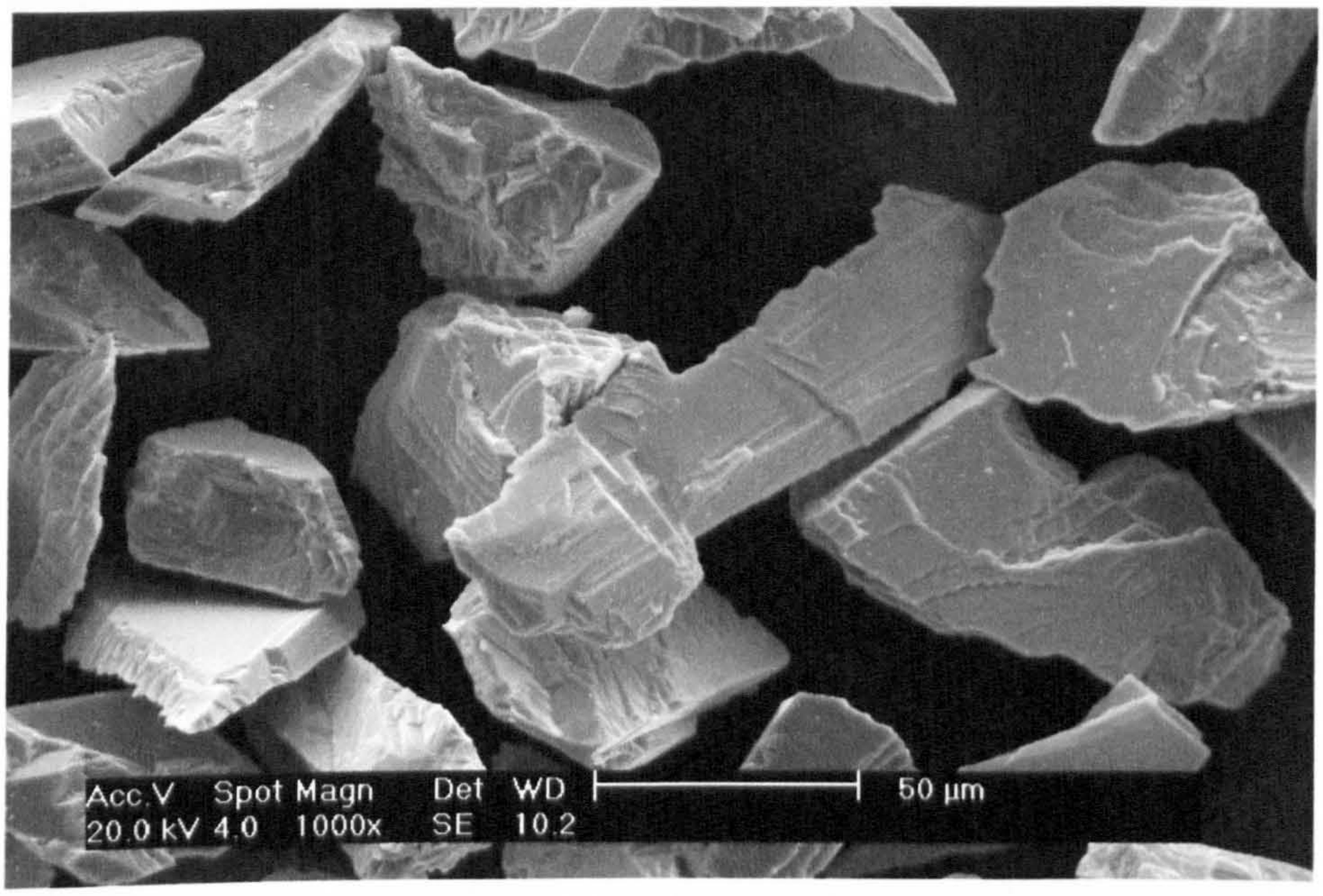

Figure 5-5 Secondary Electron micrograph of 38-53 μm sphalerite particles before leaching

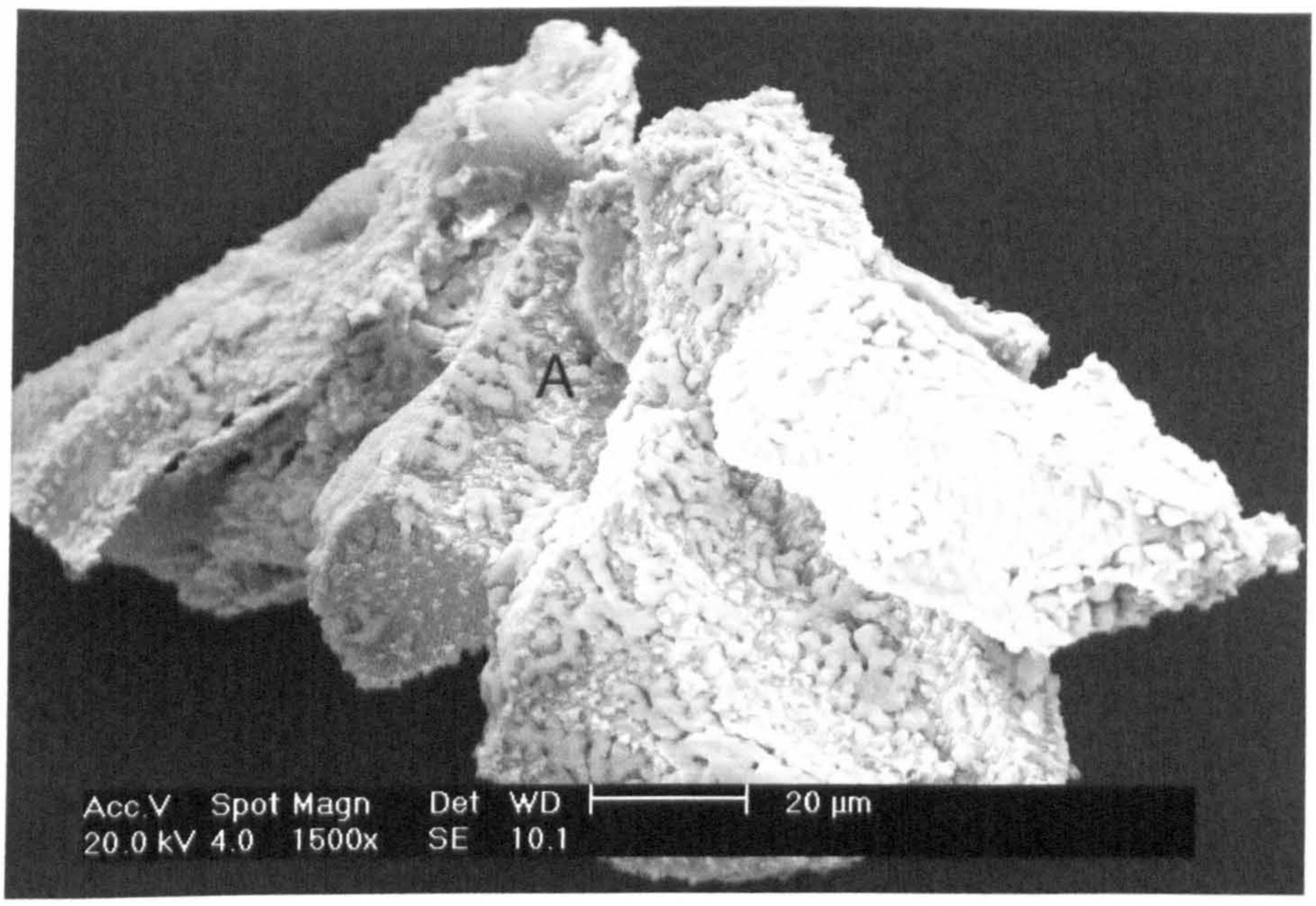

Figure 5-6 Secondary Electron micrograph showing few agglomerated sphalerite particles (38-53µm) and an extensive partially covered sulphur layer covering the particles (leached for 3 hours in 0.25 M $Fe_2(SO_4)_3$ – 0.5 M H_2SO_4 at a temperature of 90°C)

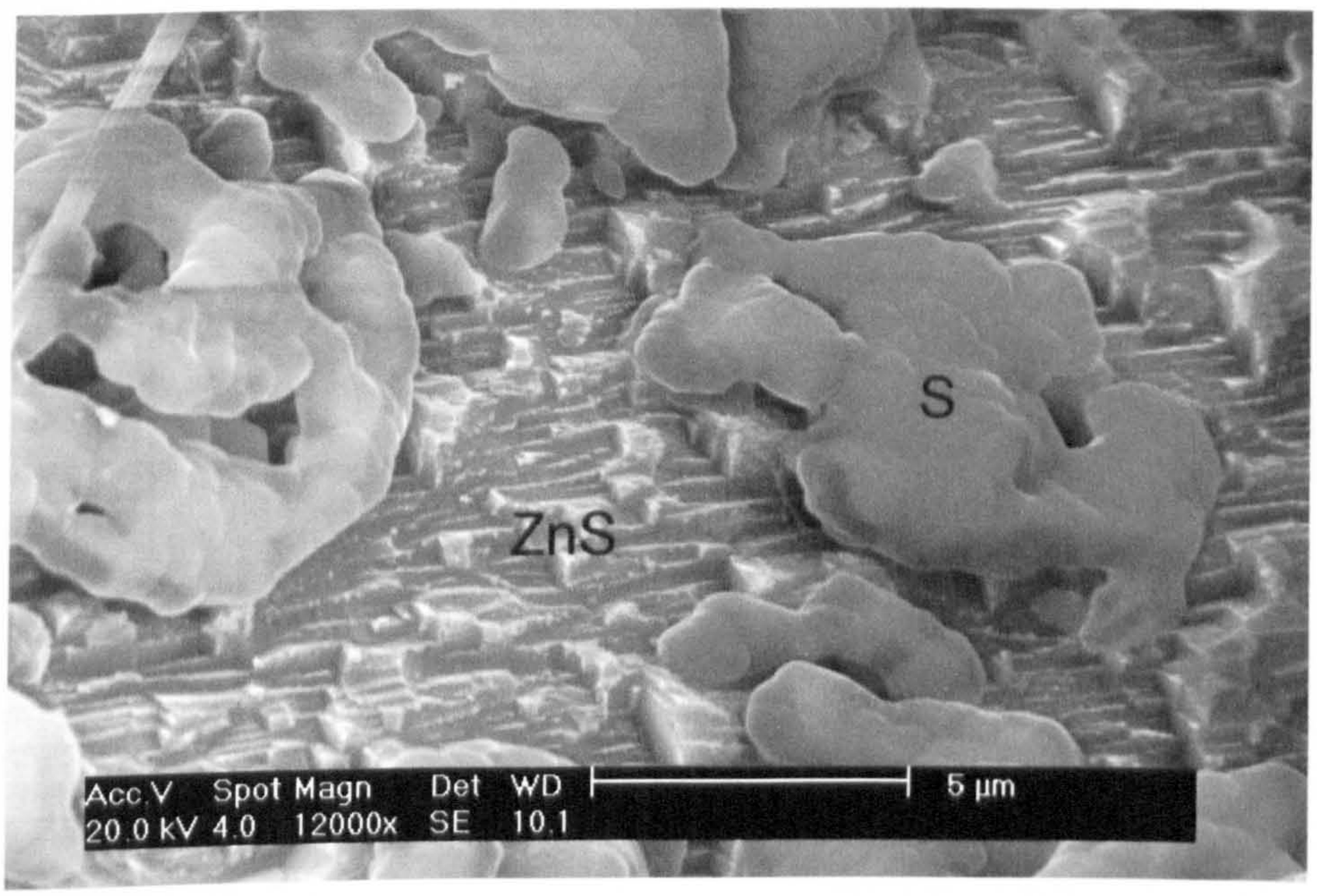

Figure 5-7 Secondary Electron micrograph showing batches of sulphur deposited on sphalerite with textured surface (the micrograph is obtained by zooming in the area marked by A in Figure 5-6 (particle size 38-53µm)

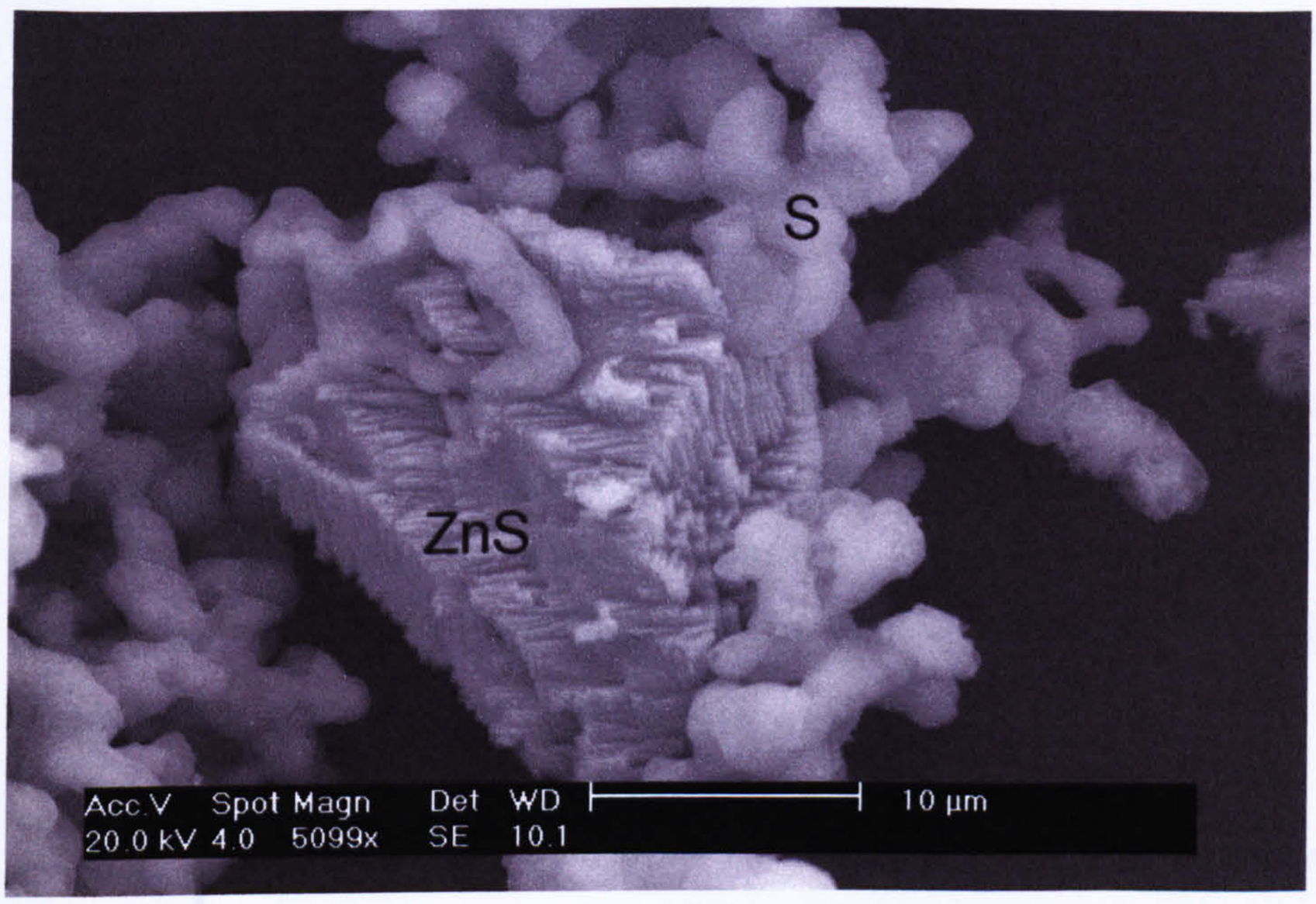

Figure 5-8 Secondary Electron micrograph of sphalerite particles (<25µm) after being leached for 3 hrs in 0.25 M $Fe_2(SO_4)_3$ – 0.5 M H_2SO_4

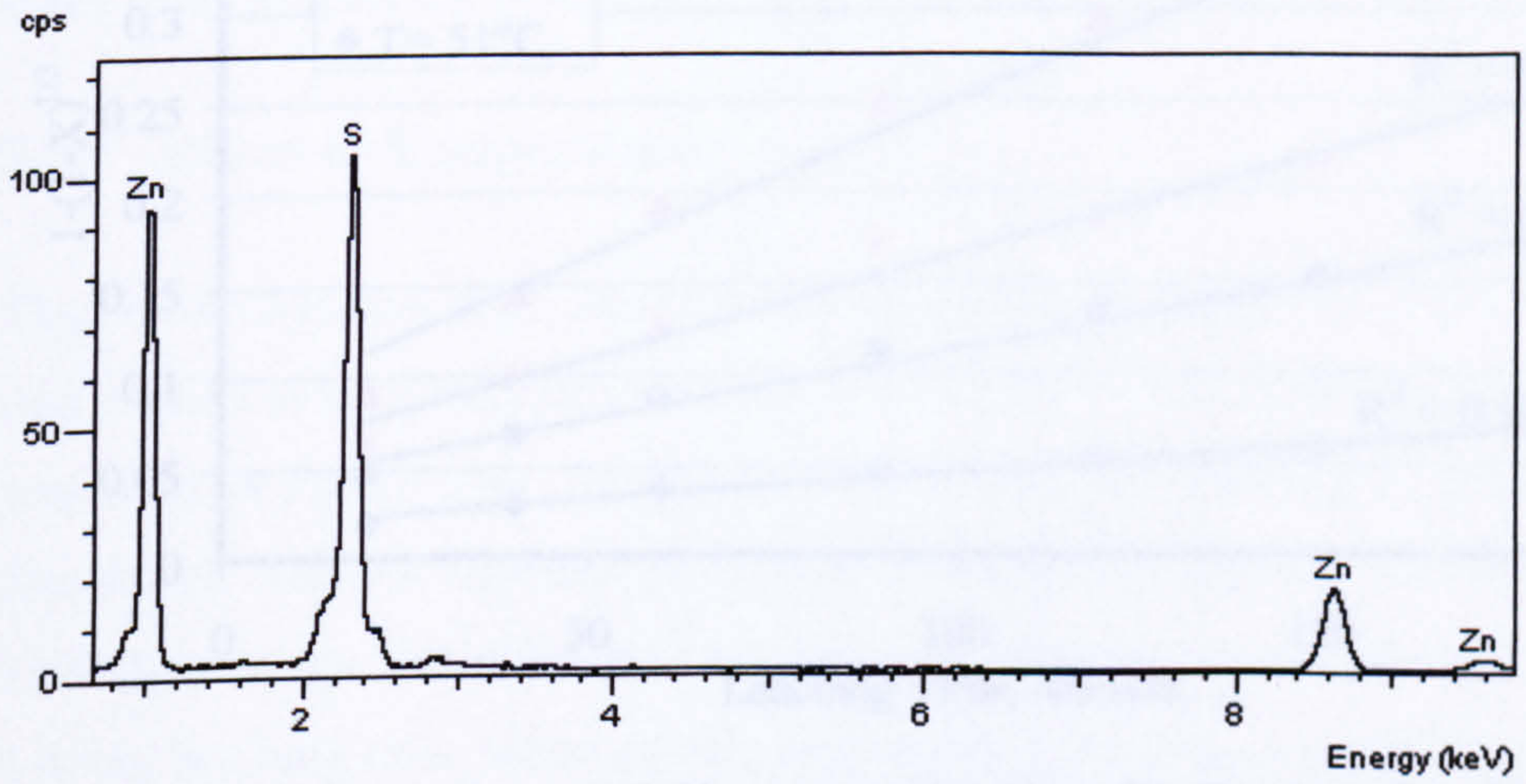

Figure 5-9 EDAX spectra of sphalerite obtained from the location marked by ZnS in Figure 5-8

5.6.5 A study of Reaction Kinetics

Previous investigations have shown that the dissolution of sphalerite in ferric sulphate is chemically controlled (Palencia and Dutrizac, 1991; Suni et al., 1989).

In the current work <25µm sphalerite particles were examined by SEM after leaching in ferric sulphate, as shown in Section 5.6.5. It was found that the elemental sulphur reaction product partially covered the reacted surface. These

observations are consistent with the observations of Jin et al (1984) and Dutrizac and MacDonald (1978) who concluded that the rate of reaction was not affected greatly by this porous sulphur. Therefore, they concluded that the reaction is chemically controlled.

When the shrinking core model (in which the rate limiting step is chemical reaction (Equation 4-11)), was applied to the data shown in Figure 5-3, a good linear fit was obtained as shown in Figure 5-10, with a correlation coefficient higher that 0.97. The quasi-linear fit in Figure 5-10 seems to support the assumption that the reaction is chemically controlled.

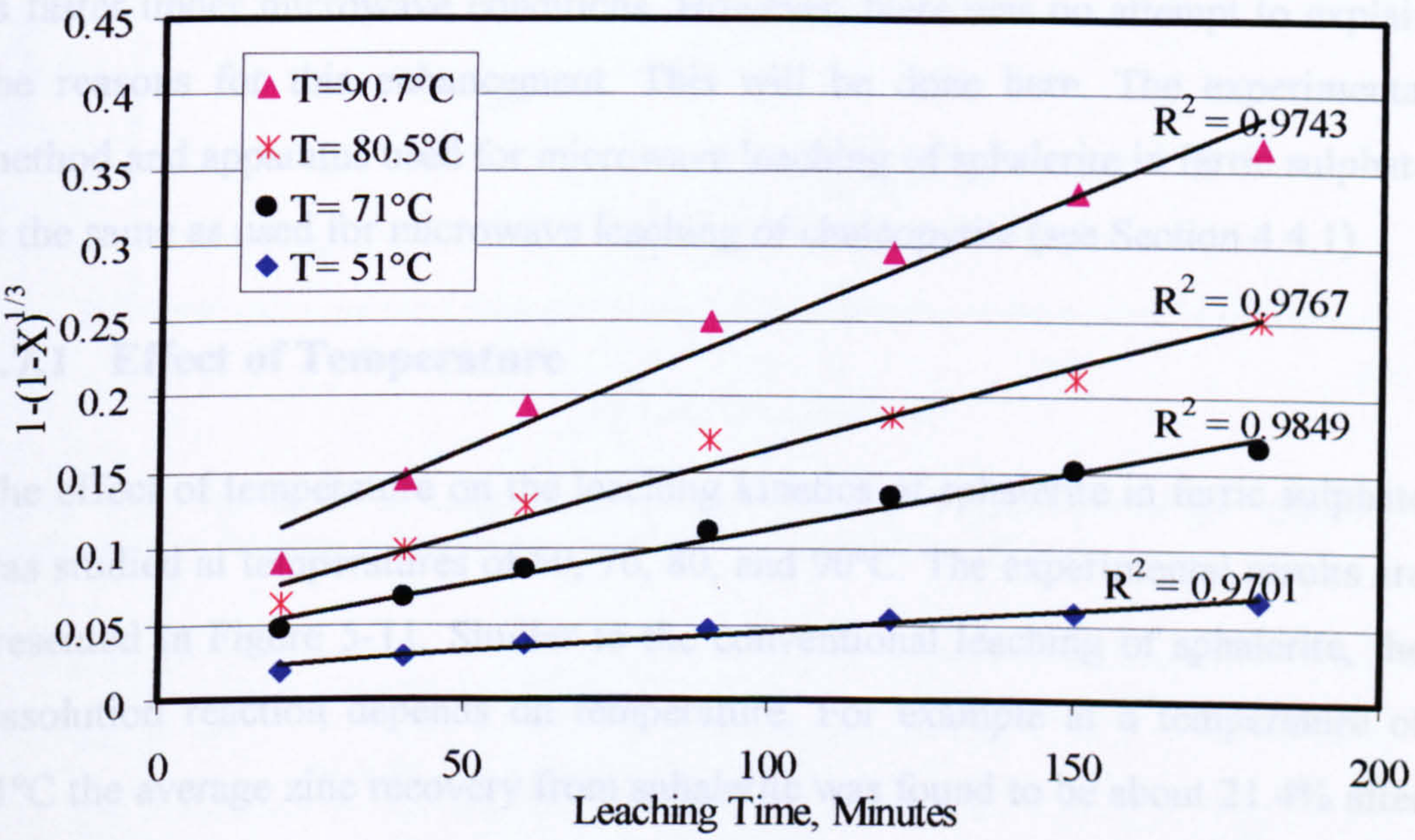

Figure 5-10 Plot fitted using a shrinking core model with a limiting step of surface reaction: conversion vs. time data in Figure 5-3 at various temperatures

The values of apparent rate constants k_s were calculated as the slope of the straight lines in Figure 5-10 and are tabulated in

Table 5-3. The value of activation energy calculated from the apparent rate constants was found to be 43 kJ/mole. This value is consistent with chemical reaction control and agrees with the values of activation energy reported in literature (Appendix 3-3). For example, Ferron (2000) reported an activation energy value of 36.5 kJ/mole and Suni et al (1989) reported a value of 46 kJ/mole.

Table 5-3 The apparent rate constants of the sphalerite dissolution in ferric sulphate

Leaching temperature, °C	Apparent rate constant $k_s \times 10^{-4}$, min^{-1}	
	Conventional	Microwave
51	2.88	3.35
71	7.47	8.26
80.5	11.3	11.9
90.7	17	18.5

5.7 Microwave Leaching of Sphalerite in Ferric Sulphate

As discussed earlier (Section 3.6.6) several reports are found regarding microwave leaching of sphalerite in ferric ion media (Peng and Liu, 1992; Peng and Liu, 1997). It was reported that the dissolution of sphalerite in ferric sulphate is faster under microwave conditions. However, there was no attempt to explain the reasons for this enhancement. This will be done here. The experimental method and apparatus used for microwave leaching of sphalerite in ferric sulphate is the same as used for microwave leaching of chalcopyrite (see Section 4.4.1)

5.7.1 Effect of Temperature

The effect of temperature on the leaching kinetics of sphalerite in ferric sulphate was studied at temperatures of 50, 70, 80, and 90°C. The experimental results are presented in Figure 5-11. Similar to the conventional leaching of sphalerite, the dissolution reaction depends on temperature. For example at a temperature of 51°C the average zinc recovery from sphalerite was found to be about 21.4% after 3 hours leaching time, whereas zinc recovery at a temperature of 91°C on average reached 81.7% after the same period of time.

5.7.2 Effect of Agitation

The effect of agitation on microwave leaching of chalcopyrite was investigated at a temperature of 90°C. The experimental results are shown in Figure 5-12. The recovery of zinc from sphalerite increased considerably as a result of agitation under microwave conditions, which was consistent with the results obtained under conventional conditions. Furthermore, the enhanced rate of reaction with agitation is also consistent with the expected mass transfer resistance under stagnant

conditions caused by the presence of a liquid boundary film layer. This is different from the observations made regarding microwave leaching of chalcopyrite in ferric sulphate (Section 4.4.2.3), where the copper recovery was found to be higher under stagnant conditions.

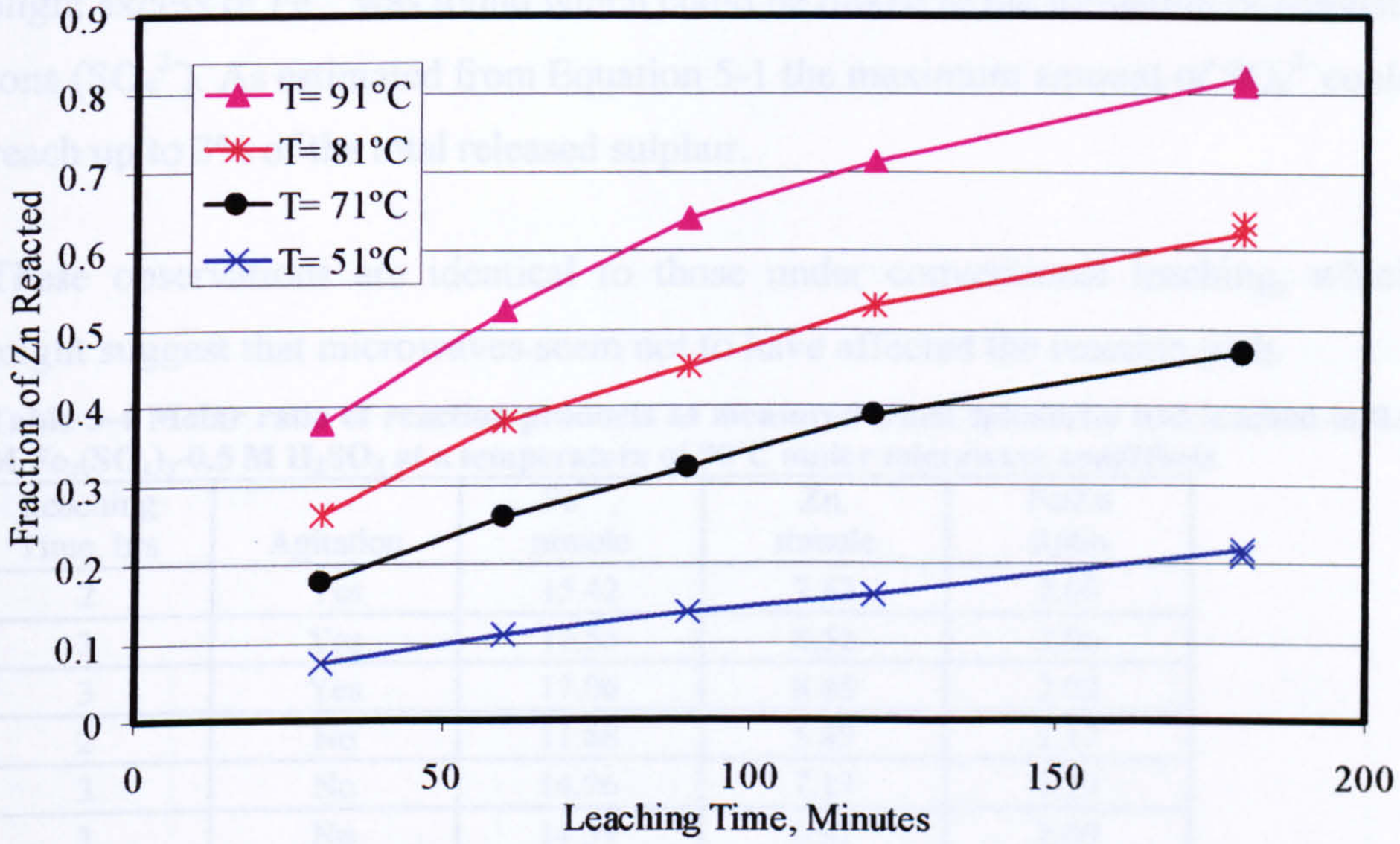

Figure 5-11 The effect of temperature on the leaching of sphalerite under microwave conditions as a function of time ($C_{Fe2(SO4)3}$: 0.25 M, particle size: <25µm)

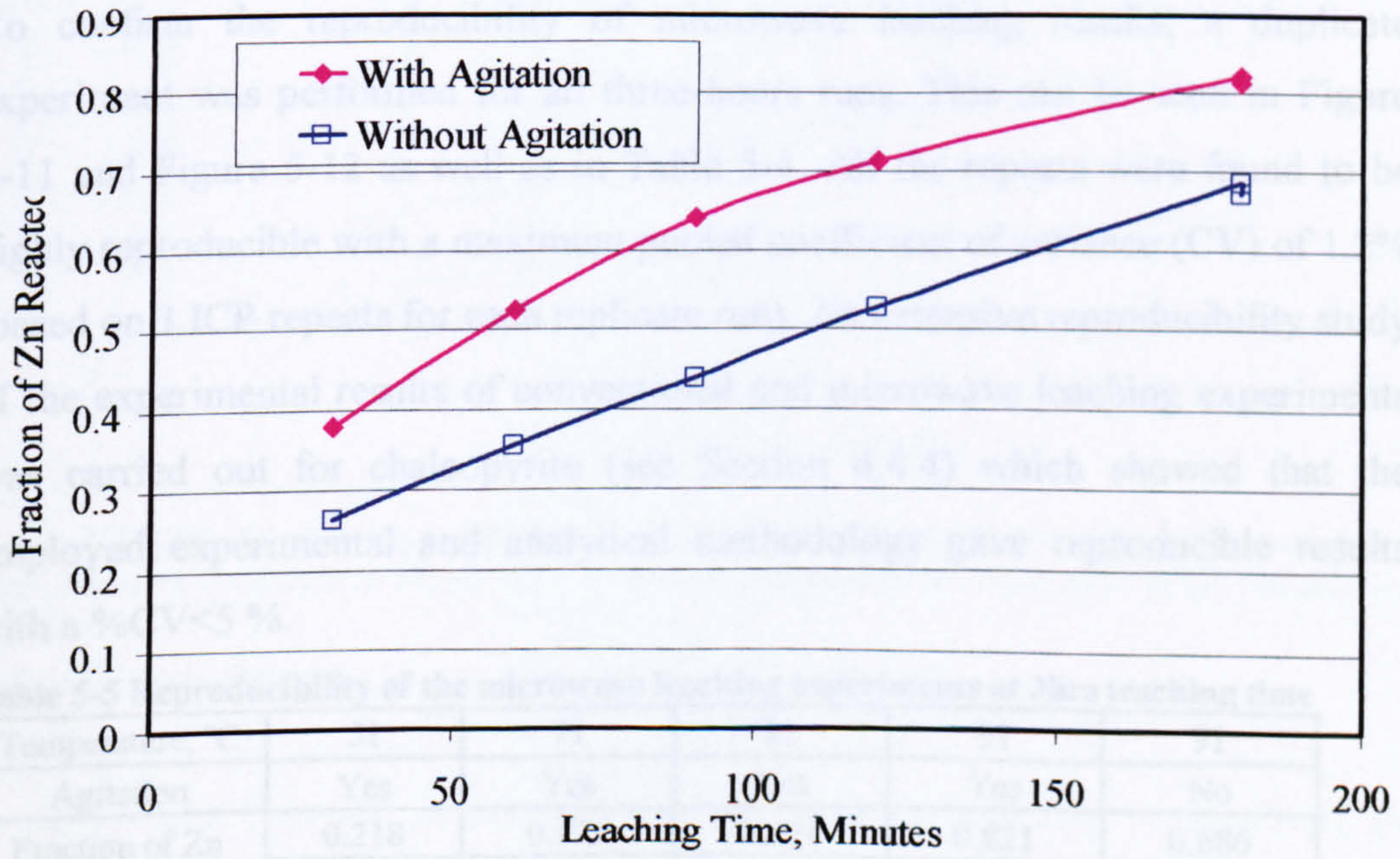

Figure 5-12 The effect of agitation on microwave leaching of sphalerite in ferric sulphate as a function of time ($C_{Fe2(SO4)3}$: 0.25 M, T=90°C, particle size: < 25µm).

5.7.3 Ratio of Reaction Products

In an attempt to check the stoichiometry of Reaction 3-18, the ratio of reaction products Fe^{2+}/Zn^{2+} were calculated (see Table 5-4). The Fe^{2+}/Zn^{2} ratio was found to be very close to the theoretical ratio calculated from Reaction 3-18. However, a slight excess of Fe^{2+} was found which could be linked to the formation of sulphate ions (SO_4^{2-}). As estimated from Equation 5-1 the maximum amount of SO_4^{2-} could reach up to 3% of the total released sulphur.

These observations are identical to those under conventional leaching, which might suggest that microwaves seem not to have affected the reaction path.

Table 5-4 Molar ratio of reaction products as measured when sphalerite was leached in 0.5 M $Fe_2(SO_4)_3$-0.5 M H_2SO_4 at a temperature of 90°C under microwave conditions

Leaching Time, hrs	Agitation	Fe^{2+}, mmole	Zn, mmole	Fe/Zn Ratio
2	Yes	15.42	7.42	2.08
3	Yes	17.55	8.52	2.06
3	Yes	17.06	8.45	2.02
2	No	11.88	5.49	2.17
3	No	14.96	7.13	2.10
3	No	14.59	6.97	2.09

5.7.4 Reproducibility of the Experimental Results

To confirm the reproducibility of microwave leaching results, a duplicate experiment was performed for all three-hours runs. This can be seen in Figure 5-11 and Figure 5-12 as well as in Table 5-4. All the repeats were found to be highly reproducible with a maximum pooled coefficient of variance (CV) of 1.2% (based on 3 ICP repeats for each replicate run). An extensive reproducibility study of the experimental results of conventional and microwave leaching experiments was carried out for chalcopyrite (see Section 4.4.4) which showed that the employed experimental and analytical methodology gave reproducible results with a %CV<5 %.

Table 5-5 Reproducibility of the microwave leaching experiments at 3hrs leaching time

Temperature, °C	51	71	81	91	91
Agitation	Yes	Yes	Yes	Yes	No
Fraction of Zn reacted	0.218	0.471	0.621	0.821	0.686
	0.209	0.468	0.635	0.813	0.671

5.7.5 A Study of Reaction Kinetics

As for conventional leaching of sphalerite, the shrinking core model (in which the rate limited is chemical reaction) was applied to the kinetic data presented in Figure 5-11. A good quasi-linear fit was obtained with a correlation coefficient of more than 0.987 (as can be seen in Figure 5-13). The apparent rate constants were calculated as the slope of the straight lines in Figure 5-13, values of which are presented in

Table 5-3. The value of activation energy was then calculated from the corresponding apparent rate constants and the inverse of the temperature and found to be 41.2 kJ/mole, which again suggests that the dissolution process is chemically controlled.

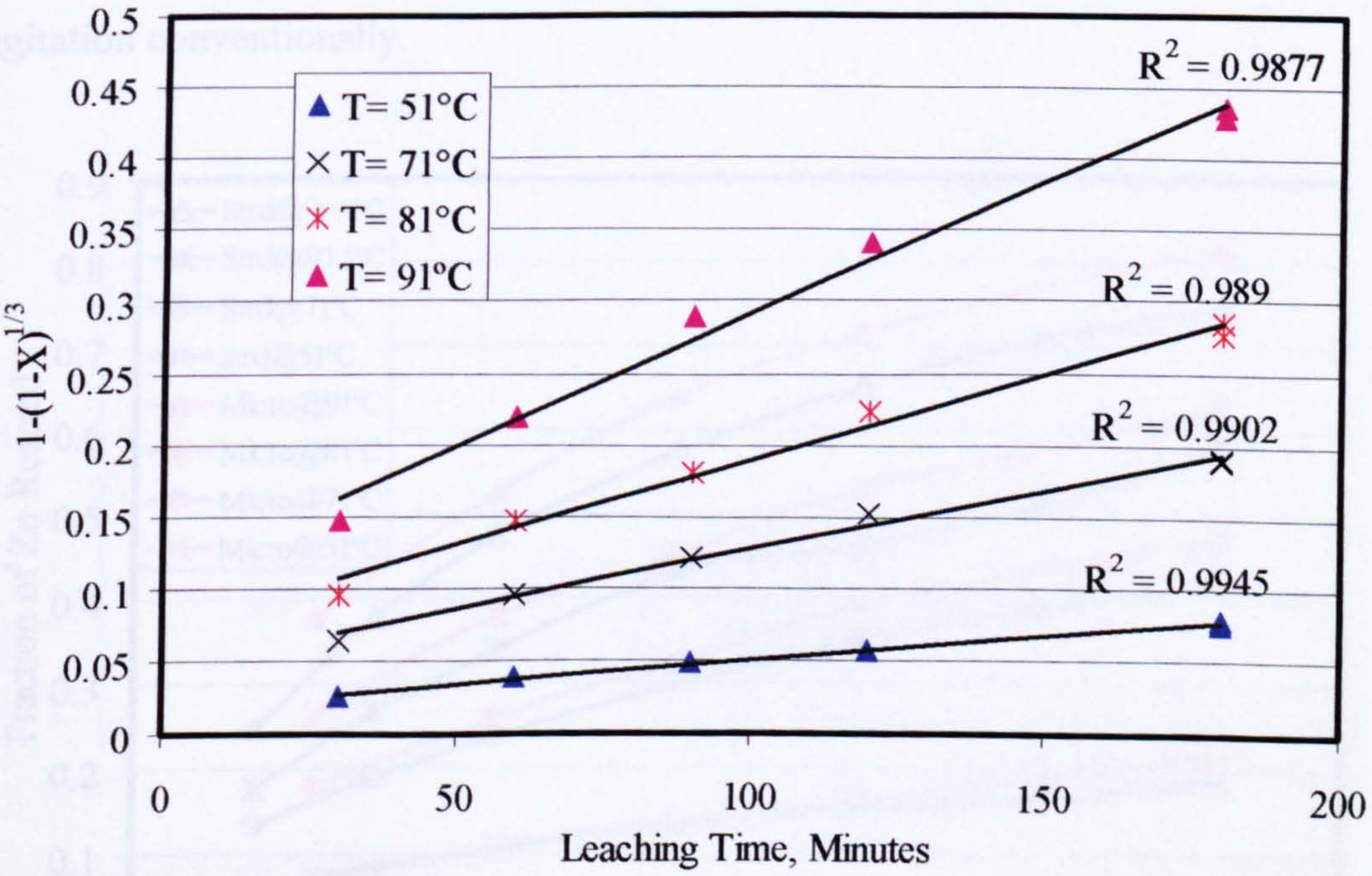

Figure 5-13 Plot fitted using a shrinking core model with a limiting step of surface reaction: conversion vs. time data in Figure 5-11 at various temperatures under microwave conditions.

5.8 Discussion

A comparison between microwave and conventional leaching of sphalerite in ferric sulphate at different temperatures is presented in Figure 5-14, Figure 5-15 and Figure 5-16. Figure 5-14 clearly demonstrates that the zinc recovery from

sphalerite is enhanced by the application of microwaves. For example, about 82% zinc was extracted from sphalerite at a temperature of 90°C under microwave conditions compared to 74% conventionally, which corresponds to about 10% increase in zinc recovery. The comparison of the apparent rate constants of the sphalerite dissolution reaction, based on the surface reaction control model, also shows an enhancement under microwave conditions (see Table 5-3). Enhancement was also observed for leaching under stagnant conditions.

The recovery of zinc with and without agitation is also higher under microwave conditions compared to the corresponding conventional conditions as can be seen in Figure 5-15. This observation is consistent with the fact that agitation eliminates the diffusion resistance due to the liquid film layer. However it is interesting to note that zinc recovery increased by more than 74% under microwaves after 3 hours without agitation compared to a 10% increase without agitation conventionally.

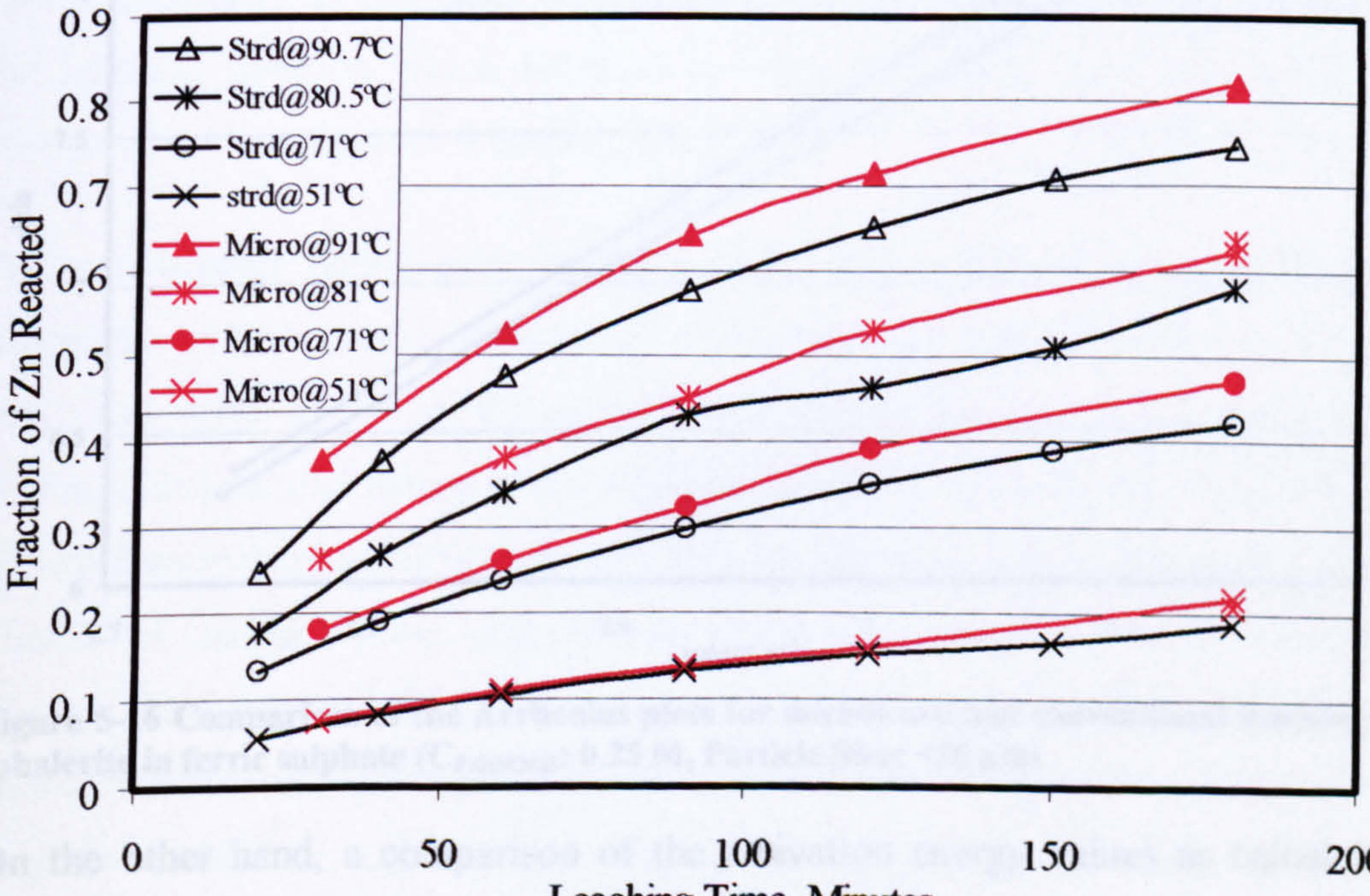

Figure 5-14 Comparison between microwave and conventional leaching of sphalerite at various temperatures as a function of time ($C_{Fe2(SO4)3}$: 0.25 M, particle size: <25 μm).

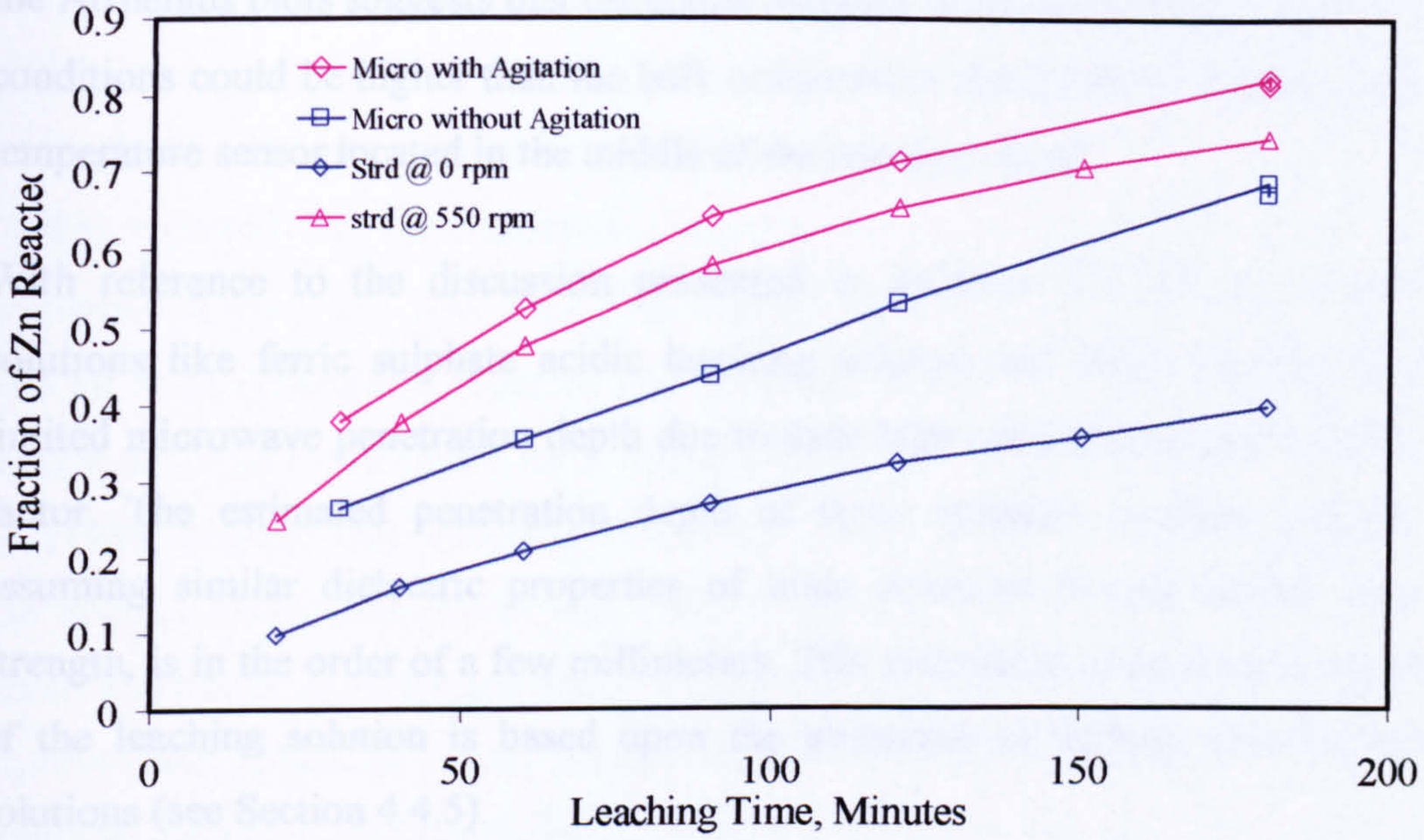

Figure 5-15 The effect of agitation on microwave and conventional leaching of sphalerite in ferric sulphate ($C_{Fe2(SO4)3}$: 0.25 M, particle size: <25 µm, T= 90°C)

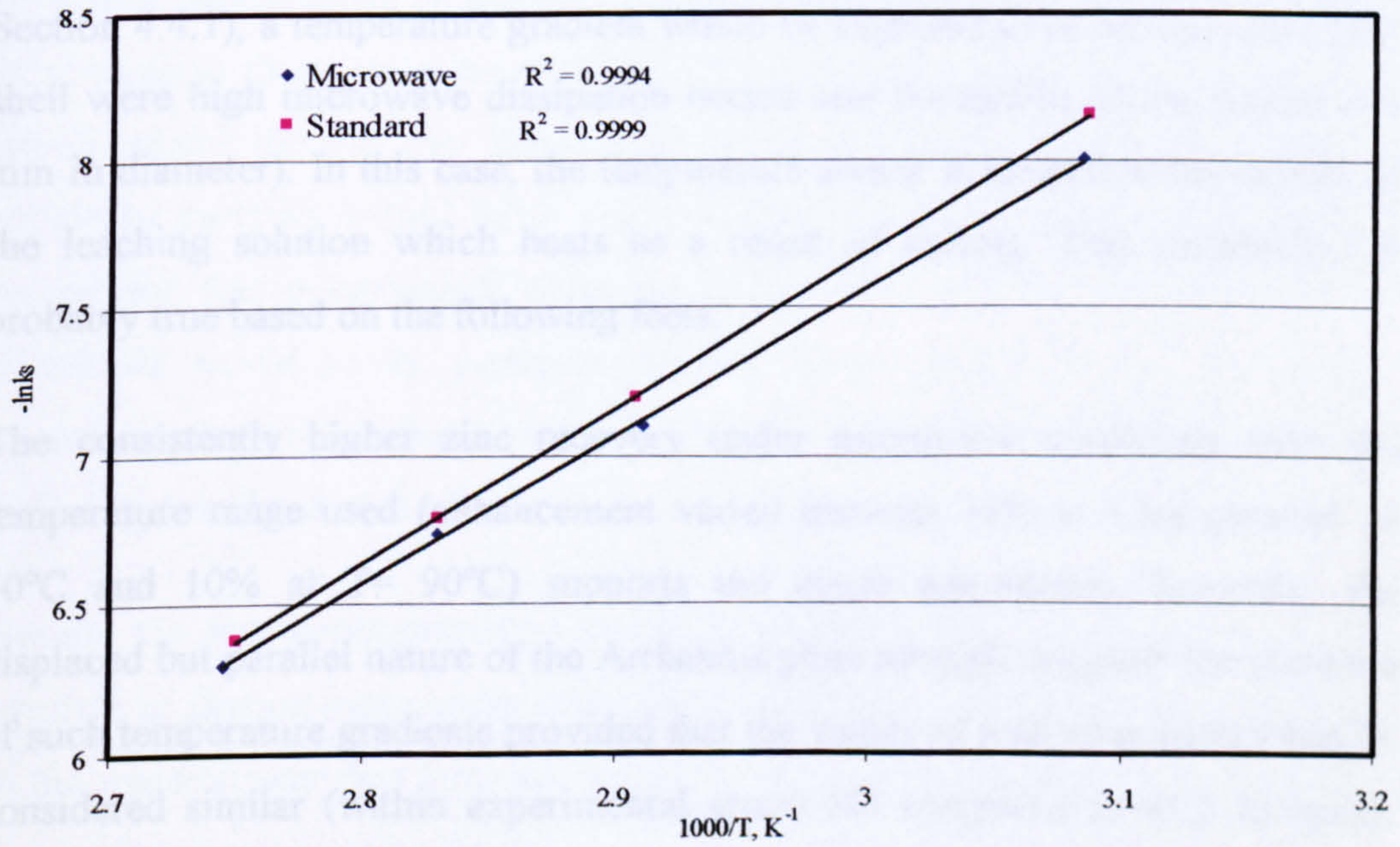

Figure 5-16 Comparison of the Arrhenius plots for microwave and conventional leaching of sphalerite in ferric sulphate ($C_{Fe2(SO4)3}$: 0.25 M, Particle Size: <25 µm)

On the other hand, a comparison of the activation energy values as calculated from Arrhenius plots (43 and 41.2 kJ/mole for conventional and microwave conditions respectively) demonstrates their similarities. Furthermore, the lines in the Arrhenius plots for microwave and conventional leaching are found to be parallel (as shown in Figure 5-16). The displaced but parallel nature of the lines of

the Arrhenius plots suggests that the actual reaction temperature under microwave conditions could be higher than the bulk temperature measured by the fiber optic temperature sensor located in the middle of the reaction vessel.

With reference to the discussion presented in Sections 2.5 and 2.2.5, ionic solutions like ferric sulphate acidic leaching solution and NaCl solution have limited microwave penetration depth due to their high conductivity and high loss factor. The estimated penetration depth of ferric sulphate leaching solution, assuming similar dielectric properties of ionic solutions having similar ionic strength, is in the order of a few millimeters. This estimation of penetration depth of the leaching solution is based upon the properties of sodium chloride salt solutions (see Section 4.4.5).

Provided that microwave energy was almost all the time in "on" mode (see Section 4.4.1), a temperature gradient would be expected to be between the outer shell were high microwave dissipation occurs and the middle of the reactor (34 mm in diameter). In this case, the temperature sensor is located in the middle of the leaching solution which heats as a result of mixing. This assumption is probably true based on the following facts:

The consistently higher zinc recovery under microwave conditions over the temperature range used (enhancement varied between 14% at a temperature of 50°C and 10% at T= 90°C) supports the above assumption. Secondly, the displaced but parallel nature of the Arrhenius plots strongly suggests the presence of such temperature gradients provided that the values of activation energy can be considered similar (within experimental error) (43 compared to 41.2 kJ/mole). Finally, clear evidence of the presence of the temperature gradient, due to the limited penetration depth, can be drawn when the recovery of zinc is compared at stagnant conditions between microwave and conventional conditions. The enhancement at these conditions was found to be 74% after 3 hours leaching time in favour of microwave stagnant conditions compared to that conventionally (as can be seen in Figure 5-15).

On the other hand previous studies on the microwave heating of sphalerite have shown that sphalerite does not heat in microwave field (800W multimode cavity) particularly sphalerite with low iron content (Chen et al., 1984). Walkiewicz et al. (1988) reported that the maximum temperature achieved (when sphalerite was microwaved using a 1 kW, 2.45 GHz multimode oven) was 88°C in 7 minutes. McGill et al. (1988) also reported that sphalerite temperature reached 139° when heated in single mode cavity for 7 minutes at a power level of 500 W. McGill et al. (1988) showed that sphalerite (unknown purity) started to heat readily when the applied microwave power was 2000 W. In the current study, however, the maximum power level applied was 7 W (see Table 4-14). Furthermore, it has been reported that sphalerite is the poorest electrical conductor among the common sulphide minerals. The conductivity of sphalerite varies from 10^{-12} to 10^{-4} S/m depending on the purity level (Shuey, 1975). In addition, the loss factor of sphalerite was found to be less than 0.006 (Church, 1988; Cumbane, 2003). These facts suggest that sphalerite could be considered as transparent to microwaves which would dismiss any assumption of the selective microwave heating of sphalerite particles within ferric sulphate solution. Therefore, the only possible reason for the enhancement observed in the zinc recovery under microwave conditions would be the presence of temperature gradient due to the shallow microwave penetration depth and probably also due to the superheating occurring in that region (Joret et al., 1997).

Despite the arguments presented in the above discussion, one could explain the increase in zinc recovery under microwave conditions due to a higher temperature at the reaction interface between sphalerite and the leaching solution caused by space charge polarisation between sphalerite and some of the reaction products (see Section 2.2.1.4). This claim could be made based on the hypothesis that the sphalerite dissolution reaction in ferric sulphate occurs in several steps involving the formation of a S_n^- chain on the surface of the sphalerite particles (Weisener et al., 2003). This polar intermediate reaction product in contact with non conducting ZnS medium would cause combined dielectric-conductive microwave heating of the solid system ($ZnS - S_{n>2}^-$). However, this theory could be rejected based on

the fact that Maxwell–Wagner (space charge) polarisation takes place at a lower frequency band than 2.45 GHz (see Figure 2-1 and Section 2.2.1.4) (Metaxas and Meredith, 1983). Furthermore there is no data available regarding the conductivity of S_n^-.

5.9 Conclusions

The leaching of sphalerite in ferric sulphate under both microwave and standard conditions has been studied. The effects of temperature and agitation on the leaching kinetics have been investigated. The dissolution reaction was found to be chemically controlled under both microwave and conventional conditions, with corresponding apparent activation energies of 41.2 and 43 kJ/mole. Therefore, it seems that there is no evidence of a so called "microwave non-thermal effect". Instead, the application of microwaves on the leaching of sphalerite was found to enhance the leaching rate due to the presence of temperature gradient between the outer shell and the middle of the leaching vessel caused by a shallow microwave penetration depth. The effect of penetration depth was more apparent on the microwave leaching outcome when leaching was conducted at stagnant conditions.

CHAPTER SIX

Understanding the Interaction of Microwave Energy with Sulphide Minerals in Leaching Solutions

6.1 Overview

It was shown in Chapters 4 and 5 that the behaviour of chalcopyrite and sphalerite in ferric ion media under microwave conditions exhibited both differences and similarities. Both systems (chalcopyrite and sphalerite) were found to be similar in terms of the enhancement in the recovery of valuable metal achieved under microwave conditions. Furthermore, comparison of activation energy values under microwave and conventional conditions for both chalcopyrite and sphalerite in ferric sulphate suggests that there is little change. However, the main differences between the two systems were observed when the leaching was carried out under stagnant conditions.

The indications from the experimental results produced support the hypothesis of selective heating of chalcopyrite over the high loss leaching solution. The results also show the effect of microwave penetration depth on the leaching of both chalcopyrite and sphalerite in terms of the recovery of the metal value.

It was felt very important to provide further supportive evidence to explain the selective heating of chalcopyrite and the effect of penetration depth on the leaching of chalcopyrite. It is the aim of this chapter to show this evidence by studying the properties and behaviour of both the leaching solution and leached

materials within the microwave field. Having done that, a numerical electromagnetic simulation of the leaching system in an electromagnetic field is presented to gain further understanding of the microwave interaction mechanism with leaching systems.

This chapter considers dielectric property measurements of chalcopyrite, sphalerite and leaching solution using the cavity perturbation and the coaxial probe techniques. Furthermore, the heating behaviour of various liquids in microwave fields was investigated.

6.2 Measurements of Dielectric Properties by the Cavity Perturbation Method

The basic theory of cavity perturbation method was described earlier (Section 2.6.1). An attempt was made here to measure the dielectric properties of chalcopyrite, sphalerite and ferric sulphate leaching solutions at different concentrations.

6.2.1 Experimental Apparatus and Method

A general schematic diagram of the measurement system is shown in Figure 6-1. It consists of a resonant circular cavity with a diameter of 373 mm and a height of 37.3 mm which resonates in the TM_{0n0} modes. The resonant frequency f and the quality factor Q of the cavity are recorded by a Hewlett-Packard 8753C Automatic Network Analyser (ANA) controlled by a PC. A vertical sample actuator is used to move the sample holder to the cavity and the furnace (for measurements at high temperatures). A detailed description of a similar measurement system can be found in (Cumbane, 2003) and (Greenacre, 1996).

The sample holder, made of silica, has an internal diameter of 3.8 mm with a wall thickness of 1 mm. A 1 mm thick flat disc was fused in the middle of the tube to provide a support for the sample under test. The empty sample holder was weighed using a four digit balance, and raised first into the cavity using the robotic sample actuator. The resonant frequency (f_0) and the quality factor (Q_0)

of the cavity with the empty sample holder were then measured. The sample holder was then filled with sample to a specified height (about 10 mm) and then weighed again. Chalcopyrite and sphalerite powdered samples (<38 and <25 μm respectively) were slightly compressed inside the sample holder. Liquid samples were filled in the sample holder using disposable glass pipettes to a height of 10 mm. The sample holder containing the sample was raised again into the resonant cavity. The resonant frequency (f_s) and the quality factor (Q_s) of the sample were then measured.

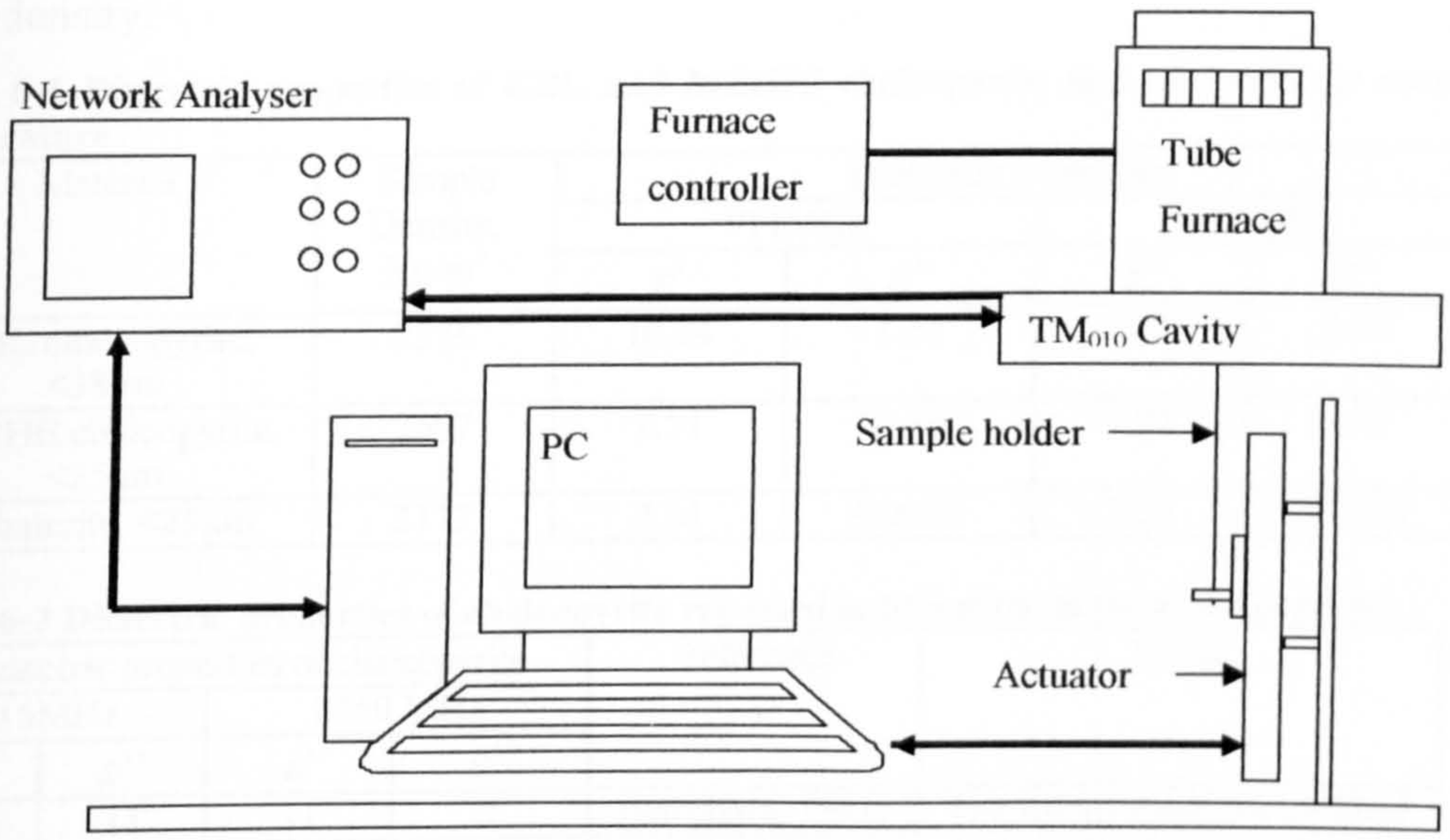

Figure 6-1 Schematic diagram of resonant cylindrical cavity at Stafford University

The measurements of frequency shift and quality factor were made at 911 MHz and 2.45 GHz at room temperature. The dielectric constant (ε') and loss factor (ε'') were then calculated using Equation 2-15 and Equation 2-16.

6.2.2 Experimental Results

6.2.2.1 Dielectric Properties of Chalcopyrite.

The measurement results of GBL and MZ2HE chalcopyrite dielectric properties are given in Table 6-1. A survey of the dielectric properties of chalcopyrite reported in literature shows great discrepancy between various sources as shown in Table 6-2. Salsmam (1991) and Holderfield (1992) used the coaxial line

technique for the measurements of dielectric properties of chalcopyrite. They used a similar procedure to extrapolate the dielectric data at the bulk density of air-mineral mixture to that at the density of solid (a summary of some empirical equations used to extrapolate dielectric properties of powdered materials to their solid density is given in Appendix 6-1). Although they used the same measurement technique, their results were very different as can be seen from Table 6-2. Florek et al. (1996a) and Harrison (1997) also used a reflection method for the measurements of dielectric properties of chalcopyrite. In their work, it is not stated clearly if the data were extrapolated to the properties of chalcopyrite at solid density.

Table 6-1 Dielectric properties of GBL and MZ2HE chalcopyrite and sphalerite at room temperature

Material	Sample Density, Kg/m^3	Dielectric properties			
		911MHz		2450 MHz	
		ε'	ε''	ε'	ε''
GBL chalcopyrite, <38μm	2375	10.24	1.12	9.65	1.35
MZ2HE chalcopyrite, <25μm	2597	7.51	0.29	7.22	0.19
Sphalerite, <25μm	2173	2.94	0.0066	2.94	0.0035

Table 6-2 Dielectric properties of chalcopyrite reported in literature at room temperature

Dielectric properties of chalcopyrite				Reference	Notes
915MHz		2450 MHz			
ε'	ε''	ε'	ε''		
12.8	11	11	7	(Salsmam, 1991)	The values were extrapolated to the solid density using the square root relationship
90				(Holderfield and Salsmam, 1992)	
5	0.33	4.75	0.26	(Harrison, 1997)	There is no data about the extrapolation procedure to the solid density
		10.3	2.28	(Florek and Lovas, 1995)	There is no data about the extrapolation procedure to the solid density
1.8	2.75			(Florek et al., 1996a)	
7.4 at 615 GHz	0.23 at 615 GHz	7.5 at 2.16GHz	0.2 at 2.16 GHz	(Cumbane, 2003)	For particle size 125 μm and bulk density of 2188 kg/m^3 (not extrapolated to solid density)
8.5 at 615 GHz	0.5 at 615 GHz	8.5 at 2.16 GHz	0.5 at 2.16 GHz	(Cumbane, 2003)	For particle size 45 μm and bulk density of 2380 kg/m^3 (not extrapolated to solid density)

Harrison (1997) highlighted the problems involved with the measurements of dielectric properties and the correlation of the results. It was shown that the

measurements must take into account physical, chemical and electric properties of the material, including the magnetic field portion of the wave that may affect magnetic materials. Cumbane (2003) used a cavity perturbation method, with a procedure similar to that used in this thesis, for the measurements of chalcopyrite dielectric properties. The raw dielectric properties data of MZ2HE chalcopyrite agree with Cumbane's (2003) raw data (see Table 6-1 and Table 6-2). However, the measured dielectric properties of GBL chalcopyrite are different, especially the values of loss factor which is 6 times higher than the one reported by Cumbane. The close examination of the XRD pattern for the chalcopyrite used by Cumbane (2003) suggests a presence of some impurities, one of these impurities being pyrite. This is probably why the dielectric properties data of MZ2HE chalcopyrite is comparable to Cumbane's data (2003) because MZ2HE chalcopyrite contains some pyrite (see Figure 4-2). It should be noted also that the packing density of the samples may also have an effect on the values obtained (Nelson, 1988). With regards to the dielectric properties reported by (Florek et al., 1996a; Florek and Lovas, 1995; Harrison, 1997; Salsmam, 1991) there is no information about the purity of samples, the extrapolation method and the packing density of the samples.

Nevertheless, the measured dielectric constant and loss factor (as shown in Table 6-1) as well as the literature values suggests that chalcopyrite is a good microwave receptor. On the other hand, chalcopyrite is known to be a good conductor (Crundwell, 1987a; Shuey, 1975). Shuey (1975) reported that the conductivity of 24 natural chalcopyrite samples varied from 20 to 1×10^4S/m and the conductivity of the majority of the samples was found to be more than 1×10^3 S/m. This value of conductivity suggests that it is probably erroneous to suggest that chalcopyrite is a dielectric material and the measured losses are mainly conductive. Furthermore, a simple test was carried out to check if GBL chalcopyrite is conductive. A piece of this chalcopyrite was placed between the two test probes of a voltmeter, the reading shorted similar to a metal object, showing continuity of the electrical signal.

Therefore, throughout this thesis, chalcopyrite is dealt with as a conductive material rather than dielectric. The measurements undertaken for this thesis should be considered indicative and undertaken for comparison purposes with the literature.

Nevertheless, the values of dielectric properties of chalcopyrite suggest that chalcopyrite is a good microwave absorber in its powder form. Furthermore, the great variations of the measured dielectric properties of chalcopyrite in literature are caused by several factors: the most important of which are the purity of the sample and the packing density.

6.2.2.2 Dielectric Properties of Sphalerite

The dielectric properties of sphalerite measured by the cavity perturbation technique are presented in Table 6-3. The value of loss factor (0.0035 at 2.45GHz) suggests that sphalerite is a poor microwave absorber because of the extremely low loss factor. This is in agreement with the reported poor heating characteristics of sphalerite in a microwave field (Chen et al., 1984; Walkiewicz et al., 1988). The dielectric properties of sphalerite reported in the literature also show that sphalerite has a very low loss factor (Table 6-3), with values similar to the data obtained in the current work.

Table 6-3 Dielectric properties of sphalerite reported in literature at room temperature

Dielectric Properties of chalcopyrite				Reference	Notes
915MHz		2450 MHz			
ε'	ε''	ε'	ε''		
9.66	0.0067			(Church, 1988)	No data about the purity and the extrapolation procedure
2.8 at 615 GHz	0.008 at 615 GHz	2.8 at 2.16GHz	0.008 at 2.16 GHz	(Cumbane, 2003)	For particle size 45 μm and bulk density of 1620 kg/m^3 (not extrapolated to solid density)
3.3 at 615 GHz	0.008 at 615 GHz	3.3 at 2.16 GHz	0.008 at 2.16 GHz	(Cumbane, 2003)	For particle size 45 μm and bulk density of 2110 kg/m^3 (not extrapolated to solid density)
2.94	0.0066	2.94	0.0035	Current work	Particle size <25μm with packing density 2173kg/m^3

Again the variations between the various literature sources are evident. This is probably due to sample purity, packing density and the method used to extrapolate dielectric data to its solid density equivalent.

Sphalerite has a very low conductivity ranging from 10^{-12} to 10^{-4} S/m depending on the purity level (Shuey, 1975). It is considered the poorest electric conductor among sulphide minerals. This probably explains the extremely low loss factor as the latter is related to the conductivity according to Equation 2-4.

6.2.2.3 Dielectric Properties of Liquids

An attempt was made to measure the dielectric properties of different solutions using the cavity perturbation method. These solutions included distilled water, 0.5 M H_2SO_4 and ferric sulphate solutions with various concentrations (0, 0.01, 0.05, 0.1, 0.2 and 0.25) prepared in 0.5 M H_2SO_4. The experimental results are shown in Table 6-4. To check for the accuracy of the measurements, a liquid with known dielectric properties was chosen. Distilled water was selected as a reference material as its dielectric properties are well documented (see Table 4-17).

Table 6-4 Dielectric properties of liquids measured at room temperature (cavity perturbation method)

Solution	911 MHz		2450 MHz	
	ε'	ε"	ε'	ε"
Distilled water	18.1	0.21	19.4	0.55
0.5 M H_2SO_4	21.5	1.94	ND	ND
0.01 M $Fe_2(SO_4)_3$	25.2	7.59	ND	ND
0.05 M $Fe_2(SO_4)_3$	23.1	2.29	ND	ND
0.1 M $Fe_2(SO_4)_3$	24.2	4.89	ND	ND
0.125 $Fe_2(SO_4)_3$	21.2	2.43	ND	ND
0.2 M $Fe_2(SO_4)_3$	24.9	4.7	ND	ND
0.25 M $Fe_2(SO_4)_3$	24.4	1.3	ND	ND
4 M NaCl	19.4	0.7	ND	ND

Unfortunately, the measured dielectric constant and loss factor of distilled water are considerably lower than those reported in literature. The reason for that could be related to the high complex permittivity of water which caused high shift in the resonant frequency of the cavity. The great shift in resonant frequency invalidates the perturbation theory, the basis of the technique (Metaxas and Meredith, 1983).To minimize the frequency shift, a very small sample volume of such a high

loss liquid is required to use. For example, Kapilevich et al (2000) used a sample volume of 0.2 μL placed in a tube with a diameter of 250μm to measure the dielectric properties of water and some saline liquid with good accuracy. However, it should be recognized that the use of such a small sample volume and very narrow tubes would involve a considerable error in sample volume determination. Furthermore, such tubes were not available at the time the measurements were conducted.

As was discussed in Section 4.4.6, the leaching solutions above have high ionic content. Therefore the conductivity of such solutions is expected to be very high, which means that such solutions would have high loss factors due to the contribution of conductive losses (see Equation 2-4). These losses again would cause a great shift in the resonant frequency of the perturbed cavity. Therefore, effort was directed toward the use of the coaxial probe method to measure dielectric properties of such high loss liquids.

6.3 Measurements of Dielectric Properties by the Coaxial Probe Method

Due to the erroneous results of dielectric property measurements of leaching solutions obtained using the cavity perturbation method, it was decided to repeat the measurements using a coaxial probe method, a more suitable technique for dielectric properties measurement of high lossy liquids. A description of the theoretical basis of the coaxial probe technique is given in Section 2.6.2.

Dielectric properties measurements were undertaken at the University of Stellenbosch in South Africa in collaborative work with the electroheating group. As part of this joint work, the author of this thesis visited the University of Stellenbosch to take part in the measurement process.

The measurements of dielectric properties of leaching solutions were carried out at different temperatures and concentrations.

6.3.1 Experimental Apparatus and Method

The measurements of dielectric properties of liquids was undertaken at the University of Stellenbosch using a flanged coaxial probe sensor developed previously by Rimbi (2003) (Figure 6-2). The flange dimensions were 20×20 mm. The principle of operation of the probe and the equivalent electric circuits are briefly described in Section 2.6.2. A detailed description of the measurement system can be found in (Rimbi, 2003) and (Louw, 2005).

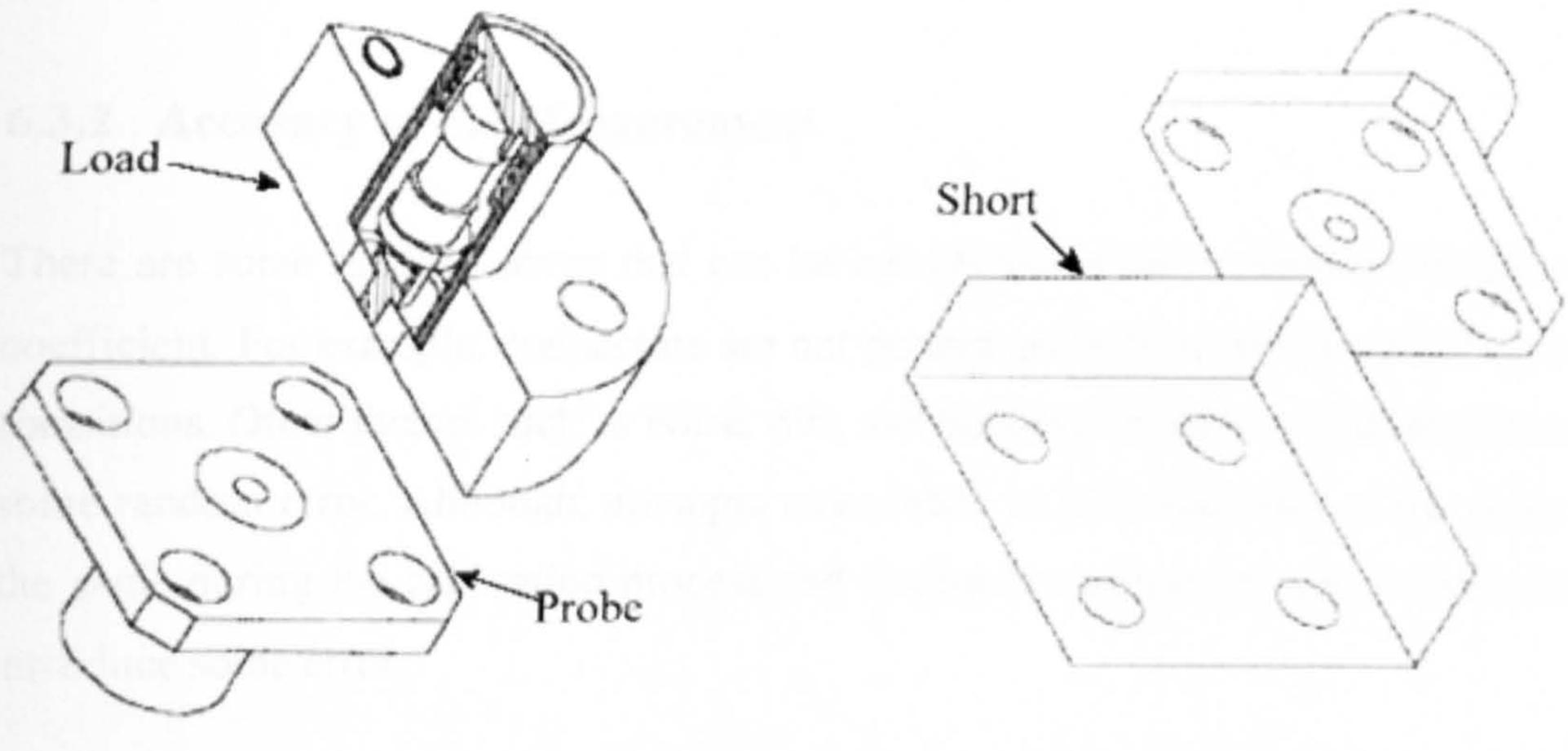

Figure 6-2 Flanged coaxial probe with calibration standards ((Rimbi, 2003)

The measurement system involves the probe which is connected to computer controlled ANA HB8510 via a 50Ω coaxial cable. The system is calibrated to eliminate systematic errors that could bias the measured reflection coefficient S_{11}. The calibration procedure of the probe includes the use of three standards: a matched load (with 50Ω load), a short circuit and an open circuit (see Figure 6-2). A full description of the coaxial probe calibration can be found in (Kingman et al., 2005).

After the calibration procedure was completed, the magnitude and the phase of the reflection coefficient of materials with well-known dielectric properties were measured to ensure accuracy. These materials include air, and distilled and saline water. Then the reflection coefficient of the liquid of interest was measured.

About 50 ml of the liquid poured in a beaker was heated to the desired temperature, the probe was then immersed in the solution where S_{11} parameters were measured. The measurements of S_{11} were carried out over a frequency ranging from 45 MHz to 3 GHz at a step of 59.1 MHz using ANA. The data are then utilised in an inversion algorithm implementing Equations 2-18 and 2-19 from Stuchly and Stuchly (1980) and Marcuwitz (1986). The analytical solution yielded dielectric constant and loss factor of the material as a function of frequency. The analytical solution was done by the University of Stellenbosch (Louw, 2005)

6.3.2 Accuracy of the Measurement

There are some random errors that can be introduced in the measured reflection coefficient. For example, connectors are not perfect and reflections occur between transitions. Other factors such as noise, dirt, and bending of cable might introduce some random error. Although, attempts were made to keep the bend of the cable the same during the calibration process and during the measurements, it can still introduce some error.

Temperature drift is an important source of error during the experiments, which influenced mainly the values of dielectric properties at high temperatures (between 50 and 90°C). This is because the temperature of the solution changes during the sweep and also because the probe itself heats up which affects its properties. Therefore the data presented is not claimed to be highly accurate, but it shows trends and the approximate values. Furthermore, the dielectric properties of air, distilled water and 0.2 M NaCl were measured to check for the accuracy of the measurements.

6.3.2.1 Air

The dielectric properties of air are given in Figure 6-3. The data presented in Figure 6-3 was obtained from two runs. The measured dielectric constant is one over the measurement frequency range. The values of loss factor are very close to

zero as can be seen from the Figure 6-3. Ideally, the value of dielectric constant and loss factor are 1 and 0 respectively.

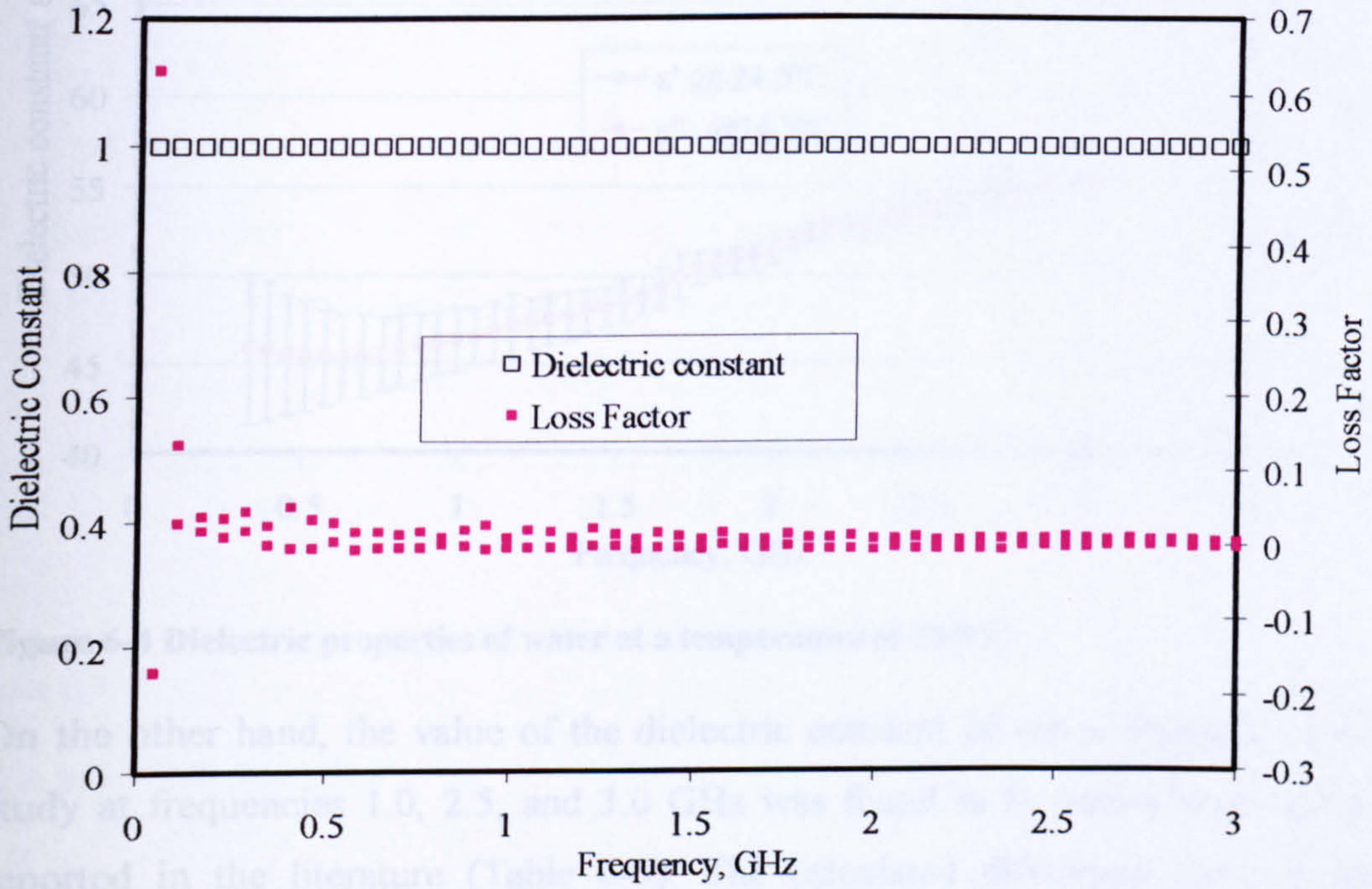

Figure 6-3 Dielectric properties of air measured by coaxial probe technique.

6.3.2.2 Distilled Water

The measured dielectric properties of distilled water at temperature 24.5°C are presented in Figure 6-4. The data point in Figure 6-4 is an average of four repeats. The CV of the dielectric constant varies between 0.14 and 3.4% over a frequency range between 0.045 and 3 GHz suggesting good precision of the measured values of dielectric constant. The CV of the loss factor at lower frequency is very high, but the amplitude of the CV drops considerably with the increase in frequency.

It was reported that the accuracy of dielectric properties measurements at low frequencies is affected by an electrode polarisation effect (Bordi et al., 2001). This effect is caused by the accumulation of charge on the surface of the probe causing the formation of an electric double layer that strongly modifies the ion distribution within the sample under investigation. At frequencies above 1.9 GHz, the CV is about 5 % giving better precision at the frequency of interest (2.45 GHz).

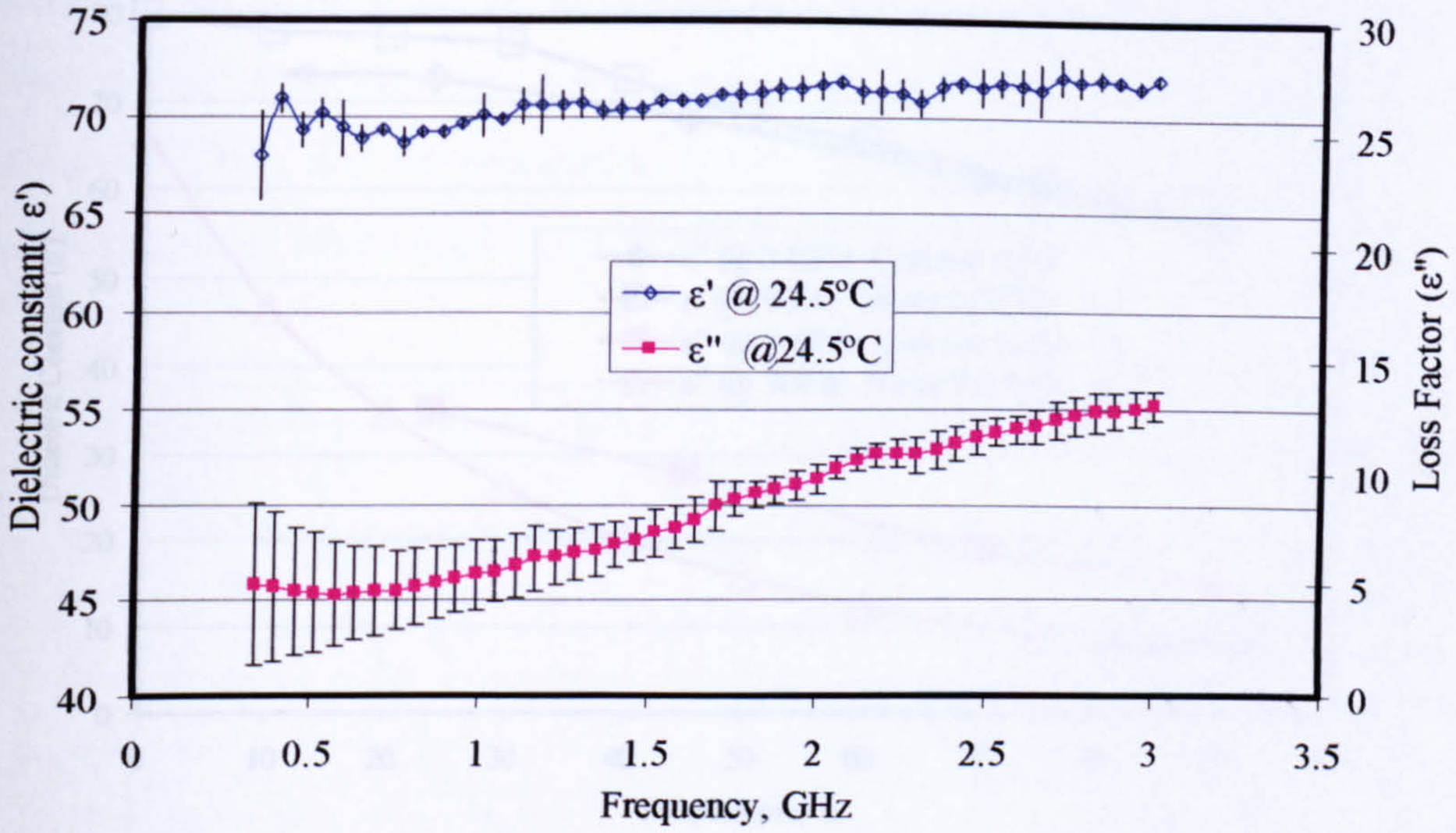

Figure 6-4 Dielectric properties of water at a temperature of 24.5°C

On the other hand, the value of the dielectric constant of water obtained in this study at frequencies 1.0, 2.5, and 3.0 GHz was found to be below those values reported in the literature (Table 6-5). The calculated difference between the literature and current values is below 9 %. The values of loss factor generally better matches the literature values with the exception of the one at 2.5 GHz when compared to the data reported by (Meredith, 1998).

Table 6-5. Comparison between measured dielectric properties of water and literature at room temperature

f, GHz	Dielectric constant (ε')		% diff.	Loss Factor (ε'')		% diff.	Reference
	Measured	Literature value		Measured	Literature value		
1.0	70.2±1.1	77	-8.8	5.4±1.5	5.2	+3.9	(Meredith, 1998)
2.5	71.6±1.0	77	-7.0	11.7±.7	13	-10	(Meredith, 1998)
3.0	72.0±0.3	77.4	-7.0	13.1±0.7	13.05	+0.4	(Hasted, 1973)
3.0	72.0±0.3	77.7	-7.3	13.1±0.7	13	+0.8	(Cook, 1952)

Furthermore, the comparison of water dielectric properties measured in this work with the literature, as a function of temperature is given in Figure 6-5. The trend of the data obtained in this work is shown to be similar to these reported by Hasted (1973). Although there is no close agreement of the absolute values of the dielectric properties of water, the general trend of the data can still be relied on and the data can be used with caution taking into account an error of up to 10%.

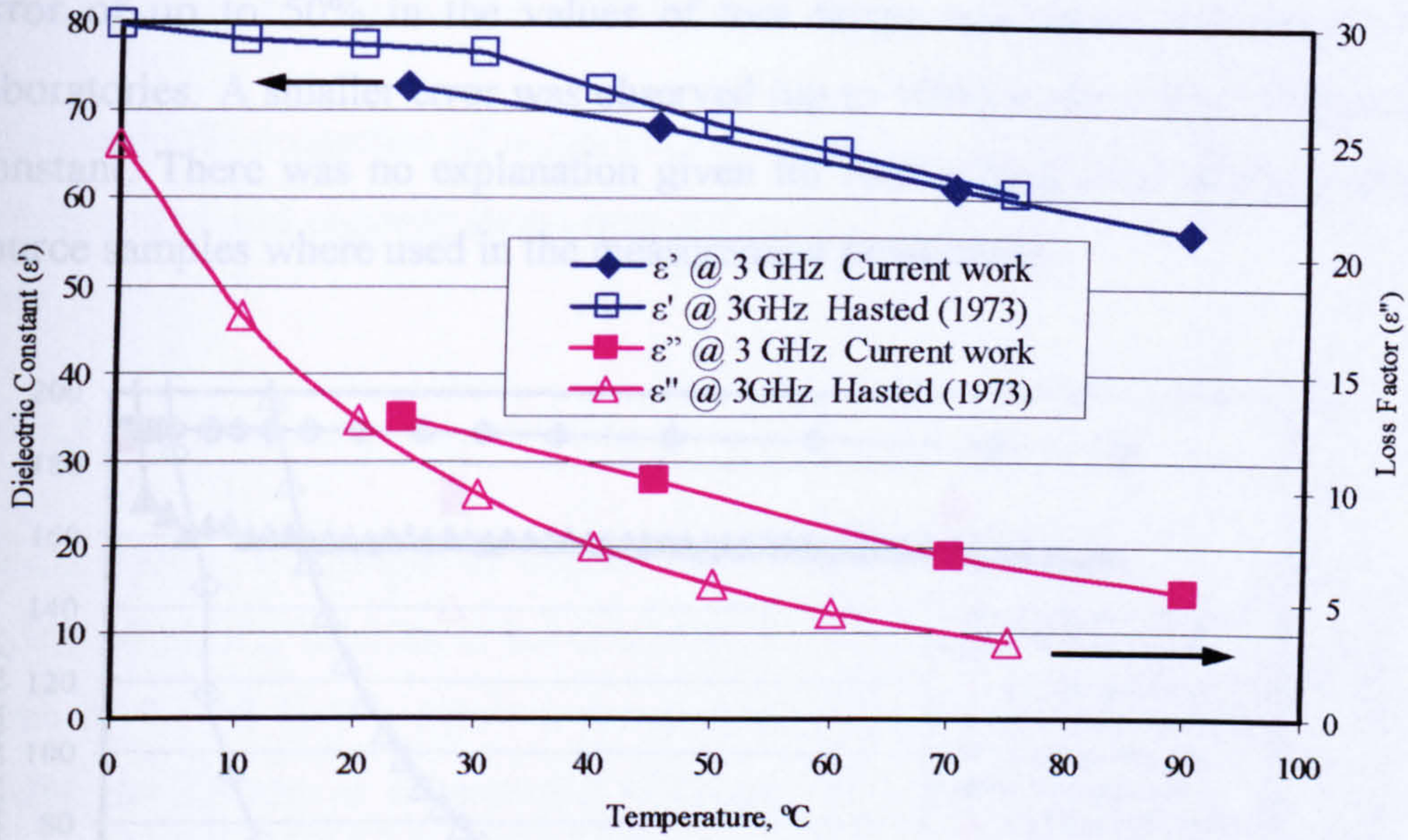

Figure 6-5 Dielectric properties of water at different temperature. Comparison with literature.

6.3.2.3 Salt Solution

It has been reported previously that the measurement of dielectric properties of ionic solutions involves considerable error, which is proportional to the frequency. The problem of high error in ionic solutions is particularly influential at lower frequencies (Bordi et al., 2001; Kaatze et al., 1987). The leaching solutions used in this work have high ionic concentrations, which would affect the accuracy of their dielectric properties. Therefore it was felt important to measure the dielectric properties of a known solution. Sodium chloride solution (0.5 M NaCl) was chosen to check the accuracy of measured data compared to the literature as the dielectric properties of this solution is documented in more than one source.

A comparison between dielectric data of the 0.5 M NaCl from various sources is presented in Figure 6-6. The dielectric constant measured in this work is generally lower than reported literature data (Meredith, 1998; Metaxas and Meredith, 1983; Salsmam, 1992) with an estimated error of between 7 and 16%. With regard to the loss factor, a greater scatter was found between various literature sources (see Figure 6-6). Batt et al. (1995) carried out a parallel measurement programme for the measurement of dielectric properties of materials using different equipment and techniques to evaluate the disagreement between various laboratories. An

error of up to 50% in the values of loss factor was found between various laboratories. A smaller error was observed (up to 10%) in the values of dielectric constant. There was no explanation given for such a high error although single source samples where used in the measurement programme.

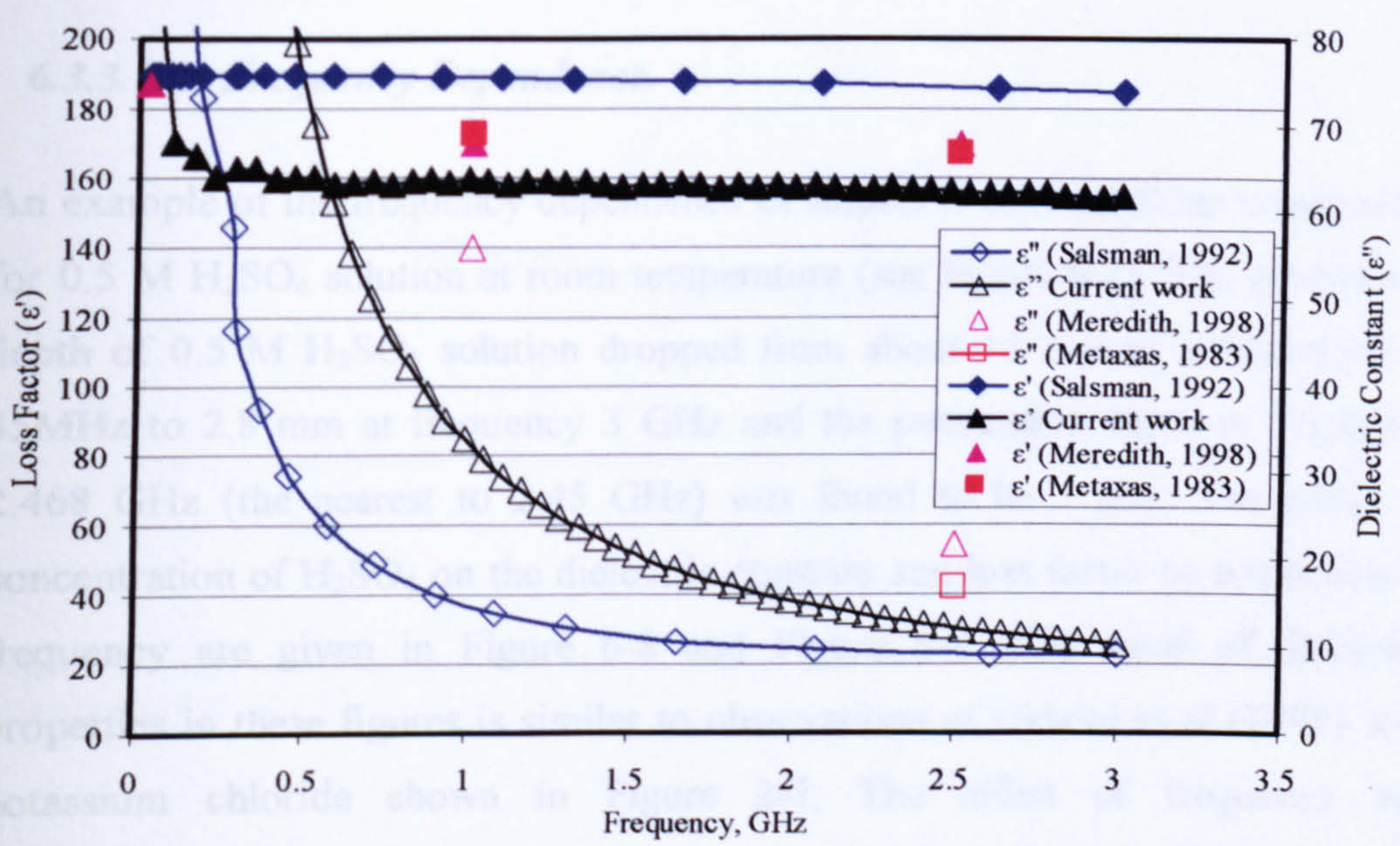

Figure 6-6 Dielectric properties of 0.5 M NaCl solution at a temperature of 24.5°C

6.3.3 Experimental Results

The results of the dielectric properties measurement of liquids include dielectric constant and loss factor of NaCl (0.01, 0.1, 0.2, 0.5, and 2.5 M), H_2SO_4 (0.01, 0.05, 0.1, 0.2, 0.5, and 1.0) and ferric sulphate (0.25 M $Fe_2(SO_4)_3$ prepared in 0.5 M H_2SO_4) solutions. Three factors are examined in this study: effect of frequency, effect of temperature and effect of concentration. As there is no direct importance of dielectric properties of sodium chloride solution, the data is given in Appendix 6-2. These properties would rather be used for comparison with the dielectric properties of the solution of interest.

6.3.3.1 Dielectric Properties of Sulphuric Acid Solutions

The dielectric properties of sulphuric acid solutions were measured at different temperatures and concentrations over a frequency range between 45 MHz and 3 GHz.

6.3.3.1.1 Frequency Dependence.

An example of the frequency dependence of sulphuric acid solutions is presented for 0.5 M H_2SO_4 solution at room temperature (see Figure 6-7). The penetration depth of 0.5 M H_2SO_4 solution dropped from about 13 mm at a frequency of 45MHz to 2.8 mm at frequency 3 GHz and the penetration depth at frequency 2.468 GHz (the nearest to 2.45 GHz) was found to be 3 mm. The effect of concentration of H_2SO_4 on the dielectric constant and loss factor as a function of frequency are given in Figure 6-8 and Figure 6-9. The trend of dielectric properties in these figures is similar to observations of Gabriel et al (1998) with potassium chloride shown in Figure 2-7. The effect of frequency and concentration of ions on the dielectric properties of liquids was discussed in some detail in Chapter 2 (Section 2.5). As the ion concentration increases, the conductivity of the liquid solution increases which in turn, contributes to the value of loss factor according to the following Equation 6-1 (Metaxas and Meredith, 1983):

$$\varepsilon''_{dc} = \frac{\sigma}{\omega \varepsilon_0} \qquad \textbf{Equation 6-1}$$

This equation shows that the increase of frequency reduces the contribution of ε''_{dc} to the effective loss factor as can be seen clearly in Figure 6-9 when comparing the change of distilled water loss factor with those containing sulphuric acid at various concentrations.

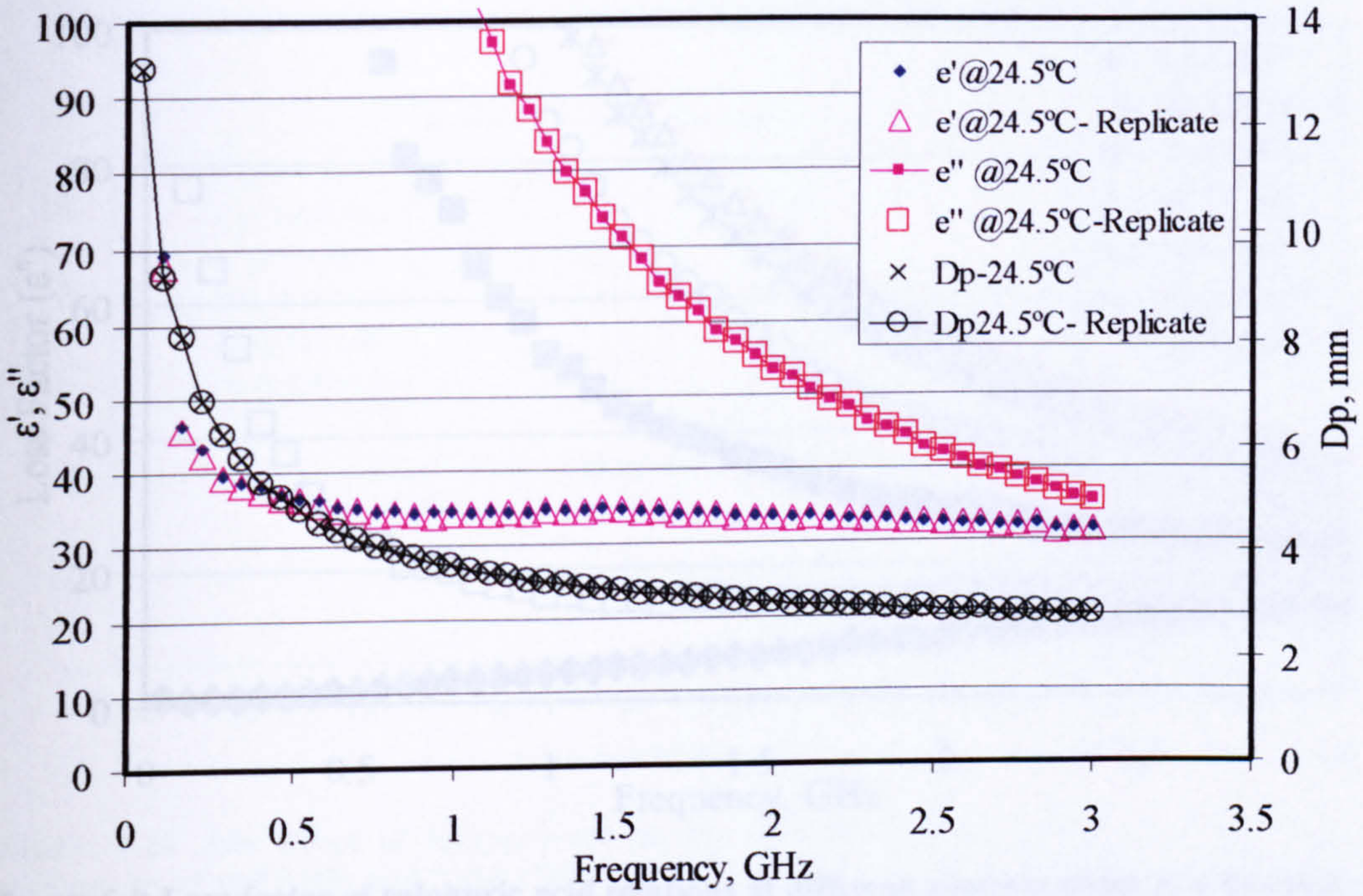

Figure 6-7 Dielectric properties of 0.5 M H_2SO_4 solution as a function of frequency at a temperature of 24.5°C

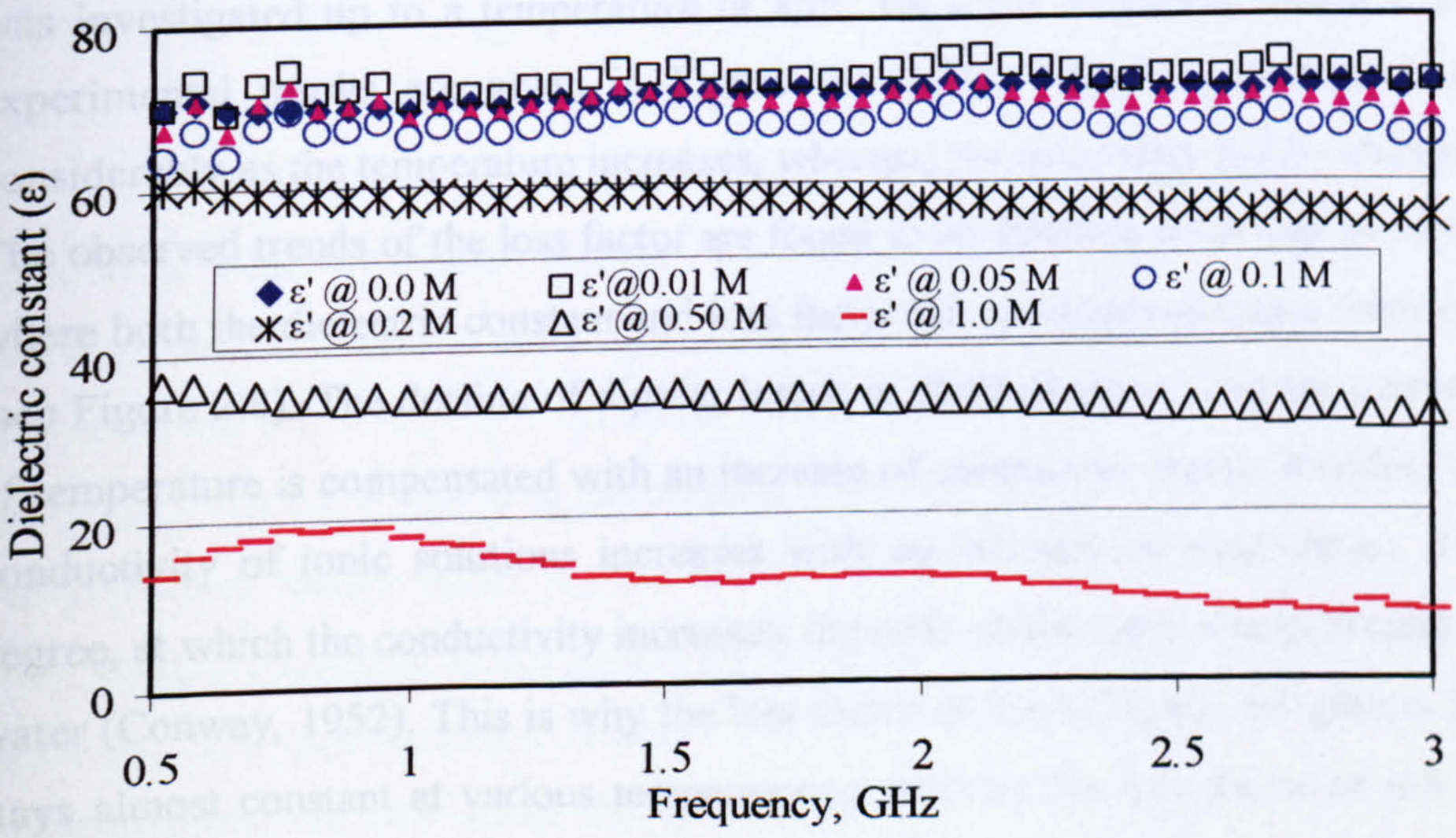

Figure 6-8 Dielectric constant of sulphuric acid solutions at different concentrations as a function of frequency at a temperature of 24.5°C

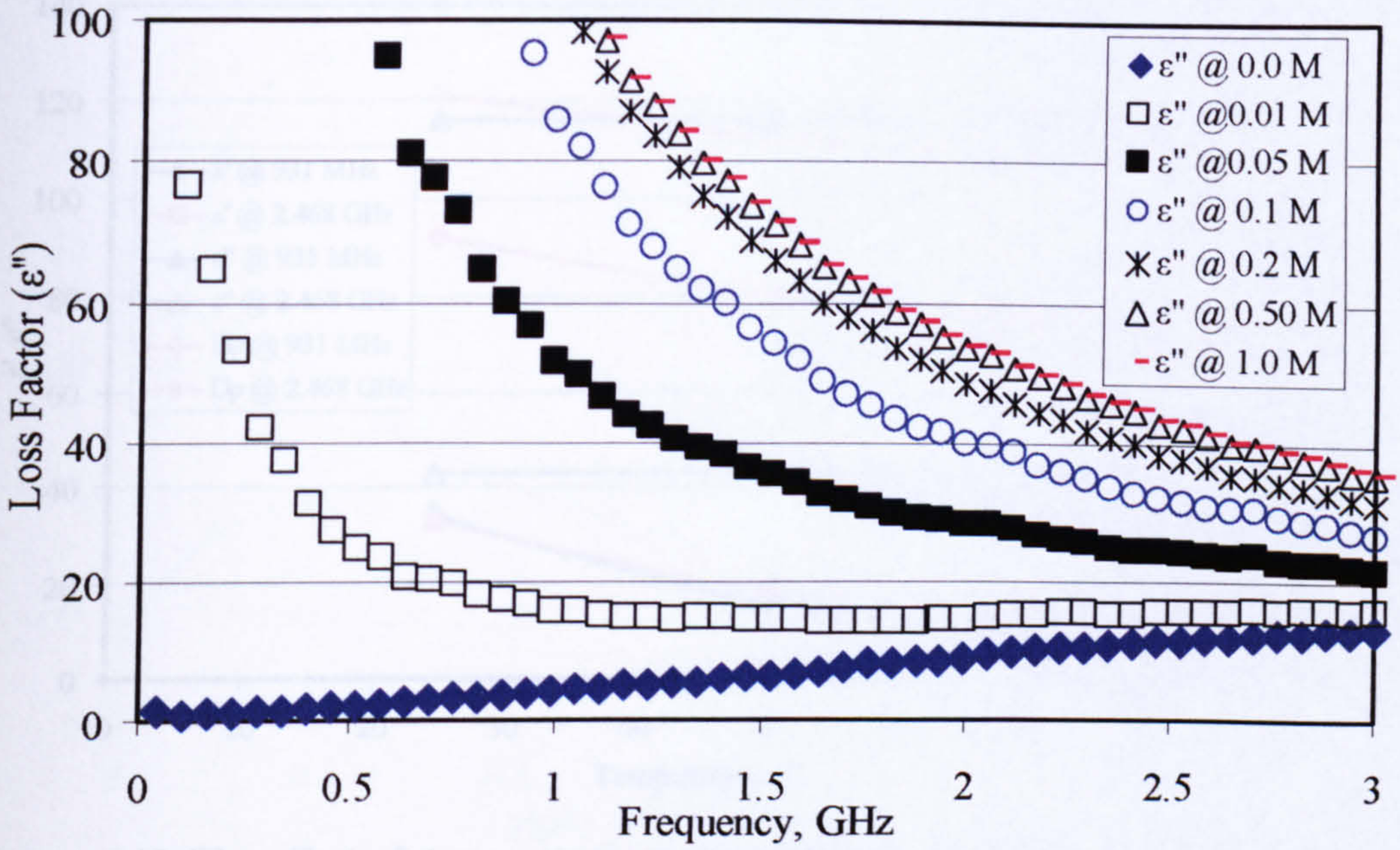

Figure 6-9 Loss factor of sulphuric acid solutions at different concentrations as a function of frequency at a temperature of 24.5°C

6.3.3.1.2 The Effect of Temperature.

The effect of temperature on the dielectric properties of sulphuric acid solutions was investigated up to a temperature of 86°C on a 0.5 M H_2SO_4 solution. The experimental results are given in Figure 6-10. The dielectric constant drops considerably as the temperature increases, whereas, the loss factor hardly changes. The observed trends of the loss factor are found to be different from that of water, where both the dielectric constant and loss factor fall as the temperature increases (see Figure 2.8). The decline of dipolar losses in distilled water with the increase of temperature is compensated with an increase of conductive losses. Besides, the conductivity of ionic solutions increases with an increase of temperature. The degree, at which the conductivity increases, depends on the type of ions present in water (Conway, 1952). This is why the loss factor of 0.5 M H_2SO_4 (Figure 6-10) stays almost constant at various temperatures, whereas the loss factor of 0.5 M NaCl (Appendix 6-2) increases with temperature. With regards to the penetration depth, a slight decrease was observed as the temperature increases. The observed trends of the changes of dielectric constant, loss factor and penetration depth as a function of temperature are similar for both frequencies; 931 MHz and 2.468 GHz.

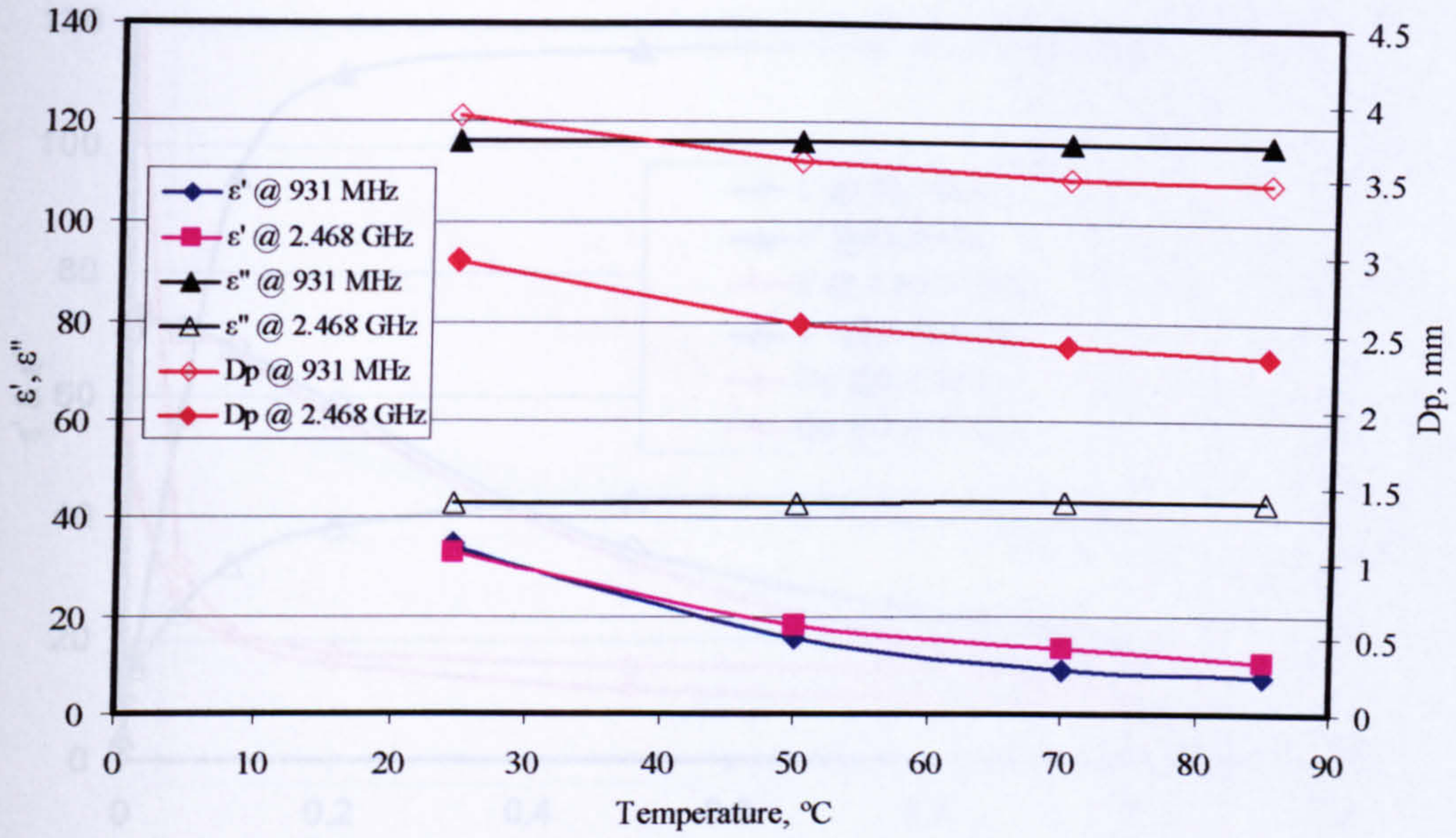

Figure 6-10 The effect of temperature on the dielectric properties of 0.5 M H_2SO_4 at frequencies of 931 MHz and 2.468 GHz.

6.3.3.1.3 Effect of Concentration

The effect of sulphuric acid concentration on the dielectric properties of water was investigated at room temperature. A summary of the experimental results is given in Figure 6-11. It can be seen that the dielectric constant falls steadily in a linear manner as the sulphuric acid concentration increases. However, at a low sulphuric acid concentration (0.01 M) the dielectric constant seems to exceed the dielectric constant of water by a small amount. This is consistent with the observed trends produced on the dielectric constant of sodium chloride (Appendix 6-2). This was also observed previously by Nortemann et al. (1997). Furthermore, a small rise in dielectric constant at low concentration is consistent with the predictions of the Debye-Huckel theory which suggests a rise in dielectric constant above that of pure water proportional to the square root of ionic concentration (Hasted, 1973). However, this approximation is only valid for very dilute solutions. At higher concentrations, the ions orient the water molecules around them, which reduces the ability of water molecules to orient in the applied electric field, reducing the dielectric constant (Hasted, 1973). The increase in loss factor is due to the high contribution of conductive losses (see Equation 2-4) from the considerable increase of conductivity with the increase of concentration.

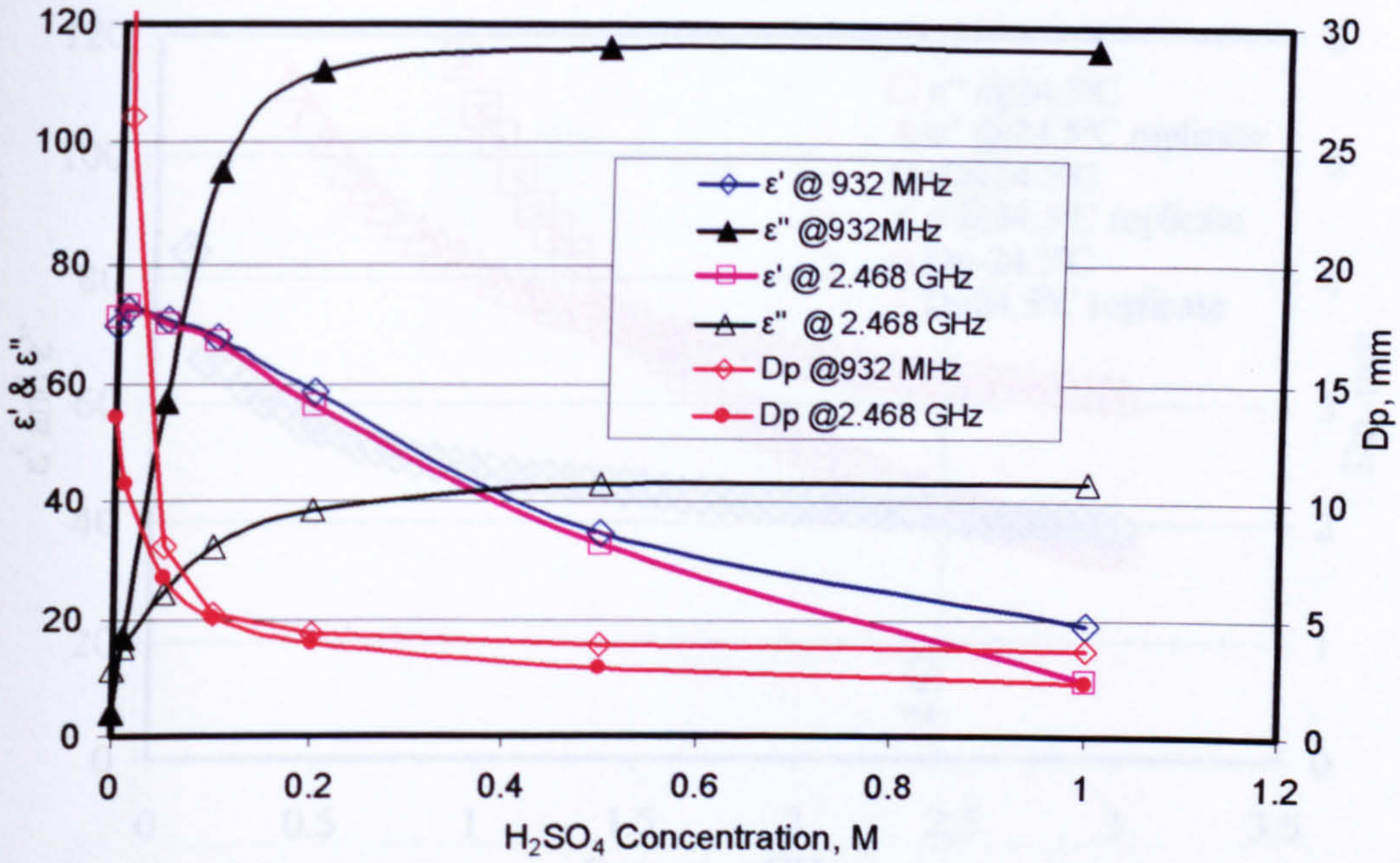

Figure 6-11 The effect of concentration on the dielectric properties of sulphuric acid solution at room temperature and frequencies 931 MHz and 2.468 GHz

6.3.3.2 Dielectric Properties of Ferric Sulphate Solution

The dielectric properties of ferric sulphate were studied using 0.5 M $Fe_2(SO_4)_3$ – 0.5 M H_2SO_4. The effects of temperature and frequency were investigated here only with only one repeat at room temperature. This is because the metallic part (made of copper) of the probe was found to react with the leaching solution which was corroded by the end of experiment.

6.3.3.2.1 Frequency Dependence

The measured dielectric properties of the ferric sulphate leaching solution are given in Figure 6-12. The measurement was repeated twice at room temperature to establish the precision of the data. It was found that the repeated runs showed excellent reproducibility. The average values of dielectric constant and loss factor at a temperature of 24.5°C for 0.25 M $Fe_2(SO_4)_3$ – 0.5 M H_2SO_4 were found to be 40.6 and 42.4 respectively at a frequency of 2.468 GHz. The calculated corresponding microwave penetration depth using Equation 2-7 was found to be 3.2 mm. The dielectric constant and loss factor were found to decrease with an increase in frequency similar to those found for NaCl and H_2SO_4 previously.

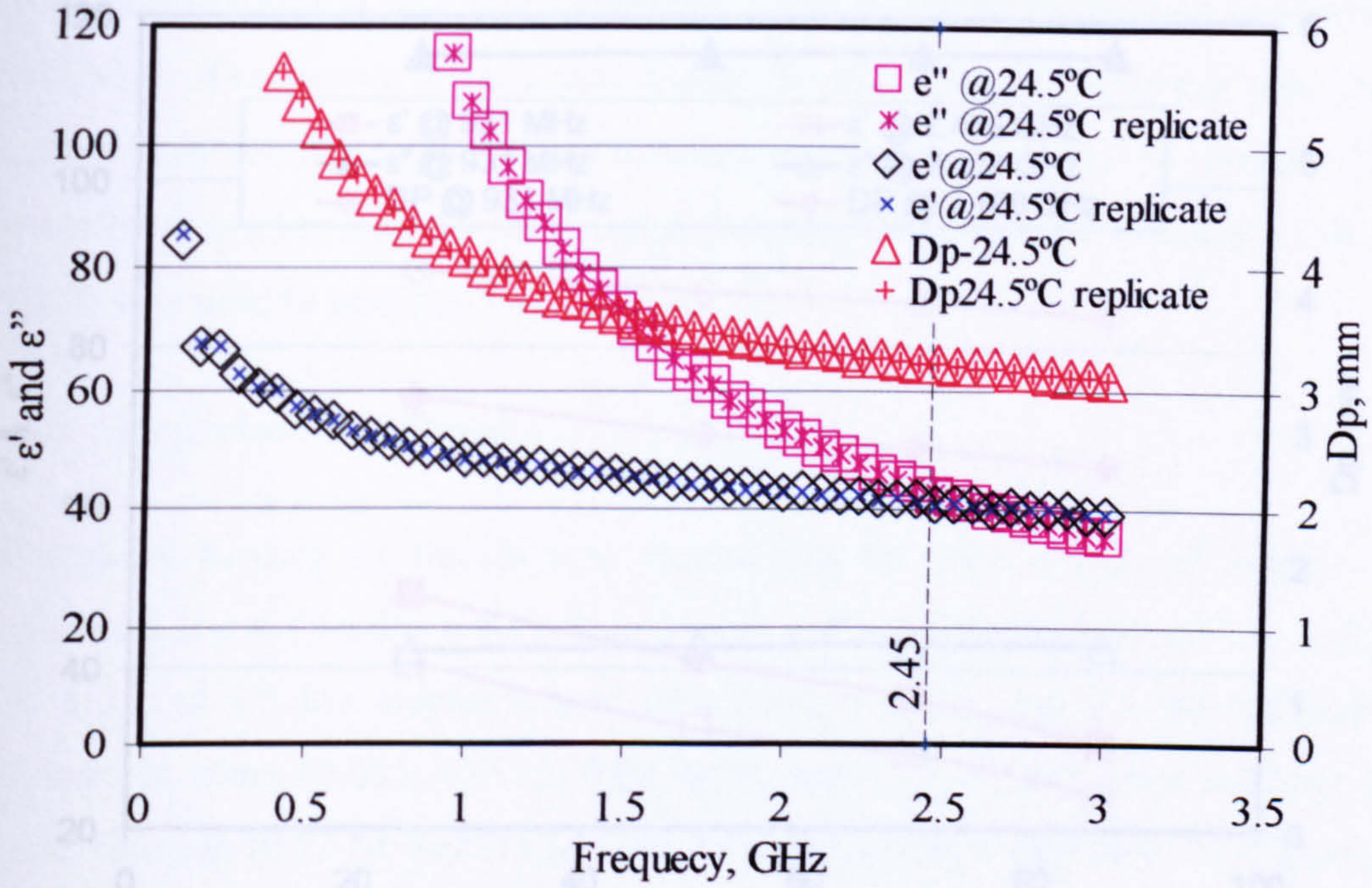

Figure 6-12 Dielectric properties of 0.25 M $Fe_2(SO_4)_3$-0.5 M H_2SO_4 leaching solution as a function of frequency

6.3.3.2.2 The Effect of Temperature

The effect of temperature on the dielectric properties of 0.25M $Fe_2(SO_4)_3$-0.5 M H_2SO_4 leaching solution is shown in Figure 6-13. It can be seen that the dielectric constant decreases with an increase in temperature, showing similar behavior to the dielectric constant of water, NaCl and H_2SO_4 solutions. However, the loss factor showed a negligible increase with an increase in temperature (42.3 at a temperature of 24.5°C and 43.1 at a temperature of 86°C) as opposed to water. This issue was discussed earlier in Section 6.3.3.1.2.

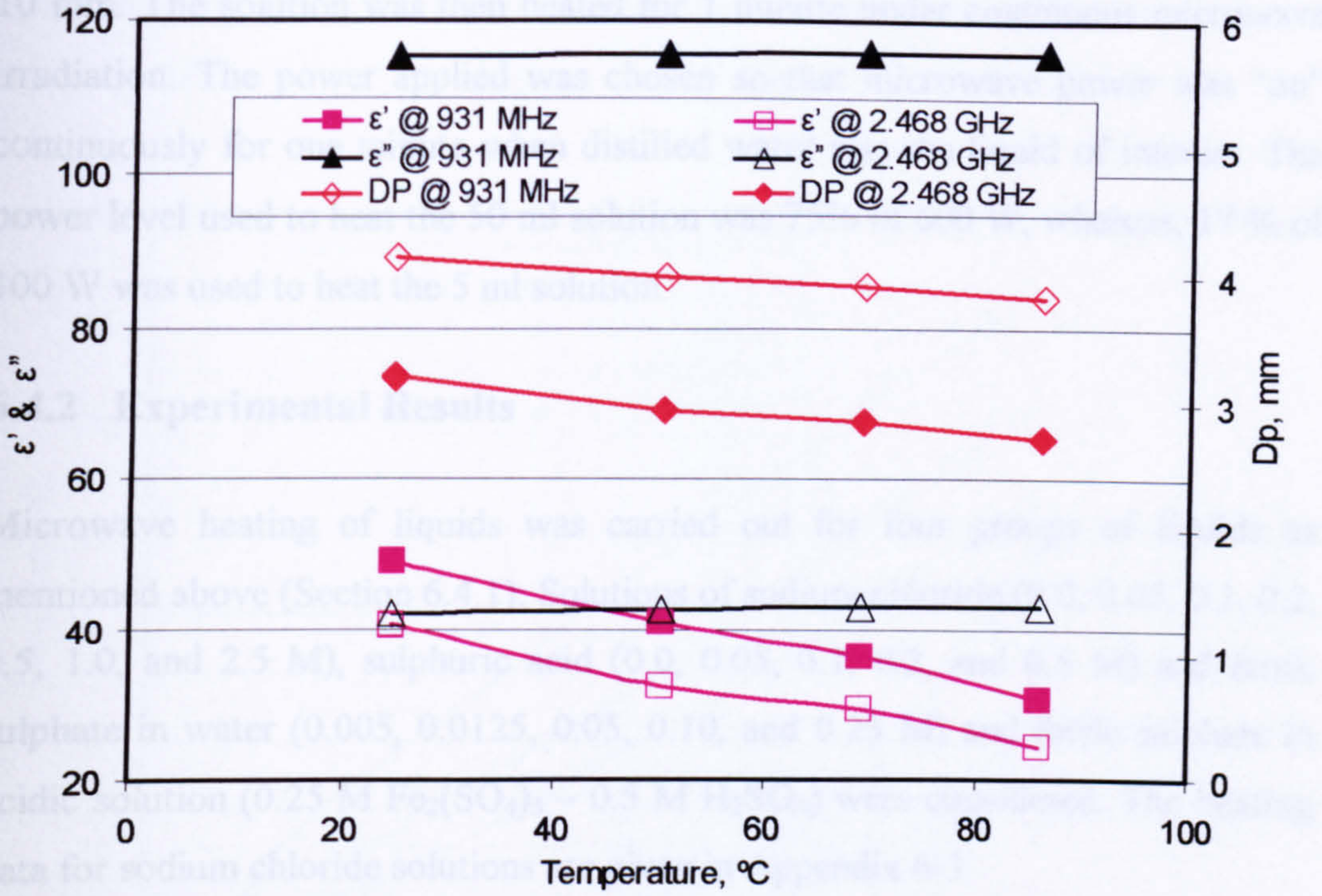

Figure 6-13 The effect of temperature on the dielectric properties of 0.25 M $Fe_2(SO_4)_3$ – 0.5 M H_2SO_4 leaching solution at frequencies 931MHz and 2.468 GHz

6.4 Microwave Heating of Liquids

This study was carried out with the aim of investigating the heating of liquids in a microwave field and, in particular, to investigate the effects of reactor size and ion concentration on the heating rate of aqueous solutions.

6.4.1 Experimental Apparatus and Method

The experiments were carried out in the MARS X® system described in Section 4.2.3.1.1. The MARS X® system was an ideal apparatus to carry out this study because of the capability to measure and record both the temperature and pressure during the heating process. Two vessels made of PFA® with diameters of 10 and 34 mm were considered, the 34 mm vessel being the one used for microwave leaching experiments (Section 4.4). This was carried out to investigate the effect of vessel diameter on the heating of liquids.

Microwave heating of liquids in the 34 mm vessel was carried out using 50 ml solution, whereas, only 5 ml was used in the case of the vessel with a diameter of

10 mm. The solution was then heated for 1 minute under continuous microwave irradiation. The power applied was chosen so that microwave power was "on" continuously for one minute when distilled water was the liquid of interest. The power level used to heat the 50 ml solution was 75% of 600 W, whereas, 17 % of 300 W was used to heat the 5 ml solution.

6.4.2 Experimental Results

Microwave heating of liquids was carried out for four groups of liquids as mentioned above (Section 6.4.1). Solutions of sodium chloride (0.0, 0.05, 0.1, 0.2, 0.5, 1.0, and 2.5 M), sulphuric acid (0.0, 0.05, 0.1, 0.2, and 0.5 M) and ferric sulphate in water (0.005, 0.0125, 0.05, 0.10, and 0.25 M) and ferric sulphate in acidic solution (0.25 M $Fe_2(SO_4)_3$ – 0.5 M H_2SO_4) were considered. The heating data for sodium chloride solutions are given in Appendix 6-3.

6.4.2.1 Microwave Heating of Sulphuric Acid Solutions

The heating rate data of sulphuric acid base solutions, carried out in the larger vessel, are presented in Figure 6-14. As the sulphuric acid concentration increases the heating rate, as well as the maximum temperature reached after 60 seconds of microwave irradiation was found to decrease. The heating rate of distilled water was found to be the highest compared to the other solutions. On the other hand, the pressure developed inside the vessel could be measured although the temperature of the liquid was well below the boiling point of the heated solutions. Furthermore, the vapor pressure developed inside the vessel increased with an increase in sulphuric acid concentration, showing opposite behaviour to the temperature change.

It can also be observed that the temperature of all solutions containing H_2SO_4 started to rise after at least 5 seconds irradiation time, whereas, the water temperature increased instantly as soon as microwave irradiation was started. The heating rate data observed here are found to be very similar to those for sodium chloride solutions as shown in Appendix 6-3. When the same experiments were

repeated using the small vessel, the heating rate and the maximum temperature reached after 60 seconds irradiation time were found to be different.

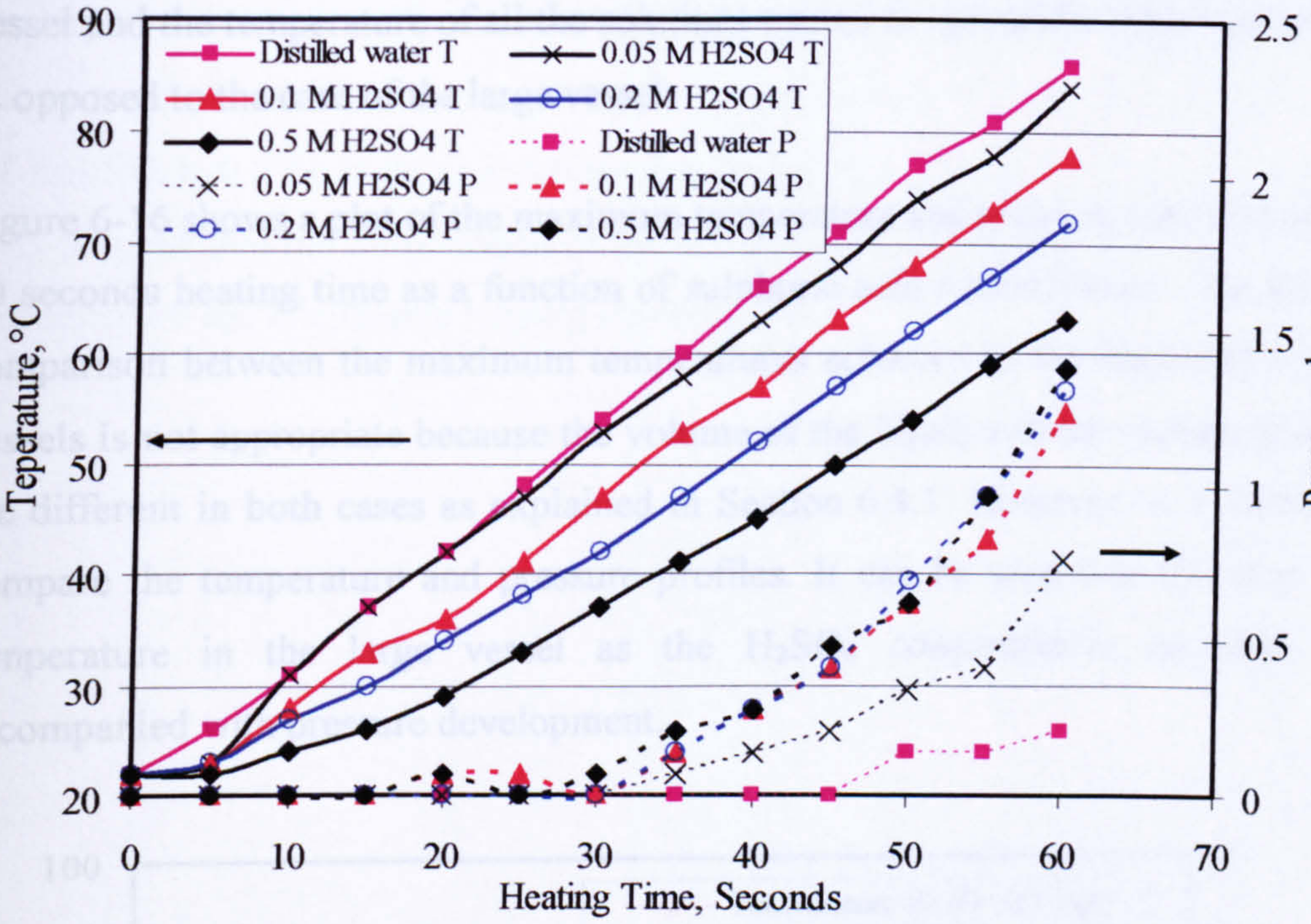

Figure 6-14 Microwave heating of 50 ml sulphuric acid solutions of various concentrations in the large vessel (D= 34 mm) for 60 seconds

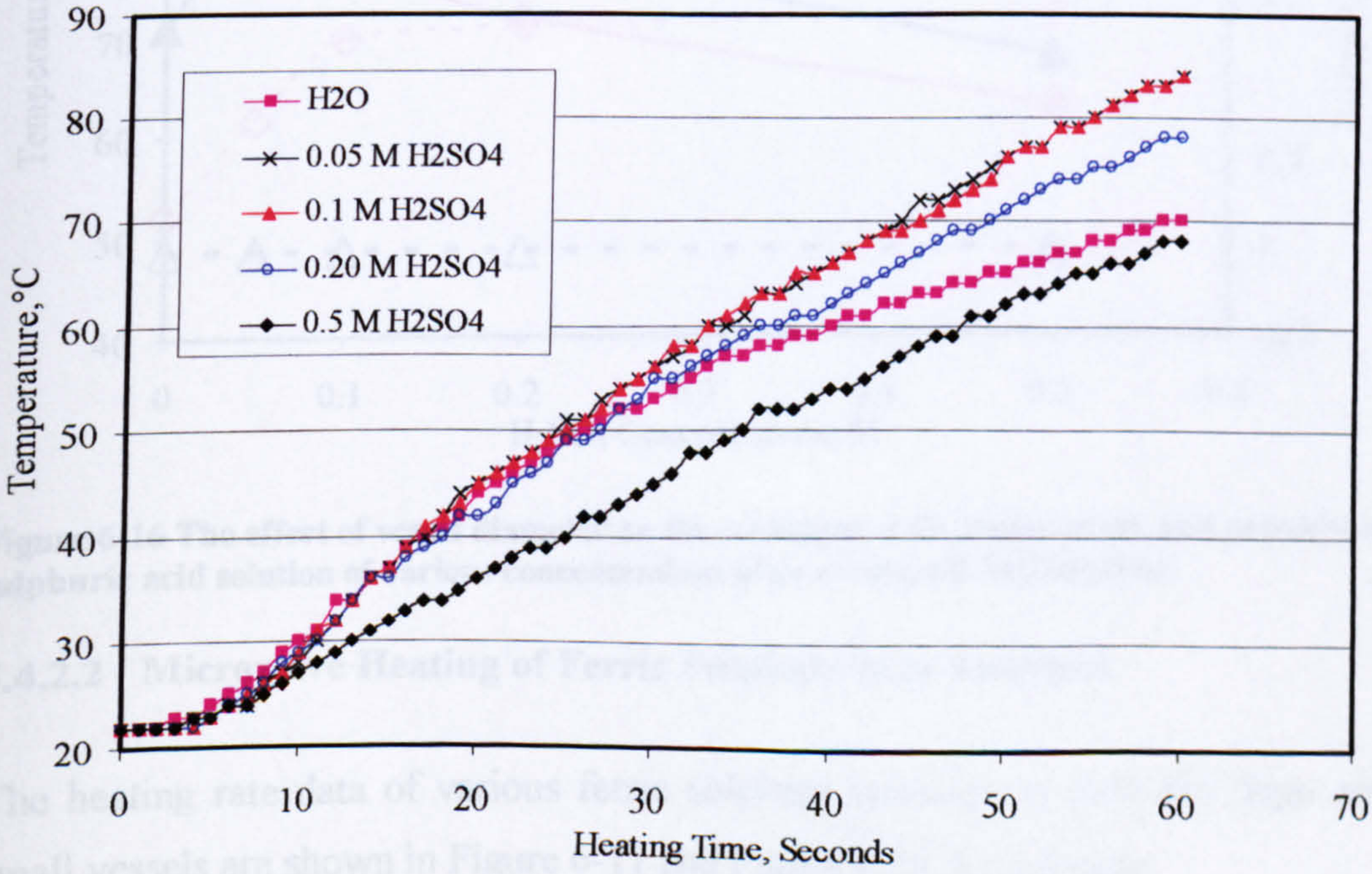

Figure 6-15 Microwave heating of 5 ml sulphuric acid solutions of various concentrations in the small vessel (D= 10 mm) for 60 seconds

The highest heating rate was achieved when heating solutions with 0.05 and 0.1 M H_2SO_4. The heating rate then decreased with an increase in sulphuric acid concentration. In this case, there was no pressure development inside the small vessel and the temperature of all the solutions started to rise earlier than 5 seconds as opposed to the case of the large vessel.

Figure 6-16 shows a plot of the maximum temperature and pressure achieved after 60 seconds heating time as a function of sulphuric acid concentration. The direct comparison between the maximum temperatures achieved in the large and small vessels is not appropriate because the volume of the liquid and the applied power are different in both cases as explained in Section 6.4.1. However, it is valid to compare the temperature and pressure profiles. It can be seen that the drop of temperature in the large vessel as the H_2SO_4 concentration increases is accompanied with pressure development.

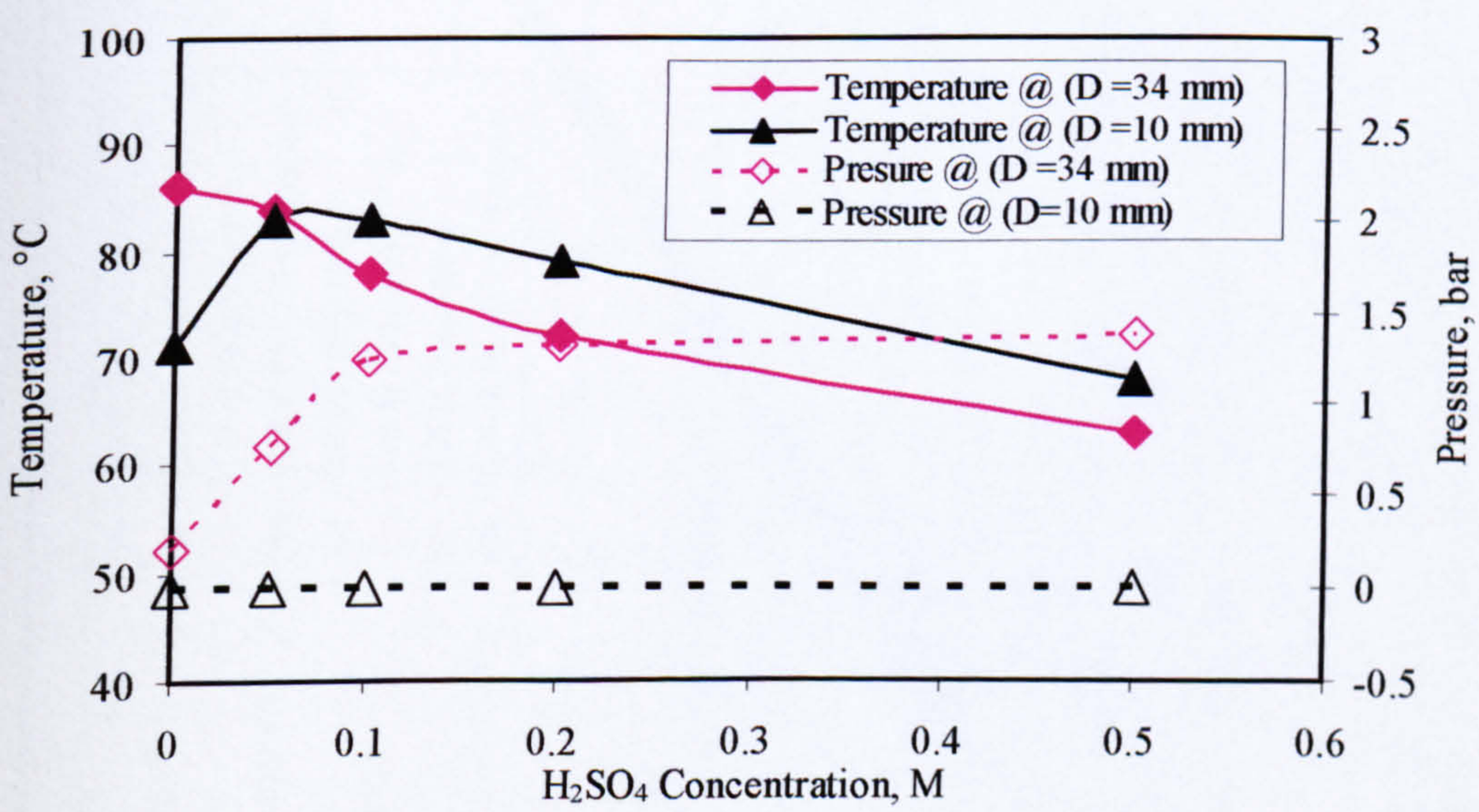

Figure 6-16 The effect of vessel diameter on the maximum bulk temperature and pressure of sulphuric acid solution of various concentrations after 60 seconds heating time.

6.4.2.2 Microwave Heating of Ferric Sulphate Base Solutions

The heating rate data of various ferric sulphate solutions in both the large and small vessels are shown in Figure 6-17 and Figure 6-18 respectively.

The heating characteristics of ferric sulphate solutions are shown to be similar to other ionic solutions (NaCl and H_2SO_4 solutions) in both the large and small vessels. However, the maximum temperature achieved after 60 seconds microwave heating for ferric sulphate solutions are found to be higher at similar ion concentrations. Furthermore, the heating rate of both (0.5 M H_2SO_4) and (0.25 M $Fe_2(SO_4)_3$-0.5 M H_2SO_4) solutions are found to be the same. These two facts may suggest that the introduction of ferric sulphate in the acidic solution has little influence on the microwave heating characteristics.

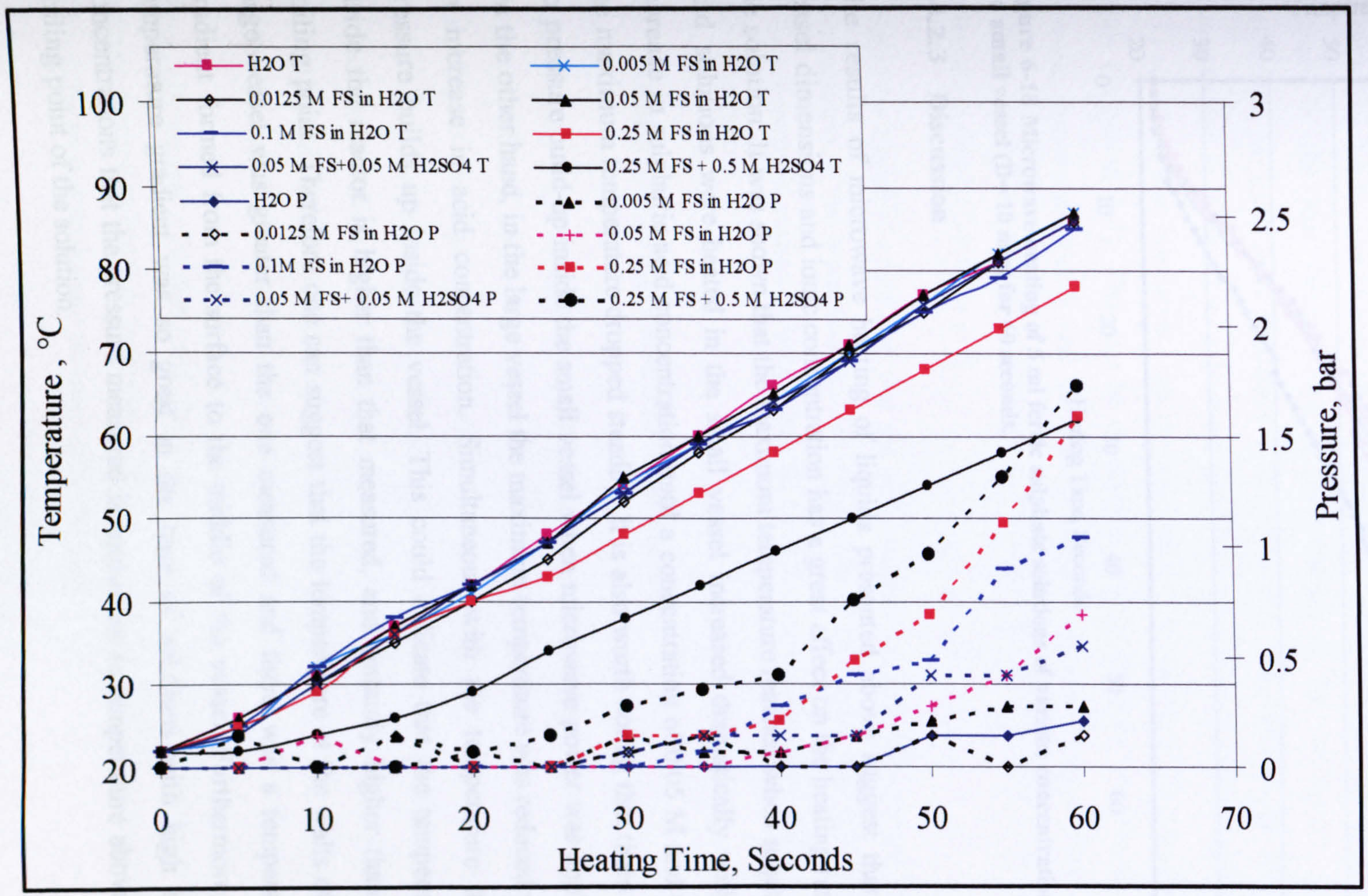

Figure 6-17 Microwave heating of 50 ml ferric sulphate solutions of various concentrations in the large vessel (D= 34 mm) for 60 seconds

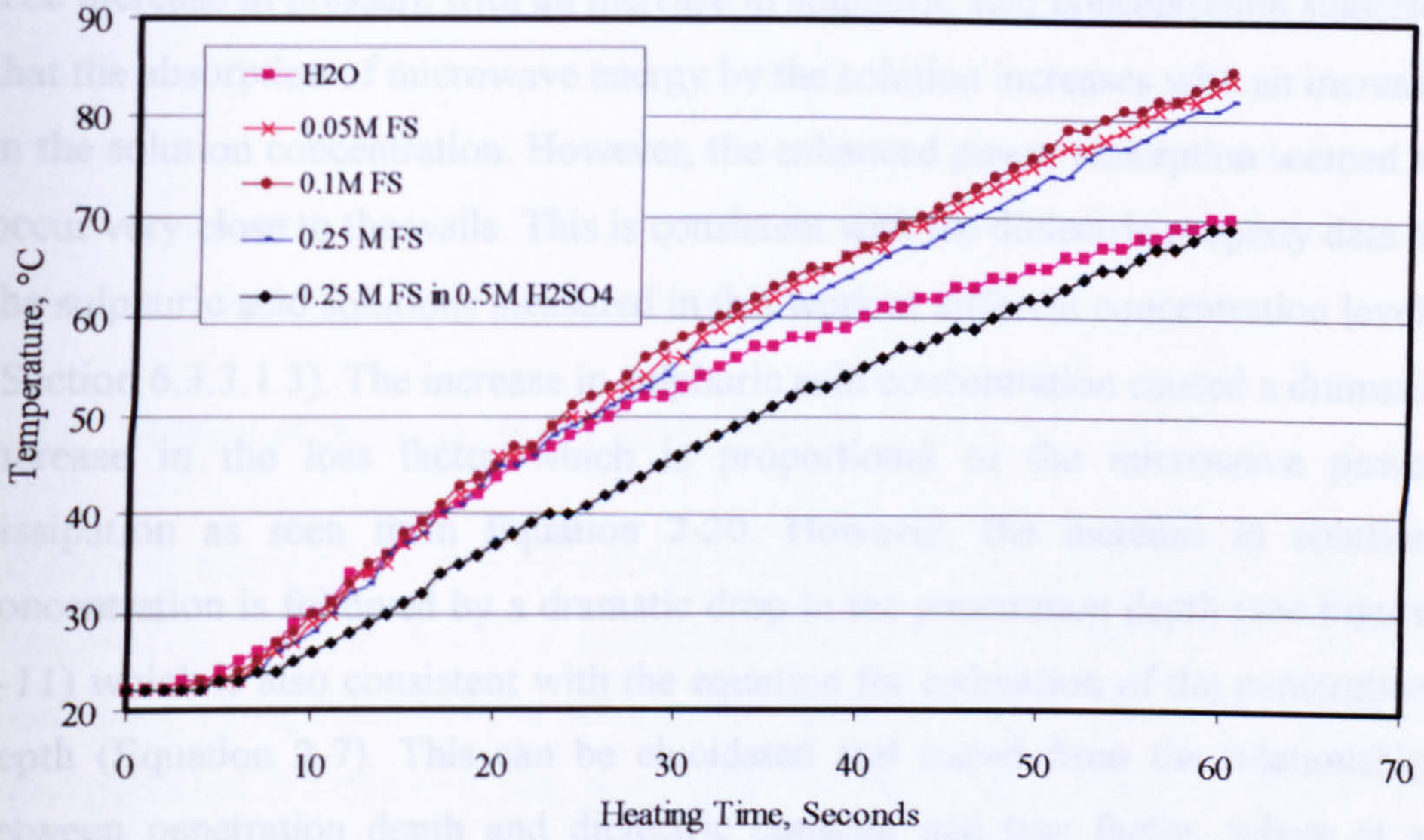

Figure 6-18 Microwave heating of 5 ml ferric sulphate solutions of various concentrations in the small vessel (D= 10 mm) for 60 seconds.

6.4.2.3 Discussion

The results of microwave heating of liquids presented above suggest that the vessel dimensions and ionic concentration has a great effect on the heating rate of the solution. It was shown that the maximum temperature reached when sulphuric acid solutions were heated in the small vessel increased dramatically with an increase in sulphuric acid concentration until a concentration of 0.05 M and then the maximum temperature dropped steadily. It is also worth noting that there was no pressure build-up inside the small vessel when microwave power was applied. On the other hand, in the large vessel the maximum temperature was reduced with an increase in acid concentration. Simultaneous with the temperature drop, pressure builds up inside the vessel. This could indicate that the temperature inside the reactor is higher than that measured, and certainly higher than the boiling point. Therefore one can suggest that the temperature at the walls of the large vessel was greater than the one measured and there was a temperature gradient formed from the surface to the middle of the vessel. Furthermore, the temperature gradient was so great in the case of solutions with high ionic concentrations that the pressure measured is equivalent to temperature above the boiling point of the solution.

The increase in pressure with an increase in sulphuric acid concentration suggests that the absorption of microwave energy by the solution increases with an increase in the solution concentration. However, the enhanced power absorption seemed to occur very close to the walls. This is consistent with the dielectric property data of the sulphuric acid solutions measured in this work at different concentration levels (Section 6.3.3.1.3). The increase in sulphuric acid concentration caused a dramatic increase in the loss factor which is proportional to the microwave power dissipation as seen from Equation 2-20. However, the increase in solution concentration is followed by a dramatic drop in the penetration depth (see Figure 6-11) which is also consistent with the equation for estimation of the penetration depth (Equation 2-7). This can be elucidated and traced from the relationship between penetration depth and dielectric constant and loss factor, where at a constant dielectric constant the increase in loss factor is followed by a decrease in penetration depth (Equation 2-7).

It could be therefore concluded that the bulk temperature inside the vessel is not representative of the actual temperature at the walls of the vessel. The introduction of ions promotes surface heating because microwaves are absorbed before they reach the centre.

6.5 Numerical Electromagnetic Simulation

Expressions for describing electric field in microwave waveguides and/or cavities are very difficult to solve analytically (Chan and Reader, 2000). Computer modelling is an important tool used to solve problems that are difficult or impossible to solve analytically. Electromagnetic numerical simulation provides valuable information about electric and magnetic field distribution, power absorbed by the material exposed to microwaves. Furthermore, the temperature distribution within the material can be determined.

There are several methods used for electromagnetic modelling such as finite element method (FEM), in frequency (FEFD) and in the time domains (FETD), finite difference time domain methods (FDTD) and others.

For the purpose of this, thesis a numerical simulation was carried out by Bradshaw (2005) at the University of Stellenbosch as part of collaborative research work. The aim of the numerical electromagnetic simulation was to provide supportive evidence for the results of microwave leaching of chalcopyrite in ferric sulphate (Section 4.4 and Section 4.7)

6.5.1 Selective Heating of Chalcopyrite

To provide support for the hypothesis of local heating of the chalcopyrite particles discussed in Section 4.4.6, a numerical simulation was performed. In this simulation, a simplified representation of the leaching system was used. A layer of cubic particles, 0.5 mm to a side, was uniformly dispersed in a regular array of 31 x 19 particles, with an inter-particle gap of 2 mm in a fluid layer with dielectric properties as given in Figure 6-13. The simulation was carried out at temperatures of 24.5 and 86°C. The particles were modelled as conductive medium with surface losses as described in Section 4.4.6 (σ = 1000 S/m). The fluid layer and particles representing chalcopyrite were assumed to be in a section of WR 284 waveguide with cross section 72 x 34 mm. The layer of particles was 2 mm interior to the leading edge of the fluid layer. A graphical representation of the simulation conditions is shown in Figure 6-19. The microwave excitation was a sinusoid at 2.45 GHz with amplitude 1 W. A finite difference time domain method (FDTD) was used for the simulation using QuickWave 3d®. Electric field and power density plots were observed once the simulation had reached steady state (Bradshaw, 2005).

Figure 6-20 shows a plot of the power density taken on the midline of the waveguide at a temperature of 24.5°C. Microwave energy is incident from the right hand side of the figure (x = 20). Spikes in the power density can be seen clearly on either side of all the particles. Most importantly it can be seen that immediately in front of the particles there is a thin layer in the leaching solution in which the power density is large, while the effect of surface conduction in the particles themselves leads to a power density that is more than double that of the surrounding fluid. This simulation, of an idealised array for particles,

demonstrates the differential heating between particles and fluid and also shows the effect of penetration depth on the power dissipation in the fluid volume.

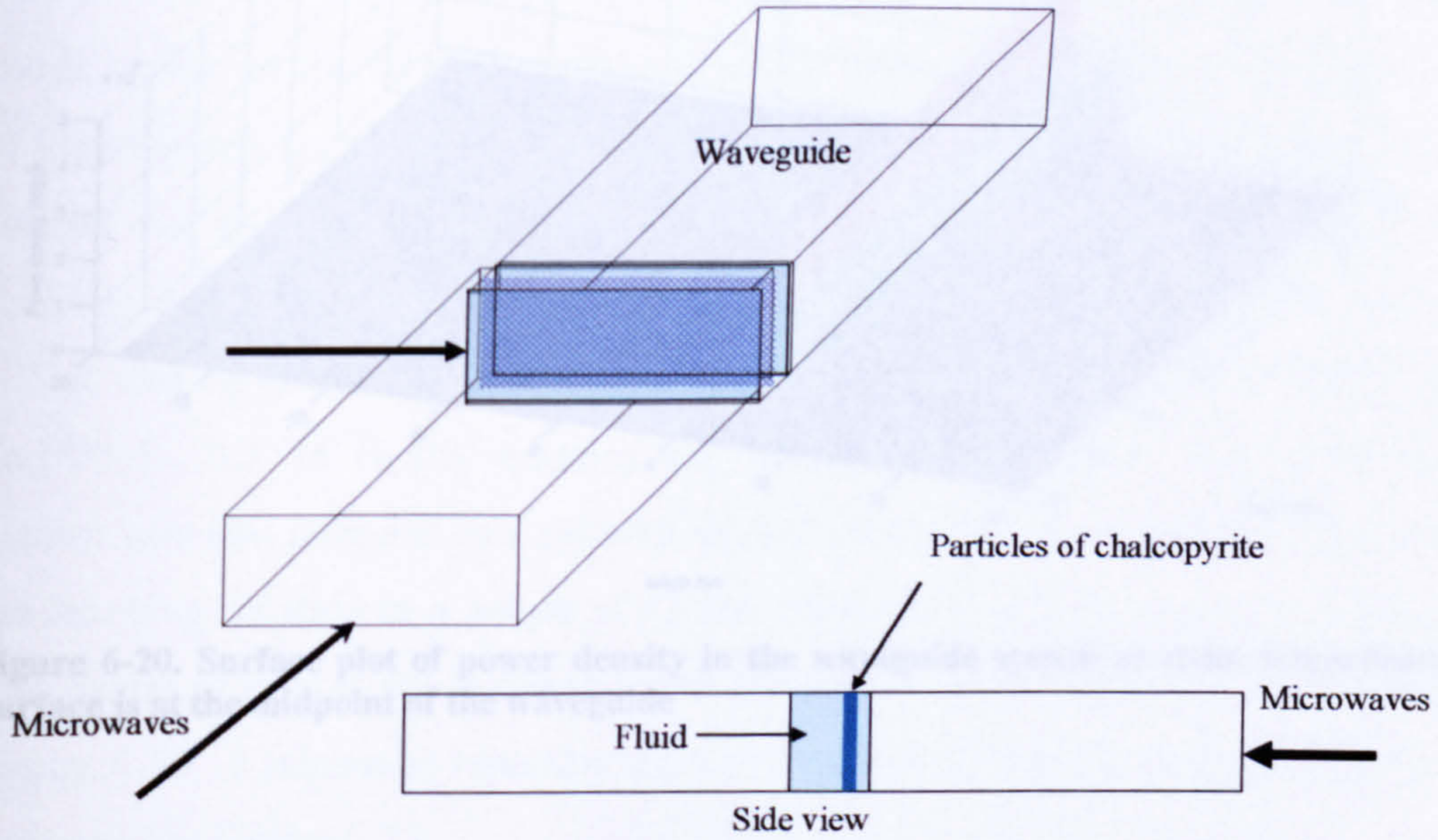

Figure 6-19 Graphical representation of the electromagnetic simulation conditions.

Figure 6-21 shows plots of the power density of side views of sections taken on the midline of the waveguide at temperatures 24.5°C (pane A) and 86°C (pane B). This figure clearly demonstrates the difference in the power density of both fluid and chalcopyrite particles. It also shows how the power density of fluid changes from the right to the left reflecting the microwave penetration depth. Furthermore, the difference between cold and hot leaching system is evident from the value of power density of both fluid and chalcopyrite particles. However, this difference is not great which is consistent with dielectric properties measurements (see Figure 6-13)

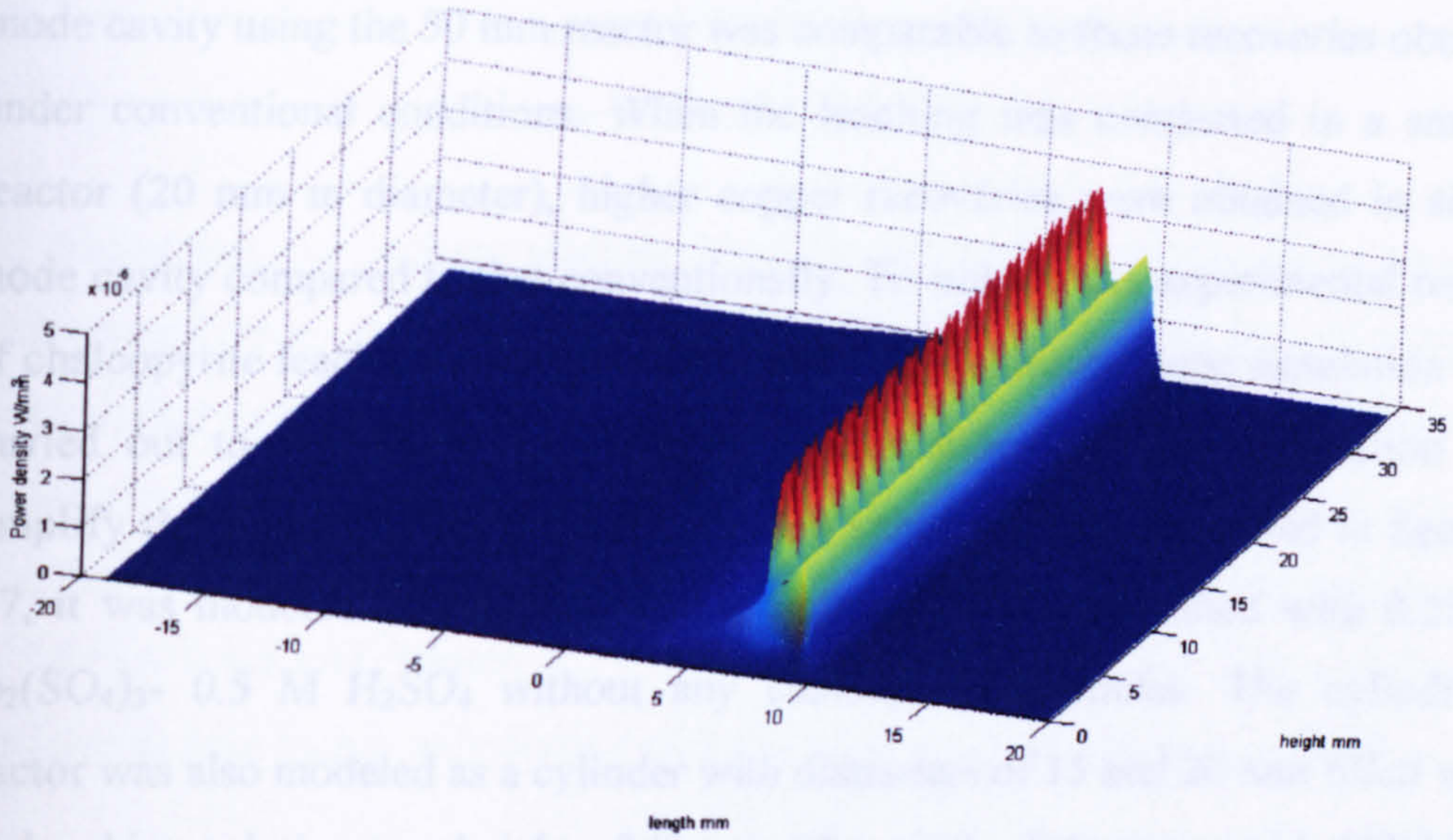

Figure 6-20. Surface plot of power density in the waveguide system at room temperature. Surface is at the midpoint of the waveguide

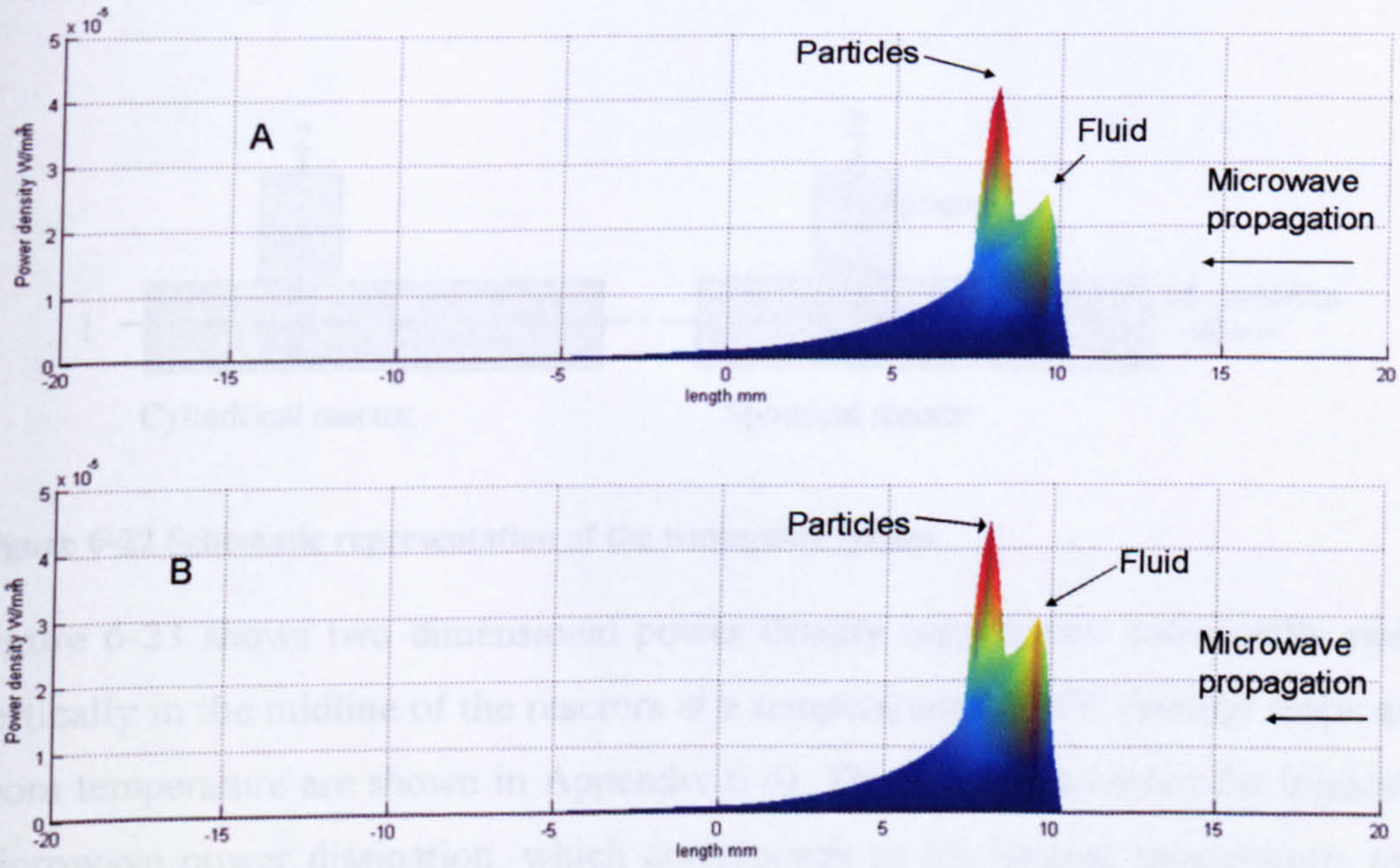

Figure 6-21 Sections of the surface plot of the power density in the waveguide system. A- at temperature 24.5°C, B- at a temperature of 86°C

6.5.2 Effect of Reactor Size in a Single Mode Cavity

It was demonstrated previously that the reactor size has a major effect on the recovery of copper from chalcopyrite (see Section 4.7). It was found that the copper recovery from chalcopyrite when leached in ferric sulphate in the single

mode cavity using the 50 mm reactor was comparable to those recoveries obtained under conventional conditions. When the leaching was conducted in a smaller reactor (20 mm in diameter), higher copper recoveries were obtained in single mode cavity compared to that conventionally. To support the experimental results of chalcopyrite leaching in single mode cavity an electromagnetic simulation was carried out to investigate the effect of reactor size on power dissipation. To simplify the simulation for the flat bottomed spherical flask described in Section 4.7, it was modeled as a sphere with a diameter of 50 mm filled with 0.25 M $Fe_2(SO_4)_3$- 0.5 M H_2SO_4 without any chalcopyrite particles. The cylindrical reactor was also modeled as a cylinder with diameters of 15 and 20 mm filled with the leaching solution to a height of 43 mm (the width of the waveguide WR340). The centre of the reactor is coaxial with the centre of the waveguide as shown in Figure 4-55. A schematic representation of the reactors in the waveguide system is presented in Figure 6-22

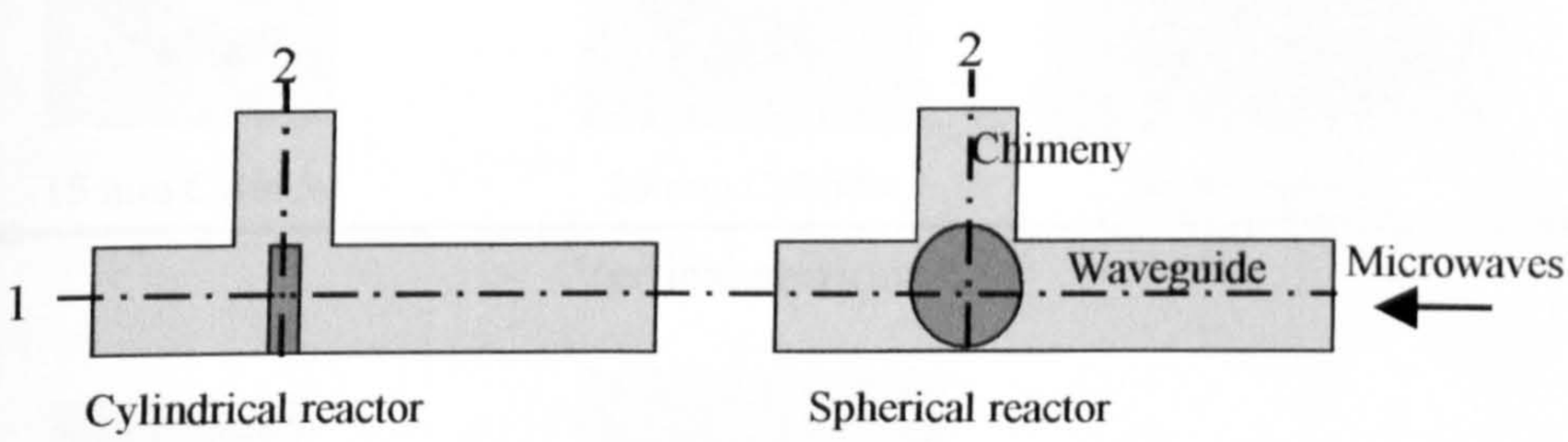

Figure 6-22 Schematic representation of the waveguide system

Figure 6-23 shows two dimensional power density maps taken horizontally and vertically in the midline of the reactors at a temperature of 86°C (similar maps at room temperature are shown in Appendix 6-4). The area experienced the highest microwave power dissipation, which corresponds to the highest temperature, as represented by red colour. Microwaves are incident from the right hand side of the maps. It can be clearly seen that the high regions of power density in the sphere are limited to a small area (< 25% in the horizontal section and < 10 % in the vertical section). The power density coverage increases with the decrease of the reactor size. For example, in the cylindrical reactor with a diameter of 20 mm, the area with high power density is estimated to be more than 40% (see Figure 6-23).

Therefore, the power distribution in the 20mm cylindrical reactor is estimated to be at least 2.5 times higher compared to the sphere.

Assuming that the leaching mixture (chalcopyrite particles and leach solution) is well mixed, one could suggest that the residence time of the particles is proportional to area. This means that the residence time of chalcopyrite particles within the area of high power density in the cylindrical reactor (20mm diameter) is at least 2.5 times higher than in the sphere. Therefore, based on the discussion in Section 4.4.6 and Section 6.5.1, there will be more chances for chalcopyrite particles to gain higher temperature than the bulk liquid in the small reactor.

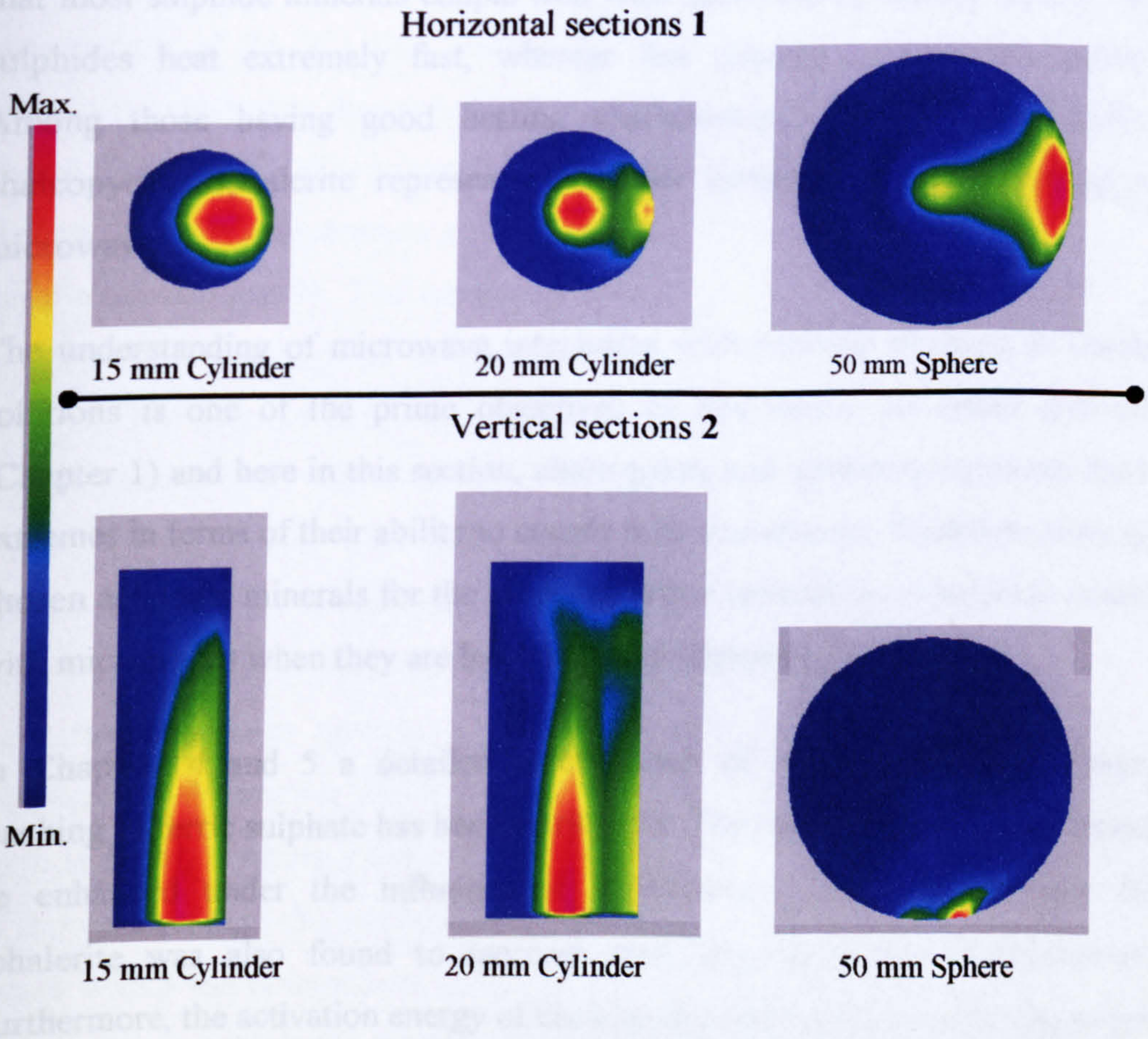

Figure 6-23 Power density maps taken along the horizontal and vertical axis of the single mode cavity (T =86°C).

The simulation results presented in this section agree with experimental results of chalcopyrite leached in a single mode cavity (Section 4.7). The limited enhancement in copper recovery from chalcopyrite when leached in the 50 ml

vessel in the single mode cavity is probably due to the short resident time of chalcopyrite particles within the region of high microwave power density. However, a higher copper recovery was observed in the small reactor due to the longer residence time as estimated from the pattern maps in Figure 6-23.

6.6 General Discussion

The behaviour of sulphide minerals in a microwave field has been investigated by many researchers (Chen et al., 1984; Harrison, 1997; Kingman and Rowson, 1998; McGill et al., 1988; Walkiewicz et al., 1988) and many others (see Appendix 3-4 for some of the heating rate data reported in literature). It was found that most sulphide minerals couple well with microwaves, heating rapidly. Some sulphides heat extremely fast, whereas few showed unresponsive behavior. Among those having good heating characteristics in microwave fields is chalcopyrite. Sphalerite represents the other extreme of poor coupling with microwaves.

The understanding of microwave interaction with sulphide minerals in leaching solutions is one of the prime objectives of this thesis. As stated previously (Chapter 1) and here in this section, chalcopyrite and sphalerite represent the two extremes in terms of their ability to couple with microwaves. Therefore, they were chosen as model minerals for the investigation of interaction of sulphide minerals with microwaves when they are leached under microwave conditions.

In Chapters 4 and 5 a detailed investigation of chalcopyrite and sphalerite leaching in ferric sulphate has been carried out. The copper recovery was found to be enhanced under the influence of microwaves. The zinc recovery from sphalerite was also found to increase with the application of microwaves. Furthermore, the activation energy of chalcopyrite and sphalerite leaching in ferric sulphate was found not to change significantly by the application of microwaves. For chalcopyrite, Ea was found to be 76.5 kJ/mole for microwave leaching conditions and 79.5 kJ/mole conventionally, and the difference between these values was found to be statistically insignificant. Similarly, the activation energy

of the sphalerite leaching process under microwave conditions was found to be 41.2 kJ/mole compared to 43 kJ/mole conventionally.

A comparison of the Arrhenius plot slopes for both conventional and microwave conditions for both chalcopyrite and for sphalerite show displaced but still quasi-linear character. This result indicated that the actual reaction temperature could be higher than the actual bulk temperature. This hypothesis was further elucidated by carrying out further specialised experimentation and numerical modelling.

First of all, the dielectric properties measurements of ferric sulphate showed that this solution is highly lossy (see Section 6.3.3.2). The calculated penetration depth corresponding to the measured dielectric properties was found to be 2.7 mm at a temperature of 86 °C. This shallow penetration depth suggests that most of microwave energy is dissipated within the first few millimeters of the leaching vessel (D= 34 mm). This suggests that the temperature at the walls of the vessel is higher than the temperature at the position of the temperature sensor (in the middle of the vessel). The temperature gradient was confirmed by microwave heating of ferric sulphate solutions in vessels of various diameters (Section 6.4.2.2). The pressure build up in the closed large vessel reached 1.7 bars after 1 minute heating time, which corresponds to a measured temperature of 63°C in the middle of the vessel. The water temperature which corresponds to a vapor pressure of 1.7 bars is reported to be 115°C ((David, 2004). It should be noted, however, that microwave heating of ferric sulphate solution was carried out deliberately without agitation. Of course agitation will minimize such great temperature difference. However, as microwave energy was almost always applied during leaching, one could expect some difference between the outer shell of the vessel where the maximum power dissipation occurs and the middle of the vessel where the temperature sensor is located. So when the particles of either chalcopyrite or sphalerite are thrown to the periphery of the vessel as a result of agitation, they fall within the region of high temperature which means that the dissolution reaction in this region will proceed at higher temperature. Now the conventional leaching of chalcopyrite and sphalerite showed that their dissolution processes are chemically controlled and the reaction rate is sensitive to

temperature change. This means that a small change in the reaction temperature will result in a sensible change in copper and zinc recoveries from their corresponding minerals. The above arguments should explain the enhanced recovery of both copper and zinc from their corresponding minerals when leaching is carried out under microwaves.

On the other hand, the leaching outcome of chalcopyrite and sphalerite under stagnant microwave conditions was found to be different. The recovery of copper from chalcopyrite under stagnant microwave conditions was found to be higher than under agitated microwave conditions, which is not consistent with the mass transfer limitations observed in conventional experiments (see Figure 4-41). On the other hand, as expected, the recovery of zinc from sphalerite under stagnant conditions is lower than the agitated case, which is consistent with the fluid film limitations demonstrated in Figure 5-4. It should be stated however, that the zinc recovery under stagnant microwave conditions is higher than that produced conventionally (as discussed in Section 5.8). Based on the experimental and literature evidence regarding the conductivity of chalcopyrite (Section 4.4.6 and Section 6.2.2.1), it is therefore suggested that chalcopyrite could be heated selectively in the ferric sulphate solution despite this solution being found to be high loss. The selective dissolution generates a temperature gradient at the reaction interface between the chalcopyrite particle surface and the leaching solution, which consequently leads to a higher copper recovery under stagnant conditions because all chalcopyrite particles were within the penetration depth of microwaves. The proposed hypothesis of the selective heating of chalcopyrite in ferric sulphate was further supported by the numerical simulation results presented in Section 6.5.1. The simulation showed that the power density in chalcopyrite layer of particles is double that of the surrounding fluid. This in turn strongly supports the hypothesis of selective heating of chalcopyrite.

Sphalerite, on the other hand, was found to be a poor microwave absorber (see Section 6.2.2.2), particularly the sample used for the current thesis which had a very low iron content (<0.1%). That is probably why the recovery of Zn under microwave agitated conditions is higher than that produced under stagnant

microwave conditions as there is no preferential microwave heating, which is similar to the trend observed under conventional conditions.

It should be considered, however, that not all the enhancement observed in Cu recovery under stagnant microwave conditions is a result of selective heating of chalcopyrite. The shallow microwave penetration depth, which results in higher temperature of the leaching solution at the walls of the vessel, may also have participated in the observed enhancement at stagnant microwave conditions. The pressure build-up in the large vessel during microwave heating of ferric sulphate (see Section 6.4.2.2) resulted from the high temperature developed at the periphery of the large vessel. This supports the idea of the enhancement being caused by a temperature gradient between the region of penetration depth and the centre of the vessel. The other experimental evidence of the temperature gradient being a cause for the enhancement is that the zinc recovery from sphalerite under microwave stagnant conditions is higher compared to that conventionally. As stated previously sphalerite is not responsive to microwaves, thus the only possible reason here for the enhancement in recovery is due to a temperature gradient between the bottom of the vessel where the particles are located and the centre of the vessel where the temperature sensor is located.

Upon further analysis of the enhanced recovery of both copper and zinc when leached from their corresponding minerals, one can notice that the overall percentage enhancement of copper recovery is generally about twice as high as the increase in zinc recovery. This is illustrated in Table 6-6 which shows further evidence to suggest that the enhancement of Cu from chalcopyrite is affected by the preferential heating of the particles and the temperature gradient across the leaching vessel.

Table 6-6. The enhancement in Cu and Zn recovery after microwave treatment

T, °C	Chalcopyrite			Sphalerite		
	Cu Recovery, %		**Enhancement, %**	Zn Recovery		**Enhancement, %**
	Conv	Micro		Conv	Micro	
50	1.05	1.38	**31.4**	18.7	21.4	**14.4**
70	4.14	5.44	**31.4**	42	46.8	**11.4**
80	8.75	10.5	**16**	58	65.8	**8.3**
90	13.5	16.9	**25.2**	74.4	81.3	**9.3**
90rep	14.7±0.8	12.0±0.2	**23±7**			

Based on the above discussion it could be concluded that the increase in copper recovery from chalcopyrite under stagnant microwave conditions is caused by at least the preferential heating of particles over the solution. The effect of temperature difference resulting from the limited depth of penetration is another possible influential factor on the observed enhancement.

The experimental results of the single mode cavity strongly support the phenomena of the preferential heating of chalcopyrite as well as the effect of penetration depth (Section 4.7.2). There was no enhancement in copper recovery from chalcopyrite when leached in the large reactor in the single mode cavity compared to the conventional leaching results presented in Table 4.16. However, copper recovery obtained in the 20 mm reactor was higher than the 50 mm reactor and it is comparable to those results obtained in the multimode cavity (Table 4.16). These results were backed up with the numerical simulation results discussed in Section 6.5.2, where it was estimated that the residence time of chalcopyrite particles in the region of high power density is at least 2.5 times higher in the small cylindrical reactor compared to the large spherical one.

6.7 Conclusions

Measurements of dielectric properties of solids and liquids used in this thesis have been carried out. The dielectric properties measurement of powdered chalcopyrite indicates that it is lossy. However, chalcopyrite was considered in this work to be a conductor based on the experimental and literature evidence. On the other hand, sphalerite showed very poor microwave absorbing characteristics. The loss factor of sphalerite was found to be about 0.0035 at room temperature and at a frequency of 2.45 GHz.

It has been shown that the cavity perturbation technique, used for the measurements of sphalerite and chalcopyrite dielectric properties, is not suitable for high loss leaching solutions. Coaxial probe techniques were found to be more suitable for solutions with high ionic concentrations. Ferric sulphate leaching

solution was found to be a highly lossy liquid with a penetration depth of about 2.7 mm at a temperature of 86°C and at a frequency of 2.45 GHz.

Microwave heating of ionic solutions of various concentrations in vessels of different diameters showed the importance of considering the effect of penetration depth and vessel diameter in the interpretation of microwave leaching data. Furthermore, the numerical simulation was used to support the experimental results. It showed clearly how chalcopyrite particles could be heated preferentially in ferric sulphate, which is suggested to be the main reason for the increase in copper recovery from chalcopyrite under microwave conditions. The simulations also showed that the smaller the reactor, the larger the specific volume of ferric sulphate affected by high power density. This concurs with the results of chalcopyrite leaching in reactors of different sizes in the single mode cavity.

CHAPTER SEVEN

Conclusions and Further Work

7.1 Conclusions

Hydrometallurgy as an alternative route for metal extraction from sulphide minerals is attractive compared to pyrometallurgy because of the lower energy demands and less gaseous emission to the atmosphere. However, this method suffers from lengthy processing time and lower recovery of metal value, particularly, for minerals like chalcopyrite and to a lesser extent sphalerite. Despite extensive research in this area and some success at the bench scale, there are still significant challenges to the scale up of copper extraction from chalcopyrite by hydrometallurgical means. Therefore, research work is still ongoing to develop processes which are less costly, and more environmentally friendly. One direction toward a cleaner environment is to use microwaves as an energy source to enhance leaching processes. A comprehensive review of microwave assisted leaching has been carried out by Al-Harahsheh and Kingman (2004) which showed that the application of microwave energy in mining and metallurgy is in the early stages. Microwaves have many potential applications in mineral processing and extractive metallurgy. However, great disagreement regarding the effect of microwaves on chemical reactions and leaching system was found.

This thesis has developed a fundamental understanding of the effect of microwaves on sulphide minerals in leaching solutions. The investigation

included conventional and microwave leaching studies of chalcopyrite and sphalerite. The understanding of conventional leaching of chalcopyrite was important for the understanding of microwave leaching because the literature survey showed that the dissolution of chalcopyrite is not completely understood, and the mechanism by which chalcopyrite is passivated is still under debate.

Therefore, a study of chalcopyrite leaching in ferric sulphate was carried out. It was found that chalcopyrite leaching in ferric sulphate is a very slow process and the kinetic data suggests that the dissolution process is chemically controlled. The apparent activation energy of chalcopyrite dissolution in ferric sulphate was found to be 79.5 kJ/mole, which agrees with the values reported in the literature. Furthermore, as revealed from SEM analysis there was no complete sulphur layer formed to envelope the leached particles. Instead, a preferential oxidation or sulphur deposition on particular fracture planes was found to occur.

ToF-SIMS analysis of freshly fractured particles showed the different abilities of some regions to absorb hydrocarbons (HC). Two types of area were identified and both seemed to have different reactivities. One area was found to be rich in HC and oxidised species. The other area resembled what might be expected from a clean, pure chalcopyrite surface. The relative ratio of some oxidised sulphur species (S_n^-, SO_n^- and MS_n^-) on those two areas was found to be up to 7 times higher on the HC area. Preliminary analysis of the ToF-SIMS data indicated different surface chemistry on both areas. This was hypothetically linked to the different chemistry of different cleavage planes of chalcopyrite with some of these planes being experienced significant alteration and oxidation thereafter. It is speculated that the area which experienced high oxidation might represent the case where the reconstruction process proposed by Klauber (2003) has occurred producing a pyrite type phase. Furthermore, it is speculated that the plane that experienced reconstruction consisted of zigzag type orthogonal micro planes based on the analogy to the observations of Shukri (1997) on $CuInSe_2$ cleavage planes. One micro plane has the properties of chalcopyrite and the other micro plane behaves electrochemically like pyrite. These two microplanes would behave similar to the case where pyrite and chalcopyrite are in an intimate contact leading

to an enhanced leaching to such planes. No conclusive evidence to support such speculation was produced and this matter is one of the areas requiring further investigation.

The effect of microwaves upon the leaching of chalcopyrite in ferric sulphate was demonstrated. A slight enhancement in copper recovery was observed when leaching was carried out under microwave conditions. For the first time, this enhancement was explained to be a result of two factors. The limitation of the solution penetration depth caused a temperature gradient to occur between the outer shell and the middle of the reactor, where the bulk temperature was measured. The temperature gradient was evident from the displaced but parallel nature of the Arrhenius plots and the similarities in the values of activation energies, within the experimental error, of both microwave and conventional leaching. This hypothetical explanation was supported by the measurements of the dielectric properties of the leaching solution, which was found to be high lossy with a penetration depth of about 2.7 mm at a temperature of 86°C. Further supportive evidence was obtained from microwave heating of liquids with various concentrations under controlled conditions and using different vessel sizes. Great temperature differences were observed between the outer shell and the middle of the large vessel based on the temperature and pressure measured inside the vessel. The temperature measured inside the vessel was much lower than the temperature equivalent to the pressure developed.

Secondly the selective heating of chalcopyrite potentially explains the enhancement of the copper recovery under microwave conditions. This was supported by the higher copper recovery when no agitation was applied. Furthermore, the high conductivity of chalcopyrite also supports the theory of selective heating, which causes chalcopyrite to heat by conduction losses. Finally the electromagnetic simulations showed that the power density of chalcopyrite particles is higher than the liquid due to the higher power dissipation in chalcopyrite particles when located within the penetration depth of the leaching solution.

The leaching of chalcopyrite in ferric chloride was also studied. The dissolution reaction was found to chemically controlled with an apparent activation energy of 69 kJ/mole. Under conventional conditions it was found that agitation had a negative effect on copper recovery. Higher copper recoveries were obtained under stagnant conditions due to the accumulation of $CuCl_2$, a reaction product, which acted as a second oxidant. The lower recovery of copper under agitated conditions was due to the reduced concentration of $CuCl_2$ at the surface of chalcopyrite particles as a result of agitation. Surprisingly, the copper recovery from chalcopyrite in closed anaerobic conditions was found to be twice as high as the open vessel. This result could not be explained and requires further investigation.

The effect of microwaves on the leaching of chalcopyrite in ferric chloride was also studied. An enhancement of the copper recovery was also observed. However, due to the complexity of the chloride system under closed conditions it was very difficult to account for the effect of microwaves on the reaction kinetics. This is because microwave leaching experiments were carried out in closed vessels. Additionally, the effect of $CuCl_2$ on the reaction rate is difficult to distinguish from the selective heating of chalcopyrite and penetration depth effects.

A study on the leaching of sphalerite in ferric sulphate was also carried out under both microwave and conventional conditions. The dissolution reaction was found to be chemically controlled under both conventional and microwave conditions with corresponding activation energies of 43 and 41.2 kJ/mole. Similar to the chalcopyrite case, the almost parallel and displaced Arrhenius plots suggests that the actual reaction temperature is higher than the temperature measured in the middle of the reactor. Therefore higher rates of chalcopyrite dissolution were observed under microwave conditions. However, as opposed to microwave leaching of chalcopyrite, sphalerite did not selectively heat within the leaching solution. This was evident because the recovery was lower at stagnant conditions. Furthermore, the percentage enhancement in zinc recovery under microwave conditions was, on average, half the percentage enhancement observed in copper recovery.

A measurement of dielectric properties of chalcopyrite, sphalerite, sulphuric acid solutions of different concentrations, and ferric sulphate leaching solution were carried out. It was found that sphalerite is a poor microwave absorber with a loss factor of about 0.0035 at room temperature, a frequency of 2.468 GHz and a packing density of 2173 kg/m^3. With regards to chalcopyrite, it was found that it behaves like a metal powder in a microwave field based on literature data and simple experiments. Nevertheless, the dielectric properties of powder samples suggest that chalcopyrite can heat readily in a microwave field due to conductive losses. The dielectric properties of ionic solutions were measured using the coaxial probe technique as the cavity perturbation technique was found not to be suitable for high loss materials. Ferric sulphate leaching solution (0.25 M $Fe_2(SO_4)_3$- 0.5 M H_2SO_4) was found to be highly lossy. The calculated penetration depth was about 2.7 mm at a temperature of 86°C and a frequency of 2.468 GHz, which corresponds to a dielectric constant of about 41 and loss factor of about 42. The dielectric properties of sulphuric acid solutions, the matrix of the leaching solution used, are strongly dependent on sulphuric acid concentration. As sulphuric acid concentration increases, the loss factor increases dramatically until a concentration of about 0.2 M, which correspond to a dramatic drop in the penetration depth. The dielectric constant also falls considerably with an increase in sulphuric acid concentration.

Microwave heating of ionic solutions in vessels of various diameters shows the importance of considering the effect of penetration depth and vessel diameter in data interpretation. This was also demonstrated experimentally when chalcopyrite was leached in a single mode cavity using vessels of various diameters.

The numerical simulation of the leaching system agreed with the experimental results. It was shown that chalcopyrite could be heated selectively in high loss solution when it is located within the penetration depth region. Furthermore, the reactor diameter affected the residence time of leached solid particles within the high power density domain.

The work for this thesis has demonstrated clearly that the main challenge of microwave application in hydrometallurgy is the limitation of microwave penetration depth. The reactor size should be comparable with the penetration depth to obtain sensible enhancement. The work at lower frequency and higher power levels would also increase the power density domain.

7.2 Recommended Further Work

The understanding of the chalcopyrite leaching mechanism is very important for the development of new hydrometallurgical processes. The work for this thesis forms a very small part of the research work undertaken in this area. Based on the results obtained in this work, one identified area of research would be further investigating the surface chemistry of a freshly cleaved and leached chalcopyrite surfaces under various conditions using ToF-SIMS, SEM and possibly XPS. Part of this work is recommended to be carried out on laboratory-grown synthetic chalcopyrite crystals. Various cleavage planes are required to be produced for a systematic study using ToF-SIMS before and after leaching for different leaching times. ToF-SIMS depth profiling would be a powerful tool to use to obtain more information from chalcopyrite surfaces, before and after leaching. The depth profiling mode provides information about the nature of the subsurface monolayer.

Leaching of chalcopyrite in ferric chloride under closed vessel conditions was also identified as a potential area of research. Such a study would involve two parts: theoretical and experimental. The theoretical study would involve a speciation study using available speciation software such as PHREEQC®. The experimental part may take into account the possibility of identifying the gaseous phase generated inside the vessel and the solubility of these gases in the leaching solution.

With regards to microwave leaching, it has been found that the dielectric properties of both leaching solution and leached material, the reactor size and the position of the leached materials in the microwave cavity have high influence on

the leaching outcome. It would be interesting to devise a simple dissolution system which would include metal powders (copper) of various particle sizes and acidic solution with a simple dissolution process. This would provide a strong evidence of the selective heating.

Another area of research would be to repeat some of the experiments at lower frequency (915 GHz) in order to work at a deeper penetration depth. More importantly is to try designing continuous systems which involve circulation of the leaching slurry through a set of narrow reactors located within a microwave cavity at high power levels.

It would also be interesting to investigate the possibility of the space charge polarisation effect on the selective heating of both chalcopyrite and sphalerite. This would ideally be carried out using a multi-frequency microwave system capable of generating low frequencies.

High pressure and temperature leaching is one hydrometallurgical route used for leaching of several minerals, including chalcopyrite and sphalerite. It would be interesting to using microwave energy to generate high temperatures and pressures inside the reactor, especially if the leached material is able to heat selectively. It should be noted, however, that at such a high temperature ferric sulphate is not recommended as an oxidant due to several reasons. First of all, there will be high risk of jarosite formation. Furthermore, to dissolve one mole of chalcopyrite, 8 moles of ferric sulphate is required producing 17 moles of ferrous sulphate against only one mole of copper sulphate. Finally, all sulphur will oxidise to its sulphate state.

References

Abkar, M. (Editor), 1998. Inductively Coupled Plasma Mass Spectrometry. Wiley-VCH, New York.

Abu-Samra, A., Morris, S.J., Koirtyohann, S.R. and., 1975. Wet ashing of some biological samples in a microwave oven. Analytical Chemistry, 47(8): 1475-1477.

Adams, R.L., Russo, R., Arnott, R.J. and Wold, A., 1972. Preparation and properties of the systems $CuFeS_{2-x}$ and $Cu_{1-x}Fe_{1+x}S_{2-y}$. National Bureau of Standards (US) Special publications, 364: 713-719.

Al-Harahsheh, M. and Kingman, S.W., 2004. Microwave-assisted leaching-a review. Hydrometallurgy, 73(3-4): 189-203.

Allen, T., 1997. Particle Size Measurements. Particle Sampling and Particle Size Sampling. 5th Edition. Chapman & Hall, London.

Andress, J.M., Ferrando, A.C. and Memrado, L., 1996. Chemical desulphurisation of coal with hydriodic acid. Fuel and Energy Abstracts, 10(2): 425-430.

Antonijevic, M.M., Jankovic, Z. and Dimitijevic, M., 1994. Investigations of the kinetics of chalcopyrite oxidation by potassium dichromate. Hydrometallurgy, 35: 187-201.

Antonucci, V. and Correa, C., 1995. Sulphuric acid leaching of chalcopyrite concentrate assisted by application of microwave energy. In: W.C. Cooper, D.B. Dreisinger, J.E. Dutrizac, H. Hein and G. Ugarte (Editors), Proceeding of COPPER 95- COBRE 95 International Conference, Vol. 3- Electrorefining and Hydrometallurgy of Copper. The Metallurgical society of CIM, Santiago, Chile, pp. 549-557.

Antonucci, V.L., 2004. Evolution of process LOXS-MW for sulphuric leaching of chalcopyritic copper concentrate, Hydrosulphide 04, Chile.

Arai, M., Binner, J.G.P. and Cross, T.E., 1993. High temperature dielectric properties measurements of engineering ceramics. American Ceramic Society, 36: 483-492.

Baghurst, D.R. and Mingos, D.M.P., 1992. Supper heating effect associated with microwave dielectric heating. The Journal of the Chemical Society, Chemical communications: 674-677.

Balaz, P., Kupka, D., Bastl, Z. and Achimovicova, M., 1996. Combined chemical and bacterial leaching of ultrafine ground chalcopyrite. Hydrometallurgy, 42(2): 237.

Batt, J. et al., 1995. Aparallel measurement progamme in high temperature dieletric propertiy measurements: an update. Ceramic Transactions, 59: 243-250.

Baur, J.B., Gibbs, H.L. and Wadshworth, M.E., 1974. RI 7823, USBM.

Beckstead, L.W. et al., 1976. Extractive Metallurgy of Copper. In: J.C. Yannopoulos and J.C. Agarwal (Editors). AIME, N. Y. (cited in Dutrizac, 1981).

Beeby, J.P., 1992. The recovery of a valuable species from an ore. Patent No. WO92/18249

Berry, V.K., Murr, L.E. and Hiskey, J.B., 1978. Galvanic interaction between chalcopyrite and pyrite during bacterial leaching of low-grade waste. Hydrometallurgy, 3(4): 309-326.

Biegler, T. and Swift, D.A., 1979. Anodic electrochemistry of chalcopyrite. Journal of Applied Electrochemistry, 9(5): 545-554.

Binner, J.G.P., Vaidhyanathan, B. and Wang, J., 2003. A comparative study of temperature measurement during microwave processing. In: J.G.P. Binner (Editor), 9th International Conference on Microwave and High Frequency Heating. Loughborough University, Loughborough University, UK.

Bobeck, G.E. and Su, H., 1985. The kinetics of dissolution of sphalerite in ferric chloride solution, Metallurgical Transactions B, pp. 413-424.

Bordi, F., Cametti, C. and Gili, T., 2001. Reduction of the contribution of electrode polarization effects in the radiowave dielectric measurements of highly conductive biological cell suspensions. Bioelectrochemistry, 54(1): 53.

Boughriet, A., Wu, Z., McCann, H. and Davis, L.E., 1999. The measurement of dielectric properties of liquids at microwave frequencies using open-ended probes, 1st World Congress on Industrial Process Tomography. Virtual Centre for Industrial Process Tomography, Buxton, Greater Manchester, pp. 318-322.

Boulton, A., Fornasiero, D. and Ralston, J., 2003. Characterisation of sphalerite and pyrite flotation samples by XPS and ToF-SIMS. International Journal of Mineral Processing, 70(1-4): 205-219.

Bradshaw, S.M., 2005. Personal Communications.

Bradshaw, S.M. and Beckmann, A., 1998. Microwave processing of chalcopyrite, Mineral Processing 98. Western Cape Branch of SAIMM, Cape Town.

Bringhurst, S. and Iskander, M.F., 1996. Open-ended metallised ceramic coaxial probe for high temperature dielectric properties measurements. IEEE Transactions on Microwave Theory and Technique, 44(6): 926-935.

Buban, K.R., Collins, M.J., Masters, I.M. and Trytten, L.C., 2000. Comparison of direct pressure leaching with atmospheric leaching of zinc concentrate. In: J.E. Dutrizac, F. Gonzalez, D.M. Henke, S.E. James and A.H.-J. Siegmund (Editors), Lead-Zinc 2000. TMS, Warrendale, PA, USA, pp. 727-738.

Buchner, R., Barthel, J. and Stauber, J., 1999. The dielectric relaxation of water between 0[deg]C and 35[deg]C. Chemical Physics Letters, 306(1-2): 57-63.

Bykov, Y.V., Rybakov, K.I. and Semennov, V.E., 2001. Topical review: High temperature microwave processing of materials. Journal of Physics D: Applied Physics, 34: 55-75.

Carranza, F., Palencia, I. and Romero, R., 1997. Silver catalyzed IBES process: Application to a Spanish copper- zinc sulphide concentrate. Hydrometallurgy, 44(1-2): 29-42.

CEM, www.cem.com [online]. Available at: <www.cem.com> [20/03/2003]

Chan, T.V.C.T. and Reader, H.C., 2000. Understanding Microwave heating Cavities. Archtech. House, London.

Chemat, F. and Esveld, E., 2001. Microwave assisted heterogeneous and homogeneous reactions., Available from: Fifth International Electronic Conference on Synthetic Organic Chemistry (ECSOC-5), http://www.mdpi.org/ecsoc-5.htm, 1-30 September 2001.

Chen, T.T., Dutrizac, J.E., Haque, K.E., Wyslouzil, W. and Kashyap, S., 1984. The relative transparency of minerals to microwave radiation, Canadian Metallurgical Quarterly, pp. 349-351.

Church, R., 1988. Dielectric properties of low-loss minerals. RI 9194, USBM.

Clark, D.E., Folz, D.C. and West, J.K., 2000. Processing materials with microwave energy, Material Science and Engineering, pp. 153-158.

Conway, B.E., 1952. Electrochemical Data. Elsevier Publishing Company, Amsterdam.

Cook, H.F., 1952. British Journal of Applied Physics, 3(249): (cited in Hasted, 1973).

Crundwell, F.K., 1987a. Kinetics and mechanism of the oxidative dissolution of zinc sulphide concentrate in ferric sulphate solutions. Hydrometallurgy, 19: 227-242.

Crundwell, F.K., 1987b. Refractory behaviour of two sphalerite concentrates to dissolution in ferric sulphate solutions. Hydrometallurgy, 19: 253-258.

Crundwell, F.K., 1988a. Effect of iron impurity in zinc sulphide concentrates on the rate of dissolution. Am. Inst. Chem. Eng. J., 34(7): 1128-1134.

Crundwell, F.K., 1988b. The influence of electronic structure of solids on the anodic dissolution and leaching of semiconducting sulphide minerals. Hydrometallurgy, 21: 155-190.

Cullity, B.D. and Stock, S.R., 2001. Elements of X-ray diffraction. 3rd. Prentice Hall, Upper Saddle River, N.J.

Cumbane, A.J., 2003. Microwave Processing of Minerals. PhD Thesis, University of Nottingham, Nottingham, UK.

Davenport, W.G., King, M., Schlesinger, M. and Biswas, A.K., 1976. Extractive Metallurgy of Copper. 4th Edition. Pergamon, Oxford.

David, R.L. (Editor), 2004. Handbook of Chemistry and Physics. CRC Press, Boca Raton, Fla.; London.

Duan, J., Fornasiero, D. and Ralston, J., 2003. Calculation of the flotation rate constant of chalcopyrite particles in an ore. International Journal of Mineral Processing, 72(1-4): 227-237.

Dutrizac, J.E., 1978. The kinetics of dissolution of chalcopyrite in ferric ion media. Metallurgical Transactions B-Process Metallurgy, 9: 431-439.

Dutrizac, J.E., 1981. The dissolution of chalcopyrite in ferric sulphate and ferric chloride media. Metallurgical Transactions B-Process Metallurgy, 12: 371-378.

Dutrizac, J.E., 1982. Ferric ion leaching of chalcopyrites from different localities. Metallurgical Transactions B-Process Metallurgy, 13: 303-309.

Dutrizac, J.E., 1989a. Elemental sulphur formation during the ferric sulphate leaching of chalcopyrite. Canadian Metallurgical Quarterly, 28(4): 337-344.

Dutrizac, J.E., 1989b. Sulphate control in chloride leaching processes. Hydrometallurgy, 23(1): 1-22.

Dutrizac, J.E., 1990. Elemental sulphur formation during the ferric-chloride leaching of chalcopyrite. Hydrometallurgy, 23(2-3): 153-176.

Dutrizac, J.E., 1992. The leaching of sulphide minerals in chloride media. Hydrometallurgy, 29(1-3): 1-45.

Dutrizac, J.E. and MacDonald, R.J.C., 1978. The dissolution of sphalerite in ferric chloride solutions. Metallurgical Transactions B, 9B: 543-551.

Dutrizac, J.E., MacDonald, R.J.C. and Ingraham, T.R., 1969. The kinetics of dissolution of synthetic chalcopyrite in aqueous ferric sulphate solutions. Transactions of the Metallurgical Society of AIME, 245(955-959).

Dutrizac, J.E., Pratt, A.R. and Chen, T.T., 2003. The mechanism of sphalerite dissolution in ferric sulphate-sulphuric acid media. In: F. Kongoli, I. K, C. Yamauchi and H.Y. Sohn (Editors), Yazawa International Symposium: Metallurgical and Materials Processing: Principles and Technologies: Aqueous and Electrochemical Processing. Minerals, Metals and Materials Society, San Diego, USA.

Eaglabs, 2005. [online]. Available at: <http://www.eaglabs.com/cai/simstheo/ionsput.htm> [15/15/2005]

Elsamak, G.G., Altuntas, N. and Yurum, Y., 2003. Chemical desulphurisation of Turkish Cayirhan lignite with HI using microwave and thermal energy, Fuel, pp. 531-537.

Ermilov, V.V., Tkachenke, O.B. and Tseft, A.L., 1969. Tr. inst Met. Obegashch Alma Ata, 30: 3.

Ferrando, A.C., 1996. Coal desulphurisation with hydroiodic acid and microwave. Fuel and energy abstracts, 37: 333.

Ferreira, R.C.H., 1972. Leaching of Chalcopyrite. PhD Thesis, Imperial College of Science and Technology, London.

Ferron, C.J., 2000. Atmospheric leaching of zinc sulphide concentrates using regenerated ferric sulphate solutions. In: J.E. Dutrizac, F. Gonzalez, D.M. Henke, S.E. James and A.H.-J. Siegmund (Editors), Lead-Zinc 2000. TMS, Warrendale, PA, USA, pp. 711-726.

Fini, A.A. and Breccia, A., 1999. Chemistry by microwaves. Pure and Applied Chemistry, 71(4): 573-579.

Fletcher, R., 1995. Investigation into Microwave Heating of Uranium Dioxide, The University of Nottingham, Nottingham, UK.

Florek, I., Labun, J., Murova, I. and Lovas, M., 1996a. The measurements of complex electric permittivity of fine grained minerals at microwave frequencies, 31st International Microwave Power Symposium, Boston USA.

Florek, I. and Lovas, M., 1995. The influence of the complex permittivity and grain size on microwave drying of the fine grained minerals. Fizykochemicze Problemy Mineralurgii, 29: 127-134.

Florek, I., Lovas, M. and Muroval, I., 1996b. Influence of microwave radiation on the leaching of tetrohedrite, Mineralia Slovaca, pp. 450- 454.

Fogler, H.S., 2000. Elements of Chemical Reaction Engineering. 3rd Edition. Prentice Hall PTR, Upper Saddle River, N.J.

Ford, J.D. and Pei, D.C.T., 1967. High temperature chemical processing via microwave absorption, Journal of Microwave Power, pp. 61-64.

Gabriel, C., Gabriel, S., Grant, E., H, Halstead, B.S.J. and Mingos, D.M.P., 1998. Dielectric parameters relevant to microwave dielectric heating. Chemical Society Reviews, 27: 213-223.

Galema, S.A., 1997. Microwave chemistry. Chemical Society Reviews, 26: 233-238.

Gill, C.B., 1980. Nonferrous Extractive Metallurgy. Wiley, New York.

Godocikova, E., Balaz, P. and Boldizarova, E., 2002. Structural and temperature sensitivity of the chloride leaching of copper, lead and zinc from a mechanically activated complex sulphide. Hydrometallurgy, 65(1): 83-93.

Goldstain, J.I. et al., 2003. Scanning Electron Microscopy and X-Ray Microanalysis. 3rd. Kluwer Academic/Plenum, New York.

Gomez, R.A., 1995. Leaching process for nickel, cobalt and manganese ores. US Patent 5393320

Greenacre, N.R., 1996. Measurements of High Temperature Dielectric Properties of Ceramics at Microwave Frequencies, University of Nottingham, Nottingham, UK.

Habashi, F., 1970. Principles of Extractive Eetallurgy. 2-Hydrometallurgy. Gorden and Breach, New York.

Habashi, F., 1993. A Text Book of Hydrometallurgy. Métallurgie extractive Québec, Enr, Sainte-Foy, Québec.

Habashi, F. and Toor, T., 1979. Aqueous oxidation of chalcopyrite in hydrochloric acid. Metallurgical Transactions B-Process Metallurgy, 10: 49-56.

Hackl, R.P., Dreisinger, D.B., Peters, E. and King, J.A., 1995. Passivation of chalcopyrite during oxidative leaching in sulfate media. Hydrometallurgy, 39(1-3): 25-48.

Hall, S.R. and Stewart, J.M., 1973. The crystal structure refinement of chalcopyrite $CuFeS_2$. Acta Crystallographica, B29: 579-585.

Haque, K.E., 1987. Microwave irradiation pre-treatment of refractory gold concentrate. In: R.S. Salter, Wysouzil, D. M., McDonald, G W. (Editor), proc. Int. Symp. on gold. Winnipeg, Canada, pp. 327-339.

Haque, K.E., 1999. Microwave energy for mineral treatment processes - a brief review. International Journal of Mineral Processing, 57(1): 1-24.

Harnby, N., Edwards, M.F. and Nienow, A.W. (Editors), 1997. Mixing in the process industries. Butterworth-Heinemann, Oxford.

Harrison, P.C., 1997. A Fundamental Study of the Heating Effect of 2.45 MHz Microwave Radiation of Minerals. PhD Thesis, the University of Birmingham, Birmingham, UK.

Hasted, J.B., 1973. Aqueous Dielectrics. Chapman and Hall, London.

Haver, F.P. and Wong, M.M., 1971. Recovery of elemental sulphur from nonferrous minerals. Ferric chloride leaching of chalcopyrite concentrate. RI 7474, USBM, Washington.

Havlik, T. and Kammel, R., 1995. Leaching of chalcopyrite with acidified ferric chloride and carbon-tetrachloride addition. Minerals Engineering, 8(10): 1125-1134.

Havlik, T., Miskufova, A. and Tatarka, P., 2001. Modern methods of oxidative leaching of chalcopyrite leaching. Acta Metallurgica Slovaca, 4(special issue): 62-68.

Havlik, T., Popovicova, M. and Ukasik, M., 2002. Use of microwave energy for chalcopyrite leaching. Metall, 56(3): 131-134.

Havlik, T., Skrobian, M., Balaz, P. and Kammel, R., 1995. Leaching of chalcopyrite concentrate with ferric-chloride. International Journal of Mineral Processing, 43(1-2): 61-72.

Havlik, T. and Ukasik, M., 2001. Leaching of chalcopyrite with acidified ferric chloride and ozone presence, Acta Metallurgica Slovaca, pp. 193-197.

Hayashi, J., Oku, K., Kusakabe, K. and Morooka, S., 1990. The role of microwave irradiation in coal desulphurisation with molten caustics. Fuel, 69: 739-742.

Hirato, T., Kinoshita, M., Awakura, Y. and Majima, H., 1986. The leaching of chalcopyrite with ferric-chloride, Metallurgical Transactions B-Process Metallurgy, pp. 19-28.

Hirato, T., Majima, H. and Awakura, Y., 1987a. The leaching of chalcopyrite with cupric chloride. Metallurgical Transactions B-Process Metallurgy, 18(1): 31-39.

Hirato, T., Majima, H. and Awakura, Y., 1987b. The leaching of chalcopyrite with ferric sulphate. Metallurgical Transactions B-Process Metallurgy, 18(3): 489-496.

Hiroyoshi, N., Arai, M., Miki, H., Tsunekawa, M. and Hirajima, T., 2002. A new reaction model for the catalytic effect of silver ions on chalcopyrite leaching in sulphuric acid solutions. Hydrometallurgy, 63(3): 257-267.

Hiroyoshi, N., Hirota, M., Hirajima, T. and Tsunekawa, M., 1997. A case of ferrous sulphate addition enhancing chalcopyrite leaching. Hydrometallurgy, 47(1): 37-45.

Hiroyoshi, N., Hirota, M., Hirajima, T. and Tsunekawa, M., 1999. Inhibitory effect of iron-oxidizing bacteria on ferrous-promoted chalcopyrite leaching. Biotechnology and Bioengineering, 64(41): 478-483.

Hiroyoshi, N., Miki, H., Hirajima, T. and Tsunekawa, M., 2000. A model for ferrous-promoted chalcopyrite leaching. Hydrometallurgy, 57(1): 31-38.

Hiroyoshi, N., Miki, H., Hirajima, T. and Tsunekawa, M., 2001. Enhancement of chalcopyrite leaching by ferrous ions in acidic ferric sulphate solutions. Hydrometallurgy, 60(3): 185-197.

Holderfield, S.P. and Salsmam, J.B., 1992. Observed trends in dielectric properties of minerals at elevated temperature. Mat. Res. Soc. Proc., 269: 589-594.

Hua, Y., Lin, Z. and Yan, Z., 2002. Application of microwave irradiation to quick leach of zinc silicate ore. Minerals Engineering, 15(6): 451-456.

Huang, J.H. and Rowson, N.A., 2000. An application of microwave pre-oxidation in improving gold recovery of a refractory gold ore. Rare Metals, 19(3): 161-171.

Huang, J.H. and Rowson, N.A., 2002. Hydrometallurgical decomposition of pyrite and marcasite in a microwave field. Hydrometallurgy, 64(3): 169-179.

Huang, L.H., 2000. The Application of Microwave Energy to Improve Grindability and Extraction of Gold Ores, University of Birmingham, Birmingham, UK.

Hwang, J., Shi, S., Xu, Z. and Huang, X., 2002. Oxygenated leaching of copper sulphide mineral under microwave-hydrothermal conditions. Journal of Minerals & Materials Characterization & Engineering, 1(2): 111-119.

Hyvarinen, O. and Hamalainen, M., 2005. HydroCopper^{TM}-a new technology producing copper directly from concentrate. Hydrometallurgy, 77(1-2): 61.

International-Zinc-Association, 2005. Zinc Guide 2004 [online]. ZincWorld. Available at: <http://www.zinc-guide.org/HTM/zgd2004.htm> [17/08/2005]

Jain, N.K., Sharma, J.M. and Kumar, D., 1993. A kinetic study of ferric chloride leaching of Khetri chalcopyrite concentrate. Transactions of Indian Institute of Metallurgy, 45(5): 323-325.

Jin, Z.-M., Warren, G.W. and Henein, H., 1984. Reaction kinetics of the ferric chloride leaching of sphalerite- an experimental study. Metallurgical Transactions B, 15B: 5-12.

Jones, D.L. and Peters, E., 1976. The leaching of chalcopyrite in ferric sulphate and ferric chloride. In: J.C. Yannopoulos and J.C. Agarwal (Editors), Extractive Metallurgy of Copper. AIME, New York, pp. 632-653.

Joret, L., Cote, G. and Bauer, D., 1997. Effect of microwaves on the rate of dissolution of metal oxides (Co_3O_4 and CeO_2) in nitric acid. Hydrometallurgy, 45(1-2): 1-12.

Kaatze, U., Lonnecke, V. and Pottel, R., 1987. Dielectric spectroscopy on aqueous solutions of zinc(II) chloride. Evidence of ion complexes. Journal of Physical Chemistry, 91: 2206-2211.

Kametani, H. and Aoki, A., 1985. Effect of suspension potential on the oxidation rate of copper concentrate in a sulphuric acid solution. Metallurgical Transactions B-Process Metallurgy, 16: 695-705.

Kametani, H. and Kobayashi, M., 1988. Correlation between dielectric properties and aqueous oxidation rate for pulverised sphalerite and zinc concentrates. Metallurgical Transactions B, 19B: 25-36.

Kammel, R., Pawlek, F., M., S. and Xi-Ming, 1987. Oxidizing leaching of sphalerite under atmospheric pressure. Metall, 41(2): 158-161.

Kapilevich, D.Y., Ogourtsov, S.G., Belenky, V.G., Maslenikov, A.B. and Abbas, S.O., 2000. Accurate microwave resonant method for complex permittivity measurements of liquids. IEEE Transactions on microwave Theory and Techniques, 48(11): 2159-2164.

Kingman, S.W., 1998. The Effect of Microwave Radiation upon the Comminution and Beneficiation of Minerals, The university of Birmingham, Birmingham, UK.

Kingman, S.W., 2005. Latest developments in microwave processing of minerals. International Materials Reviews, 50(4).

Kingman, S.W., Jackson, K., Groves, L. and Bradshaw, S.M., 2005. Microwave processing of ores: summary of investigations January 2003-December 2004, The University of Nottingham.

Kingman, S.W. and Rowson, N.A., 1998. Microwave treatment of minerals. Minerals engineering, 11(11): 1081-1087.

Kirkbride, C.G., 1978. Sulphur removal from coal. US Patent 4,123,230

Klauber, C., 2003. Fracture-induced reconstruction of a chalcopyrite ($CuFeS_2$) surface. Surface and Interface Analysis, 35(5): 415-428.

Klauber, C., Parker, A., van Bronswijk, W. and Watling, H., 2001. Sulphur speciation of leached chalcopyrite surfaces as determined by X-ray photoelectron spectroscopy. International Journal of Mineral Processing, 62(1-4): 65-94.

Kruesi, P.R. and Frahm, V.H., 1982a. Process for the recovery of copper from its ores. US Patent 4324582

Kruesi, P.R. and Frahm, V.H., 1982b. Process for the recovery of nickel, cobalt and manganese from their oxides and silicates. US Patent 4,311,520

Kruesi, W.H. and Kruesi, P.R., 1986. Microwave in laterite processing, Proceedings of CIM 25th Conference of metallurgists, Toronto.

Kuslu, S. and Bayramoglu, M., 2002. Microwave-assisted dissolution of pyrite in acidic ferric sulphate solutions. Ind. Eng. Chem. Res., 41: 5145-5150.

Laban, K.L. and Atkin, B.P., 2000. The direct determination of the forms of sulphur in coal using microwave digestion and ICP-AES analysis. Fuel, 79: 173-180.

Lester, E., Kingman, S. and Dodds, C., 2005. Increased coal grindability as a result of microwave pretreatment at economic energy inputs. Fuel, 84(4): 423.

Levenspiel, O., 1999. Chemical Reaction Engineering. John Wiley & Sons, New York.

Levich, V.G., 1962. Physicochemical Hydrodynamics. Prentice-Hall, New Jersey.

Linge, H.G., 1976. A study of chalcopyrite dissolution in acidic ferric nitrate by potentiometric titration. Hydrometallurgy, 2(1): 51-64.

Linke, W.F., 1965. Solubility of Inorganic and Metal-Organic Compounds. 4th Edition, 2. American Chemical Society.

Lochmann, J. and Pedlik, M., 1995. Kinetic anomalies of dissolution of sphalerite in ferric sulphate solution. Hydrometallurgy, 37(1): 89-96.

Lotens, J.P. and Wesker, E., 1987. The behaviour of sulphur in the oxidative leaching of sulphidic minerals. Hydrometallurgy, 18(1): 39-54.

Louw, W.J., 2005. Microwave Heating of Multiphase Materials: Modelling and Measurement. Master Thesis, University of Stellenbosch, Stellenbosch.

Lovas, M., Murova, I., Mockovciakova, A., Rowson, N. and Jakabsky, S., 2003. Intensification of magnetic separation and leaching of Cu-ores by microwave radiation. Separation and Purification Technology, 31(3): 291-299.

Lu, Z.Y., Jeffrey, M.I. and Lawson, F., 2000a. The effect of chloride ions on the dissolution of chalcopyrite in acidic solutions. Hydrometallurgy, 56(2): 189-202.

Lu, Z.Y., Jeffrey, M.I. and Lawson, F., 2000b. An electrochemical study of the effect of chloride ions on the dissolution of chalcopyrite in acidic solutions. Hydrometallurgy, 56(2): 145-155.

Lundstrom, M., Aromaa, J., Forsen, O., Hyvarinen, O. and Barker, M.H., 2005. Leaching of chalcopyrite in cupric chloride solution. Hydrometallurgy, 77(1-2): 89.

Mahan, D.G., 1976. Theoretical issues in superionic conductors. In: D.G. Mohan and L.W. Roth (Editors), Superionic Conductors. Plenun press, New York & London.

Marcuwitz, N., 1986. Waveguide Handbook. Peter Peregrinus, London.

Markus, H. et al., 2004. Reduction of ferric to ferrous with sphalerite concentrate, kinetic modelling. Hydrometallurgy, 73(3-4): 269-282.

Maurice, D. and Hawk, J.A., 1998. Ferric chloride leaching of mechanically activated chalcopyrite. Hydrometallurgy, 49(1-2): 103-123.

Maurice, D. and Hawk, J.A., 1999a. Ferric chloride leaching of a mechanically activated pentlandite-chalcopyrite concentrate, Hydrometallurgy, pp. 289-312.

Maurice, D. and Hawk, J.A., 1999b. Simultaneous autogenous milling and ferric chloride leaching of chalcopyrite. Hydrometallurgy, 51(3): 371-377.

McGill, S.L., Walkiewicz, J.W. and Smyres, G.A., 1988. The effect of power level on the heating rate of selected chemical and minerals. Mat. Res. Soc. Proc., 124: 247-252.

Mehta, A.P. and Murr, L.E., 1983. Fundamental-studies of the contribution of galvanic interaction to acid-bacterial leaching of mixed metal sulphides. Hydrometallurgy, 9(3): 235-256.

Meredith, R.J., 1998. Engineers' handbook of industrial microwave heating. Institution of Electrical Engineers, London.

Metaxas, A.C. and Meredith, R.J., 1983. Industrial Microwave Heating. Peter Peregrinus, London.

Micromeritics-Instrument-Corporation, 1992. Micropore analysis using the ASAP Accelerated Surface Area and Porosimetry System: Operator Manual V3.01, Micromeritics Instrument Corporation.

Miller, J.C. and Miller, J.N., 1993. Statistics for Analytical Chemistry. 3rd Edition. Ellis Horwood PTR Prentice Hall, Chichester.

Miller, J.D. and Portillo, Q., 1979. In: J. Laskowsky (Editor), Proceeding 12th International Mineral Processing Congress. Elsevier, Amsterdam, pp. 851-901.

Mingos, D.M.P. and Baghurst, D.R., 1991. Application of microwave dielectric heating effects to synthetic problems in chemistry. Chemical Society Reviews, 20: 1-47.

Misra, M. and Fuerstenau, M.C., 2005. Chalcopyrite leaching at moderate temperature and ambient pressure in the presence of nanosize silica. Minerals Engineering, 18(3): 293.

Mitchell, T.K., Nguyen, A.V. and Evans, G.M., 2005. Heterocoagulation of chalcopyrite and pyrite minerals in flotation separation. Advances in Colloid and Interface Science, 114-115: 227.

Munoz, P.B., Miller, J.D. and Wadshworth, M.E., 1979. Reaction mechanism for the acid ferric sulphate leaching of chalcopyrite. Metallurgical Transactions B-Process Metallurgy, 10: 149-158.

Murr, L.E. and Mehta, A.P., 1982. Electron diffraction studies on thin secondary product films on electrochemically reacting metal sulphides. Thin Solid Films, 95: 175-183.

Murr, L.E. and Mehta, A.P., 1983. The role of iron in metal sulfide leaching by galvanic interaction. Biotechnology And Bioengineering, 25(4): 1175-1179.

Nadkarni, R.A., 1984. Application of microwave oven sample dissolution in analysis. Analytical Chemistry, 56: 2233-2237.

Nelson, S.O., 1988. Estimating the permitivity of solids from measurements in granular pulverized materials. Mat. Res. Soc. Proc., 124: 149-154.

Ngoc, N.V., Shamsuddin, M. and Prasad, P.M., 1990. Oxidative leaching of an offgrade/ complex copper concentrate in chloride lixiviants. Metallurgical Transactions B-Process Metallurgy, 21: 611-619.

Nortemann, K., Hilland, J. and Kaatze, U., 1997. Dielectric properties of aqueous NaCl solutions at microwave frequencies. Journal of Physical Chemistry A, 101: 6864-6869.

O'Malley, M.L. and Liddell, L.C., 1987. Leaching of $CuFeS_2$ by aqueous $FeCl_3$, HCl, and NaCl: Effect of solution composition and limited oxidant. Metallurgical Transactions B-Process Metallurgy, 18: 505-510.

Palencia, I., Romero, R. and Carranza, F., 1998. Silver catalyzed IBES process: Application to a Spanish copper-zinc sulphide concentrate. Part 2. Biooxidation of the ferrous iron and catalyst recovery. Hydrometallurgy, 48(1): 101-112.

Palencia, P.I. and Dutrizac, J.E., 1991. The effect of iron content of sphalerite on its rate of dissolution in ferric sulphate and ferric chloride media. Hydrometallurgy, 26: 211-232.

Palmer, P.R., Nebo, C.O., Rau, M.F. and C., F.M., 1981. Rate phenomena involved in the dissolution of chalcopyrite in chloride bearing lixiviants. Metallurgical Transactions B-Process Metallurgy, 12: 595-601.

Parker, A., Klauber, C., Kougianos, A., Watling, H.R. and van Bronswijk, W., 2003. An X-ray photoelectron spectroscopy study of the mechanism of oxidative dissolution of chalcopyrite. Hydrometallurgy, 71(1-2): 265.

Parker, A.J., Klauber, C., Watling, H.R. and Van Bronswijk, W., 2001. An X-Ray photoelectron spectroscopy study of the mechanism of chalcopyrite leaching. In: V.S.T. Ciminelli and J. O. Garcia (Editors), Biohydrometallurgy: Fundamentals, Technology and Sustainable Development: Proceedings of the IBS-'01. Elsevier Scientific Publishers, Amsterdam, pp. 547-555.

Parker, A.J., Paul, R.L. and Power, G.P., 1981a. Electrochemical aspects of leaching of copper from chalcopyrite in ferric and cupric salt solutions. Australian Journal of Chemistry, 34: 13-34.

Parker, A.J., Paul, R.L. and Power, G.P., 1981b. Electrochemistry of the oxidative leaching of copper from chalcopyrite. Journal of Electroanalytical Chemistry, 118: 305-316.

Paynter, J.C., 1974. Journal of South African Institute of Mining and Metallurgy, 74(4): 158-170.

Peacey, J., Guo, X.J. and Robles, E., 2003. Copper Hydrometallurgy- Current status, preliminary economics, future direction and positions versus melting [online]. The Hatch Group. Available at: <http://www.hatch.ca/mining_mineral_processing/articles/> [16/08/2005]

Peng, J. and Liu, C., 1992. The kinetics of ferric chloride leaching of sphalerite in the microwave field. Journal of China Nonferrous Metals, 2(1): 46-49.

Peng, J.H. and Liu, C.P., 1997. Kinetics of leaching sphalerite with pyrolusite simultaneously by microwave irradiation. Transactions of Nonferrous Metals Society of China, 7(3): 152-154.

Piantadosi, C., Jasieniak, M., Skinner, W.M. and Smart, R.S.C., 2000. Statistical comparison of surface species in flotation concentrates and tails from TOF-SIMS evidence. Minerals Engineering, 13(13): 1377-1394.

Piantadosi, C. and Smart, R.S.C., 2002. Statistical comparison of hydrophobic and hydrophilic species on galena and pyrite particles in flotation concentrates and tails from TOF-SIMS evidence. International Journal of Mineral Processing, 64(1): 43-54.

Pinches, A., Myburgh, P.J. and van der Merwe, C., 2001. Process for rapid leaching of chalcopyrite in the absence of catalysts. US Patent No 6277341

Popovicova, M. and Havlik, T., 2001. Microwave leaching of chalcopyrite. Acta Metallurgica Slovaca, 7(1): 27-33.

Porch, A., 2005. Personal Communications, University of Wales, Cardiff.

Price, A.H., 1973. Dielectric measurements of liquids in the frequency range 250MHz to 140 GHz. In: J. Champberlain and G.W. Chantry (Editors), High frequency dielectric measurement. IMP Science and Technology Press Ltd, National Physical Laboratory,Teddington, UK, pp. 28-33.

Prosser, A.P., 1996. Review of uncertainty in the collection and interpretation of leaching data. Hydrometallurgy, 41(2-3): 119.

Raicu, v., 1995. A simple theoretical and practical approach to measuring dielectric properties with an open-ended coaxial probe. Measurement Science and Technology, 6: 410-414.

Rath, P.C., Paramguru, R.K. and Jena, P.K., 1981. Kinetics of dissolution of zinc sulphide in aqueous ferric chloride solution. Hydrometallurgy, 6: 219-225.

Rauwle, A., 2000. Basic princibles of particle size analysis [online]. Available at: <www.malvern.co.uk> [10/03/2003]

Rimbi, M., 2003. Wood Microwave Dielectric Heating and Measurement of Material Properties. PhD Thesis, University of Stellenbosch, Stellenbosch.

Rimstidt, J.D. and Vaughan, D.J., 2003. Pyrite oxidation: a state-of-the-art assessment of the reaction mechanism. Geochimica et Cosmochimica Acta, 67(5): 873-880.

Roman, R.J. and Banner, B.R., 1973. The dissolution of copper concentrates. Minerals Science and Engineering, 5(1): 3-24.

Romero, R., Mazuelos, A., Palencia, I. and Carranza, F., 2003. Copper recovery from chalcopyrite concentrates by the BRISA process, Hydrometallurgy, pp. 205-215.

Rowson, N.A. and Rice, N., M., 1990a. Desulphurisation of coal using low power microwave energy. Minerals Engineering, 3(3-4): 355-361.

Rowson, N.A. and Rice, N., M., 1990b. Magnetic enhancement of pyrite by caustic microwave treatment. Minerals Engineering, 3(3-4): 363-368.

Ryynanen, S., 2002. Microwave Heating Uniformity of Multicomponent Prepared Food, University of Helsinki, Helsinki.

Salsmam, J.B., 1991. Technique for measuring dielectric properties of minerals as a function of temperature and density at microwave heating frequencies. Mat. Res. Soc. Proc., 189: 509-515.

Salsmam, J.B., 1992. Measurements of dielectric properties in frequency range of 300 MHz to 3 GHz as a function of frequency and density. Ceramic Transactions, 59: 203-215.

Saltiel, C. and Datta, A.K., 1999. Heat and mass transfer in microwave processing. Advances in Heat Transfer, 33: 1-94.

Santos, J.d.l., Garcia, D. and Eiras, J.A., 2002. Dielectric characterization of materials at microwave frequency range. Materials Research, 6(1): 97-101.

Schaefer, M.D., 1999. Microwave Tempering of Shrimp with Susceptors. Master Thesis, Virginia Polytechnic Institute and State University, Virginia.

Schultze, L.E., Sandoval, S.P. and Bush, R.P., 1995. Effect of additives on chalcopyrite leaching, USBM, RI 9556.

Shibata, C., Kashima, T. and Ohuchi, K., 1996. Nonthermal influence of microwave power on chemical reactions, Japanese. Journal of Applied Physics(35): 1A.

Shuey, R.T., 1975. Semiconducting Ore Minerals. Elsevier Scientific Publishing Company, Amsterdam.

Shukri, Z.A. and Champness, C.H., 1997. Cleavage and twining in $CuInSe_2$ crystals. Acta Crystallographica, B53: 620-630.

Skoog, D.A., West, D.M., Holler, F.J. and Crouch, S.R., 2000. Analytical Chemistry An Introduction. 7th Edition. Saunders College Publishing, Philadelphia.

Skrobian, M., Havlik, T. and Ukasik, M., 2005. Effect of NaCl concentration and particle size on chalcopyrite leaching in cupric chloride solution. Hydrometallurgy, 77(1-2): 109.

Smart, R.S.C., Jasieniak, M., Prince, K.E. and Skinner, W.M., 2000. SIMS studies of oxidation mechanisms and polysulfide formation in reacted sulfide surfaces. Minerals Engineering, 13(8-9): 857-870.

Stuchly, M.A. and Stuchly, S.S., 1980. Coaxial line reflection methods for measuring dielectric properties of biological substances at radio and microwave frequencies- a review. IEEE Transactions on Instrumentation and Measurement, IM-29: 176-183.

Sturcken, E.F., 1992. Metal recovery from porous materials. US Patent 5, 154, 899

Sucher, M. and Fox, J. (Editors), 1963. Handbook of Microwave Measurements, Vol.1. Polytechnic Press, New York.

Suni, J., Henein, H., Warren, G.W. and Reddy, D., 1989. Modelling the leaching kinetics of a sphalerite concentrate size distribution in ferric chloride solution. Hydrometallurgy, 22: 25-38.

Tebble, R.S., 1969. Magnetic Materials. Wiley-Interscience, New York; Chichester.

Third, K.A., Cord-Ruwisch, R. and Watling, H.R., 2000. The role of iron-oxidizing bacteria in stimulation or inhibition of chalcopyrite bioleaching. Hydrometallurgy, 57(3): 225-233.

Thostenson, E.T. and Chou, T.-W., 1999. Microwave processing: fundamental and applications. Composites, Part A 30(30): 1055-1071.

Tiwari, B.L., Kolbe, J. and Hayden, H.W., JR., 1980. Leaching of high solids, attritor-ground chalcopyrite concentrate by in situ generated ferric sulphate solution. Metallurgical Transactions B-Process Metallurgy, 11: 89-93.

Tranquilla, J.M., 1997. Mineral extraction and the use of microwave, Presented at CIM conference, Vancouver, British Columbia, Canada.

Tromans, D. and Meech, J.A., 2002. Enhanced dissolution of minerals: Conjoint effects of particle size and microtopography. Minerals Engineering, 15(4): 263.

Tuller, W.N. (Editor), 1954. The Sulphur Data Book. McGraw-Hill, New York.

Vaughan, D.J., Becker, U. and Wright, K., 1997. Sulphide mineral surfaces: theory and experiment. International Journal of Mineral Processing, 51(1-4): 1-14.

Verbaan, B. and Crundwell, F.K., 1986. An electrochemical model for the leaching of a sphalerite concentrate. Hydrometallurgy, 16: 345-359.

Vickerman, J.C. and Briggs, D., 2001. ToF-SIMS: Surface Analysis by Mass Spectrometry. IM Publications and Surface Spectra Limited, Manchester.

Vickerman, J.C., Brown, A. and Reed, N.M. (Editors), 1989. Secondary Ion Mass Spectrometry Principles and Applications. Clarendon Press, Oxford.

Vogel, A.I., 1961. A Text-Book of Quantitative Inorganic Analysis Including Elementary Instrumental Analysis. 3. Longman, London.

von Hippel, A.R., 1954. Dielectric Materials and Applications. New York: John Wiley & Sons, Inc; London: Chapman & Hall, LTD, 3-43 pp.

Wadsworth, M.E., 1972. Advances in the leaching of sulphide minerals, Minerals Science and Engineering, pp. 36-47.

Walkiewicz, J.W., Kazonich, G. and McGill, S.L., 1988. Microwave heating characteristics of selected minerals and compounds. Minerals and Metallurgical Processing, 5(1): 39-42.

Warren, G.W., Henein, H. and Jin, Z.-M., 1985. Reaction mechanism for the ferric chloride leaching of sphalerite. Metallurgical Transactions B, 16B: 715-724.

Weian, D., 1997. Leaching behaviour of complex sulphide concentrate with ferric chloride by microwave irradiation. Rare Metals, 16(2): 153-156.

Weisener, C.G., Smart, R.S.T.C. and Gerson, A.R., 2003. Kinetics and mechanisms of the leaching of low Fe sphalerite. Geochimica et Cosmochimica Acta, 67(5): 823.

Weng, S., 1993. Mossbauer analysis of the microwave desulphurisation process of raw coal. Journal of Applied Physics, 73(9): 4680-4682.

Weng, S. and Wang, J., 1992. Exploration on the mechanism of coal desulphurisation using microwave irradiation/ acid washing method. Fuel Processing Technology, 31: 233-240.

Weng, S. and Wang, J., 1993. Mossbauer study of coal desulphurisation by microwave irradiation combined with magnetic separation and chemical acid leaching. Science in China Series B-Chemistry, 36(11): 1289-1299.

Whittaker, G., 1997. A basic introduction to microwave chemistry [online]. Available at: <http://homepages.ed.ac.uk/ah05/basicintro.html#b> [07/02/2005]

Worner, H.K., 1990. Microwave irradiation of composites. US Patent No 4906290.

www.nottingham.ac.uk, 2005. Centre for Surface Chemical Analysis [online]. University of Nottingham. Available at: <http://www.nottingham.ac.uk/csca/csca_links.htm> [15/05/2005]

Xia, D.K. and Pickles, C.A., 1997. Applications of microwave energy in extractive metallurgy - A review. CIM Bulletin, 90(1011): 96-107.

Xia, D.K. and Pickles, C.A., 2000. Microwave caustic leaching of electric arc furnace dust. Minerals Engineering, 13(1): 79-94.

Xiong X, Y., Jacob-Duliere, M. and Sterckx, J., 1989. Relation between the leachability of zinc concenrates in Fe(3)-H_2SO_4 media and their electric conductivity. In: M. Koch and J.C. Taylor (Editors), Productivity and Technology in the Metallurgical Industries. Minerals, Metals and Materials Soc., Warrendale, USA, pp. 673-693.

Yianatos, J.B. and Antonucci, V., 2001. Molybdenite concentrate cleaning by copper sulfation activated by microwave. Minerals Engineering, 14(11): 1411-1419.

Zavitsanos, P.D. and Bleiler, K.W., 1978. Process for coal desulphurisation. US Patent 4,076,607

Zavitsanos, P.D., Bleiler, K.W. and Golden, J.A., 1979. Coal desulphurisation using alkali metal or alkaline earth compounds and electromagnetic energy. US Patent 4,152, 120

Appendices

Appendix 2-1. Microwave Generators

Magnetrons

The magnetron was invented by Hull in 1921 (Reich et al., 1957). However, they were developed extensively during the Second World War as a source of high microwave power for radar application. It was then developed for heating purposes by Spencer Perch at Raytheon who presented the first version of domestic ovens (Osepchuk, 1984).

1. A schematic sketch of a magnetron is shown in Figure 1. The principal components of a high power industrial magnetron are (Meredith, 1998):
2. A cylindrical heating cathode emitting electrons;
3. A circular anode concentric with a surrounding cathode, having an array of radial slots forming resonators tuned to the desired operating frequency;
4. A high strength magnetic field aligned axially to the anode-cathode assembly. This can be provided by permanent small magnet for small magnetrons, or an electromagnet for high power magnetrons;
5. A high voltage (2-20kV) applied between anode and cathode. The anode is at high potential compared to cathode;
6. The whole system is enclosed in a vacuum envelope and sealed with a high vacuum;
7. A probe antenna, coupled to the resonator and sealed by an output window of microwave transparent material;
8. A construction which provides for easy rebuilding after end of life failure or damage.

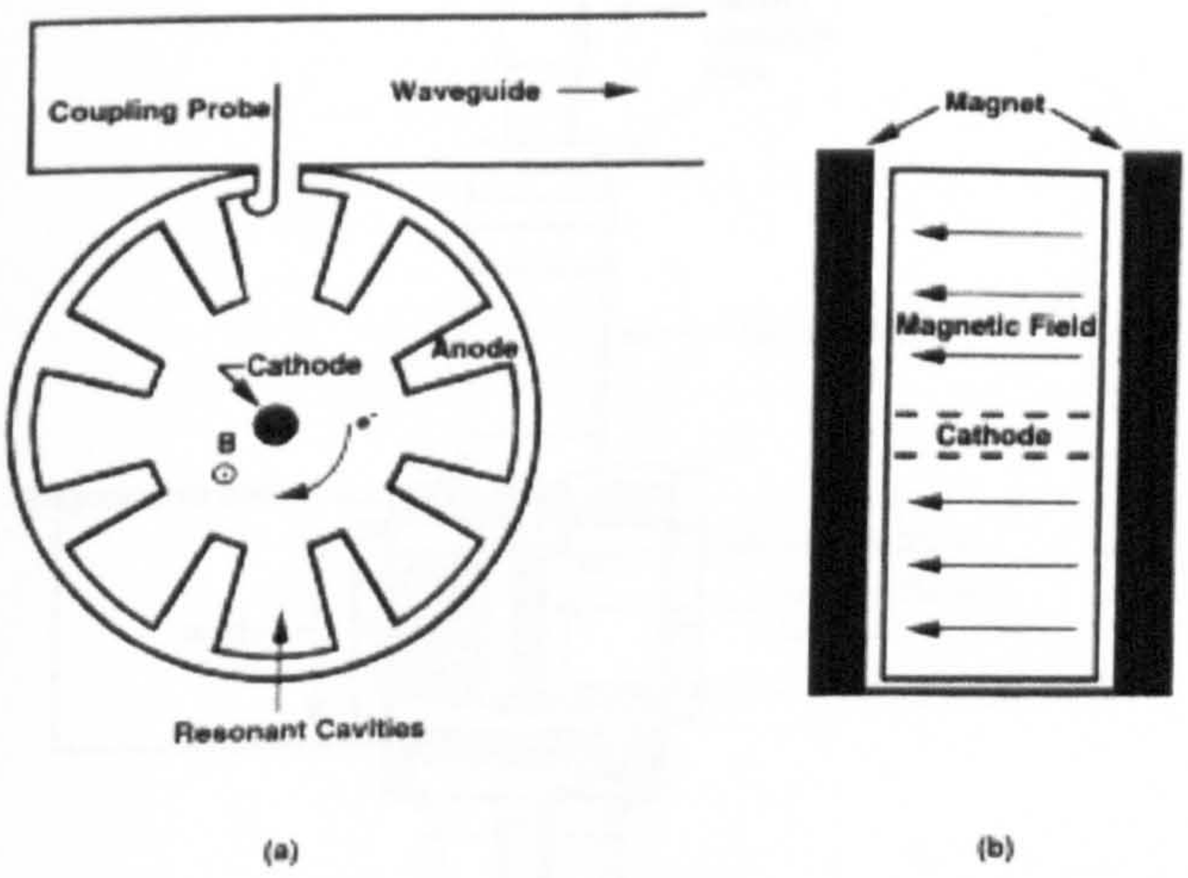

Figure 1 Schematic diagram of the magnetron microwave tube: (a) top view. (b) side view(Thostenson and Chou, 1999)

Figure 2 shows a sectional view of a high power magnetron produced by California Tube Laboratory Inc. (Meredith, 1998). In the vacuum tube, the potential difference between the anode and the cathode produces a strong electric field which causes the loosely bound valence electrons to be drawn from the heated cathode. The magnet generates magnetic field which is orthogonal to the

electrons path. In the presence of such a magnetic field, the electrons, instead of travelling outward to the anode, travel in a spiral path in the space between the cathode and the anode. The trajectory and the velocity of the electrodes are therefore controlled by the combined adjustment of both applied magnetic and electric fields (Meredith, 1998; Thostenson and Chou, 1999).

The spiral movement of electrons creates a swirling cloud of electrons. The swirling cloud of electrons, influenced by the high voltage and the strong magnetic field, forms a rotating pattern that resembles the spokes in a spinning wheel. The interaction of this rotating space-charge wheel with the configuration of the surface of the anode produces an alternating current flow in the resonant cavities of the anode. This is explained as follows: as a "spoke" of electrons approaches an anode vane (or the segment between the two cavities), it induces a positive charge in that segment. As the electrons pass, the positive charge diminishes in the first segment while another positive charge is being induced in the next segment. In another words, As these electrons sweep toward a point where there is excess negative charge, that charge tends to be pushed back around the cavity, imparting energy to the oscillation at the natural frequency of the cavity. The frequency of the alternating currents is determined by the number and the size of resonant cavities. The driven oscillation of the charges around the cavities leads to radiation of electromagnetic waves, the output of the magnetron. Electromagnetic energy is coupled from one of the resonant cavities to the transmissions through a coaxial line or waveguide launcher as shown schematically in Figure 1 (a).

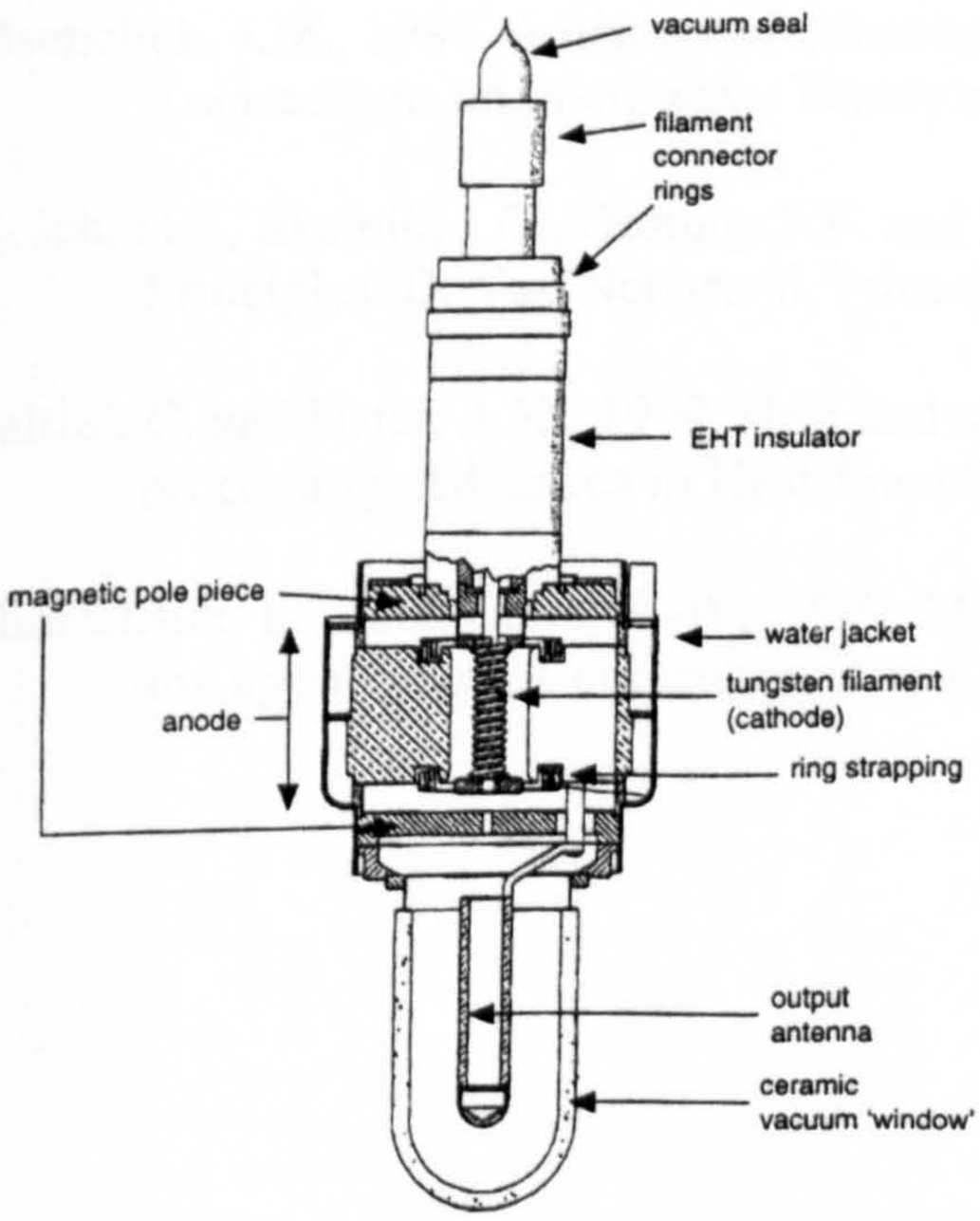

Figure 2. Sectioned view of 75 kW 915 MHz magnetron (Meredith, 1998)

The magnetron power output is adjusted either by adjusting the magnetron period of operation or by adjusting the cathode current or the strength of magnetic field.

In the first instance, the magnetron is operated at full power for a specific period of time then it switches off for another segment of the period. The average power is then reduced (Thostenson and Chou, 1999). The second instance allows variable control of the microwave power within the range of the source. It is required for example if continuous power is needed.

Klystrons

Similar to the magnetron, the klystron modulates the movement of electrons using resonant cavities. In klystrons however the cavities are arranged in a linear fashion. The use of klystrons is limited due to their high cost. However, they can produce high microwave power (over 100kW at 2.45 GHz) which may necessitate their use in certain applications (Saltiel and Datta, 1999).

Travelling Wave Tubes

Travelling wave tubes (TWT) are linear-beam tubes. Unlike magnetrons and klystrons a TWT serves only as an amplifier. The have a voltage-controlled oscillator generates the microwave signals. They are used for warfare, transmission as well as heating. A distinct feature of TWT's is that they are able to produce variable frequency microwaves (Saltiel and Datta, 1999).

Meredith, R.J., 1998. Engineers' handbook of industrial microwave heating. Institution of Electrical Engineers, London.

Osepchuk, J.M., 1984. A history of microwave heating applications. IEEE Transactions on microwave Theory and Techniques, 32: 1200-1224.

Reich, H.J., Skalnik, J.G., Ordung, P.F. and Krauss, H.L., 1957. Microwave Principles. D. Van Norstrand, Princeton, N. J.

Saltiel, C. and Datta, A.K., 1999. Heat and mass transfer in microwave processing. Advances in Heat Transfer, 33: 1-94.

Thostenson, E.T. and Chou, T.-W., 1999. Microwave processing: fundamental and applications. Composites, Part A 30(30): 1055-1071.

Appendix 3-1. Summary of investigations on chalcopyrite leaching in ferric chloride

Material	Temp rang	E_a kJ/mol.	Author	Rate limiting step
Synthetic	25-75	38±4	Ammou-Chockroum 1977)	Mass transfer
Natural	30-100	42±4	Dutrizac (1978)	Mass transfer
Synthetic	50-100	46±4	Dutrizac (1978)	Mass transfer
Natural	60-106	50	Ermilov (1969)	Not given
Natural monosize, 0.2M HCl, 0.1 $FeCl_3$	75-96	62	Palmer (1981)	
Natural, 1M HCl, 3M NaCl, 0.1 $FeCl_3$	82.5-96	83	Palmer (1981)	
Natural	55-85	69	Majima (1985)	Electrochemical
Natural of an offgrade copper concentrate in 4M $FeCl_3$- .2M HCl	~65-110	37.4	Ngoc (1990)	
Natural	40-90	73±1.5	Buttinelli (1993)	
Natural	3.5-80	55±5	Havlik (1995a)	
Natural	3.5-45	1.1	Havlik (1995b)	Diffusion controlled
Natural	45-80	69	Havlik (1995b)	Chemically controlled
Natural, with addition of CCl_4,	45-80	31.2	Havlik (1995b)	Diffusion controlled
Natural, 1.0M $FeCl_3$, 1M NaCl, 0.25 HCl	60-90	68	Maurice (1998)	
Natural, pentlandite- $CuFeS_2$ concentrate, 1.0M $FeCl_3$, 1M NaCl, 0.25 HCl	70-90	86.7±10	Maurice (1999)	

Appendix 3-2. Summary of some investigations on sphalerite leaching in ferric chloride

Experimental conditions		Iron cont.	Temperature Range	Activation energy, kJ/mole	Remarks	Reference
Natural crystals as sintered disc and untreated from Spain(-212+150μm) in ferric chloride (0.001-1.0M) in HCl		0.08	25-100	42	Surface reaction model	(Dutrizac and MacDonald, 1978)
Flotation concentrate of size 53-63 in 0.2M $FeCl_3$-0.1M HCl		3.4	27-93	58.4	Surface reaction control	(Jin et al., 1984)
Flotation concentrate of size between 91-363μm in 0.1-1.0M ferric chloride			44-90	50	Mixed surface and diffusion model proposed. Reaction order 1.0	Su (1976)[sited in(Jin et al., 1984)
Balmat/USA	In 0.3 M Fe_2Cl_3 – 0.3M HCl, Particle size 75-104 μm	1.29	50-90	50	Surface reaction control, The deviation in the activation energy varied between 2 and 4kJ/mole	(Palencia Perez and Dutrizac, 1991)
Nanisivik/Canada		6.0		49		
Geco/ Canada		7.17		57		
Long Lake/ Canada		7.5		49		
Montauban/ Canada		7.95		51		
Bluebell/Canada		12.5		38		
Chemical grade zinc sulphide powder in ferric chloride (.2M)		0	30-70	90±12.5	Parabolic kinetics: Inward diffusion of ferric ions through sulphur layer	(Rath et al., 1981)
Crystal in ferric chloride		0	45-90	64.5	Mixed control	(Bobeck and Su, 1985)
St. Joe minerals in ferric chloride		5.2	45-90	46.9	Mixed control	
Wards	0.2 M FeC_3-0.3M HCl, 0.005M $FeCl_2$ amd 2 M NaCl	0.55		59.5	Electrochemical reaction control which depends on semiconducting properties	(Crundwell, 1988a)
Rosh Pinah		1.79		44.1		
Zincor		2.56		51.6		
Black Mountain		8.02		31.7		
Gamsberg		8.62		43.3		

Appendix 3-3. Summary of some investigations on sphalerite leaching in ferric sulphate

Experimental conditions		Iron cont.	T Range	Activation energy, kJ/mole	Remarks	Reference
Santander/ Spain	In 0.3 M $Fe_2(SO_4)_3$ – 0.3M H_2SO_4, Particle size 75-104 µm	0.04	50-90	72	Surface reaction control, The deviation in the activation energy varied between 2 and 9kJ/mole	(Palencia Perez and Dutrizac, 1991)
Oklahama/ Mexico		0.19		61		
Balmat/ USA		1.29		66		
Dosun/ Canada		4.03 (cont. Cu)		67		
Nanisivik		6.0		50		
Geco/ Canada		7.17		46		
Long Lake/Canada		7.5		50		
Montauban/ Canada		7.95		52		
Europe		11.8		48		
Bluebell/ Canada		12.5		41		
sberg deposit sphalerite concentrate (44-53µm) in ferric sulphate				46	Surface reaction control	(Suni et al., 1989)
Sphalerite concentrate (Red Dog) containing 5.1% Fe in ferric sulphate		5.1	75-95	47.4	Data can be fitted to various models	(Markus et al., 2004)
Flotation concentrate in ferric sulphate 60g/L Fe^{3+}		0.4	25-80	36.4	Diffusion through reaction products	(Ferron, 2000)
Flotation concentrate from Gamsberg/SA in 0.45M Ferric sulphate + 0.1 M H_2SO_4		9.1	25-85	79.4	Electrochemical control	(Verbaan and Crundwell, 1986)

Appendix 3-4. Literature data on microwave heating of minerals and compounds

Heating time For Various Compounds			
Compound	Color	Heating Time (min.)	Max. Temp. (°C)
Al_2O_3	White	24	900
C (Charcoal)	Black	0.2	1000
CaO	White	40	200
Co_2O_3	Black	3 (B)	900
CuO	Black	4	800
CuS	Dark blue	5	600
Fe_2O_3	Red	6	1000
Fe_3O_4	Black	0.5	500
FeS	Black	6	800
MgO	White	40	1300
MnO_2	Black	(B)	See Text
MoO_3	Pale green	46	750
MoS_2	Black	0.1	900
Ni_2O_3	Black	3(B)	1300
PbO	Yellow	13	900
TiO_2	White	-	-
UO_2	Dark green	0.1	1100
ZnO	White	4	1100

Microwave heating of some minerals and compounds (after Ford and Pie, 1967)

Mineral	Power (W)	Heating response	Product examination
Arsenopyrite	80	Heats, some sparking	S and As fumes; some fusion. Pyrrhotite, As, Fe-arsenide and arsenopyrite
Bornite	20	Heats readily	Some changed to bornite–chalcopyrite–digenite; some unchanged
Chalcopyrite	15	Heats readily with emission of sulfur fumes	Two Cu–Fe–sulfides or pyrite and Cu–Fe–sulfide
Covellite/anilite (60% vol. %)	100	Difficult to heat; sulfur fumes emitted	Sintered to single composition of $(Cu, Fe)_9S_8$
Galena	30	Heats readily with much arcing	Sintered mass of galena
Nickeline/cobaltite (3 vol. %)	100	Difficult to heat	Some fused; most unaffected
Pyrite	30	Heats readily; emission of sulfur fumes	Pyrrhotite and S fumes
Pyrrhotite	50	Heats readily with arcing at high temperature	Some fused; most unaffected
Sphalerite (high Fe; Zn 58.9, Fe 7.4, S 33.7%)	100	Difficult to heat when cold	Converted to wurtzite
Sphalerite (low Fe; Zn 67.1, Fe 0.2, S 32.7%)	>100	Does not heat	No change, sphalerite
Stibnite	>100	Does not heat	No change; stibnite
Tennantite (Cu 42.8, Ag 0.1, Fe 4.8, Zn 1.7, As 12.5, Sb 10.6, S 27.5%) (90 vol% tennantite, 6% chalcopyrite, 4% quartz)	100	Difficult to heat when cold	Fused mass of tennantite–chalcopyrite; arsenic fumes emitted
Tetrahedrite (Cu 24.9, Ag 18.0, Fe 1.9, Zn 4.8, Sb 25.6, As 1.3, S 23.4%) (85 vol.% tetrahedrite, 10% quartz, 5% pyragyrite, galena, chalcopyrite)	35	Heats readily	Fused mass of Ag–Sb alloy, PbS, tetrahedrite, Cu–Fe–Zn sulfide and Cu–Fe–Pb sulfide

Chen et al (1984) notes on microwave heating of minerals

Mineral	Power (W)	Heating response	Product examination
Allanite	>150	Does not heat	No change; allanite
Cassiterite	40	Heats readily	No change; cassiterite
Columbite (40 vol. %)—pyrochlore in silicates (almandine 40%)	60	Difficult to heat when cold	Niobium minerals fused; most silicates unchanged
Fergusonite	>150	Does not heat	No change; fergusonite
Hematite	50	Heats readily; arcing at high temperature	No change; hematite
Magnetite	30	Heats readily	No change; magnetite
Monazite	>150	Does not heat	No change; monazite
Pitchblende (90 vol. %): contains chlorite, galena, calcite	50	Heats readily	Some fused to UO_2, U_3O_8, ThO_2 and Fe–Al–Ca–SiO_2 glass; others unchanged

Microwave heating of oxides and uranium minerals (after Chen et al, 1984)

Chemical	Wt, g	Vol, ml	500 W		1000 W		1500 W		2000 W	
			T, °C	Time, Min.	T, °C	Time, Min.	T, °C	Time, Min.	T, °C	Time, Min.
α-Al_2O_3	15	14	385	7	463	7	498	7	547	7
$CaCl_2$	17	14	35	7	43	7	53	7	58	7
$CaCO_3$	10	14	32	7	72	7	51	7	65	7
CuCl	25	12	425	b_3	400	b_1	400	$b_{.75}$	462	b_5
$CuFeS_2$	25	13	908	$c_{.75}$	930	d_{333}	>1150	e_{25}	>1200	e_{133}
CuO	25	8	1083	$b_{1.5}$	1088	b_{25}	1088	b_5	>1200	e_{25}
Cr_2O_3	20	13	84	7	>1200	b_4	>1250	$b_{2.5}$	>1200	b_2
$FeCr_2O_4$	30	12	110	7	>1200	$e_{6\,25}$	>1200	$e_{3\,25}$	>1200	e_2
Fe_2O_3	12	14	60	7	87	7	101	7	120	7
Fe_3O_4	25	9	1118	7	1144	$e_{3.5}$	1123	d_3	905	d_1
FeS_2	20	12	98	7	808	7	700	$d_{.75}$	375	d_{17}
$FeSO_4.7H_2O$	12	13	109	7	118	$c_{5.5}$	118	c_3	123	$c_{1.75}$
PbS	50	11	984	d_5	992	d_4	f.		f.	
SiO_2	25	14	33	7	44	7	55	7	73	7
TiO_2	10	13	67	7	109	7	150	7	228	7
$ZnCl_2$	14	g9	730	h_5	723	$h_{1\,25}$	730	$h_{.75}$	593	d_5
ZnO`	9.5	14	87	7	128	7	184	7	301	$c_{1.75}$
ZnS	30	12	139	7	236	7	>1200	e_6	>1200	$e_{3.75}$

[a] Maximum temperature obtained in indicated time interval.
[b] Test terminated because the sample melted
[c] Test terminated because the temperature began decreasing at the indicated time
[d] Test terminated because the sample arced
[e] Test terminated because the temperature passed the thermocouple limitation
[f] Sample not run because of rapid heating at lower powers- too disturbed
[g] Smaller volumes

Effect of microwave power on the heating rate of selected minerals and chemicals (After McGill et al, 1988)

Mineral	Chemical Composition	Temp., °C	Time, min
Albite	$NaAlSi_3O_8$	69	7
Arizonite	$Fe_2O_3 \cdot 3TiO_2$	290	10
Chalcocite	Cu_2S	746	7
Chalcopyrite	$CuFeS_2$	920	1
Chromite	$FeCr_2O_4$	155	7
Cinnabar	HgS	144	8.5
Galena	PbS	956	7
Hematite	Fe_2O_3	182	7
Magnetite	Fe_3O_4	1258	2.75
Marble	$CaCO_3$	74	4.25
Molybdenite	MoS_2	192	7
Orpiment	As_2S_3	92	4.5
Orthoclase	$KAlSi_3O_8$	67	7
Pyrite	FeS_2	1019	6.75
Pyrrhotite	$Fe_{1-x}S$	686	1.75
Quartz	SiO_2	79	7
Sphalerite	ZnS	88	7
Tetrahedrite	$Cu_{12}Sb_4S_{13}$	151	7
Zircon	$ZrSiO_4$	52	7

Effect of Microwave heating on the temperature of natural minerals (After Walkiewicz et al, 1988)

Chemical	Temp., °C	Time, min	Chemical	Temp., °C	Time, min	Chemical	Temp., °C	Time, min
AgBr	39	1 5	$CuCl_2 \cdot 2H_2O$	171	2.75	NH_4Cl	31	3 5
AgCl	45	4	$CuF_2 \cdot 2H_2O$	78	6	$5(NH_4)_2 \cdot 12WO_3$	88	4
AgI	64	4	CuO	1012	6.25	Ni	364	1
Ag_2S	852	5 25	Cu_2O	89	7	$NiBr_2 \cdot 2H_2O$	150	3
Al	577	6	CuS	440	4 75	$NiCl_2$	51	2.75
$AlCl_3$	41	4	Fe	768	7	$NiCl_2 \cdot 6H_2O$	168	1 75
$AlCl_3 \cdot 6H_2O$	46	4	$FeBr_2 \cdot 6H_2O$	180	4	$NiF_2 \cdot 4H_2O$	50	5
$Al(ClO_3)_3 \cdot 6H_2O$	72	5	$FeCl_2$	33	1.5	NiO	1305	6.25
Al_2O_3	78	4 5	$FeCl_2 \cdot 2H_2O$	41	4	NiS	251	7
$Al_2(SO_4)_3 \cdot 18H_2O$	206	3 75	$FeCl_2 \cdot 4H_2O$	47	4	Pb	277	7
$Al_2(SO_4)_3 \cdot K_2SO_4 \cdot 24H_2O$	56	4.5	$FeCl_3$	41	4	$PbBr_2$	56	2.75
$BaCl_2$	45	4	$FeCl_3 \cdot 6H_2O$	220	4 5	$PbCl_2$	51	2
$BaCl_2 \cdot 2H_2O$	50	0 75	Fe_2O_3	134	7	PbO	91	2.25
BaS	160	5	$Fe_2(SO_4)_3 \cdot 9H_2O$	154	6	PbS	1024	1.25
C (amorp., <1 μm)	1283	1	Hg	40	6	$PrCl_3$	30	1.25
C (graph., <1 μm)	1073	1 75	$HgCl_2$	112	7	S	163	6
C (graph., −200 mesh)	780	6	HgS	105	7	Sb	360	1
$CaBr_2 \cdot 2H_2O$	47	4	KBr	46	0.25	$SbCl_3$	224	1.75
$CaCl_2$	32	1.75	KCl	31	1	$SbCl_5$	54	6
$CaCl_2 \cdot 2H_2O$	45	0.75	$LaCl_3$	38	1.75	Sn	297	8
$CaCO_3$	61	7	$LaCl_3 \cdot 7H_2O$	34	2	$SnBr_2$	472	10
CaF_2	81	4 25	La_2O_3	119	6 5	$SnCl_2$	476	2
CaO	116	4	$LiBr \cdot H_2O$	45	1	$SnCl_2 \cdot 2H_2O$	252	5.25
CaS	102	4.5	LiCl	35	0 5	$SnCl_4$	49	8
CCl_4	34	4	Mg	120	7	$SnCl_4 \cdot 5H_2O$	151	6.75
$CdCl_2$	37	4	$MgBr_2 \cdot 6H_2O$	322	9	$SrCl_2 \cdot 6H_2O$	32	3
$CdCl_2 \cdot 2.5H_2O$	144	2 5	$MgCl_2 \cdot 6H_2O$	254	4	Ta	177	7
CdS	87	5	MgO	203	5 5	TiB_2	843	7
$CeCl_3$	48	2.75	$MgSO_4 \cdot 7H_2O$	80	4.5	$TiCl_4$	31	4
$CeCl_3 \cdot 7H_2O$	38	1.5	$MnBr_2 \cdot 4H_2O$	176	2.25	TiO_2	79	8.5
CeO_2	114	4 5	$MnCl_2$	53	1.75	V	557	1
Co	697	3	$MnCl_2 \cdot 4H_2O$	170	4	V_2O_5	714	11
$CoCl_2$	36	2	MnO	113	6	YCl_3	40	1.75
$CoCl_2 \cdot 6H_2O$	153	4	MnO_2	1287	6	Y_2O_3	115	7
Co_2O_3	1290	3	$MnSO_4 \cdot H_2O$	47	5	W	690	6.25
CoS	158	7	Mo	660	4	WCl_6	45	3
$CrCl_3$	82	6	MoO_3	69	5.5	WO_3	1270	6
$CrCl_3 \cdot 6H_2O$	181	5	MoS_3	1106	7	Zn	581	3
CrO_3	112	9	NaBr	40	4	$ZnBr_2$	574	7
Cr_2O_3	130	7	NaCl	83	7	$ZnCl_2$	609	7
Cu	228	7	Na_2MoO_4	53	4 25	ZnO	326	5 5
CuBr	722	11	Na_2SO_4	67	6	ZnS	67	3
$CuBr_2$	193	3 25	Nb	358	6	Zr	462	6
CuCl	619	13	Nb_2O_5	114	6	ZrO_2	63	4

Effect of Microwave Heating on the temperature of reagent-grade and Compounds (After Walkiewicz et al, 1988)

Appendix 4-1. The mineralogy data of the initial MZ2HE of KUCC ores provided by the supplier.

- Drums provided to Nottingham had received initial crush down to 100% passing 50 mm
- The analysis below is for material further crushed to -12 for QEM*SEM

Mineral abundance per sample

Mineral	Weight %
Chalcopyrite	2.9
Bornite	0
Other CuS	0
Pyrite	0.6
Quartz	18.7
Feldspar	42.9
Altered Feldspar/ Clay	14.4
Fe-RichMica	17.2
Other	3.3
Total	**100**

- Approximately 1/3 of the copper occurs on the outer surface of the gangue minerals
- A further 44% is associated with other sulphides or silicate gangue as inclusions
- The reminder is locked within quartz and ferdspar

SIZE BY SIZE MINERAL ABUNDANCE

Mineral	MZ2HE M2749							
Fraction	+8	+6.3	+4	+2	+500	+150	-150	Head
PSD	29.6%	13 9%	13.4%	13.3%	11.4%	5.6%	12.9%	100%
Cu Assay	0 56	0.64	0.65	0.64	0 73	1 46	1.54	0.79
QS Assay	0 53	0.61	0.62	0.61	0.69	1.38	1.46	0.75
Chalcopyrite	1.62	1.75	1.77	1.74	1.98	3.93	4.15	2.1
Bornite	0.01	0.01	0 01	0.01	0.01	0 02	0.03	0 0
Covellite	0.00	0 00	0.00	0 00	0.00	0.00	0.00	0.0
Chalcocite	0 00	0.00	0.00	0.00	0.00	0.01	0.01	0 0
Other-CuS	0 01	0.01	0.01	0.01	0.00	0.02	0.03	0.0
Pyrite	0.4	0 8	0.4	0.1	1.1	1.3	0.6	0 6
Quartz	16.5	16 4	14.3	20.4	20.3	27.7	24.9	18 9
Plagioclase	8 6	9 4	8.4	8.8	7.7	5.6	6.1	8.1
Orthoclase	35 9	35 3	40.9	34.5	38.1	33.0	25.9	35.1
Alt.Orthoclase	13 6	12.4	9 9	11.4	9.6	8 2	14.7	12.0
Muscovite/Illite	0.9	0.6	0 2	0.3	0.5	0.4	0.2	0.5
Fe-RichMica	18.2	18.0	18.4	16 9	16.2	14.4	15.9	17.3
Clays	1 7	2.3	2.6	2 8	2.1	1.1	0.9	1.9
Carbonates	0.2	0.1	0.3	0.1	0.2	1.2	1 7	0.4
S-Other	0.0	0 0	0.0	0.0	0.0	0.1	0.1	0.0
Other	2.4	2.7	2.8	2.8	2 4	3.1	4 7	2.9
TOTAL	100	100	100	100	100	100	100	100

SIZE BY SIZE % Cu DISTRIBUTION

Mineral	MZ2HE M2749							
Fraction	+8	+6.3	+4	+2	+500	+150	-150	Head
Chalcopyrite	99.3	99.3	99.2	99.1	99 4	98 2	98.4	98 9
Bornite	0 7	0.7	0.8	0.9	0.6	0.9	1.1	0.8
Covellite	0.0	0 0	0.0	0.0	0.0	0.0	0.0	0.0
Chalcocite	0.0	0 0	0 0	0.0	0.0	0.9	0 5	0.2
TOTAL	100	100	100	100	100	100	100	100

Appendix 4-2

Froth flotation of MZ2HE ore

Flotation was carried out using standard 5 litre Denver laboratory flotation cell. The rotor speed was kept constant at 1500 rpm. Potassium Iso Butyl Xanthate (SIBX) was used as a collector and was added at a dosage of 40 g/t. Frother (Procol) was used to stabilise the froth and added at a dosage of about 40 g/t. In order to add accurate amount of Xanthate and Procol a 10% and 1% solutions were prepared respectivily.

The flotation procedure was as follows:

About 1500 grams of ground ore (< 180μm) was added to the cell and about 4 litre of water was added. The machine was then switched on to mix the ore with water for a period of 3 minutes. About 0.4 ml of the 10% Xanthate solution was added and further 2 minutes were allowed for conditioning the pulp. The frother (0.5 ml) was then added and further 1 minute was allowed for conditioning. The air was then turned on and skimming of the froth was continued for 2 minutes. The air was then stopped and further 0.4 ml xanthate was added and 2 minutes were allowed for conditioning followed by the addition of 0.5 ml 1% Procol solution. After 1 minute the air was turned on again and skimming was started and continued for 5 minutes. The flotation was stopped then and the froth was then pressure filtered and dried in a vacuum dryer at temperature of 30°C.

Ten flotation experiments were done according to the procedure above. The product of all flotation experiments was mixed together and subjected to a second stage flotation. The froth was collected in a carefully cleaned tray. It was then subjected to a pressure filtration followed by vacuum drying.

Appendix 4-3. Preparation and XRD characterization of the copper ore sample used to develop the total digestion method.

The ore contains chalcopyrite, pyrite, pyrrhotite, sphalerite, quartz, calcite and miner content of other minerals was chosen. The XRD analysis of the sample is shown in Figure 1. Sample of this ore (500g) was crushed in a laboratory Jaw Crusher. A representative sample (30g) was taken by riffling. The sample was ground in a Tema® mill to a particle size 100% passing 75 μm. The maximum particle size was checked by passing the powder through 75 μm wire mesh screen. The oversize material was re-milled. The powder was manually well mixed then transferred to a clean labelled jar.

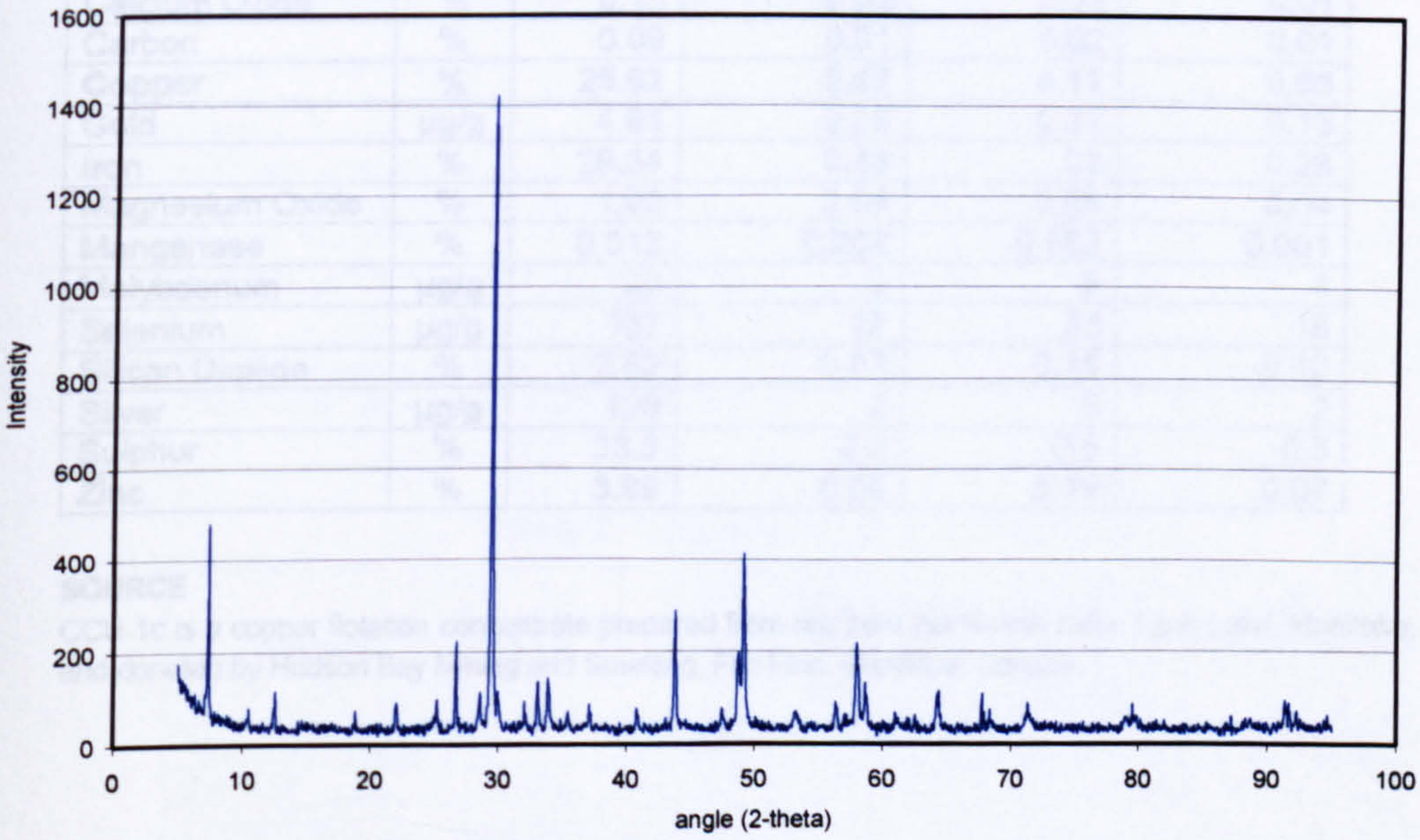

Figure 1 XRD analysis of the ore sample used to develop total digestion method.

The fine grinding was required to enhance the homogenisation of the sample prior to analysis through mixing. It also serves to enhance the digestion and to reduce the time required for total dissolution.

Appendix 4-4 Certificate of analysis for certified reference material CCU-1c

Certificate of Analysis

First issued: November 2000 Updated: January 2004

CCU-1c

Copper Concentrate

Table 1 - CCU-1c Certified Values

Element	Unit	Mean	Within-Lab Standard Deviation	Between-Lab Standard Deviation	95% confidence limit
Arsenic	µg/g	34	4	9	6
Cadmium	µg/g	136	5	12	6
Calcium Oxide	%	0.15	0.02	0.02	0.01
Carbon	%	0.09	0.01	0.02	0.01
Copper	**%**	**25.62**	**0.07**	**0.12**	**0.05**
Gold	µg/g	4.94	0.29	0.22	0.13
Iron	%	29.34	0.48	.68	0.28
Magnesium Oxide	%	1.02	0.04	0.06	0.04
Manganese	%	0.012	0.002	0.002	0.001
Molybdenum	µg/g	20	2	5	4
Selenium	µg/g	107	16	23	15
Silicon Dioxide	%	2.52	0.07	0.16	0.10
Silver	µg/g	129	2	5	2
Sulphur	%	33.3	0.2	0.5	0.3
Zinc	%	3.99	0.06	0.19	0.07

SOURCE

CCU-1c is a copper flotation concentrate prepared from ore from the Ruttan mine, Lynn Lake, Manitoba, and donated by Hudson Bay Mining and Smelting, Flin Flon, Manitoba, Canada.

DESCRIPTION

Copper concentrates generally contain chalcopyrite, pyrite, sphalerite, pyrrhotite and gangue minerals. CCU-1c is the fourth in a series, all from the same source, with predecessors, CCU-1b, CCU-1a and CCU-1. The first three materials in the series are no longer available.

INTENDED USE

CCU-1c is suitable for the analysis of copper, and other elements at major, minor and trace levels. Examples of intended use are for quality control in the analysis of samples of a similar type, method development, arbitration and the calibration of equipment.

INSTRUCTIONS FOR USE

The assigned values pertain to the date when issued. CANMET is not responsible for changes occurring after receipt by the user. CCU-1c should be used "as is", without drying. The contents of the bottle should be thoroughly mixed before taking samples. The contents of the bottle should be exposed to air for the shortest time possible. Unused material should be stored under an inert gas in a desiccator, or in a new, heat-sealed laminated foil pouch.

METHOD FOR PREPARATION

The raw material was dried at 66°C, sieved, and blended to obtain a sub-74 micron (-200 mesh) product, which was bottled in 200-gram units. This is the only size available. Each bottle was sealed under nitrogen in a laminated aluminum foil-mylar pouch to prevent oxidation.

STATE OF HOMOGENEITY

The homogeneity of the stock with respect to its antimony, copper, gold, selenium, silver and zinc was investigated using twenty-two bottles chosen according to a stratified random sampling scheme. Two splits were analysed from each bottle. The analyses for copper were performed by CANMET on 0.5g samples using a multi-acid digestion followed by a titration with thiosulphate. Instrumental neutron activation was used on 0.5g sample for antimony, selenium, silver and, zinc, and on a 5g sample for gold. A one–way analysis of variance technique (ANOVA) was used to assess the homogeneity of these elements (1). The ratio of the between-bottles to within-bottle mean squares is compared to the F statistic at the 95% level of probability. No evidence of inhomogeneity was observed for all six elements. Use of a smaller sub-sample will invalidate the use of the certified value and associated parameters. Further details are available in the certification report.

Table 2 - CCU-1c Provisional Values

Element	Unit	Mean	Within Lab Standard Deviation	Between Lab Standard Deviation	95% confidence limit
Aluminum Oxide	%	0.34	0.03	0.11	0.07
Bismuth	µg/g	70	5	9	8
Chromium	µg/g	30	3	9	8
Cobalt	µg/g	18	1	5	3
Lead	%	0.34	0.01	0.02	0.01
Mercury	µg/g	32	2	8	5
Nickel	µg/g	11	2	4	4

CERTIFICATION

Twenty-eight industrial, commercial, and government laboratories participated in an interlaboratory certification program. Various elements were analyzed by methods of each laboratory's choice. A one-way analysis of variance technique was used to estimate the consensus value and other statistical parameters (1). Fifteen elements were given recommended values and a further seven elements had provisional values assigned. Informational values for fourteen elements were derived from the mean of fifteen to forty-seven results from varying numbers of laboratories. Full details of all phases of the work, including statistical analysis, the methods and the names of the participants are contained in CCRMP Report 00-3E.

Legal Notice

CANMET has prepared this reference material and statistically evaluated the analytical data of the interlaboratory certification program to the best of its ability. The purchaser, by receipt hereof, releases and indemnifies the CANMET from and against all liability and costs arising out of the use of this material and information.

Table 3 - CCU-1c Informational Values

Element	Unit	Mean	Range	No. of Values
Antimony	µg/g	4	4-7	47
Barium	µg/g	31	6 - 76	21
Chlorine	µg/g	40	26 - 75	15
Fluorine	µg/g	294	190 - 368	30
LOI	%	16.4	15.8 - 16.8	15
Potassium	%	0.03	0.01 - 0.07	13
Scandium	µg/g	2	0.4 - 4	22
Sodium	%	0.02	0.007 - 0.08	37
Strontium	µg/g	4	3 - 5	20
Tellurium	µg/g	23	16 - 28	35
Titanium	µg/g	64	37 - 100	30
Vanadium	µg/g	15	2 - 34	20
Yttrium	µg/g	2	0.9 - 2	10
Zirconium	µg/g	17	6 - 23	15

Period of Validity

These certified values are valid until 2005. The stability of the material will be monitored every two years. Purchasers will be notified of any significant changes.

Certifying Officers

Joseph Salley

Maureen E. Leaver

For Further Information

The preparation and certification procedures used for CCU-1c, including methods and values obtained by individual laboratories, are given in CCRMP Report 00-3E. This report is available free of charge on application to:

Sales Manager, CCRMP
CANMET (NRCan)
555 Booth Street
Ottawa, Ontario, Canada K1A 0G1
Telephone: (613) 995-4738
Facsimile: (613) 943-0573
E-mail: ccrmp@nrcan.gc.ca

Reference

1. Brownlee, K.A., Statistical Theory and Methodology in Science and Engineering; John-Wiley and Sons, Inc.; New York; 1960.

Appendix 4-5 Parameters of ICP analysis of total digestion samples

Table 1 List for elements with high concentration

Element	Wavelength, °A	Concentration in the standard, ppm	Concentration in the QC, ppm	Detection limit in the rock sample, ppm	Detection limit in the solution, ppm
Al	394	100.5	20	17.5	0.035
Cu	327	1000	200	4.6	0.009
Fe	259	600	120	1.5	0.003
Pb	220	150	40	3.8	0.008
S	180.7	701	160.3	116	0.232
Zn	334(206)	1392	398	21.3(18.2)	0.042(0.037)

Table 2 List for elements with low concentration

Element	Wavelength, °A	Concentration in the standard, ppm	Concentration in the QC, ppm	Detection limit in solution, ppm	Detection limit in sample, ppm
Al	394	1	0.4	64.2	0.128
As	189	20	4	24.2	0.048
Ca	317.9	49.8	19.9	10.3	0.021
Cd	214	5	2	0.4	0.001
Cr	267	5	2	0.3	0.001
Co	228	5	2	1.0	0.002
Cu	327	10.1	2	48.7	0.098
Fe	259	6	2	13.5	0.027
Mg	279	51.5	20.6	13.4	0.027
Mn	257	5	2	0.3	0.001
Mo	202	5	2	1.6	0.003
Ni	231	25	8	1.9	0.004
Pb	220	20	4	7.8	0.016
S	180.7	8.2	2.1	51	0.103
Sb	217	10.2	2	5.8	0.012
Zn	334 (206)	16.1	4	19.6(59.6)	0.039(0.119)

Appendix 4-6 The chemical analysis of MP-1a without matrix matching in silicon content

Element	Number of replicates	Mean, %	CV, %	Max, %	Min, %	Reference values, %	Recovery, %
Zn	18	18.26	1.69	18.91	17.99	19.02	96.02
Pb	18	4.25	2.78	4.41	4.06	4.33	98.19
Cu	18	1.45	3.24	1.54	1.39	1.44	100.92
As	18	0.78	3.63	0.83	0.74	0.84	92.83
Bi	18	0.028	3.705	0.030	0.027	0.032	89.001
Mo	18	0.026	2.975	0.027	0.025	0.029	89.018

Appendix 4-7 Chemical analysis of the blank samples run along with total digestion samples

Element	Average	Maximum	Standard Deviation	%RSD
Al	2.9	27.5	9.9	347.3
As	14.8	43.5	13.8	93.0
Ca	BDL	BDL	-	-
Cd	0.1	0.5	0.2	185.1
Co	0.0	0.5	0.3	792.9
Cr	0.2	0.6	0.2	84.0
Cu	BDL	6.3	4.3	135.8
Fe	BDL	BDL	-	-
Mg	BDL	BDL	-	-
Mn	BDL	BDL	-	-
Mo	0.6	3.5	1.3	232.9
Ni	BDL	1.2	0.6	261
Pb	BDL	BDL	-	-
S	53.9	137.6	34.9	64.8
Sb	BDL	0.6	1.8	54.4
Zn	BDL	9.9	11.1	60.0
Zn	BDL	9.7	8.5	68.5

Appendix 4-8. ICP analysis of GBL chalcopyrite

Sample ID	Particle size, μm	Cu, %	Fe, %	Pb, %	S, %	Zn, %	Total content
MO-1225	<38	34.21	29.82	0.06	35.43	0.15	99.68
MO-1226		34.39	29.39	0.06	35.04	0.15	99.03
MO-1227		34.25	29.11	0.06	34.53	0.15	98.10
Average		34.29	29.44	0.06	35.00	0.15	98.94
Standard deviation		0.09	0.36	0.00	0.45	0.00	
CV, %		0.28	1.23	2.34	1.29	0.33	
MO-1233	38-53	34.62	30.03	0.06	35.47	0.14	100.32
MO-1234		34.96	29.96	0.06	35.64	0.14	100.76
MO-1235		34.94	29.96	0.06	35.65	0.14	100.76
Average		34.84	29.98	0.06	35.59	0.14	100.61
Standard deviation		0.19	0.04	0.00	0.10	0.00	
CV, %		0.54	0.13	0.46	0.28	1.16	
MO-1230	53-75	34.80	29.66	0.05	34.87	0.15	99.54
MO-1231		35.09	29.85	0.05	35.31	0.14	100.45
MO-1232		34.92	30.17	0.06	35.86	0.14	101.16
Average		34.94	29.89	0.06	35.35	0.15	100.38
Standard deviation		0.15	0.26	0.00	0.50	0.00	
CV, %		0.42	0.85	7.72	1.40	1.86	
MO-1224	75-106	33.96	28.80	0.04	33.44	0.14	96.37
MO-1228		34.55	29.53	0.05	34.53	0.14	98.80
MO-1229		34.37	29.39	0.04	33.95	0.14	97.89
Average		34.29	29.24	0.05	33.97	0.14	97.69
Standard deviation		0.30	0.39	0.00	0.54	0.00	
CV, %		0.89	1.34	8.31	1.60	0.93	0.00
MO-1223	Standard Reference material CCU-1c	25.99	29.01	0.31	34.04	4.12	93.48
MO-1236		25.60	28.46	0.31	33.41	4.02	91.79
MO-1237		25.76	28.72	0.30	33.28	4.03	92.10
Average		25.78	28.73	0.31	33.58	4.05	92.45
Standard deviation		0.20	0.28	0.00	0.41	0.06	0.90
CV, %		0.77	0.96	1.23	1.21	1.36	0.97
Reported chemical composition		25.62± 0.12	29.34± 0.68	0.34± 0.02	33.3± 0.50	3.99±0. 19	

The spectral line used to interpret ICP data are: $Cu_{327.393}$, $Fe_{259.939}$, $Pb_{220.353}$, $S_{180.669}$, $Zn_{334.501}$

Appendix 4-9 ICP analysis of MZ2HE chalcopyrite

Sample_ID	Particle size, μm	Cu, %	Fe, %	Pb , %	S, %	Zn, %
MO-1745	<25	30.73	28.87	0.14	33.27	0.16
MO-1746		31.44	29.31	0.14	33.42	0.16
average		*31.08*	*29.09*	*0.14*	*33.35*	*0.16*
pooled Standard deviation		*0.37*	*0.32*	*0.00*	*0.51*	*0.00*
CV, %		1.20	1.10	1.18	1.54	2.30
MO-1747	25-38	29.82	29.38	0.09	34.39	0.08
MO-1748		30.07	29.72	0.08	33.76	0.08
average		29.94	29.55	0.09	34.08	0.08
pooled Standard deviation		0.38	0.27	0.00	2.80	0.00
CV, %		1.27	0.93	1.62	8.21	2.78
MO-1749	38-53	28.71	29.86	0.08	34.06	0.07
MO-1750		28.84	29.81	0.08	34.02	0.06
average		28.78	29.84	0.08	34.04	0.07
pooled Standard deviation		0.27	0.55	0.00	0.42	0.00
CV, %		0.94	1.84	1.84	1.23	0.44
MO-1751	53-75	27.47	29.98	0.07	34.15	0.07
MO-1752		27.81	30.24	0.07	34.88	0.07
average		27.64	30.11	0.07	34.52	0.07
pooled Standard deviation		0.23	0.13	0.00	0.84	0.00
CV, %		0.83	0.43	2.14	2.45	2.06
MO-1753	75-106	25.28	29.26	0.08	33.64	0.08
MO-1754		25.71	29.58	0.08	34.03	0.07
average		25.49	29.42	0.08	33.83	0.07
pooled Standard deviation		0.27	0.46	0.00	0.57	0.00
CV, %		1.06	1.55	1.74	1.69	2.00

$Cu_{327.393}$, $Fe_{259.939}$, $Pb_{220.353}$, $S_{181.975}$, $Zn_{334.501}$

Appendix 4-10

Determination of Fe^{2+} in ferric sulphate and ferric chloride leaching solutions

Introduction

Ferric ions oxidises sulphide sulphur to elemental sulphur resulting in generation of ferrous ions as a result of oxidation reaction. Ferrous ions are also released into leaching solution from chalcopyrite itself in the case of chalcopyrite oxidation. Due to the presence of two forms of iron species in the leaching solution (Fe^{2+} and Fe^{3+}) and also the fact that the generated ferrous ions during leaching are negligible in comparison with ferric ion matrix, it is very difficult to determine accurately the reaction product of ferrous ions using ICP-AES. Therefore, redox titration was used to determine Fe^{2+} in the leaching solution. Potassium dichromate was chosen as a titrant. Due to the difficulty to distinguish the end point an indicator (sodium diphenylamine sulfonate) was used.

Dichromate ion is reduced to two chromium (Cr^{3+}) ions. The reduction reaction requires 6 electrons and 14 hydrogen (H^+) ions according to the following reaction:

$$Cr_2O_7^{2-} + 14H^+ + 6e^- \rightarrow 2Cr^{3+} + 7H_2O \qquad \textbf{Reaction 1}$$

On the other hand, only one electron is necessary to reduce Fe^{3+} to Fe^{2+}

$$Fe^{3+} + e^- \rightarrow Fe^{2+} \qquad \textbf{Reaction 2}$$

Therefore, 1 mole of $Cr_2O_7^{2-}$(the oxidizing agent) reacts with 6 moles of Fe^{2+} (the reducing agent) to form 6 moles of Fe^{3+} and 2 moles of Cr^{3+}. Thus, in net ionic form the redox reaction can be written as:

$$Cr_2O_7^{2-} + 6Fe^{2+} + 14H^+ \rightarrow 6Fe^{3+} + 2Cr^{3+} + 7H_2O \qquad \textbf{Reaction 3}$$

The molecular form of the reaction can be written as:

$$K_2Cr_2O_7 + 6Fe(NH_4)_2(SO_4)_2 + 7H_2SO_4 \rightarrow 3Fe_2(SO_4)_3 + Cr_2(SO_4)_3 + K_2SO_4 + 6(NH_4)_2SO_4 + 7H_2O \qquad \textbf{Reaction 4}$$

Standardisation of dichromate

Ferrous ammonium sulphate ($Fe(NH_4)_2(SO_4)_2$) was used to standardise dichromate solution. According to reaction 3 one mole of dichromate oxidises 6 moles of ferrous ammonium sulphate. The standardisation procedure is as follows:

1. Weigh about 6 g of 99.9% purity potassium dichromate in a glass or agate mortar then heat for 30-60 minutes at 140-150°C. Allow the mass to cool in a closed vessel in a desiccator (Vogel, 1961)
2. Weigh about 1.365 g of dichromate in a weighing boat using a 4 digit electronic balance and then transfer the mass into 1 litre volumetric flask
3. Dissolve the mass in 0.5 M H_2SO_4. To insure the total transformation of the mass into the flask, the boat should be washed with distilled water and transfer this water into the flask directly. The prepared solution should be used as a stock solution for titration.
4. Prepare 10% dichromate solution from the stock solution in 0.5 M H_2SO_4.
5. Weigh about 10.91 g of $Fe(NH_4)_2(SO_4)_2$ in a weighing boat and then transfer the mass into a 1 litre volumetric flask and dissolve the mass in 0.5M H_2SO_4. To insure the total transformation of the mass into the flask, the boat was wash with distilled water and transfer this water into the flask directly

6. Calculate the molarity of the prepared solutions (dichromate and ferrous ammonium sulphate).

$$molarity.of.dichromate.solution = \frac{10}{100} \times \frac{1.365}{294.19} = 4.639 \times 10^{-4}\, mole/litre$$

$$molarity.of.FerrousAmSulp.solution = \frac{10.91}{392.14} = 0.02783 \times 10^{-2}\, mole/litre$$

7. Add 1ml of ferrous ammonium sulphate solution to 2ml of acid mix(1 part of 50% sulphuric acid, 1 part of saturated boric acid and 1 part of orthophosphoric acid) and 2 drops of indicator (diphenylamine 4 sulfonic acid, sodium salt) in an Erlenmeyer flask. Acid mix and phosphoric acid is particularly important to lower the oxidation potential of the ferric-ferrous system by forming a complex $[Fe(HPO_4)]^+$ with the ferric ions (Vogel, 1961). The indicator impart a green colour to the ferrous solution which deepens to a blue-green shortly before the end of titration

8. Fill the burette with the $K_2Cr_2O_7$ solution and drain out enough so that the liquid level is just below the upper calibration mark and the burette tip is full. Read the initial volume from the calibration scale on the burette. This reading and all other burette readings should be estimated to the nearest 0.01 mL.

9. Titrate the iron solution in the flask. The intense purple color produced by the first drop of excess $K_2Cr_2O_7$ signals the end point for the titration.

10. According to reaction 3 one mole of dichromate can titrate 6 moles of ferrous ions. Based on this and using the calculated molarity of the solutions, the volume of dichromate required to titrate 1mg of ferrous ions can be found as follows:

If 1 mL of ferrous ammonium sulphate of a concentration of 0.027839 M requires 10.6 mL dichromate of a concentration of 0.000463918M (dried at 160 for 1hour), then the mass of Fe^{2+} equivalent to 1mL of dichromate is

$$m_{Fe^{+2}} = \frac{1 \times 0.02783 \times 1000 \times 55.84}{10.6} = 147\mu g$$ -this is the titration Factor (T_{Fe})

For the solutions containing higher concentration of Ferrous ions another dichromate solution was used which is 3 times more concentrated than the the first one.

If 1 mL of ferrous ammonium sulphate of a concentration of 0.027839 M requires 3.27 mL dichromate of a concentration of 0.0013916M (dried at 160 for 1hour), then the mass of Fe^{2+} equivalent to 1mL of dichromate is

$$m_{Fe^{+2}} = \frac{1 \times 0.02783 \times 1000 \times 55.84}{3.27} = 475.3\mu g$$ -this is the titration Factor (T_{Fe})

reference

Vogel, A.I., 1961. A Text-Book of Quantitative Inorganic Analysis Including elementary Instrumental analysis. Longman, London.

Appendix 4-11 Preparation of standard sulphur solution for UV spectrophotometric analysis

Procedure

1. Wash the Soxhlet extraction system (Figure below) and the fritted glass centre filter thoroughly with toluene by dummy extraction for about 5 hours.
2. Dry the glass centre filter at 100˚C for 5 hours
3. Remove the glass centre desk into dissicator until cools
4. Weigh the desk and report mass M1
5. Weigh mass of sulphur (0.2755g) in the filter and report M2
6. Conduct soxhlet extraction for about 24 hours
7. Remove the filter carefully and dry it as in steps 2 and 3
8. Weigh the filter M3
9. The mass of sulphur dissolved =M2- (M3-M1)
10. The sulphur solution is transferred to 250 ml volumetric flask
11. Prepare different solutions with different concentrations to draw a calibration curve

The sulphur used for preparing the standard is 99.998%purity and it is supplied by Aldrich. The sulphur appearance is yellow chips (crystalline)

The first series of standard solutions

1. St.1 0.2755 g in 250 ml of toluene or 1.102mg/ml
2. St.2 one ml from St. 1 in 100ml of toluene or 11.02 µg/ml
3. St.3 one ml from St2 in 100ml of toluene or 0.1102 µg/ml
4. St.3 5ml of St. 1 in 100 ml of toluene or 55.1 µg/ml

The second series of standard solutions

1. St1contains 0.3756 g in 250 ml of toluene or 1.5024mg/ml
2. St2 contains 10 ml of St1 in 25 ml toluene or 0.60096mg/ml
3. St3 contains 5 ml of St1 in 25 toluene or 0.30048 mg/ml
4. St4 contains 2 ml of St1 in 25 ml toluene or 0.12019mg/ml
5. St5 contains 0.5 ml of St1 in 25 ml toluene or 0.030048

The UV results of the two series of standards where combined together and plotted as shown in Appendix 4-12

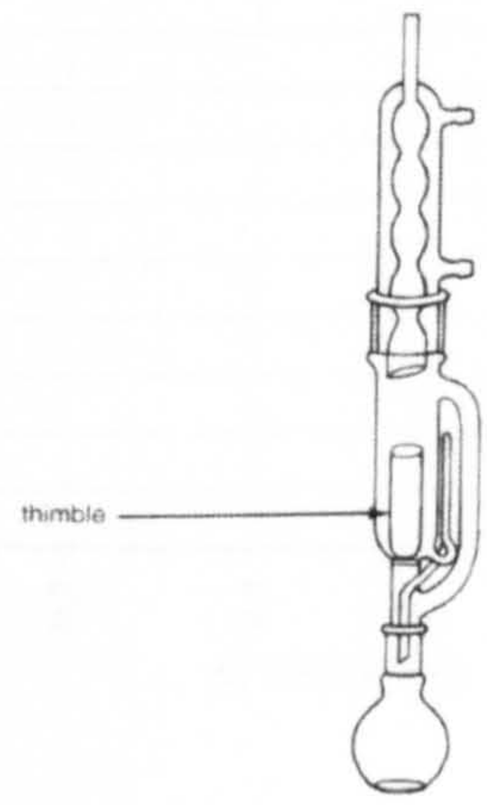

Figure 1 Schematics for Soxhlet system

Appendix 4-12.

Calibration curve for determination of sulphur by UV Spectrophotometry

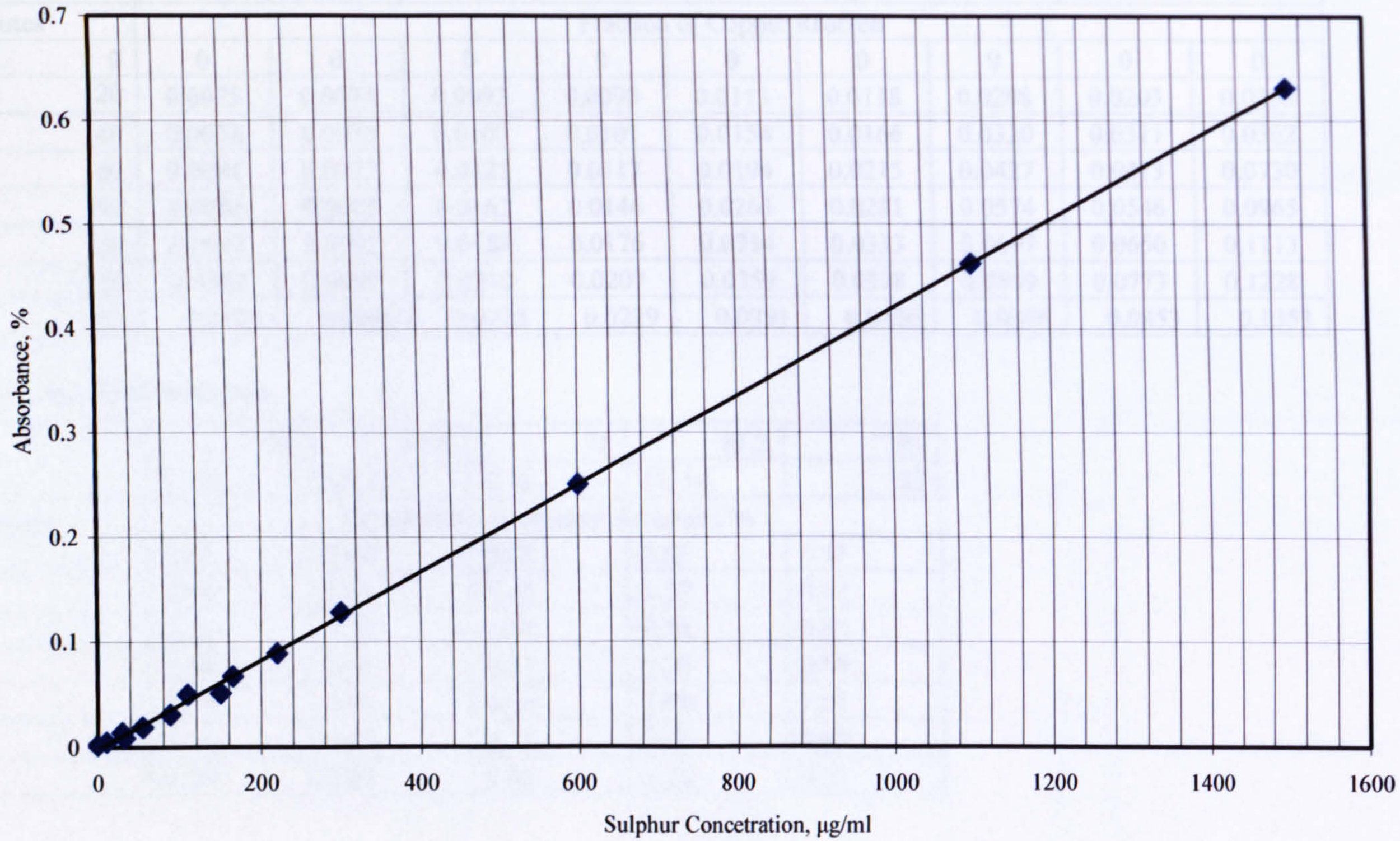

Appendix 4-13. Reproducibility of chalcopyrite leaching results in ferric sulphate under conventional conditions

Table 1 The fraction of copper reacted when GBL chalcopyrite of a particle size <38µm was leached in 0.25 M $Fe_2(SO_4)_3$ at different temperatures

Temperature, °C	52		61.5		71		81.4		91
Leach No	9	10	11	12	7	8	13	14	22
Leaching Time, Minutes	Fraction of Copper Reacted								
0	0	0	0	0	0	0	0	0	0
20	0.0075	0.0074	0.0093	0.0090	0.0113	0.0118	0.0208	0.0203	0.0355
40	0.0078	0.0076	0.0107	0.0101	0.0154	0.0166	0.0320	0.0311	0.0562
60	0.0081	0.0077	0.0125	0.0117	0.0194	0.0215	0.0427	0.0413	0.0730
90	0.0085	0.0085	0.0162	0.0146	0.0261	0.0281	0.0574	0.0546	0.0965
120	0.0093	0.0092	0.0189	0.0176	0.0314	0.0333	0.0697	0.0650	0.1113
150	0.0102	0.0099	0.0210	0.0207	0.0359	0.0378	0.0809	0.0773	0.1228
180	0.0106	0.0105	0.0235	0.0229	0.0391	0.0436	0.0896	0.0853	0.1353

Table 2 Pooled relative standard deviation

Temperature	52	61.5	71	81.2	91
Leach No	9, 10	11, 12	7, 8	13, 14	22
Leaching Time, Minutes	Pooled relative standard deviation, %				
20	0.57	0.98	0.52	0.63	1.43
40	1.02	0.93	1.42	1.17	0.67
60	1.58	1.24	1.22	0.53	0.84
90	1.90	0.60	0.83	0.28	0.86
120	1.18	0.99	0.76	1.60	1.01
150	1.34	0.87	0.72	0.63	0.85
180	1.38	0.83	1.46	1.12	0.73

Appendix 4-14 Shrinking core model

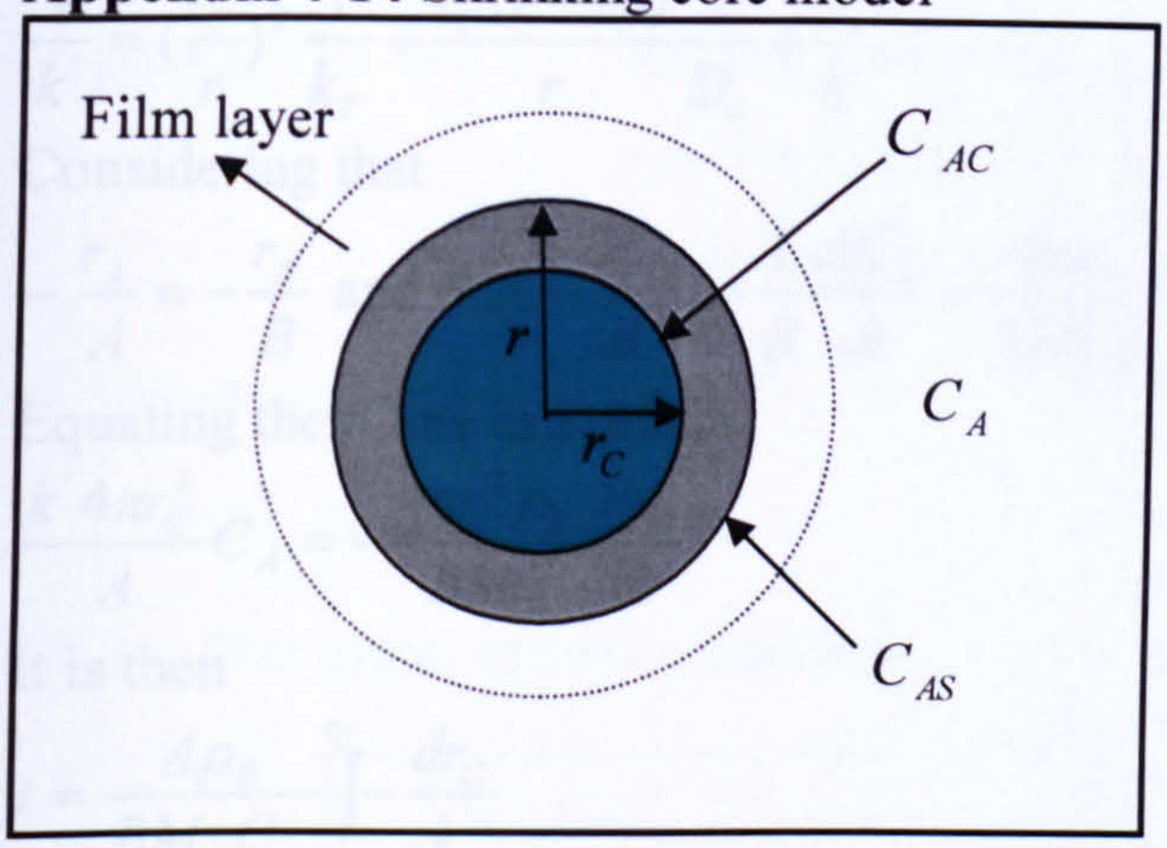

Where r is particle radius, r_C is unreacted radius, C_A is the bulk concentration of A, C_{AS} is the concentration of A at the particle surface, C_{AC} is concentration of A at the unreacted core surface.

Shrinking core model visualises 5 steps which occur in succession:

Step 1: Diffusion of reactant A through the film surrounding the particle to the surface of solid

Step 2: Penetration and Diffusion of A through the ash layer to the surface of unreacted core

Step 3: Reaction of A with solid B at this reaction surface

Step 4: Diffusion of the product through the ash to the exterior surface of the solid

Step 5: Diffusion of the product through the film layer.

The main assumptions in deriving the shrinking core model are:

The particle shape is spherical,

The bulk concentration of A is constant

The particle radius r is constant,

The reaction which occurs at the core surface is first order reaction

All the reaction steps are assumed to occur in a preudo-state conditions, i.e., the rate of diffusion through the film layer = rate of diffusion through the ash layer = the rate of reaction which occurs at the core surface.

For film diffusion process:

$$-r_A = k_T 4\pi r^2 (C_A - C_{AS})$$

For ash layer

$$-r_A = D_e \left(\frac{4\pi}{\frac{1}{r_C} - \frac{1}{r}}\right)(C_{AS} - C_{AC})$$ Which come from Fick's Law: $Q_A = D_e \frac{dC_A}{dr}$

For chemical reaction:

$$-r_A = k 4\pi r_C^2 C_{AC}$$

By eliminating C_{AC} and C_{AS} one can obtain

$$-r_A = k' 4\pi r_C^2 C_A$$

Where

$$\frac{1}{k'} = (\frac{r_C}{r})^2 \frac{1}{k_T} + \frac{r_C(r-r_C)}{r} \frac{1}{D_e} + \frac{1}{k}$$

Considering that

$$-\frac{r_A}{A} = -\frac{r_B}{B} \text{ and that } -\frac{r_B}{B} = -\frac{1}{B}\frac{dN_B}{dt} = \frac{4\pi\rho_B}{3BM_B}\frac{dr_C^3}{dt}$$

Equating them one can obtain

$$\frac{k' 4\pi r_C^2}{A} C_A = -\frac{4\pi r_C^2 \rho_B}{BM_B}\frac{dr_C}{dt}$$

It is then

$$t = \frac{A\rho_B}{BM_B C_A}\int_r^{r_C} -\frac{dr_C}{k'}$$

The conversion X can be expressed as a function of particle radius as

$$1 - X = \frac{m_C}{m} = \frac{V_C}{V} = (\frac{r_C}{r})^3 \text{ or}$$

Normally one step is limiting the reaction. If so, for Chemical reaction control where $k' = k$

$$t = \frac{A\rho_B}{BM_B C_A}\int_r^{r_C} -\frac{dr_C}{k}$$

$$t = \frac{A\rho_B}{BM_B kC_A}(r - r_C)$$

$$\boxed{t = \frac{A\rho_B r}{BM_B kC_A}(1-(1-X)^{1/3})}$$

For fluid firm diffusion controlled reaction

$$t = \frac{A\rho_B}{BM_B C_A}\frac{1}{k_T r^2}\int_r^{r_C} -r_C^2 dr_C$$

$$t = \frac{A\rho_B}{BM_B C_A}\frac{1}{3k_T}(r^3 - r_C^3)$$

$$\boxed{t = \frac{A\rho_B}{BM_B C_A}\frac{r^2}{3k_T}X}$$

For ash layer diffusion

$$t = \frac{A\rho_B}{BM_B C_A}\frac{1}{D_e r}\int_r^{r_C}(r_C^2 - rr_C)dr_C$$

$$\boxed{t = \frac{A\rho_B}{BM_B C_A}\frac{r^2}{6D_e}(1-2X-3(1-X)^{2/3})}$$

(to derive the shrinking core model (Levenspiel, 1999) was used.)

Levenspiel, O., 1999. Chemical Reaction Engineering. John Wiley & Sons, New York.

Appendix 4-15: Testing various models to fit the kinetic data of chalcopyrite leaching

Standard Leaching Data

1 Shrinkage core model

1.1 Film Diffusion control

1.1.1 Flat plate, cylinder, Sphere

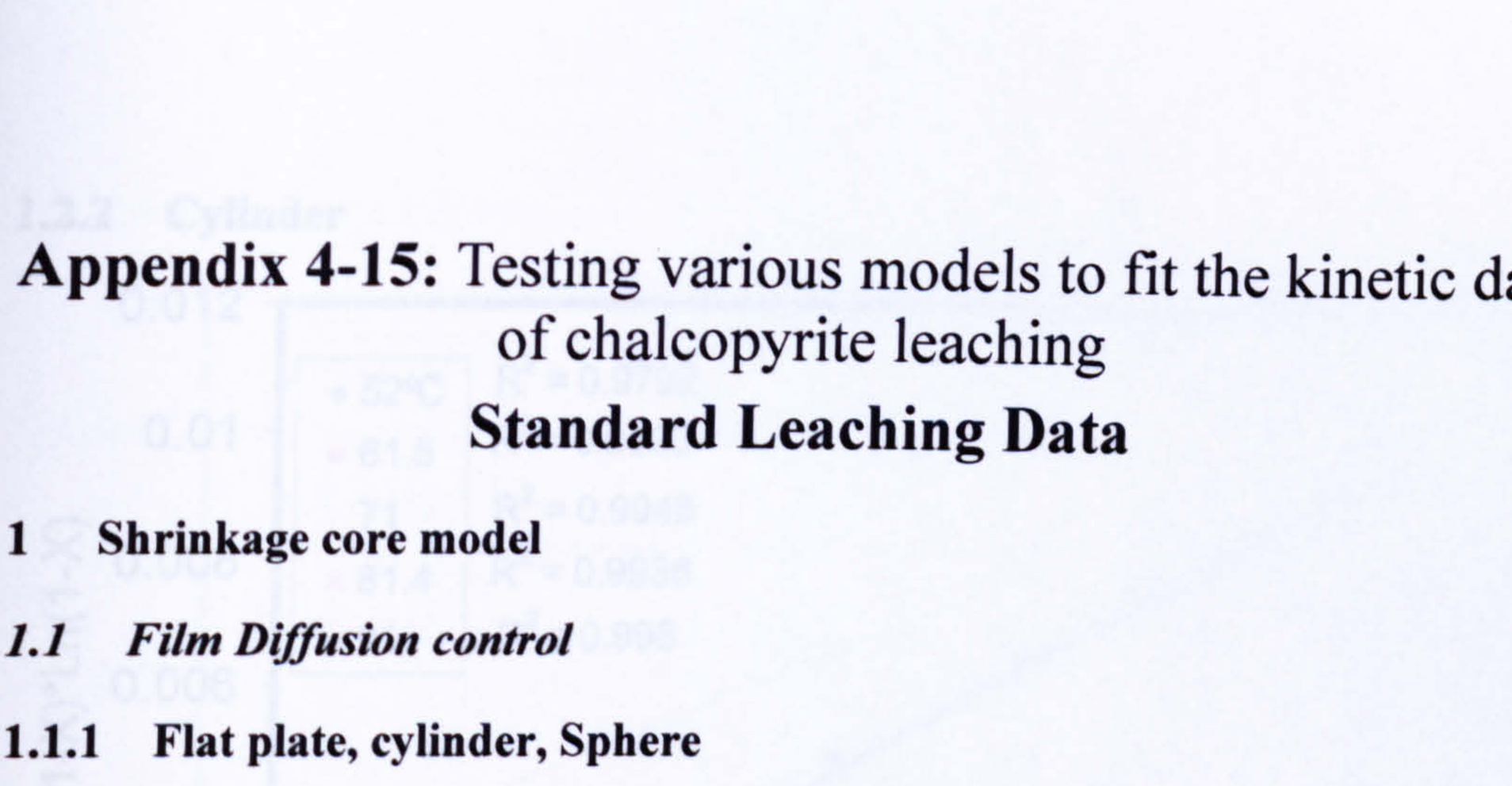

1.2 Ash diffusion control

1.2.1 Sphere

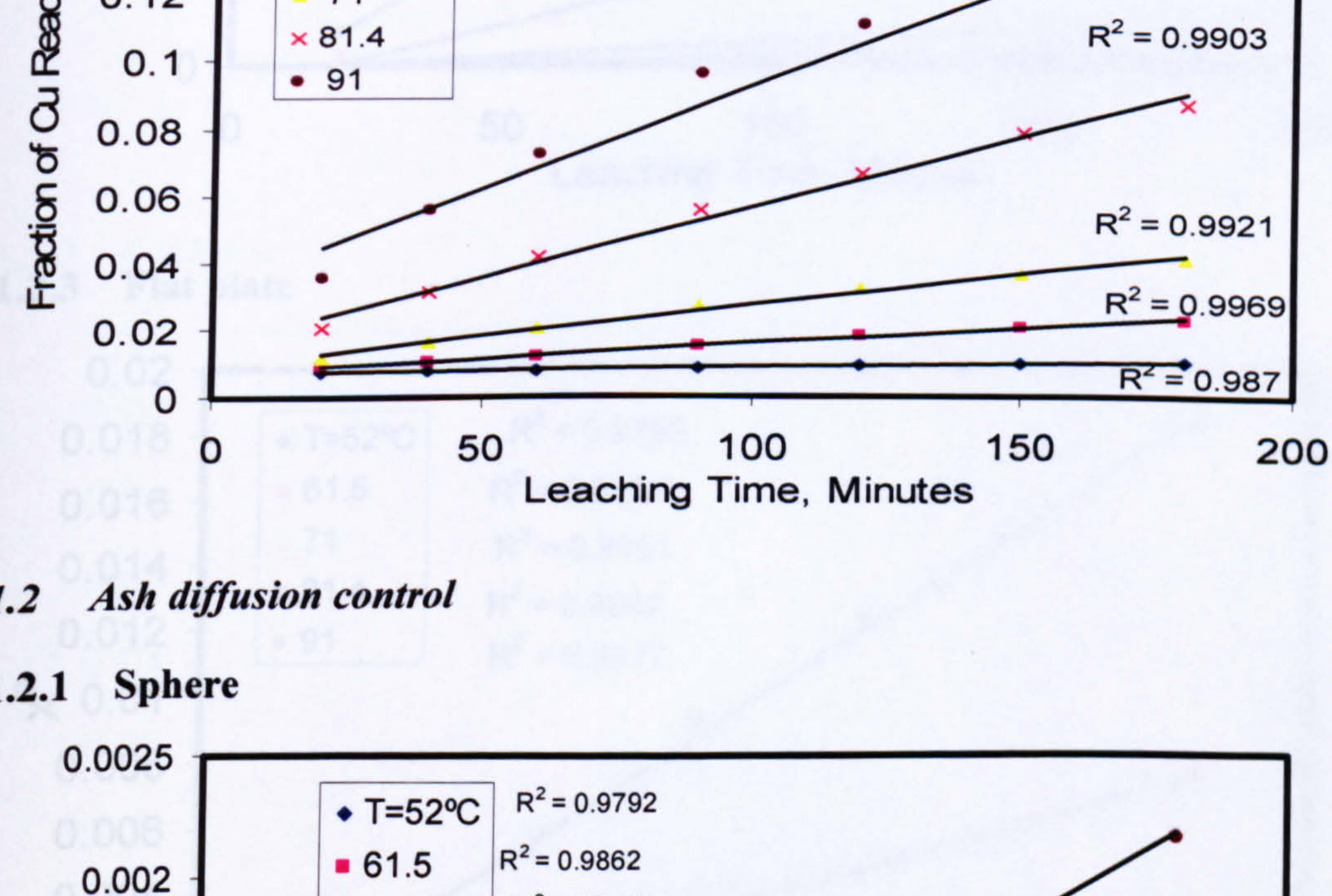

1.2.2 Cylinder

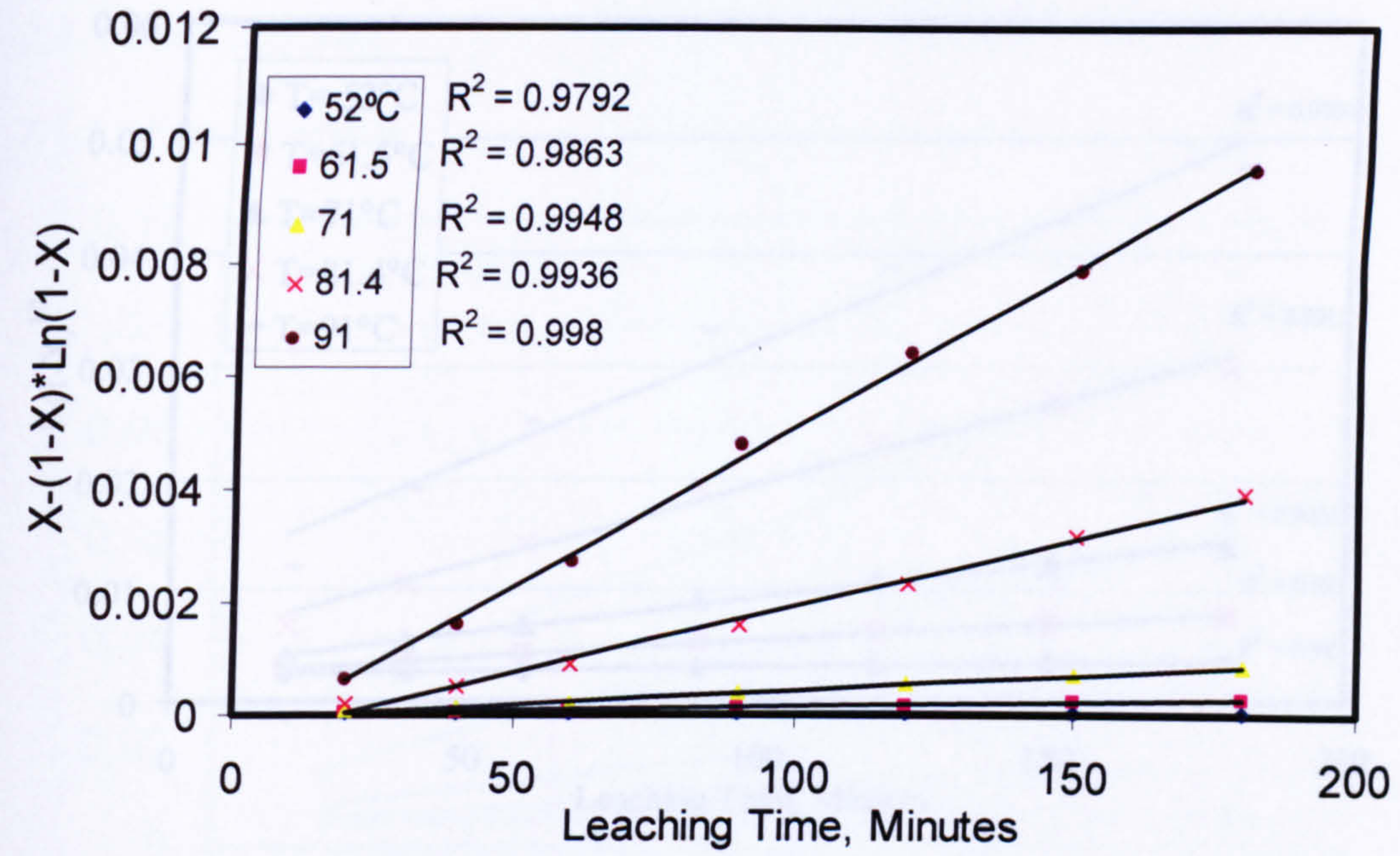

1.2.3 Flat plate

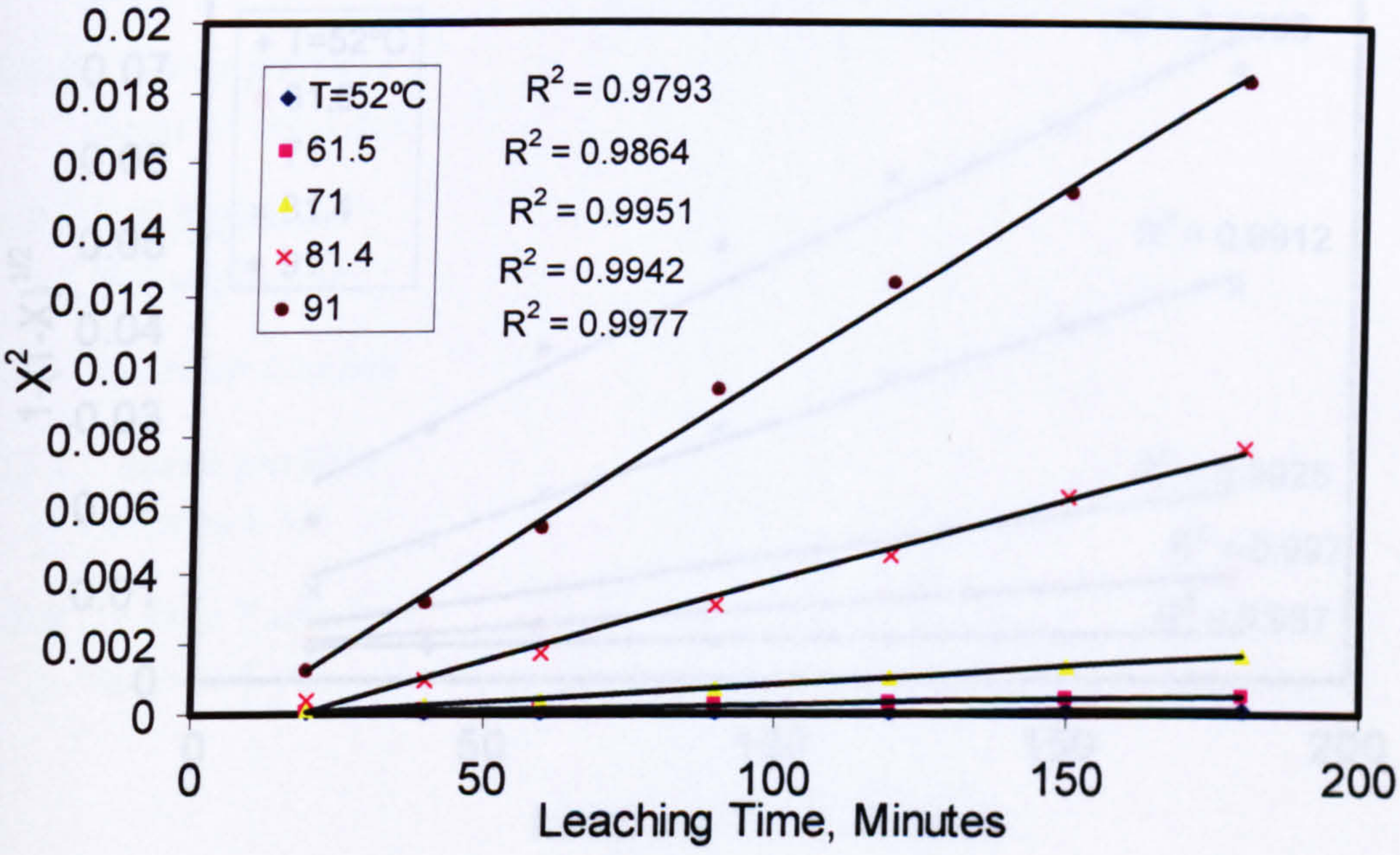

1.3 Reaction control

1.3.1 Flat plate

Same as film diffusion control

1.3.2 Sphere

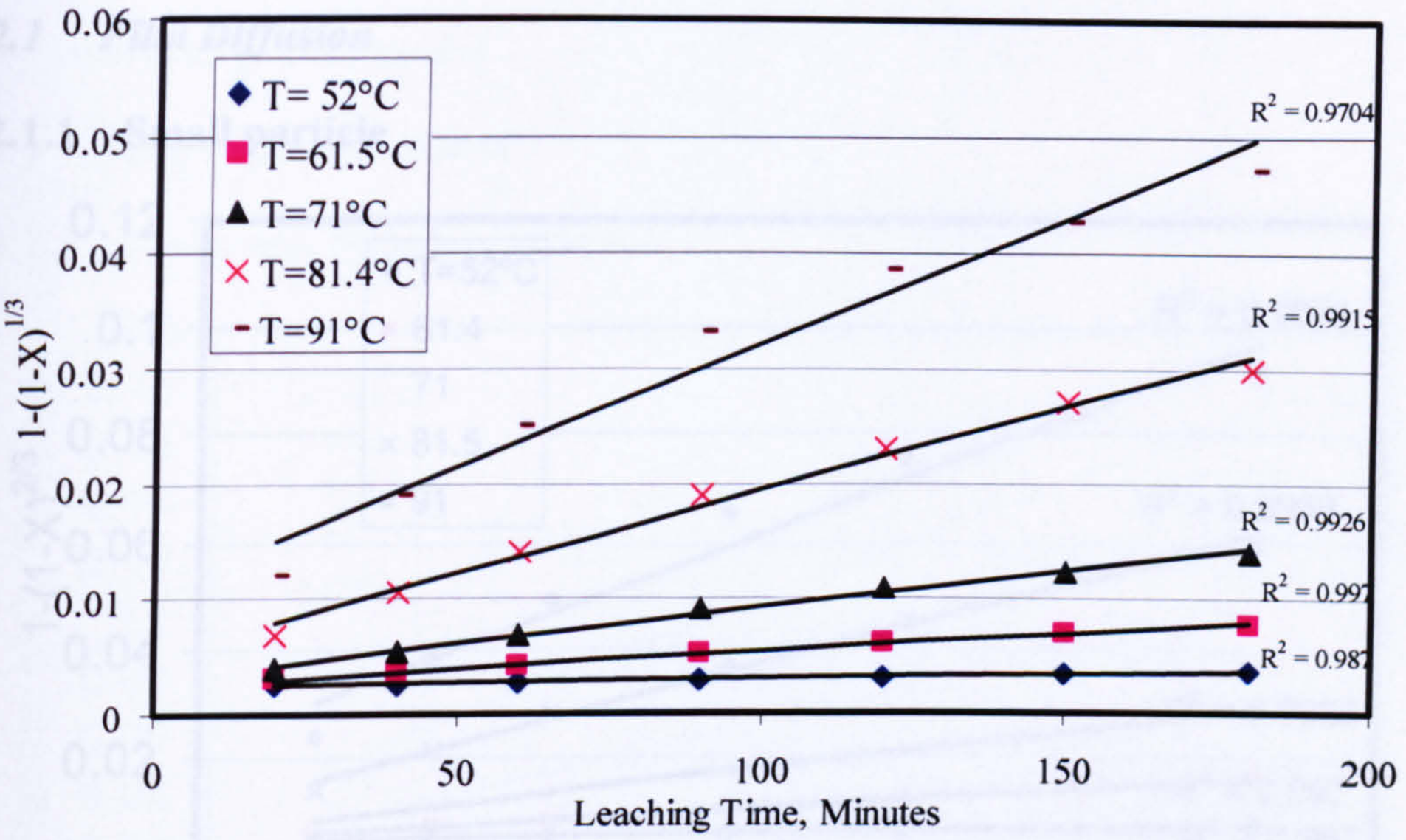

1.3.3 Cylinder

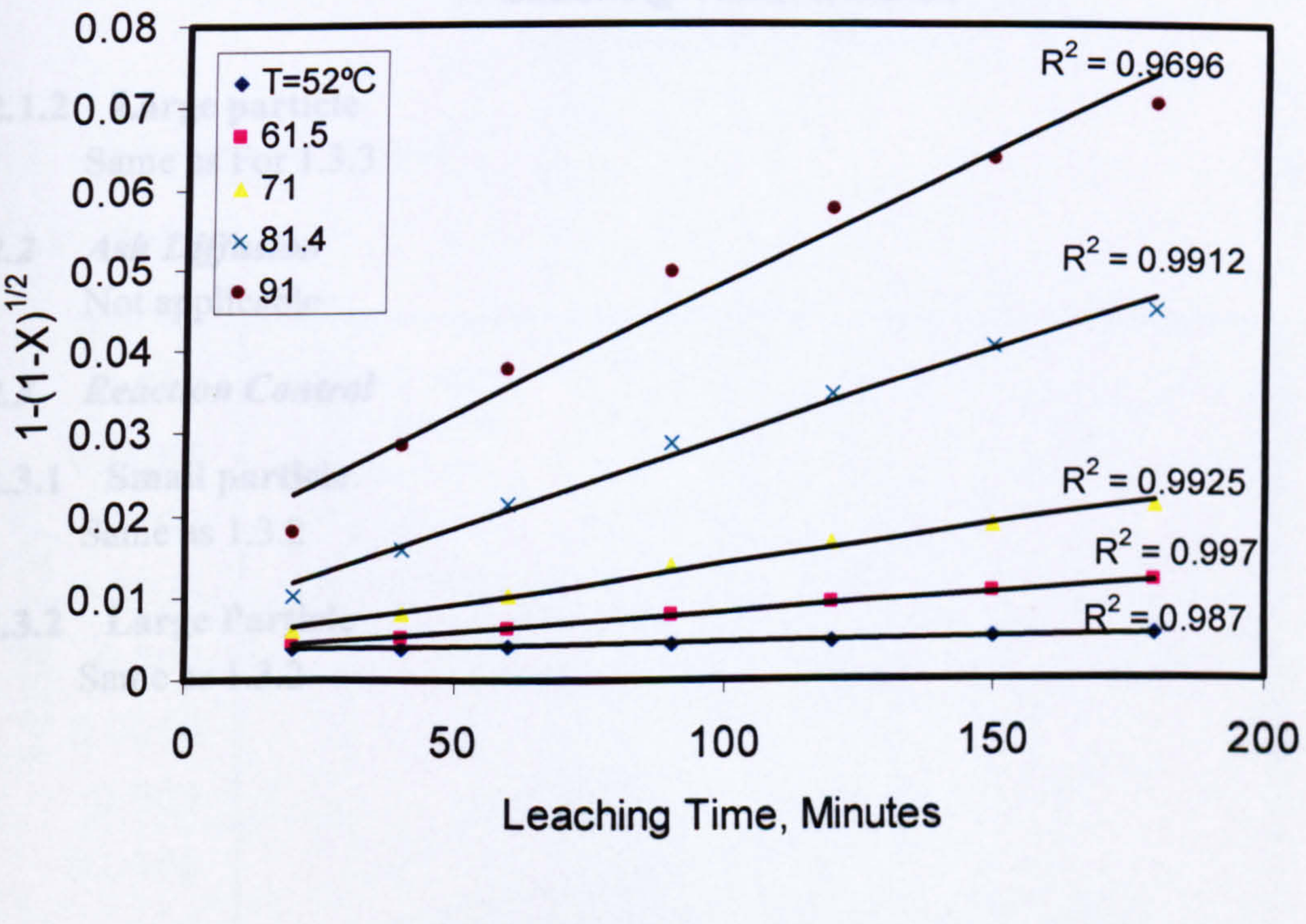

2 Shrinkage particle model

2.1 Film Diffusion

2.1.1 Small particle

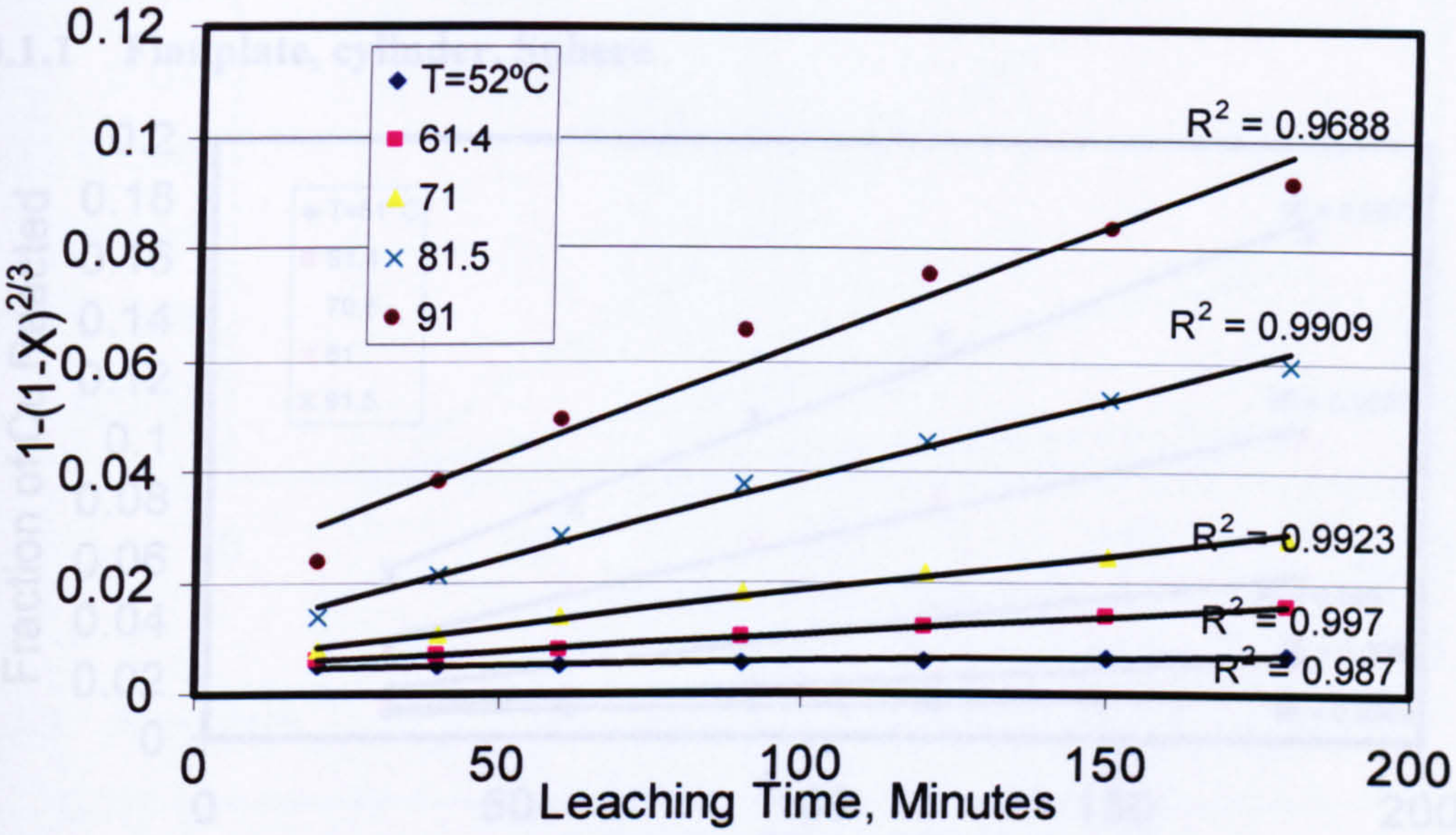

2.1.2 Large particle

Same as For 1.3.3

2.2 Ash Diffusion

Not applicable

2.3 Reaction Control

2.3.1 Small particle

Same as 1.3.2

2.3.2 Large Particle

Same as 1.3.2

3 Shrinkage core model

3.1 Film Diffusion control

3.1.1 Flat plate, cylinder, Sphere

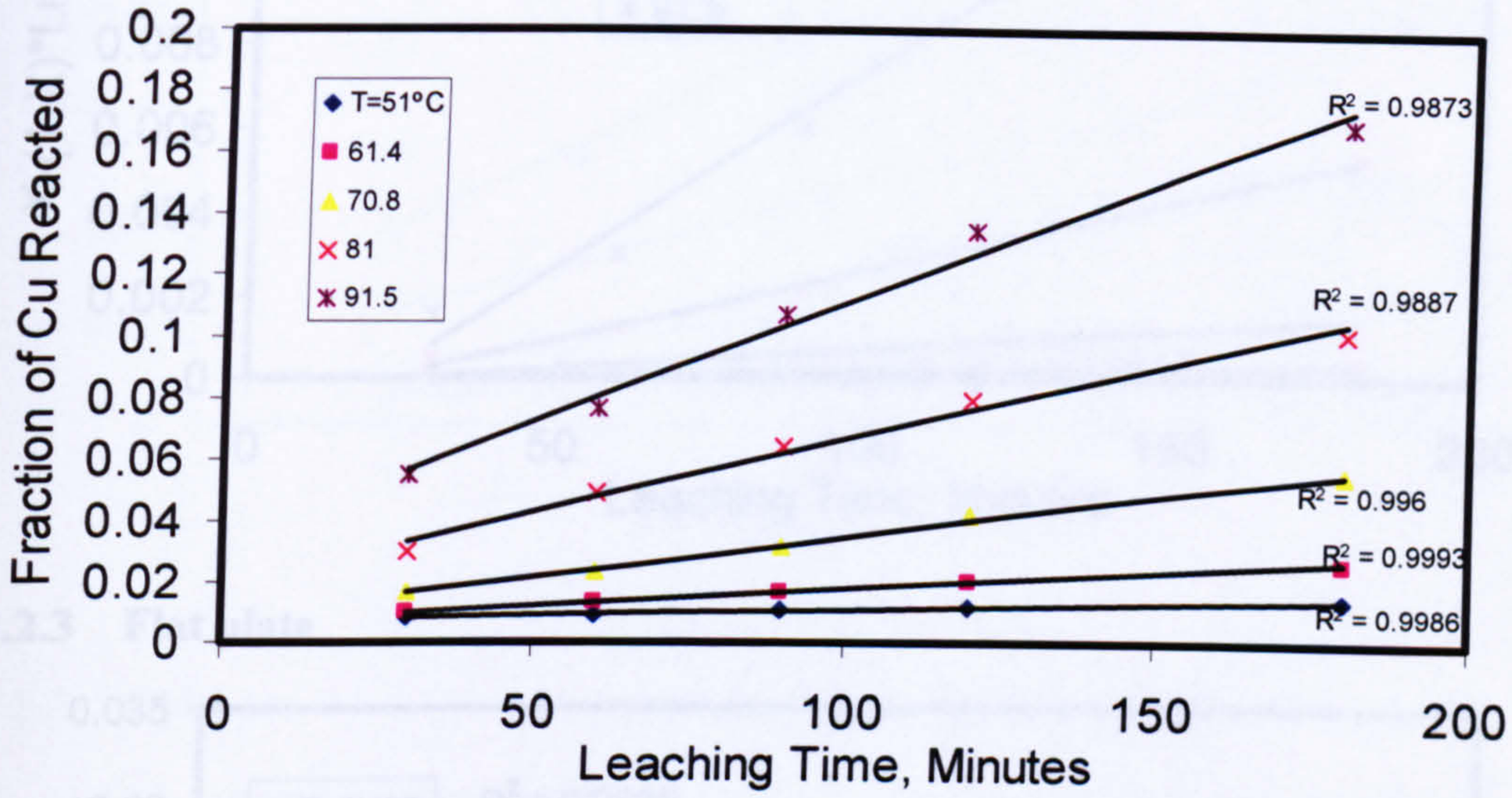

3.2 Ash diffusion control

3.2.1 Sphere

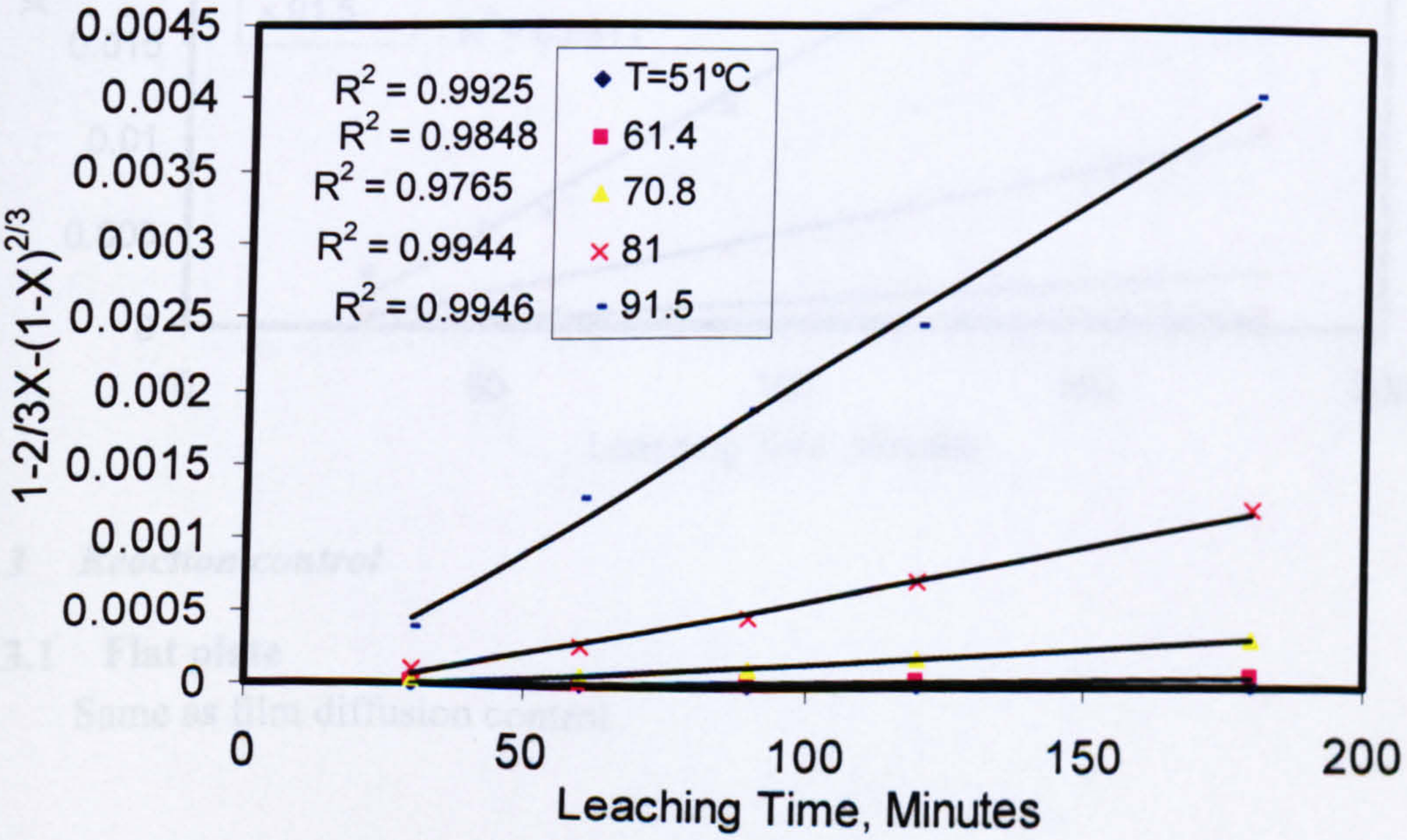

3.2.2 Cylinder

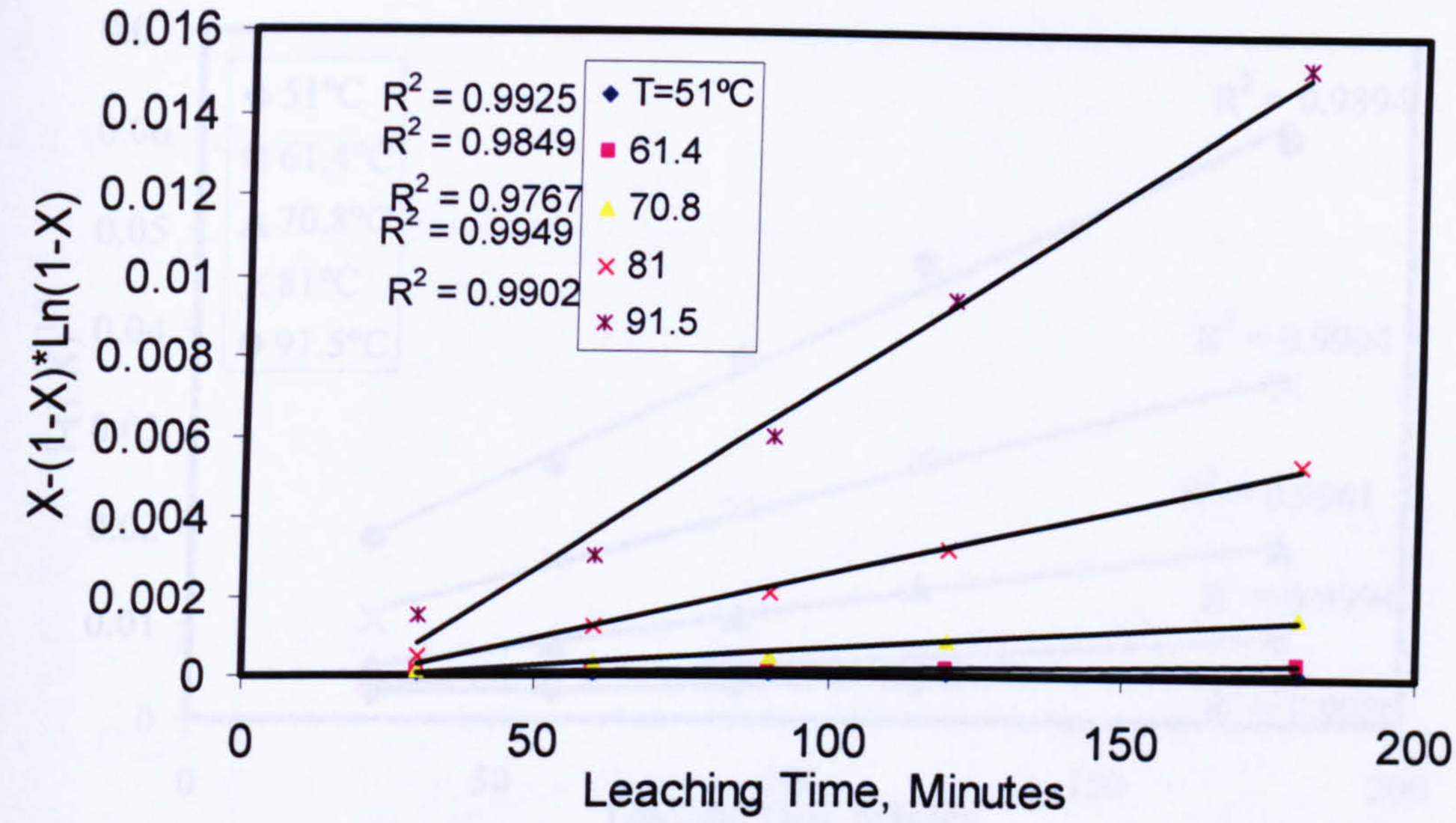

3.2.3 Flat plate

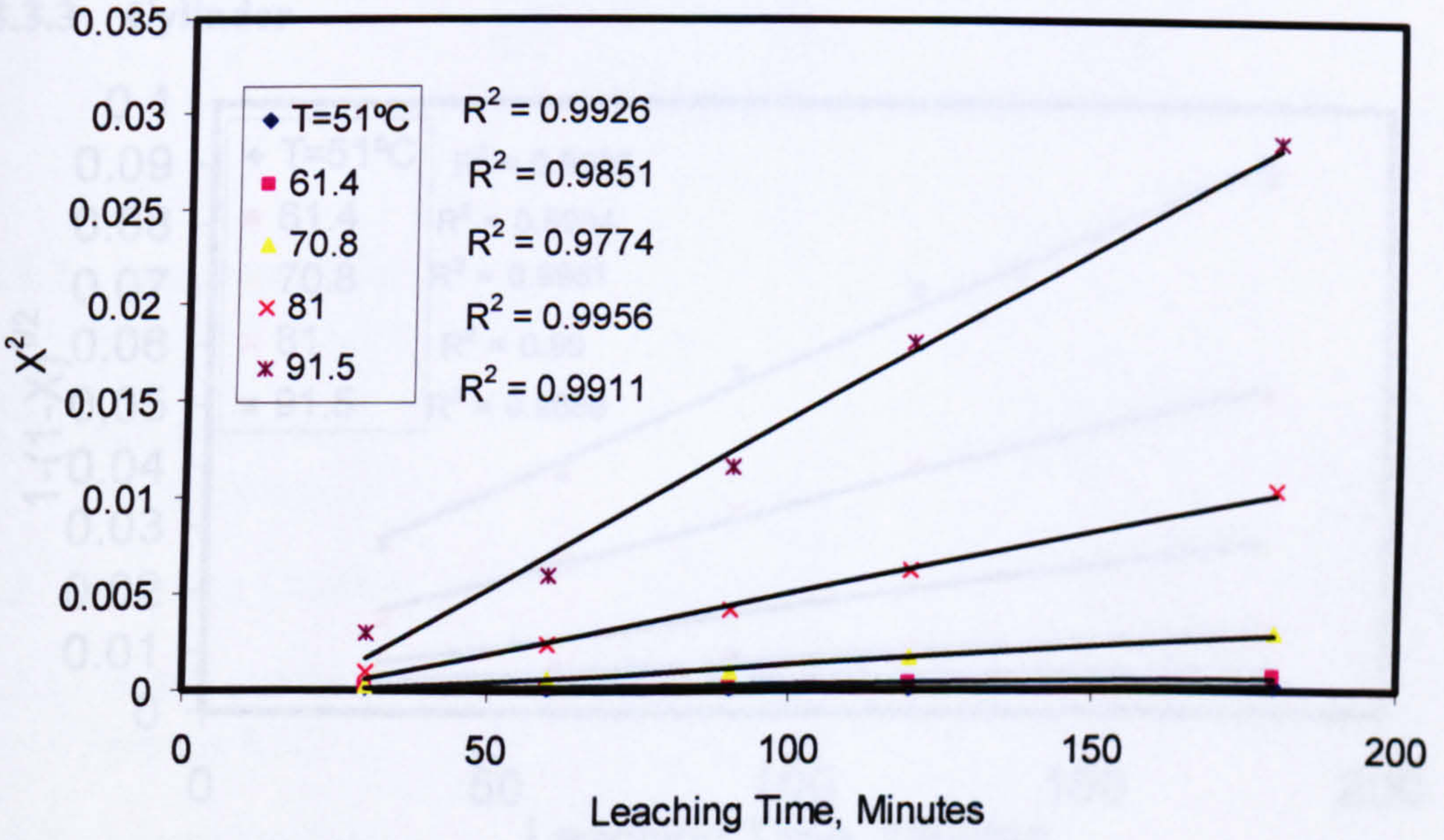

3.3 Reaction control

3.3.1 Flat plate

Same as film diffusion control

3.3.2 Sphere

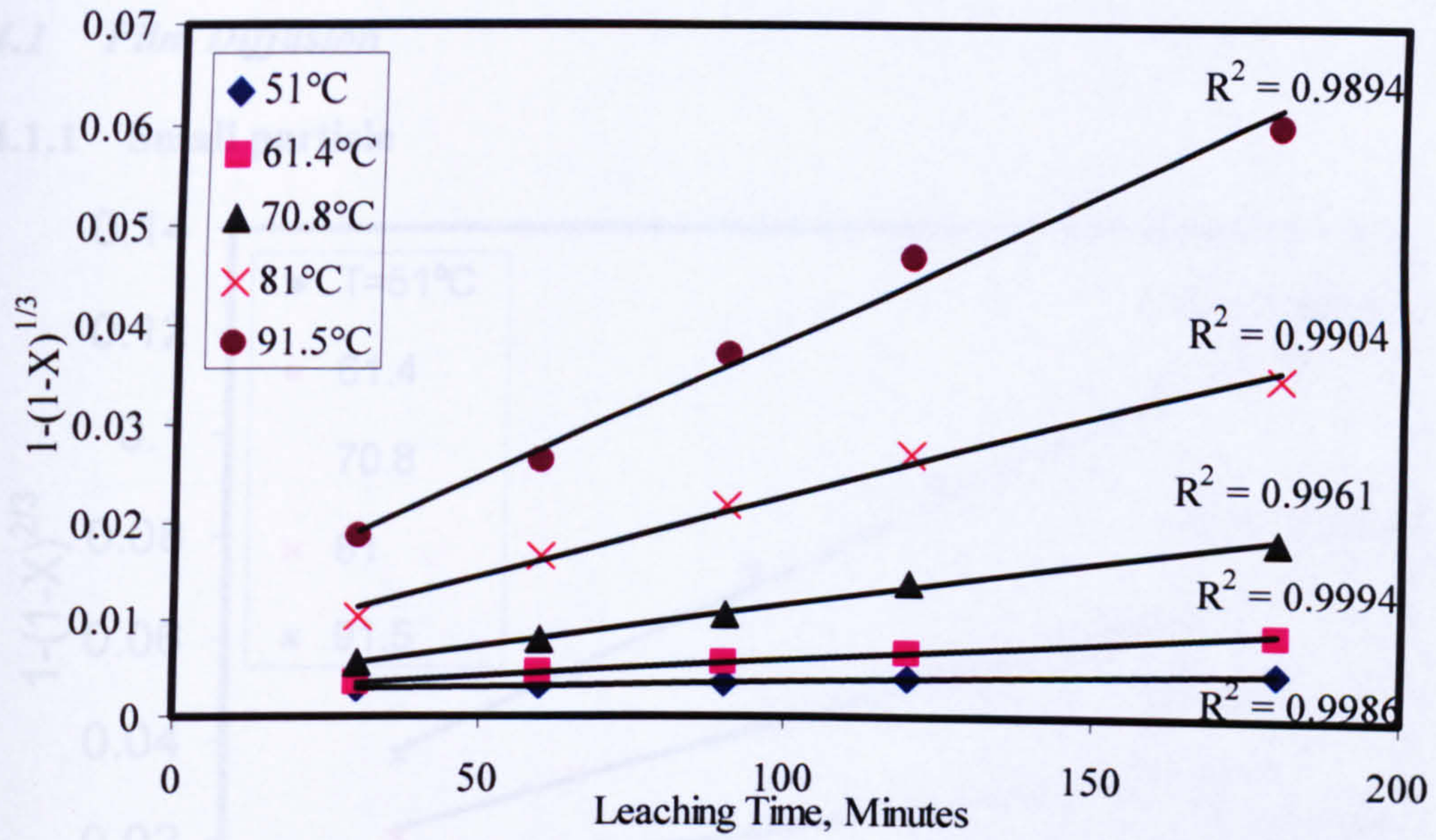

3.3.3 Cylinder

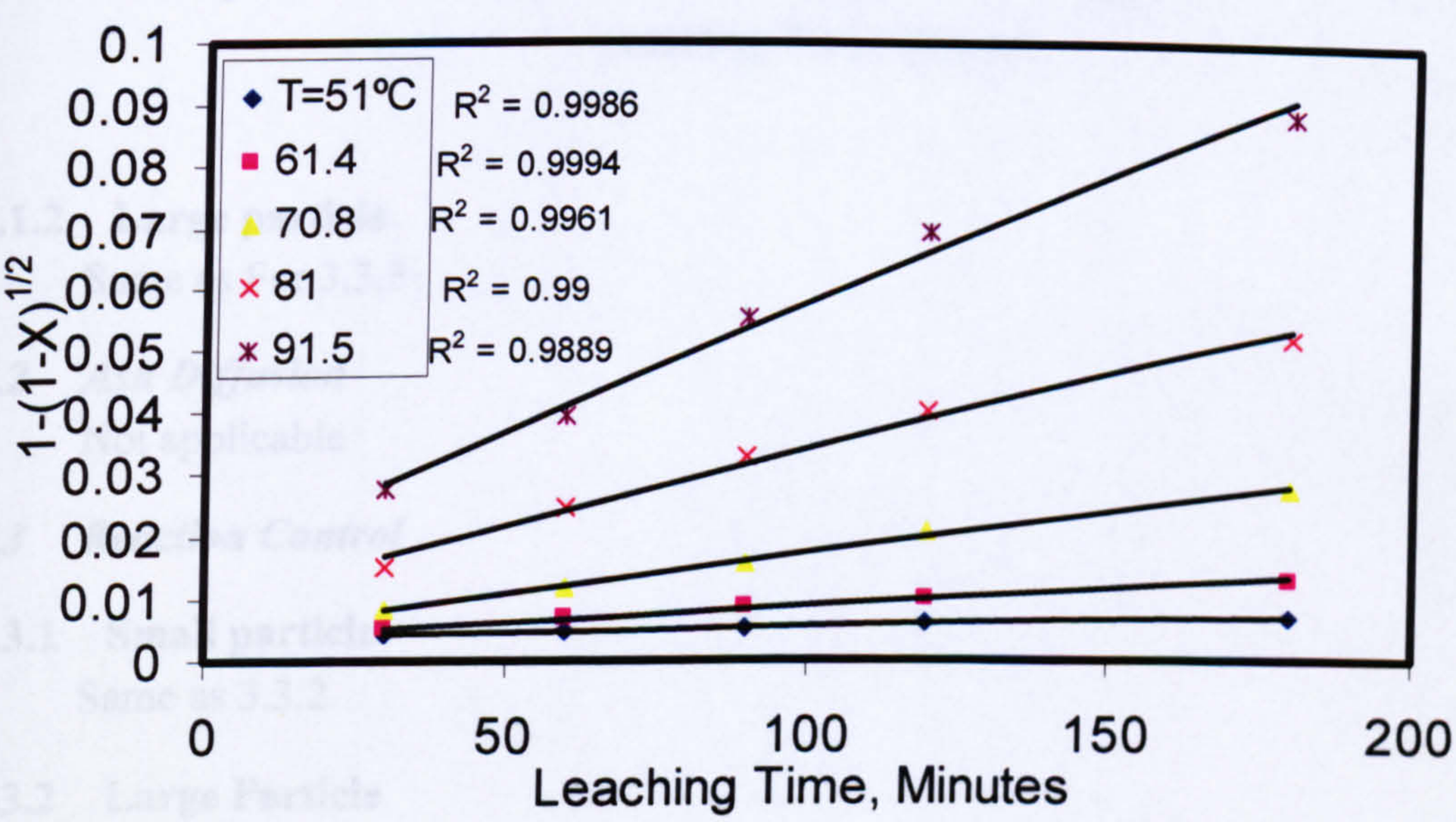

4 Shrinkage particle model

4.1 Film Diffusion

4.1.1 Small particle

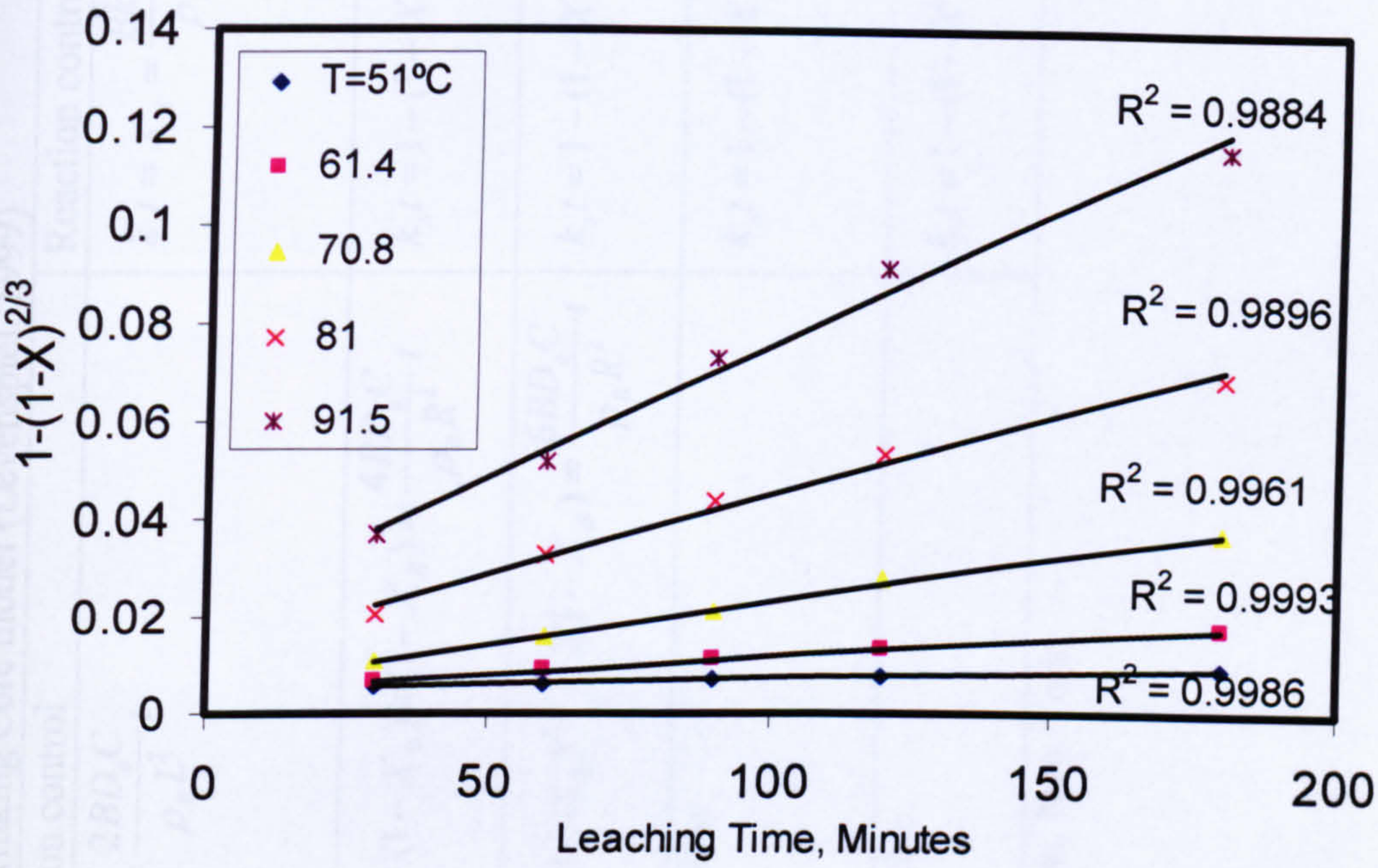

4.1.2 Large particle

Same as For 3.3.3

4.2 Ash Diffusion

Not applicable

4.3 Reaction Control

4.3.1 Small particle

Same as 3.3.2

4.3.2 Large Particle

Same as 3.3.2

Table 1 Conversion time expressions for various shapes and particles, Shrinking Core model (Levenspiel, 1999)

		Film diffusion control	Ash diffusion control	Reaction control
Constant size particles	**Flat plate** $X_B = 1 - \frac{1}{L}$ where L is half thickness	$k_f t = X_B = \frac{BkC}{\rho_B L} t$	$k_d t = X_B^2 = \frac{2BD_e C}{\rho_B L^2} t$	$k_s t = X_B = \frac{Bk''C}{\rho_B L} t$
	Cylinder $X_B = 1 - (\frac{r_c}{R})^2$	$k_f t = X_B = \frac{2BkC}{\rho_B R} t$	$k_d t = X_B + (1 - X_B)\ln(1 - X_B) = \frac{4BD_e C}{\rho_B R^2} t$	$k_s t = 1 - (1 - X_B)^{0.5} = \frac{Bk''C}{\rho_B R} t$
	Sphere $X_B = 1 - (\frac{r_c}{R})^3$	$k_f t = X_B = \frac{3BkC}{\rho_B R} t$	$k_d t = 1 - 3(1 - X_B)^{2/3} + 2(1 - X_B) = \frac{6BD_e C}{\rho_B R^2} t$	$k_s t = 1 - (1 - X_B)^{1/3} = \frac{Bk''C}{\rho_B R} t$
Shrinking sphere	**Small particle** Stockes regime	$k_f t = 1 - (1 - X_B)^{2/3} = \frac{2BDC}{\rho_B R_0^2} t$	Not applicable	$k_s t = 1 - (1 - X_B)^{1/3} = \frac{Bk''C}{\rho_B R} t$
	Large particle (u=constant)	$k_f t = 1 - (1 - X_B)^{1/2} = (const)\frac{C}{R_0^{3/2}} t$	Not applicable	$k_s t = 1 - (1 - X_B)^{1/3} = \frac{Bk''C}{\rho_B R} t$

Levenspiel, O., 1999. Chemical Reaction Engineering. John Wiley & Sons, New York.

Appendix 4-16. Concentration map of positive and negative ions acquired from a freshly cleaved GBL chalcopyrite

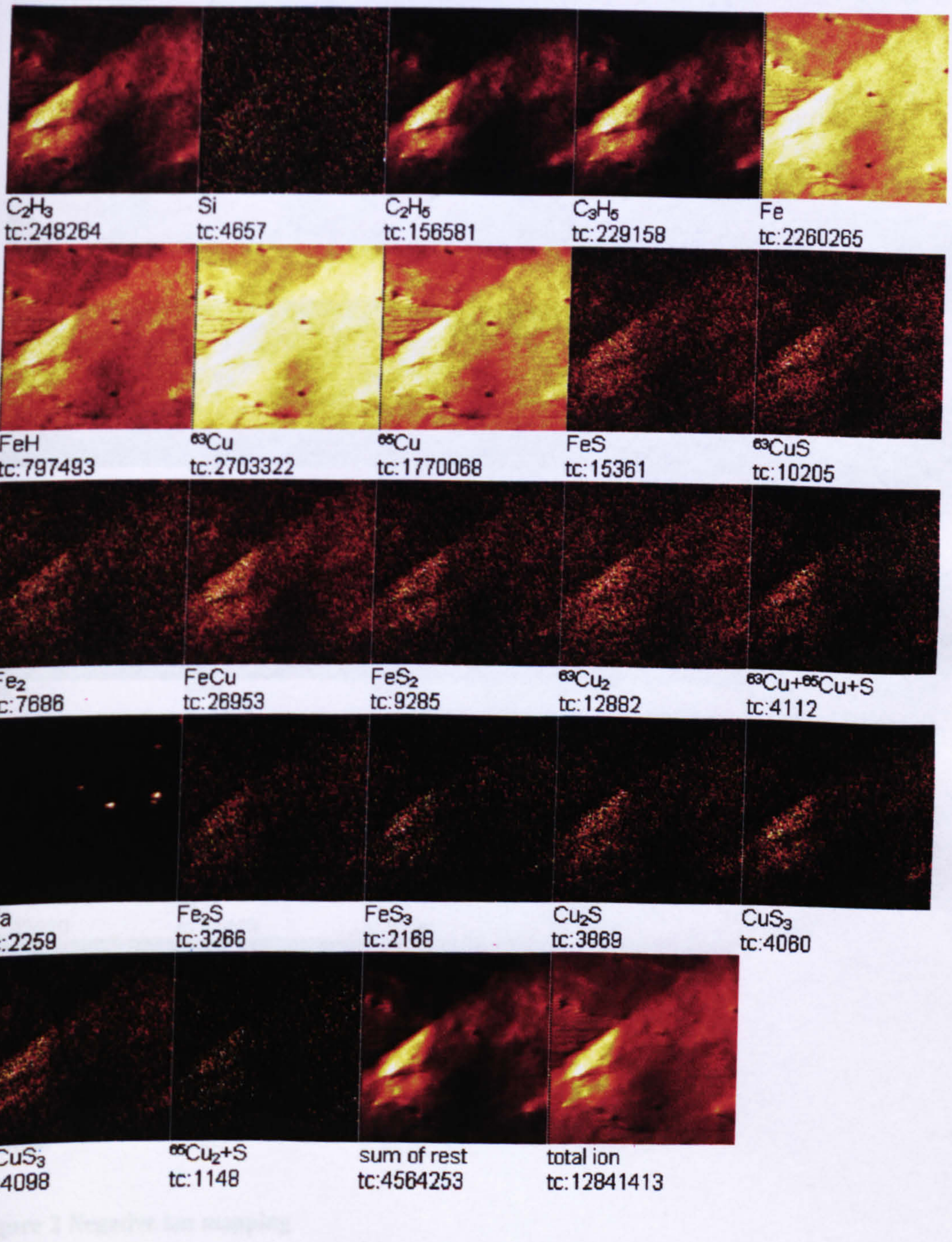

Figure 1 Positive ion mapping

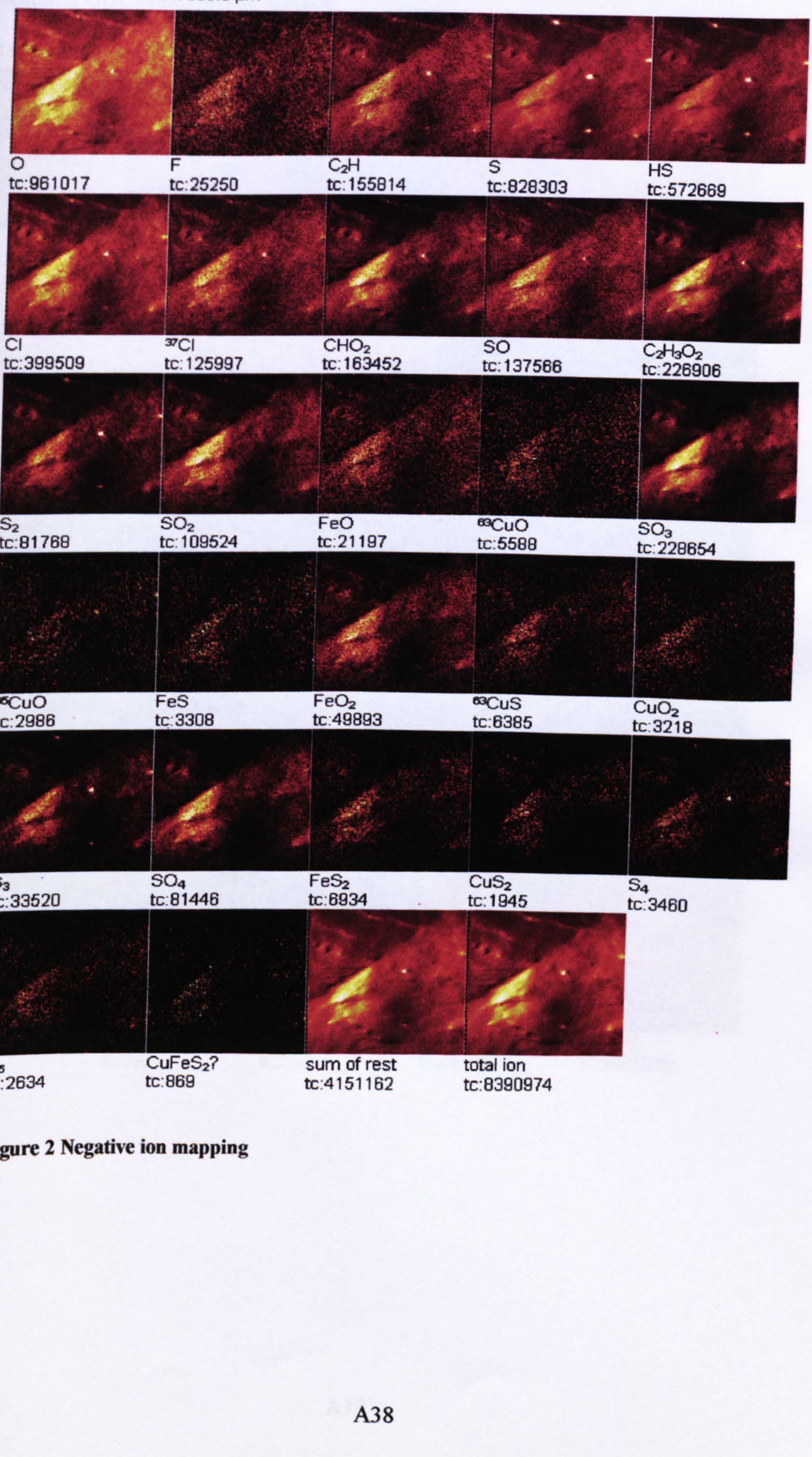

Figure 2 Negative ion mapping

Appendix 4-17. Concentration map of the positive and negative ions acquired from the leached GBL chalcopyrite surface.

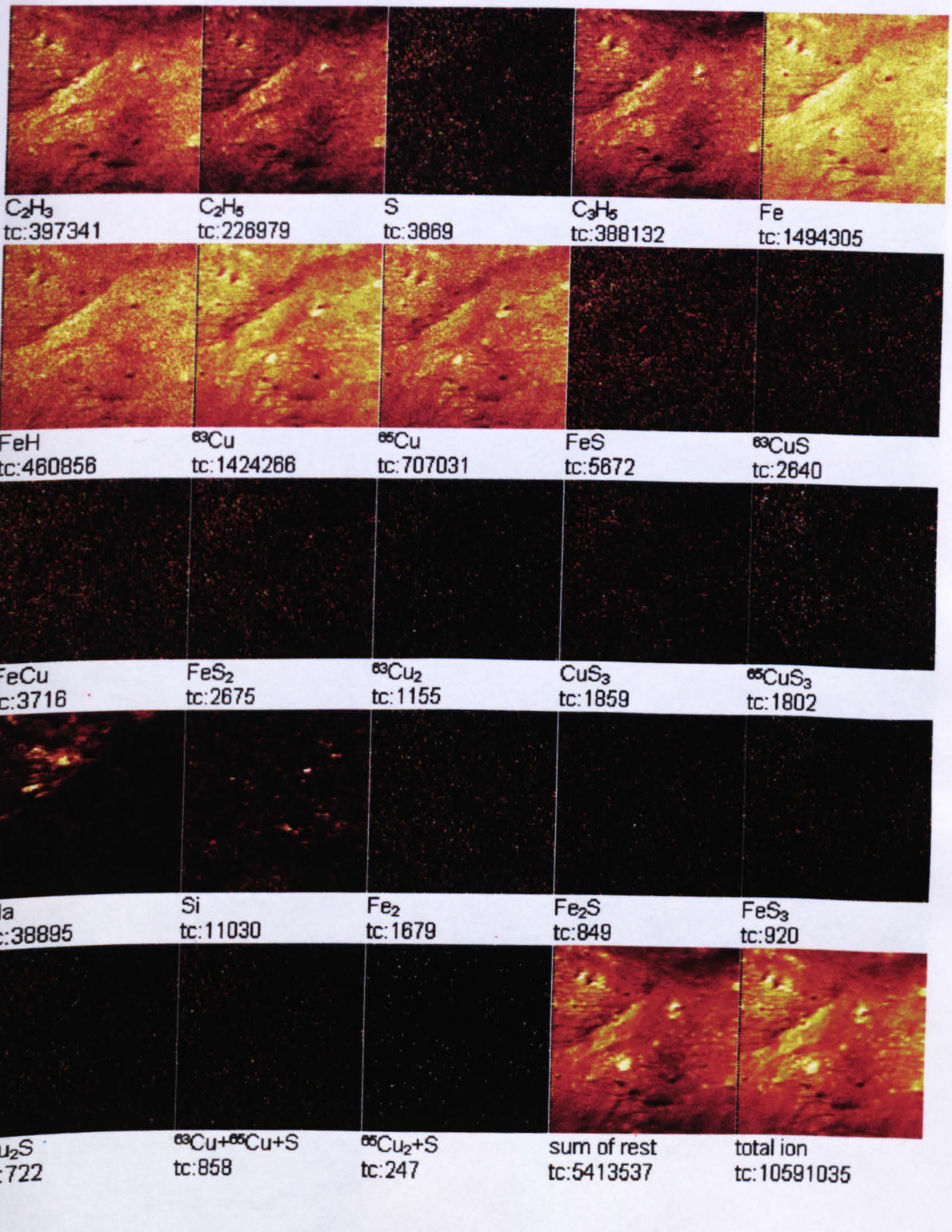

Field of view: 500.0 x 500.0 µm²

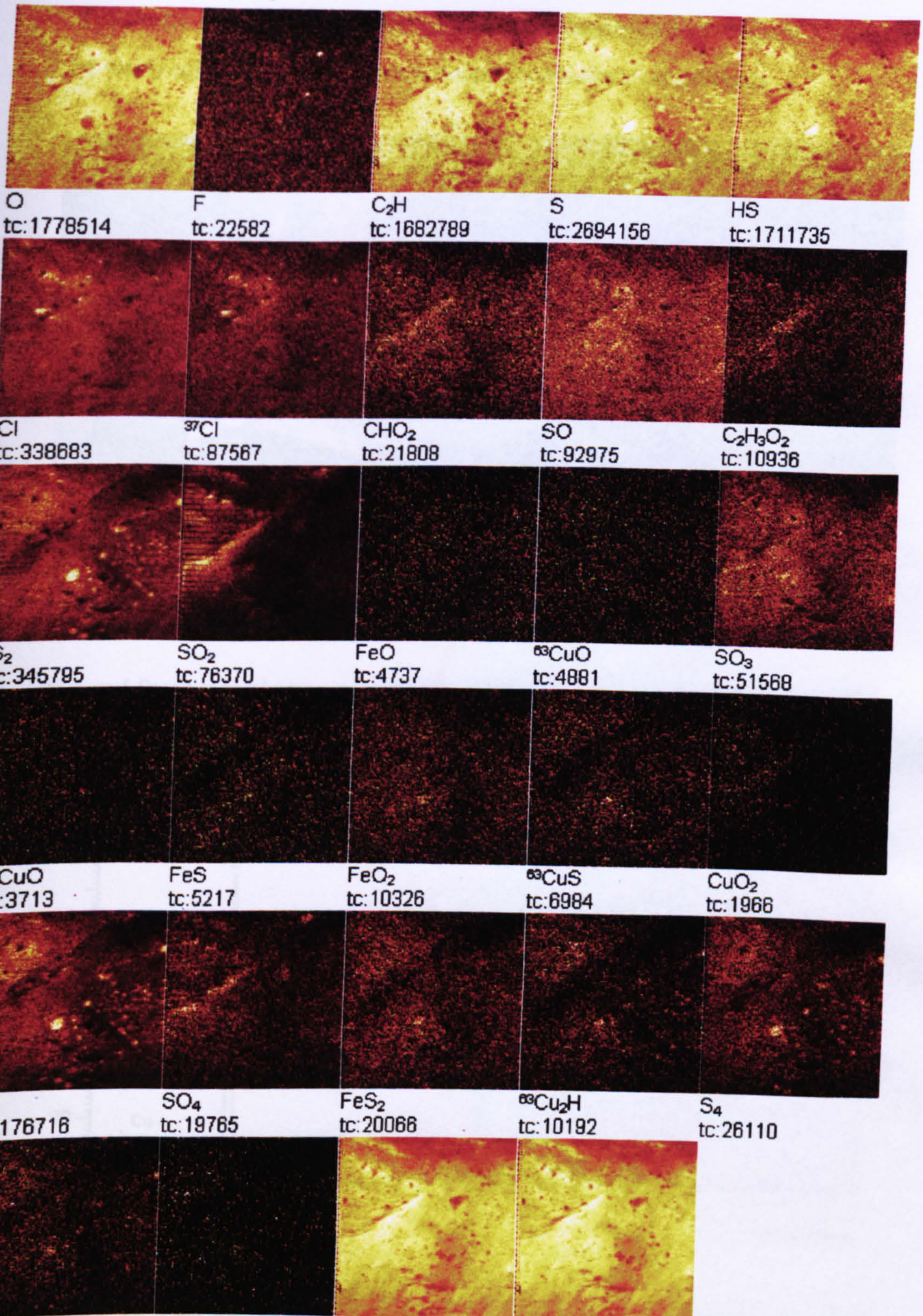

O
tc:1778514

F
tc:22582

C_2H
tc:1682789

S
tc:2694156

HS
tc:1711735

Cl
tc:338683

^{37}Cl
tc:87567

CHO_2
tc:21808

SO
tc:92975

$C_2H_3O_2$
tc:10936

S_2
tc:345795

SO_2
tc:76370

FeO
tc:4737

^{63}CuO
tc:4881

SO_3
tc:51568

^{65}CuO
tc:3713

FeS
tc:5217

FeO_2
tc:10326

^{63}CuS
tc:6984

CuO_2
tc:1966

S_3
tc:176716

SO_4
tc:19765

FeS_2
tc:20066

$^{63}Cu_2H$
tc:10192

S_4
tc:26110

S_5
tc:7845

$CuFeS_2$?
tc:1805

sum of rest
tc:13228555

total ion
tc:22444356

Positive after treatment for m14

Appendix 4-18. SEM analysis of MZ2HE chalcopyrite (<25µm) leached in 0.25 M ferric sulphate for three hours under conventional conditions.

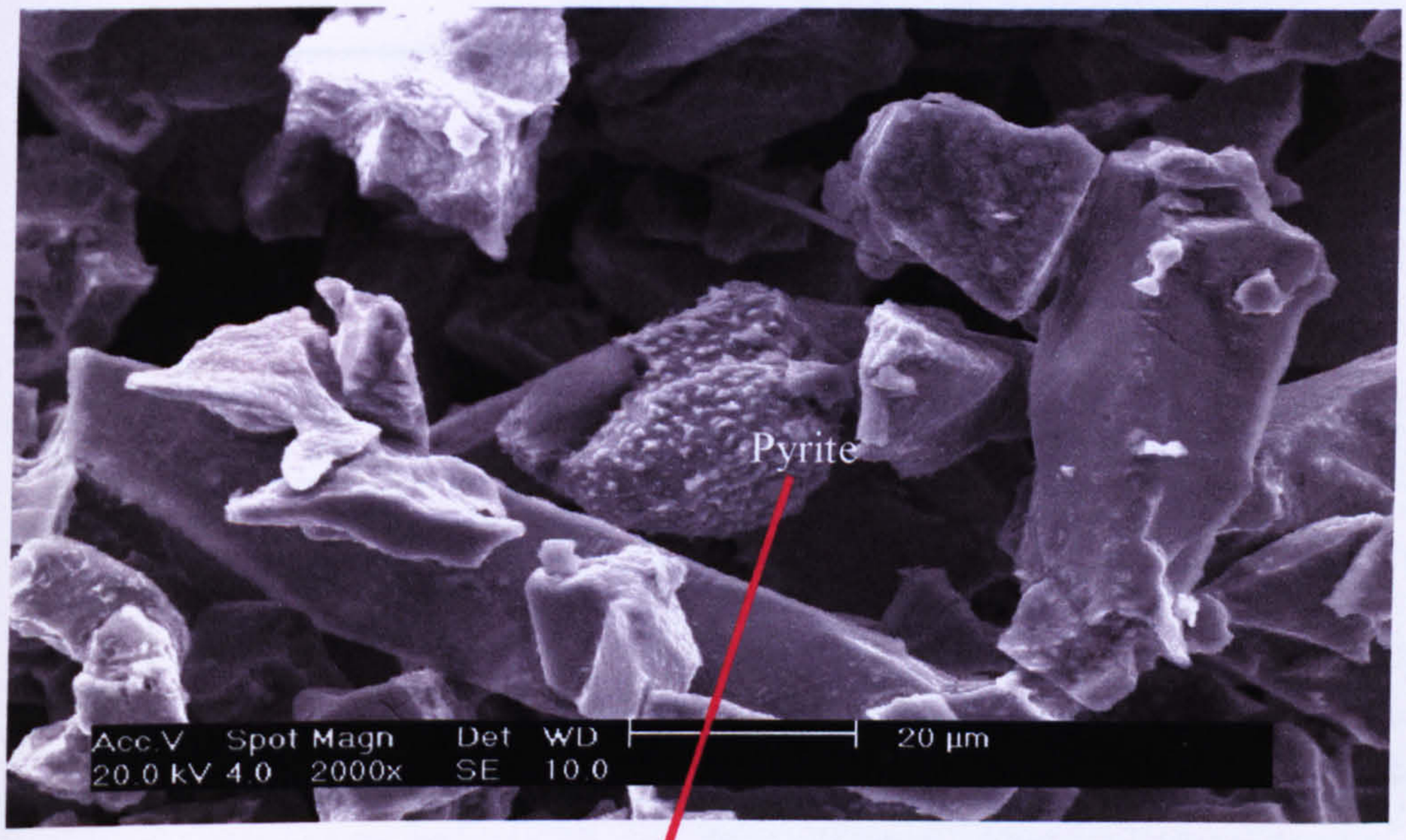

Figure 1 Secondary Electron micrograph of MZ2HE chalcopyrite (<25µm) leached in 0.25M ferric sulphate for three hours under conventional conditions. Attacked pyrite particle (middle of the graph)

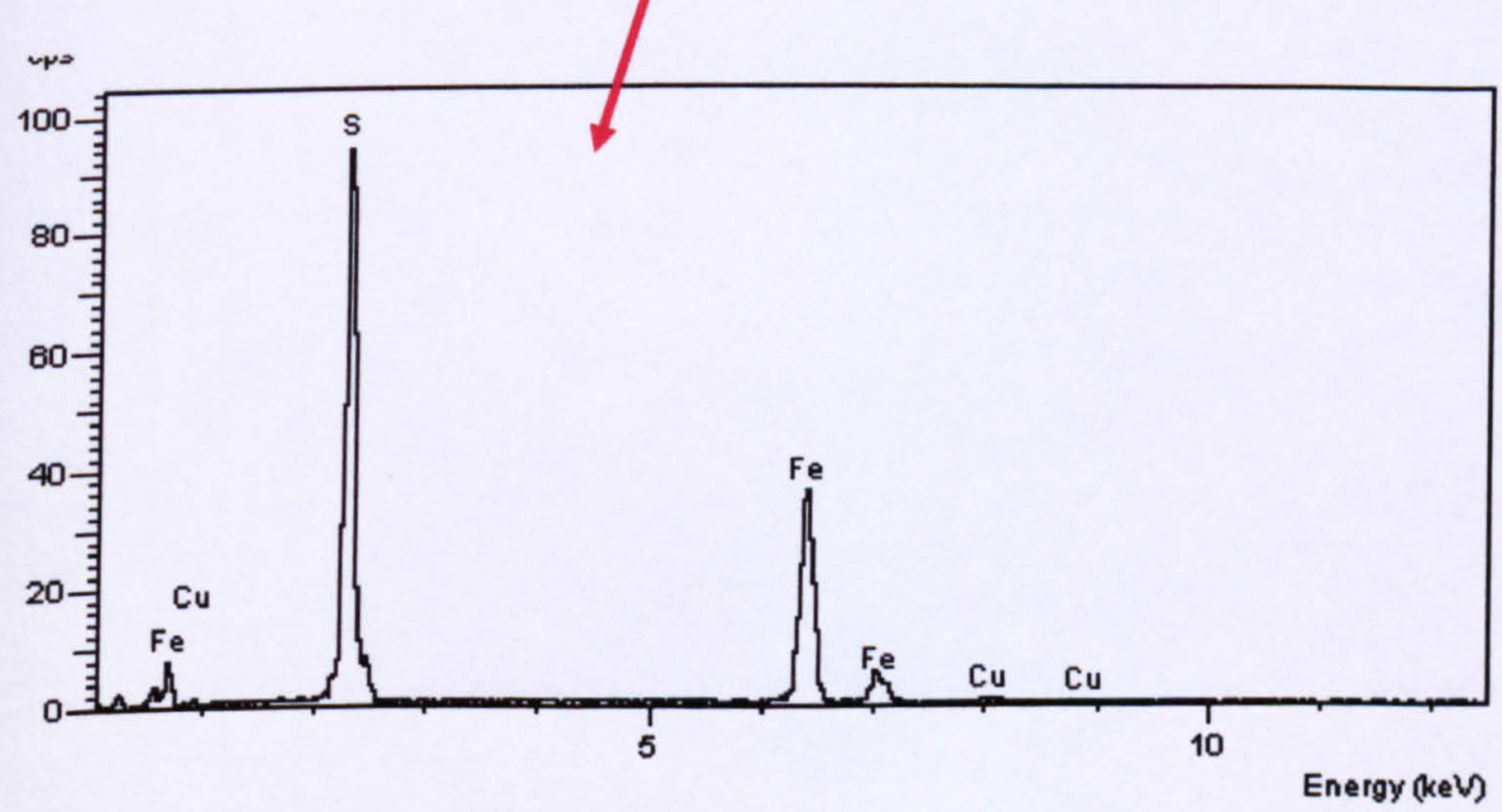

Figure 2. EDX pattern acquired from the surface of pyrite particle shown by the arrow.

Appendix 4-19. Temperature profile during microwave leaching in MARS X® at a temperature of 91°C

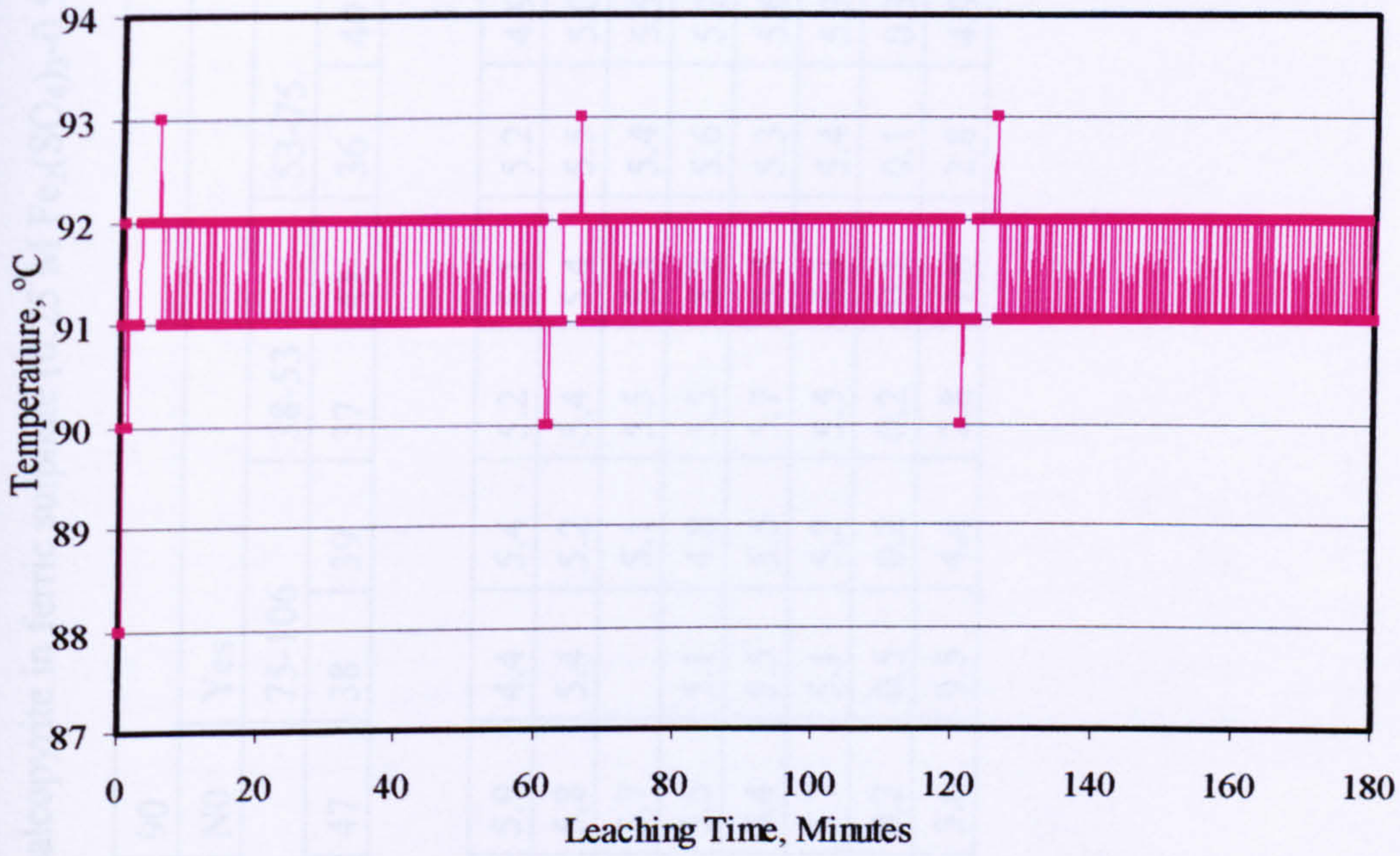

Appendix 4-20 Molar ratio of Fe/Cu calculated for microwave leaching of chalcopyrite in ferric sulphate (0.25 M $Fe_2(SO_4)_3$-0.5 M H_2SO_4)

T, °C	50	60	70	80	90	100	90						
Stirring	Yes						N0	Yes					
Particle size, μm	<38							75-106		38-53		53-75	
Leach No	43	44	45	46	35	51	47	38	39	37	41	36	40
Leaching Time, Min		Fe/Cu											
30	3.7	4.1	4.3	5.8	5.7	5.4	5.9	4.4	5.4	5.2	5.1	5.2	4.9
60	3.6	4.2	4.8	6.1	5.7	5.3	5.8	5.4	5.2	5.4	5.4	5.5	5.0
90	3.5	4.4	5.4	5.9	5.5	5.3	5.7		5.1	5.5	5.3	5.4	5.5
120	3.5	4.4	5.7	5.8	5.5	5.5	5.5	5.1	4.8	5.5	5.2	5.6	5.2
180	3.6	5.2	5.6	5.7	5.2	5.7	5.4	5.5	5.5	5.7	5.4	5.3	5.6
Average	3.6	4.5	5.2	5.9	5.5	5.5	5.7	5.1	5.2	5.5	5.3	5.4	5.3
Standard Deviation	0.1	0.4	0.5	0.1	0.2	0.2	0.2	0.5	0.2	0.2	0.1	0.1	0.3
RSD (%)	2.5	8.9	10.5	2.5	2.8	2.8	3.6	9.5	4.4	2.8	1.6	2.8	4.9

Appendix 4-21 Treatment of the kinetic data for microwave leaching in ferric sulphate ($C_{Fe2(SO4)3}$: 0.25 M, particle size: <38 μm)

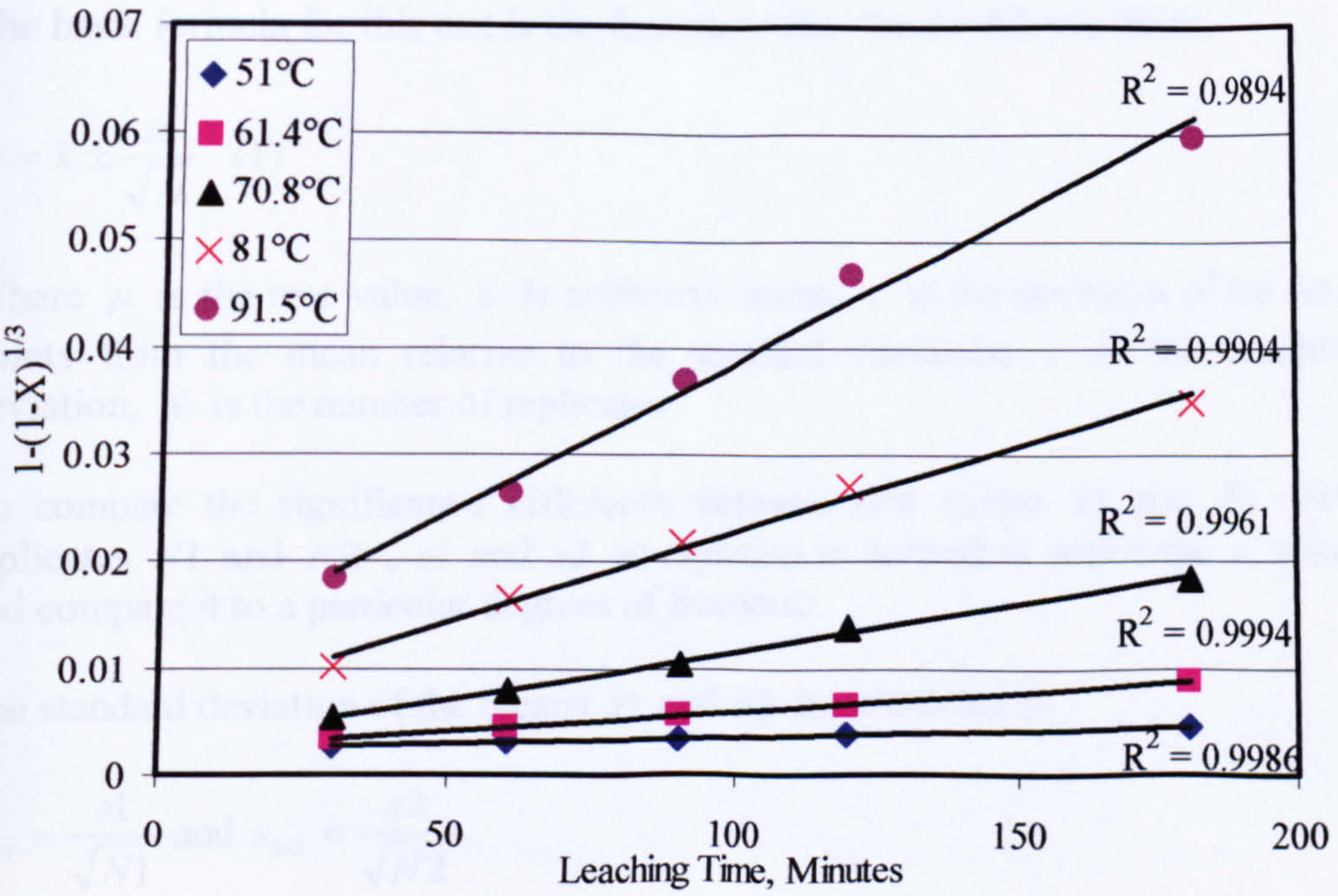

Figure 1 Plot fitted using a shrinking core model with limited step of surface reaction for rate data of microwave leaching of GBL chalcopyrite in ferric sulphate

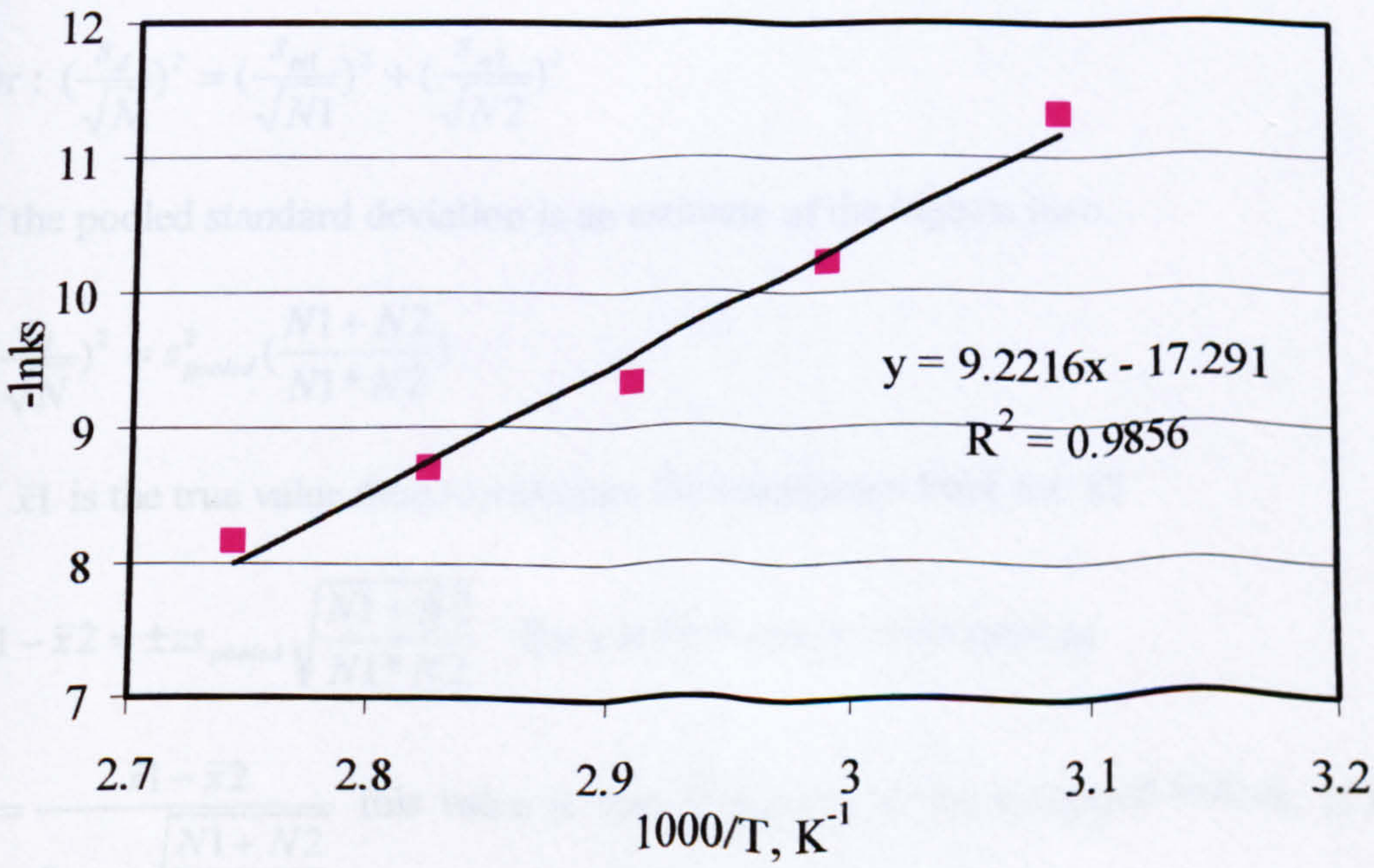

Figure 2 Arrhenius plot for microwave leaching of GBL chalcopyrite in ferric sulphate

Appendix 4-22

Testing for the statistical significance of the difference between two means:

The basic formula for this test is the formula to find the confidence limits

$$\mu = \bar{x} \pm \frac{zs}{\sqrt{N}} \quad (1)$$

Where μ is the true value, $\bar{x}$ is arithmetic mean, z is the deviation of the data points from the mean relative to the standard deviation, s is the standard deviation, N is the number of replicates.

To compare the significance difference between two means $\bar{x}1$ and $\bar{x}2$ with replicates $N1$ and $N2$, $s1$ and $s2$ an equation is derived to assess the z value and compare it to a particular degrees of freedom:

The standard deviation of the means $\bar{x}1$ and $\bar{x}2$ is calculated as

$$s_{m1} = \frac{s1}{\sqrt{N1}} \text{ and } s_{m2} = \frac{s2}{\sqrt{N2}}$$

The variance between the differences of the means can be calculated as:

$$s_d^2 = s_{m1}^2 + s_{m2}^2$$

$$\text{Or : } (\frac{s_d}{\sqrt{N}})^2 = (\frac{s_{m1}}{\sqrt{N1}})^2 + (\frac{s_{m2}}{\sqrt{N2}})^2$$

If the pooled standard deviation is an estimate of the highest then

$$(\frac{s_d}{\sqrt{N}})^2 = s_{pooled}^2 (\frac{N1+N2}{N1*N2})$$

If $\bar{x}1$ is the true value then to calculate the confidence limit for $\bar{x}2$

$\bar{x}1 - \bar{x}2 = \pm z s_{pooled} \sqrt{\frac{N1+N2}{N1*N2}}$ The z is then can be calculated as

$z = \frac{\bar{x}1 - \bar{x}2}{s_{pooled} \sqrt{\frac{N1+N2}{N1*N2}}}$ this value is then compared to the tabulated values. If the calculated z is less than the tabulated then the difference between the means is insignificant at confidence level used and vice versa.

Appendix 4-23. Coagulation of chalcopyrite at low stirring speed

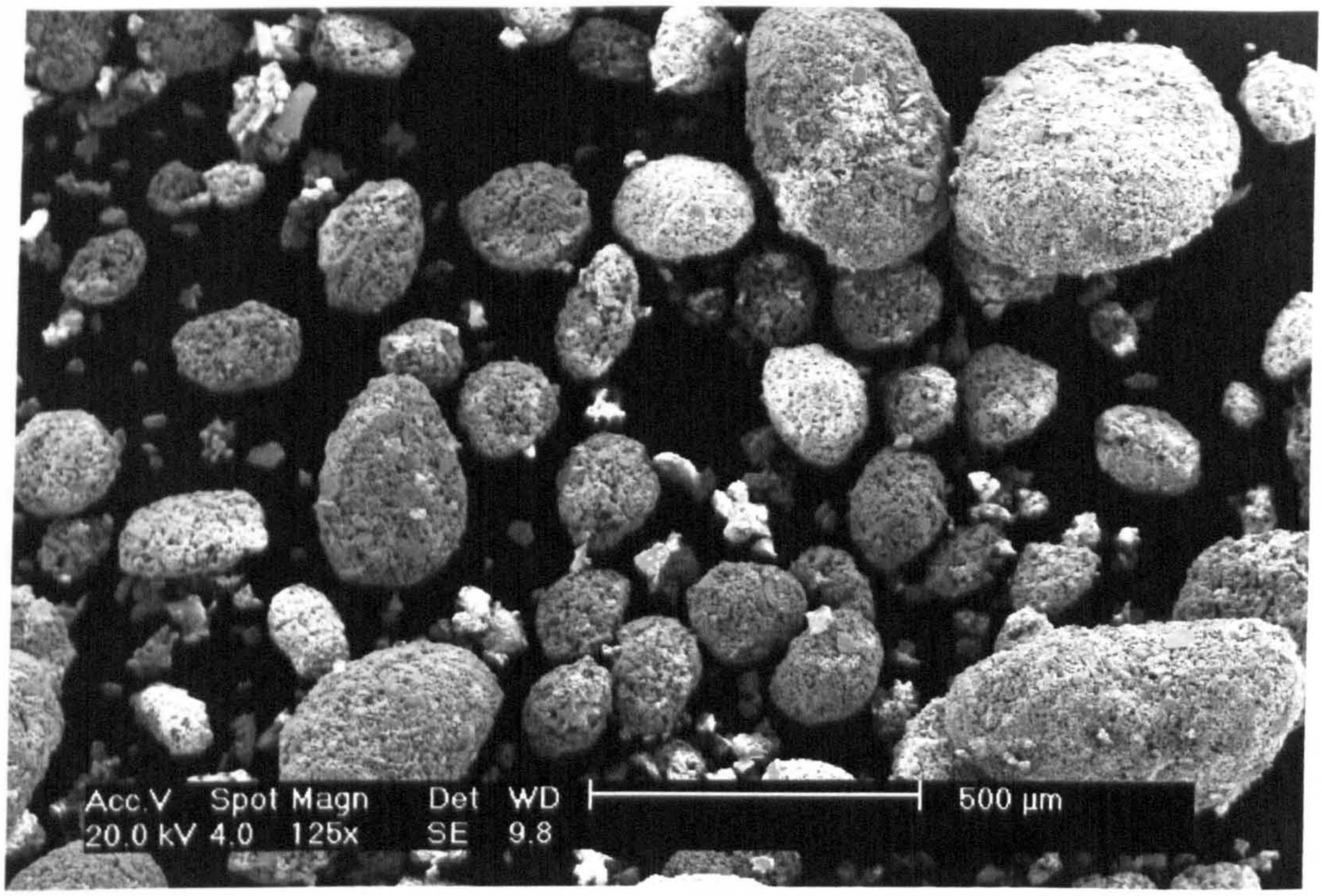

Appendix 4-24. Kinetic study on the dissolution of chalcopyrite in ferric chloride under conventional conditions.

The model involving surface reaction control was chosen to describe the kinetic data presented in Section 4.5.1.1. The plot of $1-(1-X)^{1/3}$ versus time is shown in Figure 1. The apparent rate constants calculated is presented in Table 1. The Arrhenius plot is shown in Figure 2. The calculated activation energy of the dissolution of chalcopyrite in ferric chloride is about 69 kJ/mole. This value is general agreement of the literature values presented in Appendix 3-1.

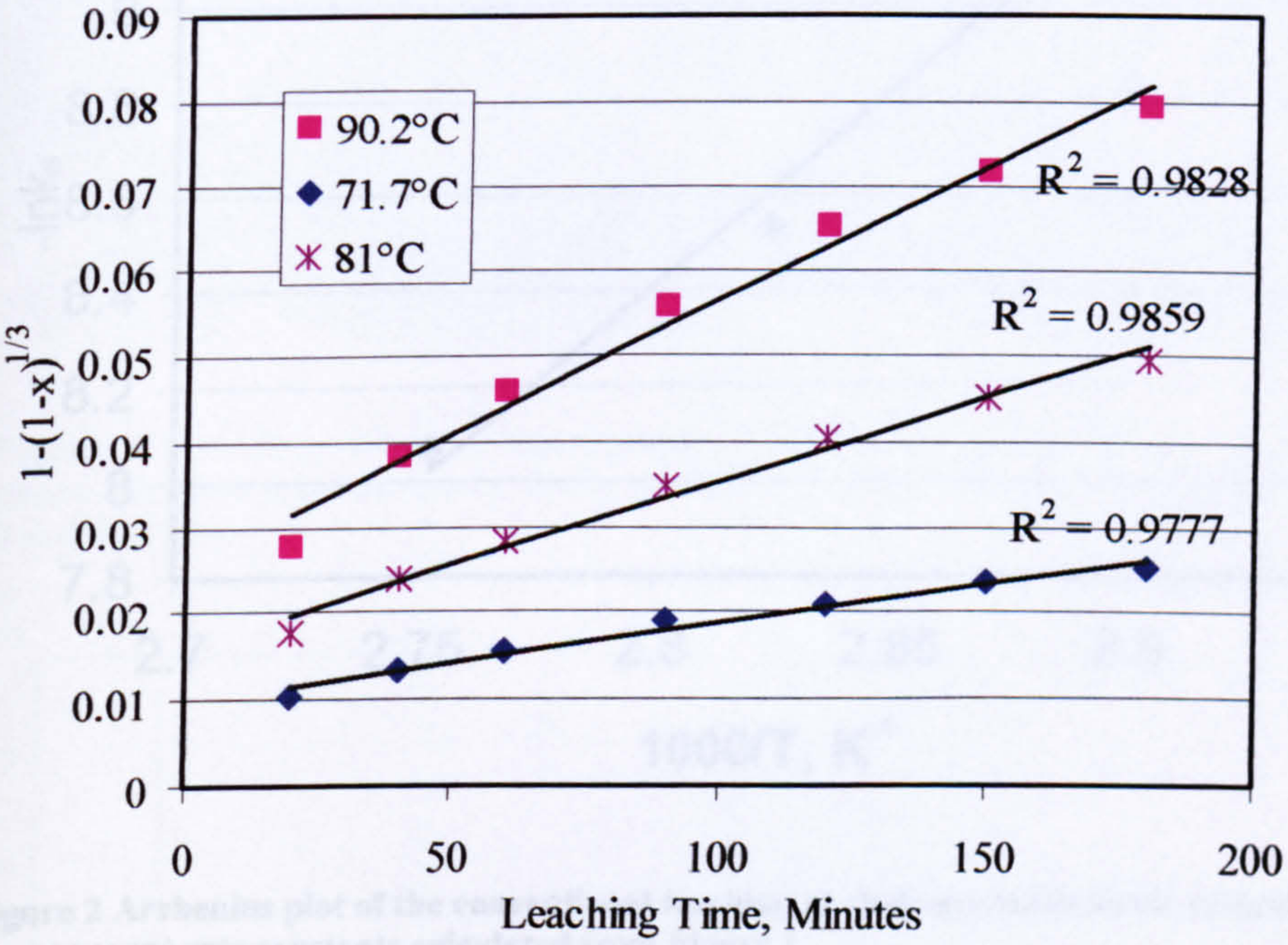

Figure 1 Plot fitted using a shrinking core model with a limiting step of surface reaction: conversion vs. time data of GBL chalcopyrite dissolution in ferric chloride at various temperatures.

Table 1 Apparent rate constant calculate for chalcopyrite leaching in ferric leaching at various temperatures

T, °C	1000*k_S , Min^{-1}	R^2
71.7	0.092	0.978
81	0.196	0.986
90.2	0.314	0.983

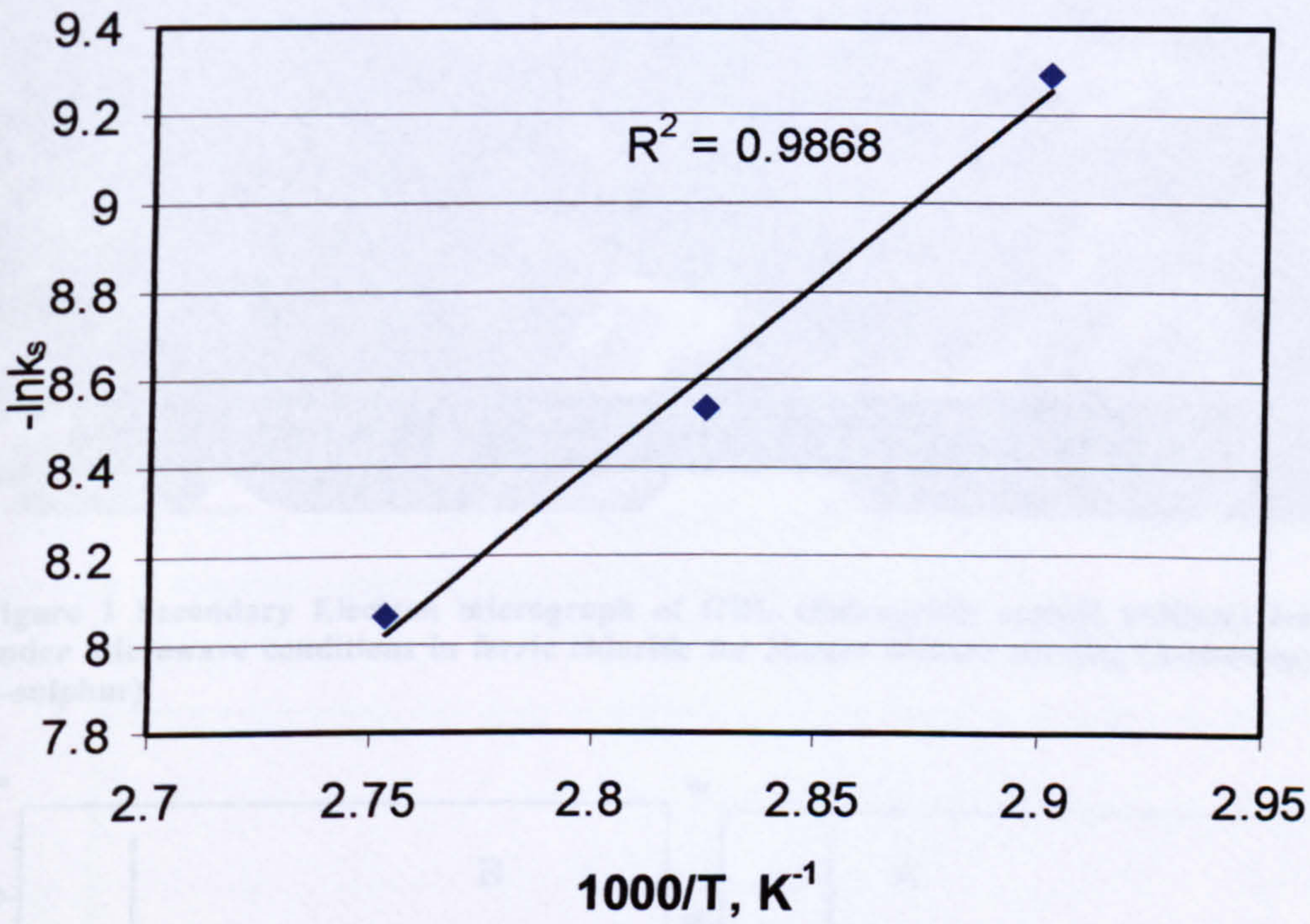

Figure 2 Arrhenius plot of the conventional leaching of chalcopyrite in ferric chloride based on the apparent rate constants calculated from Figure 1

Appendix 4-25. SEM analysis of chalcopyrite residue after being leached under microwave conditions for 3 hours in ferric chloride without agitation

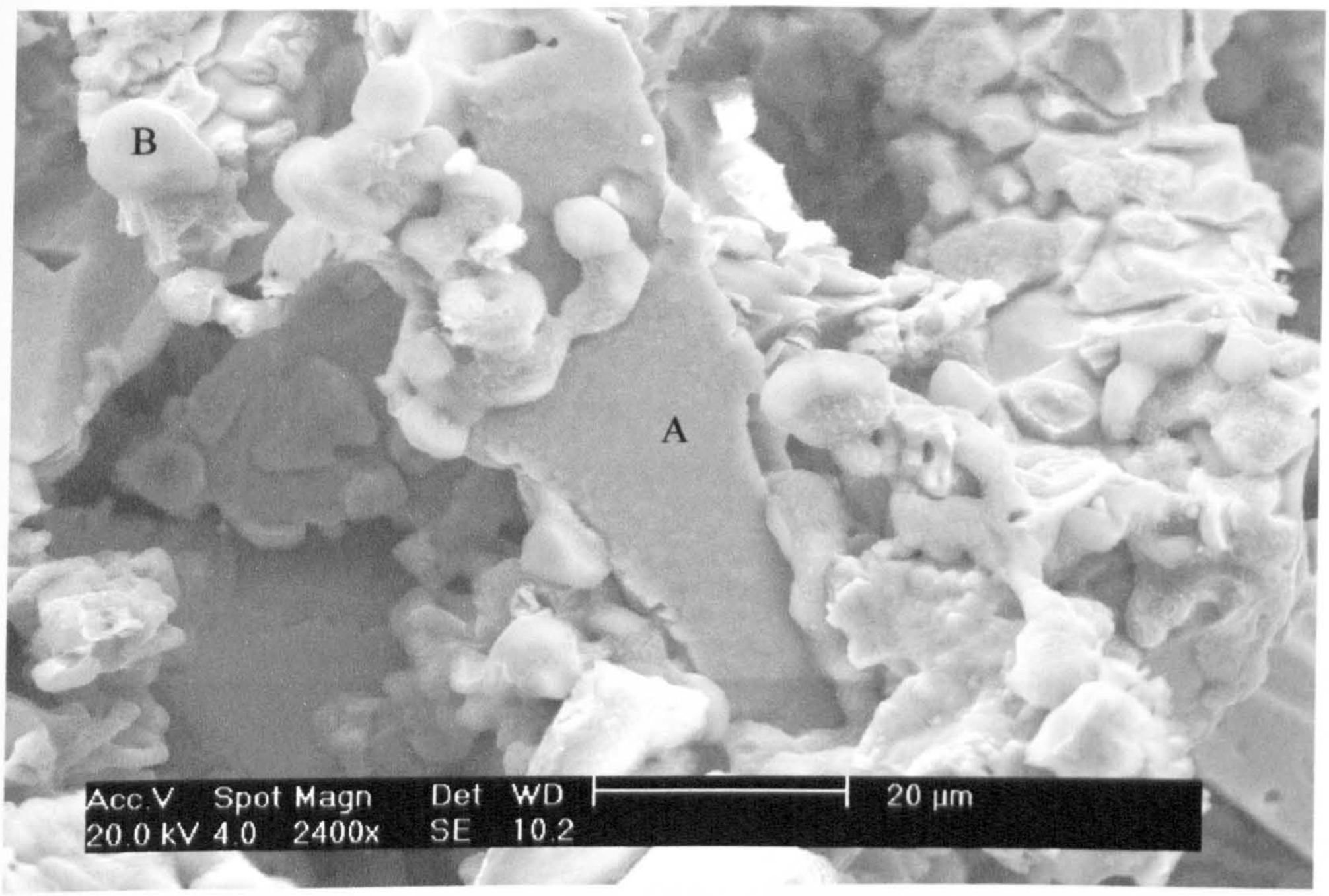

Figure 1 Secondary Electron micrograph of GBL chalcopyrite sample (<38µm) leached under microwave conditions in ferric chloride for 3hours without stirring (A-chalcopyrite, B-sulphur)

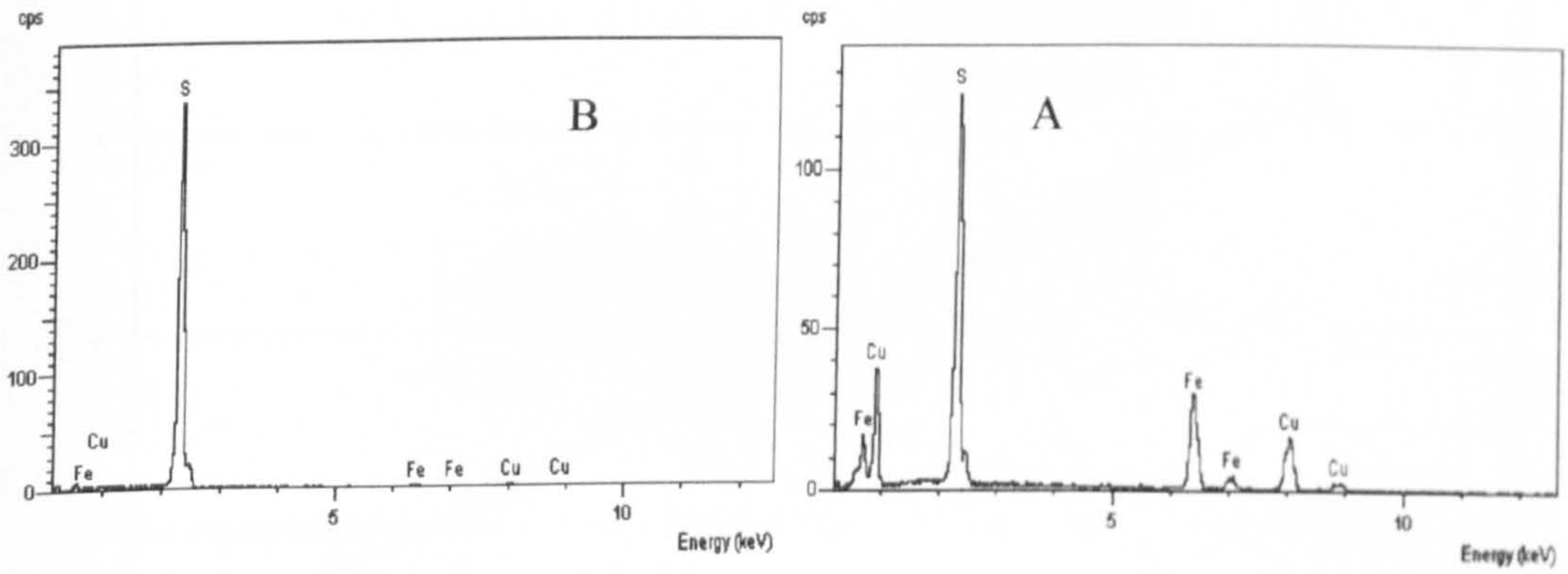

Figure 2 EDX signal obtained from locations A and B in Figure 1 showing that A is chalcopyrite particle whereas B is sulphur particle

Appendix 4-26 Treatment of the kinetic data for microwave leaching of GBL chalcopyrite in ferric chloride (C_{FeCl3}: 0.5 M, particle size: <38 μm)

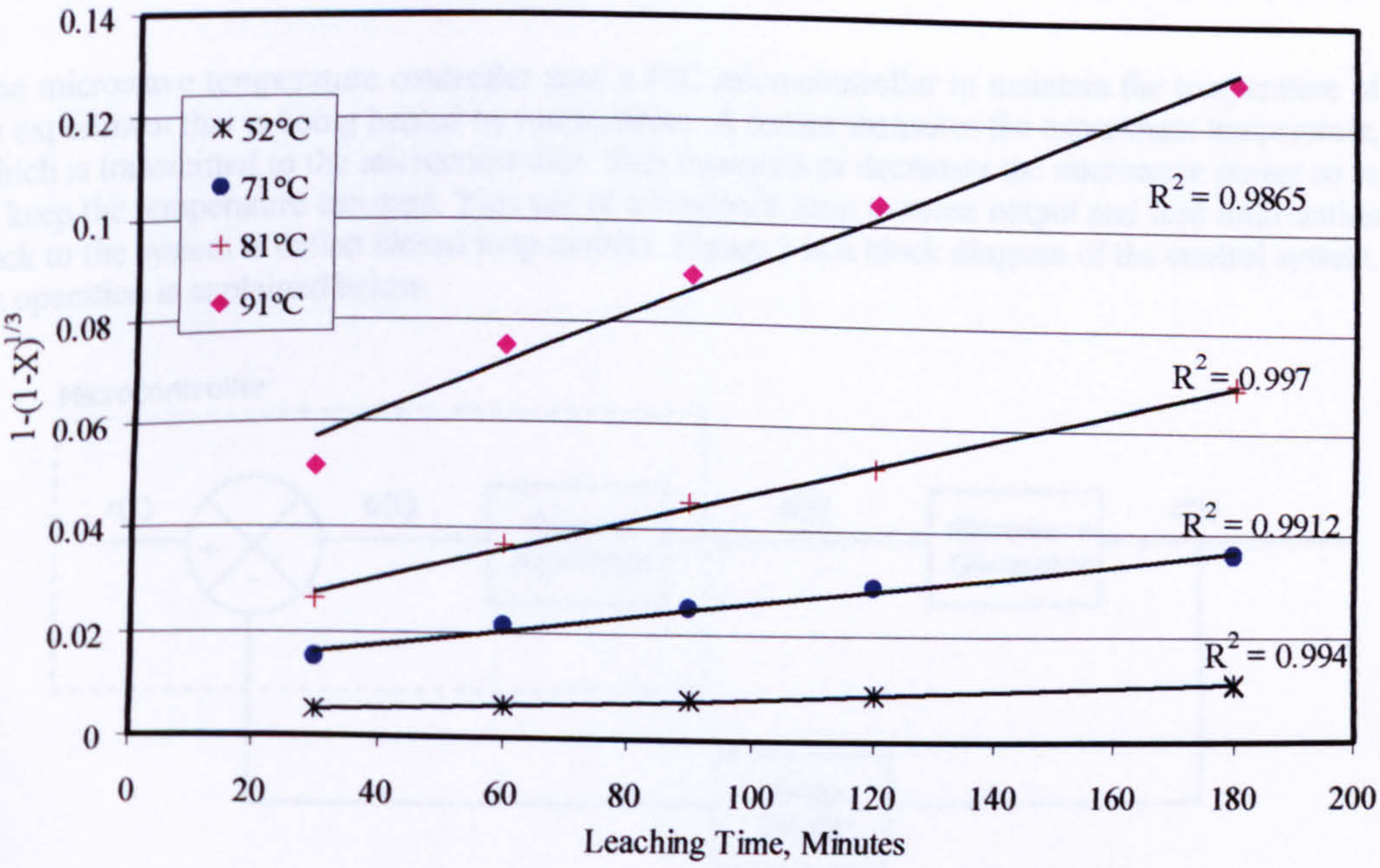

Figure 1 Plot fitted using a shrinking core model with limited step of surface reaction for rate data of microwave leaching of GBL chalcopyrite in ferric chloride

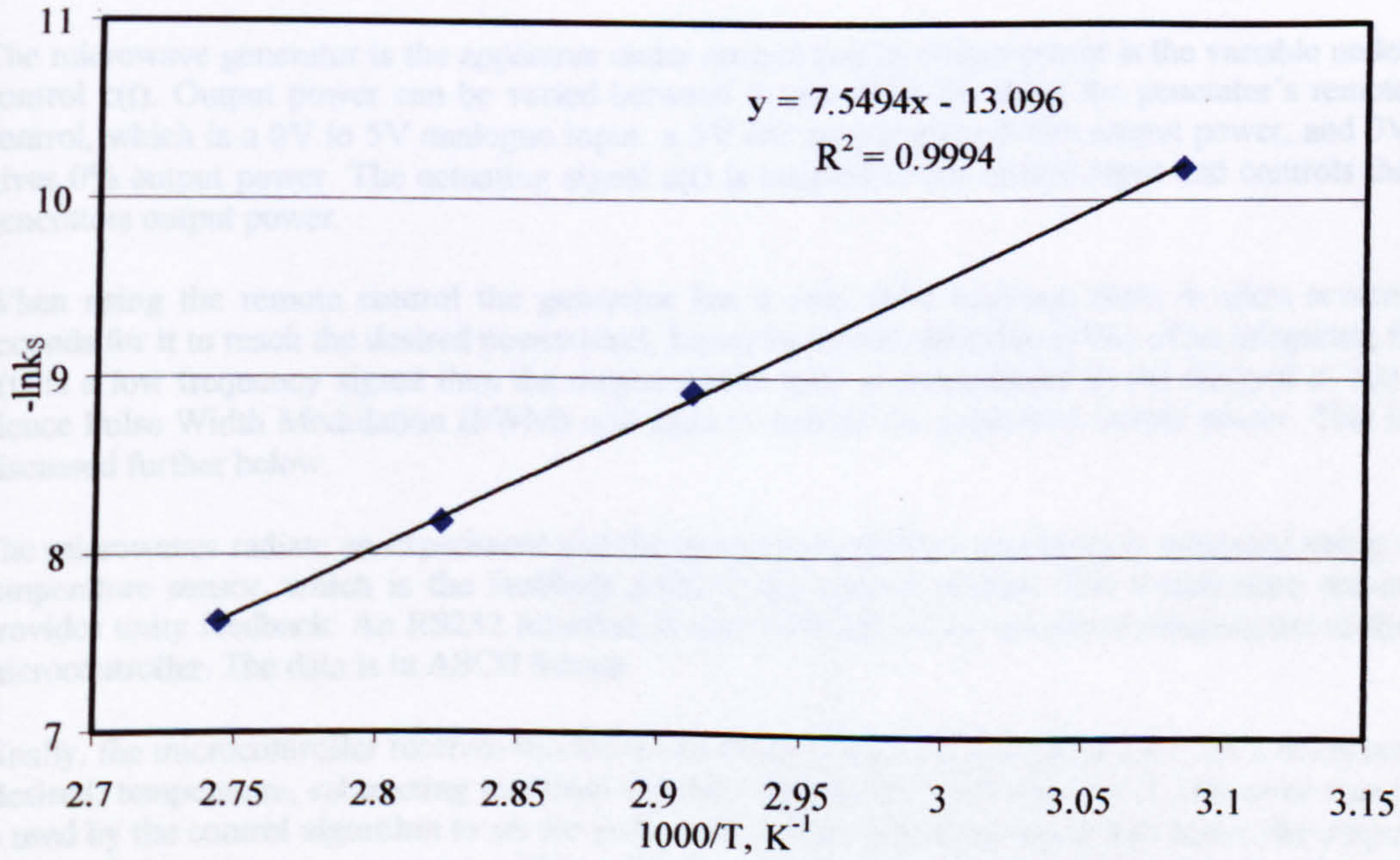

Figure 2 Arrhenius plot for microwave leaching of GBL chalcopyrite in ferric chloride

Appendix 4-27

Design of the microwave temperature controller

The Control System

The microwave temperature controller uses a PIC microcontroller to maintain the temperature of an experiment that is being heated by microwaves. A sensor measures the experiment temperature, which is transmitted to the microcontroller. This increases or decreases the microwave power so as to keep the temperature constant. This use of a feedback loop to sense output and feed information back to the system is called closed loop control. Figure 1 is a block diagram of the control system. Its operation is explained below.

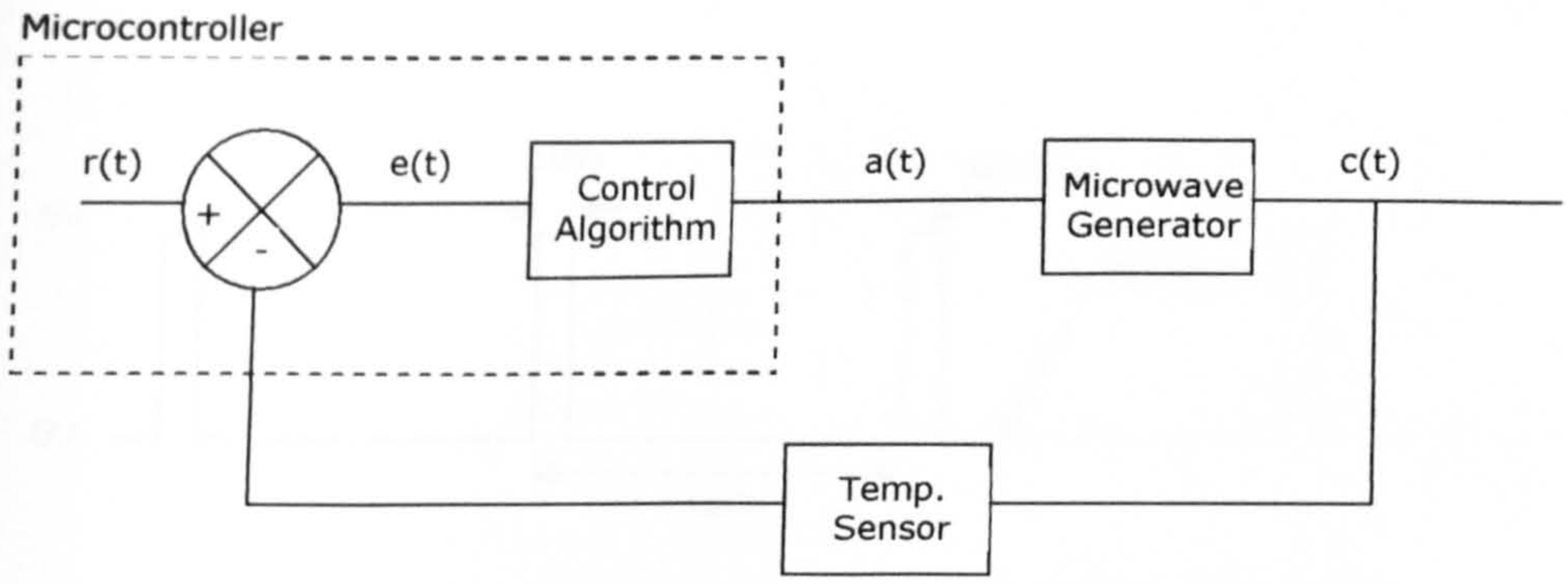

Figure 1: Block Diagram of System

r(t) = Reference Input
e(t) = r(t) – c(t) Error Signal
a(t) = Actuating Signal
c(t) = Control Variable

The microwave generator is the apparatus under control and its output power is the variable under control c(t). Output power can be varied between 0 and 100% by using the generator's remote control, which is a 0V to 5V analogue input: a 5V DC supply gives 100% output power, and 0V gives 0% output power. The actuating signal a(t) is coupled to the remote input and controls the generators output power.

When using the remote control the generator has a very slow response time; it takes several seconds for it to reach the desired power level, hence its transfer function is that of an integrator; if a(t) is a low frequency signal then the output power level is proportional to the integral of a(t). Hence Pulse Width Modulation (PWM) was used to control the generators output power. This is discussed further below.

The microwaves radiate an experiment and the temperature of the experiment is measured using a temperature sensor, which is the feedback path of the control system. The temperature sensor provides unity feedback. An RS232 interface is used to transmit the measured temperature to the microcontroller. The data is in ASCII format.

Finally, the microcontroller receives the measured temperature and compares this with a reference (desired) temperature, subtracting one from the other to give the error signal e(t). The error signal is used by the control algorithm to set the pulse width of the actuating signal and hence the output power of the microwave source, which will then 'steer' the experiment towards the desired temperature.

Pulse Width Modulation

Pulse Width Modulation (PWM) is a technique used to control analogue signal levels using a microcontrollers digital output. This is done by varying (modulating) the duty cycle of a square wave to encode a specific analog signal level, which in this case is the signal level needed to generate a given microwave power, a(t).

The control voltage, a(t), is supplied to the generators remote control input as a repeating series of on and off pulses. The on-time is the time during which the DC supply is applied to the load, and the off-time is the period during which the supply is switched off. The control voltage is switched at 1kHz. This is shown in figure 2.

Integrating under this waveform gives a signal that is 10% of 5V, or 0.5V.

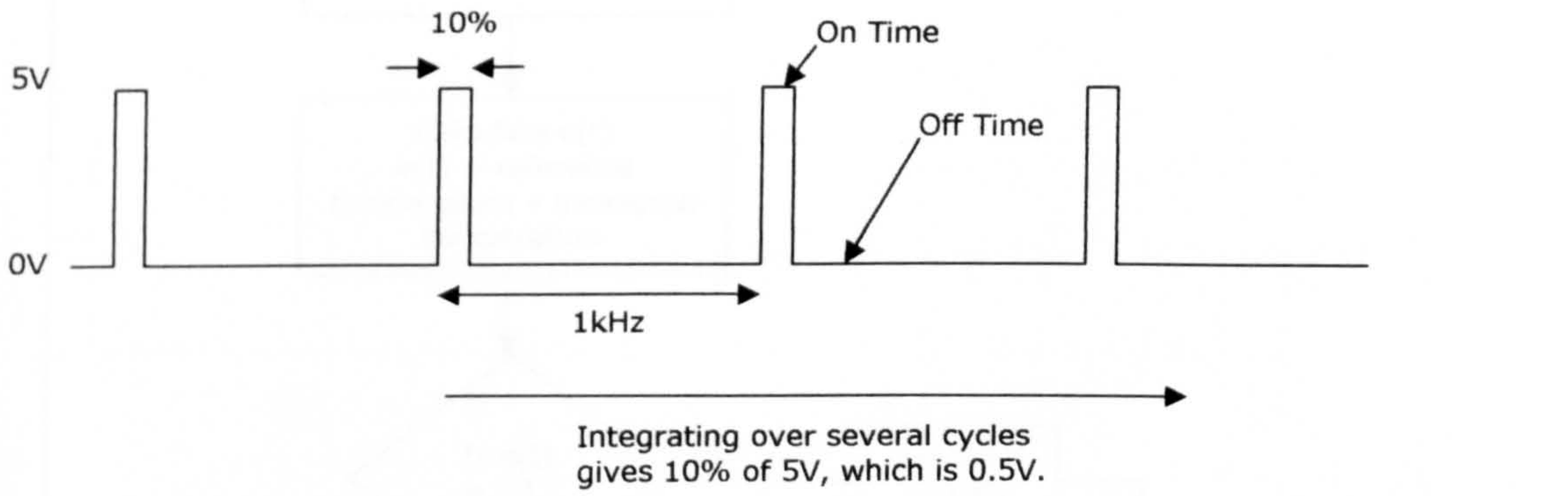

Figure 2: Pulse Width Modulation

The Control Algorithm

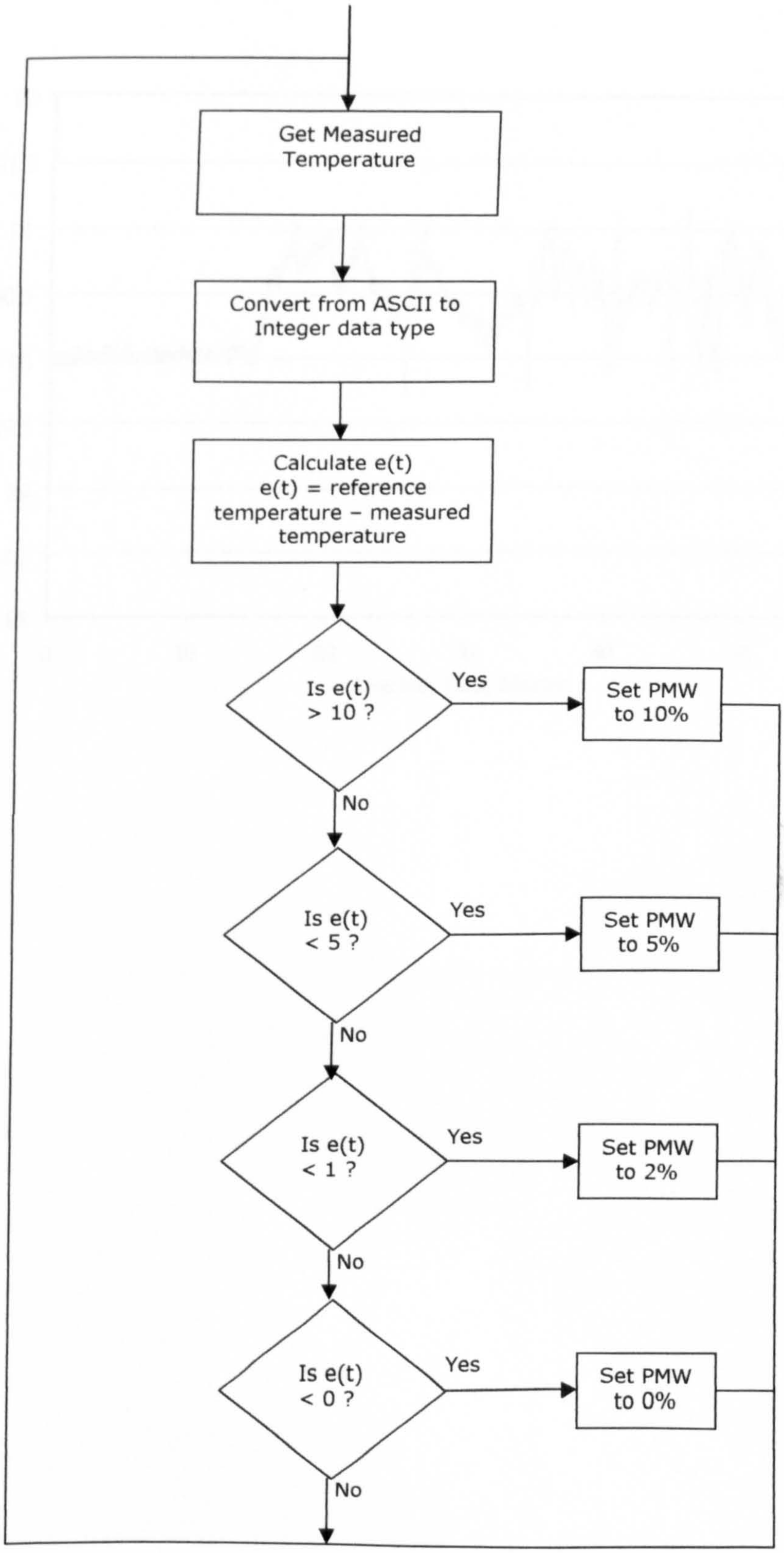

Appendix 4-27 was prepared by Mark Grub at the School of EEE –University of Nottingham

Appendix 4-28

Temperature profile in single mode cavity

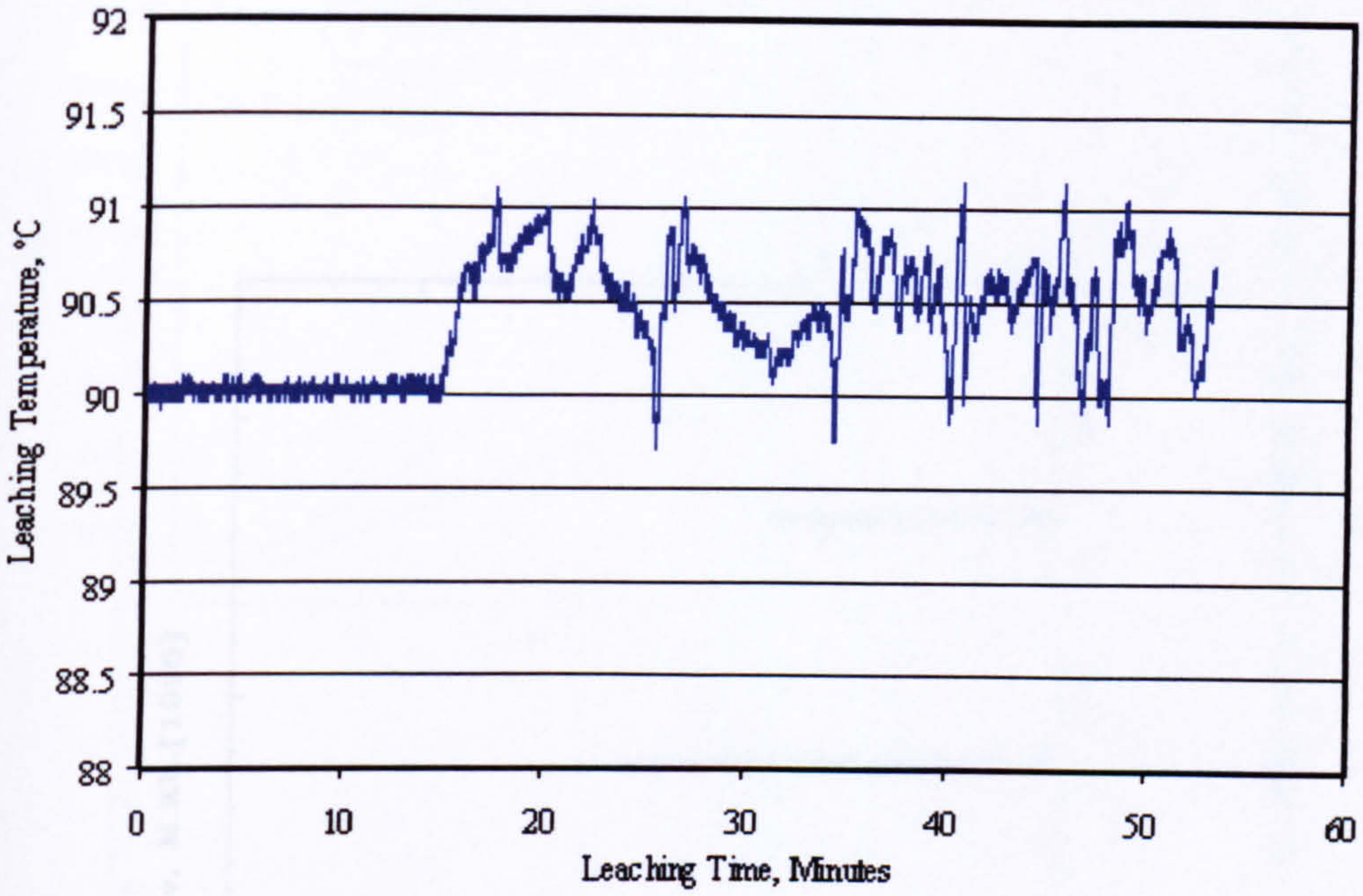

Appendix 5-1

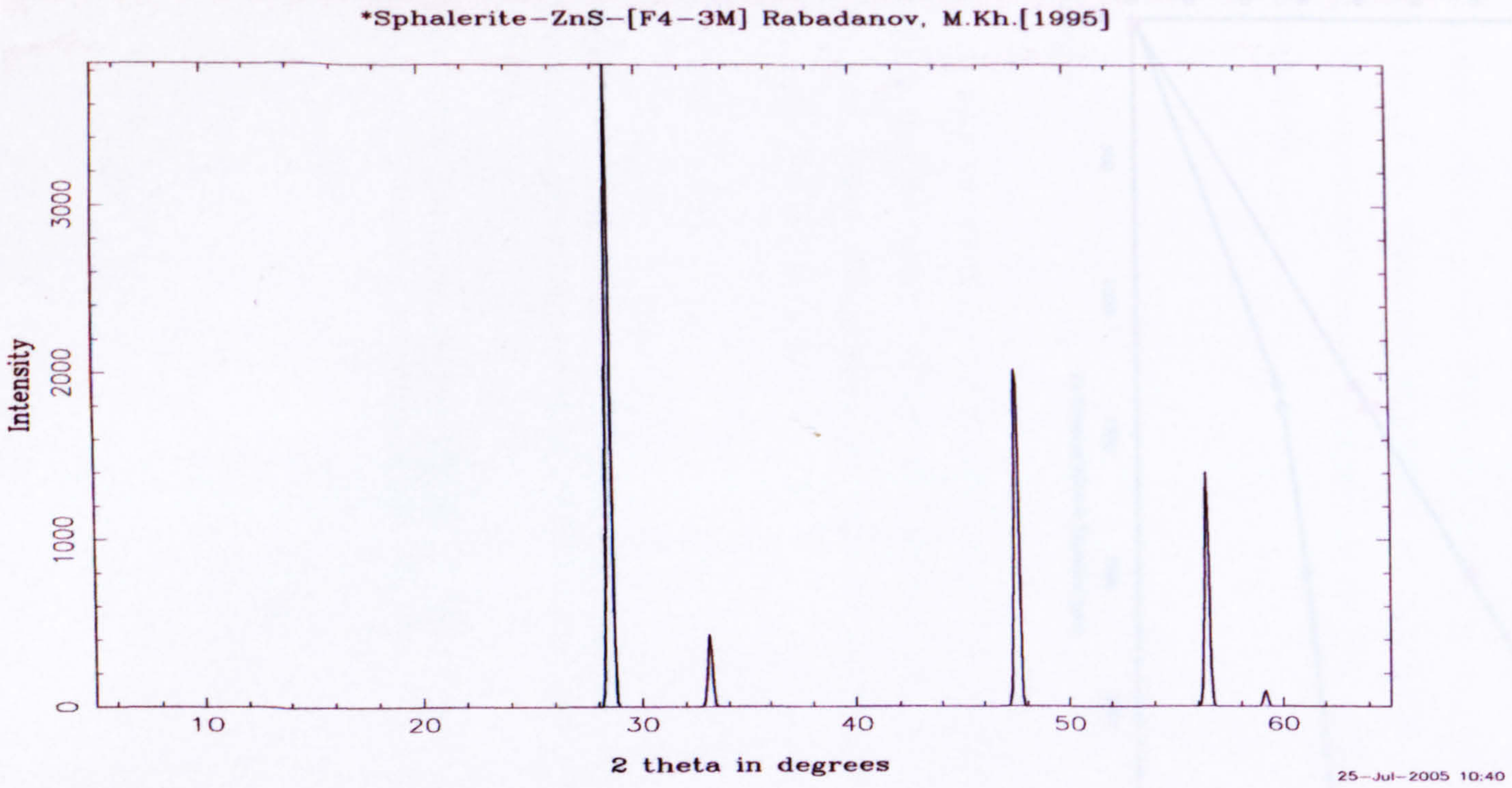

Figure 1 XRD pattern of pure sphalerite as Reported by Rabadanov (1995). The XRD pattern was obtained from Cambridge database service at **http://cds.dl.ac.uk/icsd/**

Appendix 5-2 Linearity of zinc emission lines (ICP analysis)

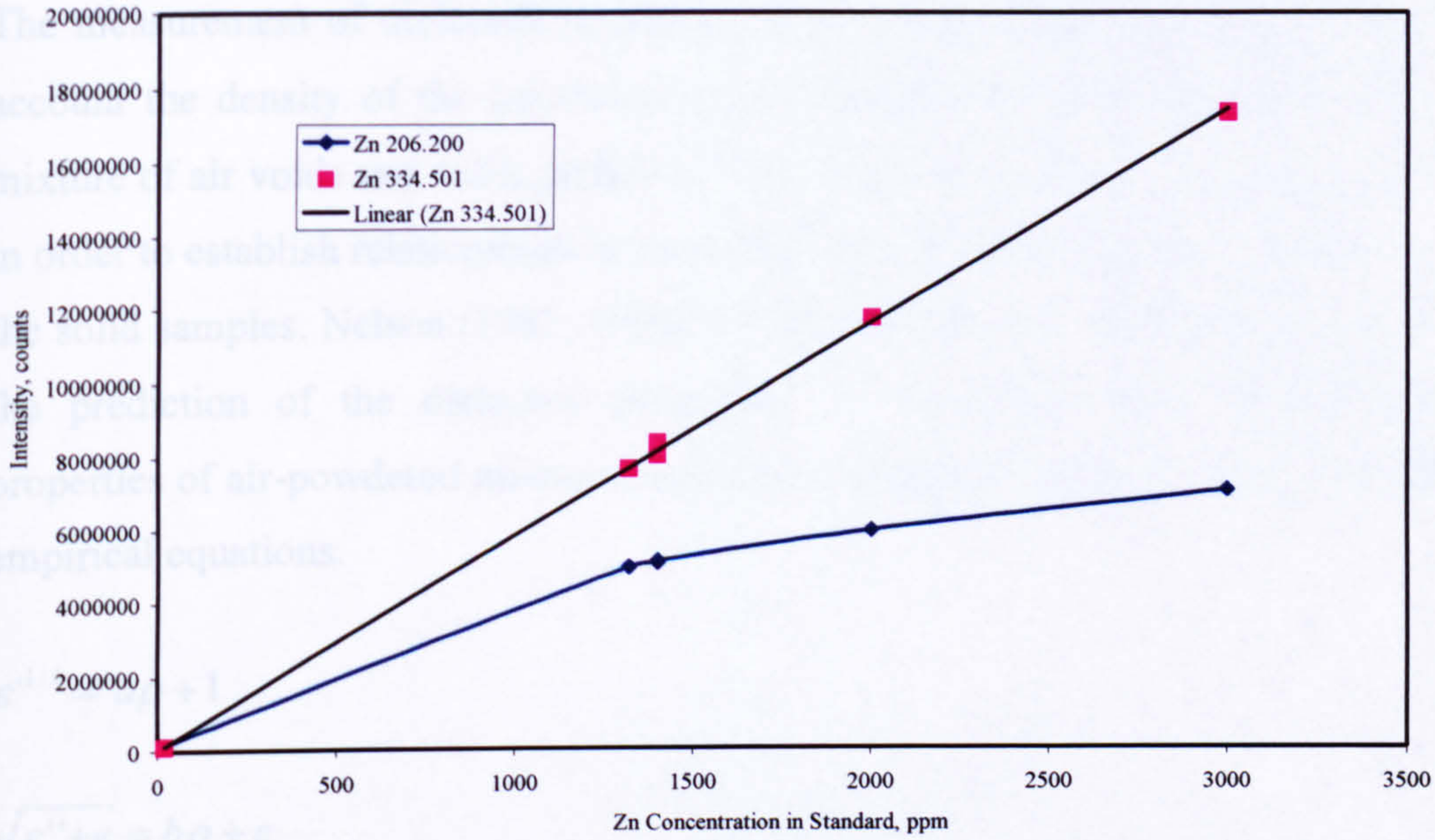

Appendix 6-1. Dependence of dielectric properties on the bulk density

The measurement of dielectric properties of powdered samples should take into account the density of the measured sample because the powdered sample is a mixture of air voids and solid particles. This issue was a subject of research work in order to establish relationships between bulk density and dielectric properties of the solid samples. Nelson (1983; 1988) has investigated the relationships to allow the prediction of the dielectric properties. It was found that the dielectric properties of air-powdered mixture could be calculated according to the following empirical equations.

$$\varepsilon''^{1/k} = a\rho + 1$$

$$\sqrt{\varepsilon'' + e} = b\rho + c$$

Where k can take values of 2 or 3 depending on the material, a, b and c are constants for a specific material at a given frequency and ρ is the density of air powder mixture. These relationships are valid only for a powder-air mixture where $\varepsilon' = 1$ and $\varepsilon'' = 0$ at zero density

Nelson, S.O., 1983. Observations on the density dependence of dielectric properties of particulate materials. Journal of Microwave Power, 18(2): 143-152.

Nelson, S.O., 1988. Estimating the permittivity of solids from measurements on granular or pulverized materials. Mater. Res. Soc. Proc., 124: 149-154.

Appendix 6-2. Dielectric properties of sodium chloride solutions

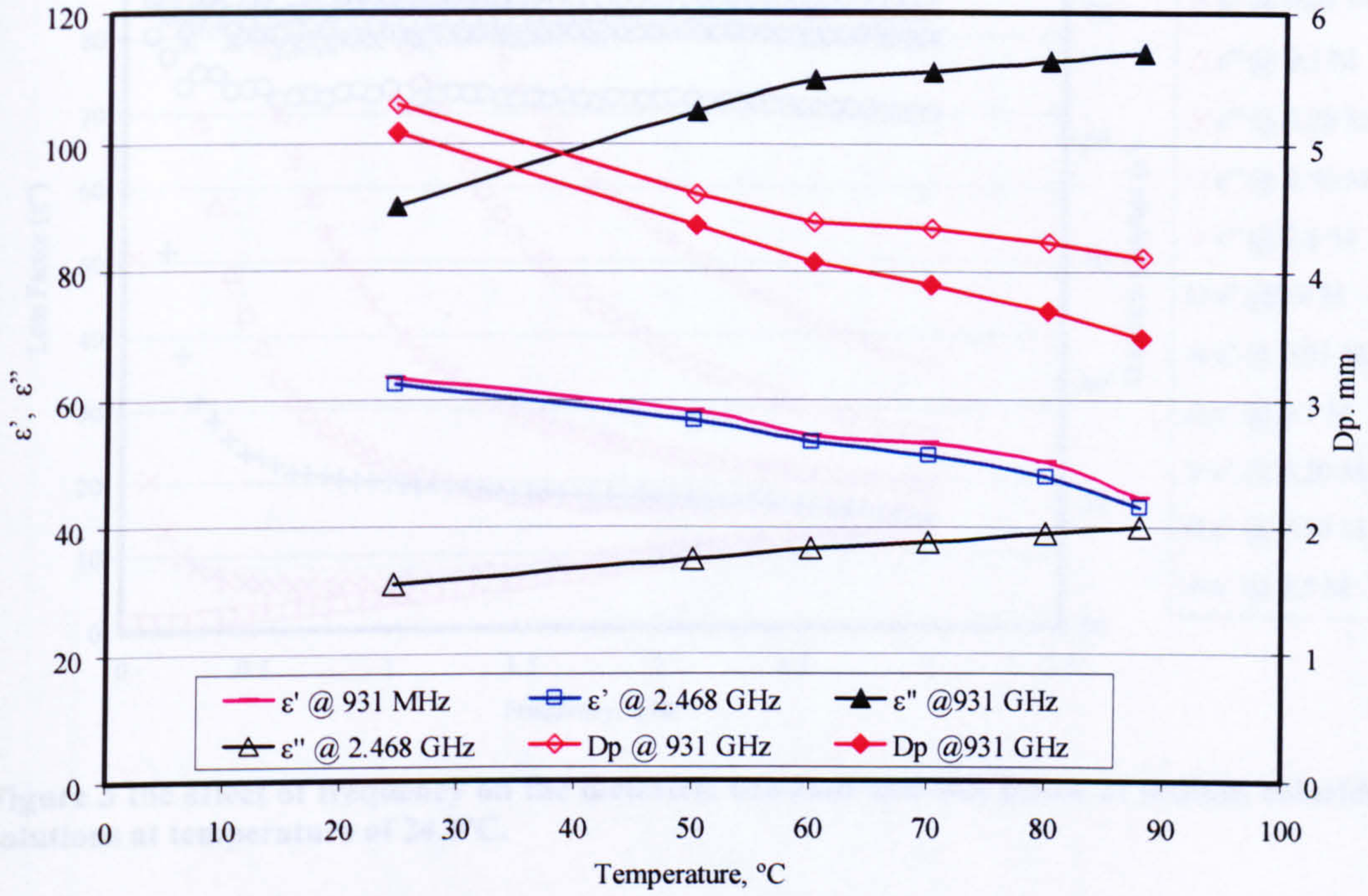

Figure 1 The effect of temperature on dielectric properties of 0.5 M NaCl solution at frequencies 931MHz and 2.468 GHz.

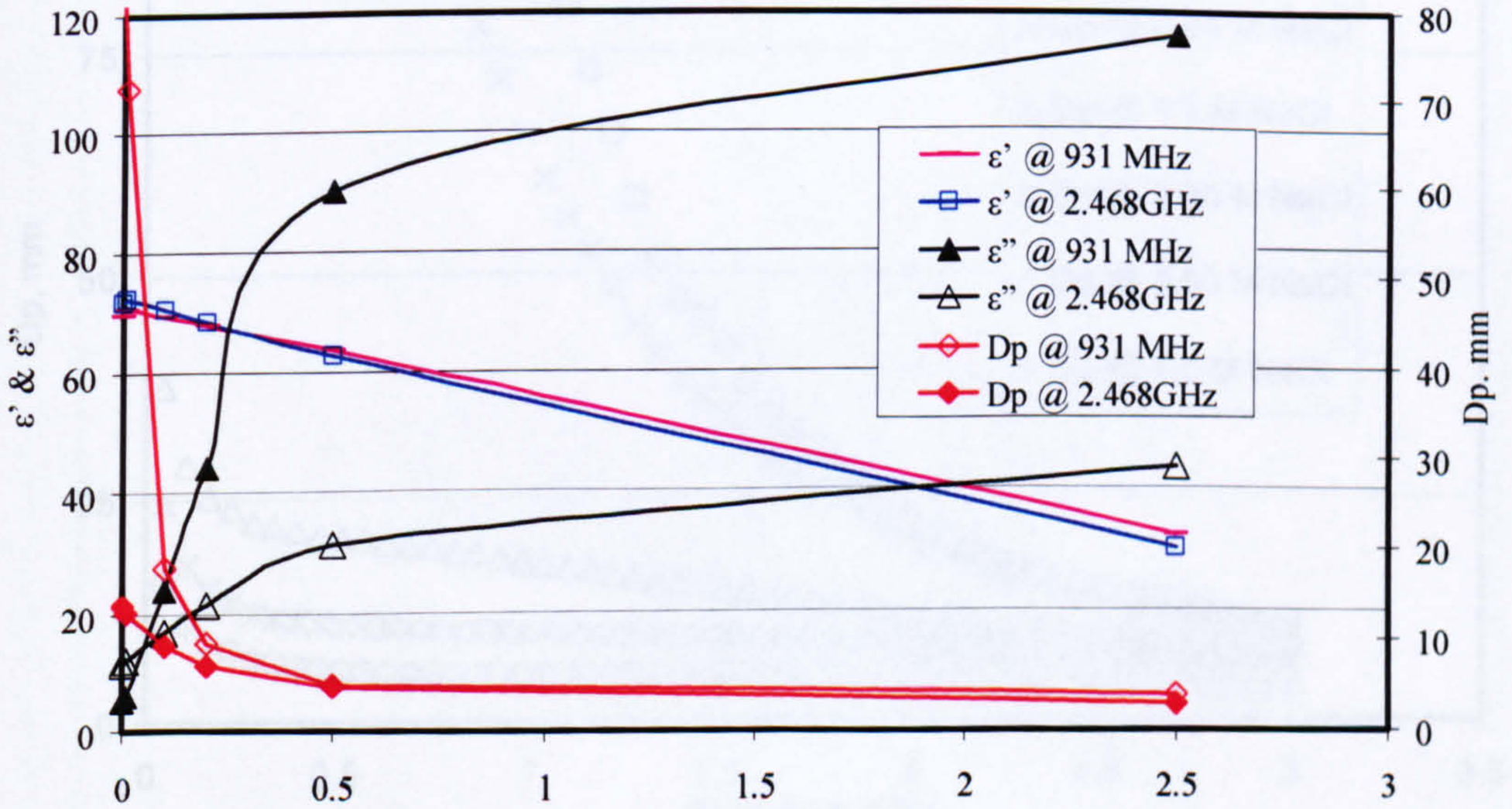

Figure 2 The effect of concentration on the dielectric properties of sodium chloride solution at room temperature and frequencies 931 MHz and 2.468 GHz

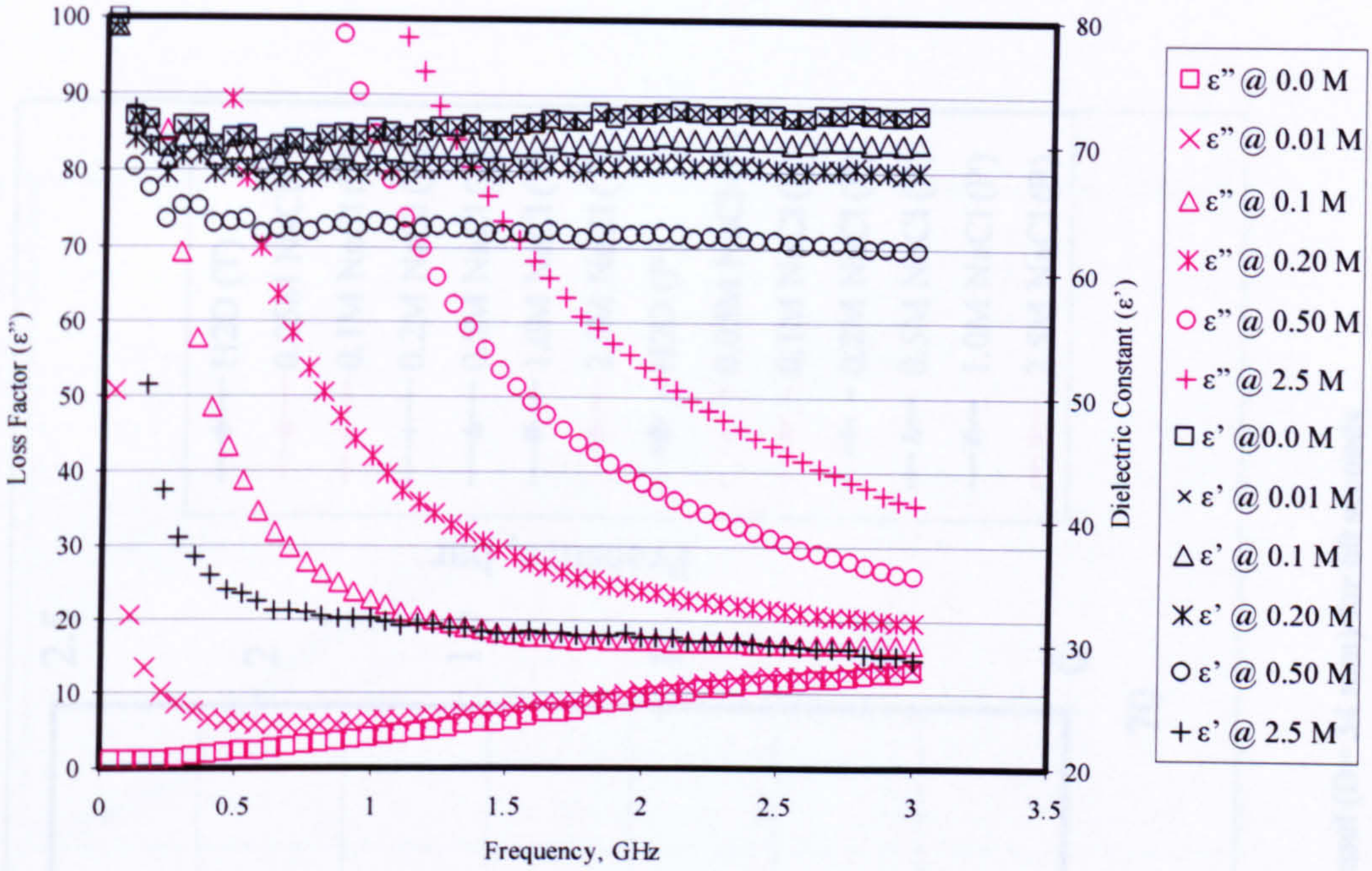

Figure 3 the effect of frequency on the dielectric constant and loss factor of sodium chloride solutions at temperature of 24.5°C.

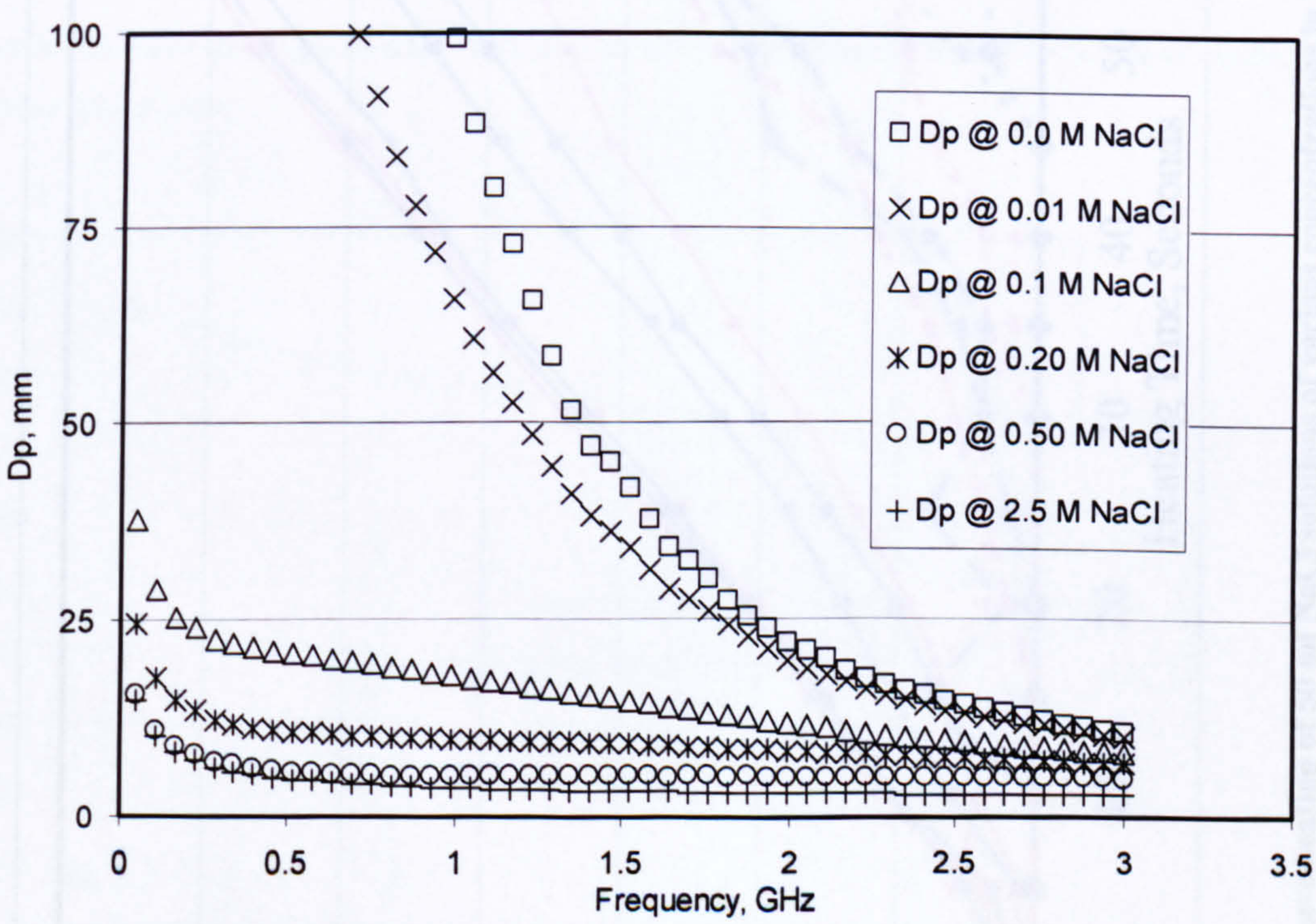

Figure 4. Penetration depth (D_P) as a function of frequency of sodium chloride solutions at temperature 24.5°C

Appendix 6-3. Microwave heating of NaCl solutions of various concentrations in the large vessel (D=34 mm)

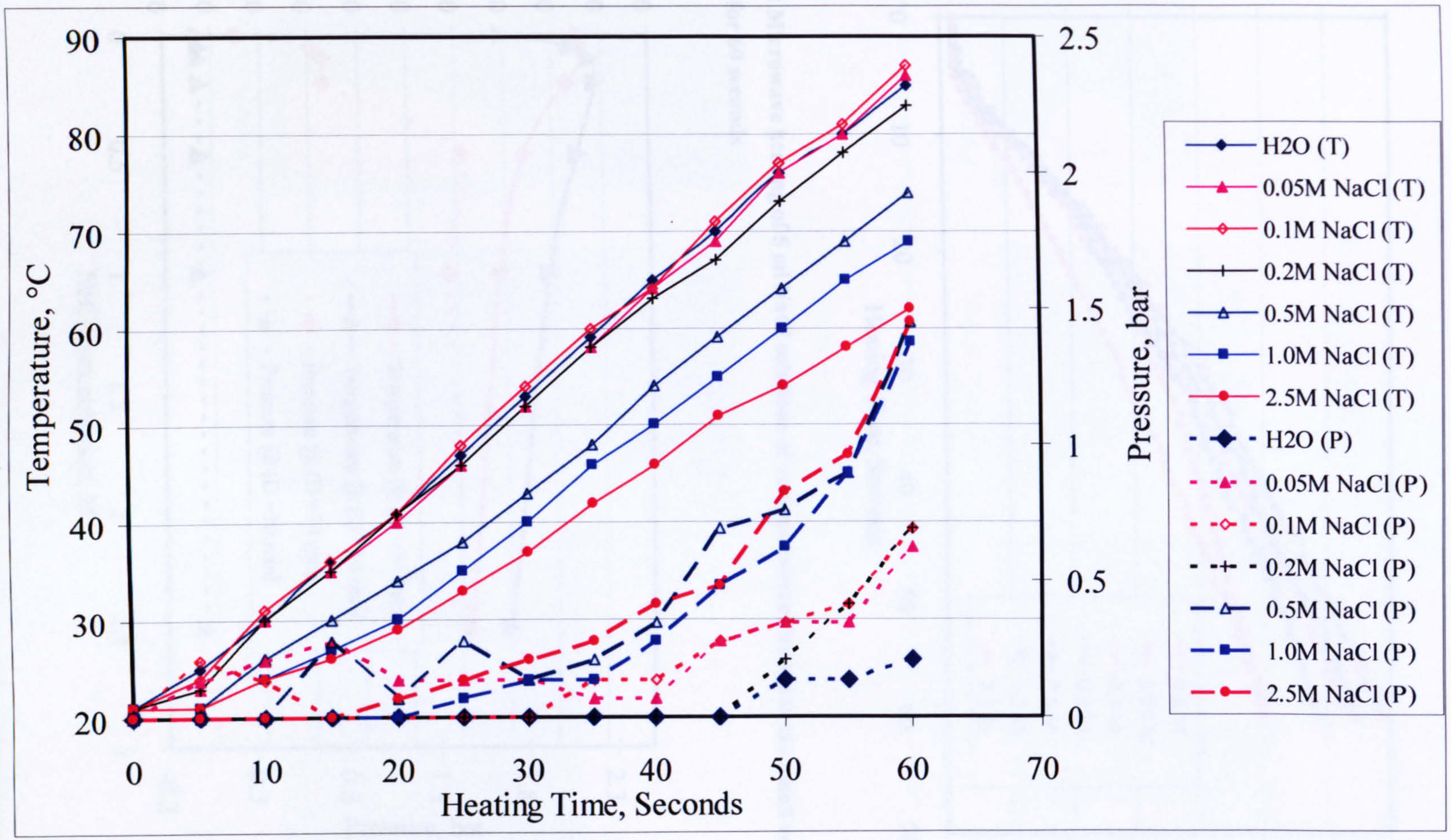

Figure 1.Microwave heating of 50 ml NaCl solutions of various concentrations in the large vessel (D= 34 mm) for 60 seconds

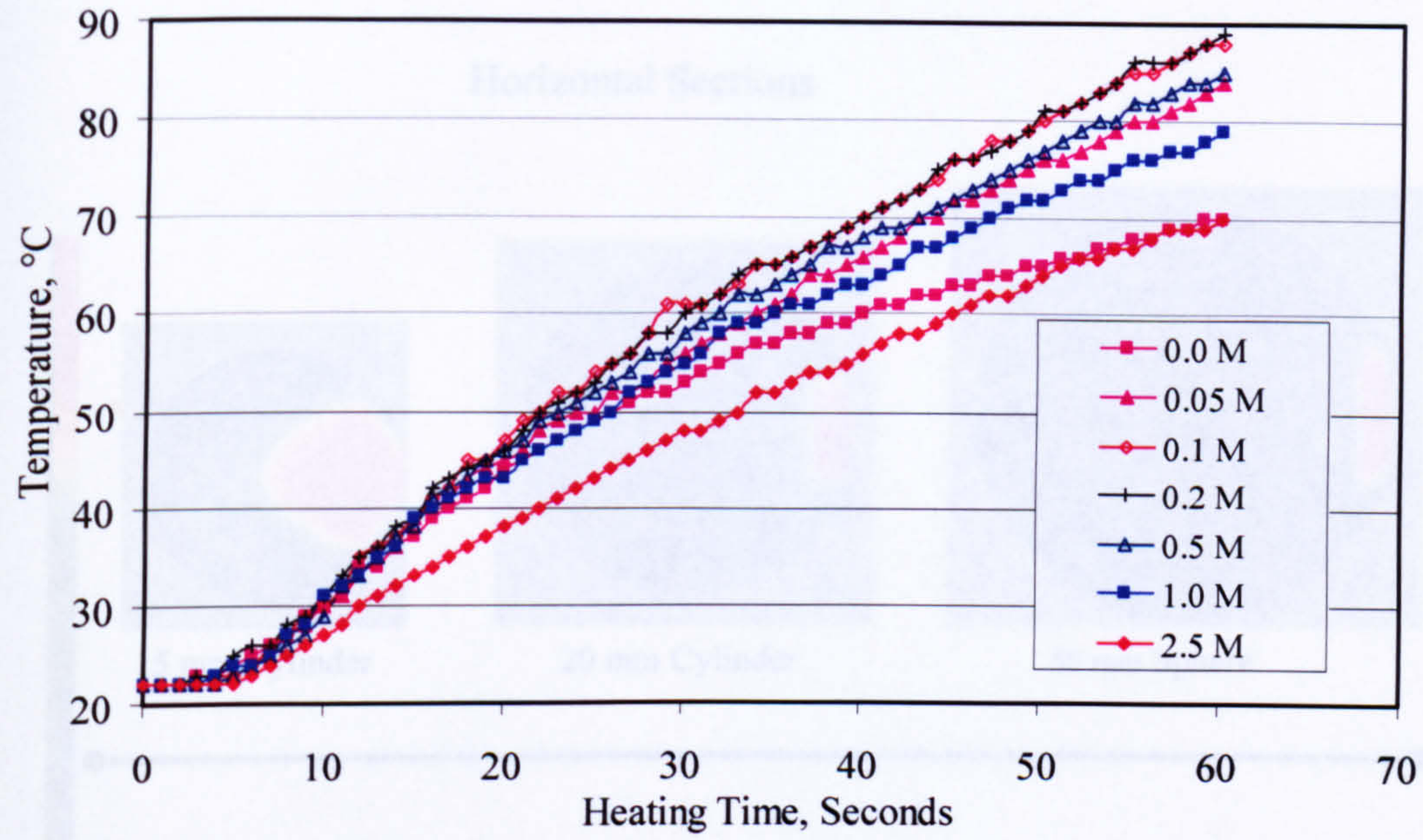

Figure 2 Microwave heating of 5 ml NaCl solutions of various concentrations in the small vessel (D= 10 mm) for 60 seconds

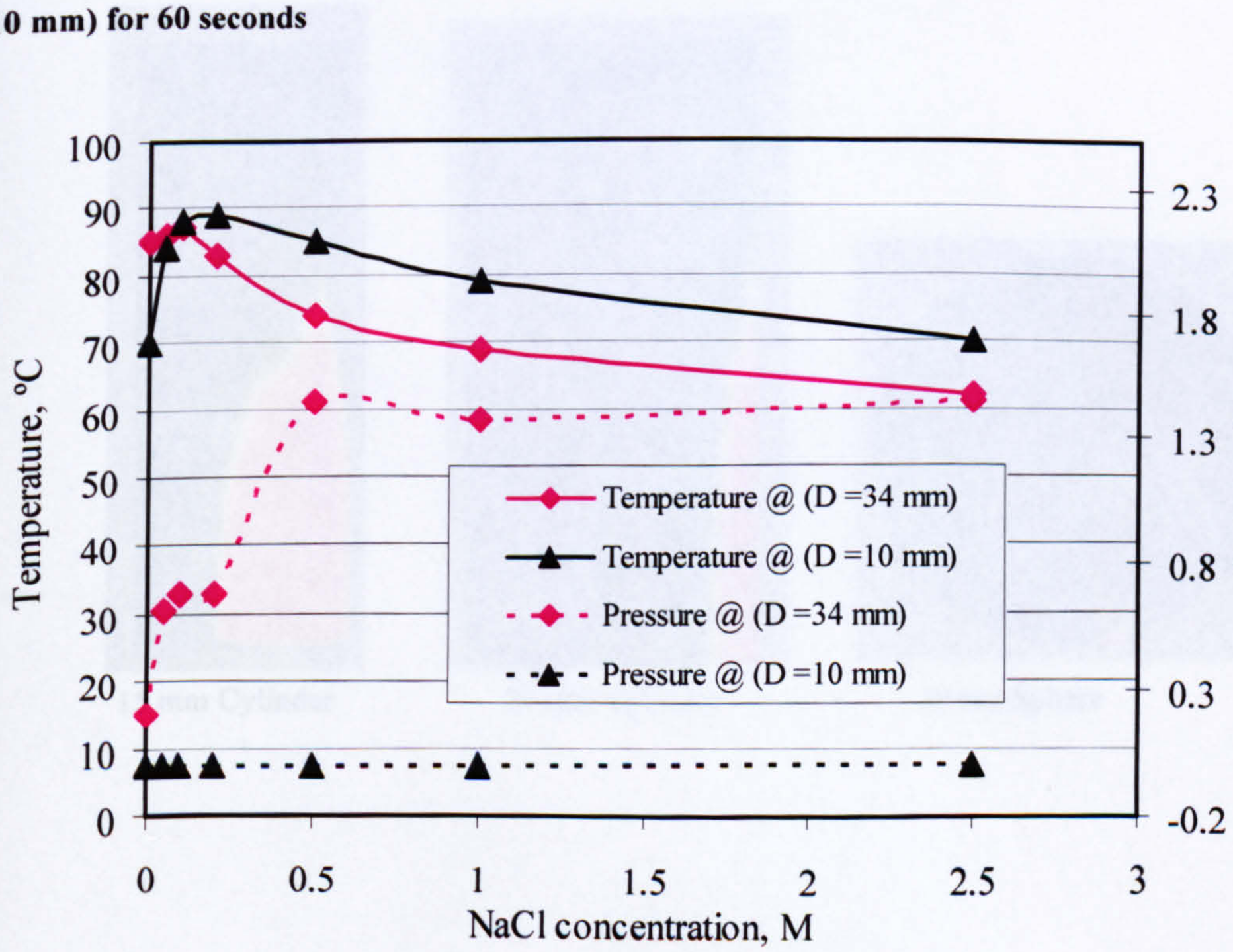

Figure 3 The effect of vessel diameter on the maximum bulk temperature and pressure of NaCl solutions of various concentrations after 60 seconds heating time

Appendix 6-4. Power density maps of reactors with various diameters in single mode cavity after being exposed to microwaves at a temperature of 24.5°C

Horizontal Sections